TECHNICAL REPORT

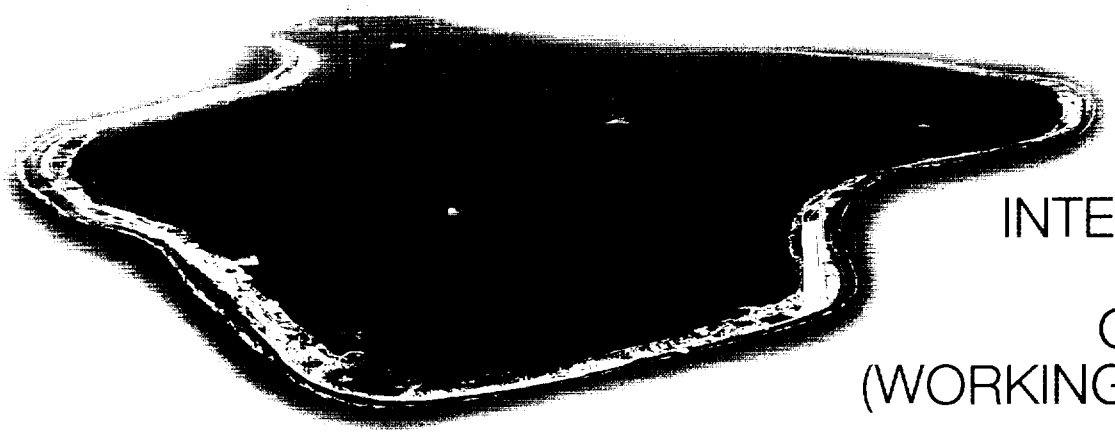

REPORT BY AN INTERNATIONAL ADVISORY COMMITTEE (WORKING GROUP 4)

THE RADIOLOGICAL SITUATION AT THE ATOLLS OF MURUROA AND FANGATAUFA

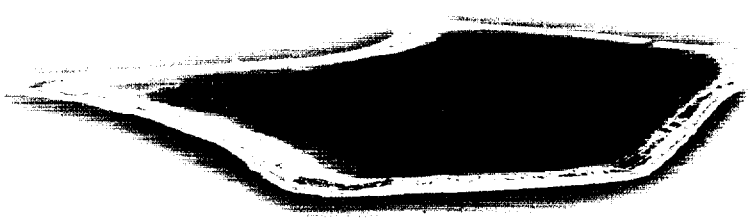

RELEASES TO THE BIOSPHERE OF RADIONUCLIDES FROM UNDERGROUND NUCLEAR WEAPON TESTS AT THE ATOLLS

Vol. 4

THE RADIOLOGICAL SITUATION AT THE ATOLLS OF MURUROA AND FANGATAUFA

TECHNICAL REPORT

In six volumes

VOLUME 4

RELEASES TO THE BIOSPHERE OF RADIONUCLIDES FROM UNDERGROUND NUCLEAR WEAPON TESTS AT THE ATOLLS

Report by an
International Advisory Committee
(Working Group 4)

THE RADIOLOGICAL SITUATION AT THE ATOLLS OF
MURUROA AND FANGATAUFA
TECHNICAL REPORT
VOLUME 4:
RELEASES TO THE BIOSPHERE OF RADIONUCLIDES FROM
UNDERGROUND NUCLEAR WEAPON TESTS AT THE ATOLLS
Report by an International Advisory Committee (Working Group 4)
IAEA-MFTR-4

Printed by the IAEA in Austria
August 1998

FOREWORD

At the present time there are various locations around the world affected by radioactive residues. Some of these residues are the result of past peaceful activities, others result from military activities, including residues from the testing of nuclear weapons. Stimulated by concern about the state of the environment, the steps taken towards nuclear disarmament, and improved opportunities for international co-operation, attention in many countries has turned to assessing and, where necessary, remediating areas affected by radioactive residues.

Some of these residues are located in countries where there is an absence of the infrastructures and expertise necessary for evaluating the significance of the radiation risks posed by the residues and for making decisions on remediation. In such cases, governments have felt it necessary to obtain outside help. In other cases, it has been considered to be socially and politically desirable to have independent expert opinions on the radiological situation caused by the residues. As a result, the International Atomic Energy Agency (IAEA) has been requested by the governments of a number of Member States to provide assistance in this context. The assistance has been provided by the IAEA in relation to its statutory obligation "to establish...standards of safety for protection of health...and to provide for the application of these standards...at the request of a State".

On 22 September 1995, a resolution of the General Conference of the IAEA called on all States concerned "to fulfil their responsibilities to ensure that sites where nuclear tests have been conducted are monitored scrupulously and to take appropriate steps to avoid adverse impacts on health, safety and the environment as a consequence of such nuclear testing".

The Study reported upon here was requested by the Government of France, which asked the IAEA to assess the radiological situation at the atolls of Mururoa and Fangataufa in French Polynesia, where France had conducted a nuclear weapon testing programme between 1966 and 1996. The IAEA convened an International Advisory Committee (IAC), under the chairmanship of Dr. E. Gail de Planque of the United States of America, to supervise the Study.

The IAC, which was given the tasks of providing scientific guidance and direction to the IAEA in the conduct of the Study, and of reporting on the Study's findings, conclusions and recommendations, met formally for the first time on 13–14 April 1996; this signalled the start of the Study of the Radiological Situation at the Atolls of Mururoa and Fangataufa. The Study has now been completed and a number of documents have been prepared. These documents are: the Main Report (which includes the Executive Summary); a Summary Report; and a Technical Report in six volumes.

I am pleased to have received these reports, which are being made available through the IAEA to a wider audience.

Mohamed ElBaradei

Director General
International Atomic Energy Agency

The Government of France covered most of the direct costs of the Study and provided invaluable logistic assistance throughout. Significant in-kind contributions were made by Argentina, Australia, Austria, Belarus, Belgium, Cuba, Denmark, Fiji, Germany, Indonesia, Japan, the Republic of Korea, New Zealand, Norway, the Russian Federation, Slovenia, Spain, Sweden, Switzerland, the United Kingdom, the United States of America, the European Commission, the South Pacific Forum, the South Pacific Regional Environment Programme, the Office of the Sub-Regional Representative for the Pacific of the Food and Agriculture Organization of the United Nations, the World Health Organization and the United Nations Scientific Committee on the Effects of Atomic Radiation.

In addition, significant in-kind contributions were made by the laboratories and other institutions involved in the Study, whose activities were co-ordinated by the Agency's Laboratories at Seibersdorf, Austria, and the IAEA Marine Environment Laboratory, Monaco. The laboratories and other institutions were: the Australian Nuclear Science and Technology Organisation (ANSTO), Sydney, and the Australian Radiation Laboratory, Melbourne, Australia; the Institute for Inorganic Chemistry and the Federal Institute for Food Control and Research, Vienna, Austria; the Institute of Radiobiology, Minsk, Belarus; the Centro de Isótopos, Havana, Cuba; the Risø National Laboratory, Roskilde, Denmark; the Physikalisch-Technische Bundesanstalt, Braunschweig, and the Federal Fisheries Research Centre, Hamburg, Germany; the National Radiation Laboratory, Christchurch, and the Institute of Geological and Nuclear Sciences, Lower Hutt, New Zealand; the Norwegian Radiation Protection Authority, Østerås, Norway; the Jožef Stefan Institute, Ljubljana, Slovenia; the Instituto del Medio Ambiente, CIEMAT, Madrid, Spain; the Radiochemistry Group, Central Veterinary Laboratory, Addlestone, Surrey, and the Centre for Environment, Fisheries and Aquaculture Science, Lowestoft, Suffolk, United Kingdom; and the Environmental Measurements Laboratory, US Department of Energy, New York, N.Y., and Lawrence Livermore National Laboratory, Livermore, California, United States of America.

The IAEA wishes to thank the large number of people who were involved in different ways in the Study. They are all acknowledged in the various reports of the IAC.

EDITORIAL NOTE

PREFACE

Between 1966 and 1996, France conducted 193 'expériences nucléaires' (nuclear experiments — a term used by the French authorities to include the full testing of nuclear weapons and the conduct of certain safety trials) above and beneath the atolls of Mururoa and Fangataufa in the Tuamotu Archipelago of French Polynesia. All French testing ceased on 27 January 1996. Before the completion of the last series of tests the Government of France requested the International Atomic Energy Agency (IAEA) to conduct a study to assess the radiological impact of the tests.

The IAEA agreed to carry out a study — the Study of the Radiological Situation at the Atolls of Mururoa and Fangataufa — for the purpose of ascertaining whether, as a consequence of the tests, radiological hazards exist now or will exist in the future, and making recommendations on the form, scale and duration of any monitoring, remedial action or follow-up action that might be required. An International Advisory Committee (IAC) was convened by the Director General of the IAEA to provide scientific direction and guidance to the IAEA in the conduct of the Study and to prepare a report on the Study's findings, conclusions and recommendations.

The IAC's first formal meeting took place in Vienna on 13–14 April 1996 and its final one, also in Vienna, on 3–5 February 1998. This publication constitutes one of several reports of the IAC to the Director General describing the conduct of the Study and its findings, conclusions and recommendations.

The terms of reference of the Study called for an evaluation of the radiological situation at the atolls (and in other involved areas). It is important to emphasize that it is the radiological situation at the atolls, both as it is at present and as it might develop in the long term, including its consequences for human health, that the Study was required to address, and not any past radiological consequences of the French nuclear testing programme. This had two implications for the Study.

First, it was not within the terms of reference of the Study to attempt to assess retrospectively doses received by inhabitants of the region as a result of the atmospheric nuclear tests at the time when those tests were carried out. Those doses were due in part to short lived fallout — for example, radioactive iodine (especially ^{131}I, which has a half-life of eight days). However, the Secretariat of the United Nations Scientific Committee on the Effects of Atomic Radiation (UNSCEAR) did provide the IAC with the results of a review of such doses that had been received by people in the South Pacific region in the past. The IAC believes that readers will be interested in these results, and it has therefore included them in an annex to the Main Report on the Study. The results are accepted by the IAC as providing an objective and balanced view of the situation.

Second, the IAC felt that the most informative indicator of the radiological situation at the atolls would be the present and future individual annual effective doses that people (real and hypothetical) at the atolls and in other involved areas might receive as a consequence both of the radioactive material that is now in the accessible environment and of that which might be released into the accessible environment over time from underground. It should be noted that while UNSCEAR has invoked other dosimetric quantities — the 'effective dose commitment' and the 'collective effective dose commitment' — in assessing the global impact of nuclear weapon testing, the IAC did not consider it appropriate to use these quantities in any reports of the Study for the reasons discussed in Section 1 of the Main Report.

The French Government provided much of the information used in the Study. This information was independently evaluated by Study participants and, where practicable, validated. For example, to provide a basis for the evaluation of French environmental monitoring data, the IAEA carried out an environmental sampling and surveillance campaign to measure independently contemporary levels of radioactive material present in the environment of the atolls. Also, with the co-operation of French scientists, samples of underground water were collected by Study participants from two test cavity–chimneys beneath the rim of Mururoa, and from deep in the carbonate layer beneath the two lagoons. These samples were analysed for a number of radionuclides, and the results provided an independent check on the validity of assumptions made in some of the Study's calculations, for example of radionuclide concentrations in the cavity–chimney of each test. The French Government allowed complete access to the atolls for these surveys and provided the necessary logistic support.

In addition to the information provided by the French Government, a small amount of information had been published in the open literature on measured levels of certain radionuclides (^{60}Co, ^{90}Sr, ^{137}Cs and $^{239+240}Pu$) in the environment of the atolls, and reports of three scientific missions to the atolls — the Tazieff Mission of June 1982, the Atkinson Mission of October 1983 and the Cousteau Mission of June 1987 — were in the public domain. Issues raised by these missions guided the IAC in the choice of certain topics to be addressed in the Study.

It is not possible to place reliable quantitative limits on the errors associated with the dose assessments carried out by the Study. The estimated upper limits to contemporary doses can be accepted with confidence as they are based on measurements of the concentrations of residual radioactive material at present in the environment of the atolls. However, considerable uncertainty is possible in the estimation of future doses because of the complexities of the physical processes involved in releases from underground sources and the limitations of the geological migration models used. Therefore, in the absence of definitive information, conservative assumptions have been made and the estimated future doses can be regarded as upper limit values. In any event, they are so small that large errors in the assumptions made would not affect the IAC's basic finding that possible radiation doses to people now, and potential doses at any time in the future, arising from the conditions at the atolls are a very small fraction of the doses people already receive from natural radiation sources.

The Main Report (which includes the Executive Summary) is a distillation of the large amount of scientific work carried out in the course of the Study, which is described in detail in the accompanying six volume Technical Report. The Summary Report presents a comprehensive summary of the Main Report, including its findings, conclusions and recommendations.

ACKNOWLEDGEMENTS

The Main Report and the Technical Report, compiled essentially between September 1997 and March 1998, represent an enormous effort by many people. All Study participants contributed, but the major load was borne by the Task Group Chairmen (A. McEwan and D.M. Levins) and the Working Group Chairmen (F. Schönhofer, D. Woodhead, L.-E. De Geer, C. Fairhurst and E. Mittelstaedt). The members of the IAEA management team, particularly A.J. González and R.M. Fry, also worked tirelessly. The Summary Report was compiled by D. Delves of the IAEA. The IAC wishes to acknowledge their dedication and that of all other participants, and also to thank the many IAEA staff members without whose efforts the Study would not have been possible. In addition, the co-operation of the French Government and the efforts of members of the French Liaison Office — G. Goutière and P. Delcourt and, in the past year, J.-F. Sornein and G. Corion — must be commended.

The IAC thanks those laboratories — all listed in the Main Report and the Technical Report — which were involved in the analysis of samples collected during the sampling and surveillance campaign, and the underground water sampling exercise, at the atolls and commends the efforts of the staff of the Agency's Laboratories at Seibersdorf, Austria, and the IAEA Marine Environment Laboratory, Monaco, who helped to co-ordinate, manage and conduct those campaigns.

The IAC expresses its appreciation for the support and encouragement of the former Director General of the IAEA, H. Blix, and the current Director General, M. ElBaradei, and for their willingness to provide the IAEA resources necessary for carrying out the Study.

The Chairman further wishes to thank all the members of the IAC for their thoughtful and competent guidance throughout the course of the Study.

E. Gail de Planque

Chairman
International Advisory Committee

NOTE FROM THE TASK GROUP CHAIRMEN

The Study of the Radiological Situation of the Atolls of Mururoa and Fangataufa, scientific details of which are presented in this Technical Report, was carried out under the scientific direction and guidance of an International Advisory Committee convened by the IAEA. It involved the efforts of a large number of scientists with expertise in many disciplines. The assessments were carried out in teams organized into two Task Groups and five Working Groups.

Task Group A evaluated the present levels of residual radioactive material in the environment of the atolls and their surrounding waters, and assessed the present and future radiation doses to people and the present radiation doses to aquatic biota attributable to this material. The Group was supported by two Working Groups dealing with Terrestrial Environmental Contamination (Working Group 1) and Aquatic Environmental Contamination (Working Group 2).

Task Group B estimated the rate at which the residual radioactive material, at present underground, might migrate through the geosphere and be released into the surrounding ocean, thereby providing the basis for the assessment of long term doses attributable to this material. The Group was supported by three Working Groups dealing, in turn, with the underground radionuclide inventory, called the Source Term (Working Group 3), Geosphere Radionuclide Transport (Working Group 4) and Marine Modelling (Working Group 5).

Each of the Working Groups produced a detailed report, which was drawn upon in the preparation of the Main Report of the Study. In addition, a sixth volume was written dealing with the estimation and assessment of radiation doses based on information provided by the Working Groups. The titles of these six volumes, which form the Technical Report of the Study, are:

Volume 1: *Radionuclide Concentrations Measured in the Terrestrial Environment of the Atolls,* A report by Working Group 1;

Volume 2: *Radionuclide Concentrations Measured in the Aquatic Environment of the Atolls,* A report by Working Group 2;

Volume 3: *Inventory of Radionuclides Underground at the Atolls,* A report by Working Group 3;

Volume 4: *Releases to the Biosphere of Radionuclides from Underground Nuclear Weapon Tests at the Atolls,* A report by Working Group 4;

Volume 5: *Transport of Radioactive Material within the Marine Environment,* A report by Working Group 5;

Volume 6: *Doses due to Radioactive Materials Present in the Environment or Released from the Atolls,* A report by Task Group A.

This document, Volume 4 of the Technical Report, describes in some technical detail the approach used by Working Group 4 to assess the rate, as a function of time into the long term future, at which radioactive material at present underground at the atolls will migrate through the volcanics and the carbonate capping of the atolls and be released to the ocean either through the lagoons, or directly from the deeper layers of the carbonate formations. This volume supplements the material presented in Section 6 of the Main Report.

Andrew McEwan
Chairman
Task Group A

Des Levins
Chairman
Task Group B

ACKNOWLEDGEMENTS

The results of this Study have been enriched considerably by the efforts of many associates. To all such colleagues, we express our sincere gratitude and hope that your contributions are adequately represented in this, the report of Working Group 4.

The Working Group owes a special debt to colleagues of the International Geomechanical Commission (IGC) who carried out an independent study on the stability and hydrology of Mururoa and Fangataufa Atolls. The report of the IGC has been drawn upon in the development of some of the material in the present Study. The work of the Working Group has also benefited immeasurably from the efforts of my colleagues and graduate students of the University of Minnesota, Minneapolis, USA, who have volunteered many hours of their time to make analyses, prepare illustrations, etc. Carlos Carranza-Torres conducted the cavity stability analysis and prepared several drawings for Section 2; Igor Jankovic and Philippe Legrand prepared the analyses for Appendix I of this report.

David Smith, a member of Task Group B, attended several meetings of the Working Group, provided valuable help throughout, responded to numerous enquiries with prompt and illuminating insights on questions of nuclear geochemistry and participated in the underground water sampling campaign. Assistance in the sampling of underground waters at the atolls was provided by Sandor Mulsow, IAEA Marine Environment Laboratory, Monaco. Wilfried Pfingsten, Paul Scherrer Institute, Villigen, Switzerland, performed many of the calculations used in Section 5 of this volume and gave invaluable professional help throughout the Study. Urs Berner and Joe F. Pearson, also of the Paul Scherrer Institute, provided valuable contributions. Pierre Perrochet and Laurent Tacher of the Ecole Polytechnique Fédérale de Lausanne, Switzerland, performed modelling calculations presented in Section 3 and provided the bathymetric profiles and sections used in the figures to illustrate testing areas. Special thanks go also to those staff members of the Accelerator Mass Spectrometry Unit of the Australian Nuclear Science and Technology Organisation at Lucas Heights, near Sydney, and of the IAEA Marine Environment Laboratory, who carried out all the analyses associated with the underground water sampling campaign at the atolls.

The Study has been particularly rewarding in providing the opportunity to be associated with outstanding professional and exceptional individuals from many countries: the IAEA Project Management and the International Advisory Committee (IAC) that oversaw the Study; Robert Fry (IAEA), Technical Project Manager for the entire Study; Des Levins, Chairman, Task Group B; Lars-Erik De Geer and Ekkehard Mittelstaedt, Chairmen of Working Groups 3 and 5, respectively; Ernst Warnecke (IAEA), Scientific Secretary to Working Group 4, who was in charge of the underground water sampling campaign at the atolls and has provided conscientious and diligent support in assembling this report, for which we are grateful; Carol Robinson (IAEA) integrated text and illustrations for various drafts of the report. Renate Boldizsar (IAEA) has provided quiet and efficient support throughout the Study. My special thanks are due to Chad Sylvain and, more recently, Katie Flynn of Itasca Consulting Group Inc., Minneapolis, who suffered through all of the many changes in the manuscript and triumphed, finally, over much adversity. Furthermore, I have to acknowledge with great appreciation the Austrian Research Centre, Seibersdorf, which provided its facilities in the Vienna city centre for Working Group 4 meetings during weekends.

Colonel P. Delcourt and G. Goutière, and, more recently, Colonel G. Corion and J.-F. Sornein of the French Liaison Office have been helpful and unfailingly courteous, especially in their attempts to provide answers to questions on topics hedged with military security. To all of these and many more, some whose names are still unknown to us, please accept our sincere appreciation.

Finally, a special word to those guardians of the English language, who have cheerfully contributed much to what we hope is an intelligible result: Kathy Sikora, Itasca Consulting Group, Inc., Minneapolis; Donna Ahrens, Consultant, Minneapolis; and my wife Margaret.

Charles Fairhurst

Chairman
Working Group 4

NOTE FROM THE WORKING GROUP CHAIRMAN

"Not a trace of radioactivity" reported the divers to Commandant Cousteau after completing their underwater survey the day after an underground nuclear test.

Walking the ocean-swept coral beach of Mururoa, looking at the fractures and surface settlements produced by underground testing, one may well ask: "How long will the coral reef remain so uncontaminated by radionuclides from the tests below?", "When will the radionuclides arrive at the surface?" and "How much will they add to the natural radiation exposure from cosmic and from terrestrial sources?".

These are essentially the questions addressed by Working Group 4, which was appointed to study radionuclide releases from the geosphere (the rock mass) to the biosphere (the living environment). Working Group 3 estimated the types and quantities of radionuclides generated by the explosions. Working Group 5 assessed how those radionuclides that reach the biosphere, the Pacific Ocean in particular, will become distributed by the ocean currents around the world. Working Group 4 must provide the link between these two groups.

Exposure to ionizing radiation from cosmic sources and the Earth is, and always has been, an inherent component of life on Earth. The possibility of levels of exposure higher than this natural background is new, a feature of the past half-century only. This generation of additional quantities of radioactive elements, or radionuclides, is a by-product of nuclear power generation and the explosion of nuclear weapons. It may have adverse health effects if radionuclides are allowed to enter the living environment, or biosphere, in high concentrations.

The initial response to the problem of nuclear weapon testing was to promote reduction of the concentration of radionuclides by dilution and dispersion in the atmosphere and/or the oceans. This solution met with strong international opposition and was finally abandoned in 1974. Nuclear testing in the atmosphere, in outer space and under open ocean was prohibited by the Limited Test Ban Treaty of 5 August 1963 and signed by the UK, USA and USSR. France ceased atmospheric testing in September 1974. Isolation from the biosphere, or containment in geological formations, became the preferred alternative.

The specific activity, and hence toxicity, of all radionuclides decay exponentially with time, so that all will become innocuous, eventually. For some radionuclides, however, the rate of decay is extremely slow. The plutonium isotope ^{239}Pu, for example, is a significant constituent of nuclear weapons and has a half-life of about 24 000 years so that ten half-lives, the period required for the activity to decay to $(\frac{1}{2})^{10}$ or 0.1% of its initial level, is approximately one quarter of a million years.

The only container considered capable of providing isolation for such long periods is the rock interior of the Earth itself, i.e. the geosphere. Isolation of highly toxic radioactive waste in excavations deep within the Earth's crust has been selected by essentially all countries where nuclear energy is being produced.

Extensive international research on radioactive waste isolation in deep underground excavations over the past 30 years has identified the principal factors affecting geological containment. The main possibility for release of radionuclides to the biosphere is by transport in groundwater that contacts the waste, takes radionuclides into solution or suspension and moves slowly through the rock to the biosphere. Although inhomogeneities and variability in the rock mass prevent accurate calculation of detailed flow paths, it is possible to make bounding estimates that will allow reliable assessments of radionuclide releases and the associated health consequences.

The extremely violent introduction of radionuclides into the geosphere by detonation of nuclear explosives at depth in rock, as at Mururoa and Fangataufa, may seem to be the very antithesis of containment, i.e. a procedure more suited to the widespread dispersal of radionuclides. Study of the physics and mechanics of underground nuclear explosions in rock reveals, in fact, that substantial containment does occur. A very large proportion (95–99%) of some of the more toxic, long lived, radionuclides, including ^{239}Pu, is captured in the molten lava created during the explosion. However, since much of the energy released by the nuclear explosion appears as heat, it adds a thermal drive to the natural system and accelerates the flow of groundwater through the explosion sites towards the biosphere.

Taking these characteristics of underground nuclear explosions into account, radioactive waste isolation experience worldwide provides a valuable point of departure from which to start the Study.

The merits of nuclear testing in South Pacific atolls cannot be assessed on technical grounds alone. It may be useful, however, to note one potentially valuable attribute with respect to underground tests conducted in these atolls. Any possible escape of radionuclides from the confines of the atolls within the next 10 000 or more years would be released into one of the world's largest bodies of salt water, the Pacific Ocean, and would be rapidly diluted. Although such a valuable fail-safe feature exists at a number of proposed radioactive waste repository sites around the world, it is not available at all of the sites currently under consideration.

Working Group 4 was composed of international authorities in the various professional disciplines associated with geological isolation of radioactive waste and included Charles Fairhurst (Chairman); Joerg Hadermann; Ghislain de Marsily; Heino Nitsche; A.S. Sastratenaya; and Lloyd Townley. The Group has worked intensively over two years to produce this report, and hopes that both the international scientific community and the public will find its analyses and conclusions to be of value in assessing the long term impact of underground nuclear testing at Mururoa and Fangataufa.

Charles Fairhurst

CONTENTS OF VOLUME 4

1. INTRODUCTION

1.1. BACKGROUND

This report is Volume 4 in the series of 6 volumes of the Technical Report on the radiological situation at the atolls of Mururoa and the Fangataufa. It is the second of the three volumes dealing with the evaluation of the long term radiological situation as a consequence of radionuclide migration from underground sources, which is the responsibility of Task Group B. This volume is based on the activities of Working Group 4 and uses, as its primary input on radionuclide inventories, the report of Working Group 3, which is Vol. 3 in this series of Technical Report.

Nuclear testing in the atmosphere, outer space and under open ocean was prohibited by the Limited Test Ban Treaty of 5 August 1963 and signed by UK, USA and USSR. France ceased atmospheric testing in September 1974. Isolation from the biosphere in geological formations, or containment in geological formations, became the preferred alternative.

The explosion of 137 underground nuclear devices in Mururoa and Fangataufa over the testing period 1975-1996, together with 10 safety trials and the burial of radioactively contaminated material gathered from the atoll surfaces, has resulted in a substantial accumulation of radionuclides in the rock beneath the two atolls. The details of all the tests are provided in Vol. 3 of this Technical Report. Fig. 1 and Table I summarise these sources of possible radionuclide releases. The sources are classified into seven categories for ease of analysis and discussion of the contribution of each to the total release from the geosphere.

Assessment of the rate at which these radionuclides move from the cavities to the environment accessible to humans, or biosphere and the total radionuclide release to the biosphere over time is the central effort of this Study. The rock mass within which the radionuclides are initially deposited, and which serves to contain or delay release of the radionuclides, will be referred to as the geosphere to distinguish it from the biosphere, where the radionuclides would be accessible either directly or through the food chain to the living environment.

This assessment of geosphere transport has been divided into the following four interrelated tasks:

(a) Geological Pathways;
(b) Hydrological Modelling;
(c) Solution Source Term; and
(d) Geosphere Transport.

The description of Geological Pathways and the Hydrological Modelling are based in large part on a more comprehensive study of the effects of underground nuclear tests on the mechanical stability and hydrology of Mururoa and Fangataufa (Fairhurst et al. (IGC) 1998).

A campaign was also carried out during summer 1997 to sample underground waters from the carbonates and also directly from the cavities produced by the explosions Céto and Aristée in Area 2 on the southern rim of Mururoa. The waters were analysed to determine the concentrations of various radionuclides in solution and, possibly, in colloidal suspension. The results of these efforts were used to validate and, where appropriate, refine the geosphere transport modelling. Details of the sampling campaign and the results are included in Section 6 and Appendix V of this report.

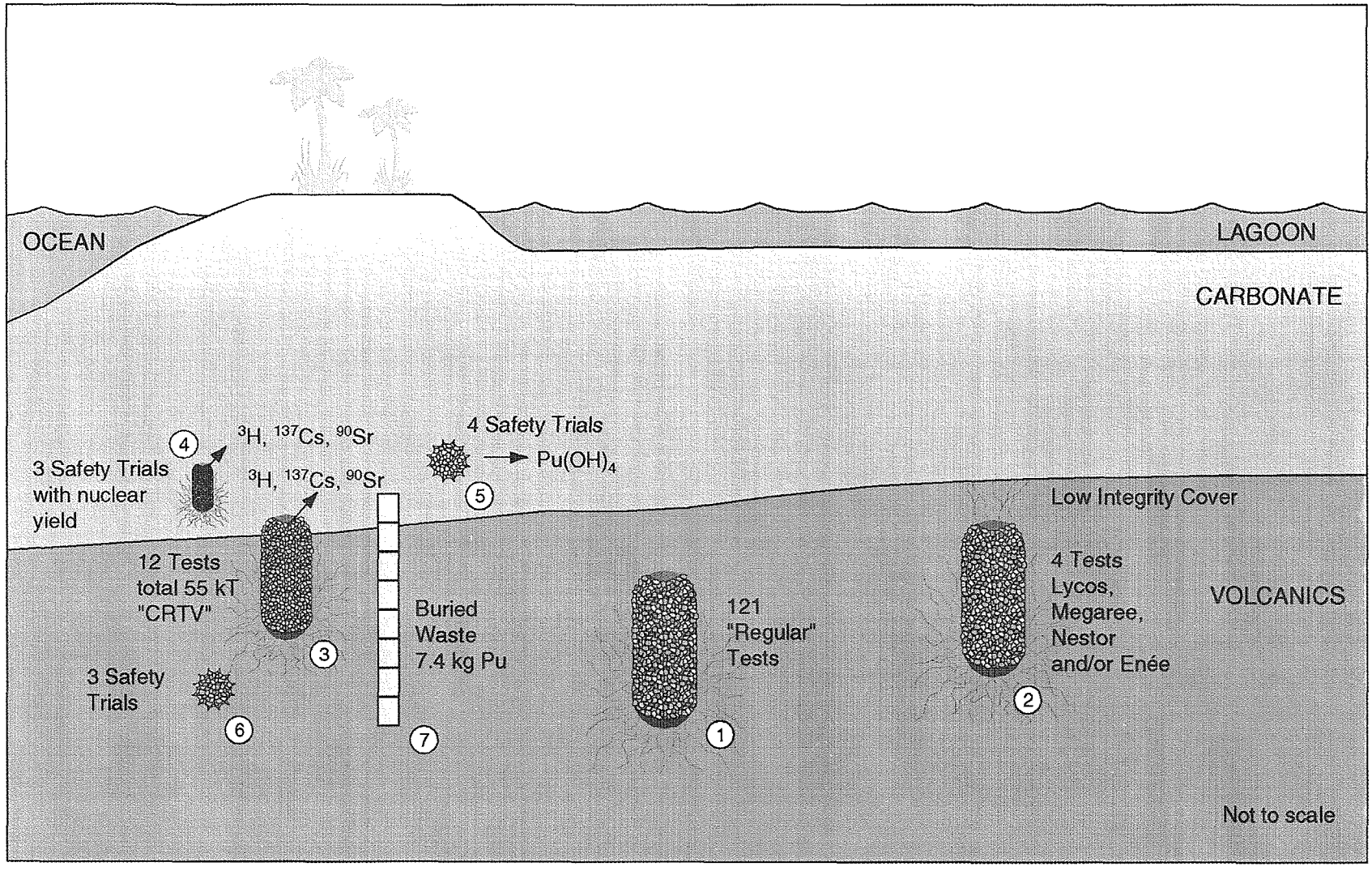

FIG. 1. The seven categories used in analysis of radionuclide transport through the geosphere. (CRTV: chimney reaching top of volcanics.) (See Table 1 for additional details).

TABLE I. CATEGORIES FOR SOURCES OF POTENTIAL RELEASE OF RADIONUCLIDES PRODUCED BY NUCLEAR TESTING IN MURUROA AND FANGATAUFA (see Fig. 1)

Category 1	the majority of the nuclear tests (121 of the 137) tests; i.e. tests where a significant thickness of essentially undamaged volcanic cover exists above the cavity-chimney (see Note 1).
Category 2	3 or 4 tests where tritium releases to the karst have been detected even though the nominal depth of (low permeability) volcanic cover should be high enough (140 m in the case of the Lycos test at Fangataufa) to prevent this. The CEA suggests that, in these cases, the original volcanic cover was relatively weak, such that drilling of the 1.5 m borehole for installation of the nuclear device at depth created an annulus of damaged rock around the hole. This annulus acts as a high permeability conduit from the cavity-chimney to the base of the carbonates, allowing early release of tritium.
Category 3	12 relatively shallow CRTV (Chimney Reaching the Top of the Volcanism) tests in which the cavity-chimney came into immediate contact with the base of the carbonates (karst). All CRTV tests are on Mururoa. 7 tests were carried out in Area 1 (1976-1981); 4 in Area 2 (1976-1980) and 1 in Area 3 (1976-1980). Together with Category 2 tests, the CRTV tests would produce a total of 16 tritium (and, to a lesser extent, ^{90}Sr and ^{137}Cs) release locations on the atolls. Measurements reported by French Liaison Office Document No. 10, 1996 (Figs 1, 3-4, 8-10) suggest at least 5 "leaks" at Mururoa, and 1 (Lycos) at Fangataufa. Some of the concentration contours shown in these diagrams, especially for Mururoa, could encircle more than one leak, i.e. the releases could be produced from several such leaks relatively close to each other.
Category 4	3 safety trials conducted in Area 2 (1976-1981, Mururoa rim) at a depth greater than 280 m in the carbonates, in which a (small) nuclear explosion (average yield 0.15 kt) resulted from each trial. Assuming that the resultant cavity radius (R_c) scales according to the same cube-root law as the cavities in the volcanic rock (i.e., $R_c = 12\ Y^{1/3}$ m, where Y is the nuclear yield in kt, we obtain, for Y = 0.15 kt, a cavity radius of approximately 7 m.
Category 5	4 safety trials conducted in Area 1 (Mururoa rim) at a depth greater than 280 m in the carbonates, without nuclear yield. In these cases, the plutonium contained in the device that was tested is estimated to be 3.7 kg plutonium per trial and remains at depth. There are essentially no cavities associated with these safety trials, but radial fracturing will occur around the seat of the chemical explosion (see Notes 2 and 3).
Category 6	3 safety trials conducted at depth in the volcanics (Mururoa rim). None of these trials resulted in a nuclear explosion. Approximately 3.7 kg of plutonium per trial remains at depth from these trials (see Notes 2 and 3).
Category 7	Radioactive waste produced by surface safety trials has been deposited in two shafts on the Mururoa rim, just west of Area 1 in the volcanic rock, at a depth of down to 1200 m. The total quantity of alpha activity in each shaft was about 10 TBq, equivalent to the plutonium from one trial. Because most of the plutonium was incorporated into cement and buried at depth in the volcanic zone, this waste represents a much lower hazard than the trials (Categories 4 and 5) carried out in the carbonate zone.

Notes

1. The 134 underground tests listed in the Appendix to Bouchez and Lecomte (1996) include the 3 Category 4 safety trials, but do not include the 6 tests (4 at Mururoa and 2 at Fangataufa) carried out in 1995–1996 (see also the table in Barrillot 1996, p. 178).

2. It is probable that explosions in the carbonates may produce compaction and pore collapse, leading to a lower permeability in the zone around the seat of the explosion.

3. The safety trials were all conducted in the general vicinity of Dora/Denise (at the westerly end of Area 1) on Mururoa, i.e. slightly east of the most northerly portion of the Mururoa rim.

1.2. GEOLOGICAL PATHWAYS

Underground testing of nuclear explosives has some similarities to the isolation of radioactive waste in geological formations. There are, however, important differences. The engineered barriers that are an important part of a waste repository do not exist in the case of a nuclear explosion. In both cases, the rock mass is a principal barrier to release of the radionuclides introduced to the underground.

In marked contrast to the isolation of radioactive waste, introduction of radionuclides in nuclear testing is inextricably linked to the release of large amounts of explosive energy, which causes substantial damage to the rock mass in the vicinity of the explosion and heat, and which, in turn, produces convective flow of groundwater through the cavity-chimney. New pathways for radionuclide releases to the biosphere may be introduced by the explosions. On the other hand, almost all of the refractory radionuclides, e.g. ^{237}Np, ^{239}Pu, ^{95}Zr and ^{147}Nd, become incorporated into the molten lava created around the cavity during the explosion. Trapped within the solidified lava, these radionuclides remain immobilised for very long periods and greatly reduce the overall hazard of radionuclide transport. Thus, the formation of lava by the explosion may be regarded as a type of "engineered" barrier.

By the nature of their volcanic formation and evolution and the subsequent accumulation of thick carbonate formations on top of the volcanics, atolls are heterogeneous rock masses. They contain a myriad of fractures, some open and others filled with clay minerals. Clearly, in order to assess the potential for releases of radionuclides as a result of the underground testing programme, it is necessary to develop an understanding of the geological framework within which the tests have been carried out and the physical and mechanical changes to the rock produced by the explosions. The details of such investigations are presented in Section 2.

1.3. HYDROLOGICAL MODELLING

The main vehicle for movement of radionuclides from their point of initial deposition within the underground rock to the biosphere is the groundwater which, under natural conditions, moves predominantly from the exterior slopes of the atoll inwards, rising through the volcanics and the carbonates towards the lagoon.

As discussed in Vol. 3, Section 7 of this Technical Report, the underground nuclear explosion creates an approximately spherical cavity in the rock, of the order of 10 m to 50 m or more in radius, depending on the energy release or "yield" of the explosion.

The explosion cavity-chimney fills with water, which becomes heated some 25–50°C above the ambient temperature of the rock. This heated water, contaminated with radionuclides, then rises as a thermal plume towards the surface. Over time, the cavity-chimney temperature drops towards the original rock temperature so that, after some 300–500 years, the thermal drive decays to insignificance and a condition approaching that of the pre-testing groundwater flow regime is re-established. However, the increased permeability in the vicinity of the tests remains.

Thus, analysis of groundwater flow and associated radionuclide transport can be conveniently divided into two sub-regimes:

(1) The long term or steady state groundwater flow system on the atoll scale, as it was before underground testing and as it is permanently changed by the tests. The steady state regime is controlled by the interaction between cold, dense ocean water on the outer flanks of the atoll, geothermal heat flowing upwards through the atoll, relatively warm water in the lagoons and the permeability of the volcanics and carbonates. Flow in the latter may be influenced by the

existence of extensive, highly transmissive karstic formations at several levels within the carbonates. There is evidence that at least some of these layers are in communication laterally with the ocean. This raises the possibility that some groundwater and also radionuclides may move laterally under the action of tidal pressure fluctuations and flow directly to the ocean without release first to the lagoon.

(2) The short term transient "thermal plume" effect which, for a period of a few hundreds of years after an underground explosion, will tend to increase the vertically upward velocity of the groundwater that flows through the cavities towards the biosphere.

The details of modelling the hydrological regime are presented in Section 3.

1.4. SOLUTION SOURCE TERM

Almost all (95–98%) of the plutonium is expected to be encapsulated within the rock lava produced at the time of the explosion (see Vol. 3 of this Technical Report). This applies also to a variety of other radionuclides produced by the nuclear reaction whose boiling points are high enough for condensation from the vapour phase to occur by the time of cavity collapse (Atkinson 1984, p. 126). The more volatile radionuclides will form part of the high pressure gaseous mass within the cavity and will largely condense onto the rubble in the cavity-chimney.

The lava is initially molten and distributed more or less uniformly (thickness of 5–10 cm) around the cavity wall. It will form a pool of the order of several metres deep at the base of the cavity. Pieces of rock dropping into this pool during chimney collapse will splash some of this lava onto the rock rubble. A small fraction of the radioactive lava is thus distributed onto the rubble surfaces, where it solidifies (see Vol. 3 of this Technical Report).

As the cavity-chimney fills with water, some of the radionuclides initially distributed in the cavity are taken into solution or may be present in suspension as colloidal particles. Determination of the concentrations of the various radionuclides in the water and how this changes with time as water flows upwards out of the cavity-chimney, to be replaced by water flowing in from the surrounding rock, is critical to the assessment of the quantity of the various radionuclides that may ultimately reach the biosphere. Estimation of the dissolution, and possible suspension in colloidal form, of radionuclides in the cavity-chimney water, i.e. the radionuclide "Solution Source Term", is the essential first step in making this assessment, which is presented in Section 4.

1.5. GEOSPHERE TRANSPORT

Radionuclides contained in solution or suspension in the groundwater may interact chemically or physically with the rock as they are transported by water through the rock microstructure and/or fractures. Some portion of the radionuclides may become attached in various ways to the rock so that they may either not reach the biosphere at all or may be delayed significantly with respect to their arrival in the biosphere. In some cases, these delays may be sufficiently long that the activity of a radionuclide has decayed to much lower levels than would have been the case if the radionuclide had moved in the groundwater with no delay.

It is thus important to consider the physical and chemical interactions between the actual pathways taken by the groundwater from the cavity-chimney to the biosphere, in order to estimate the distribution of radionuclides arriving at the biosphere, i.e. the lagoon, atoll rim and ocean, over times extending to the order of a few 10 000 years.

The physical and chemical interactions occur as a result of contact between the interstitial surfaces of the rock, by advective flow of the water along the primary interconnected voids (pores, micro and macro fractures) and by subsequent diffusion into the adjacent rock macroporosity.

Detailed discussion of radionuclide transport from the cavity-chimney through a discretely fractured volcanic rock mass (basalt) into the overlying carbonates and to the biosphere is presented in Section 5.

1.6. SAMPLING AND ANALYSES OF UNDERGROUND WATERS

Radionuclides deposited in geological formations as a consequence of nuclear weapons tests may be dissolved by underground waters from the place of deposition and be transported through the geosphere towards the biosphere. Such processes are modelled numerically for time periods appropriate to the site specific situation. Analyses of underground waters provide the opportunity to check the predictions of model calculations or specific parameters, e.g. sorption data of radionuclides under in situ conditions, important for the results of such calculations.

A system of monitoring wells is in place at the atolls of Mururoa and Fangataufa which provides the opportunity to measure radionuclide concentrations in the cavity-chimneys, the carbonates and at the top of the volcanics.

The sampling and analyses of underground waters from the cavity-chimneys produced by the explosions Céto and Aristée on Mururoa was used to check the calculated releases of radionuclides from the lava into the cavity-chimney waters, the site-specific sorption data and, in particular, the reasonableness of model calculations. Likewise, sampling of carbonate waters allows some estimates to be made of release from the volcanic rock. This can be compared with model predictions. Furthermore, measurement data obtained by CEA scientists were corroborated by IAEA scientists in an independent exercise, in particular in terms of migration of soluble, non-sorbing radionuclides as colloids.

1.7. APPENDICES

Several topics that are needed to illuminate individual items of the WG 4 Report have been included as appendices. These include:

I. Influence on ground water flow of hollow spheroidal inhomogeneities in a porous medium
II. A model of tritium release based on mixing in the carbonates
III. Models of tritium release based on piston flow or convection/dispersion in the carbonates
IV. Experimental studies of plutonium solubility in various waters
V. Underground water sampling in Mururoa and Fangataufa
VI. Excerpt from Chapter 3 of the Atkinson report 1984

2. GEOLOGICAL PATHWAYS

Some understanding of the geological structure of the atolls is necessary in order to assess (a) the strength and resistance of the rock mass to the movement of groundwater and transport of radionuclides and (b) how underground nuclear testing has affected these characteristics.

2.1. FORMATION AND STRUCTURE OF THE ATOLLS

Viewed from the air, the atolls of Mururoa and Fangataufa are thin rings of coral up to some hundreds of metres wide and two - three metres above sea level (Figs 2 and 4). Seen through the water, as in the bathymetric diagrams (Figs 3 and 5), they are revealed to consist of an accumulation of several hundreds of metres of carbonate rock (derived from coral accretions) founded upon extinct volcanoes rising some 4 km or more above the top of the ocean crust. They are underwater mountains approximately 10–12 Ma old.

Mururoa and Fangataufa are believed to have formed as the result of injection of molten magma from a fixed source or hotspot in the upper mantle into fissures or *rifts* in the crustal plate at the bottom of the 4 km deep Pacific Ocean. The magma was originally discharged under deep water to form a submarine volcanic structure which grew progressively as discharge continued. Eventually the volcano reached a height of approximately 2000 m above sea level to form a seamount.

Both atolls are of approximately the same age (Mururoa 10.6–11.8 Ma; Fangataufa 9.6–11.5 Ma) and only 45 km apart, but their distinctly different shape indicates that they formed under the influence of different fracture systems in the ocean crust. Mururoa, elongated in a N80E direction, appears to have developed by magma penetrating major fractures or rifts in the ocean crust

FIG. 2. Aerial photograph of Mururoa atoll. (By courtesy of French Liaison Office).

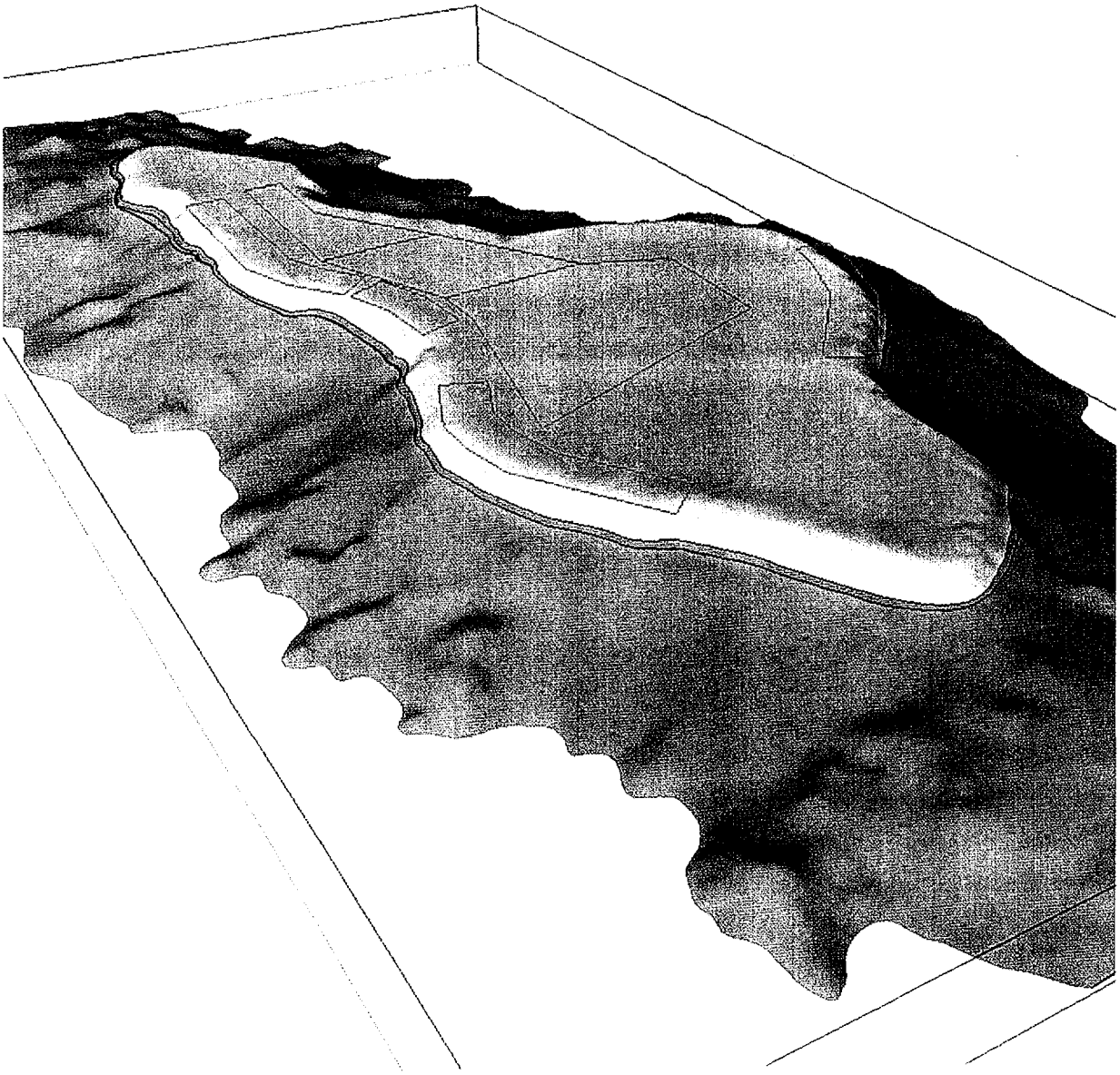

FIG. 3. Bathymetric view of Mururoa (to a depth of 2.5 km; carbonate is shown over volcanics).

in the immediate vicinity of the Austral Fracture Zone, along the now inactive Farallon Ridge, which has the same N80E orientation. Magnetic surveys of the Mururoa volcanics indicate, in fact, that the atoll consists of at least two and probably three separate magma chambers (forming a flat volcano): (a) one along the line of the Northern rim; (b) the other following the Southern rim, with an isthmus between the two in the vicinity of the natural pass on the western extremity; and perhaps (c) a third, parallel to the rims, under the present lagoon. Fangataufa is a single, classically cone shaped volcano with magma injected through fractures that follow the main rift zone trends in the South Pacific (N170E, N80E, N115E).

The period of volcanic activity ceased after approximately 2 Ma as the plate and rift zones feeding the two atolls moved away from the hot spot. Since that time, the volcanic structure has been sinking progressively, initially at a rate of 1–2 mm/a and now around 0.15 mm/a (Guille et al., 1996, p. 23) due to the combined effects of the increasing density of the seamount as it slowly cooled, flexure of the crustal plate under the weight of the volcanic edifice and possible depletion of the

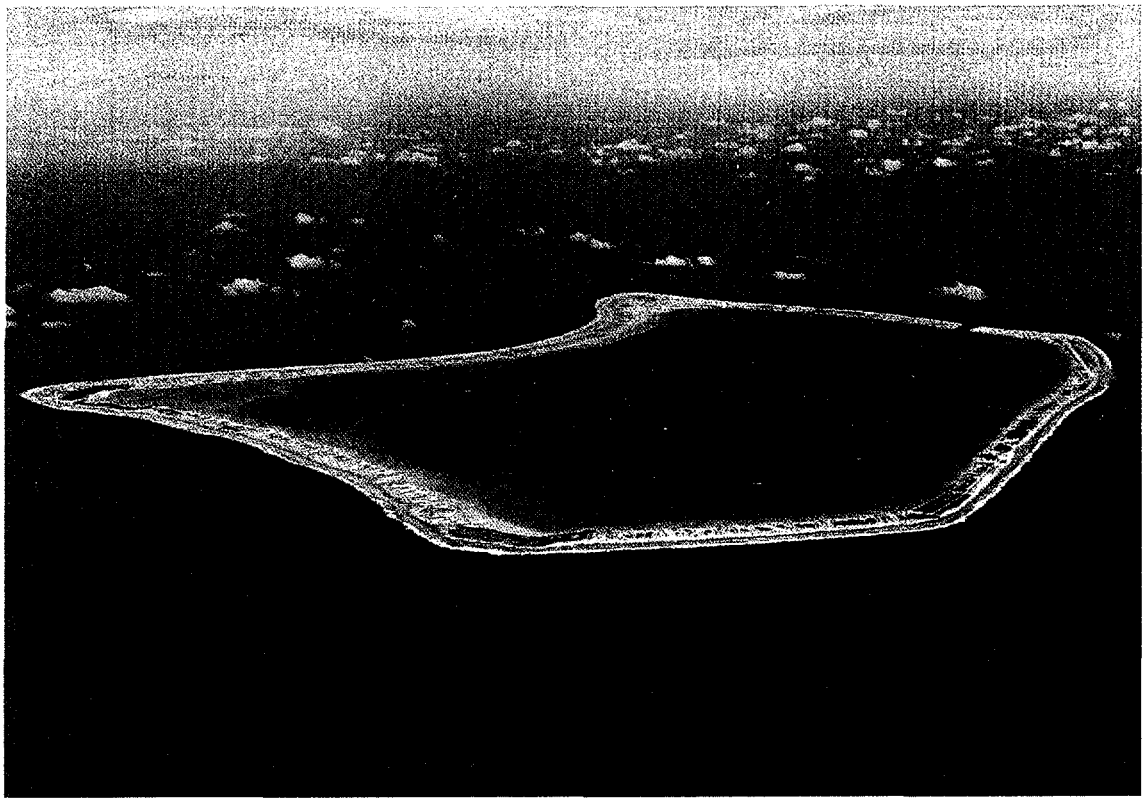

FIG. 4. Aerial photograph of Fangataufa atoll. (By courtesy of French Liaison Office).

magma chambers. The flanks, and eventually the land surface, became submerged with the shallow underwater regions then serving as sites for the growth of coral and algae. This growth has kept pace with the rate of island subsidence.

While above water level, the surfaces of the two islands were eroded by rainwater and wind, which removed preferentially the less resistant rock formations, developing a surface profile similar to that seen on the volcanic island of Mehetia today (Fig. 6).

Periodic ice ages, resulting in a relatively abrupt drop of the ocean level, by amounts varying up to 150 m or so, caused the coral topped island to re-emerge, interrupting coral growth in the above water elevations. These ocean level variations can be identified by lithological changes in the atolls. A drop of 3 m in the ocean level approximately 3000 years ago resulted in the current elevation of the atoll rim at Mururoa and Fangataufa. This drop was apparently the result of a change, at that time, from a warmer period to the present climate.

2.1.1. Volcanics

Volcanic structures, such as those of Mururoa and Fangataufa, include a variety of different lithological units. At the start of the volcano building processes, the magma was discharged onto the ocean floor under the hydrostatic pressure of 4 km of water. At this depth, gases in the lava remain in solution and the solidified rock tends to be relatively massive. Cooling, as the lava flows sub-horizontally, produces pervasive, more or less vertical fractures with a spacing that is roughly proportional to the thickness of the individual layers. As the volcano grows and the depth of water decreases correspondingly, the lava becomes progressively more eruptive. The rock from this regime is seen to contain a myriad of frozen-in gas pockets or vesicles. Eventually the volcano approaches the ocean surface. The eruptions become explosive as the magma, immediately chilled in the shallow

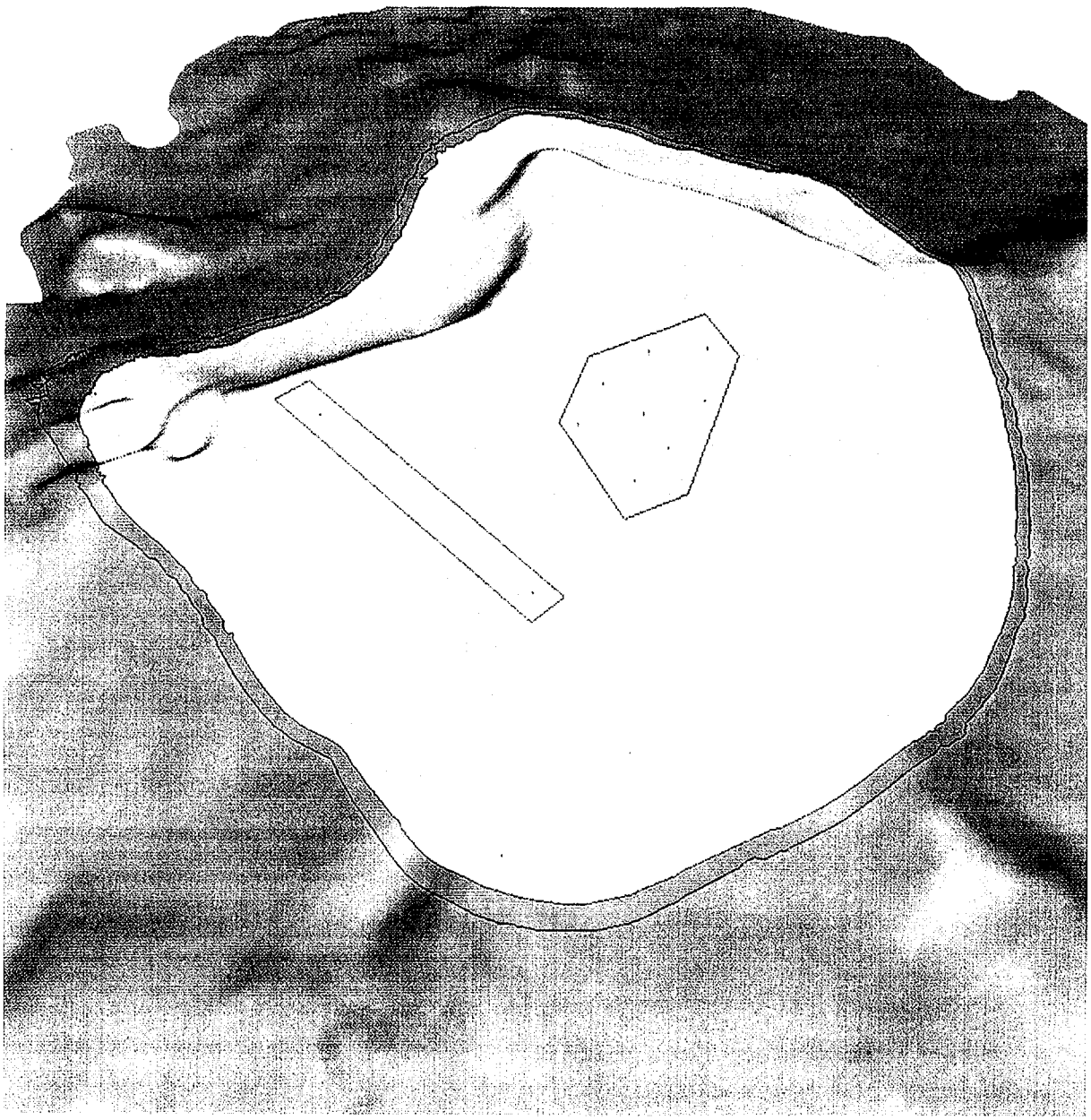

FIG. 5. Bathymetric view of Fangataufa (to a depth of 2.5 km; carbonate is shown over volcanics).

water, breaks into small, less than 2 mm fragments or breccia and ash (less than 4 mm fragments) or hyaloclastic tuff. As the volcano continues to rise, the magma ejects directly into the air to form volcanic cinders or scoriae. Once the thickness above sea level is of the order of several hundreds of metres, massive lava flows become the predominant mode of magma discharge, spreading laterally down the steep sides of the volcano towards the ocean. As with all of the magma flowing on to the surfaces of the volcano, underwater or in air, cooling produces contraction cracks perpendicular to the surface.

Superimposed on the solidified volcanic structure, later intrusive injections of magma tend to penetrate into existing fractures or layer interfaces, enlarging the apertures in the process, to form dykes (where the path is sub-vertical) or sills (where the path is sub-horizontal). Dykes, sills and related late time intrusive features can extend hundreds of metres and more, and can be several metres in thickness.

The progressive sinking of the volcanics, subsequent to the termination of volcanic activity, does not occur uniformly across the atolls. Some regions may consist of weaker, low density volcanics; some may be underlain by depleted magma chambers leading to caldera (collapse) structures, as may have occurred (Buigues 1996) in the Viviane area of the south central region of Mururoa. This differential settlement will lead to normal (sub-vertical) faulting in the volcanics, which will be obscured later by accretion of the carbonates. Hints of faulting and discontinuities in the volcanics with no dominant preferred orientation (which is consistent with the differential settlement) are seen in SISLAG seismic survey plots of Mururoa and Fangataufa (French Liaison Office Document No. 5, 1997, Figs 2a, 2b). CEA scientists noted that these "fractures" could be artifacts of the computer treatment of the seismic data.

According to the Atkinson Report (Atkinson 1984, p. 92) "*fault systems seen in seismic sections have been drilled. The drill core shows that the faults represent dyke injections, there having been no movement along the faults for many millions of years since dyke injection. The fault systems seen in seismic sections and interpreted on aeromagnetic maps therefore probably represent old fractures of the deep volcanics along which injections of lava have occurred and infilled the rifts. Their occurrence in swarms or groups is entirely consistent with this interpretation.*"

An important conclusion to be drawn from this discussion is that the volcanic base of the atoll contains an extensive network of essentially linear fissures of various sizes which combine to produce a substantial reduction, both in mechanical strength and resistance to groundwater flow, of the rock mass compared to the values obtained on small core specimens. Laboratory specimens of the basalts are found to have a hydraulic conductivity of the order of 10^{-10} m/s (or a few mm per year), whereas values of the order of 10^{-7} m/s (or a few m per year) for the conductivity of the volcanic rock mass are consistent with field evidence, i.e. the volcanic rock mass (undamaged by explosions) is about 1000 times more conductive than the intact rock.

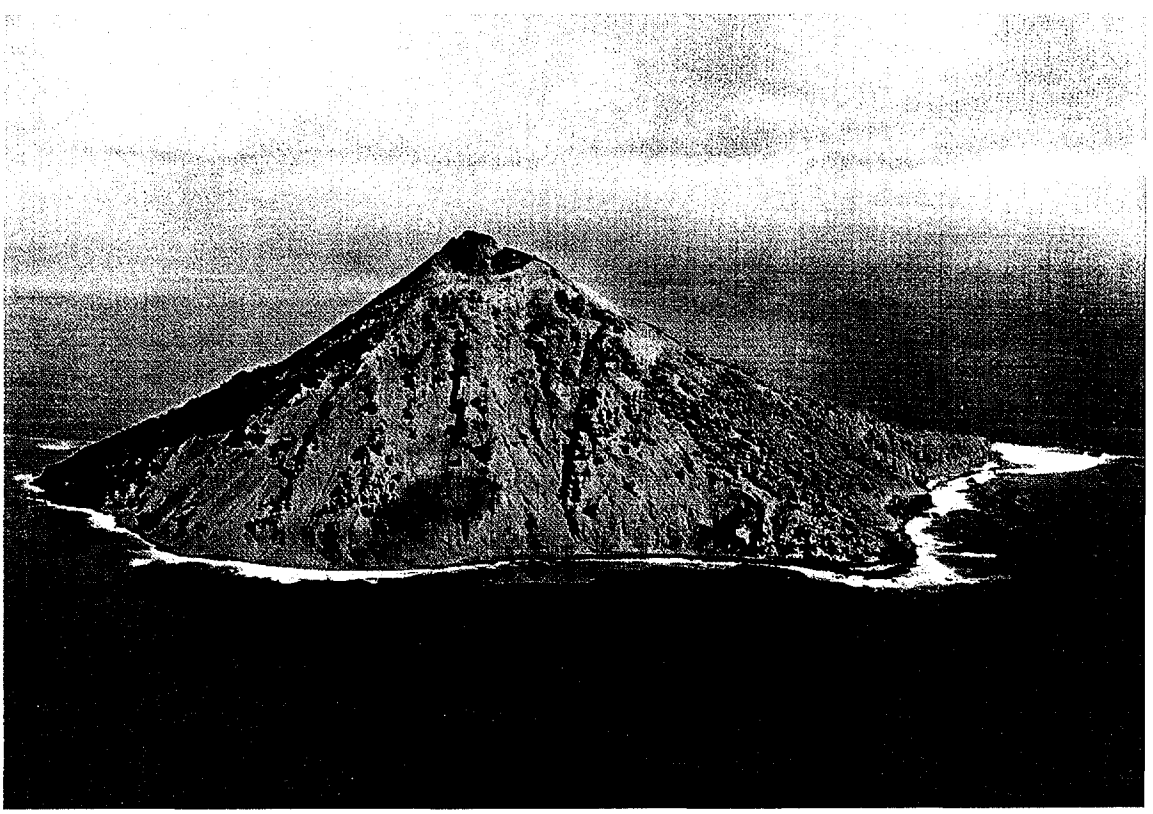

FIG. 6. Aerial photograph of Mehetia. (By courtesy of French Liaison Office).

The total flow rate of water through the rock mass, the so-called Darcy velocity (see box in Section 3.1.1), is the product of the hydraulic conductivity and the hydraulic head gradient change per unit of distance along the flow path. Head gradients in the atolls are typically a small fraction of one metre drop in pressure head per metre of water advance, so that actual flow rates of water through the rock will usually be a small fraction of the hydraulic conductivity.

If the scale of the interconnected conduits is dominated by a dense network of small pathways where the surface area exposed to flowing fluid (or the rock surface to volume ratio) becomes very large, as, for example, in a fine grained sand, it becomes appropriate to consider the rock mass as a homogeneous porous - permeable medium with equal resistance to groundwater flow in all directions and similarly for the physical and chemical processes that affect transport of radionuclides through the rock in the analysis of the physical and chemical retardation.

In the volcanics, however, the conductive pathways have evolved from a variety of sources, from (a) the large scale magmatic intrusions that emerge from fractures in the Austral fracture zone; (b) the sub-horizontal flow surfaces, varying in thickness from fractions of a metre to tens of metres; (c) cooling contraction fissures within, and generally perpendicular to, these layers; (d) the more extensive fractures, e.g. dykes and sills produced by magmatic injections that took place after cooling of the initial volcanic rock mass; and (e) settlement joints and faults. It is clear, therefore, that the properties of the volcanic base of the atolls are likely to be characterised by significant sub-vertical fracturing, sub-horizontal layering, large scale dykes and sills and normal faulting. CEA observations indicate layer thicknesses of a given facies that, in rare occasions, may be up to 35 m, e.g. submarine volcanics. The dominant thickness is in the range of less than 6 m, with the most frequent units being 2 to 3 m thick. Each of these layers contains a variety of smaller fissures and cracks, as discussed above.

The surfaces of initially large conduits in basalt become chemically altered by the flowing water and, over long time, may become sealed by alteration products such as clays or, in other cases, calcite.

Considering the intensity of discontinuities in the volcanics such as layers, cooling cracks, dykes and faulting, it was considered appropriate to assume, in the radionuclide transport calculations of Section 5, that flow in the volcanics would be dominated by flow in discrete fractures. Submarine volcanics tend to be more homogeneous but of lower mean density than the subaerial volcanics, although the spread of density values is larger.

2.1.2. Carbonates

As noted above, the carbonate cap, varying in thickness up to 500 m on the volcanic pedestal, has been built up, and continues to the present, as a result of the growth of coral and algal organisms on the flanks and the top of the volcanic mass, as it became submerged in the ocean. The organisms can live only underwater in the shallow region to which sunlight can penetrate, i.e. about 60 m maximum in the South Pacific. As the volcanic pedestal continues to subside, coral growth continues on top of the existing coral or carbonate mass. According to Guille et al., 1996, p. 69 "reef-building corals are currently proliferating at a remarkable rate" in the area of the south western rim of Mururoa (Area 4) where surface settlements produced by explosions have resulted in submergence of the rim locally. In a personal communication from CEA this rate was specified to be one or more cm per year.

Re-emergence of the carbonate, as much as 100 m or more above ocean level during periods of global glaciation, results in physical and chemical alteration of the carbonates leading, for example, to karstification. Several karstic horizons have been identified at the same depths on both atolls, indicative of previous periods of global glaciation and re-emergence of the carbonates. Such global glaciations have a dominant cycle of the order of 100 000 years, during which the level of the ocean has fallen, typically, 100–150 m, interspersed with more frequent (20 000–50 000 year period)

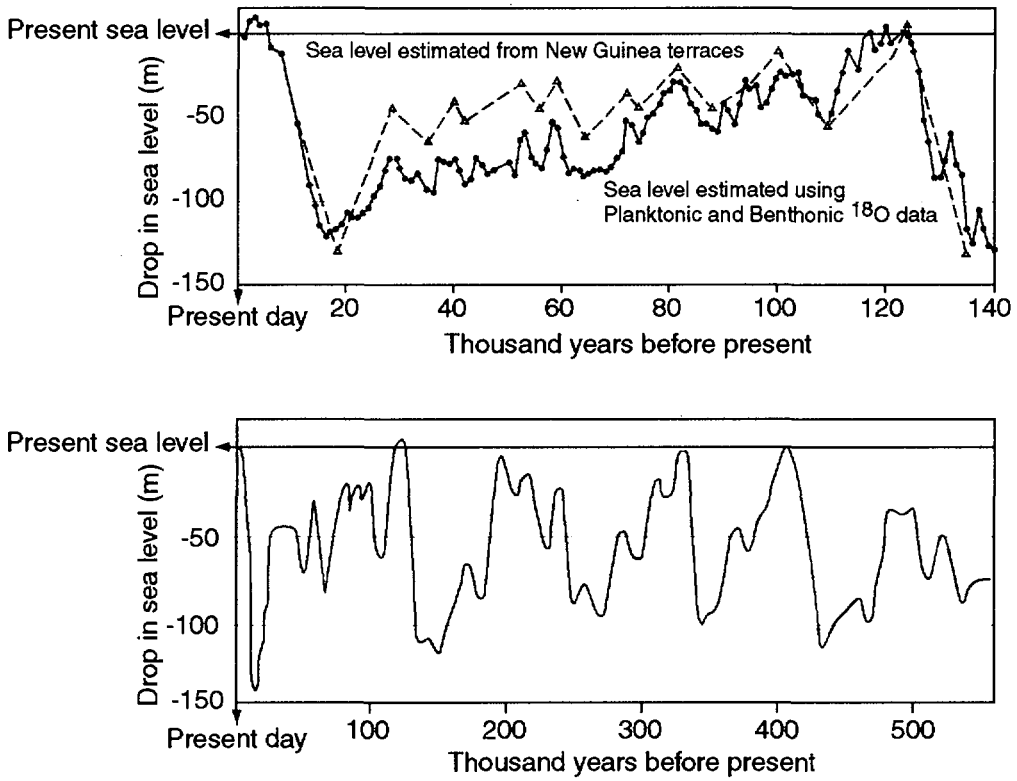

FIG. 7. Variation in sea level over the last 500 000 years. (After Shackleton (1987) and Lalou et al. (1988).)

declines of lower amplitude (Fig. 7). The last substantial ice age ended some 15 000 years ago (Guille et al.,1996).

Because of the ocean level changes the carbonates can be subject to the combined physical and chemical effects produced by rainfall and associated climatic influences and can be subject to significant chemical transformations due to the influence, at varying times, of fresh water and saline ocean water flowing through the carbonates.

Dissolution has led to the development of extensive karstic horizons (Buigues 1997). Limestones ($CaCO_3$) have been transformed to dolomites ($CaCO_3 \cdot MgCO_3$) which are often well cemented and relatively strong mechanically. An annular lens of dolomite reaching a maximum thickness of about 320 m, i.e. from near to the volcanic - carbonate interface to a minimum depth of -130 m towards the flanks, thinning to zero in the centre, has developed around Mururoa.

In other areas, dissolution by deep sea water increases the porosity, leading to a characteristic chalky limestone which is relatively weak mechanically. Cementation and dissolution of the carbonates has also taken place around the flanks (Aissaoui et al., 1986) resulting in an "apron" (Atkinson 1984) of relatively low permeability around the submerged ocean slopes and, in the Northern rim, a weak, porous "chalky limestone" (French Liaison Office Document No. 7, 1996, Figs 27–28) which appears to be a significant contributor to the continuing slope deformations in Area 1 (French Liaison Office Document No. 7, 1996, Section VI and Fairhurst et al. (IGC) 1998).

The presence of carbonate rich horizons within the volcanics also indicates that there were quiescent periods during the volcanic regime, when coral reef building activity took place on the then slightly submerged portions of the volcano.

Examination of cores from the Zoe borehole in the south western rim of Mururoa provides practical information. A log of the Zoe core is included as an Appendix to the French Liaison Office

Document No. 5, 1997. The core shows that the carbonates are bedded and vary from vuggy (large voids) and karstic (large inter-connected voids, highly transmissive to fluids) sections, to denser but still porous - permeable layers. Again, the thickness of beds appears to vary from several centimetres to 1 m or more. Evidence of vertical jointing is scarce in a vertical borehole such as Zoe. Thus, the carbonates are clearly bedded, but evidence for vertical discontinuities (fractures) is lacking.

Figure 8, modified after Buigues 1997, illustrates schematically a typical cross-section through each of the two atolls. Slope deformation and failure are part of the natural process of carbonate deposition in atoll development. Bathymetric studies of Mururoa and Fangataufa, supplemented by

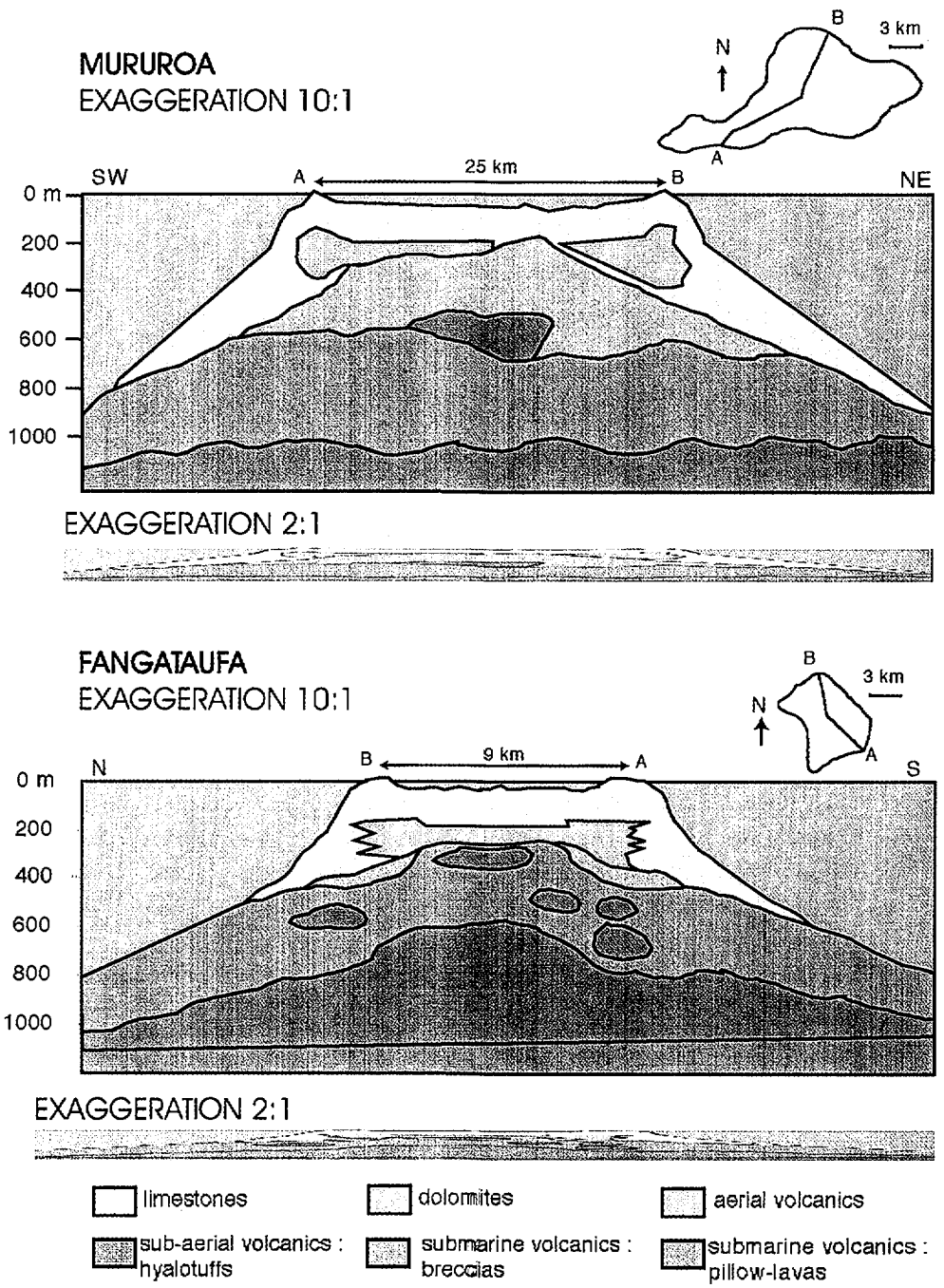

FIG. 8. *Schematic lithology of Mururoa and Fangataufa after Buigues, 1997: Exaggeration 10:1 and reduced exaggeration 2:1. Note: The true scale versions are too "thin" to be interpreted.*

photographs and video films to depths of 2000 m show considerable accumulations of carbonate sediments in valleys between submarine volcanic outcrops (Guille et al., 1996, Fig. 23). While a significant proportion of these accumulations result from erosion and slope instability produced during the period that the atolls were high above sea level, collapse of underwater slopes in the carbonates has occurred also. As noted by Goguel in his contribution to the Tazieff report (Tazieff 1982), carbonate reefal development tends to occur laterally at shallow depths (0–50 m) below water. It seems inevitable that, as the slabs so developed become "over-extended" laterally, they will break in tension and/or produce shear instabilities within the underlying carbonates, leading to periodic slope failure. Underground nuclear testing has certainly accelerated the natural process of slope deformation and has produced fractures and, in some cases (Area 4 of Mururoa) slope collapses, that would probably not have developed naturally.

In terms of modelling the geosphere radionuclide transport, it is important to note that essentially planar conduits are abundant in the carbonates, but here the conductivity of the "intact rock" is also high, so that the overall hydraulic conductivity of the mass is of the order of 10^{-4} m/s, or several km per year, i.e. much higher than in the volcanics. Again, the actual rates of water movement are considerably lower due to the typically low hydraulic gradient.

2.2. HYDROLOGICAL AND GEOMECHANICAL HETEROGENEITY

2.2.1. Hydrological heterogeneity

In discussions of the nuclear test activities the rock formations on Mururoa and Fangataufa are often referred to simply as "carbonates" and "volcanics". As seen from Fig. 8 the detailed geological structure of the atolls involves a heterogeneous array of rock types within the general "carbonates - volcanics" classification. Could these heterogeneities result in pathways for significant radionuclide releases that are not identified when simpler, homogeneous layers are assumed in the models? General modelling studies, both of the entire atoll or the region affected by an individual explosion, cannot consider these heterogeneities in detail. Neither the spatial distribution and extent of the heterogeneities nor the specific physical, hydrological, geomechanical etc. properties are known. Even if they were known, the most powerful computers could not include them in detail. In general, models represent heterogeneities as a lumped coefficient, e.g. the "scale factor" in rock mechanics or, in solute transport, accessible pore space in a double porosity model.

It is possible, however, to assess the potential significance of geological heterogeneity on potential pathways for radionuclide releases and on the likelihood that calculations based on models which do not consider this heterogeneity in detail, could be seriously in error. This is discussed in Section 3 and in Appendix I.

With respect to release of radionuclides from the underground explosions, geological heterogeneities could be important to the mechanical, hydrological and radionuclide transport characteristics of the volcanics and carbonates. There are close interrelationships between the mechanical and hydrological characteristics of a rock mass, but it is convenient here to discuss the two separately.

2.2.2. Geomechanical heterogeneity

The compressive strength of a rock mass is usually considerably lower than the strength of a small laboratory specimen. This is due largely to the presence of fractures and joints in the mass. Often, as in Mururoa and Fangataufa, these discontinuities are filled with water under pressure that can further reduce the strength. In the extreme, a rock mass that is intensively and pervasively fractured may behave, on a large scale, essentially as a cohesionless material, e.g. a soil, depending for its strength on friction between the particles or blocks, even though the blocks of rock material between the discontinuities may have a high strength.

It is also usual and conservative to assume that the tensile strength of a jointed rock mass is effectively zero. This implies that any potential development of a tensile stress in the rock mass will result in the opening of cracks in the mass. Considering the extensive fracturing in the volcanics and the relatively low tensile strength of carbonates in general, it seems appropriate to assume zero tensile strength for any analysis of atoll deformation.

The strength variability of the volcanic formations is illustrated by the relationship between the density of the volcanics and several mechanical properties measured on small laboratory specimens. The volcanic density is found to vary between 2000 and 3000 kg/m^3. The corresponding mechanical properties, as reported in French Liaison Office Document No. 5 1997, are shown below.

TABLE II. CORRELATION OF VOLCANIC ROCK PROPERTIES WITH DENSITY

Density ρ (kg/m^3)	Water content %	Elastic wave velocity km/s	Uniaxial (drained), quasi-static Compressive strength MPa
2000	24	-	-
2350	9.5	2.2	30
2800	<1	5.5	220
3000	<1	0	-

This table indicates that, from the mechanical point of view, the volcanics vary over a wide range. At one extreme, the rock strength is equivalent to a moderately weak limestone; at the other, it is the equivalent of a strong, dense granite. The corresponding values for the strength of the large scale rock mass will be substantially lower, but wave velocity, water content and density values are likely to remain more or less unchanged.

Figure 9(a) and (b), reproduced from French Liaison Office Document No. 6, 1996, Figs 15 and 16 and Fig. 7 from Appendix to Document No. 6 give additional evidence of the variability of the rock in terms of failure curves (Fig. 9(a)) and rock mechanical properties (Fig. 9(b)) as used in calculations of shock wave loading of the rock or deduced empirically from back-analysis of test results.

Thus, the volcanic formations are mechanically very variable and generally layered with extensive vertical fracturing. It is to be expected, therefore, that underground nuclear tests carried out under nominally similar conditions in the volcanics will produce variable results. Figures 10 (a) (b) (c), modified from diagrams included in the Atkinson report (Atkinson 1984), show the observed values of the scaled cavity radius and the relationship between cavity radius, cavity-chimney height and fracture radius for a number of underground tests at various depths.

The tests at approximately 700 m depth, for example, indicate a scaled radius varying approximately 20% (Fig. 10(b)). According to Vol. 3 of this Technical Report, the linear scale of effects, such as cavity radius, varies approximately as the inverse cube root of the rock strength. A 20% variation in cavity radius would be consistent with a $(1.2)^3 = 1.7$, or 70% variation in the strength. Thus, given the wide variation in strength of the volcanics indicated in Table II, it is perhaps surprising that the variation in cavity radius is not greater. This may suggest that the unconfined quasi static rock compressive strength is a secondary factor in determining the size of nuclear explosion cavities. It seems probable that the cavity size is determined more by confined strength of the rock under high values of confining stress, such as imposed during the shock loading. This behaviour may be less variable between rock types than is the unconfined compressive strength.

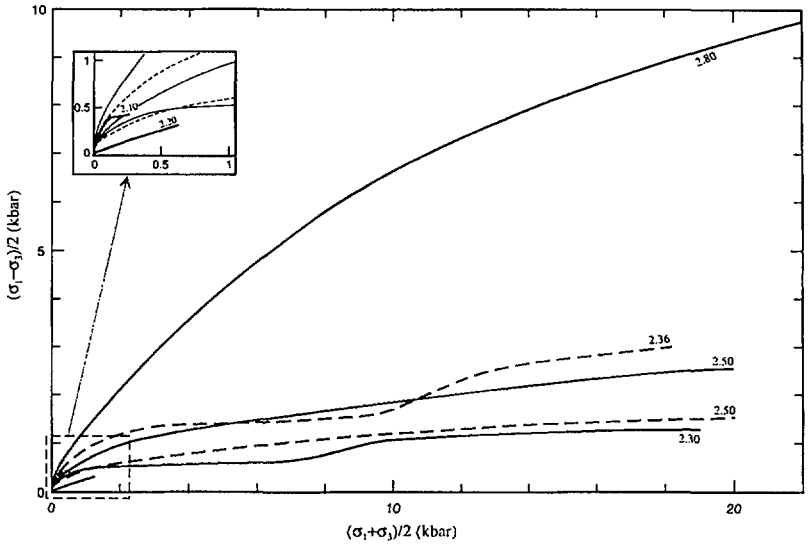

Failure curves versus density for saturated submarine volcanic formations

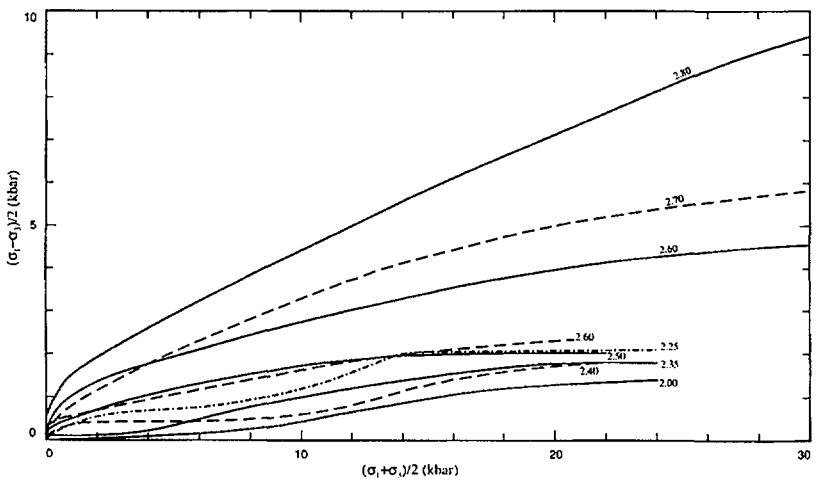

Failure curves versus density for saturated subaerial volcanic formations

FIG. 9a. *Rock mechanical properties used in calculations by CEA in analysis of shock and quasi-static loading effects. Failure curves versus density for saturated submarine and subaerial volcanic formations (reproduced from French Liaison Office Document No. 6, 1996).*

Although CEA scientists and scientists associated with other test programmes (see Vol. 3 of this Technical Report) have developed general relationships between explosive yield, cavity radius and cavity-chimney height, results in individual explosions can be expected to vary appreciably. In the case of the Lycos test at Fangataufa, for example, a nominal cover of 140 m of volcanics between the top of the cavity-chimney and the base of the carbonates was insufficient to prevent a release of tritium soon after the test. French officials acknowledge that the cover was in weak rock and that the wall of the 1.5 m diameter shaft was disturbed during drilling of the shaft. Subsequent filling with concrete and crushed rock fill did not eliminate an annulus of disturbed rock outside the filled shaft. Early leakage of tritium was attributed to the existence of this high conductivity annulus. Similar situations appear to have occurred in the Mégarée (Mururoa lagoon), Nestor and Enée tests (Mururoa rim, Area 4), since early releases of tritium have been observed from these and other test sites (French

ROCK ELASTIC MECHANICAL PROPERTIES

Material	%H_2O	ρ_0 (g/cm^3)	V_L (m/s)	V_T (m/s)	G (Mbars)	K (Mbars)	ν	$P_{H.E.L}$ (Mbars)
Limestone	16	2.20	2700.	1260.	0.035	0.11	0.36	
Dolomite	13	2.30	3010.	1450.	0.048	0.14	0.35	
Transition zone		2.20	2590.	1390.	0.042	0.092	0.30	1.E-3
Aerial volc. formation	7	2.50	4480.	2060.	0.11	0.36	0.37	3.E-3
Aerial volc. formation	15	2.20	3470.	1850.	0.076	0.11	0.30	1.7E-3
Submarine volc. form.	14	2.25	3510.	1880.	0.080	0.17	0.30	1.7E-3
Submarine volc. form.	10	2.36	3710.	2020.	0.096	0.20	0.29	1.7E-3

ROCK FAILURE SURFACE AND
PRESSURE–VOLUME RESPONSE OF A SUBMARINE VOLCANISM FORMATION

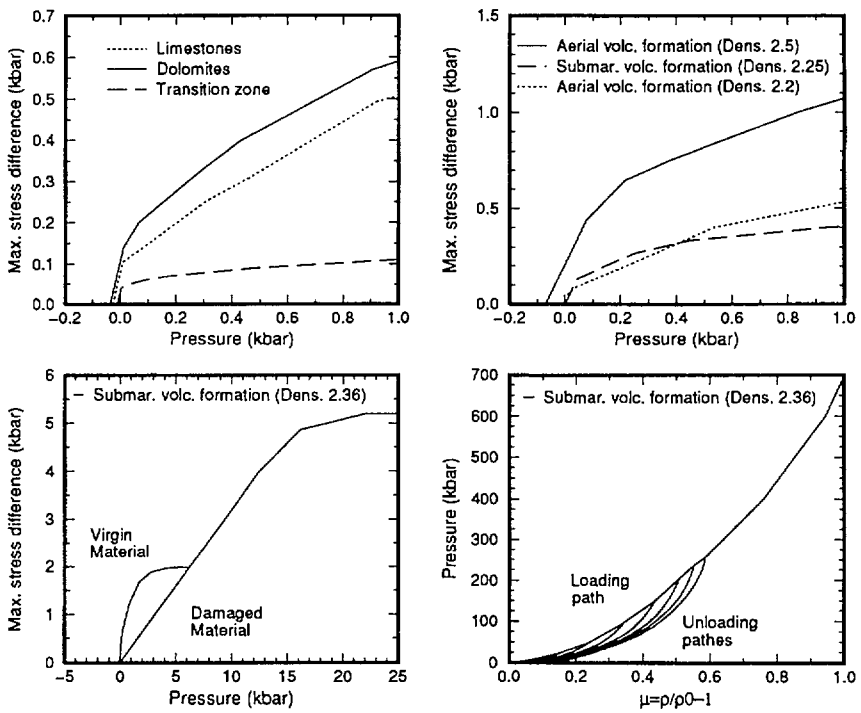

FIG. 9b. Rock mechanical properties used in calculations (reproduced from French Liaison Office Appendix to Document No. 6, 1996).

Liaison Office Document No. 9, 1996, pp. 13–16). It is also possible that the effective hydraulic conductivity of the volcanic cover at some other explosion sites could be higher than assumed, even though no tritium releases have yet been detected.

It is not possible, given the lack of available specific geological information, to consider each test in detail, nor is it necessary for the purpose of this Study. It is important, however, to be aware of geological variability and heterogeneity in examining possible variations from the conditions assumed to exist in any given situation. The early releases of tritium, strontium and caesium into the carbonates over particular areas at Mururoa and Fangataufa are probably examples of geological variability, although a substantial proportion of these early releases has been attributed to CRTV tests (French Liaison Office Documents Nos 9 and 10, 1996).

2.3. IN SITU STRESS STATE OF THE ATOLLS

The fact that original volcanic seamounts rose to a height of the order of 6 km above the top of the ocean crust by a continuing process of accretion, with molten lava flowing over the surface, solidifying and being overlain by additional lava, suggests that the in situ stresses in the atoll would be in equilibrium laterally with the hydrostatic pressure of the ocean water at that depth and with the lithostatic pressure due to the weight of the overlying rock. Thus

the lateral stresses $\sigma_x = \sigma_y = \rho_w g H$

the vertical stress $\sigma_z = \rho_r g H$

where

ρ_w is the mass density of water per unit cross-sectional area,
ρ_r is the average mass density of the overlying rock per unit cross-sectional area,
g is the gravitational acceleration, and
H is the depth below sea level.

It is unlikely that any tectonic (lateral) stresses in the ocean plate below the atoll would influence the atoll, provided there was no change in the tectonic stress subsequent to solidification of the magma in the volcanic mass. However, should the tectonic stresses increase after solidification, it is possible that the central region of the atolls would experience a small additional lateral (compressive) stress (as shown in Fig. 11). The value of this increase would decline (laterally) away from the central axis unit. At the edges of the atolls the lateral stresses (σ_x, σ_y) would be equal to the imposed hydrostatic boundary stress. Although the effect is probably small, it is interesting that lateral confining stresses on the atoll rim may be somewhat less than in the central lagoon area.

Having examined natural heterogeneity briefly, we will next consider the changes introduced to the pre-existing geological - hydrologic regime by an underground nuclear explosion.

2.4. ROCK MASS DAMAGE PRODUCED BY UNDERGROUND EXPLOSIONS

The extreme rapidity of the rates of energy release and the processes of rock deformation associated with underground nuclear explosions have no equivalent in other branches of applied rock mechanics. Chemical explosions detonate in microseconds, but the temperatures, pressures, total energy released and rate of pressure rise in a typical nuclear explosion are orders of magnitude higher. The explosion cavity, up to 50 m or more in radius for the higher yield tests, develops on the order of one tenth of a second! The fact that a substantial amount (of the order of several hundreds of tons in a test) of the volcanic rock is vaporized, eventually cooling to form a molten and then solid lava, is one indication of this difference.

This process of cavity formation and rock damage around the cavity has been discussed in Vol. 3 of this Technical Report. During passage of the explosion shock wave, the rock is subject to very high compression in every direction! As the explosion process continues, the deformation front moves radially outwards, so that a progressively larger volume of rock is involved in the crushing action, but the stress regime within the deforming region remains entirely compressive for a substantial distance into the rock. There is essentially no possibility of tensile fracturing in the region around the cavity during passage of the shock wave.

However, there is evidence that some limited amount of communication can be established between the cavity itself and the rock mass outside the cavity. This phenomenon has been termed "early time injection" (Smith et al., 1996) and is discussed below.

Early time, or prompt, injection

Post-test tunnel excavations in the vicinity of underground nuclear explosions, e.g. at the Nevada Test Site, USA, sometimes encounter veins or stringers of lava in narrow fissures, generally within one cavity radius of the explosion cavity wall. The isotopic composition of the lava in these veins is similar to that found in the cavity, indicating that the fissure lava is the result of injection of radioactive material from the cavity, i.e. directly through a fracture from the cavity. This appears to contradict the arguments above that no fractures can be generated directly from the cavity by the explosion. These arguments however, refer exclusively to the damage to the rock during passage of the outgoing shock wave. As noted above, the shock wave produces compression in every direction immediately around the cavity, so opening of fractures is not possible.

Discussions with US scientists indicate that, occasionally, and in some tests only, the form of the returning wave reflected from the surface, upon arrival at the cavity wall, may combine with the tail of the outgoing shock to produce, for a fraction of a second, a net tangential tension. This will then allow the still high pressure gases in the cavity to open and enter fractures, albeit briefly. Cavity gases can enter a few of these fractures, melting the walls and depositing radionuclides in the thin layer of lava that will then coat the fracture surfaces, forming the radioactive stringers that have been observed in post-test tunnel excavations (Smith et al., 1996).

The pressure inside a cavity can, under certain conditions, increase after an initial decline "as a direct consequence of heat transfer from condensed rock to steam vapour, i.e. a consequence of equilibration" (Peterson et al., 1991). This is referred to as a "popcorning" effect. Especially in saturated porous rocks, as in the atoll's tests, the water in the pores is vaporized as the rock is heated. The high pressure in the pores causes the rock adjacent to the cavity to spall off. Addition of heated rock and steam to the cavity can, under certain conditions, lead to an increase in cavity pressure in the order of minutes after an explosion. This rise may, in certain situations, lead to the possibility of hydraulic fracturing and possibly of venting. This is particularly the case for relatively shallow tests (see Section 2.7.2). The extent of a fracture generated in this way will depend on the in situ stress state and the (residual) gas pressure energy in the cavity.

It is unlikely, however, that this relatively late time mechanism will inject gases that are sufficiently hot to produce the stringers discussed above. French scientists indicate that, although no post-test tunnel excavations have been made on the atolls, no such radioactive *stringers* have ever been detected in their post-test radiochemical drilling.

The in situ stress state at Mururoa (see Fig. 11) is such that fractures would probably tend to propagate vertically upwards. Although they would radiate upwards from the cavity more or less as disc-shaped fractures, a considerable proportion of the fractures would be obliterated within the subsequent chimney collapse region.

There is evidence that the pressure within the cavities can fall significantly below atmospheric when the temperature drops towards the ambient rock temperature. Russian scientists (personal communication) have reported the loss of drilling equipment, sucked into a cavity as it is first penetrated by drilling after a test. French scientists (personal communication) have mentioned a sudden inrush of air at the surface into the radiochemical sampling drill hole (Bouchez and Lecomte 1996, pp. 52–53) as it penetrates into the cavity.

Shortly after the explosion, i.e. within hours, the roof of the cavity with a span (2 R_c) of 20 m for 1 kt or 100 m for 150 kt test will usually collapse, although in small explosions in massive rock such as granite the cavity may be small enough that no chimney forms. The broken rock is falling in to form a chimney filled with rubble extending up to 5 R_c above the centre of the explosion. Since broken rock, falling under gravity, tends to maintain about 30% voids, 5 R_c is usually the height at which the cavity-chimney is "filled" with rubble (Vol. 3 of this Technical Report, Section 7).

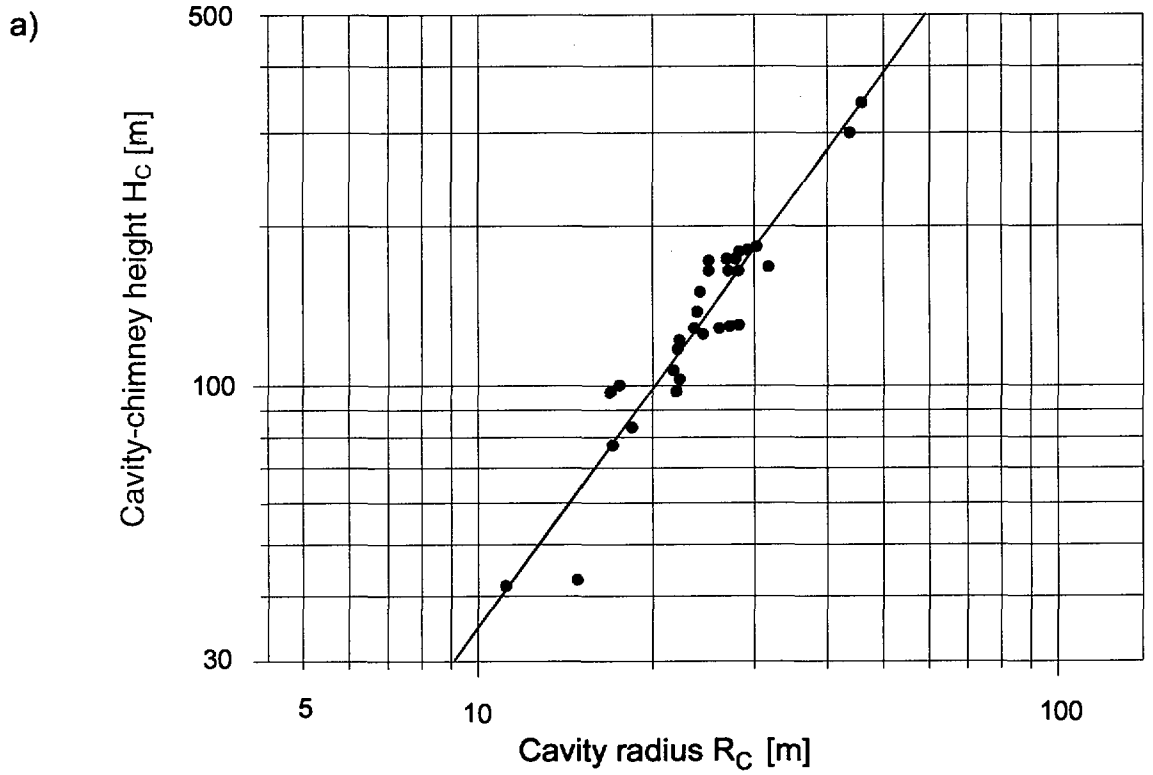

FIG. 10a. Log-log plot of measured cavity-chimney height (H_c) as a function of measured cavity radius (R_c); modified after Caristan in Atkinson 1984. Note: Logarithmic scales were omitted from original (1983) diagrams. The scales shown are estimates only from currently available data. Using the assumed scales, the straight-line fit of the data indicates the relationship $H_c = 1.1\ R_c^{1.5}$. There is no indication of an explosion depth dependency in this data or relationship.

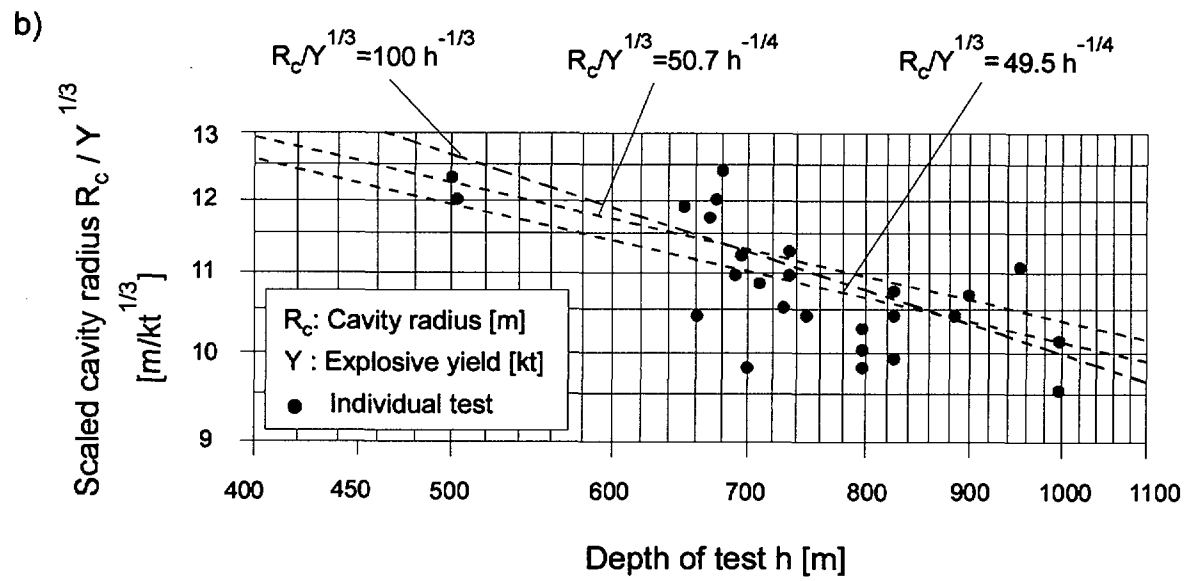

FIG. 10b. Examples of variability in cavity-chimney radius produced by underground nuclear tests in Mururoa and Fangataufa; modified after Caristan in Atkinson 1998. The underground data are given for the scaled cavity radius $R_c / Y^{1/3}$. Logarithmic scales were omitted from original (1983) diagrams. The scales shown are estimates only from currently available data. The slope relationships for the three dashed lines have been added and correspond to the estimated scales.

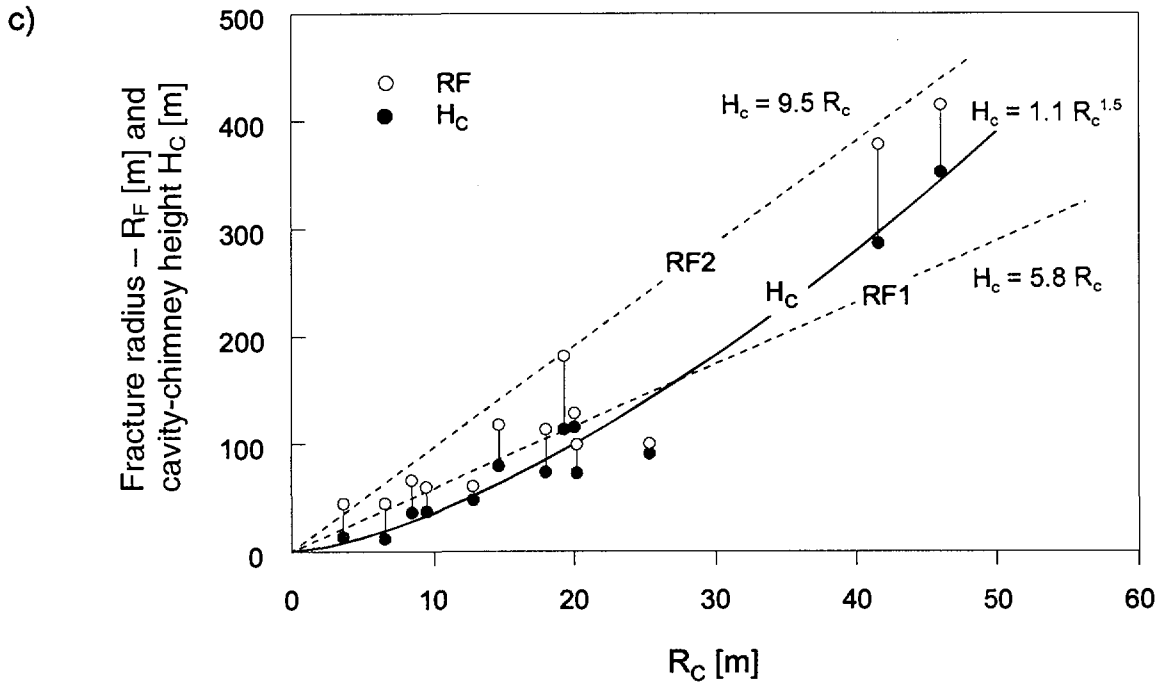

FIG. 10c. Fracture radius (R_F) and height of the cavity-chimney (H_c) as function of the cavity radius (R_c) for the volcanics of the Mururoa atoll. The indicated relationships for the three curves have been added, based on the estimated scales.

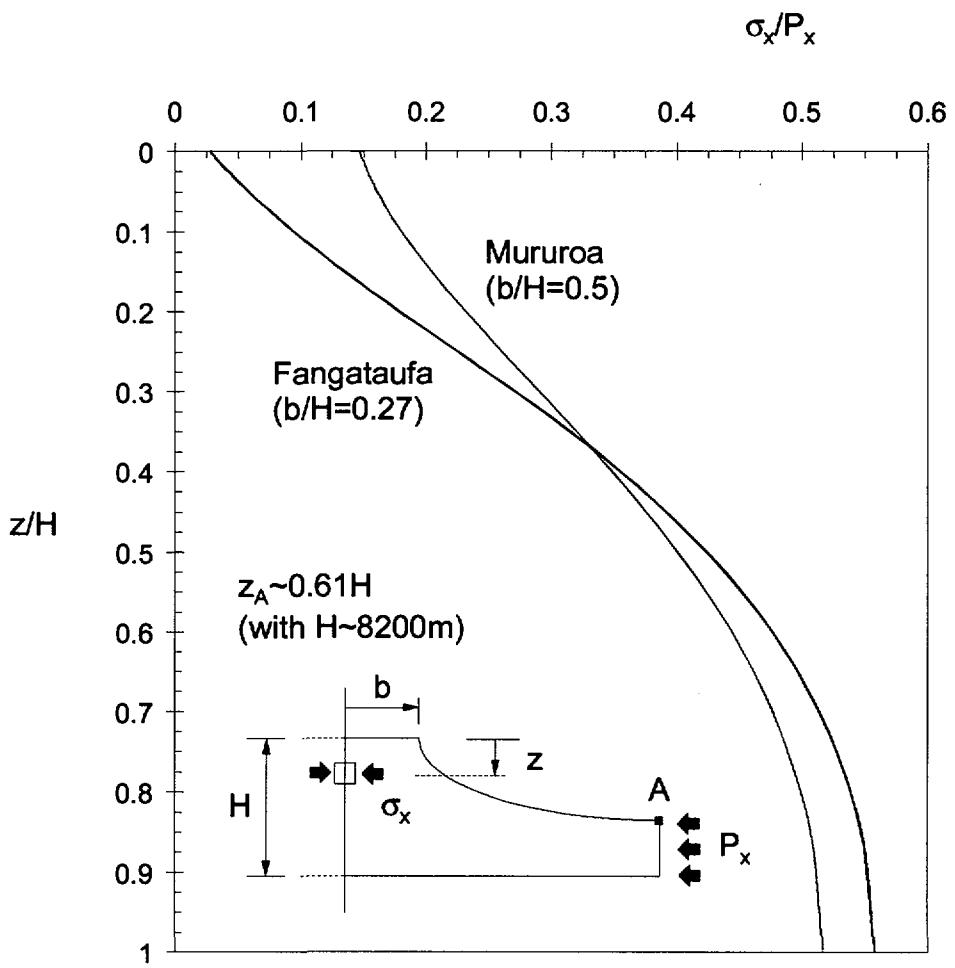

FIG. 11. Normal stress induced along the central axis of Mururoa and Fangataufa due to a change P_x in the normal stress in the ocean crust (after solidification of the seamount).

As noted in Section 3.2.3, field studies of the time required for cavity-chimneys at Mururoa and Fangataufa to refill with water have led CEA scientists to the view that a region of the order of 2.5 R_c around the explosion is enhanced in permeability due to the explosive damage. With the cavity-chimney height of 5 R_c this produces a region that is hemispherical (radius R = 2.5 R_c) on the bottom and cylindrical (height H = 5 R_c) above. Outside this region the rock permeability has not been changed significantly by the explosion.

2.4.1. Regions of fracture damage in underground tests

Although the explosion may not significantly enhance the permeability beyond a radius R = 2.5 R_c, analysis of the mechanics of damage to the volcanic rock indicates that appreciable inelastic deformation will extend further, typically to approximately R = 5 R_c with a lower level of "damage" extending to approximately 8.5 R_c (Vol. 3 of this Technical Report).

Very little comprehensive information is available on the physical appearance of the rock contained within the various zones around a cavity. Personal discussions with individuals involved in post-test excavations at the Nevada Test Site (NTS), USA indicate that, even though a large portion (more than 50–75%) of the explosion energy is dissipated in the rock within a few cavity radii of the NTS explosion, the rock (e.g. granodionite, salt) shows little visual evidence of damage beyond 0.5 R_c - R_c from the cavity. Measurements of elastic wave velocity, Schmidt hardness and other tests indicate that there is essentially no change in the region beyond R_c from the pre-test values. This could suggest that the volcanic tuff at the NTS may have undergone some degree of high temperature - high pressure recompaction and restrengthening, even though a large amount of irreversible deformation has occurred. This may not be the same for porous, saturated rock such as the volcanics on the atolls of Mururoa and Fangataufa. However, it is worth noting that dissipation of a large amount of energy in a rock under the intense loading environment of a nuclear shock may not be synonymous with complete loss of strength.

This observation does not contradict the apparent increase in permeability deduced from cavity re-filling studies (see Section 3.2.3). Interpretation of the re-filling observations is based on the assumption of spherical zones of increased permeability around the cavity. It is possible that the remaining lower hemispherical region of rock adjacent to the cavity could have reduced permeability, being associated with the lining of lava and, possibly, a small zone of compacted and reduced permeability rock adjacent to the cavity-chimney collapse region. One of the scenarios (F3) examined in Section 3.2.3 considers this situation.

Apart from the radiochemical sample holes drilled into the bottom of each cavity to obtain cores of solidified lava (Bouchez and Lecomte 1996), no post-test drilling has been performed on Mururoa and Fangataufa. Lost circulation, i.e. when drilling water, introduced to bring rock chippings to the surface, is lost into fractures rather than returned up the drill hole annulus, is seen to occur when the drill hole reaches the region corresponding approximately to R = 2.5 R_c around the explosion source. No assessments of the change in rock strength around the explosion have been made on the atolls.

Figure 12 is an attempt to indicate rock damage regions that may develop due to passage of the explosive shock wave.

(a) Starting with the vaporization and melting of the cavity walls (R_c), the outgoing shock wave causes intense crushing with, possibly, some re-strengthening, as discussed above (R_{cr} ~ 2 R_c, where R_c is the cavity radius).

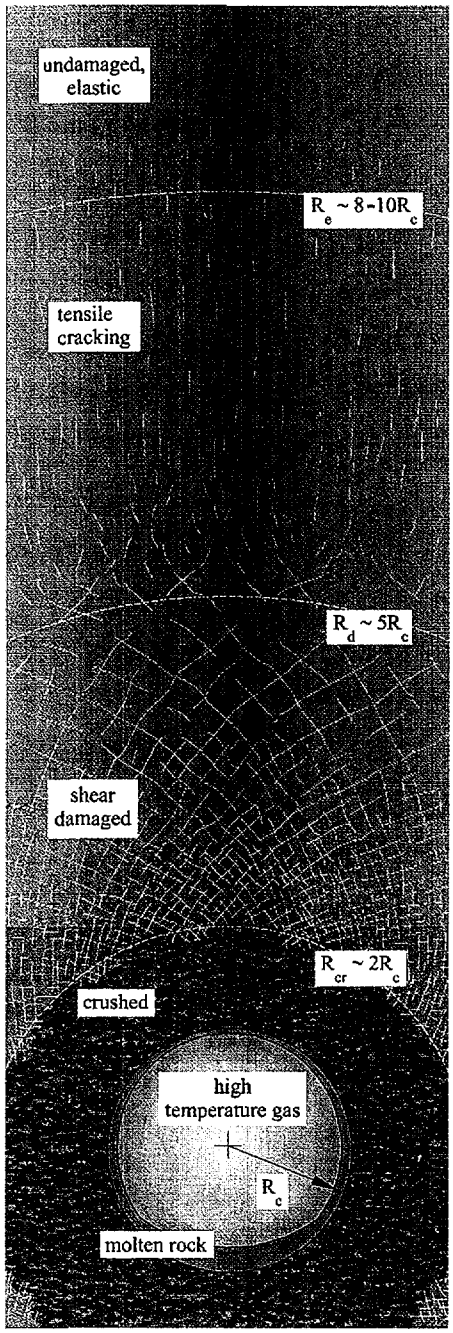

FIG. 12. Schematic illustration of zones of damage around an underground nuclear explosion.

(b) It is grading into compression induced conjugate-shear fracturing, as it is decreasing in intensity with increasing distance from the shot point ($R_d \sim 5\ R_c$). Note that shear fractures are inclined at angles of ($45° \pm \phi/2$) to each other, where ϕ is, here, essentially the angle of sliding friction between the fracture surfaces. Ideally, these fractures follow inclined logarithmic spiral paths, as indicated in Fig. 12;

(c) Eventually, as the outgoing shock wave weakens further, the tangential component of the wave will become tensile, producing individual, radially oriented, extensile fractures ($R_e \sim 8\text{-}10\ R_c$). Note that these are not, in general, connected fractures.

(d) As the intensity of the shock decreases further, fracturing will cease (estimated to be at about $R = 8\text{-}10\ R_c$), and the now low amplitude wave will propagate elastically. This elastic wave is the source of the seismic waves used to detect nuclear explosions and earthquakes at great distances, e.g. to thousands of kilometres from the source.

The important point to note is that, since the outgoing shock wave is entirely compressive, it does not, in general, produce continuous pathways of fractures that link the cavity-chimney to the undamaged region of rock beyond the damage zones (see, however, box above on early time injection).

2.4.2. Distribution of underground tests at Mururoa and Fangataufa

From the start of underground nuclear testing in Fangataufa (5 June 1975) and Mururoa (3 April 1976) until March 1981, a total of 47 tests were carried out below the rims of the two atolls (Fangataufa 2; Mururoa 45). The first test under a lagoon with the 1.5 m diameter emplacement hole drilled from a barge was conducted at Mururoa on 10 April 1981 and on Fangataufa on 11 November 1988. By 6 December 1986, when the last land (rim) based test took place, a total of 19 lagoon tests had been carried out and an additional 31 rim tests, all 50 at Mururoa. From December 1986 to the present, a total of 43 additional tests, all in the lagoons, have been conducted (Fangataufa 8; Mururoa 35).

With rim space limited at Mururoa the area close to the living quarters at the eastern end of the atoll was used for the relatively small yield tests. This is evident in Fig. 96 of the Main Report where the average yield per test in the seven test areas is seen to increase progressively to the West. Except for the first two, relatively low yield (<10 kt) rim tests, all remaining eight tests at Fangataufa were located in the central region of the atoll. This is the region of highest average yield, approaching 100 kt per test, and relatively greatest "damage", in terms of highest yield per unit plan area of the test region.

Considering the relative proximity of the sides of the atoll and neglecting any geological variations across the atoll, Area 4 in Mururoa is likely to be the most prone to explosion induced slope instability. Indeed, the development of barge drilling technology, which allowed testing under the lagoons, appears to have been stimulated by several instances of serious underwater slope collapses in Area 4 in the period 1977–1980 and the resulting hydraulic waves which, in the case of Tydée, July 1979, submerged the rim of the atoll. As noted in the report of the first scientific mission to visit Mururoa after the Tydée event, "*The conclusion of this investigation....is that the risk* [of damaging tidal waves produced by slope collapses] *is believed to be small, on the express condition that high yield tests are conducted at the maximum possible depth in the interior of the lagoon*" (Tazieff 1982, Annex 2', p. 2 last para.).

Slope instability induced by underground explosions and the consequences for release of radionuclides from the geosphere will be discussed further in Section 2.6.

Figure 13 shows the testing Area 4 of Mururoa, together with the region assumed to exhibit enhanced permeability ($R_p = 2.5\ R_c$) associated with each test, where R_c is the radius of the cavity. It is seen that, even in this most intensively damaged underground testing area of the Pacific Test Centre, there is a region of almost unchanged permeability between each test. Also, since the tests are aligned more or less parallel to the reef ocean slope, there is little or no hydraulic gradient between the tests and hence no tendency for fluid flow between cavities (see Appendix I, Fig. 6). The dashed lines in Fig. 14 show a region of fracturing damage $R_d = 5\ R_c$. It is seen that there are sections where there is overlap between the fractured rock regions. Implications of this overlap are discussed in Section 2.4.3.

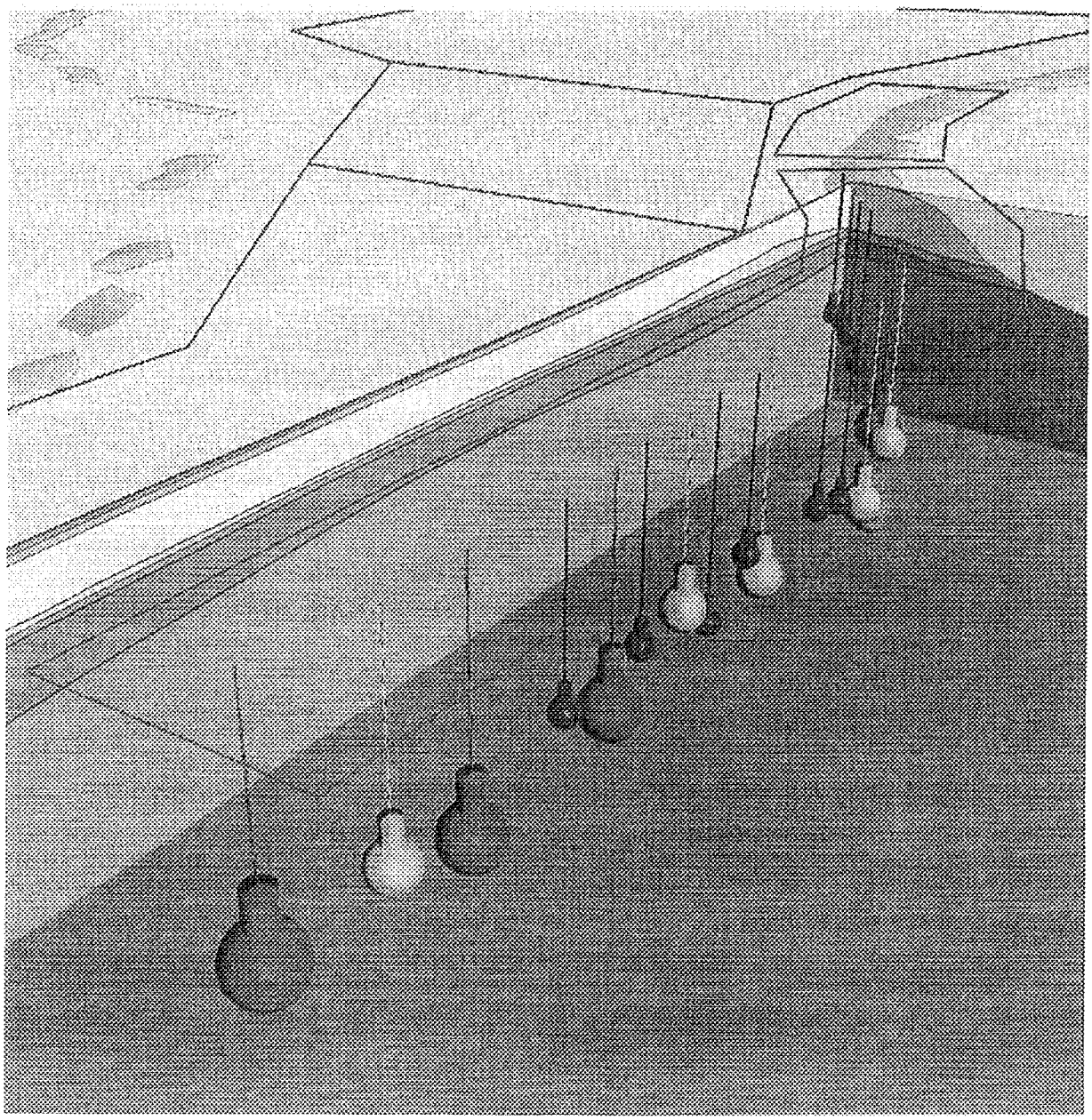

FIG. 13. Schematic illustration of cavity-chimney collapse regions associated with underground tests in Area 4 on Mururoa.

By contrast, Fig. 15 shows the extent of fracturing damage $R_d = 5\ R_c$ for the (lower yield) tests and safety trials in Area 1 on the northern rim of Mururoa viewed from the NNE. It is seen that there are substantial volumes of undamaged rock between each cavity-chimney.

2.4.3. Mechanical interaction between adjacent cavities

Within Area 4, the generally large yield and proximity of neighbouring tests suggests the possibility of structural interaction between adjacent large cavity-chimneys with a relatively small columnar pillar of damaged rock between the cavities. Some long term deformation tending to close the cavity-chimneys may occur, driven by the weight of overlying rock. This cavity-chimney closure is likely to be limited, since the large cavity-chimneys are filled with rubble and voids are filled with water under pressure, and the rock outside of the immediate cavity-chimney region, i.e. $R > 5\ R_c$,

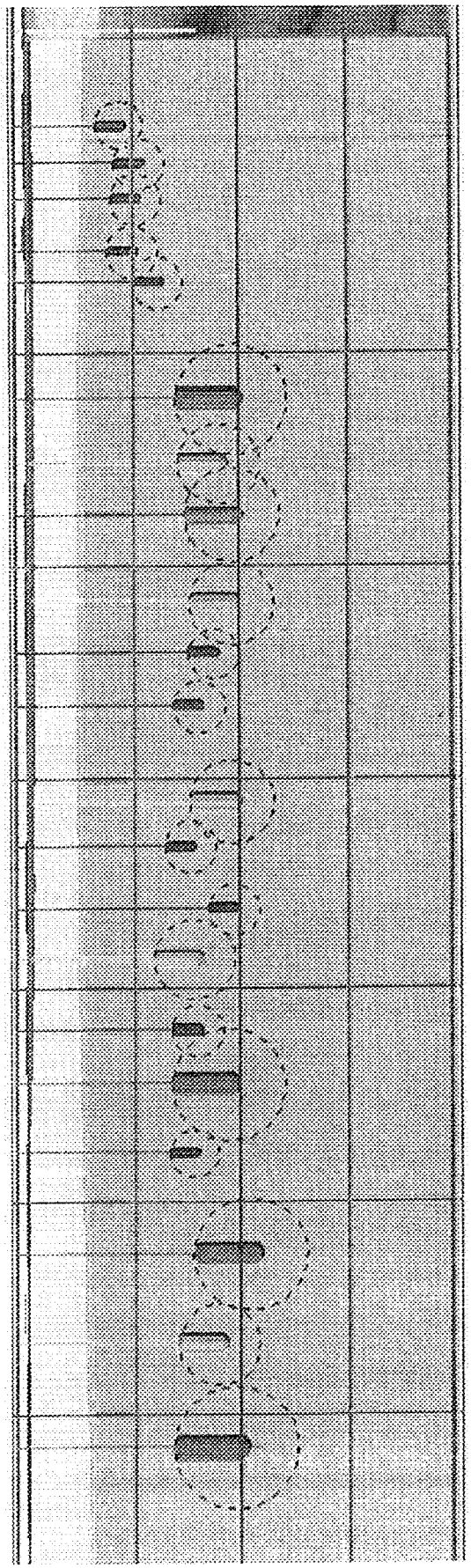

FIG. 14. Schematic illustration of regions of fracture damage (R_d = 5 R_c) associated with underground tests in Area 4 on Mururoa.

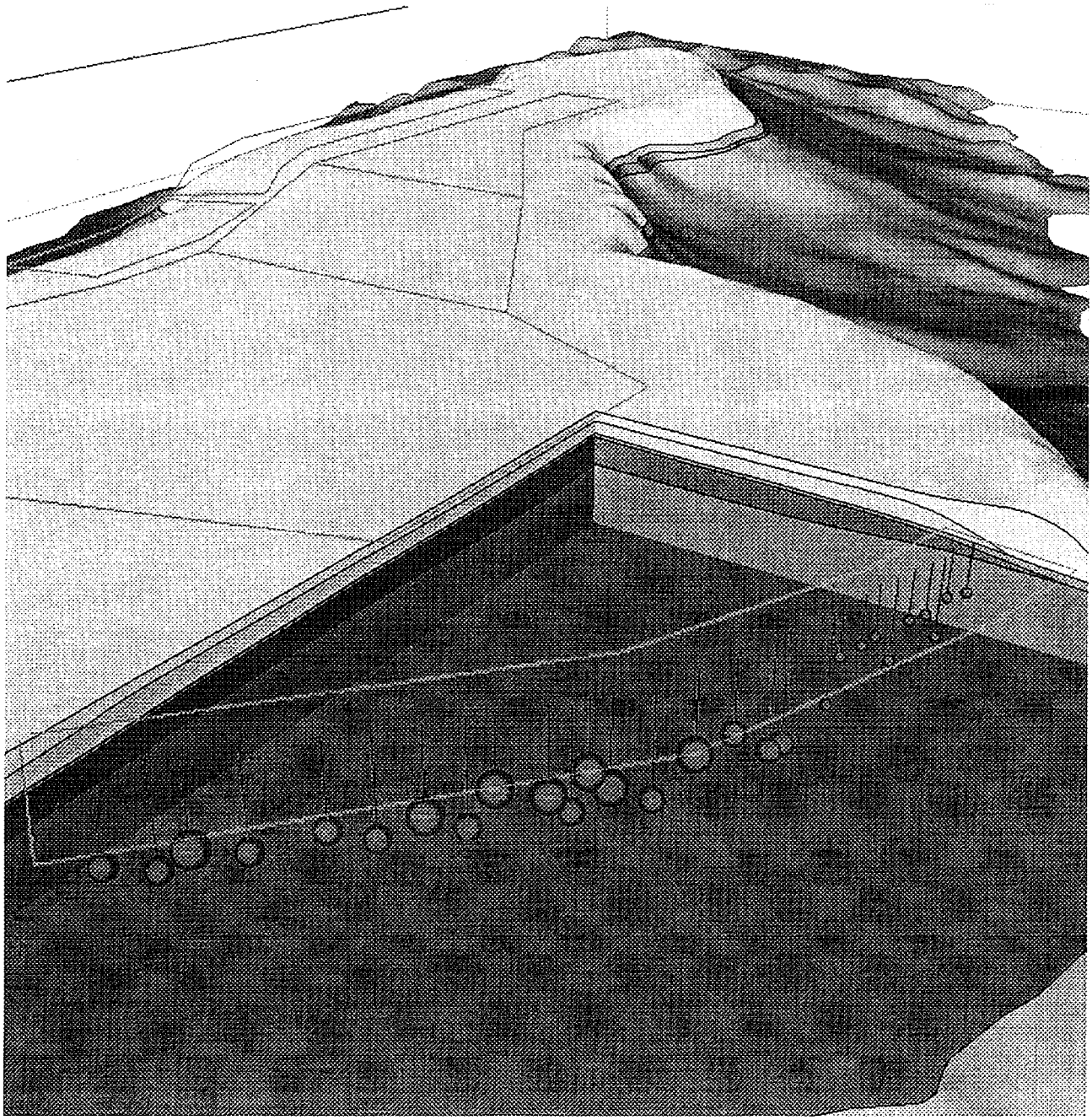

FIG. 15. Schematic illustration of regions of fracture damage (R_d = 5 R_c) associated with underground tests in Area 1 on Mururoa.

remains essentially undamaged by the explosion. This criterion for the limit of damage is probably very conservative with respect to changes in rock strength. Any such closure would be manifested in part by elastic deformations in the overlying undamaged volcanic cover and a small surface subsidence. Over time, any such surface lowering in those regions submerged by explosion induced settlements, as discussed below, would be eliminated by reactivation of coral growth.

The question of mechanical interaction between cavities has been examined by Fairhurst et al. (IGC) 1998. According to data in French Liaison Office Document No. 6, 1996, Fig. 8, no adjacent shots had a centre to centre spacing less than 5 R_c and all but 15 of the 147 underground tests conducted on the atolls had a spacing of 8 R_c or considerably more.

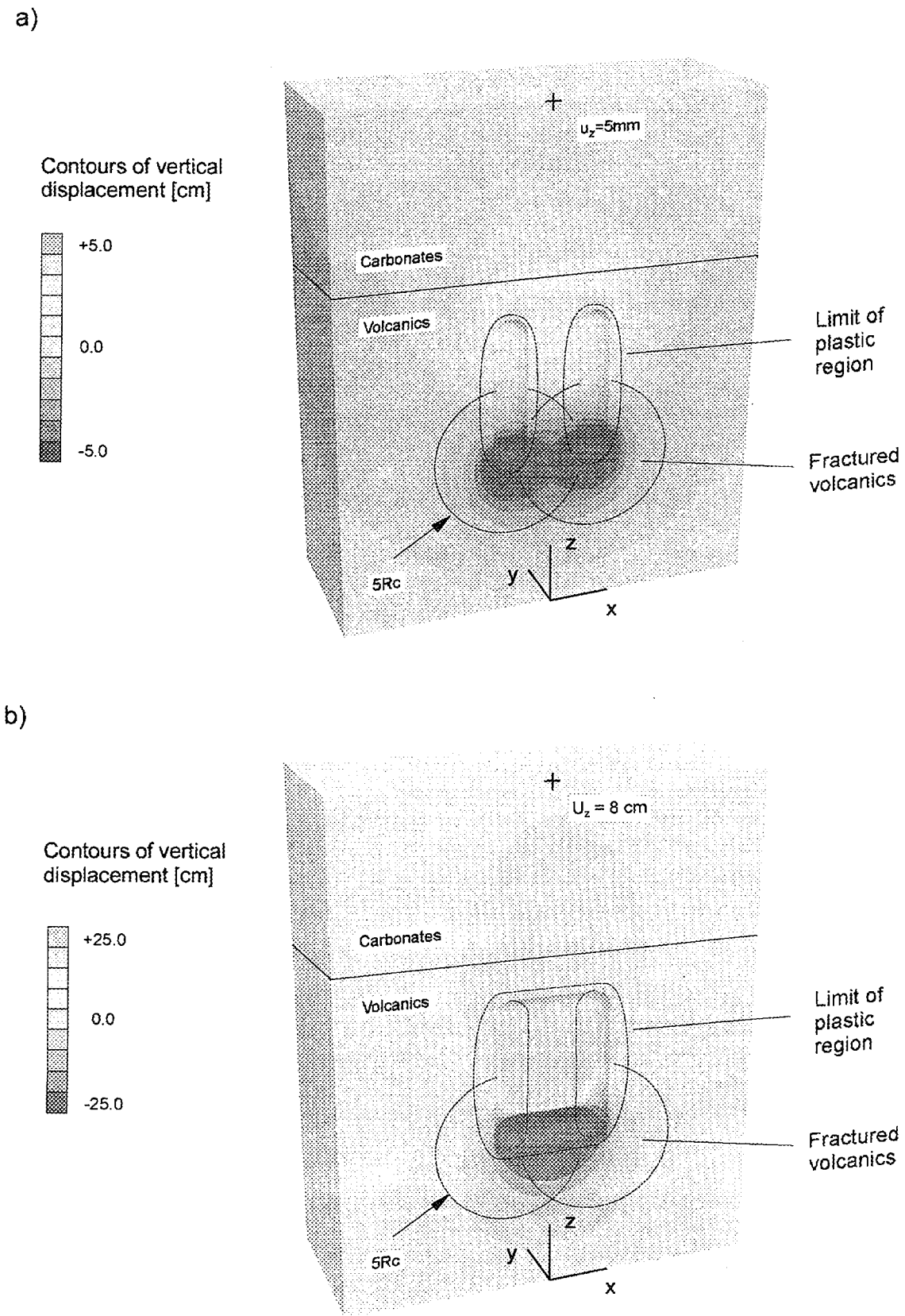

FIG. 16. Displacements induced around the cavity-chimney collapse region due to two hypothetical 150 kt nuclear explosions at 1000 m depth in the volcanics (a) for weakened rock damage zone (b) for extreme case where the pillar between cavity-chimneys is totally destroyed.

Figure 16 shows the deformations resulting from a hypothetical, extreme case of the two cavities produced by two 150 kt tests, located at the same depth and spaced 5 R_c (centre to centre) apart in weak, poor quality volcanics that have been further weakened by the explosions. The cavity-chimneys are each 8 R_c in height above the shot point. The rubble is assumed to have no influence in restricting deformation of the rock around the cavity-chimneys. This is a realistic assumption. It is seen that in both of the extreme examples shown below, the region of inelastic deformation does not extend beyond a relatively small distance from the cavity-chimneys and does not extend into the carbonates.

Figure 16(a) assumes that the rock, although significantly damaged out to a distance $R_d = 5\ R_c$ from each shot point, i.e. with overlap of the damaged regions between the two cavity-chimneys, does retain some residual strength. The calculated surface subsidence is 5 mm, approximately twice the subsidence resulting from one of the two explosions alone.

Figure 16(b) shows an even more extreme case, where the pillar between the two cavity-chimneys is assumed to lose all strength and collapse. Here, the maximum surface subsidence is calculated to be 8 cm.

Except within the region of inelastic deformation shown in the diagrams around each cavity-chimney, the deformations which are due to the large open spans of the cavity-chimneys are all elastic, i.e. no new fracture pathways are created between the cavity-chimney and the carbonates and/or the surface. The surface deformation, of the order of some mm, is to be compared with the 2 m or more of surface settlement produced by the explosion shock wave discussed in Section 2.5 below. Further details can be found in Fairhurst et al. (IGC) 1998.

2.4.4. Hydrological interaction between adjacent cavities

Hydrological interaction between closely spaced cavities produced by explosions on the rim, will be minimal, as shown in Appendix I. Since greater spacing between tests is possible under the lagoon, cavity-chimney interactions will be even less likely, although the direction of the pre-excavation flow field will differ from the simple situation on the rim. The topic of hydrologic interaction is discussed further in Sections 3.2 and Appendix I of this report.

2.5. SURFACE SETTLEMENTS

The geological structure of the atolls differs from the testing sites used in other countries, i.e. non-welded and welded tuff in the USA or granite and other media in the Former Soviet Union. The situation at the atolls is special because (a) the underground volcanics are overlain by 300–500 m of mechanically weaker carbonates; (b) the volcanics and carbonate formations are water saturated to the surface of the atoll; and (c) a substantial number of tests took place near to the underwater flanks of the atolls.

As noted earlier, the depth of burial of most of the underground nuclear tests at Mururoa and Fangataufa is sufficient to ensure that the outer radius of rock damage or, equivalently, the start of the elastic (seismic) region beyond which the wave does not damage the rock, is in most of the cases well below the top of the volcanics. This was not so for the 12 CRTV tests. However, as this elastic wave travels upwards from an explosion, it passes into the weaker carbonates. Numerical simulations (Fairhurst et al. (IGC) 1998) reveal that, as it approaches the atoll surface, near the rim, this wave is sufficiently intense to cause considerable inelastic damage to the top 150 m or so of the atoll. Since the rock is fully saturated, compaction is inhibited but the rock can fail by shear.

Assuming that the rock does not undergo any volume change during the shear process, then a lowering (settlement) of the surface (French Liaison Office Document No. 7, 1996, Fig. 11) over the

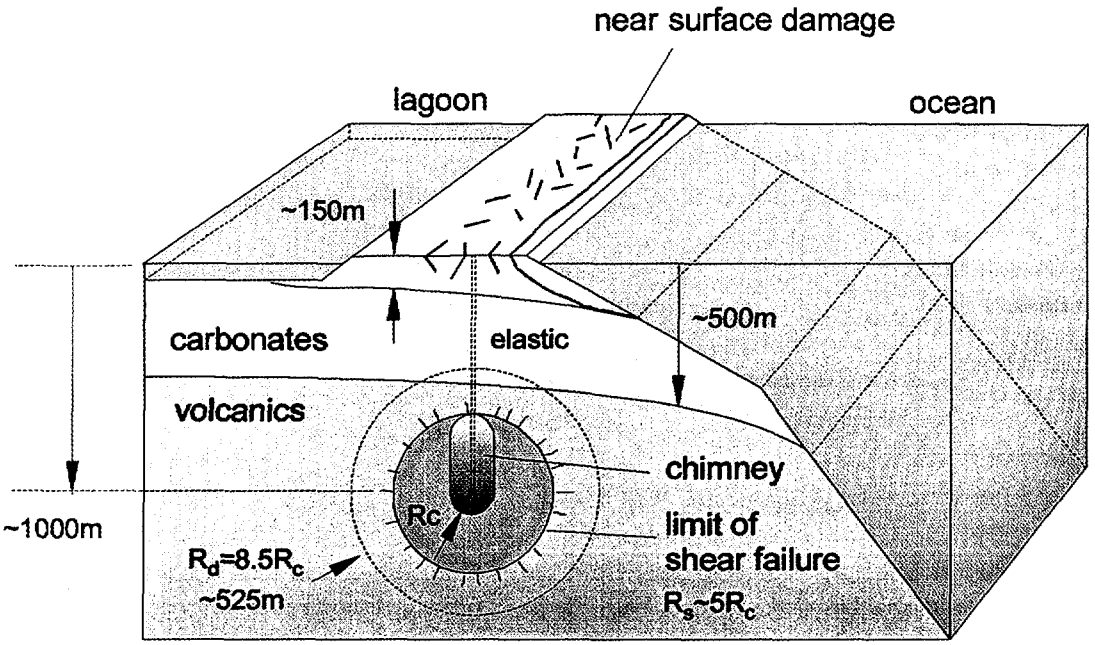

FIG. 17. Computed near surface damage due to a 150 kt explosion at 1000 m depth under the rim. Note: Cavity collapse develops minutes to hours after explosion.

cross-section of the atoll, must be accommodated by a volumetrically equal extension of the rim sides. Assuming, for example, a 300 m width of the atoll rim and no extension perpendicular to the cross-section of the atoll, then a 1 m surface settlement over the 300 m width of carbonate would produce an average lateral extension of approximately 2 m over a height of 150 m or say for illustrative purposes, 1.4 m towards the ocean and 0.6 m towards the lagoon. In reality, structural inhomogeneities, pre-existing fractures, non-uniform deformability and strength and local variations in the wave amplitudes would produce non-uniform distribution of the induced shear deformation. This lateral extension in the carbonate would tend to produce vertical fracturing, which may extend to considerable depth underwater on the sides of the atoll. This is not inconsistent with the underwater views shown on the videotape "Tahiti - l'eau de feu" prepared by the Cousteau mission 1988[1], of collapse of the underwater slopes to depths of the order of 100 m and greater. Such settlements are responsible, at least partly, for opening of the pre-existing fractures visible to anyone who walks over the various test areas. Some of the widening of these fractures is also due to deeper, ongoing, slope deformation as in Area 1 on the north side of Mururoa. A detailed analysis of surface settlements and damage to the atoll flanks by explosions is discussed in Fairhurst et al. (IGC) 1998.

Some of the fractures produced by the explosions in the Northern rim in the area currently undergoing active sliding are not visible from the surface, but may extend underground from the submerged, ocean side flank of the rim into the lagoon. This is confirmed by the statement: "*The Camélia Zone is limited by fractures crossing the coral rim and penetrating the lagoon*" (French Liaison Office Document No. 7, 1996, p. 24, VI.4.1, para. 2).

Figure 17 shows schematically the type and extent of surface settlement damage that may occur in association with a 150 kt explosion at 1000 m depth beneath the rim of the atoll. This shear settlement may be augmented somewhat by ballistic flight and subsequent fall-back, with moderate compaction of one or more slabs of rock at the surface, produced by reflection of the incident elastic compression wave from the explosion and associated expulsion of water in the near surface rock.

[1]The videotape "Tahiti — l'eau de feu" (1998) may be ordered from Equipe Cousteau, 7 rue Amiral d'Estaing, F-75016 Paris. Tel + 33 1 53 67 77 77 Fax + 33 1 53 67 77 71.

It is important to note that these "surface settlements" are restricted to the upper part of the carbonates only. Except for the CRTV tests, most of which were low yield explosions in Area 1 of Mururoa, modelling studies reveal the existence of an undamaged elastic region in both the upper volcanics and in the overlying carbonates, as shown in Fig. 17. Thus, in contrast to the subsidence craters observed in the NTS, these surface settlements do not indicate a preferred geological pathway for radionuclide release from the cavity-chimney. Even for those cases where no intact volcanic cap exists above the cavity-chimney, bulking of the collapsed carbonates will be such as to inhibit explosion-induced subsidence that extends more than a relatively short distance, i.e. less than one cavity radius, above the top of the cavity-chimney. Nevertheless, the layered and fractured nature of the carbonates will allow relatively rapid communication between the top of the cavity-chimney and the surface. The case of radionuclide releases from CRTV tests is given special consideration in Section 5.

2.6. STABILITY OF THE ATOLL SLOPES

As noted in Section 2.5, surface settlement of the rim, produced almost instantaneously when the explosion wave reaches and interacts with the near surface region (surface to about 150 m depth) of the rim, extends also to the upper levels of the underwater slopes in the carbonates (see Fig. 17). Some tens of milliseconds earlier, the same wave, radiating from the explosion, reaches the deeper parts of the slopes at the volcanic - carbonate and carbonate - ocean interfaces. Reflections of the wave at these interfaces can result in destabilisation of the deeper slope regions. The combination of high yield, greater proximity of the test to the slope, reduced strength of the carbonate rock and the volcanic - carbonate interface, increases the probability of destabilisation and collapse.

Detailed analysis of the mechanics of this destabilisation, taking into account the general carbonate - volcanic structure (Fairhurst et al. (IGC) 1998), confirms the conclusion by CEA scientists that the collapse is limited to the carbonates and the carbonate - volcanic interface. It does not extend into the volcanics.

2.6.1. Slides in the SW region of Mururoa

Several major underwater slides in Area 4, attributed to the following explosions (see Vol. 3 of this Technical Report)

-	Nestor	19 March 1977	estimated yield 47 kt;
-	Priam	30 November 1978	estimated yield 64 kt; and
-	Tydée	25 July 1979	estimated yield 112 kt.

appear to have been initiated by interaction between the explosion wave and the slopes/water interface.

Figure 18 shows a vertical cross-section, normal to the general rim line, at the (presumed) location of the Tydée test. Analysis suggests that, if this cross-section is representative of the area immediately east and west of Tydée, initial destabilisation of the slope would occur at the bottom of the carbonate - volcanic interface, immediately "in front of" the Tydée explosion source, i.e. in the cross-section shown, propagating rapidly upwards to cause a collapse to the underwater surface of the slope.

The main consequence of such rapid collapse is the generation of a hydraulic wave as water is "dragged down and pushed out" with the sliding rock towards the ocean as the rock mass descends. In the case of Tydée, the height of the wave was 2.5 m, some 90 sec after the slide, at the site of the collapse. A restaurant 10 km to the west of the explosion site was washed away. The airstrip in Fangataufa, 45 km distant, was submerged to a depth of 2 m (French Liaison Office Document No. 7,

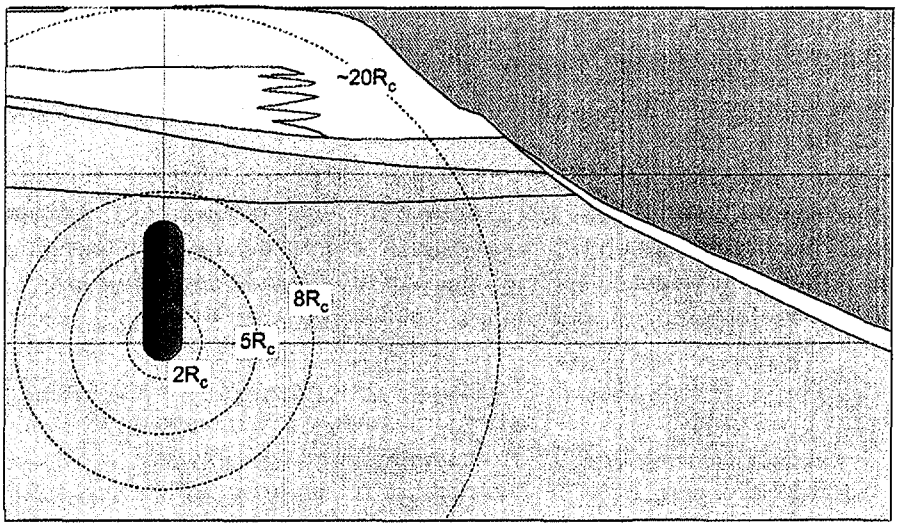

FIG. 18. Schematic illustration of the cavity-chimney (assuming H_c = 5 R_c) formed due to a hypothetical 150 kt test under the rim in Area 4.

1996, Section V.4). Similar, although less severe, hydraulic effects were associated with the Nestor and Priam events (French Liaison Office Document No. 7, 1996).

Based on bathymetric measurements, the volume of the initial Tydée slide was estimated to be approximately 0.1 km^3. This volume is consistent with the collapse, to the bottom of the carbonate - volcanic interface, of a "slab" of thickness averaging 50–100 m over a width of the order of 2–3 km. A total volume, estimated to be 0.36 km^3, slid down the slopes in a series of subsequent collapses, as a result of this explosion.

Assessment of the consequences of these events and their implications for the safety of personnel was a main concern of the Tazieff mission to the atolls (Tazieff 1982).

A puzzling feature of the Tydée slide is that it started, not directly at the slope in front of the explosion, as discussed above, but somewhat more than 2 km to the west. The explosion wave arriving along a direct path from the explosion to a point 2 km to the west would be lower in amplitude than a "direct" wave in the plane of the section and would tend to produce a shearing motion parallel to the slope, rather than a tensile or tearing action. Local inhomogeneity in the strength of the carbonates, non-uniform geometry of the rim and the "buttressing effects" of ridges in the volcanics (see Fig. 6 and Guille et al., 1996, Fig. 23) could all influence this event, complicating the wave motion and changing the local resistance to collapse.

The Nestor and Priam events, also serious, but smaller than Tydée, could have been more classical collapses, i.e. in front of the explosion, but, since the precise locations of the two explosions are not known, this question cannot be addressed.

In the case of Tydée (Bouchez and Lecomte 1996, p. 25, last para.), it is noted that the test was conducted at a depth of 987 m, i.e. 113 m above the bottom of an 1100 m deep, 1.5 m diameter emplacement hole. The device became jammed during lowering. If this 113 m was not cemented, the column of water below the device could have increased the coupling of the explosive to the rock, increasing the apparent yield. Detailed conditions of this test have not been revealed.

Geophysical monitoring of the SW region of Mururoa indicates essentially no microseismic activity since cessation of tests in this region. Based on the analysis above and this field evidence, it is

concluded that further collapse in the SW region of Mururoa is very unlikely, as microseismic activity is indicative of ongoing (micro) crack development, which, if continued, could lead to collapse.

2.6.2. Slides in the NE region of Mururoa

Slope deformations in the North Eastern area of Mururoa in the vicinity of Françoise, Camelia and Irène (Area 1) have been a continuing concern since about 1980 and have been monitored closely since that time. Although the fundamental mechanics of the slope deformation can be explained using the same analyses as for the collapses in the Southwest (Area 4) region, there are important differences.

The average yield of tests in Area 1 was approximately 2 kt, compared to 35 kt in Area 4 (see Fig. 96), with Nestor, Priam and Tydée well above this average. However, the 2 kt tests would be shallower, so that the effect on the carbonates would be greater than may be suggested by the simple ratios of yield.

The carbonate formations in the NE region contain a very weak "chalky limestone" (French Liaison Office Document No. 7, 1996, Section VI) that is very sensitive to even small disturbances, such as the pressure increase experienced by passage of the wave from remote explosions. The influence of these explosions can be seen as the short transient responses on the slope displacement records (French Liaison Office Document No. 7, 1996, Figs 35–37). Intensive slope deformation monitoring systems have been in continuous operation since around 1980. The slopes are seen to be deforming continuously. Inclinometers in vertical boreholes (French Liaison Office Document No. 7, 1996, Fig. 28) clearly reveal that the continuing "creep" displacements are taking place at about 400 m below the surface, the horizon of the chalky limestone. CEA scientists are of the opinion that the creep rate is now declining so that the system could reach equilibrium without collapse in the future. Another view is that the chalky limestone has already undergone substantial deformation (estimated from deformation measurements to total approximately 0.5% strain) and may be approaching a critical strain at which the chalk could begin to lose strength rapidly. Certainly, the data so far is not sufficient to arrive at a firm conclusion on the long term stability of the region.

As seen in Guille et al. 1996, Fig. 23, this NE region has extensive underwater accumulations of sediments, up to 300 m thick, now lying at depths of as much as 2000 m below water. This strongly suggests that the region has been subject to slope instabilities in the geological past so that, in large part, the explosions have accelerated previously slow deformation of the region, rather than causing an otherwise stable area to become unstable.

Again, the main concern is that sudden collapse could give rise to serious hydraulic wave effects. The region currently involved in the slow sliding is estimated to be 0.6 km^3, six times larger than the initial Tydée collapse. However, it is unlikely that this entire volume would collapse simultaneously. At least three distinct, but adjacent, sliding masses can be identified within the slide region. The possibility that a collapse in the NE region could involve one or more CRTV tests is mentioned in Section 2.6.4 below.

2.6.3. Fractures and microseismicity in the NE region of Fangataufa

Open fractures (tension cracks) are indicative of a deeper, probably shear, displacement. They can be seen just off-shore between the Frégate and Fox areas of NE Fangataufa. This region is unique in that no tests were ever carried out on the rim in the vicinity of the fractures. It appears that the subsurface geological condition in this region are similar to those on the NE slope of Mururoa, i.e. with a very weak, sensitive, chalky limestone. The region could have been creeping towards collapse naturally, generating surface fractures before any underground tests were conducted on Fangataufa. Relatively high yield tests in the lagoon could produce seismic pulses sufficient to accelerate this

creep deformation and fracture development. Microseismic monitoring (French Liaison Office Document No. 7, 1996, p. 38 and Fig. 47) confirms that a limiting peripheral fault which follows the rim, similar to the one at Mururoa, was activated by the Fangataufa lagoon tests beginning in 1988. Note that this is perhaps a pre-existing line of extension fractures rather than a fault with offset. The activity appears to have declined since 1992, with no significant increase in these movements due to the 1995–1996 test series. Guille et al., 1996, Fig. 60 show considerable, over 250 m underwater accumulation of sediments, extending to more than 2000 m depth in this NE region of Fangataufa. This suggests, again, that slope instability in this region is a natural process that has been accelerated by the remote, but high yield, lagoon tests of 1988–1989. According to CEA scientists (French Liaison Office Document No. 7, 1996, p. 38), the north eastern zone of Fangataufa shows very strong geological and morphological similarities to the northern zone of Mururoa. Microseismic measurements suggest however, that the deformation rate is smaller and declining.

2.6.4. Implications of slope instability for radionuclide release

In all cases of slope collapse around the atoll, an outer layer of the carbonate slope is removed. It has been suggested (Atkinson 1984) that the permeability of this outer region may be appreciably lower that the inner carbonate, due to chemical reactions, e.g. dolomitisation, between the carbonates and ocean water and that the removal of this apron could lead to earlier release of radionuclides.

As will be seen in Section 3.1.1, groundwater flow at the underwater ocean boundary of the atolls is generally from the ocean to the lagoon, so that the consequences for release into the lagoon due to removal of this apron should be negligible. Removal of the outer layer would reduce the distance between the fractured zone around the test and the slope but, again, this does not appear to have a significant release consequence.

In the NE region of Mururoa, the slide region is within Area 1. CEA scientists indicate that none of the tests in this region, including safety trials, was conducted within the actively sliding mass.

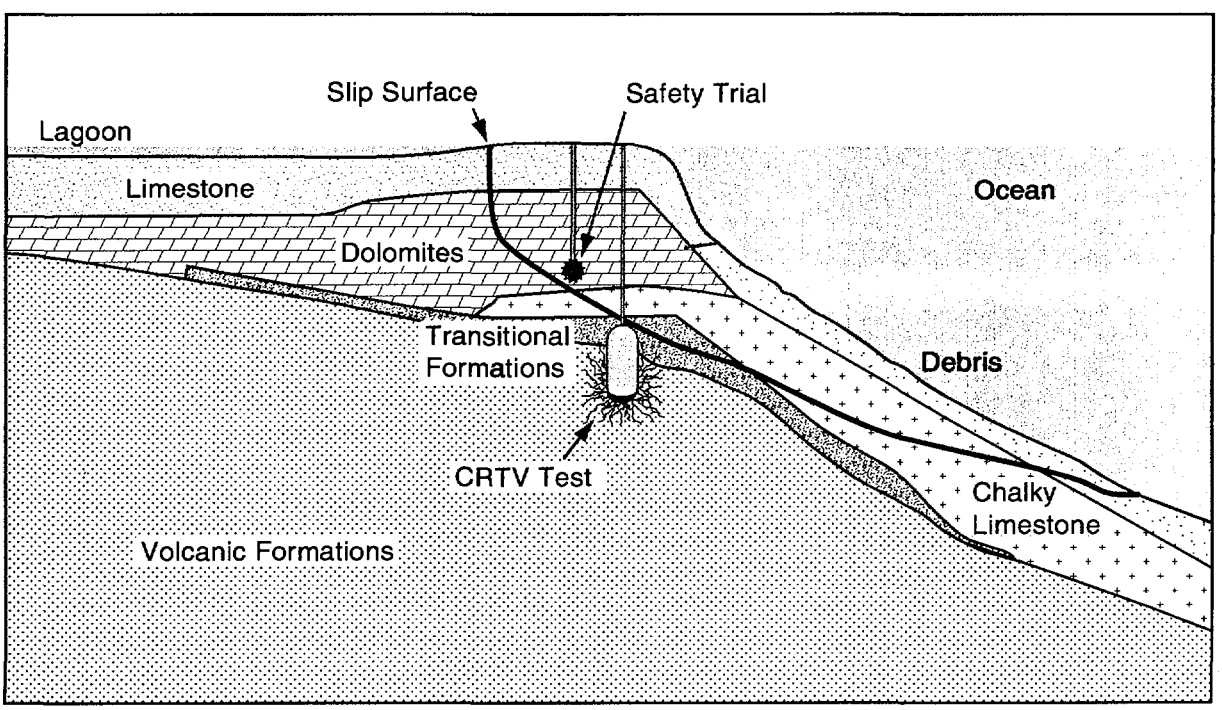

FIG. 19. Hypothetical slide of carbonate rock leading to release of radioactive material.

A number of the CRTV tests were located in Area 1. A major instability over a slide surface extending to 300 m or more in depth could perhaps bring the cavity-chimney of the CRTV tests or a safety trial into direct contact with the ocean (Fig. 19), leading to rapid release and major dilution of the radionuclides in solution in the cavity-chimney water. The possibility is discussed further in Section 7.3.1 of the IAEA Main Report.

The slope activity in the NE rim region of Fangataufa has no radiological release consequences, since no tests were conducted in the region where slope deformations are occurring.

2.7. POTENTIAL MAN MADE PATHWAYS

Much of the preceding discussion in this section has been directed at establishing the nature of the natural pathways in the geosphere between the explosion cavities and the biosphere. The process of emplacing the explosive device at depth in the volcanics via a 1.5 m diameter shaft (Bouchez and Lecomte, 1996, pp. 26–27); the taking of lava samples by inclined drill holes (op. cit., pp. 52–53); leaving of unused 1.5 m diameter shafts in the carbonates, capped only just below the lagoon (French Liaison Office Document No. 9, 1996, p. 5), all constitute potential pathways. Since most of these are primarily hydrological pathways they will be discussed in Section 3. However, plugging or "stemming" of the emplacement shafts does involve geological and mechanical issues, so it is discussed here.

2.7.1. Stemming of emplacement holes

The arrangement for stemming of the shaft above the explosive container is shown in Bouchez and Lecomte 1996, Fig. 3–8. The region around the container is filled with crushed basalt (basalt sand) and the height above that is calculated to be within the cavity-chimney collapse region is filled with consecutive layers of basalt aggregate or cuttings and cement. Above this, the shaft is filled with a homogeneous cement plug over a height of 100–200 m, i.e. a height:diameter ratio between 67:1 and 133:1. Additional basalt aggregate and cement may be placed above the plug, but it is the 100–200 m stemming plug that is expected to withstand the explosion, i.e. sustain passage of the shock wave and contain the subsequent high pressure and high temperature environment. Since the wave velocity in the cement plug will be lower than in the rock, the transient pressure adjacent to the plug - rock interface during passage of the shock effectively "clamps" the plug in the hole, so that the shock wave should not displace the plug. The large height:diameter ratio should also provide sufficient peripheral shear resistance to contain the cavity pressure. Of course, the cement will be damaged to some extent, as is the rock, by the effects of the shock wave. However, the plug is located beyond the region of intense damage, so that the upper section at least should remain essentially intact.

Drilling of the shaft in the (stressed) rock mass can result in disturbance of the rock in an annulus adjacent to the shaft, the so-called "disturbed rock zone" (DRZ), that is always a concern in the design of effective seals for nuclear waste repositories. Given the variable nature of the volcanics, it is probable that such DRZs may exist around some stemmed shafts. This appears to have been so in several cases where tritium releases have been detected in the lower carbonates soon after testing (see Fig. 1, Category 2 tests and French Liaison Office Document No. 9, 1996, esp. Figs 7 and 8). It should be noted, as discussed in Section 3.2.4, that, immediately after an explosion, the high temperature in the cavity-chimney will provide an upward drive to move the water through the region of the plug and the associated DRZ. The upward drive decreases rapidly over 50–100 years, when the temperature is decaying to the background, i.e. pre-test values after 300–500 years.

The long term (to 10 000 years) integrity of the cement as a barrier to radionuclide release will depend on the long term chemical integrity of the cement. Both the initial permeability and the porosity of the cement plug should be lower than the volcanics. There should be no system of vertical, connected cracks in the cement. Berner 1996 indicates the permeability of cement to be typically

10^{-8}–10^{-10} m/s. Although chemical alteration, involving dissolution of portlandite, $Ca(OH)_2$, will increase the porosity from 6% to ca. 10%, it seems probable that the permeability of the plug will decrease due to precipitation of brucite, $Mg(OH)_2$. Using a reasonable estimate of groundwater velocity, Berner estimates that it will take between 5000 and one million years for all of the portlandite to dissolve. Based on this analysis, it appears most unlikely that the cement plug will seriously degrade before the radionuclides produced by the explosion have decayed to insignificant levels. Furthermore, the results indicate that the plug will not act as a preferential pathway, for the release of radionuclides. Also, the cross-sectional area of the 1.5 m diameter plug is very small compared to the area of the typical cavity-chimney. It is roughly between 0.4% for a 1 kt explosion with a 24 m diameter cavity-chimney, and 0.01% for a 150 kt explosion with a 126 m diameter cavity-chimney. Thus, its influence on the total flux rising through the cover above the cavity-chimney becomes negligibly small.

2.7.2. Venting and long term leakage of explosion cavities

A principal reason advanced for switching from atmospheric to underground testing was to avoid the direct release to the atmosphere of radionuclides produced by the explosion, i.e. to avoid venting, by containing the explosion products in the underground. However, the first underground nuclear test carried out in the world was detonated at the bottom of a 499 ft (152 m) open drill hole, code named "Pascal-A". It was the 100th US nuclear test and took place at the US Nevada Test Site (NTS) on 26 July 1957.

"*Although Pascal-A marked the beginning of underground testing, above ground testing continued for another 6 years. With testing simultaneously occurring above ground, the release of radioactive material from underground explosions was at first not a major concern. Consequently, Pascal-A, like many of the early underground tests that were to follow, was an open shaft that allowed venting!* [It is interesting to note that even with an open shaft, 90% of the fission products created by Pascal-A were contained underground.]

As public sensitivity to fallout increased, guidelines for testing in Nevada became more stringent. In 1956, the weapons laboratories pursued efforts to reduce fallout...[by various approaches]. *Of these approaches only underground testing offered hope for eliminating fallout* "

(US Congress 1989)

Effective containment, i.e. such that venting does not occur, is clearly related to both an adequate depth of burial and effective sealing of the emplacement hole.

According to the US Congress 1989 report (pp. 35–36), the first scaling rule for determining how deep an explosion should be buried was derived from the Rainier test in 1957. The length unit used in US scaling rules was in foot. This has been changed to metres in the quotes of US rules, for ease of comparison with the scaling rules at the Pacific Test Centre. The depth, based on the cube root of the explosion yield, was originally

$$S_d = \frac{D.O.B.}{Y^{1/3}} = 91.5 \text{ m/kt}^{1/3}$$

where

S_d is the scaled depth in $m/kt^{1/3}$,
D.O.B. is the depth of burial in m,
Y is the explosive yield in kt.

It was not until "Blanca", 30 October 1958, that a test was conducted exactly at a scaled depth of 91.5 m to test the depth scale. The containment of the Blanca explosion, however, was

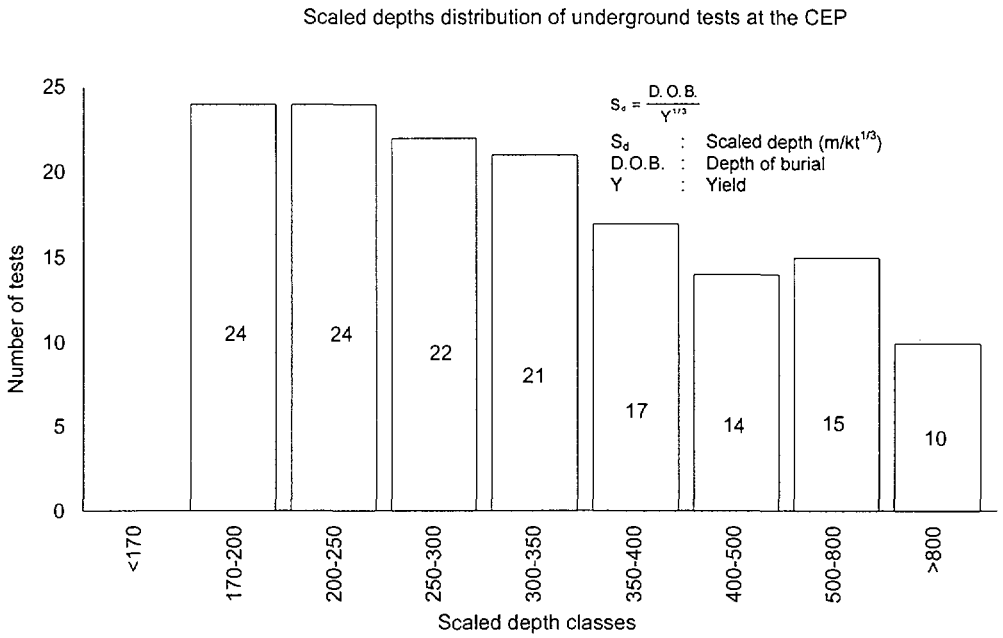

FIG. 20. Distribution of scaled depths of burial for all underground tests at Mururoa and Fangataufa (after French Liaison Office Document No. 6, 1996, Fig 6).

unsuccessful and resulted in a surface venting of radioactive material. As a result, the depth scale was increased to a rule which could be expressed, approximately as

$$D.O.B. = (91.5\ m/kt^{1/3}\ Y^{1/3}) + (60 \sim 100)\ m$$

where, of course, the actual rule in feet, was D.O.B. = 300 $Y^{1/3}$, "plus a few hundred feet".

In 1970, the "Baneberry" underground test at the NTS vented, releasing an estimated activity of 6.7×10^6 Ci (or 2.5×10^{17} Bq) into the atmosphere. This very large release led to a major review of US containment (burial) practice and resulted in the rule

$$S_d = 122\ m/kt^{1/3}$$

with a minimum depth of burial of 183 m.

Although there were some minor releases from 1971–1988, the total from all release events, including ventings (containment failures); late-time seeps; controlled tunnel purgings; and operational releases was 5.4×10^3 Ci (2×10^{14} Bq).

This indicates that a scaled depth S_d of ≥ 122 m/kt$^{1/3}$ has been successful at the NTS.

According to French Liaison Office Document No. 6, 1996, Fig. 6, the values of S_d for tests at the Pacific Test Centre range from $800 > S_d \geq 170$. This involves considerably greater depths than for the NTS, as shown in Fig. 20, which is a reproduction of Fig. 6 from French Liaison Office Document No. 6, 1996.

But can the two rules be considered comparable? The NTS rule applies to non-welded and welded tuff whereas the Pacific Test Center rule, i.e. for Mururoa and Fangataufa, applies to volcanics, i.e. basalts of various strengths and porosities.

As noted in the US Congress 1989 report "*Counter to intuition, only minimal strength is required for containment*" (p. 34).

This is a consequence of the physics of rock deformation associated with a nuclear explosion, especially in the inner regions around the cavity where the rock is vaporized and/or melted or intensely crushed and compacted, where the loading rates are extremely rapid and pressure so high that the rock strength is negligible by comparison, as explained in Section 2.4. These intense loading conditions also help to explain the relative constancy of rules for crater radius, damage radius, etc. in the various rock types around the world where underground explosions have been conducted.

Thus, it would seem that the likelihood of venting of underground tests on Mururoa and Fangataufa should be negligible, at least according to the US definition. Certainly, no mention has been made by CEA scientists of any such venting at the Pacific Test Centre.

The Atkinson Report 1984 addresses "venting" in Chapter 3.1, p. 120. The conclusion No. 9, p. 11 of the Atkinson Report 1984 states that "*venting of gaseous and volatile fission products from the test sites does occur at the time of detonation. There is evidence that the amount is greater than would be expected simply through the back-packing of the placement bore being less than perfect*".

In reading this statement, it is important, to recognise the difference in definition of the term "venting" in the Atkinson report 1984 and that followed in the US programme. The expressions "long term leakage" and "seeps" (US) are also used in association with the topic of venting.

According to the Atkinson report 1984 **venting** "*refers to the loss of radioactivity from the intended geological confinement at the time of detonation*", while **leakage** "*is restricted to the transport of radioactivity by water over any period of time after the vitrified material has cooled*".

As a consequence, venting is concerned with the inventory of fission and activation products arising from the detonation or daughter products formed within a very short period, whereas leakage is also concerned with radionuclides that may take a considerable time, e.g. 1000 years, to grow in from the decay chain that was originated by a product of the detonation.

The US definitions, as given in the US Congress (1989) report (p. 46), are as follows:

ventings "*are prompt, massive, uncontrollable releases of radioactive materials. They are characterized as active releases under pressure, such as when radioactive material is driven out of the ground by steam or gas*". "Baneberry" in 1970 is the last example of an explosion that vented.

seeps "*which are not visible, can only be detected by measuring for radiation. Seeps are characterized as uncontrolled slow releases of radioactive material with little or no energy*".

Chapter 3 of the Atkinson report 1984, relevant sections of which are included in Appendix VI of the present report, provides details of the basis for the claim that venting has occurred on Mururoa. In summary, "*the tritium concentration in the absorbed water vapour was 0.5 Bq/mL which corresponds to 4.8 Bq/m^3 in the sampled air. An acceptable derived air concentration (DAC) for members of the general public exposed continuously to tritiated water vapour is 2.7 kBq/m^3 (1/100 of the occupational DAC), a factor of 560 times higher than that measured. ..... Were it not for the weapon testing by France, the tritium levels in surface waters near Mururoa would be about 0.1 Bq/l, a factor of 5000 times lower than that measured in the absorbed water vapour*".

The sample was apparently taken in Area 2 of Mururoa, approximately 1 km west of the industrial area and between the lagoon and the road to Viviane (Atkinson 1984, p. 121) in late October 1983. Underground tests in Area 2 included 13 from 1976–1980 and 14 from 1981–1986. It seems difficult, therefore, to establish the time over which the tritium release occurred. Although the arrival at the surface of small quantities of tritium some time (months to several years) after an explosion may be considered as venting, it seems highly unlikely that ventings of the type envisaged in the US definition of the term have occurred on Mururoa or Fangataufa.

It can be concluded that long term leakages (or seeps) have definitely occurred, both on Mururoa and Fangataufa, and are reported in the French Liaison Office Documents Nos 9 and 10, 1996. Tritium release data from these documents is also used to assess the validity of the model of tritium release based on mixing in the carbonates (see Appendix II).

2.8. EFFECT OF RE-EMERGENCE ON THE STRUCTURAL STABILITY OF THE ATOLLS

As noted in Section 2.1.2, it is well established from geological evidence (Buigues 1996 and 1997) that periodic epochs of glaciation, occurring with a frequency between 20 000–100 000 years (Guille et al., 1996, p. 69) have resulted in an associated drop in sea level varying from several tens to more than 100 m. Under such drops, the atolls will re-emerge to a height corresponding to the drop in sea level and the exposed carbonate, previously saturated, will drain. The hydrostatic groundwater pressure in the portions that do not re-emerge will be reduced correspondingly.

The relative stability of a saturated rock mass is determined by the "effective stress" (σ_e) acting in the mass, defined as

$$\sigma_e = (\sigma_s - p)$$

where

σ_s is the total stress acting at a point in the rock mass, e.g. the gravitational stress due to the weight of overlying rock,
p is the pore water pressure in the rock mass.

Increase in the effective stress σ_e tends to reduce the potential for failure, both in shear and in tension. Thus, the mechanical stability of the atolls will be greater during periods of emergence than when submerged, as at present.

2.9. DISCUSSION AND CONCLUSIONS

(1) The processes involved in the development of the seamounts succeeded by a slow progressive subsidence and associated accretion of the carbonate caps, as modified by periodic global ice ages, have combined to produce rock masses at Mururoa and Fangataufa that, typical of atolls, are geomechanically, hydrologically and chemically heterogeneous.

(2) With respect to underground nuclear testing, this heterogeneity has several consequences that may be significant. Tests in one region of the atolls may produce a different response, e.g. cavity-chimney size and damage extent, than similar tests in another region. This is seen, for example in the activation of major, continuing slope deformations in the Northern rim Area 1 of Mururoa, even though all tests in this region were of low yield, while some regions of Area 4 on the southern rim have withstood much more powerful tests. The fact that the Tydée slide started some 2 km to the west, rather than on the rim directly in front of the Tydée explosion, suggests a strong influence of local heterogeneity. Leakage of radionuclides from the Lycos test in Fangataufa, even though the depth of "intact" volcanic cover above the cavity-chimney was ostensibly 140 m, is considered to be the result of an extensive thickness of weak rock above the test horizon that was "damaged" by drilling of the 1.5 m diameter installation hole, serving as a high permeability annulus around the concrete plug in the hole to the carbonates. (See Category 2 tests in Fig. 1 and Section 5.)

(3) Although geological heterogeneities have mechanical consequences in testing, they may be more important as hydrological "fast paths" along which water, containing radionuclides, can reach the biosphere.

(4) Ancillary field activities associated with the nuclear testing can introduce potential "fast paths" if not treated after completion of the activities. Such activities include exploration drillholes, post-test radiochemical sampling holes penetrating directly into the cavity, open 1.5 m diameter bored shafts not used for tests and left open over most of their depth and the concrete plug installed to fill each shaft above a nuclear device. CEA scientists acknowledge that about five unused holes remain below the lagoon at Mururoa, and that there are none at Fangataufa. In all cases, these potential pathways result primarily in hydrological consequences which will be discussed in Section 3.

(5) Although a nuclear explosion releases an enormous amount of energy, the essentially instantaneous or "shock" loading of the rock acts to eliminate the possibility of direct connection between the cavity and the rock mass via fracture pathways. Thus, virtually all of the molten lava which contains most of the less volatile radionuclides, e.g. plutonium, will remain within the cavity, where it will solidify. The minor amounts of radioactivity potentially released via the prompt or early time injection mechanism discussed in Section 2.1.4 do not change this conclusion significantly.

(6) Although underground tests at the Pacific Test Centre produce substantial settlements which are in excess of 2 m in some places, on the rim surface, these settlements do not extend directly to the underground cavity-chimney, as was the case for many tests at the NTS in the USA. A substantial thickness of underground volcanic rock usually separates the top of the cavity-chimney from the overlying carbonates.

(7) In a number of cases, i.e. the 12 CRTV tests, according to the French Liaison Office, the underground explosion has created a cavity-chimney that extends into the carbonates (Category 3 tests in Fig. I). It is probable that a substantial thickness of undamaged carbonates remain between the cavity-chimney and the surface or lagoon for most of the CRTV tests.

(8) Mechanical interactions between adjacent large cavities, will not produce inelastic deformation in the carbonates, even in Area 4, where large yield tests were carried out relatively close to each other. Hydrological interactions between adjacent cavities, together with the hydrological consequences of such features as lava tubes, boreholes, and drilled shafts, will be addressed in Section 3 and Appendix I.

3. HYDROLOGICAL MODELLING

3.1. NATURAL CONDITIONS PRIOR TO NUCLEAR TESTS

3.1.1. Natural flow of groundwater in an atoll

In very general terms, the hydrology of a natural atoll is well understood. Generally, two different flow systems are present:

(a) The first system is very superficial and consists of fresh to moderately saline water that infiltrates into the ground above sea level, due to recharge by rainfall, and flows laterally towards the ocean and the lagoon. This freshwater forms a "lens" on top of denser sea water in the sand and calcareous rim of the atoll. Its thickness can extend from a few metres to some tens of metres, mostly depending on the maximum width and ground elevation of the rim. If, for instance, the water table elevation under the rim, due to recharge, is 1 m, then, according to the Ghiben-Herzberg relation, the thickness of the freshwater lens would be in the order of 40 m. The coefficient of 40 between the elevation of the water table and the depth of the sea water interface is equal to $(\rho_s-\rho_f)/\rho_f$, where ρ_s and ρ_f represent the density of sea water and freshwater, respectively (e.g. Marsily 1986, p. 223). Because of tidal fluctuations, a gradual transition from freshwater to sea water is observed over a thickness of some 10 m (Oberdorfer et al., 1990). This freshwater lens is the unique source of freshwater for human consumption on an atoll.

(b) The second system is the deeper sea water that saturates the lower part of the calcareous cover of the atoll, underneath the freshwater lens, and the underlying volcanic rocks. Generally speaking, the permeability of the limestone is much higher than that of the volcanic, and most of the flow in this second system occurs in the limestone. Two mechanisms have been shown to generate groundwater flow in this sea water:

- the first one, known as bow pressure, is related to the general ocean current that surrounds the atoll. Because of a small pressure difference between the upstream and downstream end of the atoll (with respect to the ocean current), a small horizontal groundwater flow exists in the atoll, in the same direction as the ocean current.
- The second one is known as endo-upwelling and has a vertical component upwards. It is considered more significant than the previous one, especially in the case of interest here. This vertical flux is due to thermal buoyancy forces.

Because of the natural geothermal heat flux in the Earth's crust, the solid atoll conducts heat to the surface and is warmer than the surrounding ocean water, which typically is around 4°C at depths greater than 1 km. The water in the pores or fractures of the atoll is thus warmer than the surrounding sea water, and therefore lighter due to thermal expansion. A general circulation pattern is thus infiltration of sea water along the flanks of the atoll and flow of this water towards its centre and vertically upwards to the lagoon. This mechanism has been observed in several atolls and is thought to explain the generally high biological productivity of lagoons because the flux of deep sea water is rich in nutriments (Rougerie and Wauthy 1993; Samaden et al., 1985; Henry et al., 1996; Swartz 1958). Superposed on this upwelling flow are periodic tidal fluctuations, which can generate larger velocities than those produced by upwelling, especially if the tide inside the lagoon lags slightly behind the tide in the ocean. This oscillating velocity is, however, in general of zero average and responsible for causing mixing in the atolls, especially in the high permeability karstic layers of the carbonates.

The hydrological processes of interest in atoll hydrology include groundwater flow through porous and fractured rock, transport of heat and transport of solutes. Even though the volcanic and

carbonate rocks in atolls are generally fractured and exhibit variability at many scales, it is commonly accepted to represent the rock by an equivalent porous medium when considering groundwater flow at the atoll scale. It is thus necessary to adjust the permeability of this equivalent porous medium in such a way that it accounts, in a global sense, for the effect of fractures and heterogeneities, for the flux of water, heat and solutes. This conceptual model, used in all other hydrological studies of atolls, is adopted for all the analyses described in this report.

In mathematical terms, groundwater flow in a porous medium is described by Darcy's law (see box). The form of Darcy's law assumes that the porous medium is anisotropic and the permeability is a tensor, such that flow depends not only on the magnitude of the gradient in pressure or piezometric head, but also on its direction. If the medium is isotropic, the permeability is a scalar.

DARCY'S LAW, VELOCITY AND HYDRAULIC CONDUCTIVITY

Darcy's law may be written:

$$q = -\frac{\kappa}{\mu}(gradp + \rho g\ gradz)$$

where

q is the specific discharge (vector) or Darcy flux (m/s),
κ is the intrinsic permeability tensor (m^2),
μ is the dynamic viscosity of the fluid (Pa s or kg/m s),
p is the pore pressure (Pa), grad p is the pressure gradient,
ρ is the fluid density (kg/m^3),
g is the vector of acceleration due to gravity (m/s^2),
grad z is the unit vector oriented vertically upward.

The Darcy velocity, or specific discharge, is the volumetric rate of flow per unit area through which flow occurs (i.e. it is a hypothetical discharge rate assuming that water moves through the entire cross-sectional area in question). It has the same dimensions (LT^{-1}) as velocity, but it is not the speed at which the fluid moves.

To derive the average fluid velocity, it is necessary to divide the Darcy velocity by the effective porosity of the rock through which flow occurs. Thus, if the effective porosity of the rock is 10% of the total volume of the rock, the average fluid velocity in the pores is ten times the Darcy velocity. The flux, or fluid flowing across the cross-section over a given time, is the same for both calculations, that is, with or without porosity. For many calculations in hydrology, the total flux, or rate of fluid movement, is the most useful measure, i.e. Darcy velocities are appropriate.

The Hydraulic Conductivity (K) is the capacity of a porous medium to conduct water, and is defined by the expression

$$K = \frac{\kappa\ \rho\ g}{\mu}$$

where

K is the hydraulic conductivity, m/s,
κ is the intrinsic permeability of the porous medium (rock mass) (m^2).

The hydraulic conductivity of water is often referred to (incorrectly in the strict sense) as the "permeability". However, for constant values of ρ and μ in the equation above, K and κ are directly proportional to each other. In such cases, it is common to write Darcy's law for water using the hydraulic head:

$$q = -Kgradh$$

where

$h = p/\rho g + z$ is the hydraulic head (m)

To make predictions of groundwater flow and transport of heat or solutes, it is necessary to define the geometry of a flow system, the physical properties of the porous medium and the fluid itself, as well as boundary conditions, such as temperatures or fluctuating water levels, which drive the flow. Of these, the most difficult to determine are often the physical properties of the medium, in particular the equivalent or effective hydraulic conductivities.

3.1.2. Groundwater flow at Mururoa and Fangataufa

The general picture of flow in an atoll applies to Mururoa and Fangataufa. The superficial freshwater system is known to exist, e.g. in the "base vie" area of the rim, which is the widest section, but it is very shallow and contains brackish water. The CEA (Y. Caristan) has reported in a personal communication that the lens is only metres in thickness. Such a thin layer of freshwater under the rim of the atolls would have negligible effects on the movement of groundwater at depth within the atolls. It is presently unexploited (all water consumed in Mururoa was either imported or desalinised from sea water), but could represent a resource for a very small community or become significant if a drop in sea level, e.g. during a glaciation, made the rim wider and raised its elevation. The bow pressure flow has not been reported and would not be very significant, compared to the endo-upwelling flow, as the ocean current in this area is estimated at 0.1 m/s. However, the endo-upwelling flow is definitely present and has been shown by temperature measurements in vertical boreholes in the atoll (Fig. 21).

The hydrological system of Mururoa Atoll is described in detail in Guille et al., 1996. There are, however, no direct and compatible observations of heads and flows at Mururoa or Fangataufa that might allow the estimation of bulk scale effective hydraulic conductivities. The CEA has used a number of types of data to infer values or relative values of conductivity. These include observations of the thermal structure of the atolls, observations on flows within vertical drill holes, observations of loss of drilling fluids when oblique drill holes approached the cavity-chimney after each test, observations of the rate of refilling of the cavity-chimney after many tests and observations of tidal fluctuations of piezometric heads within the karst. An attempt was made to confirm the estimated hydraulic conductivity by geochemical measurements in the water of some boreholes. These data will be referred to below, when necessary. The CEA used the finite element code METIS (Goblet 1981) for all of its calculations. The results are presented in French Liaison Office Document No. 5, 1997,

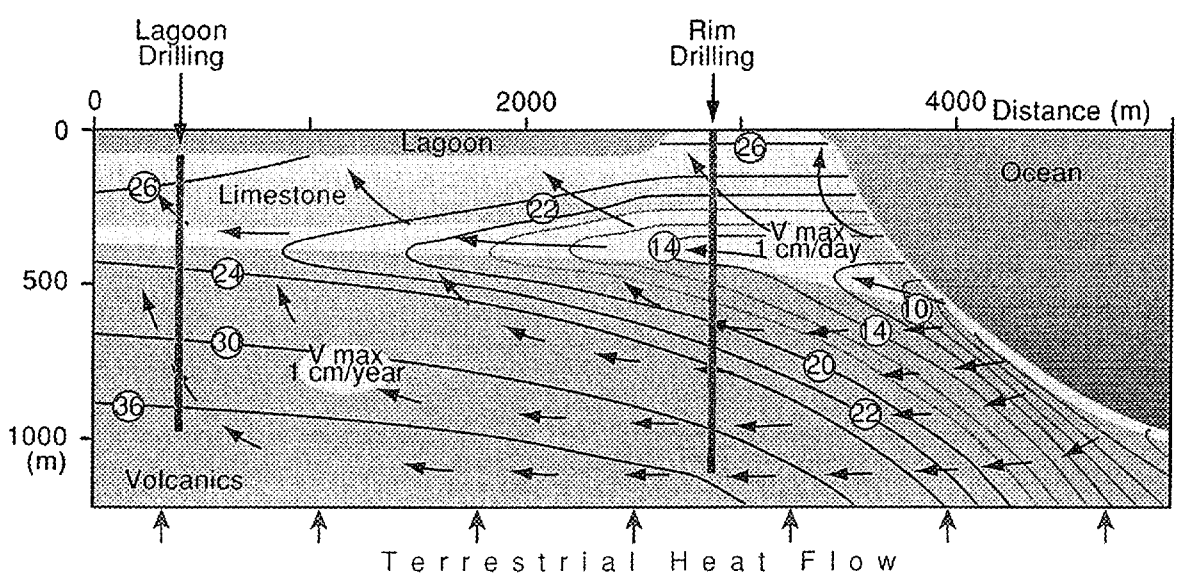

FIG. 21. Natural circulation of groundwater in the Mururoa atoll. (Adapted from Bouchez and Lecomte (1996).)

in Guille et al., 1996, Bouchez and Lecompte 1996, and Henry et al., 1996. The general conclusion from all of this work is that the volcanics and carbonates have effective (isotropic) hydraulic conductivities of about 10^{-7} m/s and 10^{-4} to 10^{-5} m/s, respectively. The values in the carbonates are consistent with those found on other atolls (Oberdorfer et al., 1990).

3.1.3. Modelling studies by the International Geomechanical Commission (IGC)

The pre-test temperature profiles used by the CEA to estimate the natural groundwater flow velocity due to endo-upwelling was also used by Perrochet and Tacher 1997, on behalf of the IGC, to estimate the rock hydraulic conductivity in natural conditions. Three temperature profiles are essentially the source of information: one in the ocean, one in a deep borehole under the rim and one in a deep borehole under the lagoon. These profiles have a particular shape and significant information can be deduced from them, as they clearly establish the existence of convective water currents in the atoll and make it possible to estimate orders of magnitude of velocities and rock permeabilities. A word of caution must be added, however: these temperature profiles, provided by the CEA (Fig. 22) are supposedly averages of several boreholes on Mururoa and not authentic raw measurements. A number of requests have been made for additional data, particularly on the thermal structure of the atolls. Confidence in the results would have been greater if these additional data had been provided as requested.

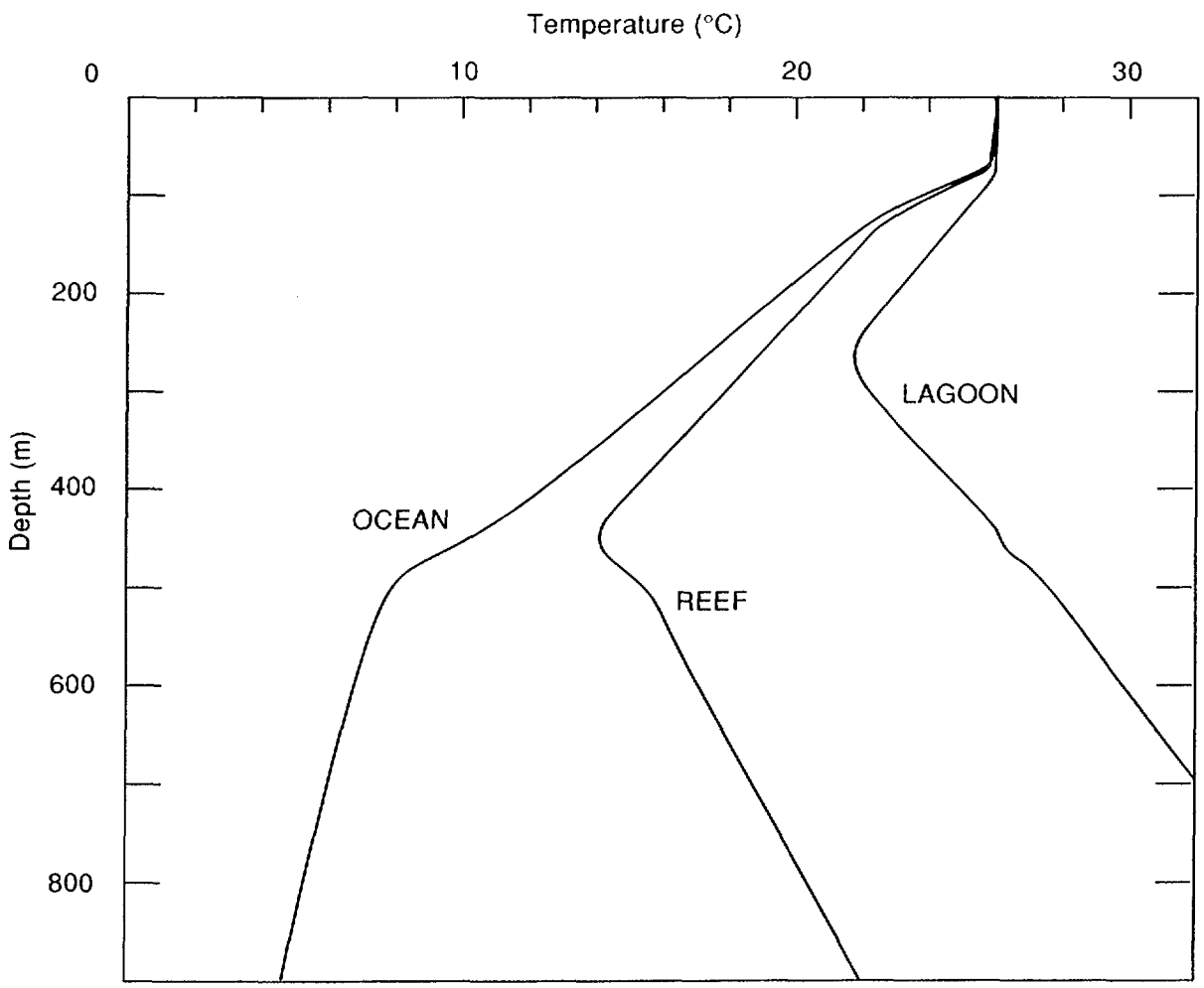

FIG. 22. Idealised temperature profiles beneath Mururoa. (Adapted from Guille et al. (1995).)

The modelling of the temperature profiles is described in detail in Fairhurst et al. (IGC) 1998, Chapter 6. To aid this modelling, the IGC used as much of the available qualitative or quantitative geological information as possible, including studies of other atolls or of relevant physical processes, and data specific for the two atolls:

- depth and nature of the volcanic rocks which are made of fine-grained basalt with a porosity of around 25% and have a permeability measured on intact cores of the order of 10^{-10} m/s or less. The basalt *in situ* contains fractures, often coated with clay from hydrothermal alteration.

- nature of the calcareous cover which is highly pervious with a permeability of up to 10^{-5} - 10^{-4} m/s and an average porosity of 20–40%. The cover is likely to contain a karstic layer at the base, as seen for instance on the Zoe core.

- estimated thermal properties of the rocks, which are known from the literature and confirm the numbers used by the CEA scientists.

The commercial code FEFLOW (Finite Element Subsurface Flow System), (Diersch 1996) was used to calculate water and heat flow in the Mururoa atoll. All calculations were performed at the Swiss Ecole Polytechnique Fédérale de Lausanne (Perrochet and Tacher 1997). The IGC first verified the calculations made by the CEA, using initially the same grid and the same assumptions, and obtained essentially similar results. The IGC then improved the model by using a much finer grid and a better definition of the variation of the water density with temperature, using a fourth order polynomial, rather than the classical linear approximation. A large number of tests were performed, in two-dimensional cross-sections, or in radial symmetry (based on the assumption of a circular atoll), or in three dimensions, as described in Table III below. Figure 23 is a comparison of the isotherms and flow paths between the CEA calculations and FEFLOW. Figure 24 is a comparison of the thermal profiles beneath the rim and the lagoon, as provided by the CEA, with cases 3–6 for the distribution of the permeability in the volcanics and the carbonates. Figures 25 to 28 are different examples of the isotherms and flow paths for the different cases 1–6 that were simulated as described in Table III.

For all simulations in the volcanics, the small effective hydraulic conductivities lead to small velocities and therefore negligible convection and dispersion. Thus the heat transport is dominated by conduction. In the carbonates the velocities are three orders of magnitude larger, and convection and dispersion dominate as the primary mechanism for transport of heat. The refined simulations do not perfectly agree with the CEA results. The latter show a minimum water temperature below the rim of about 14°C at the interface between the volcanics and the carbonates and a minimum of 22–23°C at the centre of the atoll. In contrast, the 22°C isotherm in FEFLOW simulations penetrates little further than the lagoon edge of the rim, and groundwater temperatures in the centre of the atoll are systematically higher than in CEA calculations.

In Fig. 25, case 1, the temperature inversion in the carbonates dies out about 1 km from the centre of the atoll. Near the centre of the atoll, the temperature at the base of the carbonates is higher than in the lagoon, allowing the development of local free convective cells. Rayleigh numbers, calculated *a posteriori* near the centre of the atoll, are about 100 in the carbonates, 2.5 times the critical value for such an instability. These cells are not seen in the simulations of Henry et al., 1996, because the distance from the shore to the centre of the atoll is less in that case. They are not seen in Fig. 25, case 2, because radially inwards (centripetal) velocities are greater near the centre of the atoll in the radial case and these larger velocities prevent the instabilities from occurring. The same is true in Fig. 25, case 3, where even in a non-radially symmetric case, velocities are higher because of the zone with larger hydraulic conductivity. The convective cells are possibly not seen in the CEA calculations because the resolution of the grid used by the CEA was too coarse for the cells to occur. There is no indication that such convective cells occur at Mururoa or Fangataufa, but it is nevertheless interesting that, using parameters identical to those used by the CEA, the FEFLOW

TABLE III. NUMERICAL VALUES OF PARAMETERS USED IN FEFLOW FOR FITTING TO THE THERMAL PROFILES

Parameters	Carbonates	Volcanics
Base case 1,vertical 2-D cross-section		
Horizontal hydraulic conductivity (m/s)	10^{-4}	10^{-7}
Vertical hydraulic conductivity (m/s)	10^{-4}	10^{-7}
Porosity	40%	10%
Specific storage coefficient (m^{-1})	10^{-5}–10^{-4}	10^{-5}–10^{-4}
Medium thermal conductivity (W/mK)	2	2.5
Water thermal conductivity (W/mK)	0.65	0.65
Medium volumetric heat capacity (10^6 J/m^3K)	2.2	2.2
Water volumetric heat capacity (10^6 J/m^3K)	4.2	4.2
Medium thermal longitudinal dispersivity (m)	10	10
Medium thermal transversal dispersivity (m)	1	1
Water salinity (g/l)	34	34
Water density and viscosity	High order function of temperature	High order function of temperature
Case 2, axy-symmetric version of case 1		
Case 3, vertical 2-D cross-section		
Upper carbonates, isotropic hydraulic conductivity	10^{-5}	
Porosity of upper carbonates	30%	
Lower carbonates, isotropic hydraulic conductivity	10^{-4}	
Thickness	between 75–315 m	
Porosity of lower carbonates	40%	
Case 4, vertical 2-D cross-section		
Isotropic hydraulic conductivity in carbonates	5×10^{-4}	
Case 5, vertical 2-D cross-section		
Hydraulic conductivity in carbonates - horizontal	10^{-3}	
Hydraulic conductivity in carbonates - vertical	10^{-4}	
Case 6, vertical cross-section		
Bottom karstic layer in carbonates, 10 m thick, hydr. conduct.	10^{-2}	
Remaining isotropic carbonate layer, hydr. conductivity	10^{-5}	
Case 7, three-dimensional calculations		
Upper carbonates isotropic hydraulic conductivity	10^{-5}	
Upper carbonates porosity	40%	
Lower carbonates anisotropic horizontal conductivity, 100 m thick	10^{-3}	
Lower carbonates anistropic vertical conductivity, 100 m thick	10^{-4}	
Lower carbonates porosity	40%	

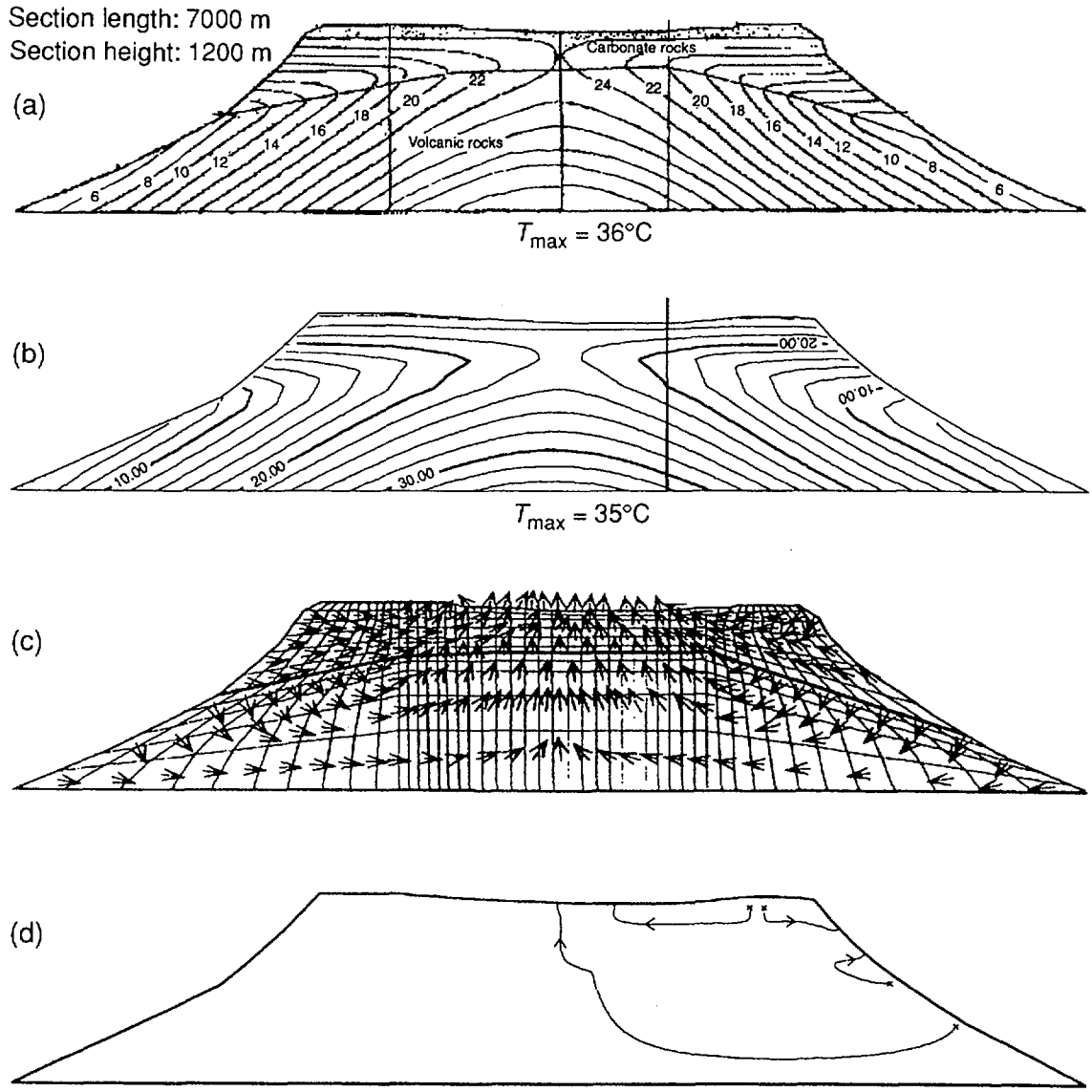

FIG.23. Comparison of isotherms and flow paths simulated by METIS (Henry et al. 1996) and FEFLOW (Perrochet and Tacher 1997): (a) original isotherms after Henry et al.; (b) isotherms given by FEFLOW using original parameters from Henry et al.; (c) original velocity vectors after Henry et al.; (d) typical flow paths given by FEFLOW using original parameters from Henry et al.

simulation with a fine mesh in a non-radially-symmetric cross-section shows a behaviour quite different from that observed or predicted by the CEA.

Figure 26 shows corresponding flow paths for the three simulations shown in Fig. 25. The flow patterns are rather similar and horizontal and vertical velocities are very similar to those computed by the CEA. Horizontal Darcy velocities are of the order of 6 or 7 mm/a in the volcanics, and of the order of 1 m/a in the carbonates. Vertically upward velocities in the carbonates are of the order of 0.5 to 2 m/a in those parts of the atoll where significant upward flow occurs. Figures 27 and 28 present the same results for cases 4–6.

3.1.4. General assessment of CEA results

In general, modelling performed by the CEA using METIS is consistent with the available data and has been verified by comparison with independent calculations using FEFLOW. Modelling by

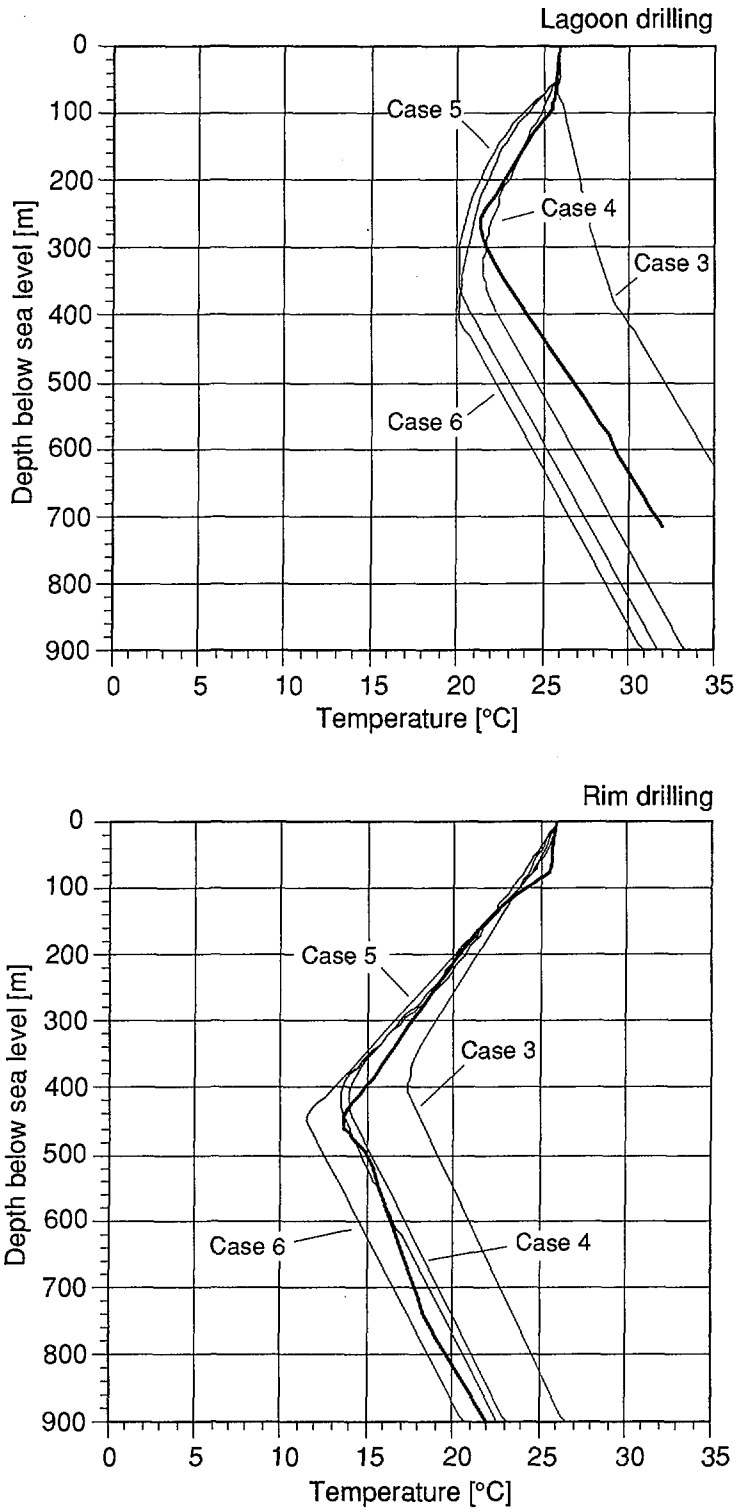

FIG. 24. Comparison of temperature profiles from drill hole measurements with simulations for cases 3–6 (observed profiles are shown in bold) (Perrochet and Tacher 1997).

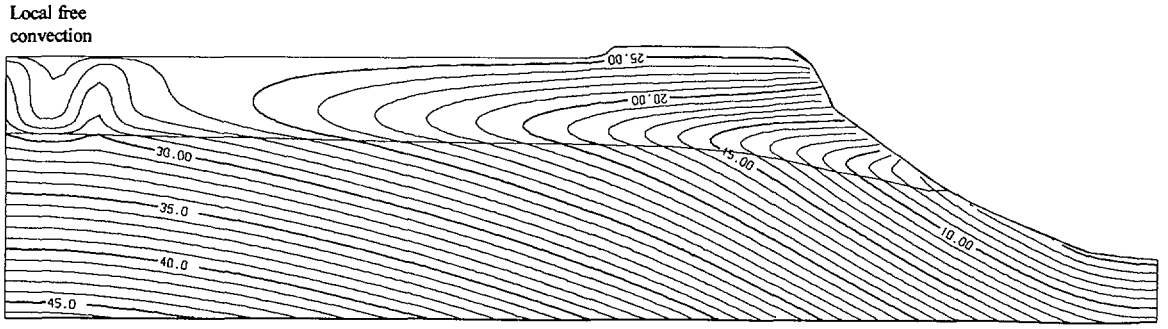

Case 1 : Reference data set with homogeneous carbonates ($K_0 = 10^{-4}$ m/s, $\phi = 0.4$).

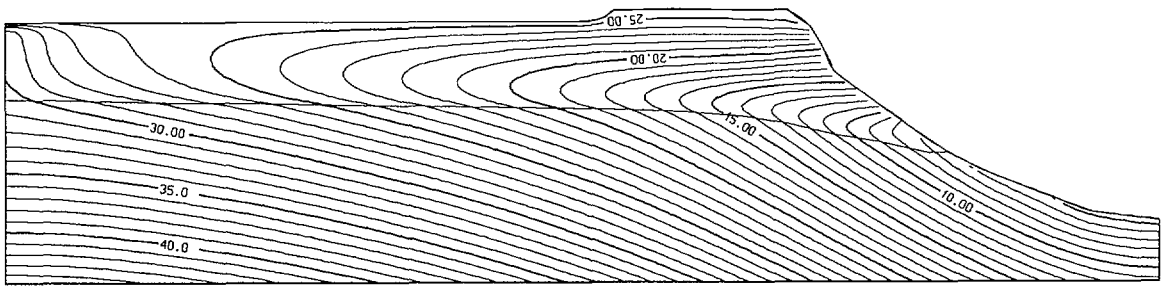

Case 2 : Axi-symmetric version of Case 1.

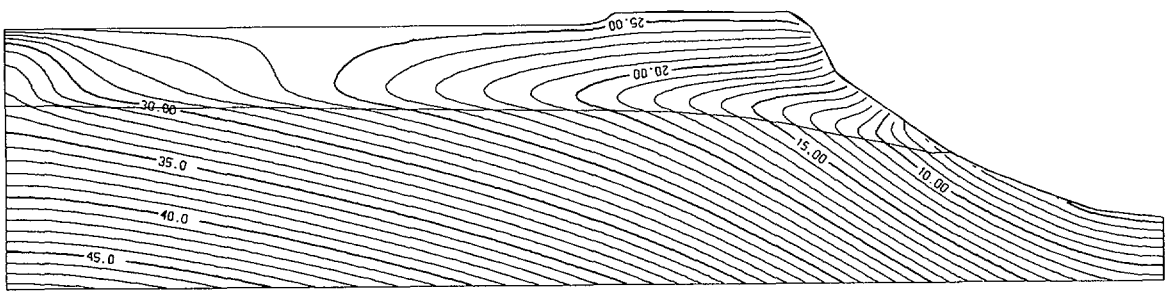

Case 3 : Reference data set with upper ($K_0 = 10^{-5}$ m/s, $\phi = 0.3$) and lower carbonates ($K_0 = 10^{-4}$ m/s, $\phi = 0.4$).

FIG. 25. Simulated isotherms for cases 1–3 to study the effect of changes in model parameters in the carbonate formations (Perrochet and Tacher 1997).

the CEA used coarse grids and adopted the Boussinesq assumption, whereas FEFLOW now allows calculations with much higher resolution, and is based on non-linear constitutive relations which express the dependence of fluid density and viscosity on temperature. In principle, FEFLOW is capable of producing more accurate results, in the sense of being more consistent with the true solution for any given combination of geometry, material properties and boundary conditions. Nevertheless, from many points of view, the results obtained and published by the CEA are good results, that support the phenomenon of endo-upwelling and suggest that long term average groundwater flow directions are generally inwards, from the ocean towards the lagoon.

3.1.5. Sensitivity analyses of two-dimensional thermal models

The atolls of Mururoa and Fangataufa are, of course, three-dimensional and neither a two-dimensional plane section nor a radially symmetric section is a good approximation of any section through either of the atolls. It could be argued that parts of Mururoa, particularly towards the western end, behave more like a plane section, whereas the eastern end of Mururoa and possibly all of Fangataufa behave more like a radially symmetric section. However, given the computational effort

required to make any of the groundwater simulations and due to the lack of a full three-dimensional description of the atolls, sensitivity analyses were made with the idealised two-dimensional and radially symmetric sections. These sensitivity studies (Fairhurst et al. (IGC) 1998) demonstrate that:

- decreasing the hydraulic conductivity in the volcanics by one order of magnitude to 10^{-8} m/s does not significantly affect the spatial distribution of temperatures, from which it is inferred that for any hydraulic conductivity of less than about 10^{-7} m/s, heat transfer within the volcanics is dominated by conduction;
- increasing the hydraulic conductivity in the volcanics by one order of magnitude to 10^{-6} m/s decreases the temperature at the interface between volcanics and carbonates at any particular distance from the centre of the atoll. More importantly, however, temperature profiles in both the volcanics and the carbonates are curved and not like the observations shown in Fig. 22;
- increasing the hydraulic conductivity in the carbonates by one order of magnitude to 10^{-3} m/s significantly increases the extent to which ocean water is drawn into the atoll, resulting in a temperature inversion at all distances from the centre of the atoll and not only near the rim;

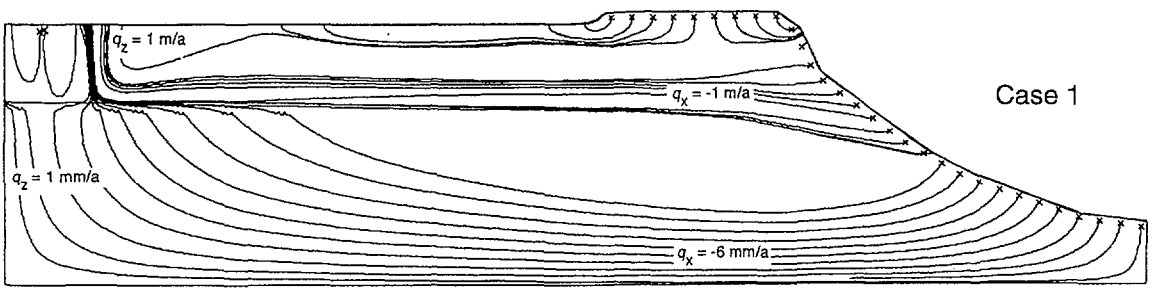

Case 1 : Reference data set with homogeneous carbonates ($K_0 = 10^{-4}$ m/s, $\phi = 0.4$).

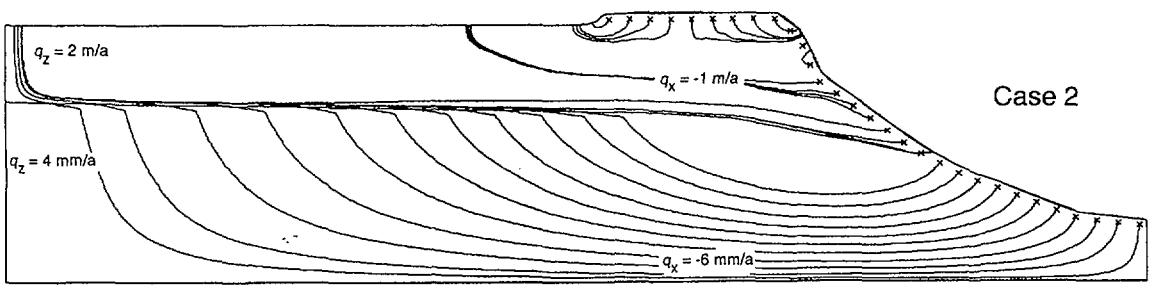

Case 2 : Axi-symmetric version of Case 1.

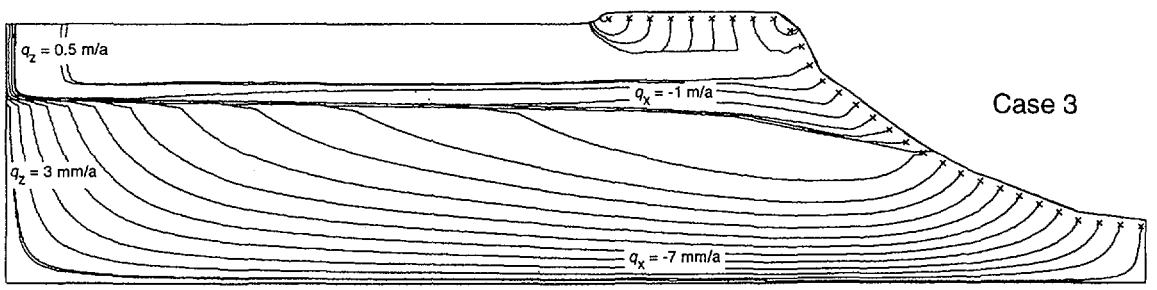

Case 3 : Reference data set with upper ($K_0 = 10^{-5}$ m/s, $\phi = 0.3$) and lower carbonates ($K_0 = 10^{-4}$ m/s, $\phi = 0.4$).

FIG. 26. Simulated flow paths and typical Darcy velocities for cases 1–3 shown in Fig. 25 (Perrochet and Tacher 1997). Crosses denote starting points for flow paths.

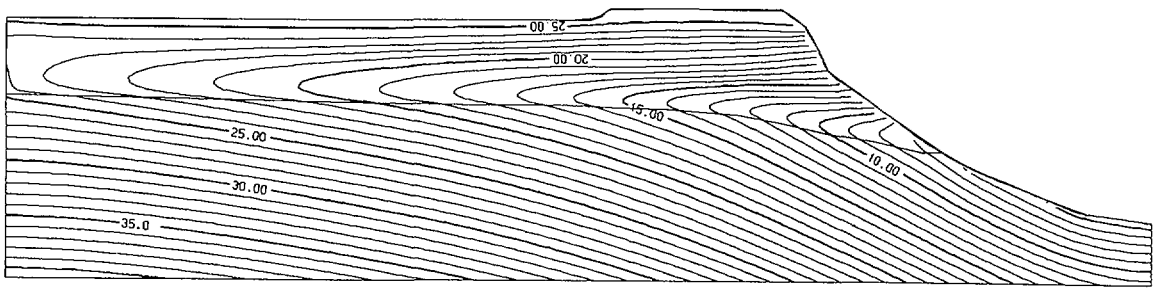

Case 4 : Reference data set with homogeneous carbonates and K_{carb} increased by a factor 5 to $5 \cdot 10^{-4}$ m/s.

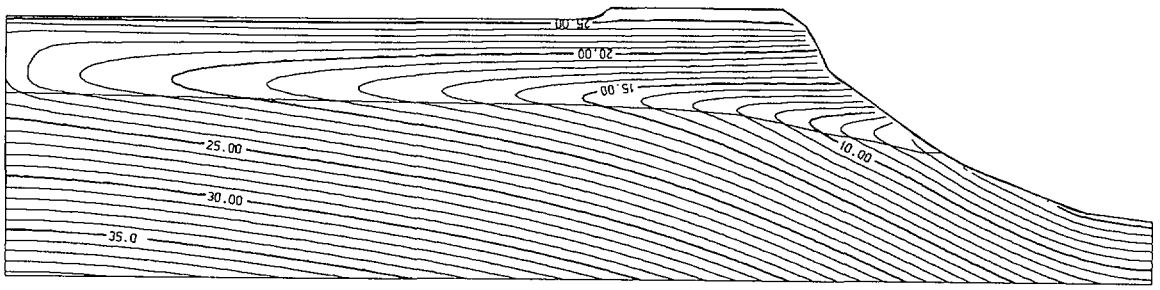

Case 5 : Reference data set with anisotropic carbonates $K_H / K_V = 10^{-3} / 10^{-4}$.

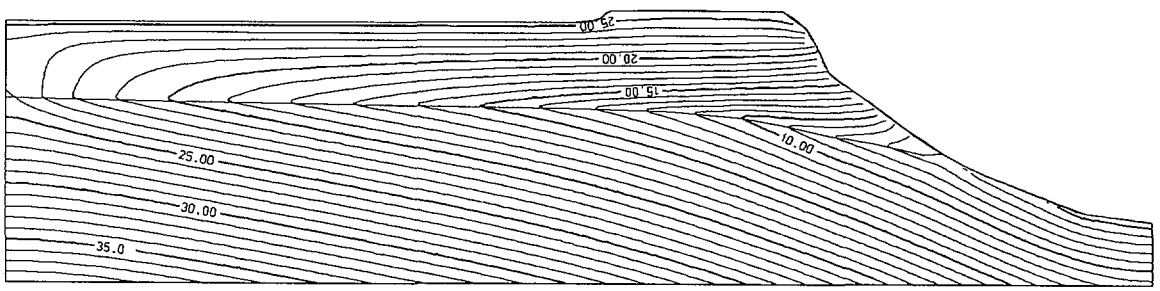

Case 6 : Reference data set with a karstic layer and K_{carb} decreased by a factor 10 to 10^{-5} m/s.

FIG. 27. Simulated isotherms for cases 4–6 to study the effect of changes in model parameters in the carbonate formations (Perrochet and Tacher 1997).

- introducing into the carbonates a thin layer of extremely high conductivity, 10^{-2} m/s, to represent a karst near the interface between the volcanics and the carbonates has a similar effect and ensures that the minimum temperature in any temperature profile occurs in that layer;
- increasing the depth of the domain of simulation from 1200 m to 2000 m has negligible effects on the spatial distribution of temperatures;
- decreasing the geothermal heat flux from 4500 to 3000 J/d m^2 decreases temperatures deep in the volcanics, and changes the slope of the geothermal profile within the volcanics to a value that is too small compared to observations, but does not have a significant impact on temperatures within the carbonates, which are more influenced by ocean temperatures along the flank of the atoll.

3.1.6. Alternative assumptions that match observed thermal profiles

Four simulations with different combinations of aquifer properties were made in an attempt to "calibrate" the model, i.e. by selecting the parameters in such a way that the results are closest to the observations. The temperature logs are shown in Fig. 24 and the corresponding thermal profiles in Figs 25–28. It could be argued that all four of these simulations fit the observations. They agree well

under the rim, but do not agree so well under the lagoon because the elevation of the position of the interface between the volcanics and the carbonates is poorly known since the exact location of the temperature logs is unknown. The assumed position in the model is uncertain. Thus the elevation of the minimum temperature in Fig. 24(a) is conceptually not as important as the slope of the thermal gradient in the carbonates. The different simulations clearly indicate significantly different velocities in different parts of the model domain. Nevertheless, all of these simulations are generally consistent with existing data and must be accepted as possible alternatives to other scenarios, at least in the absence of further information.

3.1.7. Three-dimensional simulations

Toward the end of the Study, the CEA provided ocean bathymetric data and a digital representation of the base of the carbonates at Mururoa, with approximately 100 m spacing, and a map of the temperature at the base of the carbonates, interpolated from an unknown number of measurements. These data allowed simulation of geothermal convection in three dimensions.

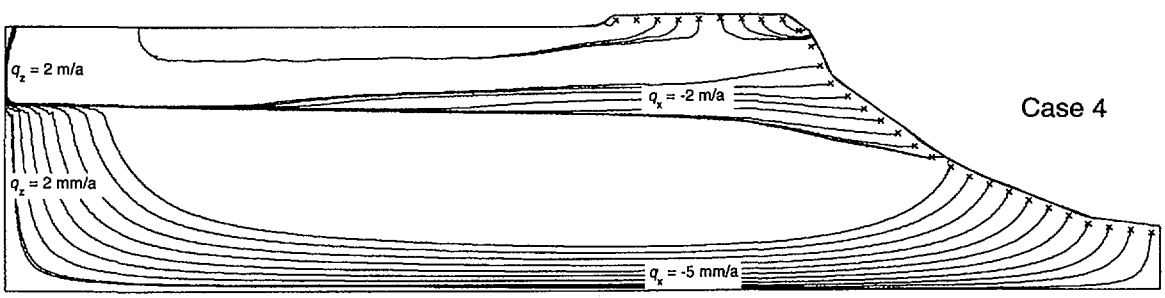

Case 4 : Reference data set with homogeneous carbonates and K_{carb} increased by a factor 5 to $5 \cdot 10^{-4}$ m/s.

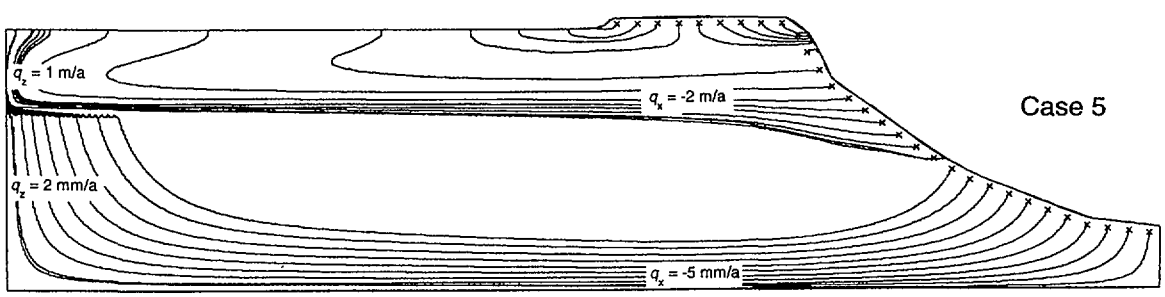

Case 5 : Reference data set with anisotropic carbonates K_H / K_V = 10^{-3} / 10^{-4}.

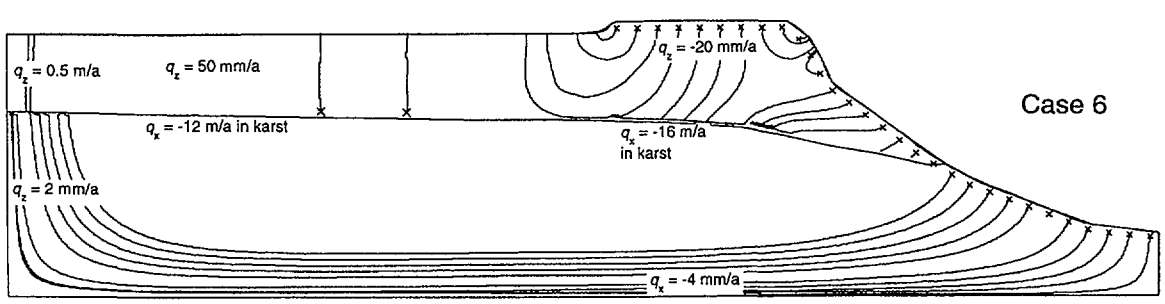

Case 6 : Reference data set with a karstic layer and K_{carb} decreased by a factor 10 to 10^{-5} m/s.

FIG. 28. Simulated flow paths and typical Darcy velocities for cases 4–6 shown in Fig. 27 (Perrochet and Tacher 1997). Crosses denote starting points for flow paths.

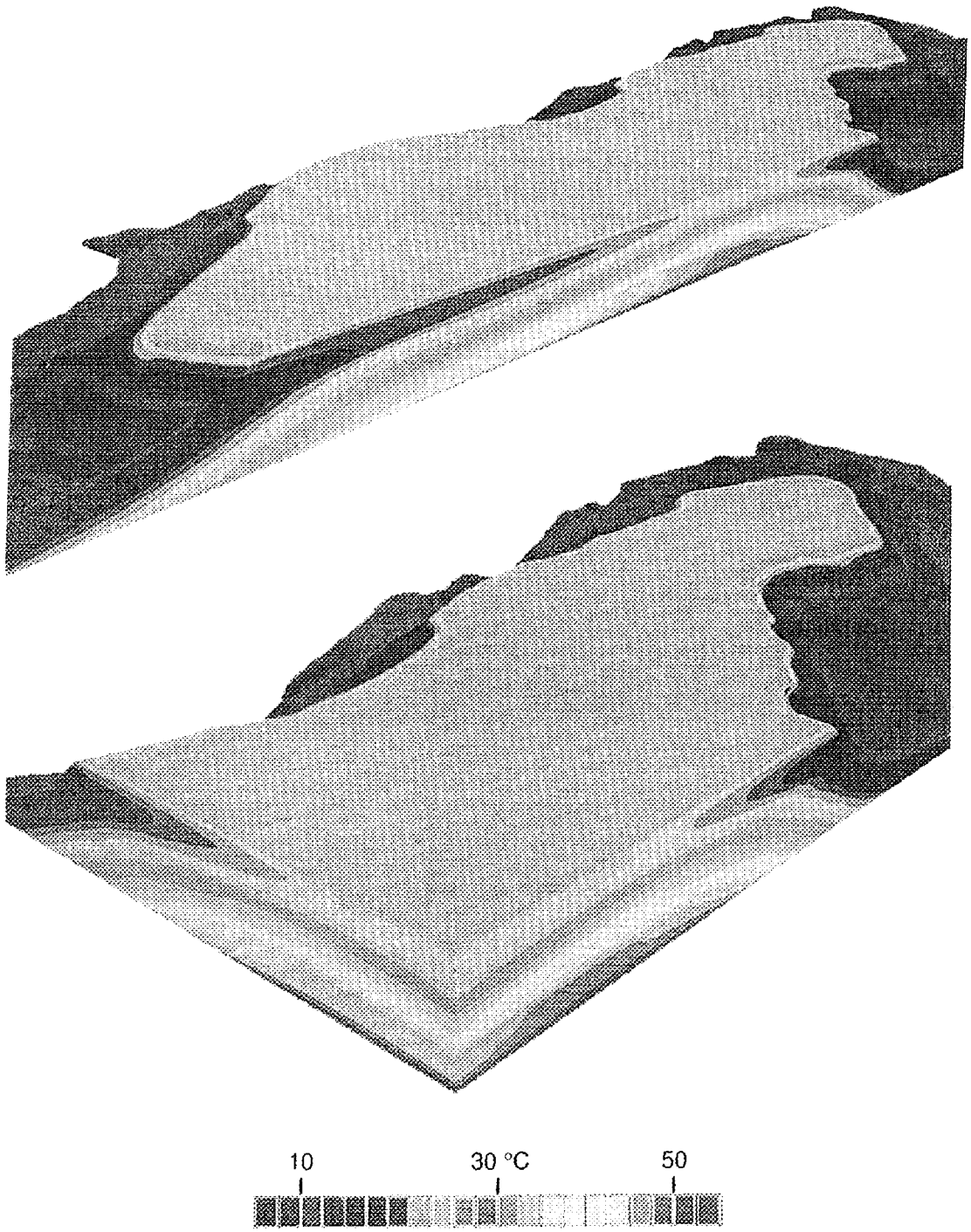

FIG. 29. Northeast–southwest section through 3-D model of Mururoa atoll showing simulated underground isotherms viewed from the northwest (vertical and horizontal scales are the same).

A three-dimensional model was constructed using FEFLOW to a depth of 1700 m below sea level (case 7). The three-dimensional finite element grid has a resolution of the same quality as that used by Henry et al., 1996. Figure 29 shows three-dimensional images of the Mururoa atoll illustrating the thermal structure inside the atoll. The temperature inversion in the carbonates is clearly evident as is the fact that the penetration of cooler water into the atoll depends on the three-dimensional geometry of the atoll. The simulation shown is qualitatively in agreement with the temperature data shown in Fig. 30.

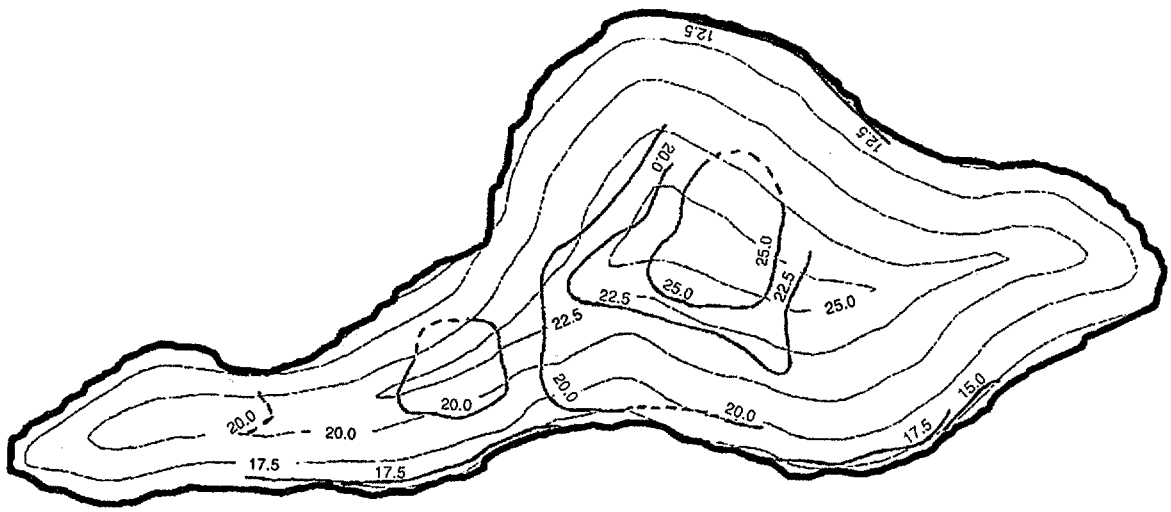

FIG. 30. Simulated and measured isotherms (shown in red) at the interface between the volcanic and carbonate formations.

3.1.8. Magnitude and effects of tidal fluctuations

As discussed in Section 3.1.1, several authors have found evidence that salinity distributions within atolls are significantly influenced by tidal oscillations within atolls. There is also a theoretical explanation for this phenomenon, at least conceptually, in that an oscillatory motion can be shown to cause mixing, at least in the presence of some kind of trapping or exchange mechanism. Oberdorfer et al., 1990, showed that in order to simulate the observed mixing of salt with a steady flow and transport model, it would be necessary to use large dispersivities, that in other circumstances would be considered unreasonably large. The same would be expected to apply to transport of heat, because the transfer of heat by conduction to the solid matrix provides an exchange mechanism, which could lead to increased effective spreading in a similar manner.

The use of dispersivities to represent physical dispersion is problematic, because appropriate values of dispersivities depend on the scale of the problem, on the precise nature of the quantity being transported and on the way that quantity interacts with the surrounding medium. All the steady-state results presented above use dispersivities α_L and α_T in the classical way because, without new research, there is no theoretical basis for representing dispersion in any other way. At the same time, it is possible to provide some insight into how dispersion could or should be represented. Perrochet and Tacher (personal communication) have used FEFLOW to simulate flow, decoupled from geothermal transport, using small time steps to compute tidal fluctuations within the atoll. An alternative approach is to use a finite element which represents tidal fluctuations in terms of sinusoids and computes the spatial distribution of amplitudes and phase lags directly, without time stepping (Townley 1993).

Tidal fluctuations and the associated velocities are not trivial, and a significant volume of water can flow into and out of an atoll during each tidal cycle. Consider a vertical cross-section perpendicular to the rim of 5000 m in length and 1200 m in depth with a specific storage coefficient of 10^{-5}/m. If the range in heads at all points in the aquifer during each tidal cycle (twice the amplitude) were 0.8 m, then the total volume of water flowing into and out of a 1 m slice (vertical to the water flow direction) of aquifer in each tidal cycle would be 48 m^3. If such a volume were to enter the carbonates in thin karstic layers, the corresponding velocities would be much greater than steady velocities due to geothermal convection.

3.1.9. Summary and discussion of pre-test hydrology

Mururoa and Fangataufa are typical examples of many of the atolls with a volcanic core (comprising submarine and subaerial basalts) overlain by carbonates (limestone and dolomite) derived from corals. The volcanic rocks, although fractured to some extent, have a very low effective hydraulic conductivity. The carbonates are highly variable, with regions of very low conductivity and layers of highly conductive karst. Groundwater flows naturally from the flanks of the atolls inwards and upwards towards the lagoon. Rates of water movement are much lower in the volcanics, typically three orders of magnitude lower than in the carbonates. Tidal fluctuations are believed to cause enhanced mixing of salt and heat, although appropriate theoretical models for this phenomenon are not available. The implication of tidal mixing is that dispersion coefficients at any point in space would probably depend on the amplitude of tidal velocities rather than on the steady velocity at that point.

The FEFLOW simulations of natural hydrogeothermal convection are generally in agreement with earlier simulations by the CEA and show that the observed geothermal profiles can be matched with a number of possible combinations of hydraulic conductivities in the volcanic and carbonates zones.

The major conclusions that can be drawn with confidence from this modelling work and which are not very different from those presented by the CEA are as follows:

(1) The large-scale natural permeability of the volcanic rock mass is in the order of 10^{-7} m/s. This very important piece of information is well established. In fact, this value is an upper limit and lower values could also be used. The reason is that with a higher volcanic permeability the lower part of the temperature profiles would no longer be linear which is the case when heat transfer occurs mostly by conduction, but would show an upward convexity due to heat transfer by convection. The permeability of the volcanic rock, as measured on cores, is about 1000 times lower than the rock mass, indicating that flow in the volcanics occurs mainly in a set of fractures with an unknown density and aperture distribution. For example, assuming smooth fractures with parallel walls, a permeability of 10^{-7} m/s could result, e.g. from one vertical fracture with an aperture of 0.1 mm every ten metres or one fracture with an aperture of 0.02 mm every metre.

(2) Different arrangements of permeabilities in the carbonates can explain the observed temperature profiles. The one considered to be the most likely by the IGC is a lower, highly permeable karstic layer above the volcanics, with a transmissivity of 0.1 m^2/s, e.g. a 10 m layer with a 10^{-2} m/s permeability, covered by a thick series of carbonates with an average isotropic permeabilty of 10^{-5} m/s. Alternatively, the carbonates could be made of one single equivalent isotropic layer of 5×10^{-4} m/s or of a single anisotropic layer with horizontal/vertical permeabilities of $10^{-3} / 10^{-4}$ m/s. These permeability data produce the following estimates of the natural Darcy fluxes at the centre of the atoll:

- in the volcanics: 2 mm/a in the vertical, 5 mm/a in the horizontal direction; and
- in the carbonates: 0.5 to 2 m/a in both the vertical and horizontal direction.

(3) The Darcy fluxes can be transformed into pore water velocities, if the rock porosity is known. For the carbonates, a reasonable estimate is 20–40%, say 30%. For the volcanics, an average value of 25% is given to the matrix porosity, i.e. the small-scale pores in the basalt. However, if the flow takes place in the fracture network without any exchange with the matrix porosity on the fracture walls, then a fracture porosity as low as 10^{-4}, e.g. an open fracture with a

0.1 mm aperture every metre, could be used. Using these numbers for Darcy fluxes, we obtain the following pore water velocities:

- in the volcanics, with matrix porosity: 10 and 20 mm/a, vertically and horizontally;
- in the volcanics, with fracture porosity: 20 to 50 m/a, vertically and horizontally; and
- in the carbonates, 2 to 7 m/a, both vertically and horizontally.

The whole focus of this section has been on the Mururoa Atoll, or idealised cross-sections intended to represent sections through Mururoa. Although no specific calculations were carried out for Fangataufa, it seems reasonable to expect that the behaviour at Fangataufa will be fundamentally similar.

3.2. HYDROLOGICAL IMPACTS OF UNDERGROUND NUCLEAR TESTS

3.2.1. Impacts of underground nuclear explosions

The effects of underground nuclear explosions are both local, i.e. in the vicinity of each test, and at the atoll scale. The complex rock-mechanical effects of cavity expansion during a nuclear explosion are described in Vol. 3 of this Technical Report. In this section, we focus on the effects resulting from nuclear explosions on hydrological processes, i.e. the movement of water and heat. Our primary interest is in the net effect of the explosion, in terms of creating a cavity and possibly a zone or zones of enhanced permeability, but we are also interested in the possibility of movement of fluids and radionuclides over significant distances in very short time periods. Scaling relationships for the radius R_c of a spherical cavity and the height of a cavity-chimney produced by an underground test are discussed in Vol. 3 of this Technical Report. Of particular interest is the fact that the volume of the combined cavity and chimney is, approximately, directly proportional to the energy or yield of the explosion, (i.e. to R_c^3).

Figure 7.3 in Vol. 3 of this Technical Report shows a general view of the regions of deformation produced by the shock wave from an underground explosion in the volcanics at Mururoa and Fangataufa, as deduced from numerical modelling studies. Although the shock wave itself does not produce fractures in the immediate vicinity of the cavity, subsequent chimney collapse and the associated communication with fractured rock farther away from the cavity-chimney tend to result in an effectively increased permeability of the rock mass around the cavity-chimney.

Under natural conditions before a test, the rock throughout the atoll is saturated with water of approximately sea water salinity. Because of the natural thermal gradient and the natural geothermal circulation, the groundwater pore pressures are slightly higher than the hydrostatic values, thus driving the upward flow from the flanks of the atoll towards the lagoon. The nuclear explosion produces a cavity within which all water is vaporised. At the same time, the process of cavity expansion causes pressures in the pore fluids of the surrounding rock to rise above their ambient levels. The extent to which this occurs has not been estimated and no direct data were obtained in the course of French nuclear testing.

Concern has often been expressed about a phenomenon known as venting, i.e. the transport of gases from the cavity-chimney to the biosphere via fractures or other pathways created by an underground nuclear explosion. The CEA has maintained that venting did not occur at Mururoa and Fangataufa atolls, because there was always sufficient geological cover to ensure that the cavity-chimney did not rise to the land surface or floor of the lagoon. Based on our predictions of R_c and H_c as a function of P, it is likely that these claims are correct (see also Section 2.7.2).

Television coverage of nuclear explosions under the Mururoa lagoon showed bubbling of the ocean surface, and water spouts are known to have occurred to heights of tens of metres above the lagoon water surface. These phenomena are caused by seismic shock waves and, as they reach the floor of the lagoon, the transfer of energy to the water column above. Irregularities of the topography of the lagoon floor result in "focussing" of the energy in the water to produce localised spouting. There is no evidence that these phenomena involve any movements of water, even in small amounts, from deep within the atoll to the lagoon. In reality, energy is propagated from the cavity to the floor of the lagoon as seismic energy which causes the physical disturbances observed in the lagoon. In the same way, there is no possible mechanism for heat to be transported from the cavity to the lagoon, thus references to the "boiling" lagoon in television coverages are probably translations from the French word "bouillonnant", which can be used to describe the bubbling surface of a water body, without any implication of temperature.

3.2.2. Explosion-induced processes inside the cavity-chimney

When the roof of a spherical cavity starts to collapse, the cavity is filled with hot gases at high pressure, and the walls of the cavity are lined with molten or rapidly crystallising rock. The roof of the cavity collapses often during a period of hours. Collapse continues until the rubble touches and supports the roof of the cavity-chimney or until a volcanic layer is reached that is able to span the cavity-chimney region without collapse. Thermal energy contained within the initial spherical cavity becomes distributed throughout the rubble because, even though heat is transferred outwards through the walls of the cavity-chimney, the temperatures within small pieces of rock inside the cavity-chimney rapidly equilibrate with the temperatures of the surrounding gases. As a first approximation, all the thermal energy inside the spherical cavity at the time when chimney formation starts becomes distributed throughout the volume of the combined cavity and chimney, including the volume of the rubble.

The temperature reached inside the cavity-chimney depends on how much of the energy released in an explosion remains initially as thermal energy inside the cavity. There is no precise way of determining the distribution of energy, but it is known that in general 20–60% of the energy remains inside the cavity. Less than 1–5% of the energy escapes the region of plastic deformation to become elastic or seismic energy which propagates far from the explosion. The remainder of the energy is consumed by deformation processes that cause the rock to flow and fractures to be formed. The energy used in deformation processes is ultimately converted to thermal energy, i.e. high pressures in the growing cavity cause the rock to deform, and in doing so, cause them to gain in temperature. We can therefore argue that even though 20–60% of the energy remains inside the cavity, more than 95–99% of the energy remains inside the damaged zone, extending to a radius of perhaps 8–10 R_c. The transfer of energy to radii outside R_c is very rapid, but it seems reasonable to ignore this initial distribution of heat outside R_c for hydrological calculations, because heat would be conducted from the cavity-chimney to the same radii relatively rapidly, thus achieving almost the same result. The temperature is also dependent, to some extent, on the initial porosity of the rock, but the net result is that the increase in temperature due to a nuclear explosion in basalt is between 25 and 50°C, whatever yield of test, as the volume of the cavity and its chimney scales with the yield. For instance, if an explosion were to occur at a location with an ambient temperature of 30°C, the temperature in the cavity-chimney a short time after the explosion would be 55–80°C. This temperature would be reached even before the cavity-chimney had refilled with water. The temperature is well below boiling point, especially at the depths of the explosion, where the high ambient pressures cause the boiling point of water to be much higher than 100°C.

During a period of days to weeks after each nuclear test, the cavity-chimney refills with water. A small portion of the water comes from condensation of gaseous water in the cavity-chimney, but most of it flows into the cavity-chimney from the surrounding rock. As the gases in the cavity-chimney cool down, the pressure inside the cavity-chimney drops to less than ambient pressure and groundwater from the surrounding region is effectively sucked back into the cavity-chimney.

Once the cavity-chimney is filled with water, the temperature of the water inside the cavity-chimney is almost constant everywhere within the volume of the cavity-chimney, because of natural convection. A cavity-chimney created by a nuclear explosion contains rubble and has an overall porosity of about 30% but the volume of the cavity-chimney is more like rockfill in a dam wall or ocean breakwater than a porous medium. Convection will occur as it would in a free body of water rather than in a porous medium. As a result, even small temperature differences of the order of 1°C are probably sufficient to cause rapid overturning and mixing, which act to equalise temperatures within the cavity-chimney.

3.2.3. Cavity-chimney filling — interpretation of observations

After the majority of the tests, the CEA used directional drilling techniques to bore a drill hole, which started vertically near the surface and deviated obliquely to intersect the cavity-chimney and ultimately the lava at the bottom of the cavity.

Cores of solidified lava were taken for later radiochemical analysis in order to determine the yield of the explosion. During construction of the first drill holes of this type, water entered the cavity-chimney via the drill hole and in a couple of cases, gases are believed to have escaped. When techniques were used to prevent blow-out of gases, it was possible to obtain usually qualitative, but sometimes quantitative information about the rate at which gas pressure increased within the cavity-chimney due to the refilling of the cavity-chimney. Data of this kind made it possible to estimate the aquifer properties of the rock near the cavity-chimney similar to a large-scale pumping test.

The data obtained were not always precise. For large tests, they were generally limited to an observation of whether or not refilling was complete by the time of completion of the inclined drill hole. For small tests, pressure was sometimes measured in a gas sampling line installed into the

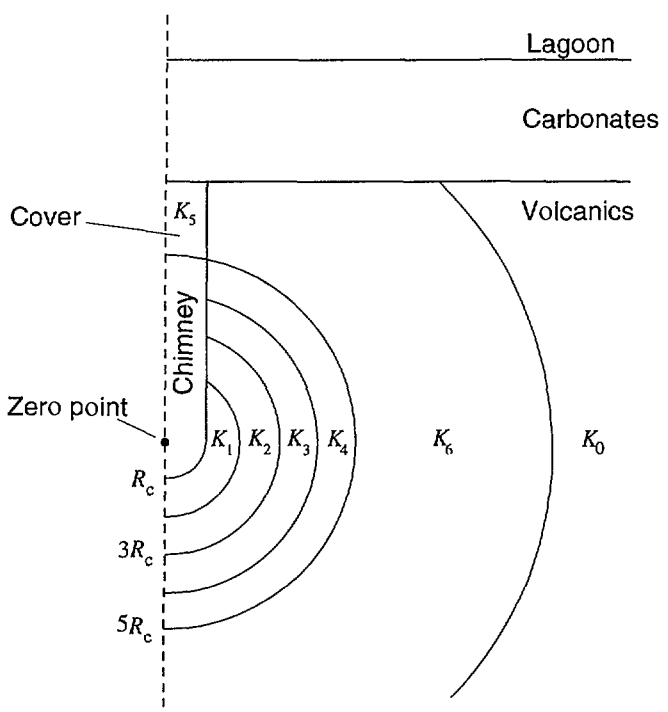

FIG. 31. Representation of post-test hydraulic conductivity zones for modelling purposes (Perrochet and Tacher 1997).

TABLE IV. SCENARIOS FOR DISTRIBUTIONS OF HYDRAULIC CONDUCTIVITY IN THE VOLCANICS TO REPRESENT POSSIBLE FRACTURING IN DAMAGED ZONES AROUND A CAVITY-CHIMNEY

Hydraulic conductivity (m/s)	F0 (no fracturing)	F1 (radially decreasing intensity of fracturing)	F2 (no fracturing except in volcanic cover above cavity-chimney)	F3 (extensive fracturing)	Radii
K_0	10^{-7}	10^{-7}	10^{-7}	10^{-7}	Regional background
K_1	10^{-7}	10^{-5}	10^{-7}	10^{-3}	R_c - 2 R_c
K_2	10^{-7}	5×10^{-6}	10^{-7}	5×10^{-4}	2 R_c - 3 R_c
K_3	10^{-7}	10^{-6}	10^{-7}	5×10^{-4}	3 R_c - 4 R_c
K_4	10^{-7}	5×10^{-7}	10^{-7}	5×10^{-4}	4 R_c - 5 R_c
K_5	10^{-7}	10^{-6}	10^{-6}	10^{-4}	Volcanic cover
K_6	10^{-7}	10^{-7}	10^{-7}	10^{-4}	5 R_c - 10 R_c

cavity-chimney. In some cases, measurements were made of static water levels within the drill hole at different times. In general, it was found that refilling times were longer for large tests, essentially because the ratio of volume to surface area of the cavity-chimney increases with the power of the test, and water to refill the volume can only flow in through this surface area.

In order to analyse these data, the CEA used the numerical METIS code described earlier. As examples of this kind of analysis, the French Liaison Office Document No. 5, 1997, has released a number of sensitivity analyses showing the effects of hydraulic conductivity K and specific storage coefficient S_0 on the filling rates, as well as data and simulations for a 14.5 kt and a 3.2 kt test. Even though only a limited amount of data is available, the methodology used by the CEA to interpret effective hydraulic properties near the cavity-chimney following nuclear explosions has been checked (Fairhurst et al. (IGC) 1998) using the FEFLOW code.

As a first stage of this exercise, an attempt was made to reproduce the results of sensitivity runs for two tests with yields of 10 kt and 100 kt (French Liaison Office Document No. 5, 1997, Fig. 17). Whereas the CEA simulations were based on a homogeneous hydraulic conductivity of 10^{-7} m/s, the present Study considered four different spatial distributions of hydraulic conductivity, as a function of the distance to the centre of the explosion (resulting from the discussion in Vol. 3 of this Technical Report) in order to assess the sensitivity of the results to possible fracturing in damaged zones surrounding the cavity-chimney. Figure 31 defines the individual zones assigned with different hydraulic conductivities. Four possible combinations, identified as scenarios F0 to F3, are defined in Table IV.

Comparisons were performed using one single value of specific storage coefficient, $S_0 = 10^{-5}$/m, because the CEA sensitivity analyses showed that this was the best value and also because this value could be reasonably expected for basalt. For both yields, scenario F0 led to filling rates somewhat slower than that calculated by the CEA, probably because of slight differences between the two calculations, due to an incomplete definition of the problem in the French Liaison Office Document No. 5, 1997. Scenario F1 led to significantly faster filling, and scenario F3 was so fast that it could not be compared on the same plot. Scenario F2, as expected, led to slightly faster filling than F0. This phase of the comparisons simply confirmed that the modelling techniques being

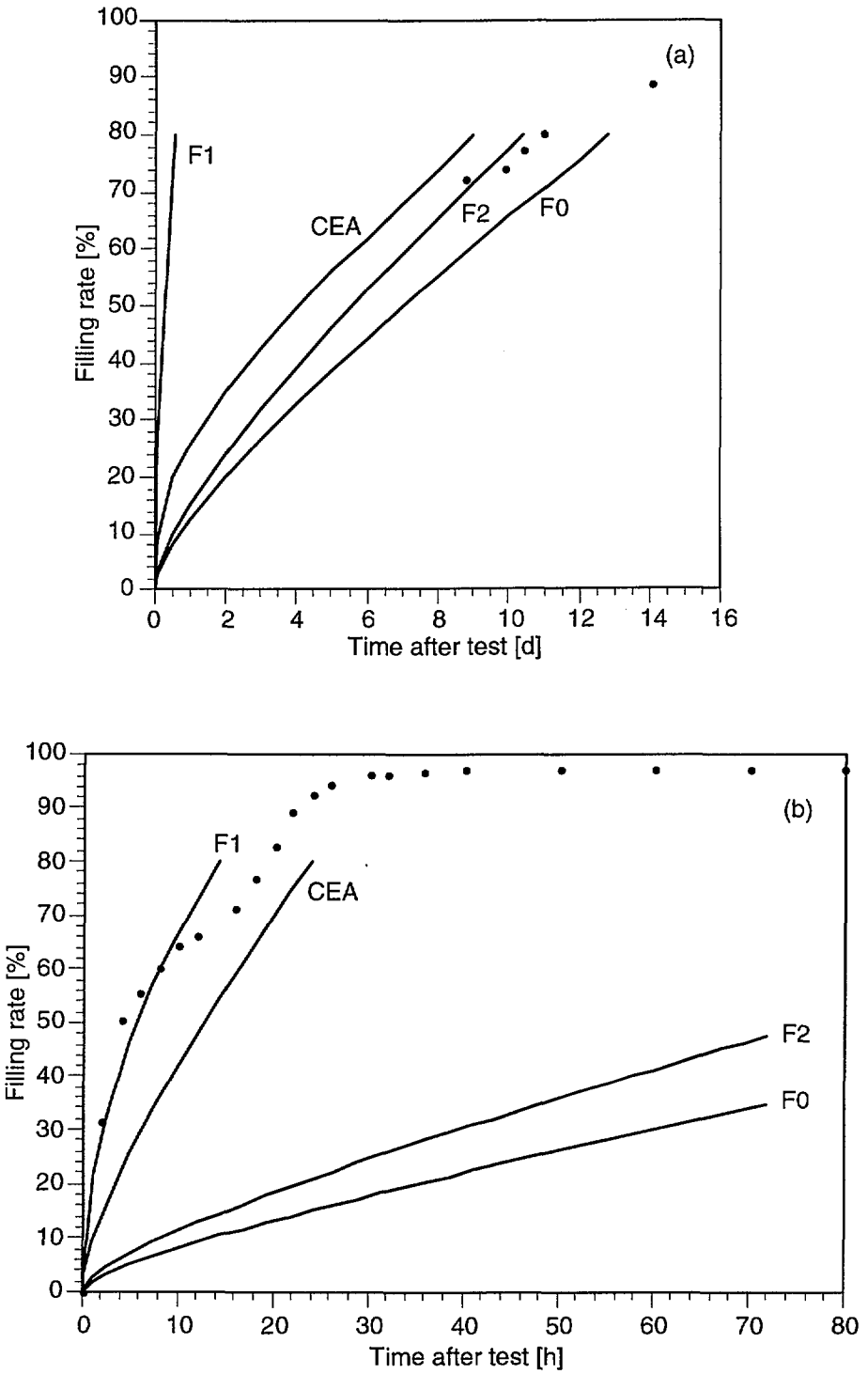

FIG. 32. Comparison of measured filling rates predicted by the French Liaison Office, with three permeability scenarios used in the Study for: (a) 14.5 kt test, (b) 3.2 kt test (Perrochet and Tacher 1997).

used were comparable with those used previously. They showed that filling times (to 95% full) would be of the order of 10 days for a 10 kt test and 60 days for a 100 kt test, if there was little damage to the rock surrounding the cavity-chimney.

Five data points are available for the filling rate of a cavity-chimney from a 14.5 kt test (French Liaison Office Document No. 5, 1997, Fig. 21). The CEA matched the filling rate with a model based on a regional background hydraulic conductivity of 6×10^{-8} m/s and an increased conductivity of 2×10^{-6} m/s within a radius of 2.3 R_c from the site of the explosion. Calculations of three scenarios are shown in Fig. 32(a), together with FEFLOW calculations based on the CEA scenario (Fairhurst et al. (IGC) 1998). The CEA scenario recalculated with FEFLOW does not perfectly match the observations, whereas the match was better in the CEA calculations. This is because not enough information was available to allow a complete definition of the problem. Scenarios F0 and F2 agree reasonably well with the data. Scenario F1 would result in much faster filling than that observed. It appears that the data obtained in the field for this 14.5 kt test are consistent with very little damage to the rock surrounding the cavity-chimney.

The only other available data are observations of pressure in the cavity-chimney for a 3.2 kt test (French Liaison Office Document No. 5, 1997, Fig. 22). These data have been converted to filling rates. Calculations are shown in Fig. 32(b). In order to match the observations, the CEA used a conductivity of 5.5×10^{-7} m/s as a regional background value and 2×10^{-6} m/s within a radius of 2.5 R_c. The FEFLOW scenario F1 matched the data far better than scenarios F0 and F2 in this case. This finding is consistent with the CEA finding that hydraulic conductivity needed to be greater, in order to explain the faster filling rate. However, it is interesting that the CEA chose to modify the regional background value rather than the near field distribution of conductivities, especially when it is known that the explosion is likely to affect rock in a spherically symmetric manner, with damage decreasing with distance from the explosion.

Estimates of filling times are available for nearly half of the underground nuclear tests carried out at Mururoa and Fangataufa Atolls. The CEA used the technique described above to estimate effective hydraulic conductivities, and has provided the results in the form of a histogram (French Liaison Office Document No. 5, 1997, Fig. 22). The histogram shows the range of values of regional background conductivity, given an assumed value of 2×10^{-6} m/s within a radius of 1.6 R_c. Although the parameter on which the calibration has been performed is perhaps contrary to what might have been expected, the results are nonetheless interesting. More than half of the estimates of regional conductivity are lower than 10^{-7} m/s, and another 40% are between 10^{-7} and 3×10^{-7} m/s. These results suggest that if the background conductivity were chosen as a fixed parameter and if filling rates were used to calibrate an effective conductivity within a radius of 1.5 or 2 R_c, nearly all tests would imply values lower than 10^{-5}/m in that zone and scenario F1 would significantly overestimate the extent of the fracturing in the zone surrounding the cavity-chimney.

3.2.4. Explosion-induced geothermal convection cells (0–500 years)

Once the cavity-chimney is full of water, the dominant process of interest hydrologically is the growth and decay of a geothermal convection cell caused by the temperature and density differences between hot water in the cavity-chimney and cooler ambient water in the surrounding basalt. This phenomenon has been described by Bouchez and Lecomte 1996, both qualitatively and, to some extent, quantitatively. The convection cell is essentially radially symmetric, with hot water rising vertically above the cavity-chimney and cool ambient water entering the bottom and sides of the cavity-chimney. Convection provides a mechanism for dissipation of heat, because heat is carried upwards by the rising water, at the same time as being transported outwards by conduction.

Numerical modelling by the CEA was referred to by Atkinson et al., 1984, Fig. 22, but few details were provided. An attempt was made by Hochstein and O'Sullivan 1985 and 1988 to model

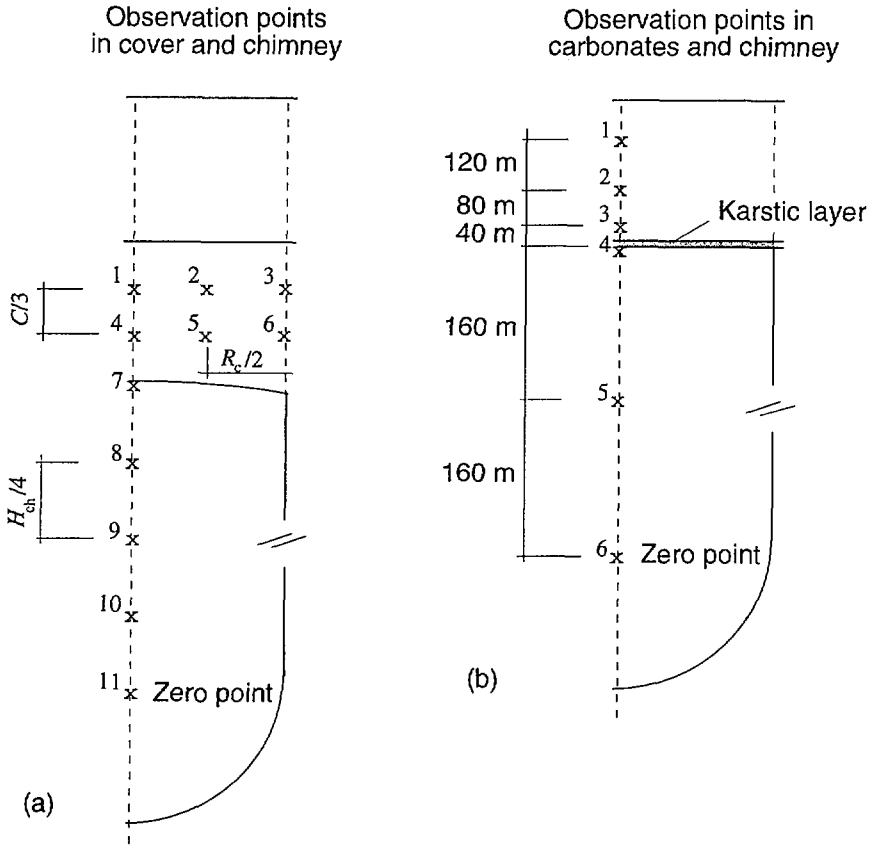

FIG. 33. Locations of points where temperatures and Darcy velocities are computed for: (a) tests with volcanic cover; (b) tests without volcanic cover (150 kt tests only, H_{ch} = 320 m, C is cover thickness) (Perrochet and Tacher 1997).

the thermal convection, but their results were obtained with a very coarse finite differences grid, and without access to accurate information from the CEA. Another effort is currently being made by Booker and Leo (personal communication). In the absence of relevant theoretical results, the best way to proceed to understand the geothermal convection cells is to use numerical methods, and this is the approach used by the CEA and the present Study.

Modelling of convection near a cavity-chimney by the CEA (Bouchez and Lecomte 1996; pp. 58–62) shows that for a 100 kt test with 140–150 m of volcanic cover and with hydraulic conductivity enhanced by a factor of 10 relative to the background conductivity of 10^{-7} m/s, i.e. scenario F2 in Table IV, the initial temperature difference of 25°C in the cavity-chimney decays to zero over a period of about 500 years. The vertical velocity in the volcanic cover decays less slowly initially, but relatively faster later on. The upward velocity induced by the natural geothermal gradient will be reached after 400 years. During the first five years, the Darcy velocity exceeds 0.25 m/a.

To check the CEA results, simulations were performed by Fairhurst et al. (IGC) 1998, using FEFLOW for a number of combinations of power, initial temperature increase in the cavity-chimney, thickness of volcanic cover and spatial distribution of hydraulic conductivity. The power of a test was considered to be either 5 kt (a relatively small explosion, requiring a small thickness of cover) or 150 kt (which is larger than the power reported at Mururoa and Fangataufa). Initial temperature differences were assumed to be either 25°C or 50°C, as discussed earlier. Volcanic cover was assumed to have thicknesses of 15 m or 100 m, which are reasonable values for small and large powers tests, respectively, or 0 m, in the case of a cavity-chimney that touches the carbonates (CRTV tests). Hydraulic conductivity distributions were considered to be F0 to F3, as defined in Table IV.

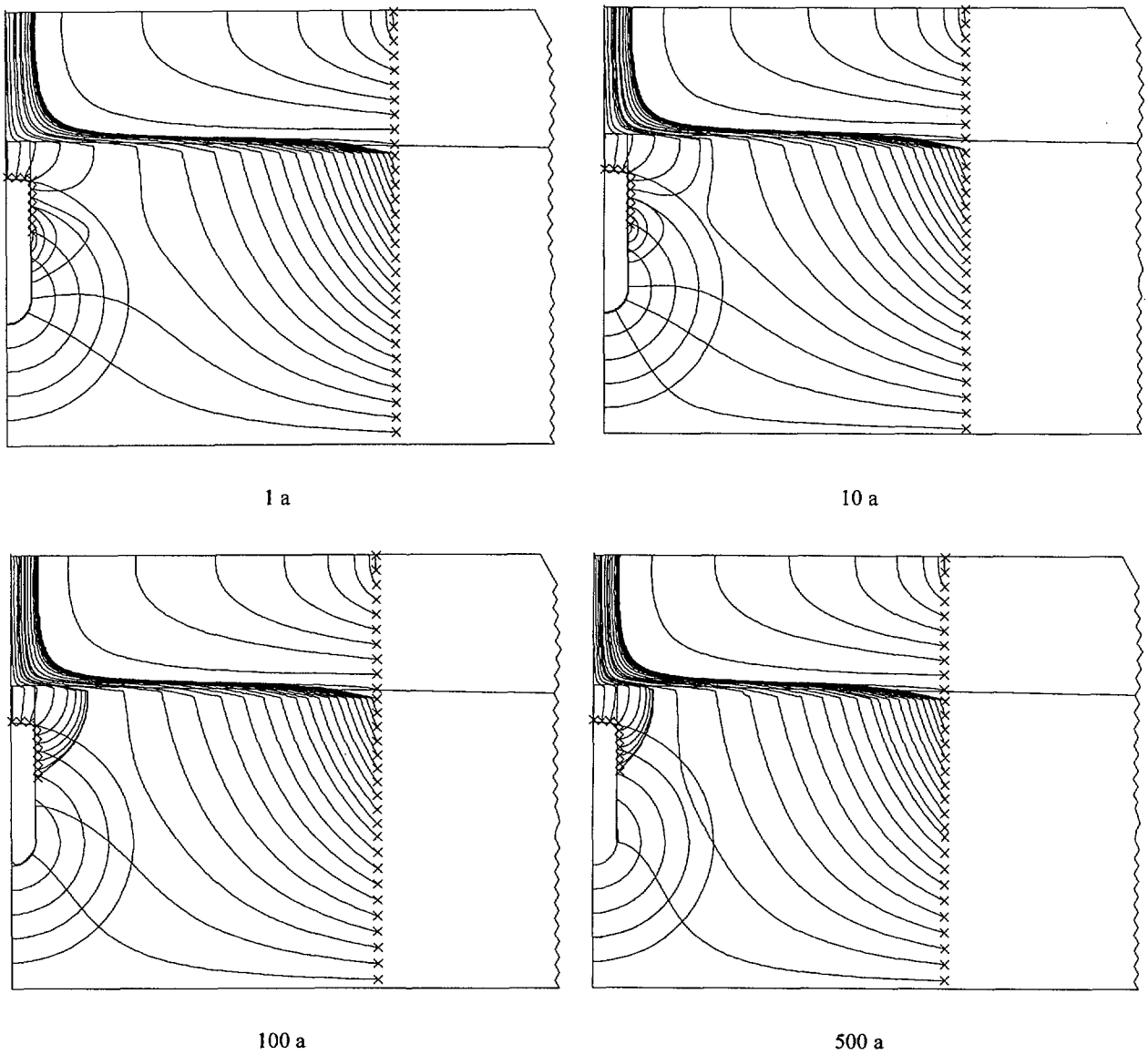

FIG. 34. Evolution of instant flow paths around a cavity-chimney.

Simulations were carried out to calculate the temperatures and velocities at a 3 × 3 array of observation points (Fig. 33) distributed uniformly (a) in the volcanic cover above the cavity-chimney, (b) in the carbonates up to 120 m above the cavity-chimney where no cover existed (CRTV tests). It was found that, during the first year, peak vertical Darcy velocities at the observation points are in the range 6-9 cm/a (F0), 100–200 cm/a (F1), and 50–60 cm/a (F2). The velocity ratios between the three cases are very similar to those observed with a 5 kt test, i.e. 5 between F2 and F0, and 10 between F1 and F0. Moreover, the average peak vertical velocities detected during the first year for the 5 kt test with shallow cover and for the 100 kt test with thicker cover show the same orders of magnitude, i.e. 10 cm/a for scenario F0, 100 cm/a for F1, and 50 cm/a for F2.

Figure 34 is an example of flow field produced around an explosion for periods of 1 to 500 years after the explosion. It shows that the vertically upward flow path above the cavity-chimney does not cease to exist even when the thermal pulse has decayed to a very low level. Figures 35 and 36 show colour plots of the migration of the thermal plume vertically above the cavity-chimney for

Text cont. on p. 72.

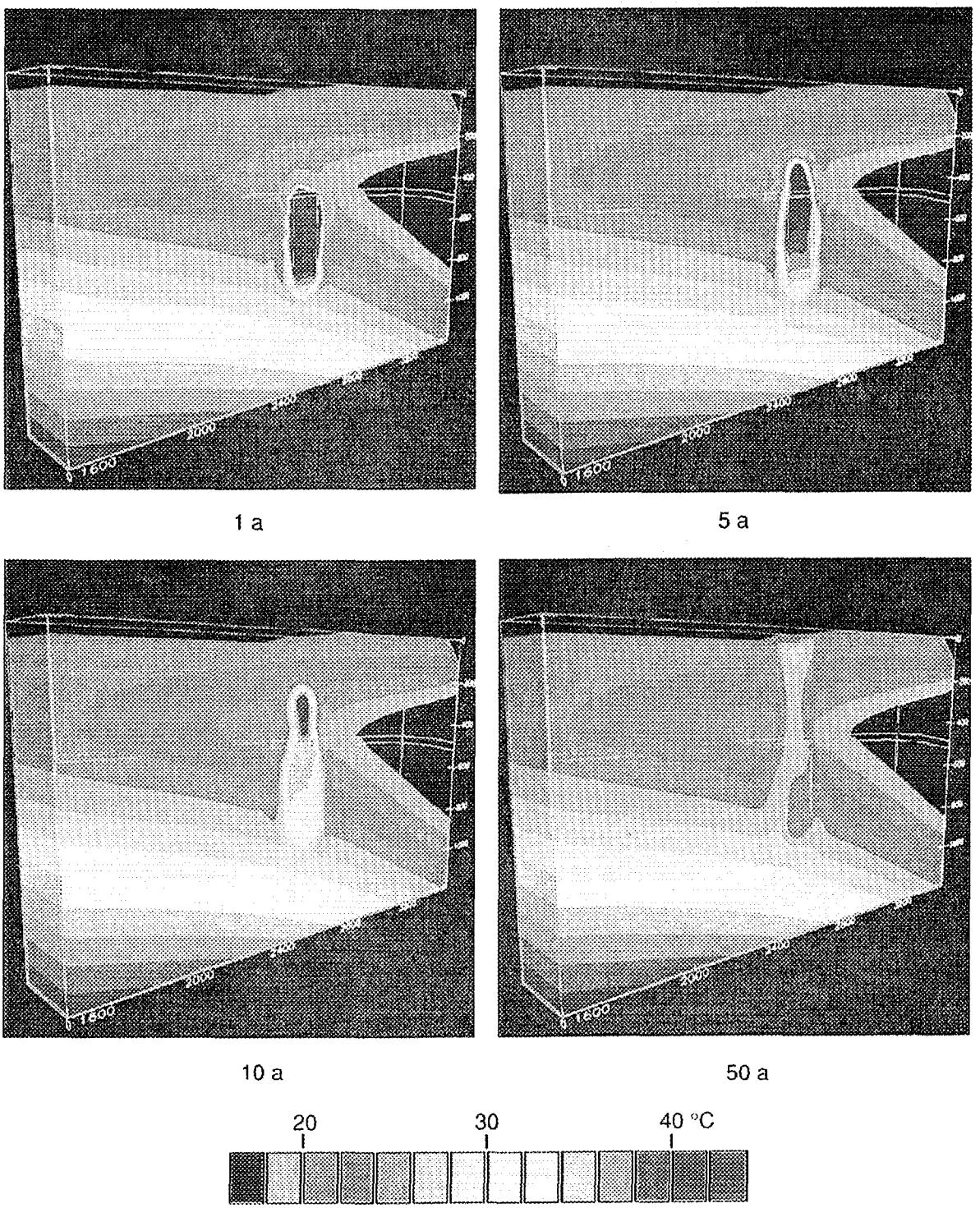

FIG. 35. Three dimensional simulation over time of isotherms for a 150 kt test with no volcanic cover, a temperature rise of 50°C in the chimney, no increase in hydraulic conductivity above the pre-test level (scenario F0) and no karst layer at the volcanic–carbonate interface (Perrochet and Tacher 1997). The test modelled is a hypothetical extreme: a 150 kt test with an initial temperature rise of 50°C and with no cover (no such tests were ever carried out).

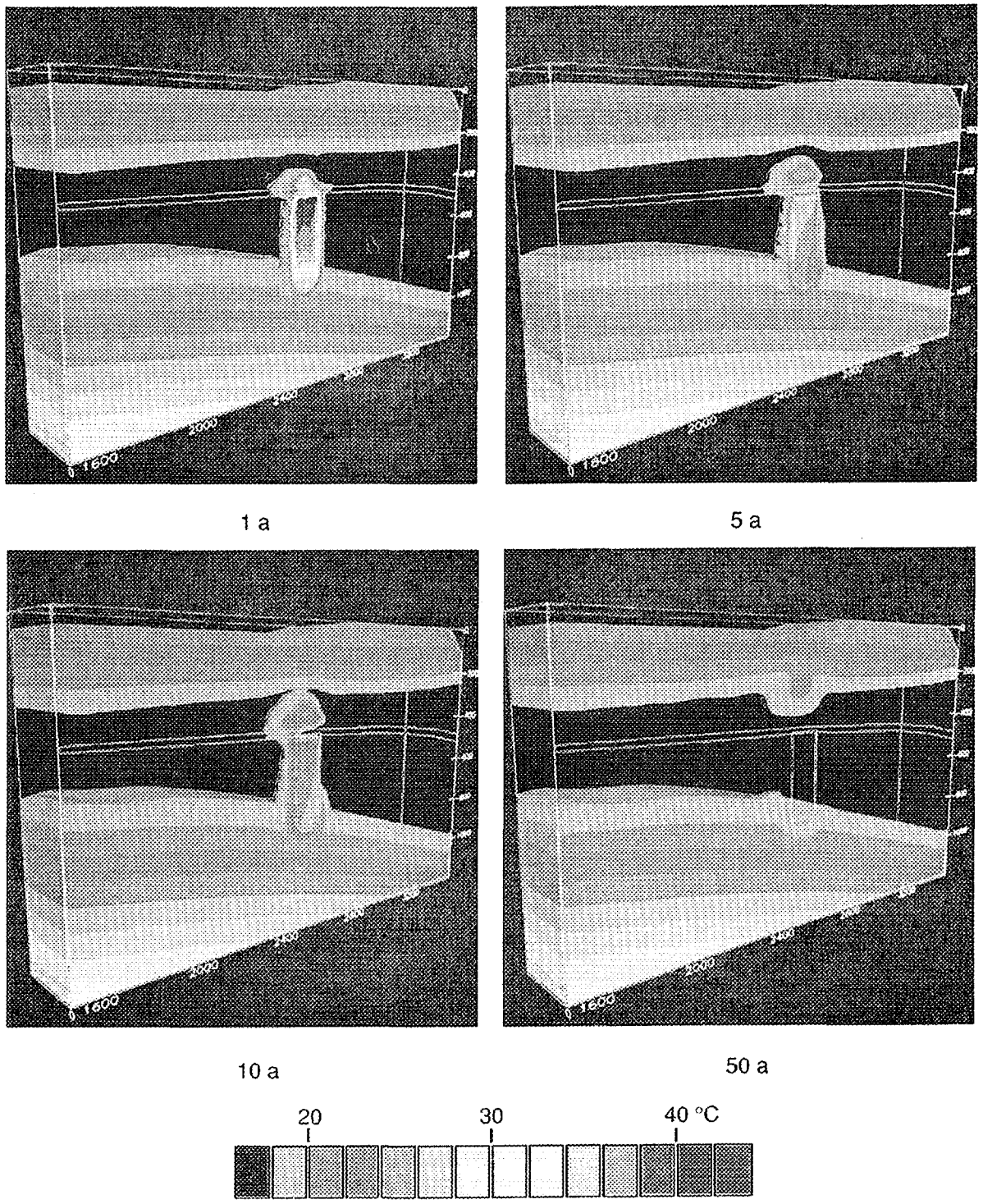

FIG. 36. Same scenario as Fig. 35 but with a karst layer and large longitudinal dispersivity (α_L = 1000 m) (Perrochet and Tacher 1997). The test modelled is a hypothetical extreme: a 150 kt test with an initial temperature rise of 50°C and with no cover (no such tests were ever carried out).

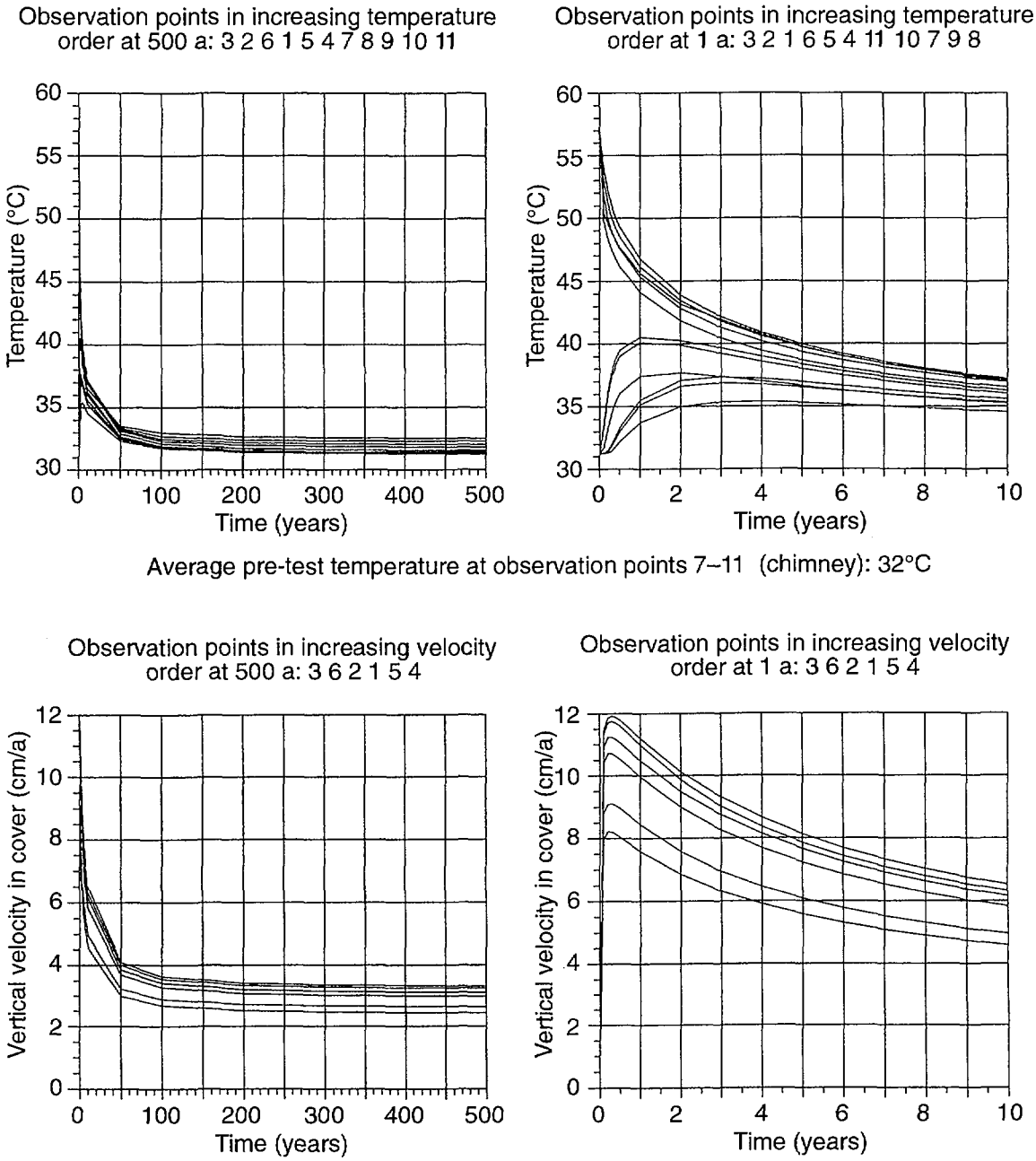

FIG. 37. Variation of temperature and Darcy velocity with time following a 5 kt test with 15 m of volcanic cover, a temperature rise of 25°C and no increase in hydraulic conductivity above pre-test level (scenario F0) (Perrochet and Tacher 1997). Observation points are shown in Fig. 33.

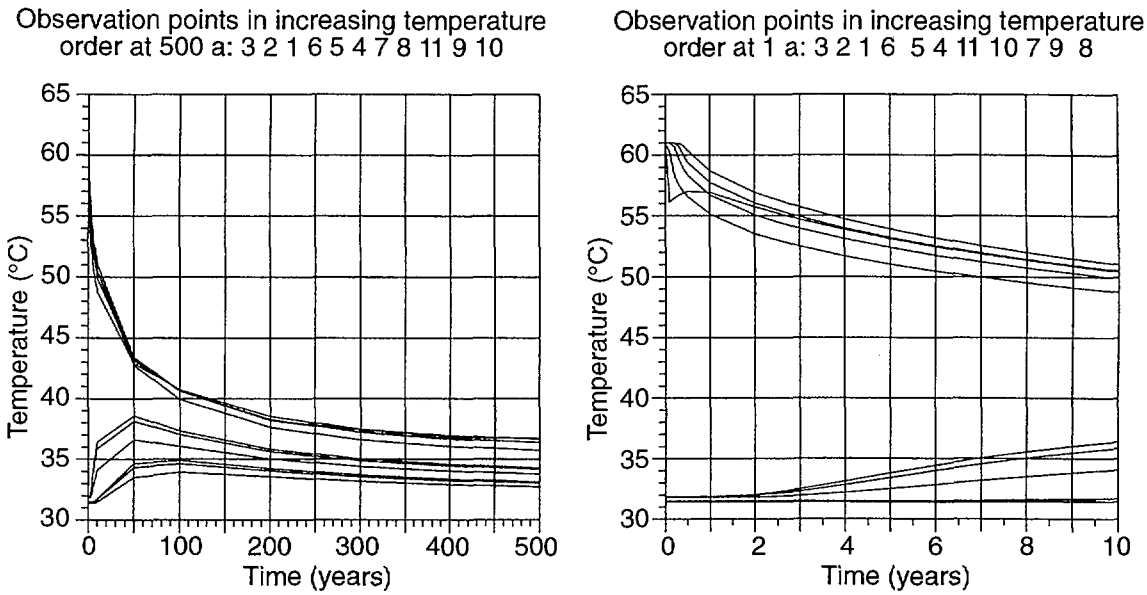

Average pre-test temperature at observation points 7–11 (chimney): 36°C

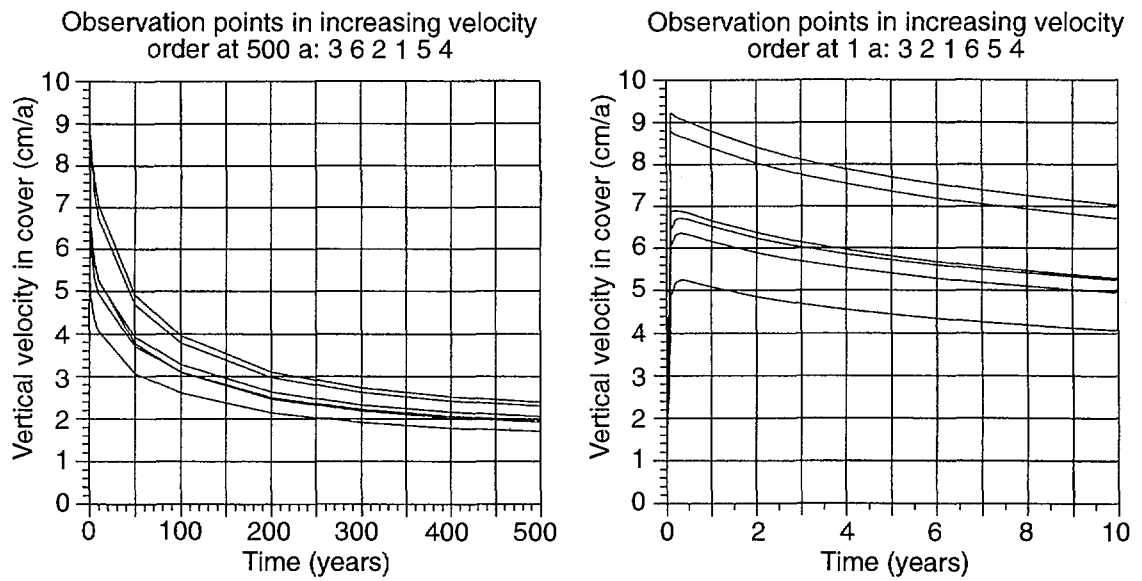

Average pre-test vertical Darcy velocity at observation points 1–6 (cover): 0.73 cm/a

FIG. 38. Variation of temperature and Darcy velocity with time following a 150 kt test with 100 m of volcanic cover, a temperature rise of 25°C and no increase in hydraulic conductivity above pre-test level (scenario F0) (Perrochet and Tacher 1997). Observation points are shown in Fig. 33.

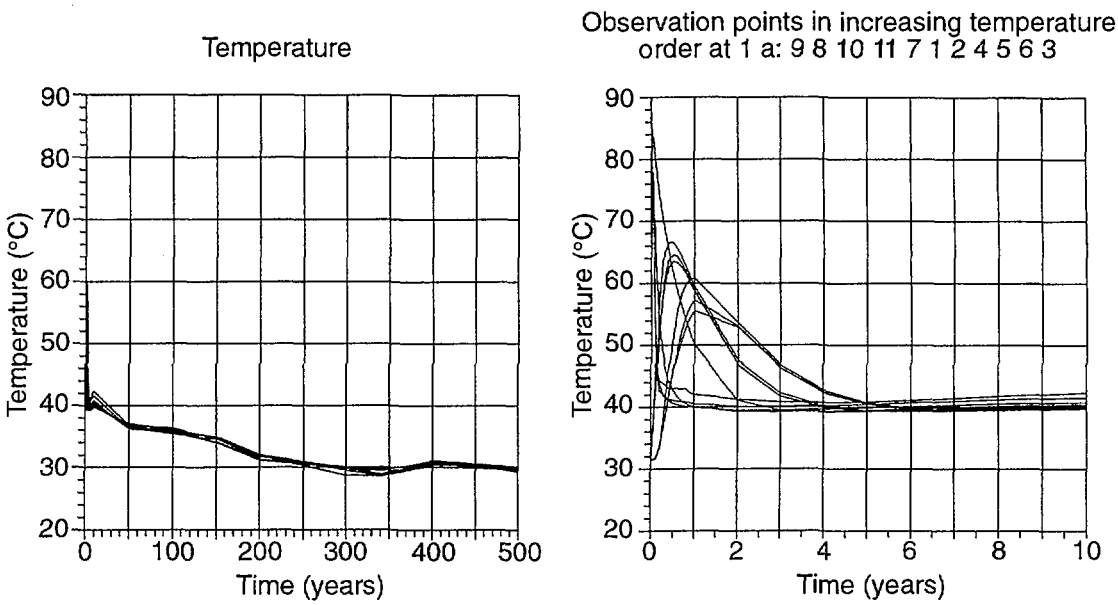

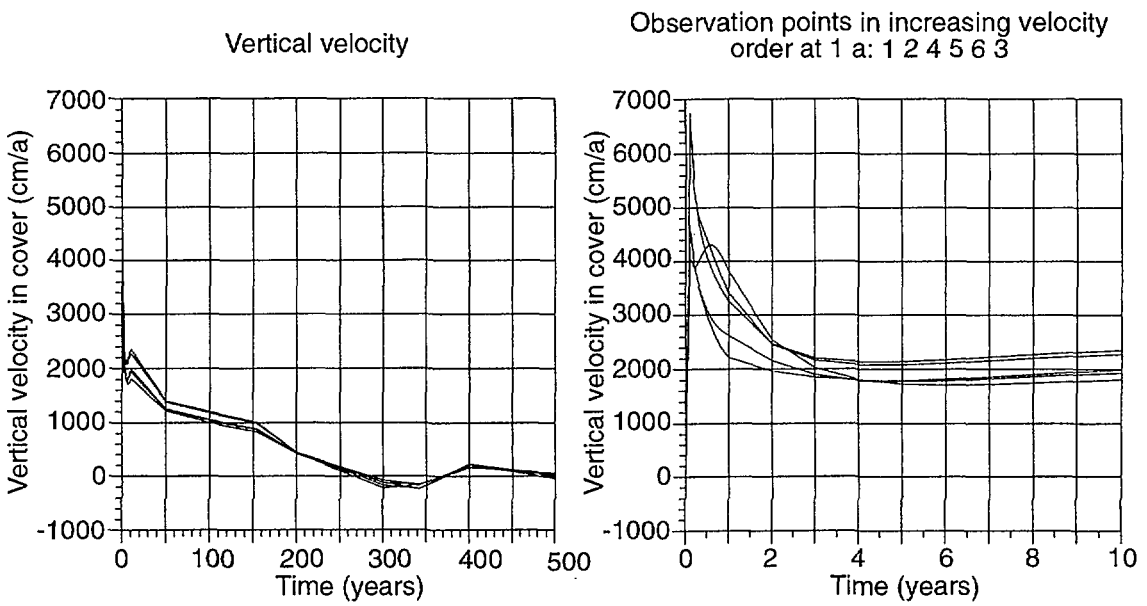

FIG. 39. Variation of temperature and Darcy velocity with time following a 150 kt test with 100 m of volcanic cover, a temperature rise of 50°C and significantly higher conductivity to $10R_c$ (scenario F3) (Perrochet and Tacher 1997). Observation points are shown in Fig. 33.

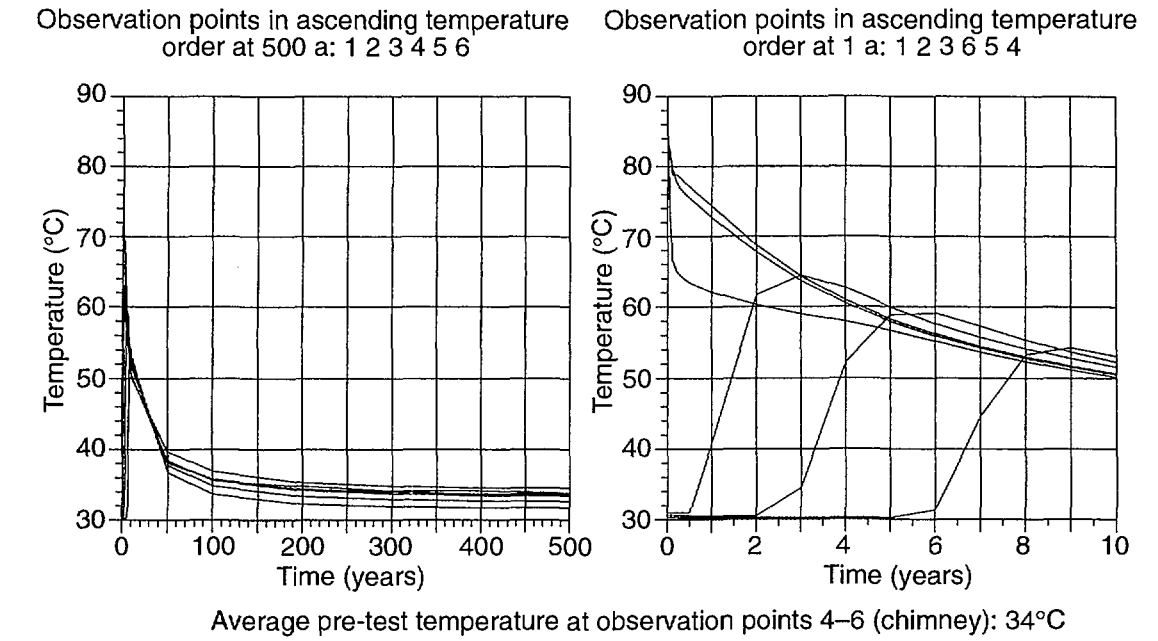

FIG. 40. Variation of temperature and Darcy velocity with time following a 150 kt test with no volcanic cover, with a pre-test temperature of 34°C, a temperature rise of 50°C and no increase in hydraulic conductivity above pre-test level (scenario F0) (Perrochet and Tacher 1997). The test modelled is a hypothetical extreme: a 150 kt test with an initial temperature rise of 50°C and with no cover (no such tests were ever carried out). Observation points are shown in Fig. 33.

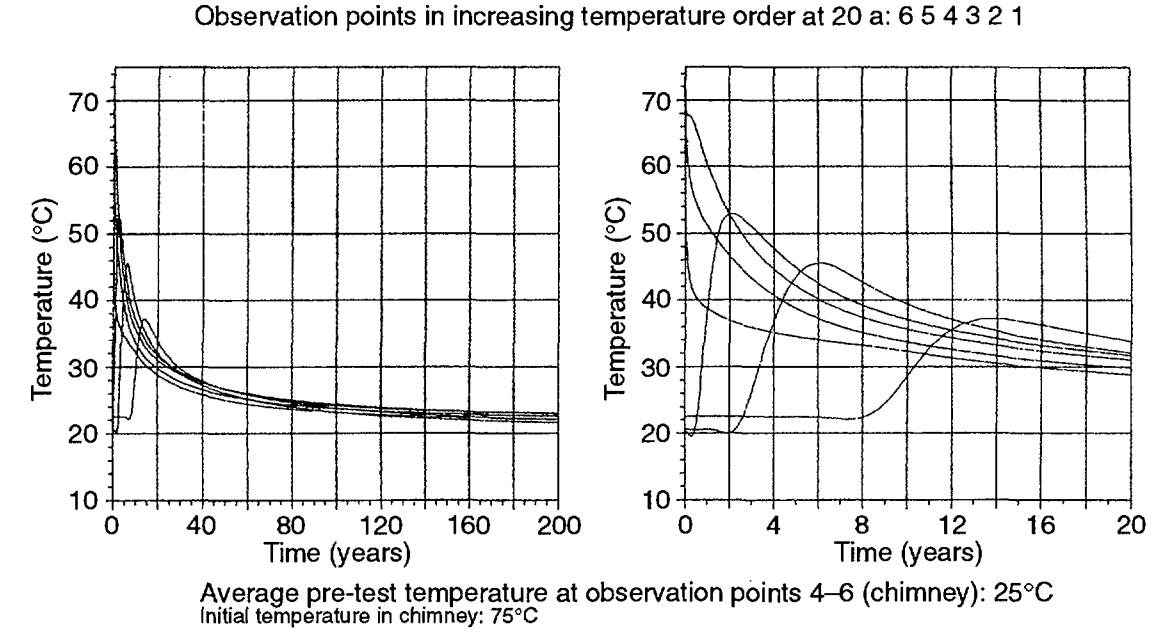

FIG. 41. *Variation of temperature and Darcy velocity with time following a 150 kt test under the rim with no volcanic cover, an initial temperature increase of 50°C and no increase in hydraulic conductivity above the cavity-chimney (scenario FO) (Perrochet and Tacher 1997). The tests modelled is a hypothetical extreme. No such tests were ever carried out. Observation points are shown in Fig. 33.*

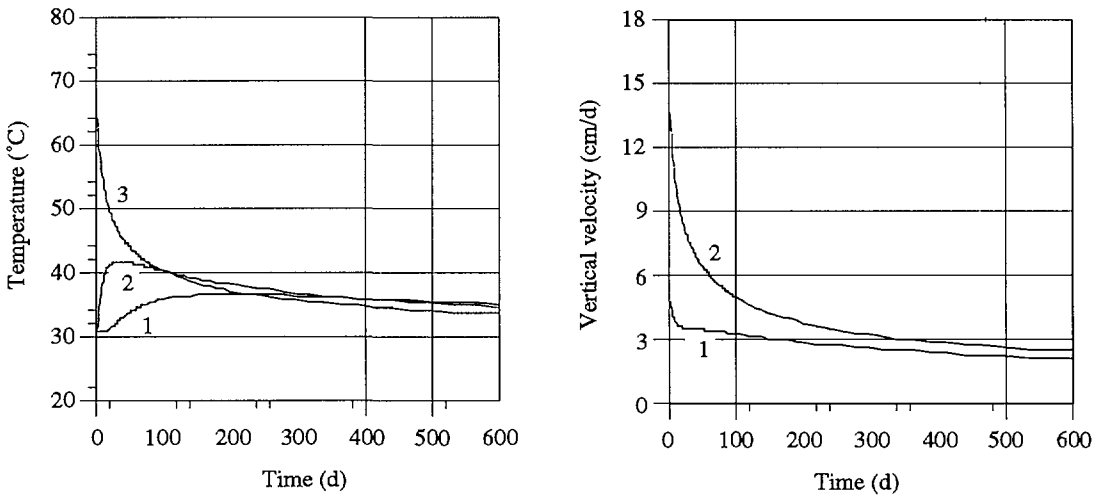

FIG. 42. Temperature and vertical Darcy velocities above a critical safety trial (0.2 kt).

the cases where there is no karstic layer at the base of the carbonates (Fig. 35) but a karst layer with large lateral dispersivity (α_L = 1000 m) (Fig. 36) exists. It shows that the karst is very effective in dissipating the thermal plume.

Figures 37–41 give the evolution with time of the velocities at the different observation points, shown in Fig. 33, for different yields, thickness of cover, temperature increase, and permeability scenario around the cavity-chimney.

3.2.5. Hydrological factors associated with safety trials

The safety trials conducted in the carbonates involved several that did not produce a nuclear yield and others that did. For the former there is no perturbation of the steady state hydrological regime. Given the lack of precise location of the trials on the one hand and the great sensitivity of flow paths in 2-D simulations on the atoll scale, a conservative estimate is required. With a karstic layer, flow paths in the carbonate below the lagoon are essentially vertical, with Darcy velocities of a few tens of cm per year. For conservative travel time estimates the Darcy velocities can be converted to appropriate pore velocities applied to the shortest, i.e. vertical, route between the source and the lagoon.

In the second case, a cavity is created. Simulation for an explosion of 0.2 kt[2] at a depth of 280 m below sea level results in a cavity-chimney of 7 m radius and 35 m height. Figure 42 gives the time evolution of temperatures and vertical Darcy velocities at 20 m (point 1) and 10 m (point 2) above the top of the cavity-chimney. Point 3 is located at the top of the cavity-chimney. The temperature at point 2 is found to be 42°C after about one month. After 100 days the temperature at this point is higher than in the cavity-chimney. The results for the temperature breakthrough at point 1 are more diffuse but the fact that the temperature stays at about 36°C between 200 and 600 days after the test indicates that after the test advection is dominant for the heat plume.

Peak vertical velocities at points 1 and 2 are detected immediately after the trial. At point 2 it is close to 18 cm/d, i.e. 65 m/a. This peak value is of the same order of magnitude as that observed for a 150 kt test reaching the carbonates. Here, however, due to the very small size of the safety trials, velocity declines faster and the average value between points 1 and 2 is in the range of 2–3 cm/d, i.e. 9-10 m/a, in the period of 200-600 days after the test. Quasi steady state velocities of about 1.3 cm/d, i.e. 5 m/a are obtained 2000 days after the test.

[2]The yield of these safety trials was rounded off from 0.15 to 0.2 kt in this assessment.

For the critical safety trials, vertical Darcy velocities are thus larger by a factor of about 100 in the early dates and by a factor of 10 at the end of the cooling period than the unperturbed steady-state velocities.

3.2.6. General comments

3.2.6.1. Flow regime above the cavity-chimney

Short term pathways from the explosions are seen to be dominated by vertically upward flow through the top of the cavity-chimney roof. Although the existence of karstic horizons in the carbonates interrupts the thermal convection cells from the explosions, flow remains vertically upward. Long term releases of radionuclides still tend to flow dominantly upwards through the top of the cavity-chimney, but beyond this region the releases tend to follow flow paths involving a significant horizontal flow component before they reach the lagoon.

3.2.6.2. Flow regime in the cavity-chimney

Between the beginning and the end of the cooling period, the simulations of flow in the cavity-chimney indicate high rotational Darcy velocities throughout the cavity-chimney, with strong convection cells (toroidal in axi-symmetry). Corresponding pore velocities typically range from about 10 m/d down to about 1 m/d at the end of the cooling. In this context cavity-chimneys may be considered as well-mixed reactors at all times.

3.2.6.3. Influence of 137 underground tests on long term hydrological regime

Steady state three-dimensional simulations (case 7 of Table III) including all the underground nuclear tests were performed to assess possible long term hydrological perturbations. According to French Liaison Office Document No. 6, 1996, Fig. 1, 137 tests were carried out in specific areas of the Mururoa atoll. In the model, each area is included as well as the number of tests per area. In each area, test locations are chosen at random and damaged zones are introduced into the volcanics. The damaged zones have been standardised to a prismatic shape of a size of 20 000 m^2 in plan area and 350 m height with the top reaching the carbonates. Homogeneous hydraulic conductivities have been assigned to all of them. The total volume of the 137 damaged zones is thus 0.96 km^3, namely 0.15% of the volume of the volcanics within the test horizons.

Successive simulations with hydraulic conductivities of 10^{-6} m/s, 10^{-5} m/s, and 10^{-4} m/s in the damaged zones yield temperature distributions virtually identical to the pre-test distributions. The steady state total discharge into the lagoon is in the order of 60 000 m^3/d. This value shows very little sensitivity to the presence of all 137 tests and the associated damaged zones in the model. With hydraulic conductivities of 10^{-4} m/s in all the damaged zones, for example, the total discharge into the lagoon is increased by less than 1%. This is consistent with the very limited influence of "local" inhomogenities on the global groundwater flow regime found in the respective analysis presented in Appendix I.

3.2.7. Summary and discussion — post-test hydrology

The major findings of the post-test hydrological assessment can be summarized in the following way:

(1) The vertical water velocity above a test site is not as sensitive to permeability variations as expected. The reason is that the water leaving the cavity-chimney towards the surface must be replaced by water flowing radially towards the cavity-chimney. Even if the rock is damaged to a larger distance from the cavity-chimney, the bottle neck is finally the water that must

eventually be discharged by undamaged zones where the permeability in the volcanics is small. For instance, for a 150 kt test, if the extreme scenario F3 (permeability increase by a factor of 10 000) is used, the vertical water velocity above the cavity-chimney is increased by a factor of 5 compared to a scenario F2 (permeability increase by a factor of 10).

(2) The cavity-chimney is a "well-mixed reactor" because of the constant internal convection. Thus, the uncontaminated water entering the cavity-chimney is instantly mixed with the contaminated water inside the cavity-chimney. As a result, it can easily be shown that the concentration in the cavity-chimney decreases exponentially with time. The time needed to transfer, e.g. 90% of the initial activity of a non-sorbing radionuclide, such as tritium, to the carbonates can be calculated. It is a function of the ratio of the Darcy velocity above the cavity-chimney to the height of this cavity-chimney (see Section 5). Typical values are tens to hundreds of years. Sorbed radionuclides would take much longer.

(3) The vertical water velocity above a test site is almost independent of the yield of the test. This is also due to the fact that the volume of the cavity-chimney scales linearly with the yield, so that the temperature increase is constant, independent of the yield. The buoyancy forces are thus of the same order whatever the yield. On the other hand, when the temperature increase is changed from 25° to 50°C, the vertical velocity is increased almost by a factor of two.

(4) The main velocity values obtained for a five selected cases are summarized as follows:

(a) Case with a volcanic cover of 15 m

For a test with a 5 kt yield, the peak vertical Darcy velocity in the volcanics above the cavity-chimney ranges from 0.1 to 1.3 m/a depending on the assumed permeability and the initial temperature increase. After 100 years a steady velocity is reached, ranging from 0.03 to 0.3 m/a. In the carbonates, above the cavity-chimney, the Darcy velocity remains in the order of the natural velocity prior to the test, i.e. 2 m/a.

We assumed a fracture porosity in the volcanics of 10^{-4}, i.e. a fracture with an aperture of 0.1 mm every metre of rock. This is conservative because a fracture porosity of, e.g. 10^{-2}, i.e. a fracture with an aperture of 1 mm every 10 cm, would be conceivable but be less conservative. With a porosity in the carbonates of 30%, a non-sorbing radionuclide such as tritium would reach the volcanic - carbonate interface in less than a year and the lagoon in 45 years, assuming 300 m of carbonates. The time for emptying the cavity-chimney of 90% of its content of a non-decaying and non-sorbing tracer is in the order of 275 years for the highest Darcy velocity. Note that tritium would almost totally disappear by decay in ten half-lives, i.e. 120 years.

(b) Case of a volcanic cover of 100 m

For a test with a 150 kt yield, the respective numbers are:

Peak vertical Darcy velocity in the volcanics: 0.6 to 1.2 m/a.
Steady state vertical Darcy velocity in the volcanics, after 200 years: 0.3 m/a.
Darcy velocity in the carbonates: 2–3 m/a at all times.
Time for a non-sorbing tracer to reach the carbonates: less than one year.
Time for a non-sorbing tracer to reach the lagoon: 30 years.
Time for emptying 90% of a non-sorbing tracer from the cavity-chimney: on the order of 800 years.

It can easily be seen that these numbers are indeed very similar to those for the 5 kt test, thus showing that the results are relatively independent of the yield and thickness of the volcanic cover. An estimated number of 121 tests of different yields fall into the category of tests with volcanic cover.

(c) Case of no volcanic cover; the cavity-chimney reaches the carbonates (CRTV tests)

For a test with a 150 kt yield, the extensive fracturing scenario (F3) and the largest temperature increase, i.e. 50°C, the respective numbers are:

Vertical Darcy velocities in the volcanics: irrelevant; only the carbonates offer confinement.
Vertical Darcy velocity in carbonates: 58 m/a at peak (1 month), decaying rapidly to 18 m/a on average, over 100 years.
Time for a non-sorbing tracer to reach the carbonates: almost immediately.
Time for a non-sorbing tracer to reach the lagoon: 2 years.
Time for emptying 90% of a non-sorbing tracer from the cavity-chimney: about 15 years.
An estimated number of 12 tests are in this category, mostly with much lower yields (5–10 kt).

(d) Case of a damaged volcanic cover with increased permeability (F3 scenario)

For a test with a 150 kt yield and the largest temperature increase (50°C), the respective numbers are:

Vertical Darcy velocity in the volcanics: 68 m/a at peak (1 month), decaying rapidly to 20 m/a on average over 50 years.
Vertical Darcy velocity in the carbonates: in the order of 30 m/a for the first tens of years.
Time for a non-sorbing tracer to reach the carbonates: almost instantly.
Time for a non-sorbing tracer to reach the lagoon: 3 years.
Time for emptying 90% of a non-sorbing tracer from the cavity-chimney: around 12 years.
An estimated number of 4 tests fall into this category. Note that these numbers are very similar to those of the CRTV case discussed above.

(e) Case for safety trials conducted in the carbonates with or without a yield

If the safety trials did not have a yield, the vertical Darcy velocity in the carbonates remains on the order of 2-3 m/a. The pore water velocity is on the order of 9 m/a and the time for the tracer to reach the lagoon on the order of 30 a, depending on the depth of the trial.

For safety trials at a depth of 280 m with a yield of 0.2 kt[3], the peak vertical Darcy velocity is in the order of 55 m/a for a few days, and stabilises at 11 m/a after one year. The vertical pore water velocity is 180 m/a, initially, and decreases to 35 m/a after one year. Time for a tracer to reach the lagoon is about 8 years.

An estimated number of 7 safety trials is in this category with 3 that went critical and 4 that did not (see Fig. 1).

(f) Implications of these flow calculations for radionuclide transport

The calculated velocities make it possible to estimate the fate of radionuclides generated in the underground by a nuclear explosion. In order to simplify and group the various tests that were performed over the years, it was decided to select a few typical values of the vertical Darcy velocity above the cavity-chimneys for use in transport modelling. The following basic data are recommended:

- For a normal test, independent of the yield: 1 m/a in the volcanics and 2 m/a in the carbonates.
- For a CRTV test, or a test with a damaged volcanic cover, independent of the yield: 20 m/a in the carbonates and the volcanics.
- For safety trials in carbonates: 11 m/a if they went critical, 2 m/a if they did not.

Further information on the refinement of these basic data and data variations for the purpose of sensitivity analyses can be found in Section 5.2.

[3]The yield of these safety trials was rounded off from 0.15 to 0.2 kt in this assessment.

3.3. TRITIUM TRANSPORT CALCULATIONS AND COMPARISON WITH CONCENTRATIONS MEASURED IN THE KARSTIC LAYER ABOVE THE VOLCANICS

In order to validate the final outcome of all the above calculations and their underlying assumptions, comparisons have been made of the predicted release of tritium to the carbonates and to the lagoons, both at Mururoa and Fangataufa, with the measurements made by the CEA from 1987 onwards and by the IAEA in 1996 (see Vol. 1 and 2 of this Technical Report) and 1997 (see Section 6 and Appendix V).

To this end, a simplified "mixing model" was developed for tritium transport, and compared with a "piston flow model" and a "advection - dispersion model". These comparisons are reported in Appendix II and III. Of these, the "mixing model" was found to be the one most consistent with the observations. This model assumes:

- continuous mixing of tritium in the cavity-chimney water of each test and release of this water to the carbonates with the calculated Darcy velocities given in Section 3.2. The release decreases exponentially with time, because of the tritium half-life and the mixing in the cavity-chimney. The initial tritium inventory for each test was taken from Vol. 3 of this Technical Report.

- the tritium leaving the volcanics enters the carbonate layer which is represented in this model as a well-mixed "reservoir". The rationale for using a mixing model in the carbonates is based on the observation that the tritium is spread over a considerable thickness and volume of the carbonates throughout each test zone, but that the amount of tritium reaching the lagoons is very small. The cumulated release over 20 years is limited to only a few percent of the total inventory of the carbonates. This shows that the distribution of the residence times of tritium in the carbonates is uneven: a small fraction is released rapidly while a large fraction stays in the porewater. A mixing model is one simple way to represent this residence time distribution. The cause of the mixing may be the tidal effect and, possibly, the effects of the drilling of new test wells during the period of active testing.

- release of tritium from the carbonates to the lagoons by the average natural Darcy flux for natural conditions, which globally is not affected by the tests (see Section 3.2.6); this Darcy flux is assumed to have the tritium concentration of the mixed carbonate "reservoir".

- release of the tritium from the lagoons to the ocean because of the daily tidal flow in and out of the lagoons. The lagoons are again assumed to be well-mixed and the knowledge of the average water residence time in the lagoons, estimated by both the CEA and the IAEA, makes it possible to estimate the total annual flux of tritium to the lagoons from the measurement of the average tritium concentration of the lagoon waters.

All the parameters of this simplified "mixing model" can be independently estimated, in general within a factor of two, from the estimated yield of the tests and the hydrological calculations, in particular the values selected for the Darcy velocities for each test category. The complete set of 137 tests on Mururoa and 10 tests on Fangataufa as given in Vol. 3 of this Technical Report were taken into account and grouped together in periods of 5 years. The calculated inventory in the carbonates and the annual release to the lagoons on both atolls were then compared with the estimated inventories in the carbonates, obtained by sampling of waters from a total of 16 boreholes in Mururoa and 4 boreholes in Fangataufa, and the estimated flux of tritium to the lagoons based on the measured concentrations in the lagoon waters. The agreement was surprisingly satisfactory. It resulted in an overestimate of the flux to the lagoons by a factor of less than two and an overestimate of the tritium inventory in the carbonates by a factor of 2 to 10. Overestimating the flux and inventory is, of course, conservative with respect to the radionuclide release. Figure 43 and 44 give the calculated evoiution of the tritium flux to the Fangataufa and Mururoa lagoons over the years.

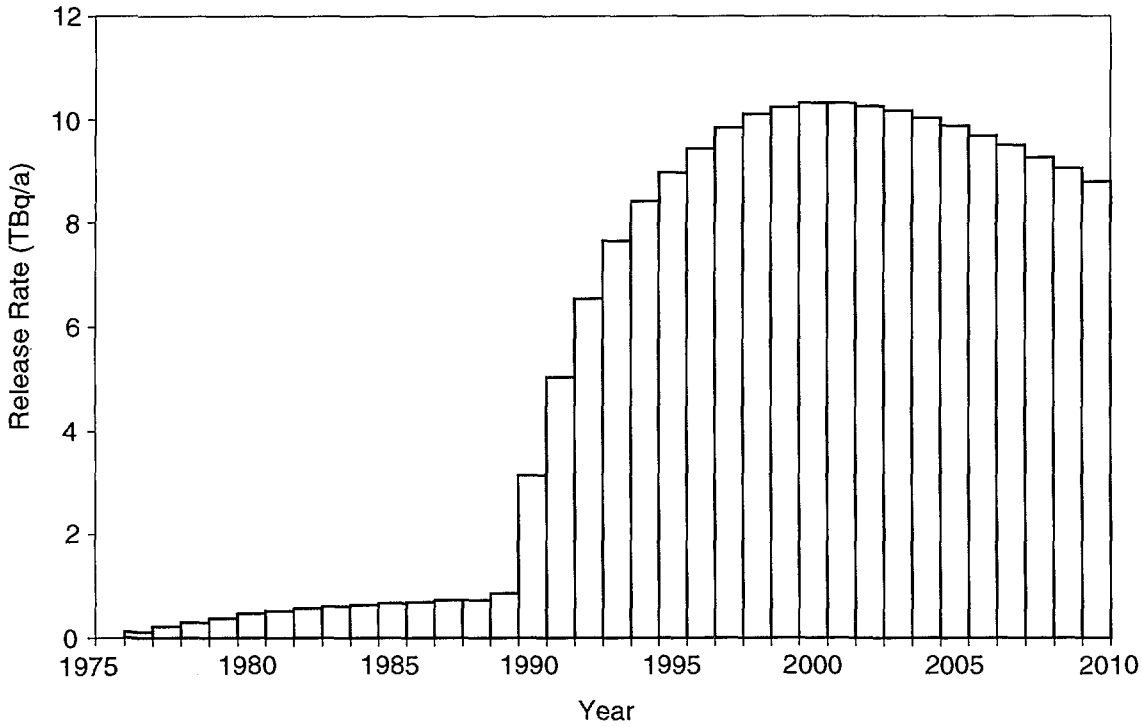

FIG. 43. Predicted rates of ^{3}H release into Fangataufa lagoon based on mixing model (reference case).

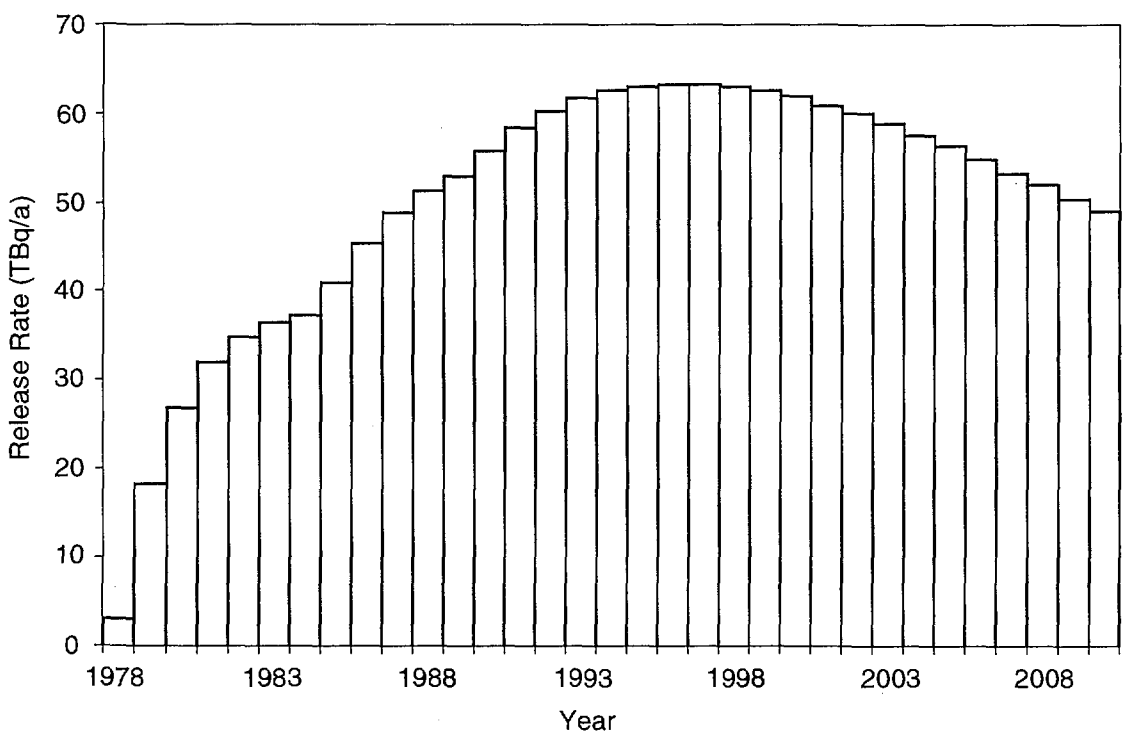

FIG. 44. Predicted rates of ^{3}H release into Mururoa lagoon, based on mixing model (reference case).

This result is considered to offer a strong indication that the estimated velocities for the flow of the contaminated water from the cavity-chimneys to the carbonates are reasonable. These numbers are clearly very important for estimating the radiological consequences of the tests.

In Section 5, the radionuclide transport was calculated with the velocities in the volcanics above the cavity-chimney as defined in Section 3.2 and used in the "mixing model" in Section 3.3, but assuming transport in the carbonates as in a 1-D single porosity porous medium, with a Darcy velocity of 2 m/a. The reasons for this assumption and the further details of the calculation are discussed in Section 5. This is equivalent to using, in the carbonates, the "advection - dispersion model", also tested for tritium release (see Appendix III). It is shown in this appendix that the "advection - dispersion model" generates a too rapid release of tritium to the lagoon, compared with the "mixing model". The assumption used in radionuclide transport calculations is thus conservative.

3.4. HYDROLOGICAL CONDITIONS OF A RE-EMERGING ATOLL DURING A PERIOD OF GLOBAL GLACIATION

3.4.1. Development of a freshwater lens

In this section, we investigate the likely hydrologic situation in Mururoa and Fangataufa in the case of a hypothetical future climatic situation, i.e. that of a new glacial period world wide which would be associated with a drop in sea level and thus would affect the hydrology of the atolls. Such a scenario is almost certain to occur in the future; it is however rather difficult to predict when. Several climate models have been developed, e.g. SKI 1997 and Provost et al., 1998, based on the Milankovich theory, which suggest that the climate may become colder within 10 000–20 000 years and even colder within 50 000–60 000 years after a brief warmer phase. Based on what happened during the last glaciation, which ended about 10 000 years ago, the sea level can drop by as much as 100 m or 150 m, due to the accumulation of ice in the cold regions. The climate of the atolls will also change, although this is less predictable (probably colder and wetter) and of a lesser consequence than the drop in sea level. Note that, during a glaciation, a 100 m drop in sea level can happen in a few thousand years, whereas the 100 m subsidence of the atolls by re-adjustment of the mantle would need about three million years (Guille et al., 1996, Chapter 4, para. 1), which is negligibly slow compared to the former one.

We will estimate the extent of the freshwater lens that will develop on the atolls, after they have become islands with a ground elevation between 50 and 150 m above sea level, receiving recharge from rainfall.

The shape of a freshwater lens in a carbonate island has been studied extensively (see e.g. Raeisi and Mylroie 1995). Because of the difference in density between sea water and freshwater, sea water is "pushed" down by the rainfall recharge water that infiltrates the porous limestone and a sharp interface develops, separating the two types of water. In natural conditions, the thickness of the transition zone between the two types of waters at depth on an island in an ocean with tides can be in the order of a few metres and up to 10 m. When pumping wells are installed, this thickness can increase up to some 10 m.

To predict the shape of the interface, common simplifications are to assume the medium to be homogeneous and isotropic, the interface to be sharp, i.e. neglecting the transition zone thickness, and to neglect the vertical components of the velocity field with respect to its horizontal components, the so-called classical "Dupuit" assumption. Based on the density difference of the two types of waters, the Ghyben-Herzberg relation states that the depth of the sharp interface below sea level is

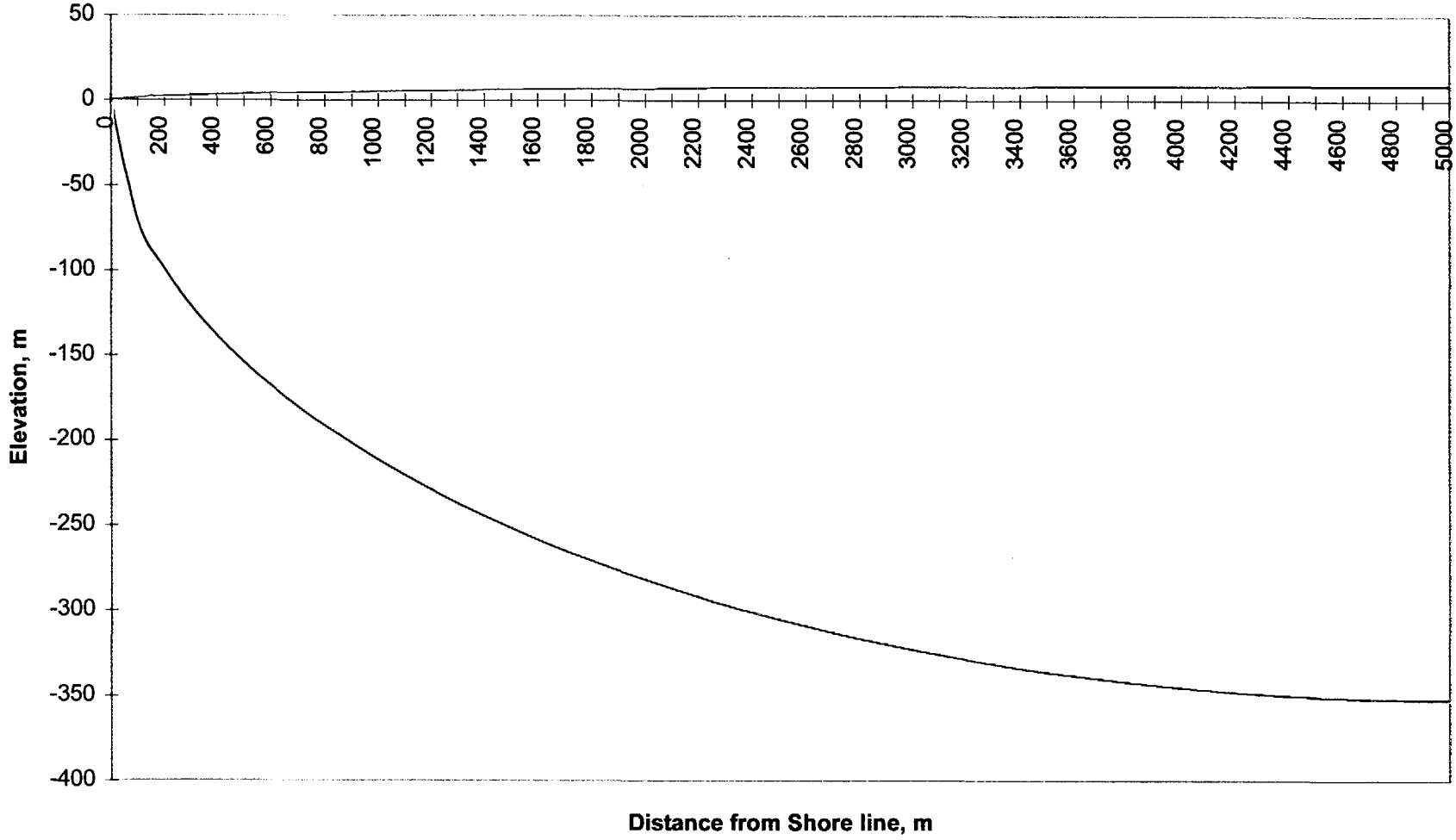

FIG. 45. Elevation of water table and sea water interface compared to sea level at Mururoa - Glaciation scenario.

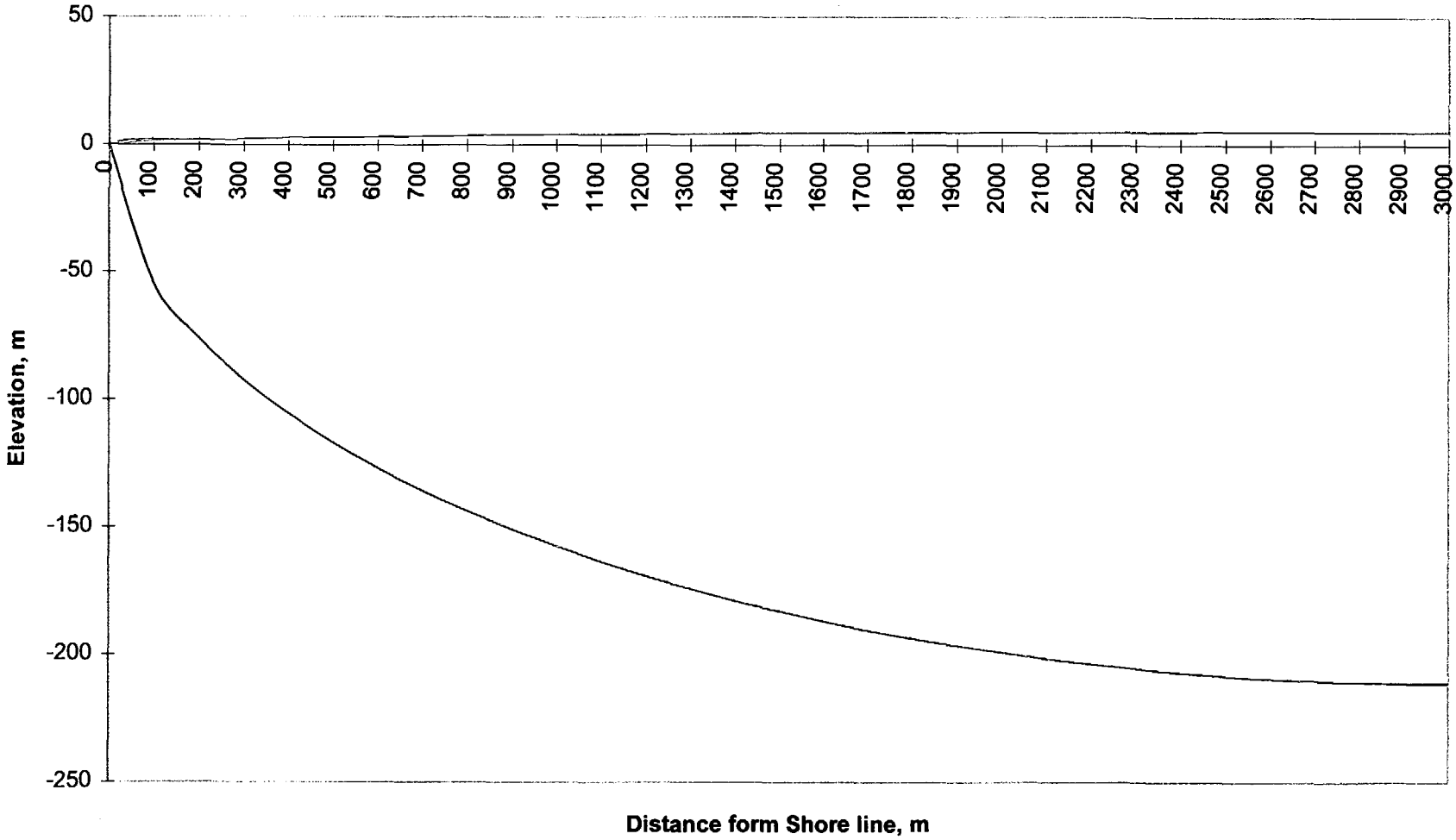

FIG. 46. Elevation of water table and sea water interface compared to sea level at Fangataufa - Glaciation scenario.

equal to 40 times the elevation of the water table above sea level (Henry 1964; Fetter 1972; Bear 1972, Vacher 1988, etc.). With this assumption the following equation can be derived:

$$h^2 = \frac{R}{K(1+\alpha)}\left(2Mx - x^2\right)$$

$$z = \alpha h$$

where

h is the elevation of the water table above sea level (m),
z is the depth of the interface below sea level (m),
R is the mean annual recharge rate by infiltration (m/s),
K is the limestone permeability (m/s),
x is the distance inland from shoreline (m),
M is the half width of the island (m),
α is the density difference $\rho_f/(\rho_s-\rho_f)$, in this case $\alpha = 40$,
ρ_s, ρ_f are the mass per unit volume of sea water (1025 kg/m^3) and freshwater (1000 kg/m$^{3)}$.

The shape of the water table and of the interface for Mururao and Fangataufa, were calculated, using the following parameters:

- Half width of the island M: Mururoa 5 km, Fangataufa 3 km.
- Recharge rate R: 0.4 m/a, as in Vacher 1988 for carbonate islands in a similar climate.
- Permeability K: 10^{-4} m/s, as estimated from fitting of the flow model against temperature data.

The results of this calculation are presented in Figs 45 and 46, and show that the depth of the interface can be as much as 350 m below the future sea level for Mururoa, and as much as 200 m for Fangataufa.

3.4.2. Potential contamination of a freshwater lens

Given the likely time of occurrence of this scenario, i.e. more than 10 000 years in the future, only plutonium is of concern, since all the ^{137}Cs and ^{90}Sr will have decayed.

The seven safety trials performed in the carbonates, four of which did not go critical while three did, were conducted between 1976 and 1980 on the rim of Mururoa at a depth greater than 280 m. If the sea level were lowered by 100 m or 150 m, the safety trials would be at a depth of 130 m to 180 m below the future sea level. As can be seen from Fig. 45, the trials would be in the freshwater lens at Mururoa if they were exploded at a distance of 350 m inland from the future shoreline, for the 150 m drop in sea level, or 700 m inland for the 100 m drop. The rim is about 400 m to 600 m wide, and the trial holes were on the lagoon side of the rim, sometimes even built on a platform some tens of metres into the lagoon. Furthermore, a drop in sea level of 100 m or 150 m would displace the shore line seaward by about 200 m to 240 m given a seaward slope of the atoll of 50° (see French Liaison Office Document No. 5, 1997, Fig. 9). Thus, there is every reason to believe that the sites of the safety trials would be inside the freshwater lens during a period of glaciation.

Will there still be plutonium from the safety trials available for dissolution at the time of the next glaciation? Given the centripetal flow velocity in the carbonates before the glaciation, the plutonium will have been transported inland. If we assume, for example, a Darcy velocity of 1 m/a, a porosity ε of 30%, a K_d for plutonium of 0.5 m^3/kg in the carbonates (see Section 5) and a carbonate density ρ_s of 2 200 kg/m^3, we obtain a retardation factor for plutonium transport of 2 500 and a

transport distance inland of 13 m per 10 000 years. It can thus be concluded that plutonium will still be in the vicinity of the sites of the safety trials after 10 000 or even 50 000 years in the future.

We can also estimate the volume of carbonate rock that will be contaminated with plutonium for a non-nuclear safety test (Category 5). In order to be conservative it is assumed that this plutonium will be at the solubility limit of 10^{-7} mol/L, i.e. 56 MBq/m^3 (with 1 mol of ^{239}Pu equal to 5.6×10^{11} Bq), although the range of solubility is 10^{-7}–10^{-9} mol/L and the value of 10^{-8} mol/L is recommended in Section 4.3.1. When plutonium is dissolved at the solubility limit, it migrates and sorbs on the carbonates with a K_d of 0.5 m^3/kg; in each m^3 of carbonates, there is thus $(\varepsilon + (1-\varepsilon) \rho_s K_d)$ C of plutonium in solution and sorbed, where C is the plutonium concentration in solution, i.e. 43 GBq of plutonium per m^3 of rock. As each safety test contains about 8 TBq of ^{239}Pu (Vol. 3 of this Technical Report), the plutonium contaminated volume of rock will be in the order of 200 m^3. This rock will contain about 70 m^3 of water with a plutonium concentration at the solubility limit. If we assume that the thickness of the contaminated zone is 10 m, the plutonium plume of each safety test in the carbonates will be spread over 20 m^2. Given that the time of occurrence of this scenario is uncertain, e.g. between 10 000 and 100 000 years from now, we do not take benefit of plutonium decay in the following assessment.

The presence of plutonium in the carbonates under the rim is therefore of concern for a glaciation scenario. It is, however, difficult to determine the plutonium concentration in the water pumped from a well in the freshwater lens that would intersect the plutonium contaminated plume. First, the wells will probably be drilled towards the centre of the island rather than towards the shoreline, since the sea water interface is at greater depth in the centre and the risk of upconing of the saltwater interface is lower. Second, if a well is drilled close to the shoreline, the resulting drawdown may raise the level of the interface by upconing and thus bring the site of the safety trials below the sea water interface and hence outside the freshwater lens. Third, the likelihood that a well would be drilled exactly at the location of a safety trial is rather small. Finally, not all the water extracted from the well will come from the deeper section contaminated with plutonium. We will assume, for example, that only 3% of the water extracted is plutonium contaminated. This is consistent with the assumption of a 10 m thick plutonium contaminated zone, compared with the 300 m thick freshwater layer in the carbonate. The plutonium concentration is at the assumed solubility limit, i.e. 10^{-7} mol/L, in the contaminated area since it is in contact with plutonium sorbed on the carbonate, resulting from the retarded transport from the near-by location of the safety test. If we calculate the concentration of plutonium in such a well, without taking into account any of the first three considerations, but taking the assumed dilution factor into account, we would obtain a concentration of plutonium in the well water of 3×10^{-9} mol/L, i.e. about 1.7 MBq/m^3. The corresponding radiological assessment is carried out in Vol. 6, Section 4.2 of this Technical Report.

However, the probability that a well will be drilled in the contaminated area is rather small: the total area of the emerged island will be on the order of 150 km^2, and the contaminated area is only 20 m^2 for each safety test. Since there are 4 safety trials that did not go critical, and since there may be more than one well drilled in the island in the future, let us say for instance 100 wells, the probability of having one well in a contaminated area could be about 5×10^{-5}. Of course the probability of drilling a well may not be uniformly distributed, and this number may be an underestimation. However, as seen in Fig. 45, the emerged island would be quite flat, with the major portion of the surface consisting of the former lagoon floor.

There are other sources of plutonium in the carbonates. First, the safety trials in the carbonates that did produce a small nuclear yield (3 tests in Category 4), should also be considered. The plutonium is then enclosed in the lava, but, with the assumed yield of 0.2 kt[4], the plutonium contamination is spread over an area of 150 m^2 (the cavity radius is 6.6 m). The calculations show

[4]The yield of these safety trials was rounded off from 0.15 kt to 0.2 kt in this assessment.

that the concentration of plutonium in the water of the contaminated zone is lower (around 0.15 MBq/m^3, see Section 5). The dose from a drinking water well would then be lower than for the previous case.

Finally, there will be plutonium released from the volcanics to the carbonates before the glaciation occurred. Indeed, the plutonium delivered to the carbonates from the volcanics will be mostly sorbed to the carbonate rocks and very slowly released to the lagoon. In the time frame of some 50 000 years, it can be assumed that most of the plutonium released from the volcanics will still be in the carbonates. When the freshwater lens develops, this plutonium sorbed on the rock will be slowly released to the freshwater. The concentration of the plutonium in the water released from the volcanics is on the order of 0.01 MBq/m^3 and will be in equilibrium with the sorbed plutonium. Therefore, plutonium in the freshwater will also be at this concentration. The area of concern is much larger than for the safety trials. The area corresponding to the 12 CRTV and the 3 Category 2 tests amounts in total to about 40 000 m^2. The category 1 tests release very little plutonium. The dose for a well drilled above a contaminated test site would be lower than for the areas close to the safety test, even without considering the effect of dilution and the probability of the drilling.

In summary, after a worldwide drop of sea level of 100-150 m due to a future glaciation, a freshwater lens would develop in the carbonates. This may generate doses to those inhabitants of the islands who would exploit the groundwater in the freshwater lens if a well was drilled into a contaminated area.

These doses could be large (see Vol. 6, Section 4.2 of this Technical Report) if a water supply well was drilled in the area contaminated by a safety trial that did not have a nuclear yield (a total of 4 such tests were done at Mururoa, and none at Fangataufa). However, the probability of drilling a well in a contaminated area is in the order of 5×10^{-5} and thus rather small. Other plutonium contaminated areas (safety trials that went critical or release of plutonium from the volcanics) would give doses much below the non-nuclear safety trials. It would appear, therefore, that it is only the case of the non-nuclear safety trials that may deserve more attention.

It should be noted that estimation of both, the probability and the consequences of events so far into the future, is extremely difficult. Thus, estimation of the probability of the emerged atolls being populated 10 000 to 50 000 years hence and the consequences of the plutonium contaminated water on humans at that time involve highly conjectural assumptions about many influential factors concerning the nature of civilisation at that time, their habits, awareness of (then "ancient") history, state of medical science (will cancer still be a serious disease?) and many more. Currently, we have no scientifically credible way to establish these probabilities.

As noted earlier, the probability that one or more groups of inhabitants of the atolls would drill into the plutonium plume is likely to be small. At even larger times into the future, when the period of glaciation has ended, the atoll would resubmerge, and the plutonium would also become progressively leached away and decay. The WG 4 recommends that the dose assessment group includes consideration of the possible dose implications of the glaciation scenario for a future population of the emerged atoll (see Vol. 6, Section 4.2 of this Technical Report).

4. SOLUTION SOURCE TERM

The purpose of this section is to estimate the leaching rate of radionuclides from the lava and the desorption of radionuclides from the rubble into the water of the cavity-chimney. This task is divided into the following four sub-tasks:

1. A review of radioanuclide release from the lava and rubble and comparison with independent data for natural basaltic and nuclear waste glasses.

2. Interpretation of CEA and IAEA measurements on the composition and the chemical form of radionuclides in the cavity-chimney.

3. Selection of appropriate sorption coefficients, K_d or other sorption parameters for the selected set of radionuclides and comparison with CEA data for Mururoa and other available data for similar radionuclide - rock systems.

4. Estimation of the initial radionuclide concentration in the carbonates.

4.1. RADIOACTIVITY RELEASE FROM LAVA

Radionuclides will migrate away from the cavity-chimney region by flowing groundwater. The dissolution or leach rate of radionuclides from the lava and rubble into the groundwater determines the source term for transport. This process depends on the available surface area of the rock matrix, composition, pH and temperature of the groundwater and the chemical properties of the particular element. Modelling the release is further complicated by the distribution of the radionuclides between the lava and the rubble.

A number of leaching studies on nuclear melt glass and rock debris have been conducted to determine the rate at which melt glass reacts and releases radionuclides (Kersting 1996, and references herein, Smith 1993). As can be expected, due to the large surface area, higher leach rates were determined with smaller than with larger size fractions. Measured average leach rates ranged from 1×10^{-1} kg-glass/m^2 d for ^{22}Na to 1×10^{-4} kg-glass/m^2 d for ^{54}Mn. Determined average leach rates are:

$$^{131}\text{I}\ (9 \times 10^{-2}\ \text{kg/m}^2\ \text{d}) > {}^{129+132}\text{Te} > {}^{124+127}\text{Sb} > {}^{137}\text{Cs} > {}^{237}\text{U} > {}^{58+60}\text{Co} > {}^{103+106}\text{Ru} > {}^{141+144}\text{Ce} > {}^{54}\text{Mn} > {}^{95}\text{Zr} > {}^{239+240}\text{Pu}\ (3 \times 10^{-6}\ \text{kg/m}^2\ \text{d})$$

Experiments showed that the leach rates from both lava and rubble are low. More than 98% of the radionuclides remained in the glass or in the rubble after one year of leaching. The leach rates were higher from the rubble than from lava.

A vast body of data obtained from leaching studies of glasses designed for the long term disposal of high level nuclear waste show that, after an initial time dependent leaching period which was also observed in the above described experiments, the radionuclides are leached at the dissolution rate of the glass (Grauer 1983, Grauer 1985 and references herein). The following corrosion rates of high level waste glasses were observed in long term experiments at:

90°C: 3.7×10^{-2} kg/m^2 a; and
55°C: 3.7×10^{-4} kg/m^2 a.

The Swiss Kristallin-I HLW repository study assumes a glass corrosion rate of 3×10^{-4} kg/m^2 a (NAGRA 1994, p. 39). The CEA study estimates 3×10^{-6} kg/m^2 a. If the lava is at 20°C, a further

TABLE Va. SELECTED K_d (m^3/kg) VALUES FOR CAVITY-CHIMNEY WATERS AND COMPARISON WITH THE CEA AND OTHER LITERATURE DATA, FOR FISSION PRODUCTS

Element	Selected Value	French Data	Basalt[a]	Tuff[a]	Granite	Dome Salt[a]	Granite[b] (low salinity)	Granite[b] (high salinity)
^{79}Se (reducing)	0-0.01		0.02	0.003	0.003	0.1	0.0005	0.0001
(oxidising)			0.005	0.001	0.001	0.07		
^{85}Kr	0		0	0	0	0	-	-
^{90}Sr	0.008 - 0.1	0.02	0.1	0.1	0.012	0.008	-	-
^{93}Zr	0.5		0.5	0.5	0.5	0.5	1 - 2	1 - 2
^{93m}Nb	0.01 - 0.03		0.1	0.1	0.1	0.05	1 - 2	1 - 2
^{99}Tc (reducing)	0 - 0.01		0.02	0.005	0.004	0.005	0.05 - 0.2	0.05 - 0.2
(oxidising)			0	0	0	0	0.0002	0.0002
^{106}Ru	0.01 - 0.03[c]							
^{107}Pd	0.05		0.05	0.05	0.01	0.005	0.001 - 0.1	0.0001 - 0.1
^{126}Sn (reducing)	0.01 - 0.03		0.05	0.005	0.01	0.01	0.001 - 0.2	0.0001 - 0.5
(oxidising)			0.5	0.5	0.5	0.1		
^{125}Sb	0 - 0.01							
^{129}I	0		0	0	0	0	0.0002 - 0.0008	0.0001 - 0.0002
^{134}Cs	0.3		-	-	-	-	-	-
^{135}Cs	0.3		0.3	0.1	0.3	0.8	0.05 - 0.4	0.01 - 0.1
^{137}Cs	0.3	0.2	0.3	0.1	0.3	0.8	0.05 - 0.4	0.01 - 0.1
^{147}Pm	0.05							
^{151}Sm	0.05		0.05	0.05	0.1	0.05	-	-
^{155}Eu	0.05							

[a] Serne and Releya 1981, Tables 6 and 7.
[b] Hakanen and Hölttä 1992, Appendix I, Table I.
[c] Value from ^{126}Sn.
- No data available.

TABLE Vb. SELECTED K_d (m^3/kg) VALUES FOR CAVITY-CHIMNEY WATERS AND COMPARISON WITH THE CEA AND OTHER LITERATURE DATA, FOR ACTIVATION PRODUCTS

Element	Selected Value	French Data	Basalt[a]	Tuff[a]	Granite	Dome Salt[a]	Granite[b] (low salinity)	Granite[b] (high salinity)
^{14}C	0		0	0	0	0	0.0001 - 0.001	0.0001 - 0.001
^{36}Cl	0		0	0	0	0	0.00001 - 0.0001	0.00001
^{55}Fe	0.01 - 0.03[c]		-	-	-	-	-	-
^{60}Co	0.01 - 0.03[c]		-	-	-	-	-	-
^{59}Ni	0.01 - 0.03		0.05	0.05	0.01	0.01	0.1 - 0.2	0.05 - 0.1
^{63}Ni	0.01 - 0.03		0.05	0.05	0.01	0.01	0.1 - 0.2	0.05 - 0.1
^{152}Eu	0.05		0.05	0.05	0.1	0.05	-	-
^{154}Eu	0.05		-	-	-	-	-	-
^{205}Pb	0.005		0.025	0.025	0.005	0.005	-	-

[a] Serne and Releya 1981, Tables 6 and 7.
[b] Hakanen and Hölttä 1992, Appendix I, Table I.
[c] Value from ^{126}Sn.
- No data available.

reduction by a factor of 27 of the 55°C corrosion rate can be calculated by using an activation energy of 75 kJ/mol. The calculation results in a leach rate of 1.1×10^{-5} kg/m^2 a. This is only a factor of 3.7 different from the CEA estimate of 3×10^{-6} kg/m^2 a and is a reasonable estimate which will serve as a base value in Section 5.1.2 in conjunction with lifetime estimates for the lava glass.

4.2. K_d VALUES FOR SELECTED RADIONUCLIDES AND COMPARISON WITH CEA AND OTHER DATA

4.2.1. Selected radionuclides

Working Group 3 has provided a list of 40 radionuclides that were generated in the CEA tests at Mururoa and Fangataufa (Vol. 3 of this Technical Report).

4.2.2. K_d values

As with stable isotopes, radionuclides can undergo a variety of chemical and physical reactions and processes as they come into contact with the solid and liquid phases that make up the saturated rock mass. Although these reactions and processes are not all well understood in detail, the net result, which is of special significance to the study of radionuclides releases, is that some radionuclides may effectively move through the geosphere at a much lower rate than the groundwater, i.e. the radionuclides are retarded relative to the groundwater by sorption onto the rock. Their effectively longer passage time also allows greater decay of the radioactivity before it can reach the biosphere.

The nature and intensity of the chemical and physical interactions between the rock and the radionuclides can be strongly dependent on both the magnitude and chemical nature of the surfaces

TABLE Vc. SELECTED K_d (m^3/kg) VALUES FOR CAVITY-CHIMNEY WATERS AND COMPARISON WITH THE CEA AND OTHER LITERATURE DATA, FOR FUEL PRODUCTS

Element	Selected Value	French Data	Basalt[a]	Tuff[a]	Granite	Dome Salt[a]	Granite[b] (low salinity)	Granite[b] (high salinity)
^{3}H	0	0	0	0	0	0	-	-
^{229}Th	0.5		0.5	0.5	0.5	0.1	0.02 - 0.5	0.2 - 0.5
^{233}U (reducing)	0.01		0.01	0.005	0.005	0.003	0.1 - 1	0.1 - 1
(oxidising)			0.003	0.001	0.001	0.0015	0.001 - 0.005	0.001 - 0.005
^{236}U (reducing)	0.01		0.01	0.005	0.005	0.003	0.1 - 1	0.1 - 1
(oxidising)			0.003	0.001	0.001	0.0015	0.001 - 0.005	0.001 - 0.005
^{237}Np (reducing)	0.2 - 0.5		-	-	-	-	0.2 - 0.5	0.2 - 0.5
(oxidising)			-	-	-	-	0.002 - 0.005	0.002
^{238}Pu (reducing)	0.5		0.5	0.5	0.5	0.5	0.5 - 2	0.5 - 2
(oxidising)			0.04	0.04	0.1	0.05	0.1 - 1	0.1
^{239}Pu (reducing)	0.5	10	0.5	0.5	0.5	0.5	0.5 - 2	0.5 - 2
(oxidising)			0.04	0.04	0.1	0.05	0.1 - 1	0.1
^{240}Pu (reducing)	0.5	10	0.5	0.5	0.5	0.5	0.5 - 2	0.5 - 2
(oxidising)			0.04	0.04	0.1	0.05	0.1 - 1	0.1
^{241}Pu (reducing)	0.5		0.5	0.5	0.5	0.5	0.5 - 2	0.5 - 2
(oxidising)			0.04	0.04	0.1	0.05	0.1 - 1	0.1
^{242}Pu (reducing)	0.5		-	-	-	0.5 - 2	0.5 - 2	-
(oxidising)			-	-	-	0.1 - 1	0.1	-
^{241}Am	0.05	10	0.05	0.05	0.2	0.3	0.04 - 0.5	0.04 - 0.5

[a] Serne and Releya 1981, Tables 6 and 7.
[b] Hakanen and Hölttä 1992, Appendix I, Table I.
- No data available

TABLE VI. SELECTED K_d (m^3/kg) VALUES FOR CHEMICAL ELEMENTS IN CAVITY-CHIMNEY WATERS

Element	K_d
^3H (H_2O)	0
C	0
Cl	0
Fe	0.01–0.03
Co	0.01–0.03
Ni	0.01–0.03
Se	0–0.01
Sr	0.008–0.1
Zr	0.5
Tc	0–0.01
Ru	0.01–0.03
Pd	0.05
Sn	0.01–0.03
Sb	0–0.01
I	0
Cs	0.3
Pm	0.05
Sm	0.05
Eu	0.05
U	0.01
Np	0.2–0.5
Pu	0.5
Am	0.05

which are contacted by the radionuclides during flow. Although the detailed nature of the reactions is often very complex, several simple models have been used to attempt to assess the significance of these processes in affecting radionuclide transport. Sorption processes are usually described by a linear isotherm, i.e. a constant distribution coefficient K_d which is defined as

$$K_d = \frac{\textit{concentration of species sorbed on the solid (mass per unit mass of solid)}}{\textit{concentration of species in solution (mass per unit volume of solution)}} .$$

K_d values describe the equilibrium distribution between a solid phase and liquid phase solute concentration and assume reversibility of the sorption reaction. Because often a fraction of the solute reacts irreversibly with the surface, and distribution coefficients may not have been experimentally determined strictly at equilibrium, a distribution ratio R_d is normally used instead of the thermodynamic constant K_d. To indicate such possible differences, for reasons of comparability with the CEA data, this paper uses the CEA K_d nomenclature.

Tables Va to Vc list the K_d values for cavity-chimney waters for the selected radionuclides together with the CEA and other literature data. Because sorption is mostly independent of the isotopic composition, the K_d values are summarised in Table VI for the chemical elements of interest to this Study. These values were derived for modelling the radionuclide migration through the volcanics. They are also applied to the carbonates because the results of experimental investigations into the sorption of radionuclides on carbonatic rocks made available by the Bundesamt für Strahlenschutz (BfS), Germany were consistent with these data.

4.3. PLUTONIUM CONCENTRATIONS IN THE CARBONATES

As noted earlier, a number of safety trials were conducted in the carbonate rock at Mururoa which constitute a major source of radionuclides, in particular plutonium, in the carbonate zone. These tests are shown in Fig. 1 and described in the accompanying text (Table I). The chemical behaviour of plutonium in terms of solubility and speciation (colloids) in the carbonates is of particular interest because of the proximity to the biosphere.

4.3.1. Plutonium concentration/solubility

The remaining plutonium from the four safety trials that had no nuclear yield (Category 5, Fig 1) should be considered as a source for potential release to the biosphere. After chemical detonation of a safety trial, approximately 3.7 kg plutonium remain, totalling about 15 kg of uncontained plutonium in the carbonate zone. It can be assumed that the conventional explosive ruptured the device container and the metallic plutonium oxidises upon contact with the water of the carbonates which is almost of sea water composition. The reaction occurs immediately and produces either a) PuO as an intermediate product and hydrous Pu(IV) oxide that is finely dispersed by the hydrogen gas stream stemming from the metal oxidation reaction (Lai and Goya 1996) or b) PuOH, plutonium monoxide monohydride (Haschke 1992, Haschke 1995). PuO and PuOH are not stable in water and undergo further oxidation mainly to plutonium dioxide, PuO_2, and/or hydrous plutonium (IV) oxide, PuO_2 xH_2O and, to a lesser extent to amorphous plutonium (IV) hydroxide, $Pu(OH)_4$(am), often referred to as Pu(IV) polymer. Hydrous plutonium (IV) dioxide and Pu(IV) polymer are known to form colloidal solutions under certain conditions and are therefore often referred to as Pu(IV) colloid. Hydrous Pu(IV) oxide is considered an intermediate form between PuO_2 and $Pu(OH)_4$(am). It is much less crystalline than PuO_2 but more ordered than $Pu(OH)_4$(am). The solubility of plutonium (IV) oxide and hydroxide depends on the crystallinity of the solid. Plutonium (IV) hydroxide or Pu(IV) polymer is a green gelatinous amorphous solid and is, in strict thermodynamic terms, a non-defined solid. Its solubility depends strongly on the genesis and age of the solid. This leads to large solubility variation (Nitsche et al., 1992a, Nitsche 1992c). The solubility product constant, log K_S, for the dissolution reaction

$$Pu(OH)_4(am) = Pu^{4+} + 4OH^-$$

ranges between -56.30 and -57.85.

The experimentally determined log K_S values for the dissolution of crystalline PuO_2 according to the reaction

$$PuO_2(c) + 2H_2O = Pu^{4+} + 4\ OH^-$$

range between -60.20 and -62.5.

The solubility of radionuclides in sea water depends not only on the solubility controlling radionuclide-bearing solid phase but also on the oxidation state of the radionuclides in solution and the concentration of water constituents that can form soluble radionuclide complexes (Silva and Nitsche 1995). Complexation of radionuclides increases their concentration in solution and may also increase release rates. In water, inorganic ligands such as hydroxide, chloride, sulphate and carbonate can form soluble complexes with plutonium.

A number of studies of the solubility of plutonium in various waters including artificial sea water have been conducted in connection with the nuclear waste repository selection in the USA. Details are given in Appendix IV. These experiments show that the solubility controlling phase in supersaturated solutions of tetravalent plutonium is, to a large degree, amorphous $Pu(OH)_4$ that is also called Pu(IV) polymer. Its solubility in water depends on the chemical composition of the water

and therefore varies between 1.1×10^{-6} mol/L (6.2×10^{8} Bq/m^3) and 4.5×10^{-7} mol/L (2.5×10^{8} Bq/m^3). In a brine with a composition close to that of sea water, 3.5×10^{-7} mol/L (1.9×10^{8} Bq/m^3) was determined. An undersaturation experiment where amorphous $Pu(OH)_4$ was brought in contact with a "seawater-like" brine determined a somewhat lower solubility of 8×10^{-8} mol/L (4.6×10^{7} Bq/m^3).

Different dissolution tests of plutonium metal in sea water have shown that either a) amorphous $Pu(OH)_4$ and PuO_2 of, at best, very low crystallinity (Lai and Goya 1966) or b) crystalline PuO_2 (Haschke 1995) is produced. It cannot be excluded that the low crystalline PuO_2 may convert to amorphous $Pu(OH)_4$. Based on the solubility measurements of $Pu(OH)_4$ in laboratory experiments, the solubility of plutonium that may be released from the safety trials should be about 10^{-8} mol/L (5.6×10^{6} Bq/m^3) which is about the value for $Pu(OH)_4$(am). This is, of course, a very conservative assumption and does not consider the much lower solubility of crystalline PuO_2(c). The solubility assumptions in the CEA study were based on an initial measurement where practically all of the deposited activity is present as plutonium (IV) dioxide and less than 1% exists as plutonium hydroxide. This may be supported by the results of Haschke, but is by no means conservative.

Modelling calculations (Puigdomènech and Bruno 1991), using the program EQ3NR, determined a solubility of 10^{-8} mol/L (5.6×10^{6} Bq/m^3) for amorphous $Pu(OH)_4$ in granitic groundwater at pH 8, and about 10^{-10} mol/L (5.6×10^{4} Bq/m^3) as the lowest solubility using the lowest possible Eh at this pH. Solubility calculations for highly crystalline plutonium dioxide, PuO_2(c) in the Yucca Mountain J-13 water determined a solubility of about 5×10^{-13} mol/L (2.7×10^{2} Bq/m^3) (Wilson and Bruton 1989).

CEA modelling calculations (French Liaison Office Document No. 8, 1996, IV, p. 3) show a somewhat higher plutonium concentration in sea water (7.3×10^{-8} mol/L or 4×10^{7} Bq/m^3 for Eh = + 500 mV and 3.1×10^{-7} mol/L or 1.7×10^{8} Bq/m^3 for Eh = –300 mV) than the calculations of Puigdomènech and Bruno. This may be due to a different data set for the aqueous complexes. The stability constants of the plutonium (IV) carbonate complexes are too high in several databases.

The CEA scientists report maximum $^{239+240}$Pu concentrations of 8 Bq/m^3 (1.5×10^{-14} mol/L ^{239}Pu) that were measured at a distance of 10 m from a non-yield safety trial 15 years after the test was conducted (French Liaison Office Document No. 8, 1996). This result may indicate that (a) only very small amounts of plutonium are dissolved and most of the plutonium is still in solid form, or (b) dissolved plutonium is retained on the surface of the rocks in the carbonates, or (c) the dissolved plutonium is diluted by sea water far below the solubility limiting concentration. Using the $Pu(OH)_4$ (am) solubility of 10^{-8} mol/L that is recommended by this report, 6.3×10^{6} m^3 or 1.1×10^{7} m^3 water would be required to dissolve the overall plutonium mass of about 15 kg involved in the four safety trials without criticality or the about 26 kg involved in the 7 safety trials in the carbonate. This includes the mass of ^{239}Pu that underwent fission is included. For a dilution of the respective plutonium masses to 10^{-14} mol/L, the required sea water volumes would be 6.3×10^{12} m^3 and 1.1×10^{13} m^3.

4.3.2. Speciation of soluble plutonium and colloidal plutonium

In aqueous solution, plutonium can exist in four different oxidation states, Pu(III), Pu(IV), Pu(V), and Pu(VI). The distribution between the oxidation states depends on the pH and Eh of the water. Low pH values tend to favour the lower oxidation states, whereas the higher oxidation states become more accessible at near neutral and basic pH. The same behaviour can be observed for reducing or oxidising Eh conditions where the oxidation states Pu(III) and Pu(IV) or Pu(V) and Pu(VI), respectively, are stabilised (Silva and Nitsche 1995).

Pentavalent plutonium has been found to be the main oxidation state in various natural waters (Choppin and Kobashi 1990). 77% of plutonium was present as Pu(V) in 0.22 μm filtered waters from the Irish sea near a nuclear fuel reprocessing plant. Laboratory experiments showed that mainly pentavalent and small amounts of hexavalent plutonium species in solution are in steady state equilibrium with solid $Pu(OH)_4$ (am) (Rai and Swanson, 1981, Nitsche et al. 1992a and 1992b). The solutions were filtered through filters of a few nanometres in size (2 or 4 nm) to exclude suspended colloidal plutonium. In surface and sea waters, ratios of colloidal plutonium to dissolved plutonium were up to 250:1 when the colloidal material was separated by filtration through 0.22 μm filters.

Penrose et al., 1987, observed reduction of Pu(V) in laboratory solutions of near neutral pH (5–7) by sediment suspensions that were obtained from a deep, high sedimentation area of Lake Michigan. The sediment had less than 3% of organic matter, which may be enough to act as the potential reducing agent. As little as 0.1 mg humic material in filtered sea water was sufficient to reduce Pu(VI) at a concentration of 10^{-10}mol/L to 30% Pu(V) and 70% Pu(IV) (Choppin 1991). Such mechanisms may reduce the soluble plutonium to $Pu(OH)_4$ (am) or even $Pu(OH)_3$. If the reduced plutonium remains bound to the sediments, it would less likely take part in the dissolution process.

The CEA report is in agreement with this observation. Plutonium was mainly present as Pu(V) and Pu(VI) in lagoon surface waters and as Pu(IV) and Pu(III) in the lagoon sediments (French Liaison Office Document No. 8, II, 1996, p. 21).

4.3.3. Plutonium (IV) colloid

Tetravalent plutonium can exist in groundwater under certain conditions in colloidal form. Two different types of colloids have been identified in groundwater: (1) intrinsic plutonium or real colloids that are mainly produced through plutonium hydrolysis, and (2) pseudo colloids that are formed by sorption of either plutonium ions or intrinsic colloids on groundwater colloids. Groundwater colloids are composed of inorganic water constituents or a mixture of both or of microorganisms (Kim 1991, Silva and Nitsche 1995). Their size is usually below 0.45 μm.

During the process of dissolution of glassy lava, intrinsic and pseudo plutonium colloids can form. Their migration behaviour can be very different from that of soluble species and precipitates and their role in the plutonium transport process is not well understood (McCarthy and Zachara, 1989). Colloid formation can increase the plutonium concentration above the solubility limit, and therefore, increase the overall amount of plutonium that is available for transport.

The stability of Pu(IV) colloid depends on its size, the pH and the ionic strength of the solution. Rai and Swanson 1981 found that the stability of intrinsic Pu(IV) colloids decreases with decreasing pH and ionic strength. The colloids are most stable at low pH and low ionic strength. Rai and Serne 1979 found that, if the plutonium concentration in solution at a given pH falls below the $Pu(OH)_4$ solubility line, the colloid would not form. This may most likely be the case for the CEA tests. Zhao et al. 1997 experimentally determined, however, a somewhat surprising and contradictory result, namely that the relative Pu(IV) colloid stability increases in the pH range of 7 to 11 with increasing ionic strength of the solution.

Intrinsic Pu(IV) colloids can have a size ranging from 1μm to 1 nm in diameter, depending on the method of colloid generation (Rundberg et al., 1988, Triay et al., 1991, Ichikawa and Sato 1984). Colloids larger than 1 μm tend to agglomerate and precipitate.

Intrinsic and pseudo colloid transport can play an important role for a variety of radionuclides in addition to plutonium. The CEA study does not address colloidal radionuclide transport which is probably due to the fact that it is not sufficiently well understood in order to model it. As one can

most likely exclude intrinsic plutonium colloid formation, the formation of plutonium pseudo colloids may still occur.

In a very recent abstract of a paper, Kersting and Thompson (1997) state: *"In order to investigate the migration of radionuclides via colloids we carried out a series of filtration experiments using groundwater pumped from wells down gradient from an underground nuclear test event. We analysed unfiltered groundwater, colloidal material caught on a series of filter sizes, and the ultrafiltrate for gamma-emitting radionuclides, tritium and plutonium. Tritium, ^{60}Co, ^{137}Cs, $^{152+154+155}Eu$ and Pu isotopes were detected in the unfiltered groundwater samples. Most of the activity was caught on the filters; the ultrafiltrate had only a few percent of the radionuclides other than tritium.*

The colloidal material consists of zeolites (mordenite), clays (illite), and cristobalite (SiO_2). These minerals are consistent with the lithology of the host aquifer (volcanic tuff). We conclude that radionuclides can and do bind to colloids that then may be transported significant distances in the saturated zone."

5. GEOSPHERE TRANSPORT

5.1. INTRODUCTION

As noted earlier in this report, the only mechanism by which radionuclides from the explosion cavities can reach the biosphere naturally, i.e. except through some form of human intrusion, such as drilling into the cavities, is by transport in the groundwater. Determination of the natural rate of groundwater movement through the geosphere and its change by the explosions, is an essential first step towards establishing the rate at which the radionuclides will move towards the biosphere. This topic has been discussed in Section 3.

The water flow through the geosphere can be characterized by the Darcy velocity. This is a value given by the ratio of the total volume (or flux) of water passing through a given cross-sectional area in unit time, i.e. it is assumed that flow occurs across the entire area. In reality, of course, flow can occur only through the connected pathways within the rock. Thus, if the connected porosity is 10% (i.e. 10% of the area is available for flow) the velocity through the particle spaces (or particle velocity) will be 10 times greater than the Darcy velocity. The situation is complicated further when the detailed structure of the connected pathways, usually referred to as pore spaces, is considered. Some pores may be isolated from the flow.

Sorption of radionuclides, (see Section 4), is another effect that has to be taken into account when geosphere radionuclide transport is assessed. As a consequence of sorption, most radionuclides do not move through the geosphere at the same rate as the groundwater. The transport of radionuclides by groundwater and the retardation of radionuclides on the rock has to be modelled. The simplest way of doing this is by the application of the single porosity model which assumes one dimensional flow through a homogeneously porous medium. The mean rate of transport is described by a velocity (assumed constant) and a dispersion term which accounts for mechanical dispersion and molecular diffusion, if this is considered significant. Radioactive decay is normally incorporated into the model. Single porosity models are popular because of their simplicity and the ability to obtain analytical solutions for simple boundary value problems. They are most applicable where the pore distribution in the rock is uniform.

The single porosity model has been used in all calculations of radionuclide transport in Mururoa and Fangataufa by CEA scientists. A single porosity model is used in this report for analysis of radionuclide migration through the carbonates.

The single porosity model is not an adequate representation of transport where flow occurs predominantly along discrete fractures with preferred orientation, and where much of the porosity within the much more conductive fracture network is "dead volume", in which the water is stagnant. The dual porosity model was introduced to account for flow in such systems. In this model, the fluid phase is divided into a mobile component, the water that flows through the conductive fractures, and an immobile component, the porous matrix. Interchange between the mobile and immobile phases occurs only by molecular diffusion.

The dual porosity model has been chosen for modelling radionuclide transport through the volcanics in this study because of the fractured nature of these rocks. It is possible that the fracturing could be sufficiently pervasive so that the rock mass tends to behave effectively as a homogeneously permeable medium to which a single porosity may be applicable. However, for similar circumstances, double porosity or fracture flow models tend to predict earlier releases of radionuclides with less retardation than predicted by the single porosity models. It was felt, therefore, that the dual porosity model, by over predicting releases, would be a conservative way to estimate releases to the biosphere at Mururoa and Fangataufa.

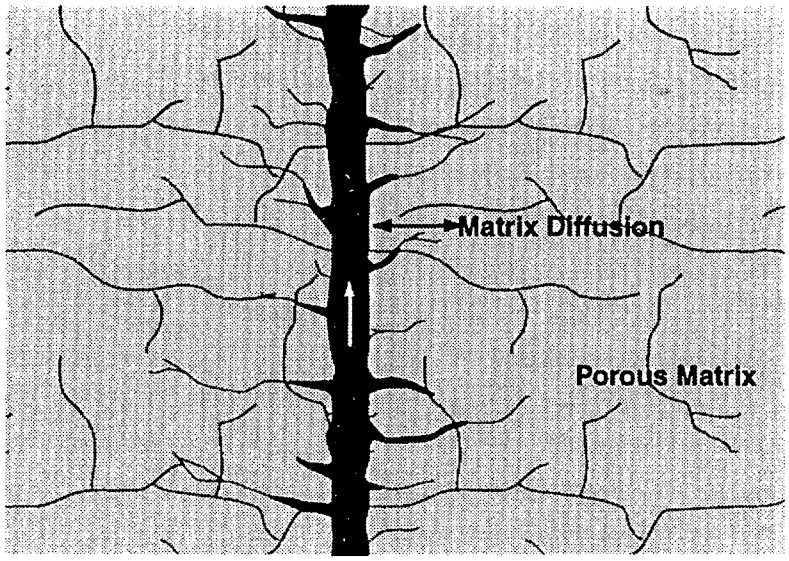

Transport along Fractures with Diffusion into Porous Matrix

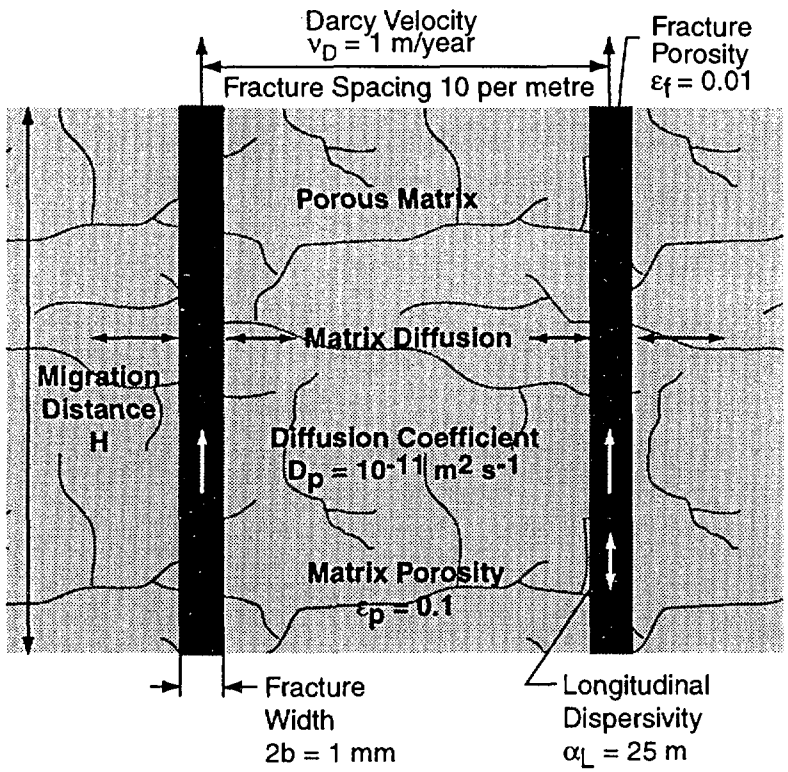

Idealized Dual Porosity Model

FIG. 47. Transport in fractured rock and idealized dual porosity model.

Figure 47 depicts transport in fractured rock along with the idealised dual porosity model. The parameters required for the model are shown on the diagram together with the selected values considered appropriate to model transport in the volcanic rock above a normal (Category 1) test. Details of the various categories of test are described below, and have been defined in Fig. 1 and Table I.

Figure 47 shows the base case, in which a fracture width of 1 mm and a fracture frequency of 10 per metre is assumed. This case represents a fracture porosity of 0.01 and a velocity of water in

the fractures that is 100 times the Darcy velocity. This results in a relatively high advective transport of radionuclides. In this respect, as noted earlier, this model is conservative with respect to a single porosity model.

With this background, we will now turn to a more detailed discussion of the model and its application to the study of radionuclide transport through the geosphere for the particular case of Mururoa and Fangataufa.

The starting point for the transport calculations is the radioactively contaminated water that fills the cavity-chimney volume.

As mentioned earlier the list of radionuclides generated by the explosion (see Table X in Vol. 3 of this Technical Report) was reduced to those 33 that may need to be considered as contributors to the overall release (see Table IX). The relevant chemical properties of these radionuclides are the subject of Section 4.

Particular attention is paid to plutonium. In the release calculations a conservative approach has been applied as it was assumed that 95% of the plutonium is initially immobilized in the lava and 5% is assumed to be deposited in an exchangeable form on the rubble or in solution in the cavity-chimney waters. CEA scientists assumed that 100% of the plutonium was trapped in the lava. The assessment provided in Vol. 3 of this Technical Report concluded that only 98% of the plutonium is trapped in the lava and that 2% are associated to the rubble. This is an important difference. On the other hand, the consequences of the differences between the 95% and 98% fractionation of plutonium are negligible.

The transport calculations are based on the concentration of radionuclides in the cavity-chimney waters (Solution Source Term) as a function of time (Section 5.2). They consider the flow of the radionuclide contaminated water from the explosion cavity-chimney to the top of the volcanic formations, i.e. the interface with the overlying carbonates (Section 5.3.1). Movements through the carbonates to the lagoon and/or to the ocean are discussed separately (Section 5.3.2).

The number of calculations necessary to assess the possible contribution of each radionuclide to the total release to the biosphere, for several combinations of assumed conditions in each case, is large. The result of each calculation is presented as a breakthrough curve, which is a graph showing the radionuclide release to the biosphere (usually taken to be the bottom of the lagoon) as a function of time. A selection of the most relevant breakthrough curves is provided in the text below. However, it does not seem appropriate or realistic to include all of these figures. The comprehensive collection of calculations of the solution source term and the geosphere transport of radionuclides can be found in Hadermann and Pfingsten 1998.

5.2. THE SOLUTION SOURCE TERM FOR LONG TERM GEOSPHERE TRANSPORT CALCULATIONS

The release of radionuclides into the cavity-chimney water as a function of time is based on two contributing sources:

(a) the radionuclides dispersed in the cavity-chimney and, for a subset of elements, sorbed on the rubble.

(b) the radionuclides incorporated into the lava meniscus at the bottom of the cavity-chimney.

Simple analytical expressions were derived to calculate the release rate. Given the uncertainties associated with each stage of the model calculations, from release into the cavity-chimney water to

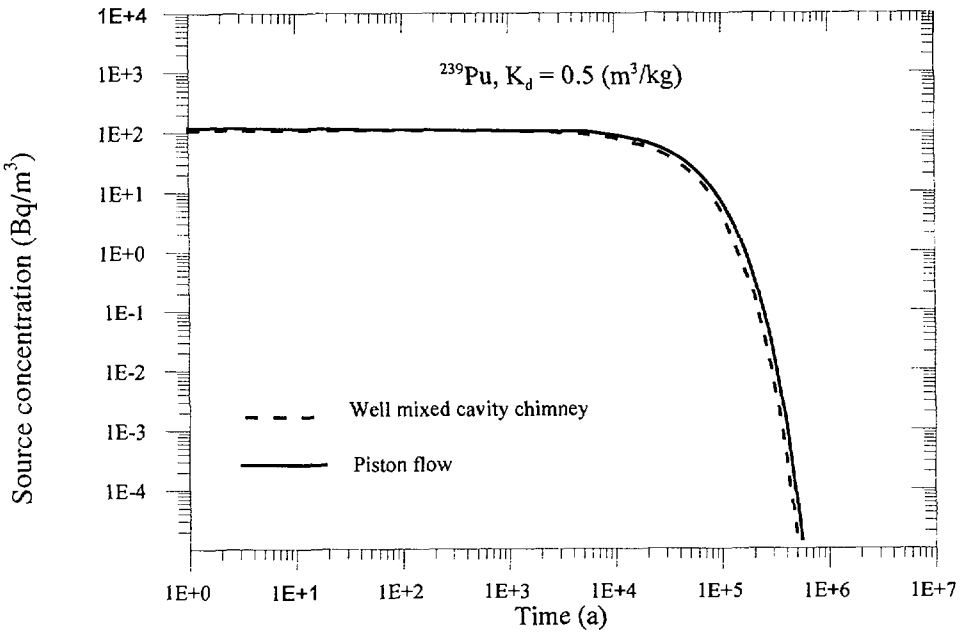

FIG. 48 Comparison of "piston flow" and "well-mixed cavity-chimney" concepts for the determination of the "Solution source term", exemplified for the rubble contribution to the ^{239}Pu concentration.

potential dose commitments, more refined models, although possible, are not considered to be justified.

Although the basic concept behind the models used here does not differ strongly from the approach taken by CEA scientists, there are marked differences in some of the details. These differences are noted in the text as they arise.

5.2.1. Release of radionuclides initially dispersed in the cavity-chimney

Those radionuclides that are not incorporated into the lava meniscus are initially dispersed in the cavity-chimney, in particular the rubble. We assume a homogeneous distribution within the cavity-chimney brought about by convection cells during the initial thermal phase of the explosion (see Section 3). After filling of the cavity-chimney with water the radionuclides are distributed between the liquid phase and the rubble surfaces, according to the sorption coefficient (K_d) provided in Section 4.

The well-mixed cavity-chimney is a key issue in the sense that freshwater entering the cavity-chimney from the bottom and the sides is assumed to instantaneously dilute the cavity-chimney waters. A more conservative model which is, however, inconsistent with the hydrological modelling results of Section 3, would consider piston flow from the bottom to the top of the cavity-chimney. The actual differences between those two modelling approaches in terms of plutonium release rate are indeed minor (Fig. 48).

The concentration in the cavity-chimney water C is given by

$$C = \frac{A}{V \varepsilon R} \quad , \qquad (1)$$

TABLE VII. COMPARISON OF DECAY CONSTANT λ AND MODIFIED DECAY CONSTANT $\tilde{\lambda}$ FOR THE VALUES h = 400 m, ρ = 2430 kg/m^3 AND ε = 0.3 (Hochstein and O'Sullivan 1985, Table 2.1)

Radio-nuclide	Decay constant λ (a^{-1})	Sorption coefficient K_d (m^3/kg)	Decay constant modified by sorption and Darcy flow $\tilde{\lambda}$ (a^{-1})		
			$v_D = 10^{-1}$ m/a	$v_D = 1$ m/a	$v_D = 10$ m/a
^{241}Am	1.604×10^{-3}	0.5	1.60×10^{-3}	1.61×10^{-3}	1.63×10^{-3}
^{240}Pu	1.060×10^{-4}	0.5	1.06×10^{-4}	1.09×10^{-4}	1.35×10^{-4}
^{239}Pu	2.875×10^{-5}	0.5	2.90×10^{-5}	3.17×10^{-5}	5.81×10^{-5}
^{237}Np	3.300×10^{-7}	0.2	1.06×10^{-6}	7.67×10^{-6}	7.38×10^{-5}
^{3}H	5.622×10^{-2}	0	5.75×10^{-2}	6.50×10^{-2}	1.40×10^{-1}
^{90}Sr	2.39×10^{-2}	0.01	2.39×10^{-2}	2.40×10^{-2}	2.53×10^{-2}
^{137}Cs	2.31×10^{-2}	0.3	2.31×10^{-2}	2.31×10^{-2}	2.31×10^{-2}
^{135}Cs	3.013×10^{-7}	0.3	7.91×10^{-7}	5.20×10^{-6}	4.93×10^{-5}
^{129}I	4.332×10^{-8}	0	8.33×10^{-4}	8.33×10^{-3}	8.33×10^{-2}

where A is the total activity in the cavity-chimney, V is the cavity-chimney volume, ε is the porosity of the cavity-chimney and R is the retardation factor, given by the expression

$$R = 1 + \frac{\rho(1-\varepsilon)}{\varepsilon} K_d \quad , \tag{2}$$

where, ρ is the rock density and K_d is the sorption coefficient (see Table VI).

From mass balance considerations we can deduce the following relationship for the change in cavity-chimney concentration with time:

$$\frac{dC}{dt} = -\lambda C - \frac{v_D}{h\varepsilon R} C \quad , \tag{3}$$

where h is the cavity-chimney height, λ is the decay constant, and v_D is the specific discharge (or Darcy velocity) from the cavity-chimney. The first term on the right describes radioactive decay within the cavity-chimney. The second term on the right describes the loss of activity by advection through the water. The solution to Eq. (3) is readily found to be

$$C = C_0 e^{-\tilde{\lambda} t} \quad , \tag{4}$$

where C_0 is the initial cavity-chimney water concentration, Eq. (1) at t = 0, and

$$\tilde{\lambda} = \lambda + v_D / \left(h\rho(1-\varepsilon) K_d + \varepsilon h \right) \tag{5}$$

Obviously, the second term on the right hand side of Eq. (5) is a correction to the radioactive decay term λ, which depends on the rate of water flow through the cavity-chimney.

Table VII lists the values of λ and $\tilde{\lambda}$ for various values of specific discharge (Darcy velocity) for a cavity-chimney height of 400 m, a rock density of 2430 kg/m^3 and porosity of 30% in the cavity-chimney. It is seen that $\tilde{\lambda}$ differs from λ only for very long lived sorbing radionuclides. This means that most of the activity of the sorbing radionuclides decays within the cavity-chimney and is not transported to the surrounding rock, i.e. beyond the walls of the cavity-chimney. This is especially the case for most of the short lived radionuclides. For non-sorbing radionuclides, the situation is different as, for example, even short lived tritium is transported out of the cavity-chimney in appreciable amounts.

The model described above has two main weaknesses:

(a) It assumes sorption equilibrium between the liquid phase and the bulk rock in the cavity-chimney. The size of the rock blocks in the rubble varies considerably, so that considerable time may be required before overall equilibrium is reached. Given the lack of detail regarding the size of the rock blocks in the rubble and the associated sorption process, it is not possible to quantify the time required to achieve equilibrium. This lack of detail is certainly compensated to some extent by neglecting irreversible sorption and choosing relatively low K_d values.

(b) The double porosity model used for the transport calculations described in this report assumes a constant rate of water flow into the overlying rocks. In reality, increases of temperature in the vicinity of each explosion increases the upward component of the natural groundwater velocity. The increase declines exponentially as the heat is dissipated. In the volcanics the pre-test Darcy velocity of 6-7 mm/a for Category 1 tests is increased to between 0.1 m/a to 1.3 m/a during the first year. It is declining to about half of this value after 10 a and to approximately 3 cm/a after 500 years. The velocity in the carbonates above the volcanics is not significantly affected by the tests. For Category 2 or Category 3 tests, the velocities above are increased by a factor of almost 50 and the velocities in the carbonates increase from 2 m/a prior to the tests to about 60 m/a after one year. They are declining to 5 m/a after 500 years (see Section 3). This variation of velocity with time has been taken into account in the model by selecting a high Darcy velocity.

Equation (3) is valid for a single decaying radionuclide only. For the actinides, which are members of decay chains, Eq. (3) is modified to

$$\frac{dC^i}{dt} = -\lambda^i C^i + \lambda^i \frac{R^{i-1}}{R^i} C^{i-1} - \frac{v_D}{h\varepsilon R^i} C^i \qquad (3a)$$

where i denotes the radionuclide in a decay chain

$$1 \rightarrow 2 \rightarrow \ldots\ldots i-1 \rightarrow i \rightarrow \ldots\ldots$$

This is a system of modified Bateman equations, for which an analytical solution can be obtained.

5.2.2. Radionuclide release from the lava

The model used to describe radionuclide release from the lava is, again, simple. The lava is assumed to consist of uniformly sized spheres with a constant dissolution rate and a congruent release of radionuclides (Hartley 1985). For these assumptions the release rate, $\hat{A}$ is given by

$$\hat{A}(t) = \frac{L}{\rho_L} \frac{S(t)}{V(t)} A(t) \quad , \qquad (6)$$

where L is the leach rate, ρ_L is the lava density, S(t) and V(t) are, respectively, the surface area and volume of the lava spheres, and A(t) is the radionuclide inventory in the lava. Please note that this equation is essentially a definition of the leach rate. The activity mass balance can then be written

$$\frac{dA}{dt} = -\frac{3}{\tau - t} A(t) - \lambda A \qquad for\ t \le \tau\ . \tag{7}$$

Here, $\tau = \rho_L r_o / L$ is the lava lifetime and r_0 the initial radius of the lava spheres. The analytical solution is

$$\hat{A}(t) = \frac{3A(t=0)}{\tau}\left(1 - \frac{t}{\tau}\right)^2 e^{-\lambda t} \qquad \text{for } t \le \tau. \tag{8}$$

The radionuclides released from the lava are assumed to be distributed instantaneously and homogeneously between the liquid and solid phase in the cavity-chimney according to the sorption coefficient K_d. This is a very conservative approach for those radionuclides that are strongly sorbing since their transport to the top of the cavity-chimney would, in reality, require considerable time.

Again, Eq. (7) is derived for a single radionuclide. For an isotope in a chain, the term $+\lambda^i A^{i-1}$ must be added on the right hand side of Eq. (7). Instead of solving the set of coupled differential equations, we added the inventories of all precursors to the radionuclide under consideration. This is conservative and has little effect on the total release rate to the geosphere since, as discussed below, the contribution of the lava to the release rate is small compared to that of the rubble.

The estimates provided in French Liaison Office Document No. 8, 1996, Chapter I are considered to be reasonably conservative, i.e. will overestimate the rate of dissolution. In applying density ρ_L = 2430 kg/m^3, a leach rate L = 3 × 10^{-6} kg/m^2 a and a radius of the particle spheres r_o = 5 × 10^{-4} m a lava lifetime of 405 000 a is calculated. Thus, release from the lava continues over very long periods of time.

A comparison of this lifetime to that of waste glass in a deep geological repository, e.g. 150 000 a (Nagra 1994, p. 209), shows that, except for an initial period of some tens of years, the ambient temperatures in a cavity-chimney are considerably lower (around 20°C compared to 55°C in a repository), but the surface to volume ratio of the glass spheres is higher. In addition, for the waste repository, bentonite as a backfill constitutes a silica sink, further increasing the leach rate. It is not clear whether or not the rubble also constitutes such a sink.

5.2.3. Analytical expression for the combined release

The total concentration of radionuclides in the cavity-chimney water is determined by contributions from both the dissolving lava and the rubble in the water filled cavity-chimney. Thus, the mass balance equation for the concentration of an individual radionuclide (Eq. 3) in the cavity-chimney includes an additional source term, $\hat{A}^{lava}$ (t) to take into account the lava contribution (Eq. 8), where A^{lava} (t = 0) is the initial radionuclide inventory stored in the lava. The mass balance equation for the total activity in the cavity-chimney, sorbed on the rubble and in the cavity-chimney water, A^{ch}, may then be written

$$\frac{dA^{ch}}{dt} = -\lambda\ A^{ch} - QC^{ch,m} + \hat{A}^{lava}(t) \tag{9}$$

where $\hat{A}^{lava}$(t) is the activity released from the lava into the cavity-chimney. Using $A^{ch} = \tilde{A}^{ch} e^{-\lambda t}$, $C^{ch,m} = \tilde{C}^{ch,m} e^{-\lambda t}$ *and*; $\tilde{C}^{ch} = \tilde{A}^{ch} / V = \varepsilon R \tilde{C}^{ch,m}$; *where* $R = 1 + \rho K_d (1-\varepsilon)/\varepsilon$, *where* V is the

cavity-chimney volume and ε is the porosity in the cavity-chimney, the mass balance equation becomes

$$\frac{d\widetilde{C}^{ch,m}}{dt} = -\nu_D \frac{1}{\varepsilon hR}\widetilde{C}^{ch,m} + \frac{3A^{lava}(t=0)}{\varepsilon VR\tau}\left(1-\frac{t}{\tau}\right)^2 \quad \text{for } t < \tau\ , \tag{10}$$

and

$$\frac{d\widetilde{C}^{ch,m}}{dt} = -\nu_D \frac{1}{\varepsilon hR}\widetilde{C}^{ch,m} \qquad \text{for } t \geq \tau \tag{11}$$

Equations (10) and (11) may be written

$$\frac{d\widetilde{C}^{ch,m}}{dt} = -\alpha\widetilde{C}^{ch,m} + \beta\left(1-\frac{t}{\tau}\right)^2 \quad \text{for } t < \tau, \text{ and} \tag{12}$$

$$\frac{d\widetilde{C}^{ch,m}}{dt} = -\alpha \cdot \widetilde{C}^{ch,m} \qquad \text{for } t \geq \tau, \tag{13}$$

where the constants are: $\alpha = \frac{\nu_D}{\varepsilon hR}$ and $\beta = \frac{3A^{lava}(t=0)}{\varepsilon VR\tau}$.

The solution of this inhomogeneous differential equation is:

$$C^{ch,m}(t) = e^{-\lambda t}\left(\frac{\beta}{\alpha} - \frac{2\beta}{\alpha}\frac{t}{\tau} + \frac{2\beta}{\alpha^2\tau} + \frac{\beta}{\alpha}\frac{t^2}{\tau^2} - \frac{2\beta}{\alpha^2}\frac{t}{\tau^2} + \frac{2\beta}{\alpha^3\tau^2} + e^{-\alpha t}\left(-\frac{\beta}{\alpha} - \frac{2\beta}{\alpha^2\tau} - \frac{2\beta}{\alpha^3\tau^2} + C^{ch,m}(t=0)\right)\right)$$

for $t < \tau$,

and $$C^{ch,m}(t) = C^{ch,m}(t=\tau)e^{-(\lambda+\alpha)(t-\tau)} \qquad \text{for } t < \tau, \tag{15}$$

where $C^{ch,m}$ (t = 0) is the initial concentration in the cavity-chimney (with no contribution from the lava) at t = 0 and $C^{ch,m}$ (t = τ) is the concentration in the cavity-chimney after dissolution of all the lava.

A similar equation for the source term may be derived for the following decay chain

$$^{241}\text{Pu} \xrightarrow{14.35\text{a}} {}^{241}\text{Am} \xrightarrow{432.1\text{a}} {}^{237}\text{Np} \xrightarrow{2.144\cdot10^6\text{a}} {}^{233}\text{Pa} \xrightarrow{27\text{d}} {}^{233}\text{U} \xrightarrow{1.529\cdot10^5\text{a}} {}^{229}\text{Th} \xrightarrow{7880\text{a}} \ldots {}^{209}\text{Bi}\ .$$

If the half-life of the isotope is short, the initial radionuclide activity is added directly to that of the daughter nuclide. The contributions of individual radionuclides to the activity in the lava and the rubble/water in the cavity-chimney are then as follows:

(a) For the lava, the activity contributions of the short lived radionuclides ^{241}Pu (14.35a) and ^{241}Am (432.1a) were added to the long lived daughter activity of ^{237}Np (2.144×10^6 a).

$$\overline{A}^{Np,lava} = A^{Pu,lava} + A^{Am,lava} + A^{Np,lava} \tag{16}$$

This is reasonable since all the short lived radionuclides in the lava will decay within the lava before it is dissolved, even for lava dissolution times of only ≥10 000 a. Thus, the contribution

of short lived radionuclides to the total source term contributed by lava dissolution is negligible.

(b) For the rubble and water, the initial ^{241}Pu (14.35a) was added to its daughter ^{241}Am (432.1a) because of its much shorter half-life.

$$\overline{A}^{Am,ch} = A^{Pu,ch} + A^{Am,ch} \tag{17}$$

(c) Differences in K_d values for ^{241}Pu and ^{241}Am are ignored: the K_d for ^{241}Am is used. This is a conservative step since the K_d value for ^{241}Pu is higher than that for ^{241}Am, and the radionuclide concentration in the mobile water would be (conservatively) higher than in the actual case. In the cavity-chimney, decay products of ^{237}Np were ignored because its half-life is long compared to the mean residence time in the cavity-chimney.

With this simplification only the equations for the source term of the ^{241}Am and ^{237}Np chain have to be considered. ^{241}Am is the mother nuclide. Its source term is that of the single radionuclide with the rubble/water contribution plus the contribution from the additional activity of ^{241}Pu rubble/water at t = 0:

$$\overline{C}^{Am,m}(t=0) = \overline{A}^{Am,ch}(t=0)/(\varepsilon V) \tag{18}$$

$$\overline{C}^{Am,m}(t) = \overline{C}^{Am,m}(t=0)\, e^{-\tilde{\lambda}^{Am} t} \quad , \tag{19}$$

where $\tilde{\lambda}^{Am} = \lambda^{Am} + \dfrac{v_D}{h\rho(1-\varepsilon)K_d^{Am} + \varepsilon h}$ is the water flow corrected decay constant.

The decay of ^{241}Am generates ^{237}Np within the cavity-chimney. The ^{237}Np produced from dissolution of the lava defines the concentration of $C^{Np,m}$ in the (mobile) cavity-chimney water. Together with Eqs (3, 3a, 7, 8, 9) these considerations lead to the balance equation

$$\frac{dA^{Np,ch}}{dt} = -\lambda^{Np} A^{Np,ch} - Q C^{Np,m} + \hat{A}^{Np}(t) + \lambda^{Am} \overline{A}^{Am,ch}(t) \quad , \tag{20}$$

where $\hat{A}^{Np}$ is the ^{237}Np activity released from the lava into the cavity-chimney for, $t < \tau$, $\overline{A}^{Np,lava}$ (t = 0) is the initial ^{237}Np activity in the lava, including the ^{241}Pu and ^{241}Am contributions from the lava for t = 0.

Using $\overline{A}^{Np,ch} = \tilde{A}^{Np,ch} e^{-\lambda^{Np} t}$, $\overline{C}^{Np,m} = \tilde{C}^{Np,m} e^{-\lambda^{Np} t}$ and $\tilde{C}^{Np,ch} = \tilde{A}^{Np,ch}/V = \varepsilon R^{Np} \tilde{C}^{Np,m}$,

where $R^{Np} = 1 + \rho(1-\varepsilon)/\varepsilon K_d^{Np}$, ε is the porosity in the cavity-chimney and V is the cavity-chimney volume, the mass balance equations become

$$\frac{d\tilde{C}^{Np,m}}{dt} = -v_D \frac{1}{\varepsilon h R^{Np}} \tilde{C}^{Np,m} + \frac{3\overline{A}^{Np,lava}(t=0)}{\varepsilon V R^{Np} \tau}\left(1 - \frac{t}{\tau}\right)^2 + e^{\lambda^{Np} t} \frac{\lambda^{Am} R^{Am} \overline{C}^{Am,m}(t)}{R^{Np}} \quad \text{for } t < \tau, \text{ or} \tag{21}$$

$$\frac{d\widetilde{C}^{Np,m}}{dt} \approx -v_D \frac{1}{\varepsilon h R^{Np}} \widetilde{C}^{Np,m} + \frac{3\overline{A}^{Np,lava}(t=0)}{\varepsilon V R^{Np} \tau}\left(1-\frac{t}{\tau}\right)^2 + \frac{\lambda^{Am} R^{Am} \overline{C}^{Am,m}(t)}{R^{Np}} \quad \text{for } t < \tau, \qquad (21a)$$

since $e^{\lambda^{Np} t} \approx 1$ for $t < 10^6$ a, and

$$\frac{d\widetilde{C}^{Np,m}}{dt} = -v_D \frac{1}{\varepsilon h R^{Np}} \widetilde{C}^{Np,m} + \frac{\lambda^{Am} R^{Am} \overline{C}^{Am,m}(t)}{R^{Np}} \approx -v_D \frac{1}{\varepsilon h R^{Np}} \widetilde{C}^{Np,m} \quad \text{for } t \geq \tau, \qquad (22)$$

since $\overline{C}^{Am,m}(t) \approx 0$ for $t \geq \tau$.

Alternatively, Eqs (21, 22) may be written as

$$\frac{d\widetilde{C}^{Np,m}}{dt} = -\alpha^{Np} \widetilde{C}^{Np,m} + \beta^{Np}\left(1-\frac{t}{\tau}\right)^2 + \gamma \overline{C}^{Am,m}(t) \qquad \text{for } t < \tau \text{, and} \qquad (23)$$

$$\frac{d\widetilde{C}^{Np,m}}{dt} = -\alpha^{Np} \widetilde{C}^{Np,m} \qquad \text{for } t \geq \tau, \qquad (24)$$

where the constants are:

$$\alpha^{Np} = \frac{v_D}{\varepsilon h R^{Np}}, \qquad \beta^{Np} = \frac{3\overline{A}^{Np,lava}(t=0)}{\varepsilon V R^{Np} \tau} \qquad \text{and} \qquad \gamma = \frac{\lambda^{Am} R^{Am}}{R^{Np}}$$

Further information on the mathematical tools and the release calculations can be found in Hadermann and Pfingsten 1998.

TABLE VIII. NUCLIDE INDEPENDENT PARAMETERS FOR DIFFERENT TEST YIELDS

Parameter	Base case values							
Yield (kt)					Enée	Lycos	Mégarée	Nestor
	5	25	60	100	53	87	54	47
h (m)	102.5	175	235	278.5	225	265	225	215
R_c (m)	20.5	35	47	55.7	45	53	45	43
v_D	1 m/a				20 m/a			
ε	matrix 0.1 carbonate 0.3				carbonate 0.3			
ρ, ρ_L	2430 kg/m^3							
L	3×10^{-6} kg/m^2 a							
r_0	5×10^{-4} m							

TABLE IX. NUCLIDE DEPENDENT PARAMETERS

Radio-nuclide	Half-life	Inventory (TBq) for different tests yields (kt)								K_d (m^3/kg) [a]
		5	25	60	100	Enée	Lycos	Mégarée	Nestor	
^{3}H	12.33	1300	2668	5256	8200	4770	7134	4860	4230	0
^{14}C	5730	0.2			0.25		0.25			0
^{36}Cl	301 000	0.0016			0.045		0.039			0
^{55}Fe	2.73	76			1500		1305			0.01–0.03
^{59}Ni	76 000	0.006			0.12		0.1			0.01–0.03
^{60}Co	5.27	200			4100		3567			0.01–0.03
^{63}Ni	100.1	0.75			15		13.05			0.01–0.03
^{79}Se	650 000	1.5×10^{-5}			3.9×10^{-4}		3.4×10^{-4}			0–0.01
^{90}Sr	28.78	11	114.1	302	520	265	452	270	235	0.008–0.1
^{93}Zr	1.53×10^{6}	4×10^{-4}			0.011		0.0096			0.5
^{99}Tc	211 100	0.0045			0.083		0.072			0–0.01
^{106}Ru	1.023	680			2700		2349			0.01–0.03
^{107}Pd	6.5×10^{6}	0.001			0.0035		0.003			0.05
^{121}Sn	55	0.0029			0.0038		0.0033			0.01–0.03
^{125}Sb	2.758	10			120		104.4			0–0.01
^{126}Sn	100 000	4.2×10^{-4}			0.0043		0.0037			0.01–0.03
^{129}I	15.7×10^{6}	1.5×10^{-5}			1.7×10^{-4}		1.7×10^{-4}			0
^{134}Cs	2.06	0.077			0.1		0.1			0.3
^{135}Cs	2.3×10^{6}	5.2×10^{-4}			0.0085		0.0074			0.3
^{137}Cs	30.1	35	156.1	365.7	600	318	522	324	282	0.3
^{147}Pm	2.62	110			2400		2088			0.05
^{151}Sm	90	1.4			15		13.05			0.05
^{152}Eu	13.54	2.8			56		48.7			0.05
^{154}Eu	8.60	0.55			11		9.6			0.05
^{155}Eu	4.76	7			36		31			0.05
^{236}U	3.42×10^{6}	7.2×10^{-4}			0.0026		0.0023			0.01
^{237}Np	2.14×10^{6}	5.6×10^{-4}			0.0042		0.0037			0.2–0.5
^{238}Pu	87.7	1.6			1.6		1.6			0.5
^{239}Pu	24 110	7.9	7.9	7.9	7.9	7.9	7.9	7.9	7.9	0.5
^{240}Pu	6 564	2.1			2.1		2.1			0.5
^{241}Pu	14.35	85			85		85			0.5
^{241}Am	432.1	2.7			2.7		2.7			0.05
^{242}Pu	373 300	6×10^{-5}			6×10^{-5}		6×10^{-5}			0.5

[a] The first value is the base case value; the second value is a variation.

Using the values of the parameters defined in Tables VIII and IX, the radionuclide concentration in the cavity-chimney is calculated as a function of time for each radionuclide, depending on K_d, cavity-chimney geometry parameters, Darcy velocity, radionuclide inventory and its distribution between lava, rubble and cavity-chimney water.

The results of such calculations in terms of radionuclide concentrations in the cavity-chimney waters are shown for selected radionuclides in Figs 49–8. Radionuclides with a short half-life make a negligible contribution to the cavity-chimney concentration at all times since they will decay within the lava. The contribution of radionuclides with a longer half-life to the radionuclide concentration in the cavity-chimney dominates at later times.

5.2.4. Test categories and assumptions made in calculations

The concentrations of radionuclides in the cavity-chimney water were used as input values for the calculation of the transport of radionuclides through the volcanics. The release rate from the cavity-chimney is calculated using Eq. (25). This is consistent with the model concept and the mass balance as described by Eq. (3). It indicates simply that the total release rate is the product of the volume of groundwater leaving the cavity-chimney per unit time and the radionuclide concentration in that volume.

$$j^i = \pi\, R_c^2\, v_D\, C^i, \tag{25}$$

where j^i is the release rate of the top of the cavity-chimney and R_c is the cavity radius.

The calculations for tests in the volcanics were done for yield clusters of 5 kt, 25 kt, 60 kt, and 100 kt tests conducted at nominal depths of volcanic cover ranging between 25 m and 250 m. The initial inventories as well as the initial radionuclide distribution on lava and rubble were taken from Vol. 3 of this Technical Report. The inventories of Enée, Lycos, Mégarée and Nestor were interpolated linearly from values given in the tables. The parameters presented in Tables VIII and IX were used for the calculation of the radionuclide transport through the volcanics. Parameter variations were made in order to identify individual parameter sensitivities. The calculations were carried out per test category and the respective parameter variations are summarized in the box included in this Section.

Test categories and parameter variations

The various test categories considered in the calculations are described below (see also Fig. 1 and Table I).

Category 1:	121 normal test with yield clusters of 5 kt, 25 kt, 60 kt and 100 kt at depths of 25 m, 75 m, 100 m, 150 m and 250 m for ^{3}H, ^{90}Sr, ^{137}Cs and ^{239}Pu. Variables: Darcy velocity in the volcanics for ^{3}H release calculations; K_d for ^{90}Sr, ^{137}Cs and ^{239}Pu
Category 2:	4 "leaky" tests (Enée, Lycos, Mégarée and Nestor) in a disturbed rock zone with a high premeability reagion above the cavity-chimneys. Variable: Darcy velocity
Category 3:	12 CRTV tests (each about 5 kt) where the cavity-chimney reaches the top of the volcanics. Variable: Darcy velocity
Category 4:	3 safety trials with nuclear yield in the carbonates (0.15 kt each). Variables: Darcy velocity, comparison of fractured versus porous medium approach.
Category 5:	safety trials without nuclear yield in the carbonates. Variables: ^{239}Pu solubility limit (see note below).
Category 6:	safety trials without nuclear yield in the volcanics. Variables: ^{239}Pu solubility limit (see note below)
Category 7:	^{239}Pu release from 1200 m deep waste shafts. Variables: ^{239}Pu solubility limit (see note below).

Note: In the case of Categories 5, 6 and 7, tests calculations were made for ^{239}Pu only because:
(i) for the "non-nuclear yield" safety trials, no ^{3}H, ^{90}Sr and ^{137}Cs would be produced;
(ii) for the two waste shafts, the inventory was not known.

5.2.5. Results and discussion

Concentrations in cavity-chimney waters and release rates into the surrounding rock through the top of the cavity-chimney were calculated for all isotopes given in Table IX.

Figures 49–52 show the time dependent concentrations in the cavity-chimney waters of the four most interesting radionuclides. For ^{3}H, the specific discharge to the geosphere has little influence in terms of overall safety considerations because of the short half-life of this radionuclide. The same is true for the other two short lived radionuclides, i.e. for ^{90}Sr and ^{137}Cs. For both, the source term is fully dominated by the contribution of rubble and the lava contribution can be neglected because leaching is so slow that these radionuclides decay before release. For ^{239}Pu, the contribution from the rubble inventory dominates for the first 1000 years, whereas at later times the lava contribution becomes more important. This contribution of the rubble is a major difference to the approach used by CEA scientists who did not take the release from the rubble into account (see Section 5.1).

For the other radionuclides a few selected concentration curves are presented in Figs 53-58. The general conclusions to be drawn are the same as mentioned in the paragraph above. For radionuclides with short half-lives the contribution of the lava to the radionuclide concentrations in the cavity-chimney water can be neglected. The short lived radionuclides are ^{55}Fe, ^{60}Co (Fig. 58), ^{63}Ni, ^{90}Sr, ^{106}Ru, ^{125}Sb, ^{134}Cs (Fig. 53), ^{137}Cs, ^{147}Pm, ^{151}Sm, ^{152}Eu, ^{154}Eu, ^{155}Eu, ^{238}Pu, ^{241}Pu, ^{241}Am (Fig. 54).

For those radionuclides with longer half-lives, the lava contribution dominates at longer time periods, i.e. ^{79}Se (Fig. 55), ^{99}Tc (Fig. 56), ^{126}Sn, ^{129}I, ^{236}U, ^{237}Np (Fig. 57), ^{239}Pu (Fig. 52) and ^{240}Pu.

The variation of the sorption coefficient K_d has a direct effect on the radionuclide concentration in the cavity-chimney. For sorbing radionuclides, the concentration is, as can be seen from Eqs (2, 3), a linear function of K_d. This is seen in the concentrations of ^{55}Fe, ^{60}Co (Fig. 58), ^{63}Ni, ^{90}Sr (Fig. 50), ^{106}Ru, ^{125}Sb, ^{126}Sn and ^{237}Np (Fig. 57) in the cavity-chimney water.

The influence of K_d on the geosphere transport of radionuclides is very important, as will be seen later.

If the half-life of a radionuclide is sufficiently long the radionuclide inventory of the rubble starts to decrease significantly at times comparable to the residence time of the water (t_w) in the cavity-chimney, whereas radionuclide releases from the lava extend over the lifetime (τ) of the lava. This residence time is given by Eq. (26)

$$t_w = \varepsilon h / \nu_D \tag{26}$$

where, as defined earlier, h is the height of the cavity-chimney, ε is the porosity of the rubble, and ν_D is the Darcy velocity.

Furthermore, it should be noted that the build-up of ^{237}Np from ^{241}Pu through ^{241}Am has been taken into account as explained in Section 5.2.3, although it has a negligible contribution to the ^{237}Np concentrations in the cavity-chimney waters.

The main differences between the results of the WG 4 and the CEA scientists in describing the source term are twofold:

(a) for the first 1000 years the contribution of plutonium and americium from the rubble dominates over that from the lava in the WG 4 calculations.

(b) the sorption coefficients used by the CEA are appreciably higher than those used by WG 4.

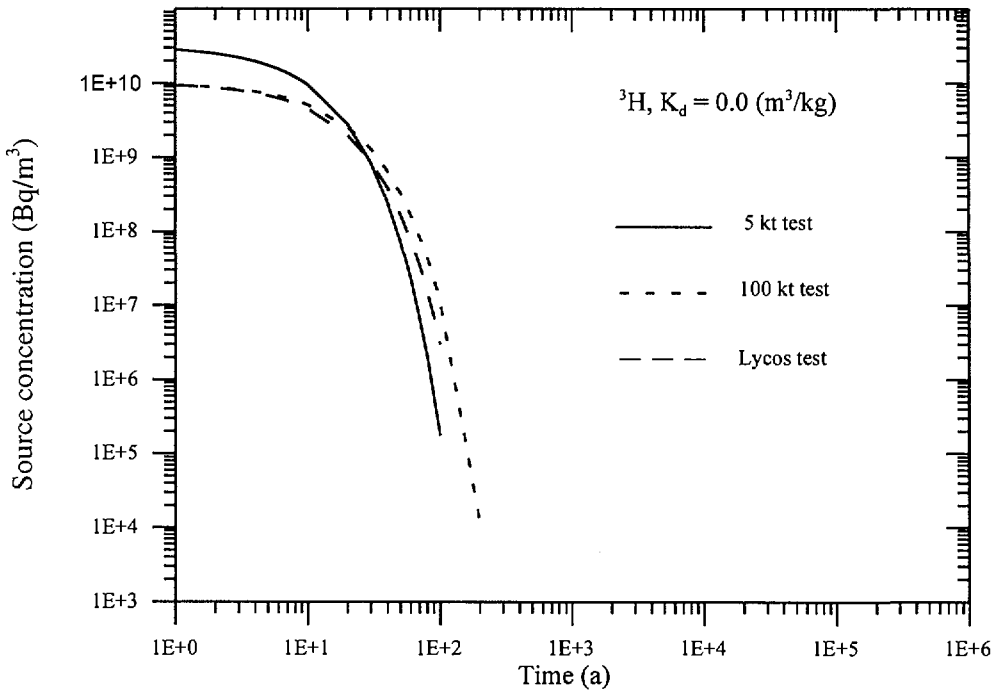

FIG. 49. *^{3}H concentration of water leaving the cavity-chimney into the fractured basalt for different test yields.*

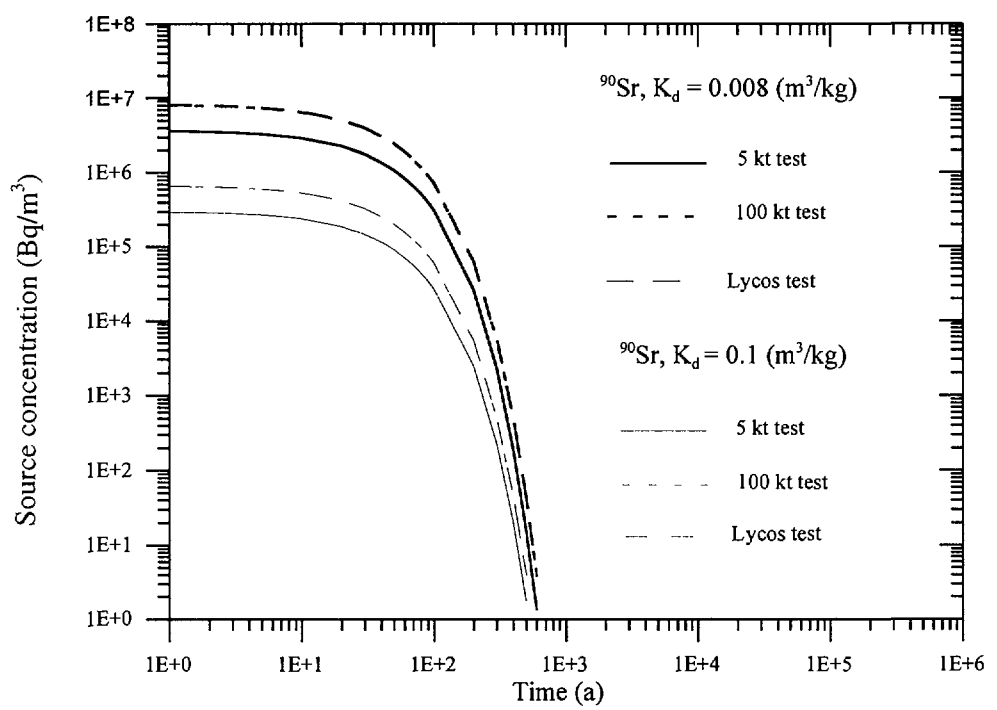

FIG. 50. *^{90}Sr concentration of water leaving the cavity-chimney into the fractured basalt for different test yields.*

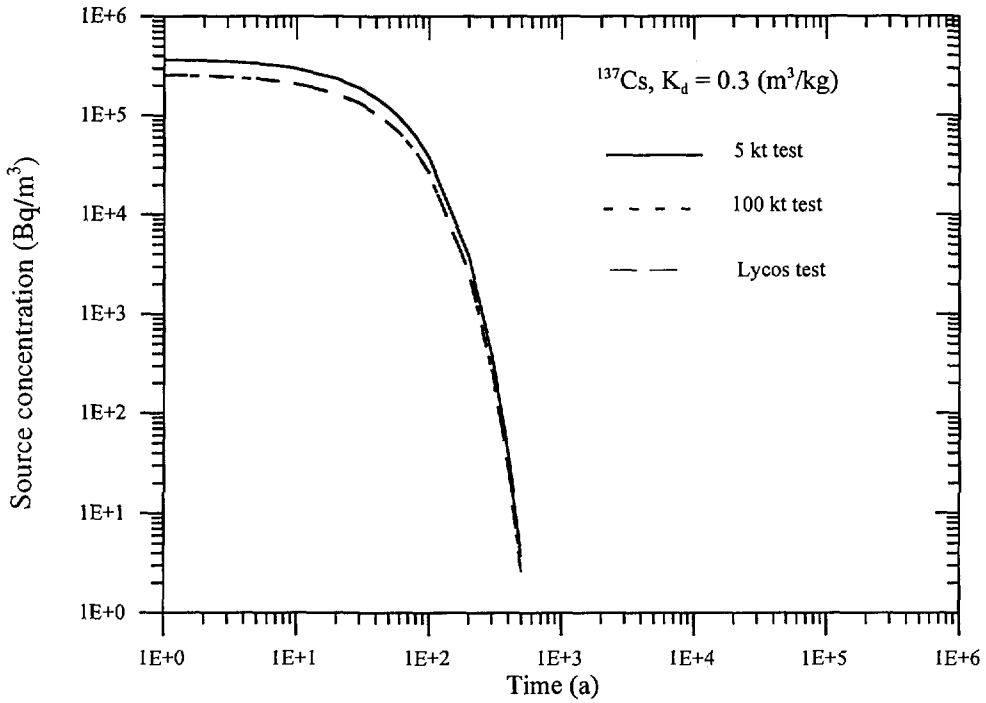

FIG. 51. *^{137}Cs concentration of water leaving the cavity-chimney into the fractured basalt for different test yields.*

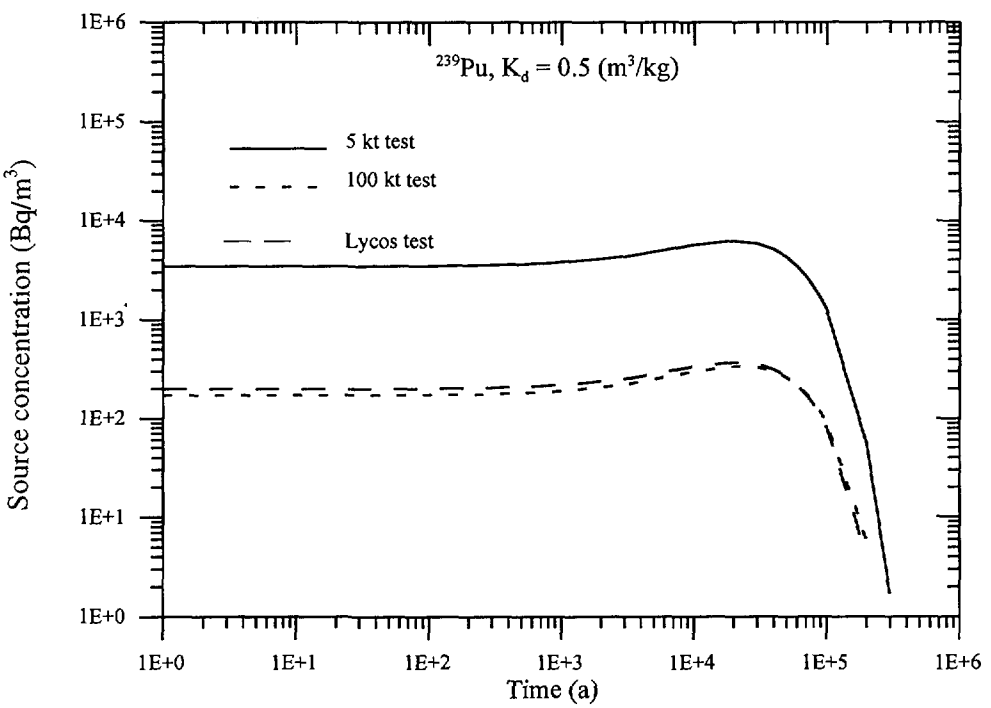

FIG. 52. *^{239}Pu concentration of water leaving the cavity-chimney into the fractured basalt for different test yields.*

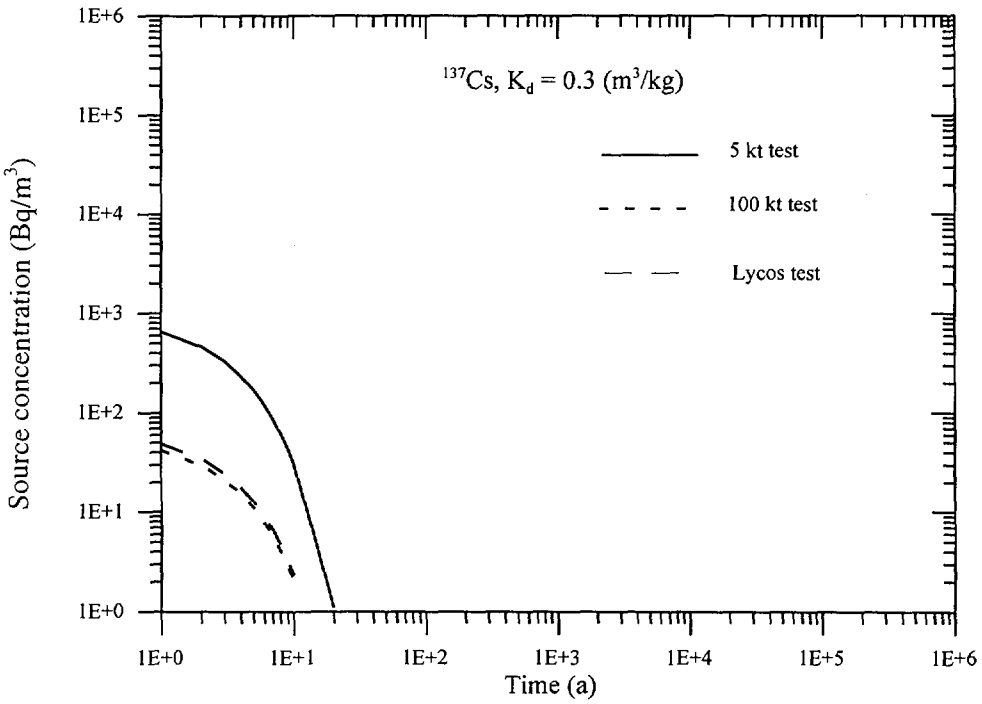

FIG. 53. *^{137}Cs concentration of water leaving the cavity-chimney into the fractured basalt for different test yields.*

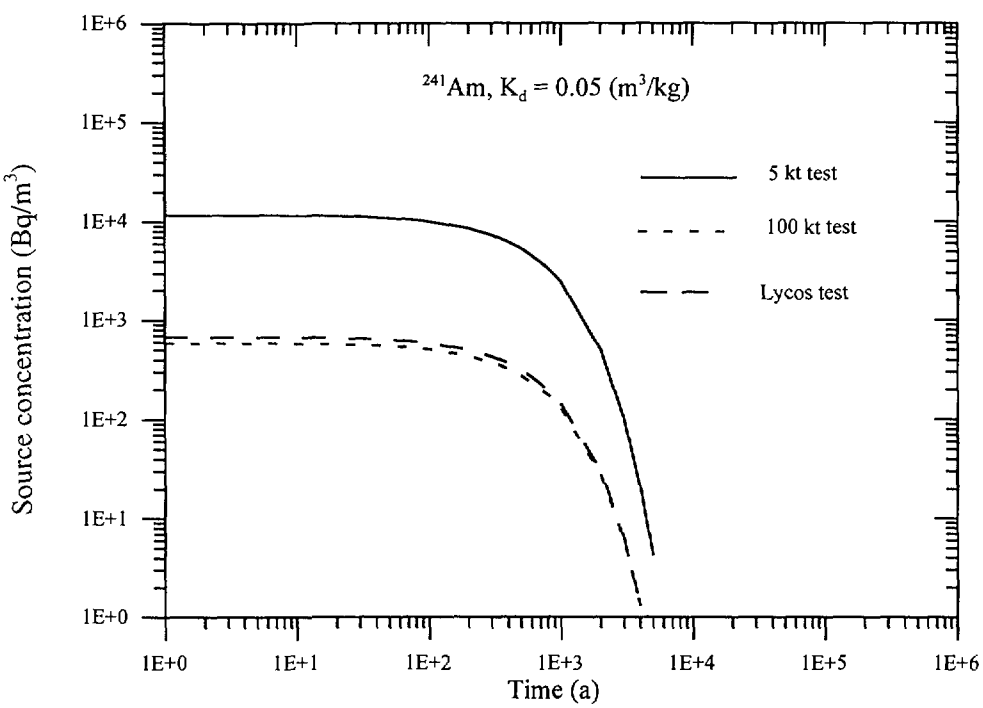

FIG. 54. *^{241}Am concentration of water leaving the cavity-chimney into the fractured basalt for different test yields.*

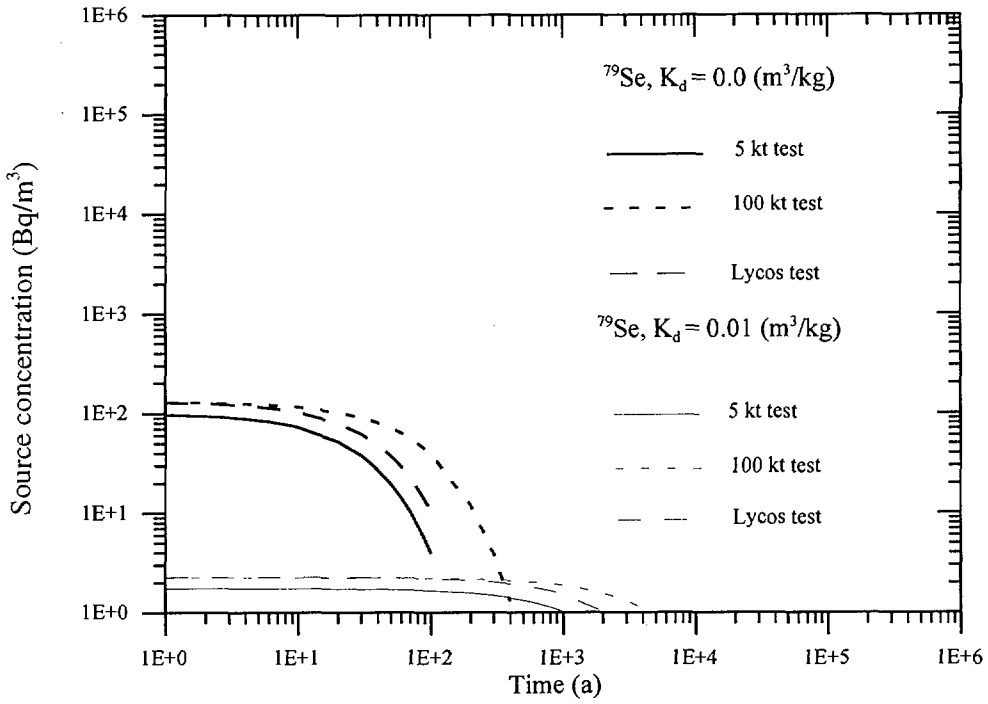

FIG. 55. *^{79}Se concentration of water leaving the cavity-chimney into the fractured basalt for different test yields.*

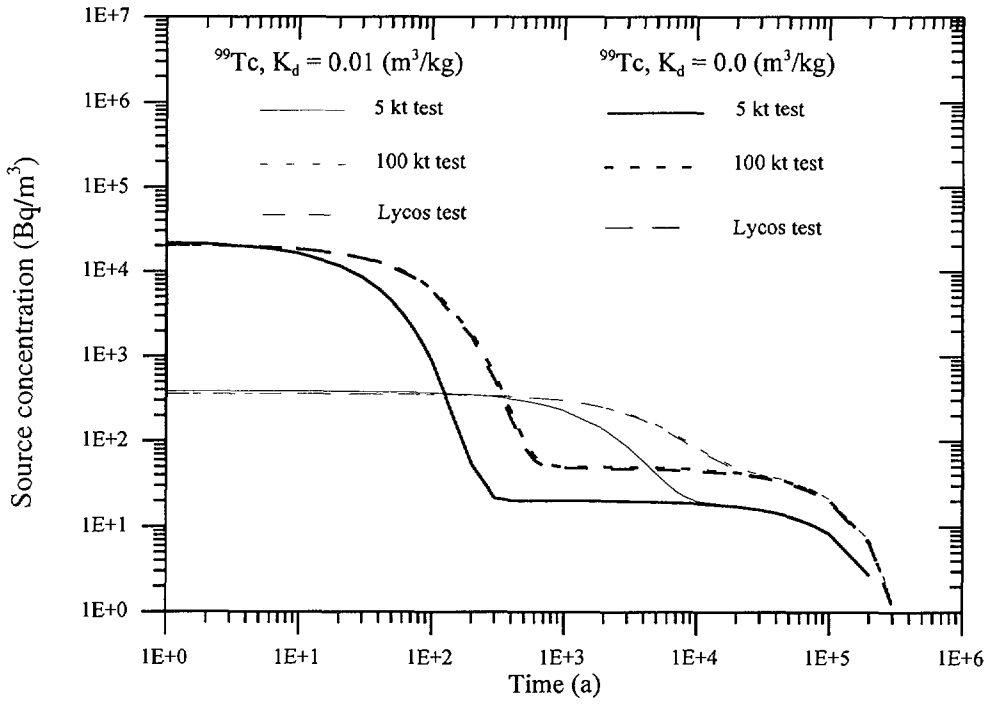

FIG. 56. *^{99}Tc concentration of water leaving the cavity-chimney into the fractured basalt for different test yields.*

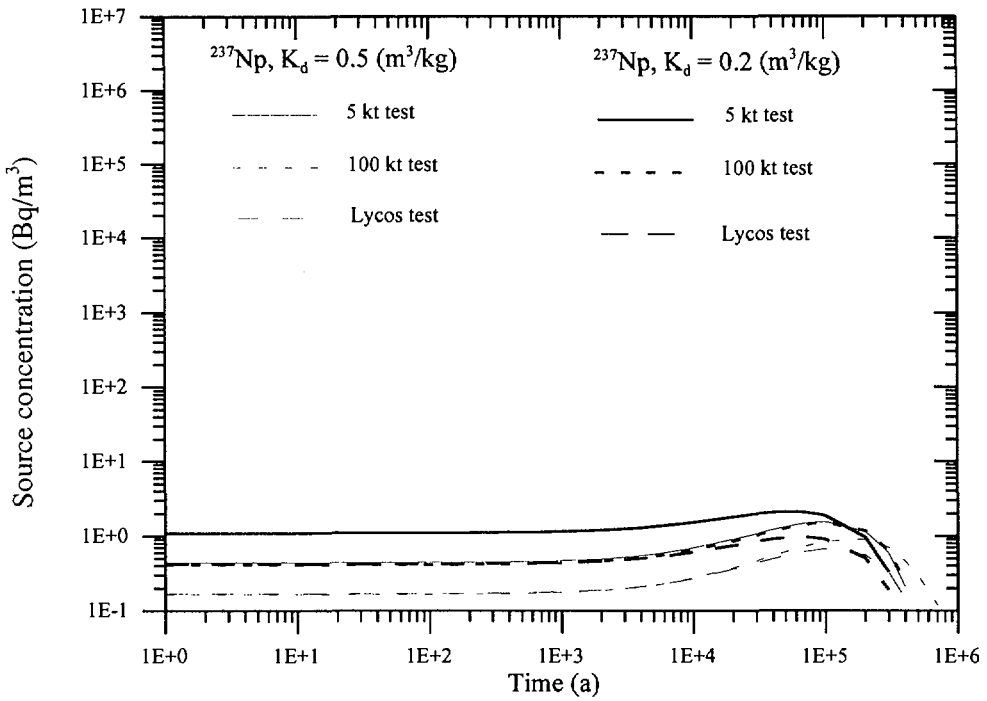

FIG. 57. *^{237}Np concentration of water leaving the cavity-chimney into the fractured basalt for different test yields.*

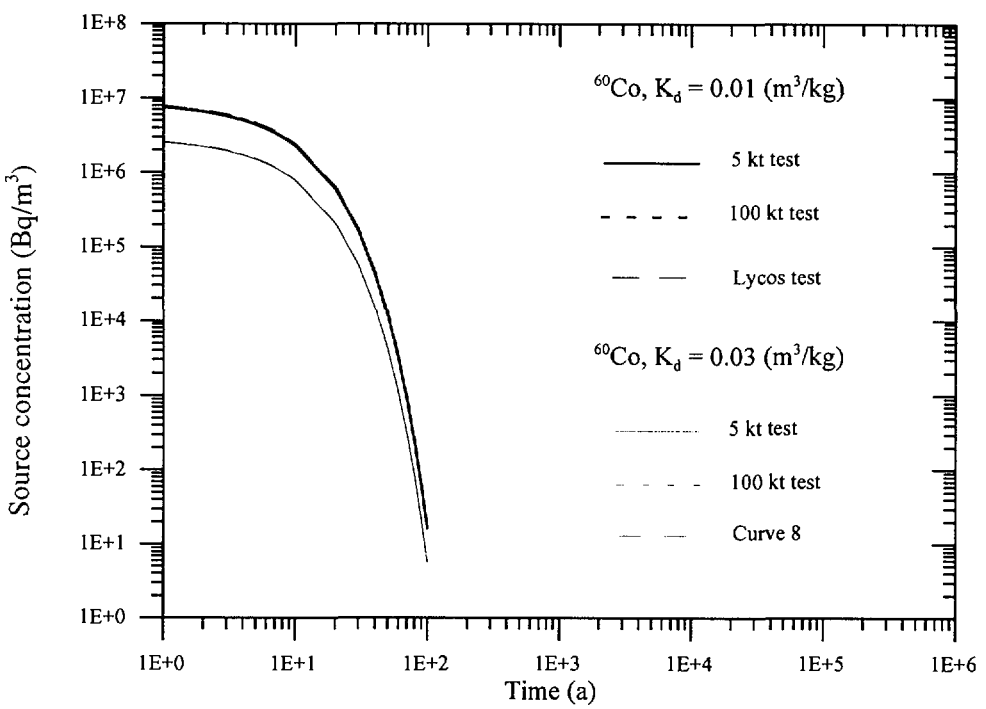

FIG. 58. *^{60}Co concentration of water leaving the cavity-chimney into the fractured basalt for different test yields. Note: There are two bundles of curves, one for K_d = 0.01 (m^3/kg) and one for K_d = 0.03 (m^3/kg), respectively.*

Measurements of the concentrations of ^{3}H, ^{90}Sr and ^{137}Cs in the cavity-chimney have been made by the CEA for several of the tests. These measurements provide an opportunity for a comparison with the present calculations. The measured and the calculated values, extracted from Figs 49–51, are summarized in Table X. It is interesting to note that the radionuclide concentrations in the cavity-chimney waters are almost independent of the yield since the cavity-chimney volume scales directly with yield.

TABLE X. COMPARISON OF CEA MEASUREMENTS IN CAVITY-CHIMNEY WATERS WITH CALCULATED RESULTS (all concentrations are in Bq/m^3)

Radionuclide	Measured				Calculated initial concentration
	Lycos[a]	Aristée[b]	Boros[c]	Ajax[d]	
^{3}H	5.5×10^{9}	10^{10}	4×10^{8}	-	10^{10}
^{90}Sr	4×10^{5}	8×10^{5}	10^{7}	7×10^{5}	6×10^{5} - 8×10^{6} [e]
^{137}Cs	1.4×10^{5}	2×10^{5}	2×10^{6}	1.3×10^{6}	2.5×10^{5}

[a] French Liaison Office Document No. 8-III, p. 8 (1996).
[b] French Liaison Office Document No. 8-II, Fig. 4 (at 10 years) (1996).
[c] French Liaison Office Document No. 8-II, Fig. 6 (at 1500 days) (1996).
[d] French Liaison Office Document No. 8-II, p. 25 (at 17 years) (1996).
[e] The range results from different K_d's used in the calculations.

The Lycos and Aristée tests are confined within the volcanics. The calculated radionuclide concentrations agree well with the measurements. Boros and Ajax are CRTV tests. The radionuclide concentrations calculated for these two tests underpredict the measured ^{137}Cs concentration for Boros. The reasons for this difference are unclear. As the ^{137}Cs sorption coefficient depends largely on the mineral composition of the rock and varies correspondingly (see Section 4) it may be speculated that actual sorption coefficients could be lower than assumed. On the other hand it is also possible that the sorption equilibrium in the cavity-chimney may not have been reached or that the cavity-chimney volume may have been smaller than expected. However, since the comparison is made without any fitted parameters and the calculation is for a generic test of 100 kt with generic parameters, the agreement is considered to be satisfactory. Further information on the comparison of measured and calculated data can be found in Section 6.

5.2.6. Release of plutonium from the safety trials - a special case

Following the CEA approach, it is appropriate to consider the release of plutonium from the safety trials as a special case. Due to the low amount of plutonium at the source and the relatively low groundwater flow, the release is solubility limited and the radionuclide flux, j^{Pu}, into the geosphere is given by

$$j^{Pu} = Q\, C_L . \tag{27}$$

where Q is the water flux and C_L is the solubility limit, taken to be 10^{-9} mol/L or 10^{-7} mol/L, respectively.

The inventory of one safety trial is assumed to be 3.7 kg of ^{239}Pu. The total water flux (Q) at the source was calculated as follows: The Darcy velocity (or specific discharge) was taken to be 2m/a (with alternative values of 10 and 100 m/a). The area (A) through which the water (coming into contact with the plutonium contaminated region) flows was estimated to be approximately 20 m^2.

This estimate is based on the assumption that plutonium contamination will occur in an area of 0.75 m around the 1.5 m diameter borehole and the 5 m effective height of the device. Thus, the area is 3 m × 6.5 m, which is about 20 m^2.

The total mass M and the radionuclide flux given in Eq. (27), are related through conservation of mass in the following way:

$$\int_0^T Q\ C_L\ dt = M\ . \tag{28}$$

This equation defines the leach time T. Although Eq. (28) neglects radioactive decay it was considered in the actual calculations. This decay is important in cases where the low solubility limit was applied because the period of radionuclide release is long compared to the half-life of plutonium.

5.3. GEOSPHERE TRANSPORT

The next step after establishing the source term, i.e. the concentration of each of the radionuclides in the cavity-chimney water as a function of time, is to determine the radionuclide transport through the geosphere, i.e. from the top of the cavity-chimney through the volcanics and the carbonates, as appropriate, to either the lagoon or the ocean.

5.3.1. Transport from the explosion cavities through the volcanics

5.3.1.1. Model concept

As noted in Section 5.1, in contrast to the modelling of groundwater flow, the modelling of mass transport requires detailed consideration of the geometrical structure of water carrying features and on transport processes.

From the evolution of the atolls it is clear that both the volcanics and the carbonates contain many fractures on varying scales (see Section 2 of this report) and that transport takes place in a fractured medium. Hence, a model for transport in a double porosity medium, i.e. fracture porosity and rock matrix porosity, is appropriate.

This is a major difference to the approach followed by CEA scientists who used a single porosity model concept. In a double porosity medium, transport in the fractures is relatively fast, and retardation of the transported radionuclides is produced principally by diffusion into and possibly sorption in the rock matrix (Jakob 1997, and references therein).

The transport equations, including decay and build-up of radionuclides are given by Eqs (29, 30) (see Jakob et al., 1989) for transport in the fractures

$$\frac{\partial C^i}{\partial t} = \frac{l}{R^i}\left(a_L v \frac{\partial C^i}{\partial z^2} - v \frac{\partial C^i}{\partial z} + \frac{l}{b} \varepsilon_p D_p \frac{\partial C_p^i}{\partial x}\Big|_{(x)=b} \right) - \lambda^i\ C^i + \lambda^{i-1} \frac{R^{i-1}}{R^i} C^{i-1} \tag{29}$$

and for transport in the rock matrix

$$\frac{\partial C_p^i}{\partial t} = \frac{l}{R_p^i} D_p \frac{\partial^2 C_p^i}{\partial x^2} - \lambda^i\ C_p^i + \lambda^{i-1} \frac{R_p^{i-1}}{R_p^i} C_p^{i-1}\ . \tag{30}$$

Here, the index p denotes matrix quantities; a_L is the dispersivity in the longitudinal direction, b the fracture half width and D_p the diffusion constant. It should be noted that the fracture half widths is actually the fracture volume divided by the fracture surface. The fracture half width b is thus related to the flow wetted surface.

The water velocity is given by

$$v = v_D / \varepsilon_f , \tag{31}$$

where ε_f is the fracture porosity and can be calculated by the expression

$$\varepsilon_f = n\,2b \tag{32}$$

where n is the fracture frequency (m^{-1}) and 2 b is the fracture aperture.

Note that, in Eq. (32), b represents the hydraulic aperture, whereas in Eq. (29), b is the mass transport aperture. The values for these two quantities might differ significantly but we do not take such differences into account. Note also that the concentrations in the transport equations are in molar units (e.g. mol/m^3) and not in activity units (Bq/m^3). For all calculations, we have neglected sorption on the fracture surfaces, i.e. $R^i = 1$, since the fracture surface is much smaller than the inner matrix surfaces. D_p is the diffusion constant and the retardation factor R_p is defined by Eq. (2).

The assumed boundary conditions are as follows: (a) upstream, the nuclide flux is given by the source term (b) downstream, we assume infinite dilution in the carbonates and (c) within the matrix, a no-flow boundary is assumed to exist at the plane of symmetry between the two fractures. As a variation a penetration of radionuclides into the rock matrix to a depth of 1 cm was also assumed. Given the large porosity of 10% in the volcanics, this is believed to be unrealistically low and thus very conservative.

Whereas advective transport is usually very fast in such a double porosity system, matrix diffusion and sorption within the matrix are powerful retardation mechanisms. Provided that the residence time in the geosphere is long compared to the release time and that the rock matrix will not be loaded to saturation with the radionuclide in question, the retardation by matrix diffusion $\hat{R}$ can be expressed as

$$\hat{R} = 1 + \frac{2}{3}\tau_0 (L/v)^{-1} \tag{33}$$

where L is the transport distance and the time shift τ_0 (Hadermann and Heer 1996), is given by the expression

$$\tau_0 = \left(\frac{\varepsilon_p}{b}\right)^2 \left(\frac{L}{v}\right)^2 \frac{D_p R_p}{4} \quad . \tag{34}$$

As noted in Section 5.2.1 on the second weakness of the model, the code used to solve Eqs (29, 30) has one main disadvantage with respect to simulation of the short term flow from the cavity-chimneys, i.e. the water velocities v must be assumed constant. The code was developed primarily for nuclear waste repository analysis, where groundwater flow velocities tend to be constant. For some years after an explosion and up to several hundred of years for the high yield test, the actual velocity tends to vary, declining exponentially from an initially high value. For this reason, we have varied v in broad ranges.

TABLE XI. GENERIC CALCULATIONS

Radio-nuclide	150 kt				10 kt[a]	CRTV and Lycos	
	K_d (m^3/kg)	Matrix depth (m)	v_D (m/a) (volcanics)	v_D (m/a) (carbonates)		v_D (m/a) (cavity-chimney)	v_D (m/a) (carbonates)
^{3}H	0	0.0495–0.01	1 (0.1, 10)	1	X	20 (2)	20 (2)
^{14}C	0	0.0495	1	1		20 (2)	20 (2)
^{36}Cl	0	0.0495–0.01	1	1		20 (2)	20 (2)
^{55}Fe	0.01–0.03	0.0495–0.01	1	1		2	2
^{60}Co	0.0–0.03	0.0495–0.01	1	1		2	2
^{63}Ni	0.0–0.03	0.0495–0.01	1	1		2	2
^{79}Se	0–0.01	0.0495–0.01	1	1		20 (2)	20 (2)
^{90}Sr	0.008–0.1	0.0495–0.01	1 (0.1, 10)	1	X	20 (2)	20 (2)
^{99}Tc	0–0.01	0.0495–0.01	1	1		20 (2)	20 (2)
^{106}Ru	0.0–0.03	0.0495–0.01	1	1		2	2
^{125}Sb	0–0.01	0.0495–0.01	1	1		20 (2)	20 (2)
^{126}Sn	0.0–0.03	0.0495–0.01	1	1		2	2
^{129}I	0	0.0495–0.01	1	1		20 (2)	20 (2)
^{134}Cs	0.3	0.0495–0.01	1	1		2	2
^{135}Cs	0.3	0.0495–0.01	1	1		2	2
^{137}Cs	0.3	0.0495–0.01	1 (0.1, 10)	1	X	20 (2)	20 (2)
^{147}Pm	0.05	0.0495–0.01	1	1		2	2
^{151}Sm	0.05	0.0495–0.01	1	1		2	2
^{152}Eu	0.05	0.0495–0.01	1	1		2	2
^{154}Eu	0.05	0.0495–0.01	1	1		2	2
^{155}Eu	0.05	0.0495–0.01	1	1		2	2
^{236}U	0.01	0.0495–0.01	1	1		2	2
^{237}Np	0.2–0.5	0.0495–0.01	1	1		2	2
^{238}Pu	0.5	0.0495–0.01	1	1		2	2
^{239}Pu	0.5	0.0495–0.01	1	1	X	2	2
^{240}Pu	0.5	0.0495–0.01	1	1		2	2
^{241}Pu	0.5	0.0495–0.01	1	1		2	2
^{241}Am	0.05	0.0495–0.01	1	1		2	2
^{241}Am chain	radionuclide specific	0.0495–0.01	1	1	X	2	2

[a] Calculations were carried out for the radionuclides identified by an "X" using the same parameters as for the 150 kt tests.

5.3.1.2. Parameters used

Although site-specific information on the parameters important for modelling radionuclide transport is scarce, especially for the parameters characterising the flow paths, data have been selected and used which seem to be representative and adequate in order to assess the overall situation at the atolls conservatively.

In this context, it is important to note that the solutions to Eqs (29, 30) are determined by four independent parameters. Hence, it is more or less a matter of choice as to which of the physical parameters to fix, and which to vary.

We have chosen to fix $L/a_L = 10$, where L is the transport distance and a_L the longitudinal dispersivity in the volcanics. Though dispersion is not fully understood, this seems to be a reasonable number, based on a wealth of field experiments (e.g. Marsily 1986). We also found it reasonable to

TABLE XII. DETAILED CALCULATIONS FOR ^{3}H, ^{90}Sr, ^{137}Cs AND ^{239}Pu

Radio-nuclide	K_d (m^3/kg)	Matrix depth (m)	5 kt, 25 kt, 60 kt, 100 kt (Category 1)		Enée, Lycos, Mégarée, Nestor (Category 2)	CRTV tests (Category 3)	3 safety trials in the carbonates with nuclear yield (Category 4)[a]	Safety trials in the carbonates without nuclear yield (Category 5)[a, b, c]	Safety trials in the volcanics without nuclear yield (Category 6)[c]	Release from 1200m deep waste shaft (Category 7)[c]
			v_D (m/a) cavity-chimney; volcanics	v_D (m/a) carbonates	v_D (m/a) carbonates	v_D (m/a) cavity-chimney; carbonates	v_D (m/a) carbonates	v_D (m/a) carbonates	v_D (m/a) carbonates	v_D (m/a) carbonates
^{3}H	0	0.0495	1, 0.1, 10	1, 2	1, 2, 20	20, 2	2, 1, 100	-	-	-
^{90}Sr	0.008–0.1	0.0495	1	1, 2	1, 2, 20	20, 2	2	-	-	-
^{137}Cs	0.3	0.0495	1	1, 2	1, 2, 20	20, 2	2	-	-	-
^{239}Pu	0.5	0.0495	1	1, 2	1, 2, 20	20, 2	2	2, 10, 100	1	1

[a] Comparison double / single porous medium.
[b] "Exchange cross section" = 20 m^2 (45 m^2).
[c] Solubility limit = 1×10^{-7} mol/L (1×10^{-9} mol/L).

fix the fracture frequency n = 10/m. The actual value of the fracture frequency cannot be known on the scale of the atolls. Atkinson 1984, p. 103 mentions frequencies between 100/m and 25/m but such a high frequency seems unlikely to be widespread (see French Liaison Office Document No. 5, 1997). We assume that all the water is flowing through these fractures. The fracture aperture was fixed at 1mm. This results in relatively fast advective transport of radionuclides. Diffusion into the matrix was fixed at $D_p = 1 \times 10^{-11}$ m^2/s, a value based on a wealth of laboratory measurements, though not site-specific. Sorption coefficients were taken to be identical to those of the cavity-chimney rubble (see Tables IX and XI). There is no reason to assume different values since the rock matrix is of the same material, except for the possible existence of alteration layers in the water conducting fractures in the rock mass which would tend to enhance sorption.

The variables were (a) the Darcy velocity, (b) the depth of penetration for diffusion into the matrix, and (c) the sorption coefficients of some of the radionuclides.

Detailed calculations over a wide range of parameters were made for ^{3}H, ^{90}Sr, ^{137}Cs and ^{239}Pu (see Table XII). For other radionuclides, calculations were made for a nominal 150 kt test at 250 m in the volcanics and a nominal 10 kt test at 25 m in the volcanics with a limited set of parameter variations (see Table XI).

5.3.2. Transport through the carbonates

5.3.2.1. Model concept

In order to develop a realistic model to describe radionuclide transport through the carbonates it is essential to have

(a) information on the geometrical structure of the flow paths, and
(b) an understanding of the influence of tidal effects in the karst.

CEA scientists have adopted a phenomenological approach to the analysis of transport in the karst. To date, however, there is little validation of this approach. Thus, there are at least two approaches that could be taken to estimate the transport of radionuclides through the carbonates into the lagoon.

1. It could be assumed that a radionuclide transfer from the top of the volcanics or from a source in the carbonates to the lagoon or ocean occurs instantaneously, i.e. there is no delay in the carbonates. This is not an appealing option. It is obviously incorrect physically and must lead to inaccurate results. In such an approach, short lived radionuclides from Categories 2, 3 and 4 tests would be released to the lagoon or the ocean instantaneously and contribute to the overall dose without delay. However, it is well known from experience that even a minor geologic barrier will result in the complete decay of short lived radionuclides during transport through the geosphere. Direct transfer to the lagoon also contradicts the experimental evidence from measurements of radionuclides in the lagoon (see Vol. 2 of this Technical Report).

2. It could be assumed that the radionuclide behaviour in the carbonates is described by a mixing tank model. This approach is discussed in detail in Section 3.3 and Appendix II.

We have opted to use a standard advection - dispersion single porosity model in the absence of site specific information on fractures, and in view of the considerable uncertainty concerning the influence of the karsts on radionuclide release pathways and release rates. In order to check the viability of this approach a comparison with the results from an analysis using a double porosity model (Section 5.3.1.1) has been made.

It should be noted that the one dimensional advection - dispersion model overestimates the radionuclide concentrations in the carbonates since dilution by transverse dispersion and mixing with uncontaminated waters are not taken into account. Each of these two mechanisms will reduce the concentrations.

5.3.2.2. Parameters used

In the absence of detailed site specific data for the carbonates and their natural variability, a "generic" thickness of 300 m for the carbonates was assumed, even though the actual cover thickness is variable. Furthermore, it was assumed that the sorption coefficients K_d for the carbonates have the same values as for the volcanics (see Section 4). Arguments in support of this choice were presented in Section 4.2.2. The assumed Darcy velocities are given in Table XII. These values overestimate the transport velocities, as does the porosity which was assumed to be 30% in the calculations.

5.3.3. Transport of plutonium from the safety trials - a special case revisited

CEA scientists assumed (French Liaison Office Document No. 10, 1996), the existence of a 4 m thick diffusion barrier for the plutonium transport away from the source. This assumption would suggest that safety trials were conducted in a large rock block with a hydraulic conductivity many (6 to 8) orders of magnitude below the average conductivity of carbonates. Since no acceptable justifications have been provided it was decided not to pursue the CEA approach. After an evaluation of other approaches, the model used for the transport through the carbonates (see Section 5.3.2.1.) was deemed to be the most reasonable. There was also no reason to follow the CEA assumption that plutonium would not sorb on the carbonates. As discussed earlier (Section 4), a value of $K_d = 0.5$ m^3/kg is assumed for plutonium (see Table XII). This leads to very slow migration of plutonium.

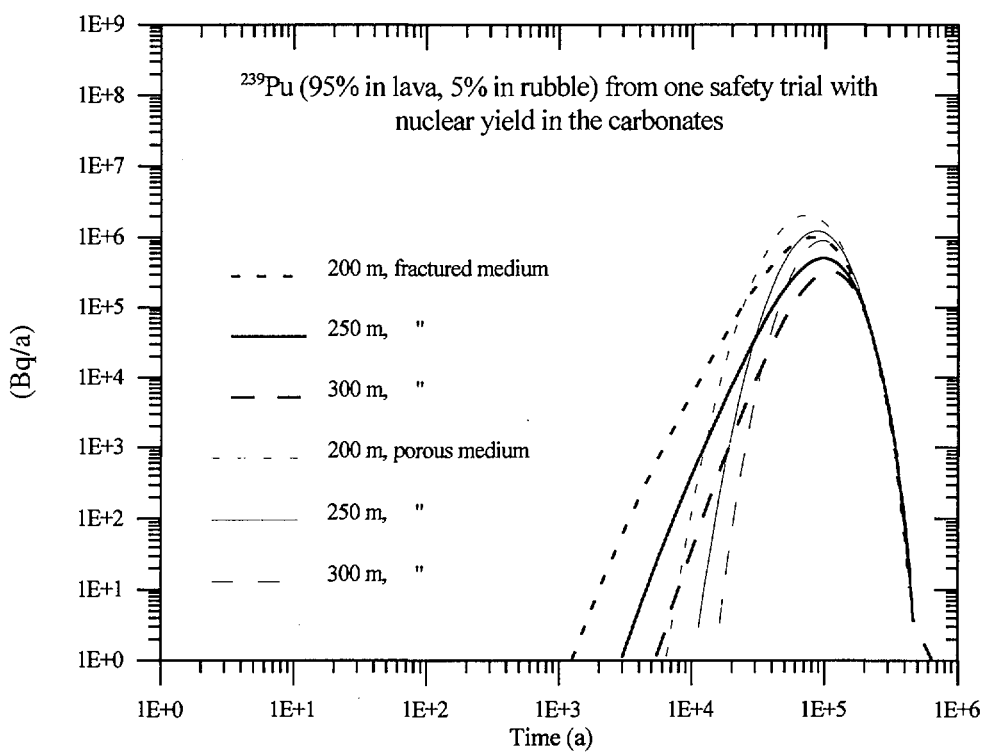

FIG. 59. Comparison of flow in a fractured (double porosity) and porous (single porosity) medium, examplified for ^{239}Pu breakthrough curves for one safety trial with nuclear yield in the carbonates.

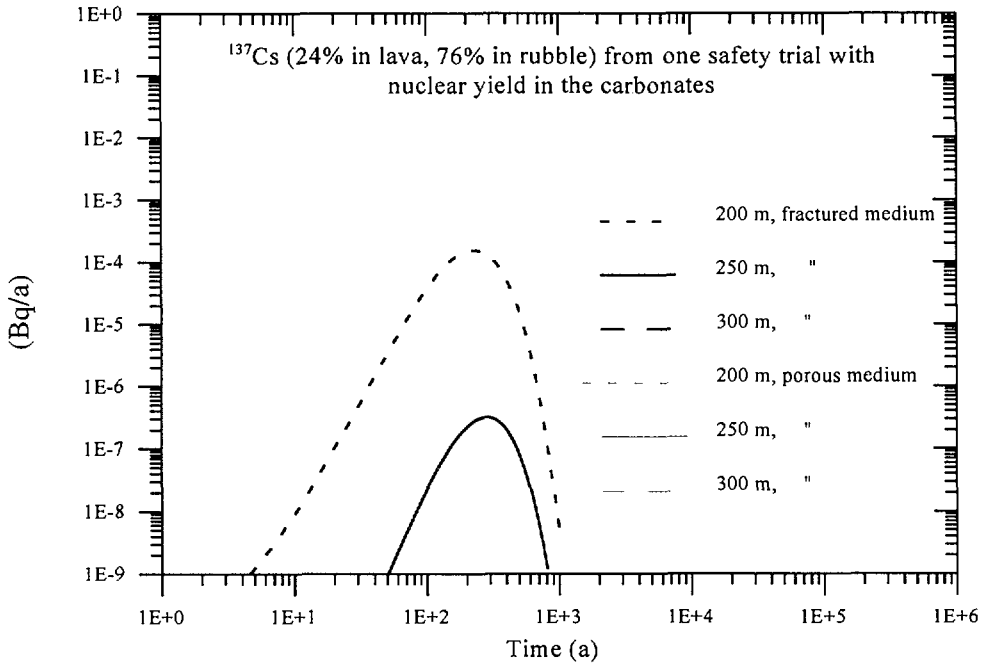

FIG. 60. *Comparison of flow in a fractured (double porosity) and porous (single porosity) medium, ^{137}Cs breakthrough curves for one safety trial with nuclear yield in the carbonates. Note: The calculated releases for four of the six cases are below the scale of this figure.*

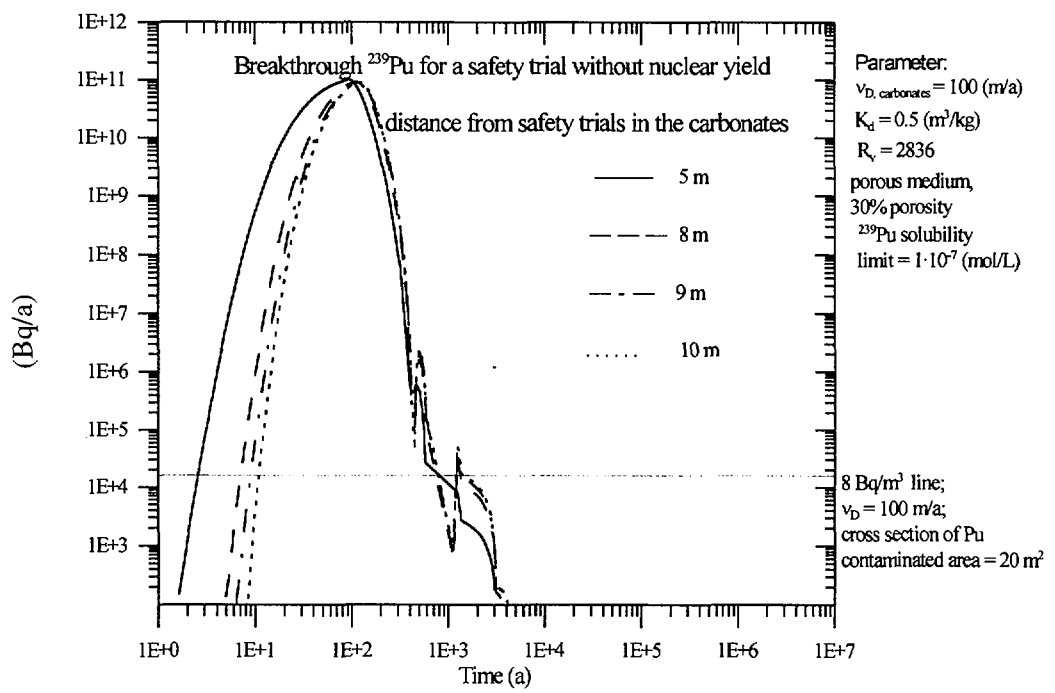

FIG. 61. *Breakthrough curves for ^{239}Pu for a safety trial without nuclear yield at different distances from the source. Note: The value based on a concentration measurement of 8 Bq/m³ at 10 m distance from the safety trial is indicated by the horizontal line.*

According to the French Liaison Office Document No. 8, 1996, plutonium concentrations in the carbonates have been measured. A plutonium concentration of 8 Bq/m^3 was found at a distance of 10 m from a safety trial 15 years after the trial. Using the single porosity model, the plutonium breakthrough was calculated at various distances from the source in the carbonates. Figure 59 shows that the calculated and the measured plutonium concentrations are compatible. This lends credibility to the model concept. However, this result should not be given too much credence because the breakthrough curves are still rising very steeply after 15 years and the calculated concentrations are very sensitive to the specific values chosen for individual parameters in the model.

With respect to the possibility of direct transfer of radionuclides from a safety trial via the karst into the ocean all the computations have assumed a minimum distance to the karst of 10 m.

5.3.4. Results and discussion

Assuming reasonable values for the fracture parameters, the comparison between the single porosity model and the double porosity model reveals the following:

(a) For ^{3}H and ^{239}Pu, there is good agreement between the results of the two calculations (Fig. 60). The differences in the rising part of the breakthrough curves are unimportant and negligible. The similarity in the results is due simply to the fact that the matrix becomes saturated.

(b) For ^{90}Sr, the difference in peak height is roughly one order of magnitude. The single porosity model overestimates retardation since the rock matrix is not fully saturated. However, the value of the peak breakthrough is extremely low for both models.

(c) For ^{137}Cs, the results of the two models differ by several orders of magnitude, but both cases show insignificantly low release levels (Fig. 61).

5.3.4.1. The base case

The discussion of results in terms of release to the carbonates and to the lagoons is based on the base case parameters, i.e. low sorption coefficients K_d, large penetration depths, high porosity in the volcanics and an assumed interconnected network of diffusion pathways. The numerous parameter variations, although not presented here, provided detailed insight into the sensitivity of the system. They are the technical support for the base case. The aim of the base case is to overestimate radionuclide release rates. The parameter variations performed show that the Darcy velocity, the flow path characterisation, the migration distance and the sorption coefficient have a major influence on the results (Hadermann and Pfingsten, 1998).

The base case calculations were carried out with the following Darcy velocities:

(a) Category 1: 1 m/a in the volcanics and the carbonates;

(b) Categories 2 and 3: For radionuclides ^{3}H, ^{90}Sr, ^{137}Cs and ^{239}Pu 20 m/a. In order to take account of the initial thermal pulse, this high value is assumed which overestimates the consequences. This assumption leads to a rapid release of radionuclides from the cavity-chimney. For the other radionuclides, a Darcy velocity of 2 m/a was assumed since the thermal pulse is of short duration. The short lived radionuclides decay in the carbonates and the long lived sorbing radionuclides show a late breakthrough;

(c) Category 4: 2 m/a;

(d) Category 5: 100 m/a; and

(e) Categories 6 and 7: 1 m/a in both the volcanics and the carbonates.

These values are consistent with the results of the hydrological modelling (Section 3) and err on the conservative side.

In terms of releases to the biosphere, two alternative scenarios have been considered:

(a) Release to the lagoons. This is the realistic scenario, since water flow is upwards towards the centre of the atoll (see Section 3).

(b) Release to the ocean. Here the assumption is that the carbonates do not present a barrier to radionuclide migration. Radionuclides are assumed to be transferred instantaneously by tidal mixing, in the karst, to the ocean when they reach the top of the volcanics.

In this scenario, the Category 2 and 3 tests dominate because of the lack of a geological barrier. This scenario has to be considered as an unrealistic worst case scenario.

From the perspective of geosphere transport scenario (b) has similarities to the worst case scenario presented in the French Liaison Office Document No. 4, 1996, with the main difference that it assumes the transfer of radionuclides to the ocean whereas the CEA assumes transfer to the lagoons. Further information on the discharge of radionuclides into the ocean and into the lagoons is presented in Section 6.10, which deals with the refinement of the geosphere transport model.

In terms of modelling the transport of radionuclides through the geosphere and generating the respective breakthrough curves, the following approach has been taken, which is distinctly different from that taken by the CEA:

(a) for normal tests (Category 1) and the safety trials (Category 6), both carried out in the volcanics, the volcanic barrier is taken into account. The transport of radionuclides from these tests through the carbonates has been modelled for ^{3}H, ^{90}Sr, ^{137}Cs and ^{239}Pu. The results are not presented here because the radionuclide releases to the lagoon or ocean were finally assessed with the "mixing model" (see Section 6.10). The information on modelling of the radionuclide release through the carbonates can be found in Hadermann and Pfingsten 1998.

(b) for Category 2 and 3 tests which reach the carbonates or have a low integrity volcanic cover and the Category 4 tests which are located in the carbonates, the radionuclides are assumed to be released directly from the cavity-chimney into the carbonates. The transport of radionuclides in the carbonates is modelled as described in Section 5.3.2 and 5.3.3. The time dependence of the radionuclide release into the cavity-chimney water and into the carbonates was taken into account.

(c) for Category 5 safety trials in the carbonate we have assumed a distance of 10 m from the karstic zone. Since the depth of the safety trials is unknown, the radionuclides were assumed to be discharged into the karst.

(d) for Category 6 safety trials in the volcanics a distance of 25 m to the top of the volcanics is assumed, which corresponds to the depth of the uppermost normal tests.

5.3.4.2. Breakthrough curves

The total releases of radionuclides to the biosphere have been assessed in such a way that the individual tests were lumped together in test categories and the releases for all the test categories added. Special attention has been given to releases of ^{3}H, ^{90}Sr, ^{137}Cs and ^{239}Pu. Other radionuclides were also examined but found not to be of the same importance. The results of these investigations will be presented in terms of non-sorbing/sorbing radionuclides and short lived/long lived radionuclides.

A selection of breakthrough curves for the base case calculations are presented in Figs 62–73 for ^{3}H, ^{90}Sr, ^{137}Cs and ^{239}Pu and in Figs 74–85 for other radionuclides. Furthermore, the release of chain members into the carbonates and the lagoon is presented in Figs 86-87, on the example of the Lycos test on Fangataufa. The full set of breakthrough curves can be found in Hadermann and Pfingsten 1998.

The overall results of these assessments are described below. They have been the fundamental input for the refinement of the geosphere transport model and the development of the time dependent radionuclide release rates into the lagoon and into the ocean (see Section 6.10).

1. Tritium

The release of ^{3}H from the geosphere is dominated by the tests with a low integrity cover and the CRTV tests (Category 2 and 3) as ^{3}H is released from the test cavities into the carbonate where it is not well contained.

Fangataufa

On Fangataufa, the main individual contributor to ^{3}H release from the geosphere is the Lycos test (Category 2) carried out in 1989. As seen in Fig. 62 its contribution to the ^{3}H release is calculated to be as high as that from all the Category 1 tests. Peak releases of ^{3}H to the lagoon were calculated to occur some tens of years after the test.

It should be noted, however, that recent measurements of ^{3}H concentrations in the lagoon indicate a decrease of ^{3}H in the lagoon waters seven years after the test (Vol. 3 of this Technical Report, Fig. 58). A comparison of this result with the calculation provided in Fig. 62 clearly shows that velocities assumed in the carbonates do not reproduce the actual ^{3}H fluxes into the lagoon as the peak is both too late and not broad enough. Furthermore, the calculated ^{3}H release rate overestimates the actual releases by a factor of about 40. This is conservative.

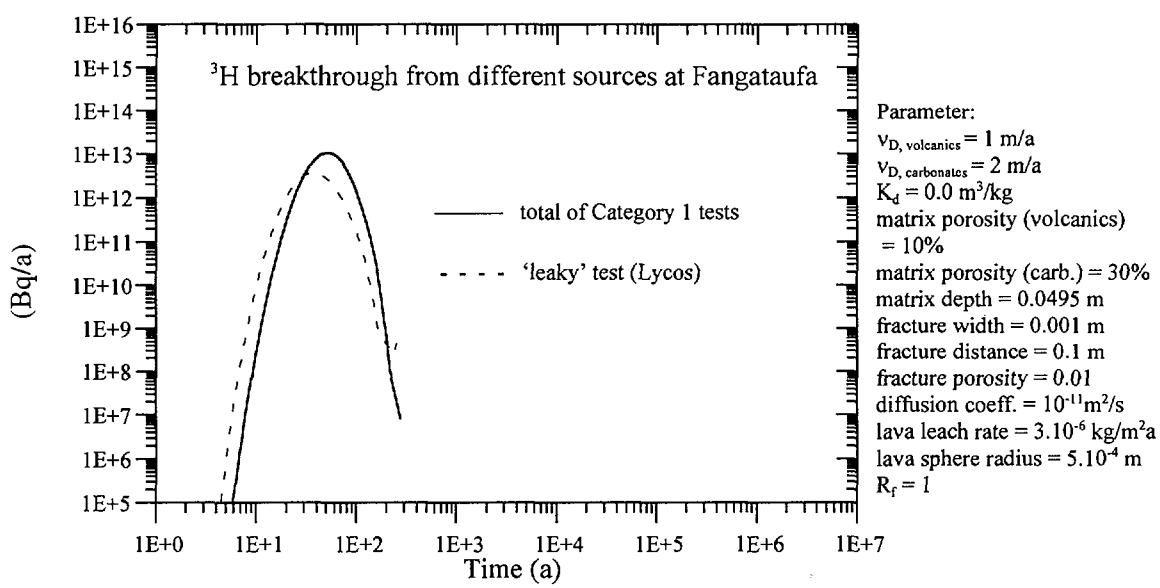

FIG. 62. *^{3}H release into the Fangataufa lagoon for Category 1 tests and Lycos test ($v_{D, carbonates}$ = 2 m/a).*

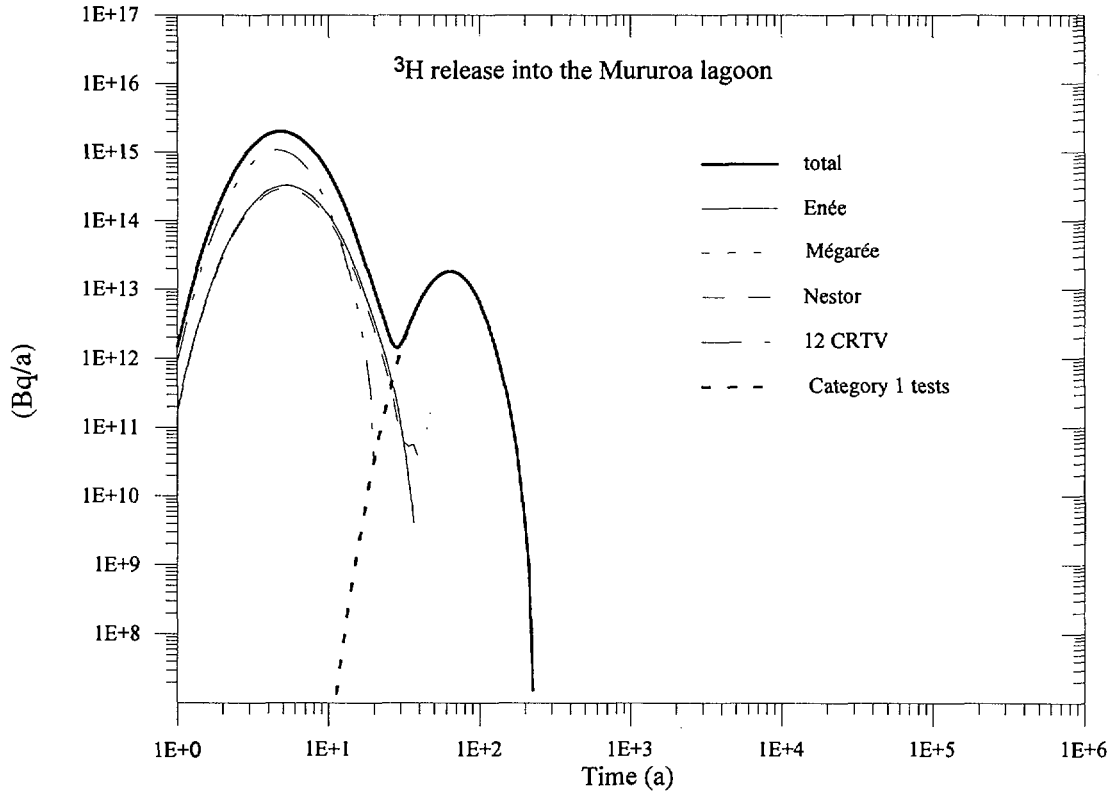

FIG. 63. *^{3}H release into the Mururoa lagoon for different tests. Note: Enée, Mégarée and Nestor have essentially the same ^{3}H release rates.*

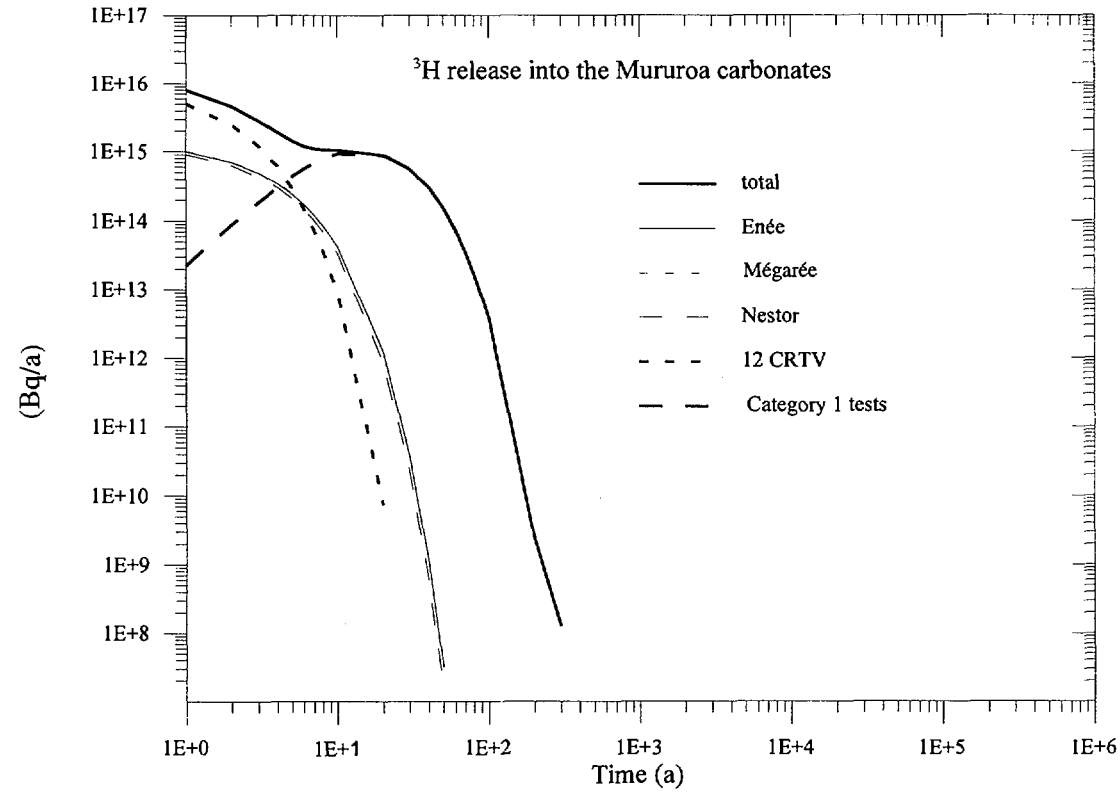

FIG. 64. *^{3}H release into the Mururoa carbonates for different tests. Note: Enée, Mégarée and Nestor have essentially the same ^{3}H release rates.*

In principle, it would be possible to obtain a better match between calculated and observed fluxes by varying the Darcy velocity in the carbonates. This was not done because the present results err on the side of conservatism and the model and the parameters are uncertain.

Concentrations in the carbonates were also assessed. It has to be noted that these are difficult to estimate in a 1-dimensional (1D) model, such as the single porosity model used here. If we adhere rigorously to the 1D model, assuming a vertical flow tube from the test site to the lagoon, the pore water concentrations are of the order of 6×10^8 Bq/m^3, which is an overestimate comparable to that for the actual flux. If we distribute the tritium over the area of 12 km^2, as is done in the compartment model, the concentration is underestimated by about one order of magnitude. Overestimation of the fluxes to the lagoon or the ocean is important in the context of a consequence analysis, since this quantity enters the dose calculations.

Mururoa

The calculated releases into the lagoon and the carbonates are given in Figs 63 and 64. The major source of the releases are the Category 2 test (Enée, Mégarée and Nestor) and the 12 CRTV tests (Category 3). It should be noted that the fact that the Mégarée test was performed 7 years later than the other tests was neglected. This would have reduced the first peak slightly (by about 16%), and would make the decrease less steep. Again the peak release into the lagoon seems to have already occurred, which is indicated by the observed ^{3}H concentrations in the lagoon (see Vol. 2 of this Technical Report).

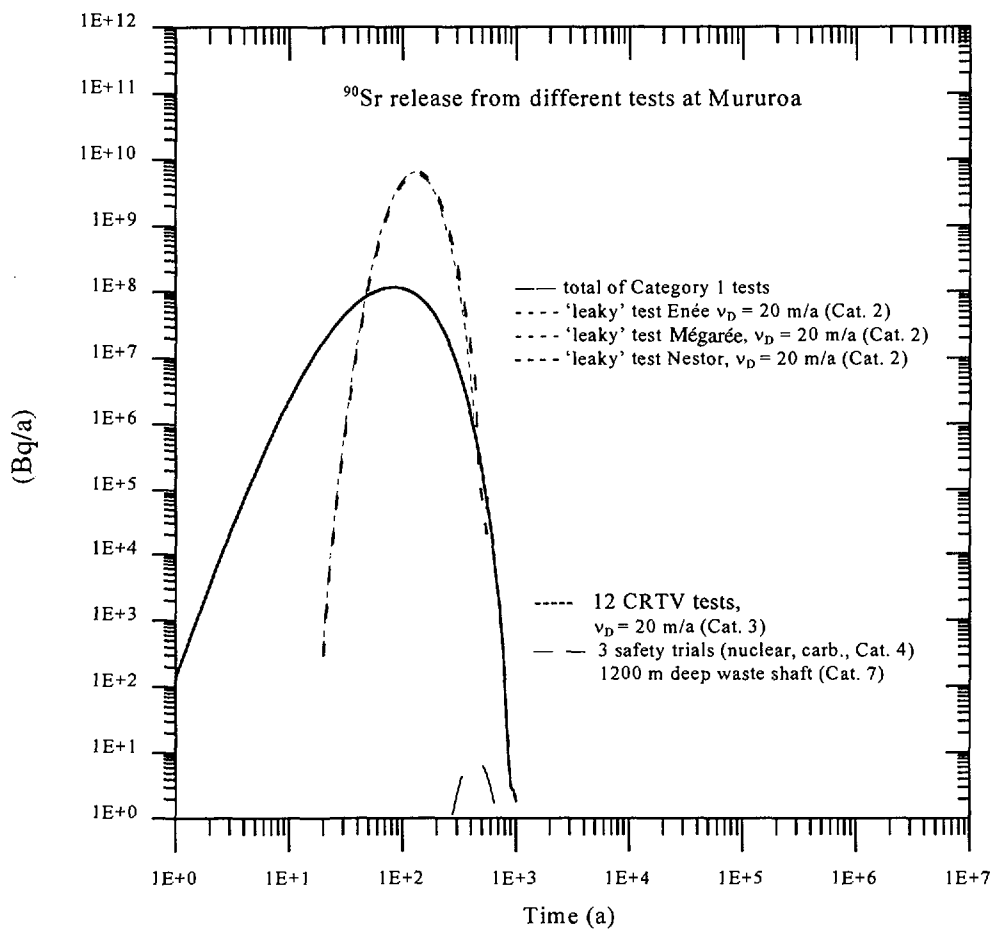

FIG. 65. ^{90}Sr release into the Mururoa carbonates for Category 1 tests and release into the Mururoa lagoon for Enée, Mégarée, Nestor and the CRTV tests. Note: The ^{90}Sr releases of Enée, Mégarée, Nestor and the CRTV tests are essentially the same. Releases of ^{90}Sr from the deep waste shaft, if any, are below the scale of this figure.

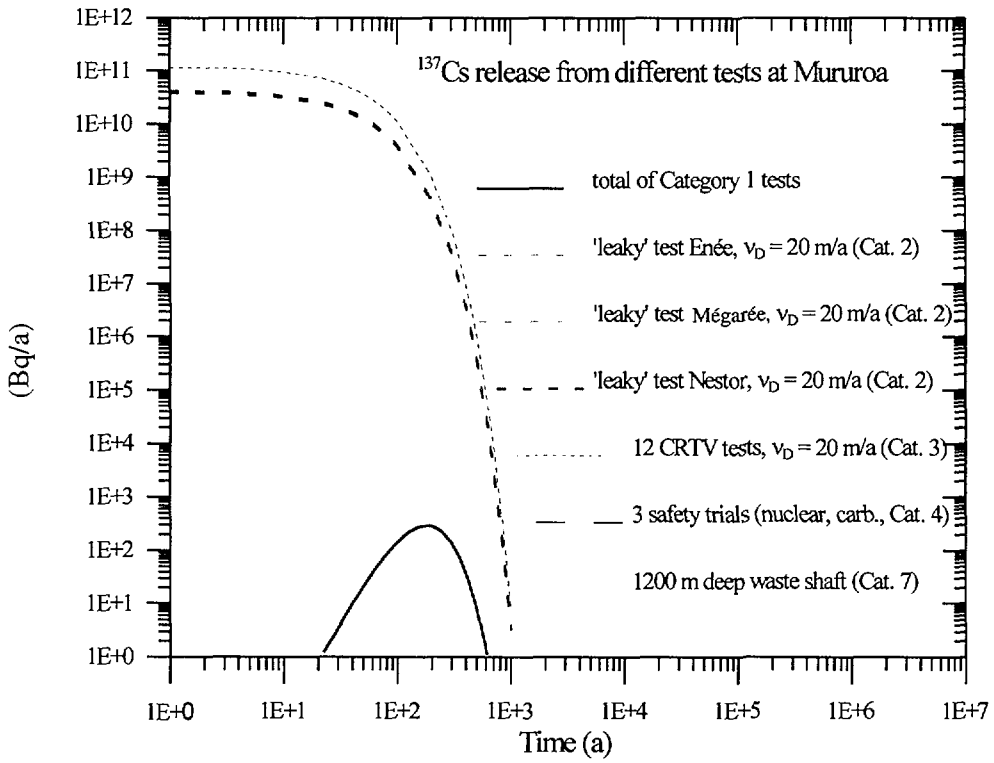

FIG. 66. *^{137}Cs release into the Mururoa carbonates from different tests. Note: The ^{137}Cs releases of Enée, Mégarée, Nestor and the 12 CRTV tests are essentially the same. Releases of ^{137}Cs from the 3 safety trials with nuclear yield in the carbonates and the deep waste shaft, if any, are below the scale of this figure.*

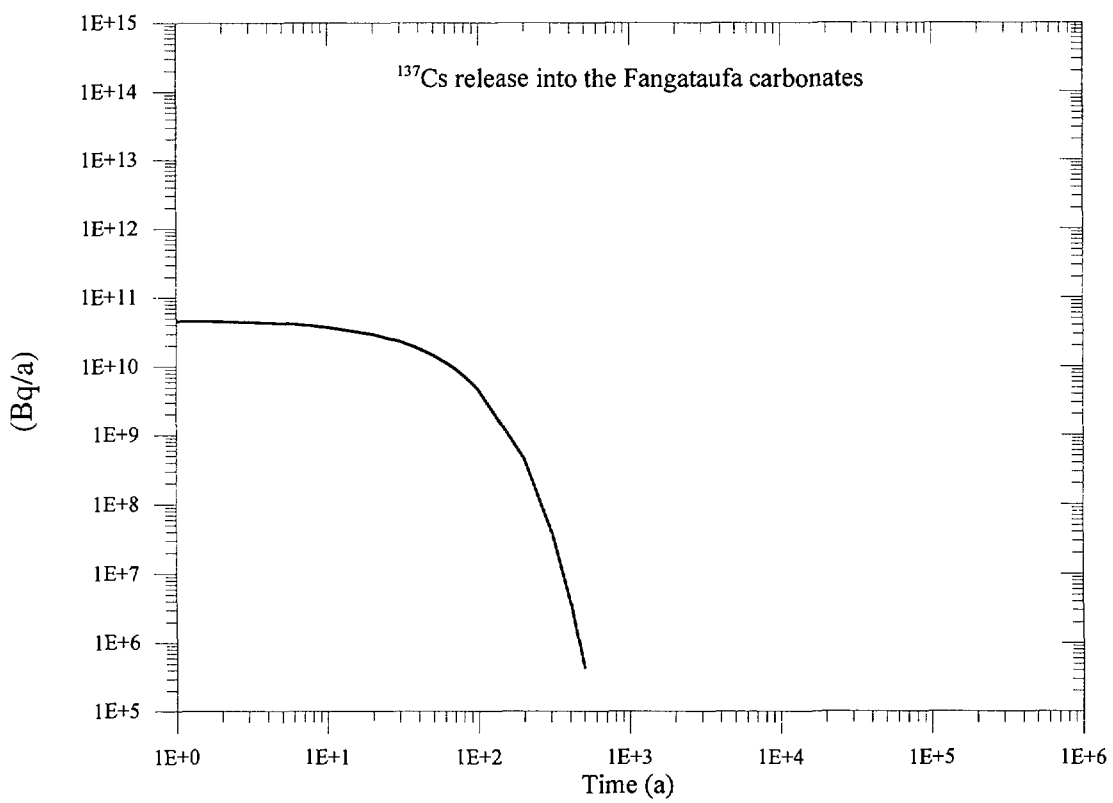

FIG. 67. *Total ^{137}Cs release into the Fangataufa carbonates.*

However, we again overestimate the fluxes to the lagoon by about a factor of 10 if the later test date of Mégarée is taken into account. Measurements of concentrations in the lagoon do not show the strong decrease seen in the calculations. This difference is only partially attributable to the above-mentioned neglect of different test times. We have not been able to account for this discrepancy but, since the calculated result overestimates the measured values, it is conservative.

2. ^{90}Sr

The ^{90}Sr release into the carbonates is presented in Fig. 65 for the Category 1 tests. It also includes the releases into the lagoon for the Catogeries 2 and 3 tests. ^{90}Sr is relatively short lived and sorbing. Retardation in almost any geological barrier is sufficient to reduce and retard the breakthrough significantly. Consequently, the releases to the carbonates and to the lagoon are dominated by the Category 2 and Category 3 tests. Peak releases of ^{90}Sr from these tests to the lagoon are calculated to occur at about 100 years after the tests. Peak releases from Category 1 tests into the carbonates occur at about the same time at a much lower rate. According to these results ^{90}Sr should still be contained in the carbonates. This result suggests that the ^{90}Sr concentrations measured in the lagoons (see Vol. 2 of this Technical Report) must be relics of the atmospheric tests. Neglecting sorption on lagoon sediments or assuming that sorption sites become saturated over time, we would calculate a maximum ^{90}Sr concentration in the Mururoa lagoon of 1 Bq/m^3 in the future and the same order of magnitude for Fangataufa. This value is similar to the present day concentrations in the lagoons.

3. ^{137}Cs

The ^{137}Cs releases into the carbonates are presented in Figs 66 and 67 for Mururoa and Fangataufa. This radionuclide is also relatively short lived and more strongly sorbing than strontium. Releases into the carbonates are dominated by Category 2 and 3 tests. As a consequence of the ^{137}Cs sorption, almost any geological barrier will reduce the breakthrough level of caesium to insignificance. This is consistent with the fact that no breakthrough to the lagoons has been observed. All ^{137}Cs is retained in the carbonates and decays there. Consequently, the measured concentrations in the lagoons (see Vol. 2 of this Technical Report) are interpreted as relics of the atmospheric tests.

It cannot be emphasised sufficiently that, for short lived and sorbing nuclides such as ^{137}Cs, assumed releases of this radionuclide into the marine environment are an extreme overestimation of the fluxes of this radionuclide to the biosphere. In our view, this assumption goes beyond reasonable conservatism and borders on incredibility. This opinion holds also for the assumption that a few percent of the flux of this radionuclide into the carbonates is instantaneously transferred to the ocean. In this regard it shows that the outlet flux from the carbonates is not a linear function of the inlet flux for such radionuclides.

4. ^{239}Pu

The ^{239}Pu releases to the carbonates and to the lagoon are presented in Figs 68–72. The results of taking an assumed fast colloid transport of 10% of the ^{239}Pu into account has to be discussed separately (Fig. 73). The ^{239}Pu has three properties which differentiate it from the previous ones. (a) It is relatively long lived, (b) it sorbs strongly, and (c) its major part of the inventory is in the lava. As a consequence, its release to the geosphere will extend over very long periods of times.

The early release of ^{239}Pu into the carbonates is dominated by the Category 3 tests (see Figs 68 and 70) and, to a lesser extent, by Category 2 and Category 4 tests (Fig. 68). For times beyond 100 years, releases from these tests are overestimated because a constant high water flux through the cavity-chimney and in the carbonates is assumed in the model calculations.

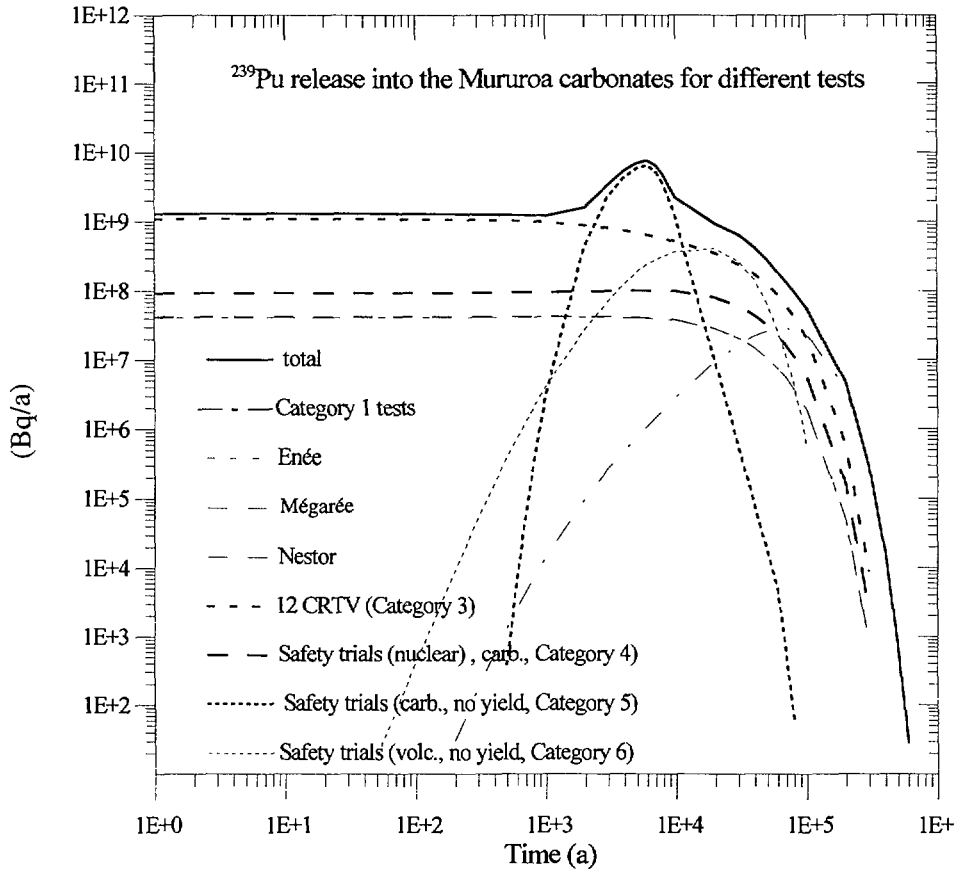

FIG. 68. *^{239}Pu release into the Mururoa carbonates from different tests. Note: The ^{239}Pu releases of Enée, Mégarée and Nestor are essentially the same. The ^{239}Pu release from the safety trials without nuclear yield in the carbonates is given for a distance of 10 m from the source.*

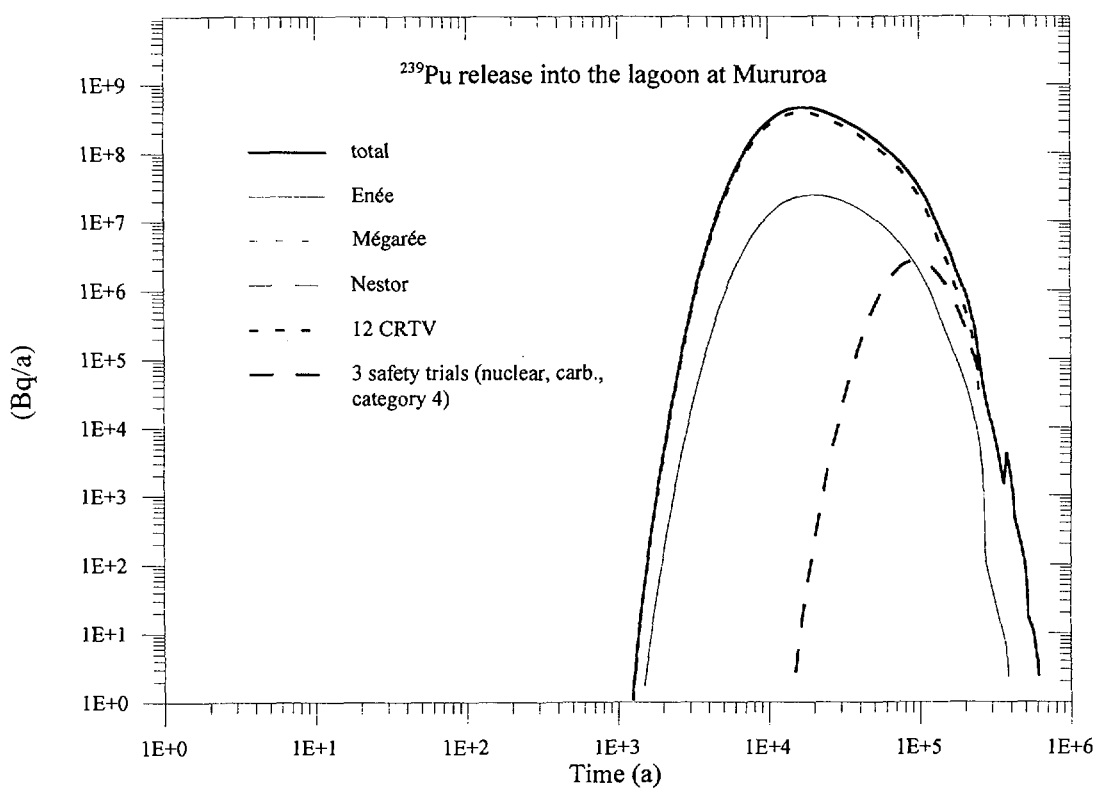

FIG. 69. *^{239}Pu release into the lagoon at Mururoa from different tests. Note: The ^{239}Pu releases of Enée, Mégarée and Nestor are essentially the same.*

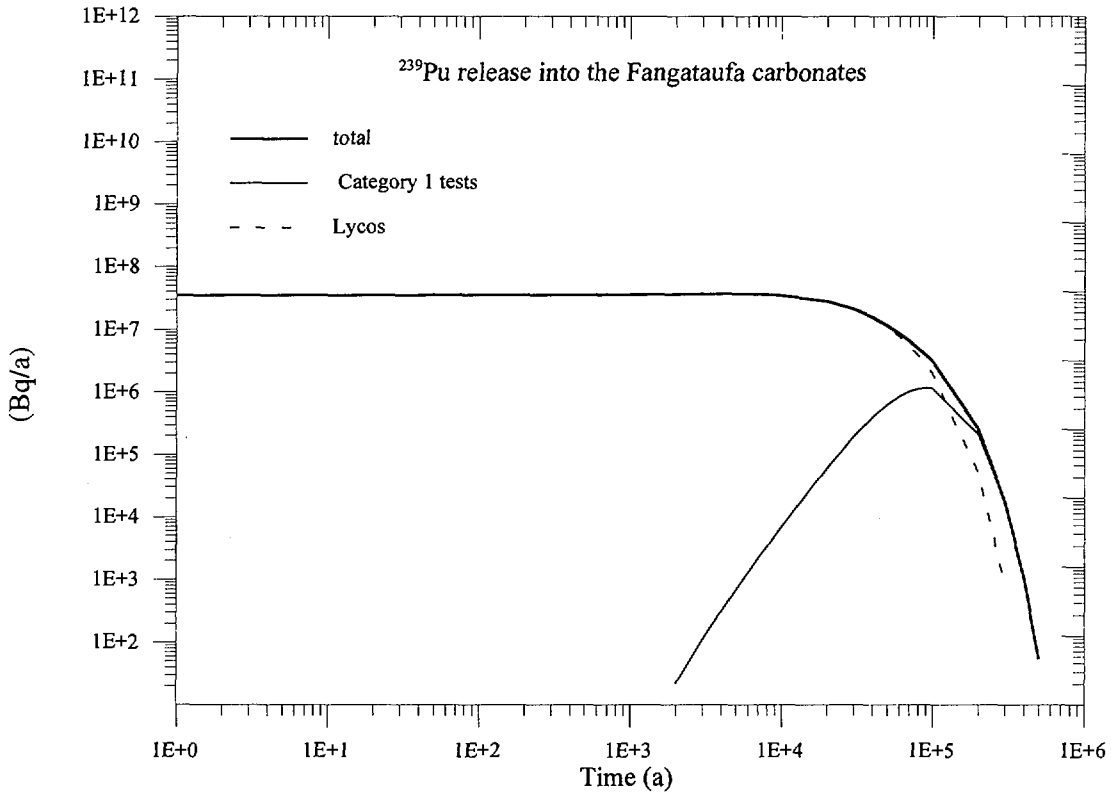

FIG. 70. ^{239}*Pu release into the Fangataufa carbonates for different tests.*

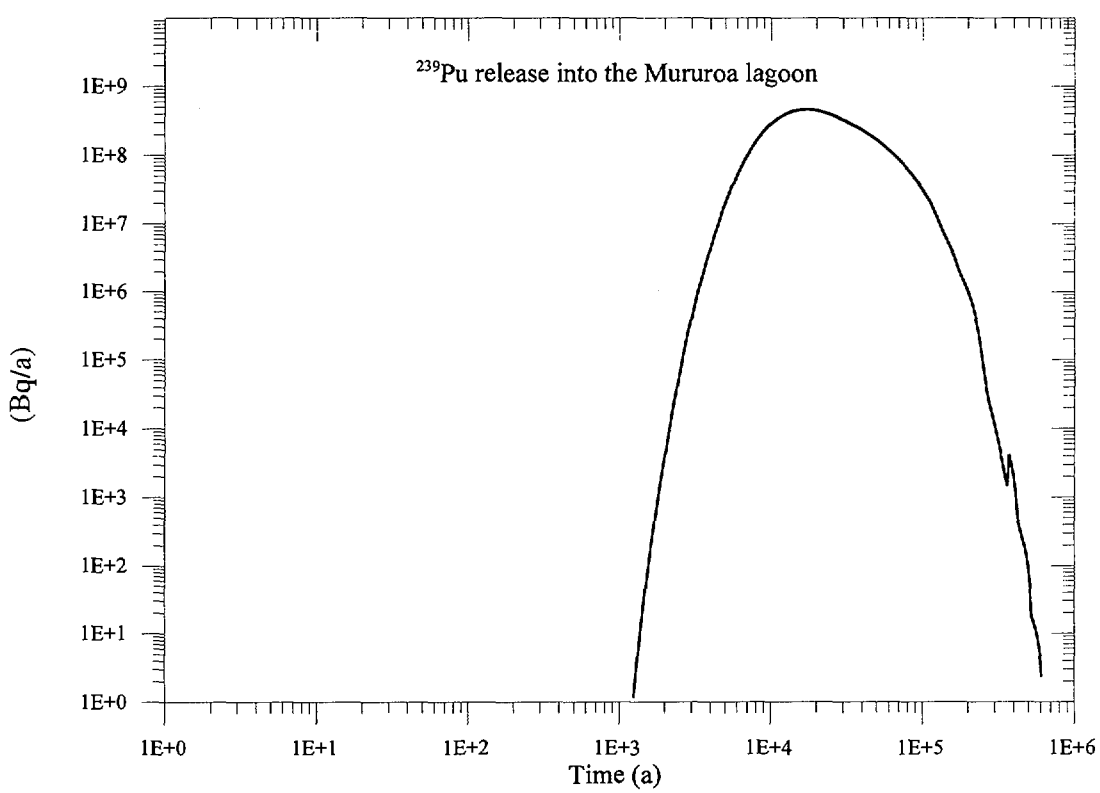

FIG. 71. Total ^{239}*Pu release into the Mururoa lagoon.*

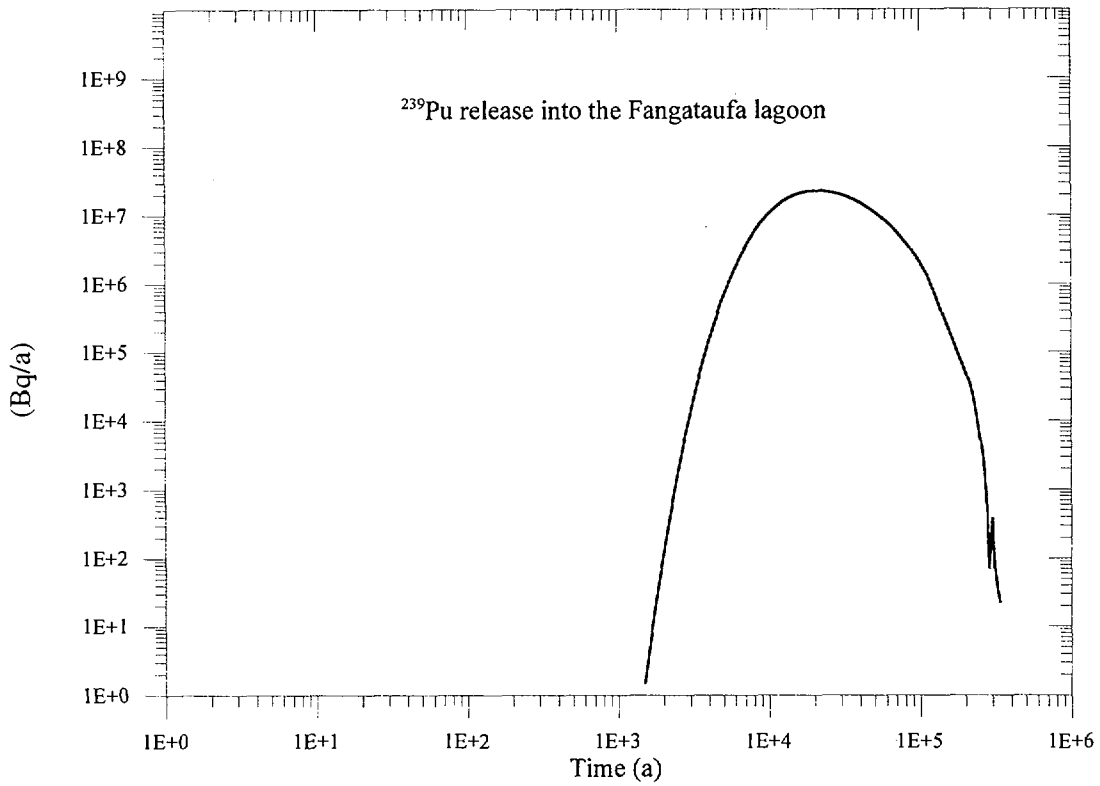

FIG. 72. Total ^{239}Pu release into the Fangataufa lagoon.

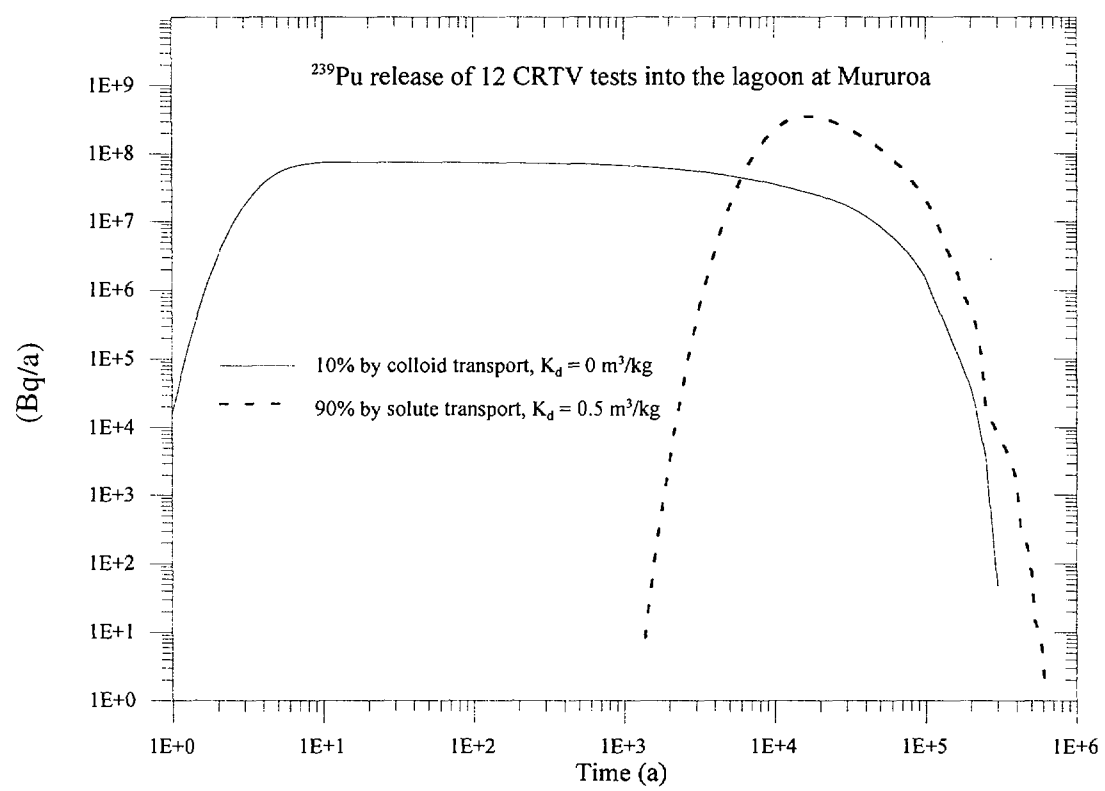

FIG. 73. ^{239}Pu release into the Mururoa lagoon for 12 CRTV tests with an assumed colloid transport of 10% of the ^{239}Pu. Note: It is assumed that ^{239}Pu is irreversible sorbed on colloids which are assumed not to sorb on the carbonates (K_d = 0 m^3/kg).

After a few thousand years and up to about 10 000 years, Category 5 tests dominate the ^{239}Pu release (Fig. 68). This result is a consequence of assuming a high plutonium solubility and a 10 m migration barrier (advection - dispersion and sorption) in the carbonates. These assumptions are not realistic but they are much less conservative than those used by CEA scientists, who assumed a diffusion barrier for these tests.

The ^{239}Pu breakthrough to the lagoons is calculated to begin to occur beyond 1000 years (Figs 69, 71–72). Thus, the presently measured plutonium concentrations in the lagoons must be relics of the atmospheric tests. The releases to the lagoons are dominated by Category 3 tests at Mururoa (Fig. 69) and (Fangataufa) with peak releases calculated to occur after about 20 000 years. It should be noted that Category 5 tests do not contribute appreciably to releases to the lagoon at Mururoa although they are the peak contributor to the release into the carbonates for a few thousand years. This result is caused by the fact that dispersion smears out the breakthrough curve into the carbonate and decreases the ^{239}Pu concentration. Furthermore, the total plutonium inventory of these tests is small compared to the other categories.

A special modelling approach has been used for colloidal plutonium transport through the geosphere in order to deal with the issue of fast plutonium transport via natural colloids. These may carry plutonium but may not undergo sorption. It should be noted that the underground water sampling provided no evidence of the presence of natural colloids (see Section 6). As no quantitative information is available on the concentration of natural colloids in the groundwater and on their characterisation, we have made the speculative assumption that 10% of the plutonium is assumed to be irreversibly sorbed on natural colloids which are mobile in the liquid phase ($K_d = 0$).

The calculation of this scenario was simplified in such a way that only the 12 CRTV tests on Mururoa have been taken into account as a source for ^{239}Pu release. This simplification can be made because the total ^{239}Pu release to the lagoon and the respective release from the CRTV tests are almost identical (Fig. 69).

As expected, a rapid breakthrough of ^{239}Pu into the Mururoa lagoon is calculated. The maximum flux involves 10% of the dissolved plutonium fraction (Fig. 73). The conclusion is that colloids, if they would occur on the atolls and if they did not undergo sorption, could induce an early breakthrough of plutonium. The magnitude is proportional to the proportion of plutonium fixed on such colloids and the release rate from Category 2 and 3 tests into the carbonates. For Fangataufa, which does not have CRTV tests, the maximum flux of such a colloidal plutonium transport into the lagoon would be about 40 times lower than for Mururoa. For times beyond a few thousand of years, such a colloid transport would become negligible compared to the transport of dissolved plutonium.

5. Other radionuclides

Radionuclides other than the four above are divided into two classes: non-sorbing and sorbing. Non-sorbing radionuclides are rapidly transferred from the cavity-chimney, either to the ocean or to the lagoon. The release of non-sorbing radionuclides is mainly determined by that part of the inventory which is mobile in the cavity-chimney. In this case, the assumption of a constant, high Darcy velocity in the cavity-chimney (Category 2) and in the carbonates, i.e. 20 m/a, is reasonable.

Short lived sorbing radionuclides decay during geosphere transport within a short distance away from the source. Therefore, it is very conservative, or even unreasonable, to use the release from the cavity-chimney for Category 2 and 3 tests as the release rate into the ocean.

Long lived sorbing radionuclides show a late breakthrough into the lagoon. In this case, it seems to be too conservative to assume an initially high Darcy velocity of 20 m/a in the carbonates. Hence, for these radionuclides a Darcy velocity of 2 m/a was applied.

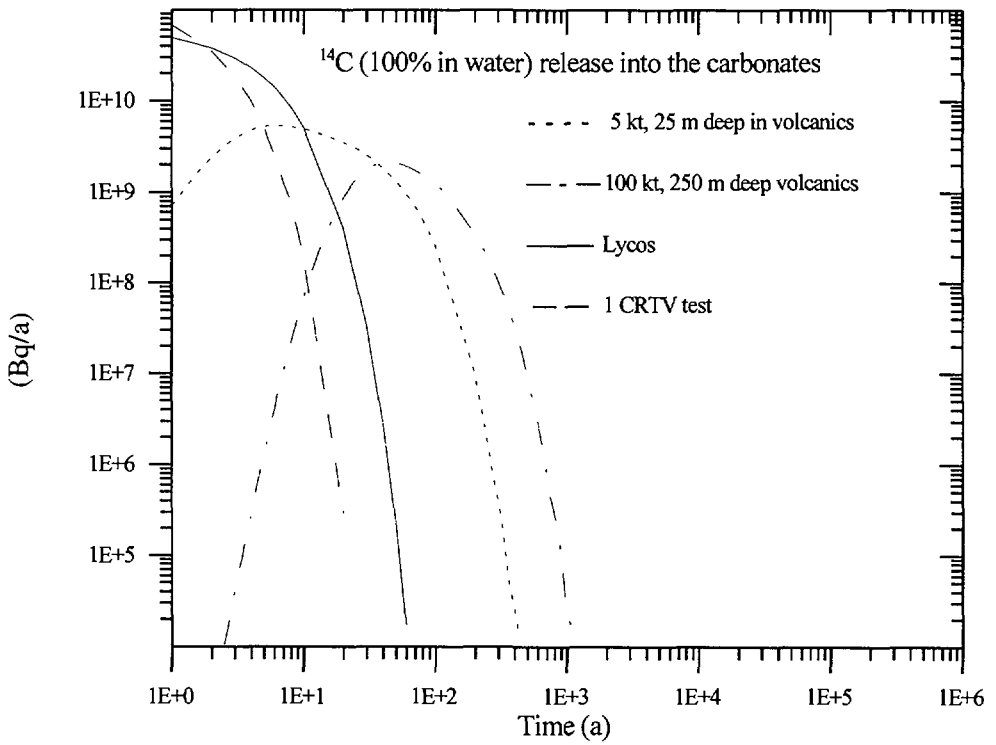

FIG. 74. *^{14}C release into the carbonates for different tests.*

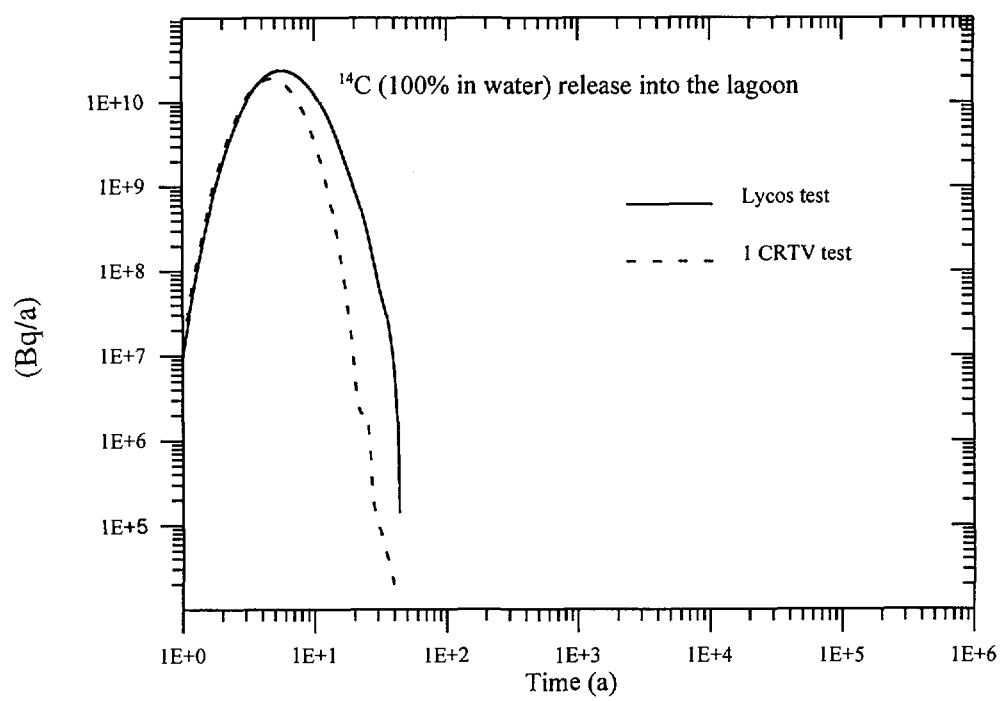

FIG. 75. *^{14}C release into the lagoon for different tests*

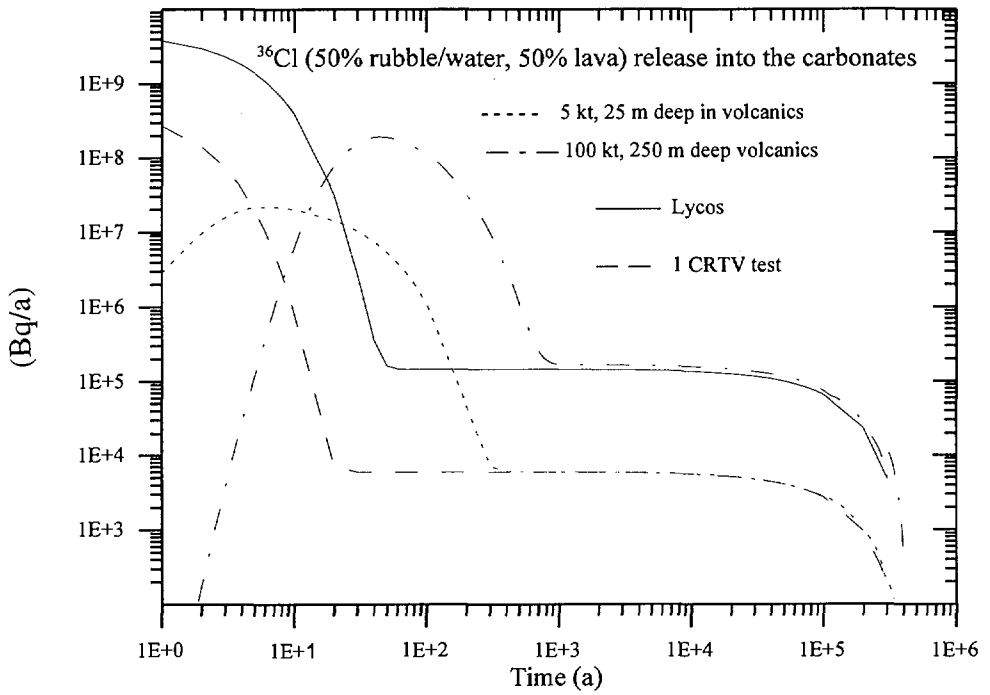

FIG. 76. *^{36}Cl release into the carbonates for different tests.*

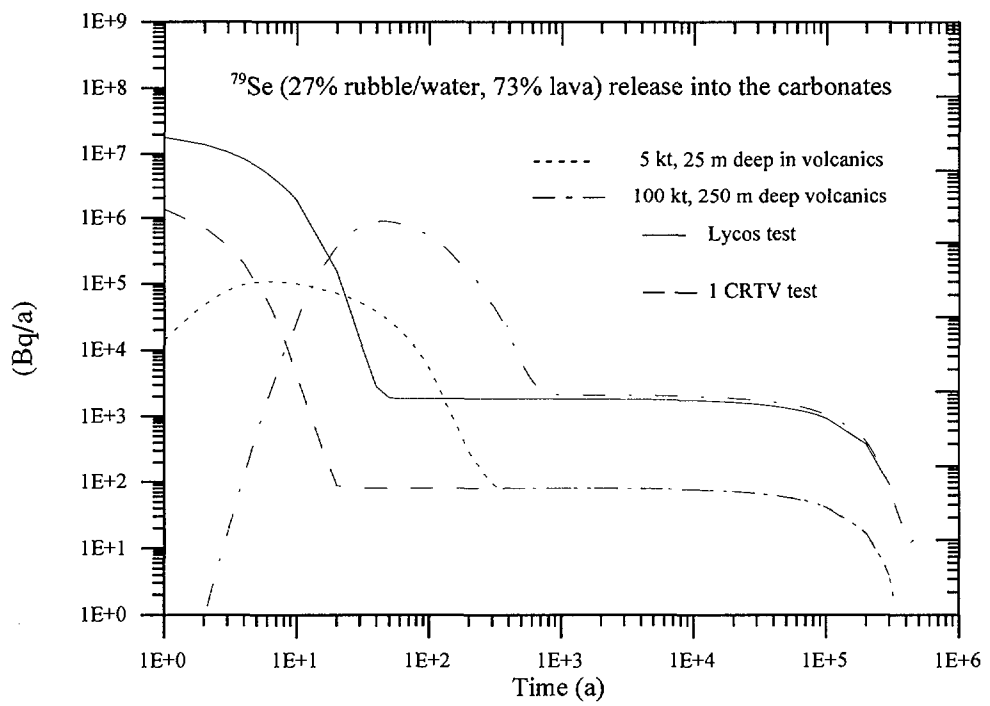

FIG. 77. *^{79}Se release into the carbonates for different tests.*

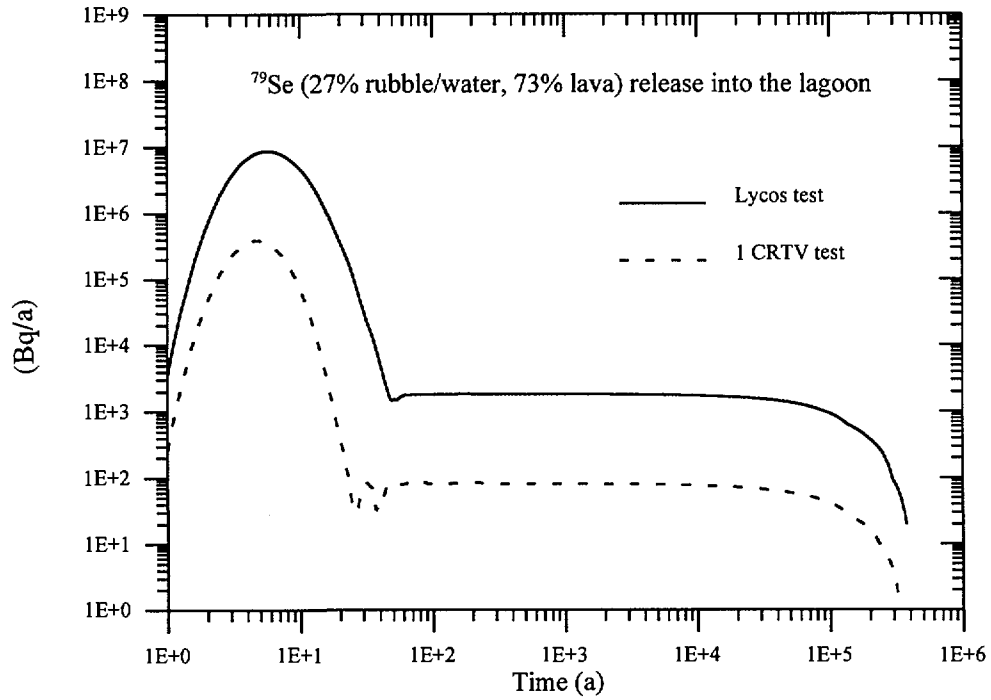

FIG. 78. *^{79}Se release into the lagoon for different tests.*

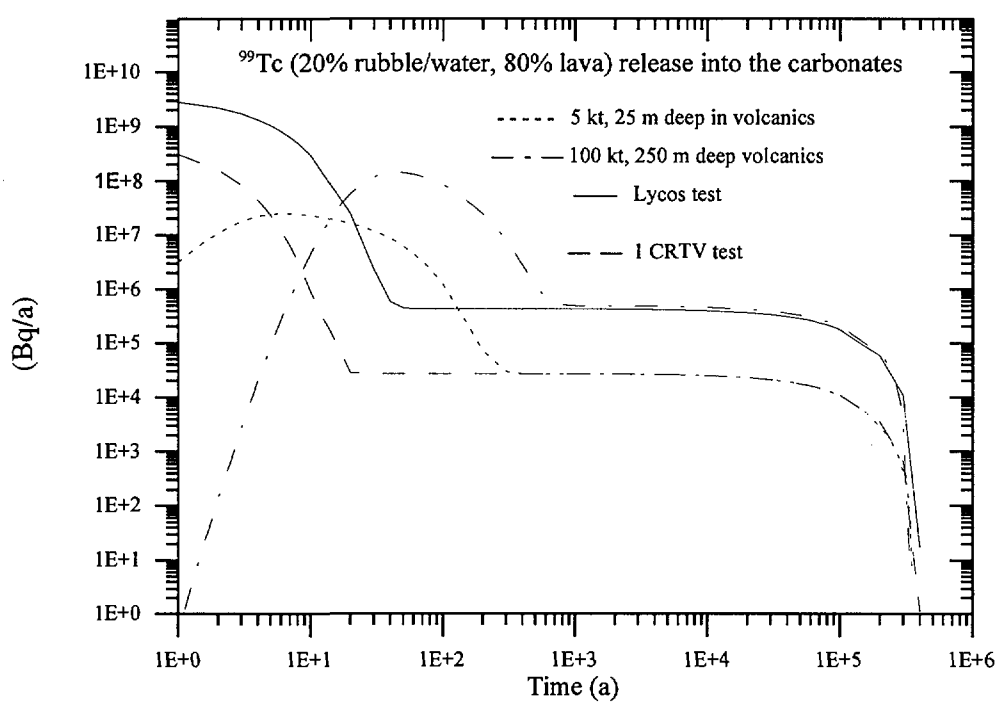

FIG. 79. *^{99}Tc release into the carbonates for different tests.*

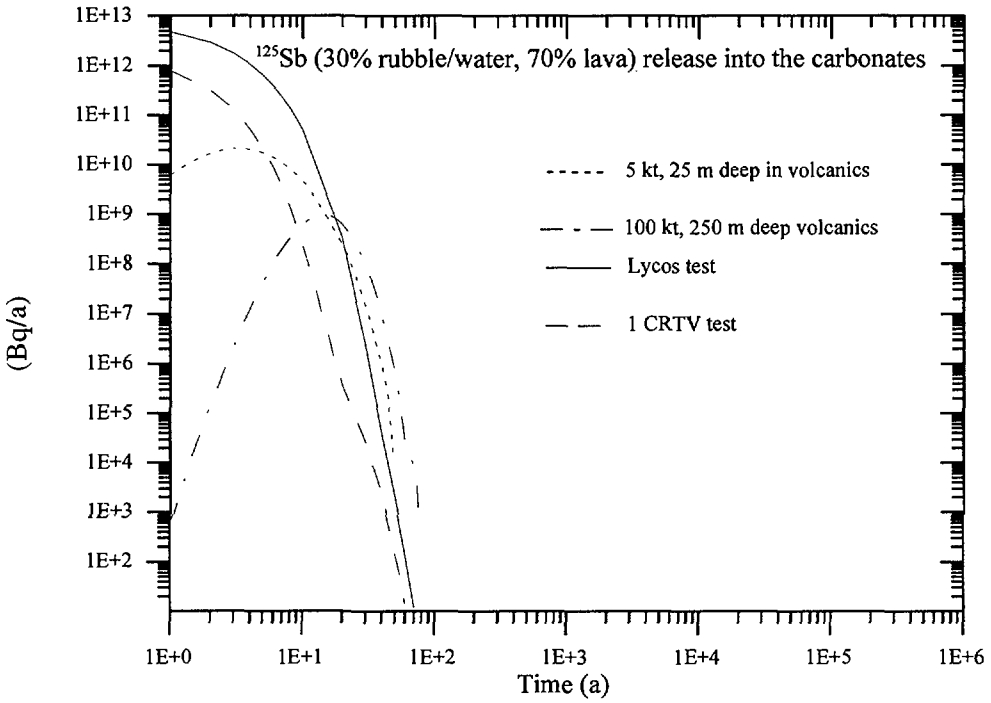

FIG. 80. ^{125}Sb *release into the carbonates for different tests.*

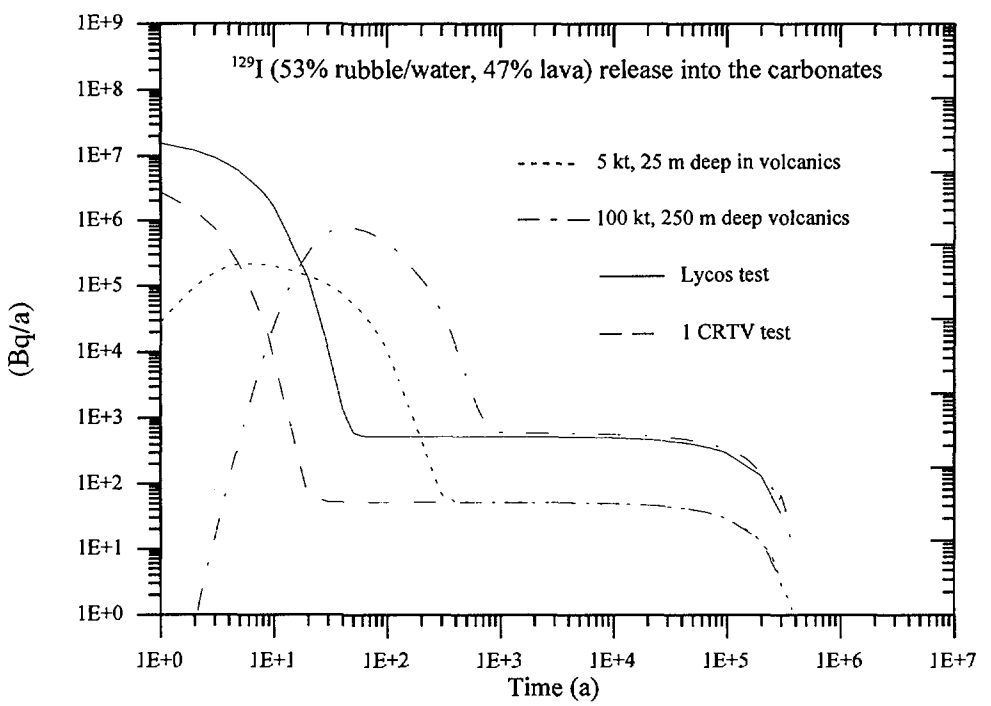

FIG. 81. ^{129}I *release into the carbonates for different tests.*

(a) Non-sorbing radionuclides

The assumption of non-sorption for the radionuclides ^{14}C, ^{36}Cl, ^{79}Se, ^{99}Tc, ^{125}Sb and ^{129}I is certainly a conservative approach. ^{14}C for example, would be expected to undergo an exchange with the non-radioactive isotope ^{12}C and thus be retarded.

For all these radionuclides a Darcy velocity of 20 m/a was assumed for Category 2 and 3 tests. The cavity-chimneys empty rapidly and the contribution from lava leaching, if any, can be neglected.

Release rates into the carbonates were calculated for typical tests, i.e. for Lycos (Category 2) and for a CRTV test (Category 3) at two different depth with different yield. The results are presented in Figs 74–81. In order to calculate the total releases, it would be necessary to multiply the release rates of the above mentioned tests by the following factors and sum up the various totals

- for Mururoa: deep volcanics by 20 (Category 1)
  shallow volcanics by 90 (Category 1)
  Lycos by 3 (Category 2)
  CRTV by 12 (Category 3)

- for Fangataufa: deep volcanics by 8 (Category 1)
  Lycos by 1 (Category 2).

An evaluation of the breakthrough curves shows that a simplified, but fair estimate of release rates to the lagoons is obtained for Mururoa by taking the Lycos curve multiplied by 3 plus a single CRTV curve multiplied by 12. The release rate to the Fangataufa lagoon is represented by the Lycos curve.

This estimate gives reasonable results with respect to the maximum release rates to the lagoon, although it overestimates releases and results in a rapid decrease of radionuclides in the geosphere. This is deemed to be of minor importance because the resulting maximum exposures will be overestimated.

It should be noted that the long term releases in the case of ^{36}Cl, ^{79}Se, ^{99}Tc and ^{129}I are the result of the slow dissolution process of the lava.

(b) Sorbing radionuclides

The release behaviour of more than 20 sorbing radionuclides was assessed. In order to ensure that the fluxes to the carbonates and to the lagoon are not underestimated, the lower sorption coefficient has been used in the calculations whenever two values are given in Table IX. Since even a small sorption coefficients delays transport appreciably, and as breakthrough is further delayed when the relatively short thermal phase is over, a Darcy velocity of 2 m/a was assumed in the carbonates.

The results of the calculations are presented for the same two typical tests (Lycos and CRTV) as mentioned earlier. In order to calculate the total release rates, the same arithmetic as mentioned for the non-sorbing radionuclides has to be applied.

Amongst the sorbing radionuclides ^{55}Fe, ^{60}Co, ^{63}Ni, ^{106}Ru, ^{121}Sm, ^{134}Cs, ^{147}Pm, ^{151}Sm, ^{152}Eu, ^{154}Eu, ^{155}Eu, ^{238}Pu, ^{241}Pu and ^{241}Am have relatively short half-lives. These decay during transport in the carbonates, but the inventory transferred to the carbonates from Category 2 and 3 tests in the first years following the tests might be appreciable. Examples of release curves for these radionuclides are given in Figs 82–84. It can be seen that the ^{60}Co release into the carbonate decreases rapidly (Fig. 82). This is true because of the short half-life of this radionuclide (about 5 years). The release curves of ^{63}Ni (half-life about 100 years) into the carbonates and into the lagoon provide another

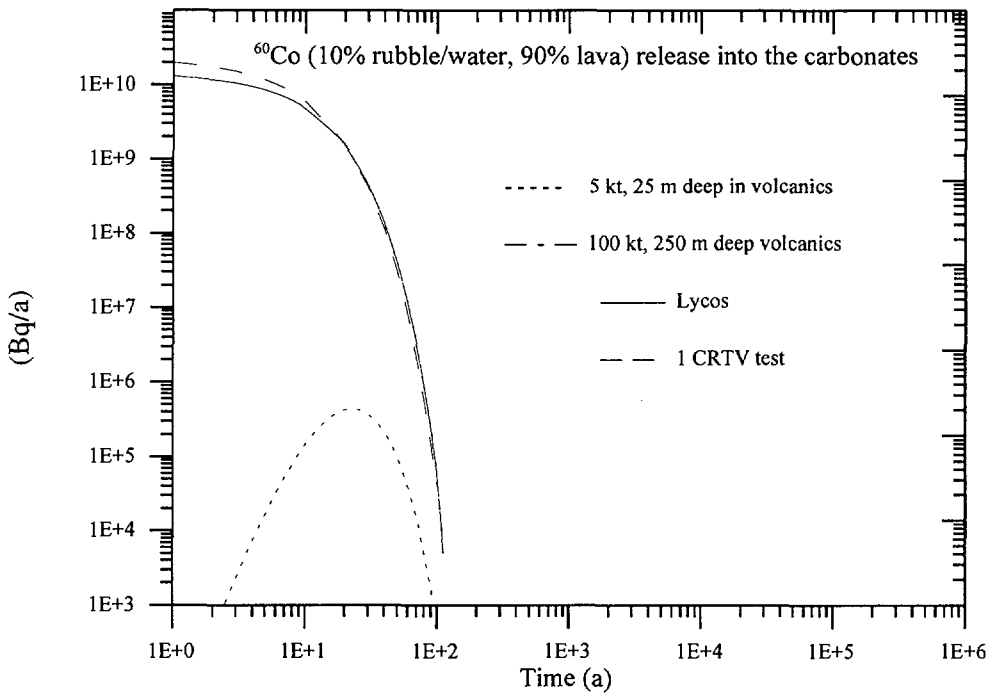

FIG. 82. *^{60}Co release into the carbonates for different tests. Note: The 100 kt test is below the scale of this figure.*

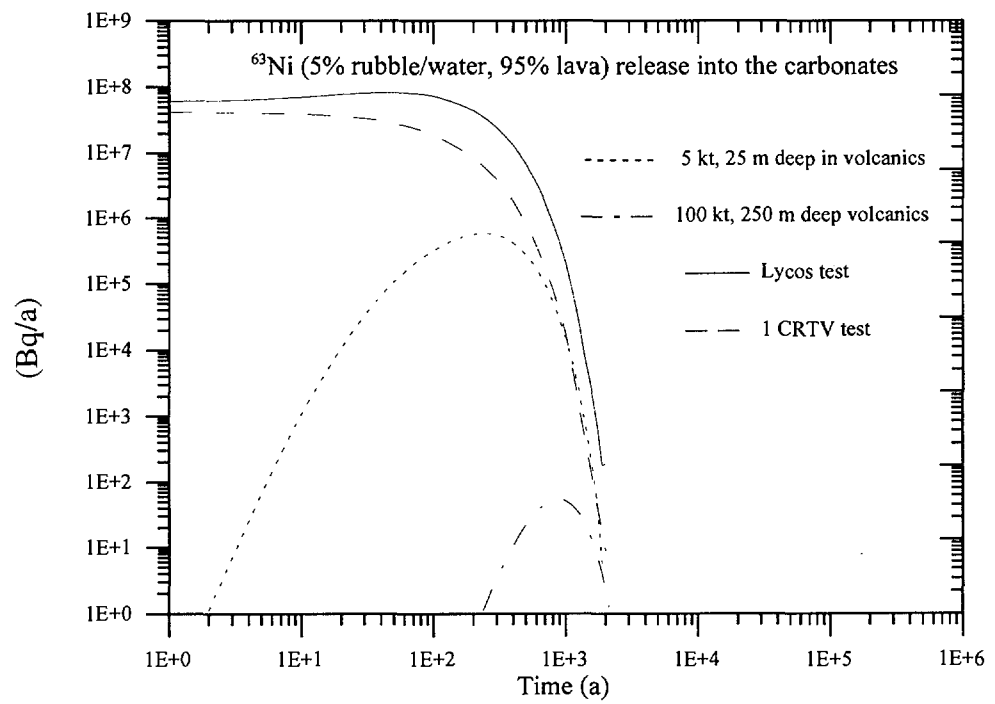

FIG. 83. *^{63}Ni release into the carbonates for different tests.*

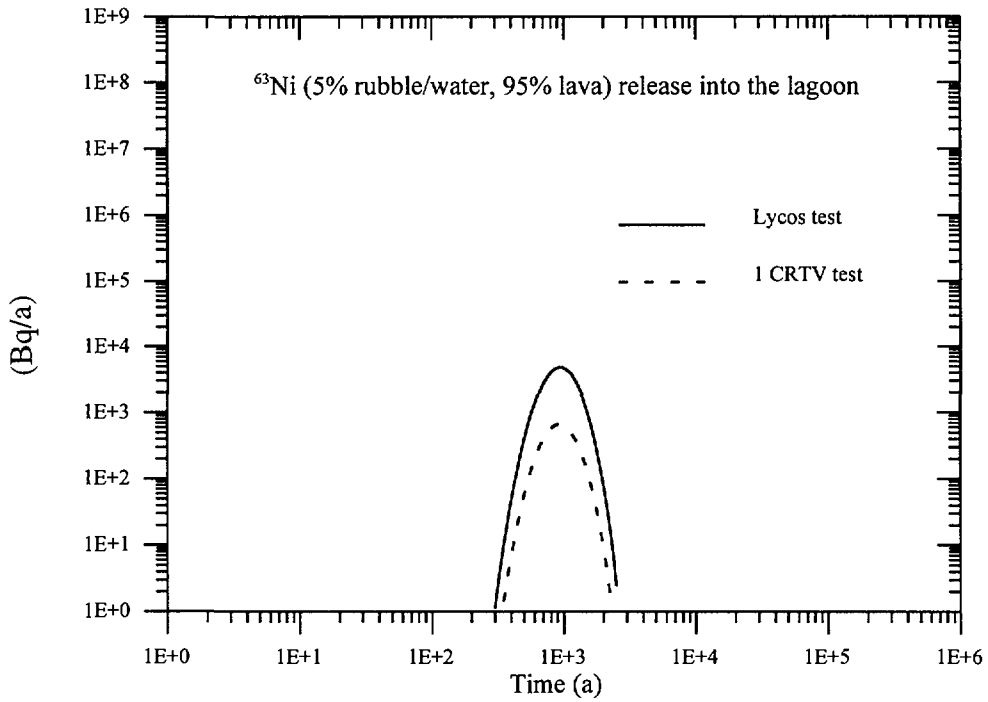

FIG. 84. *^{63}Ni release into the lagoon for different tests.*

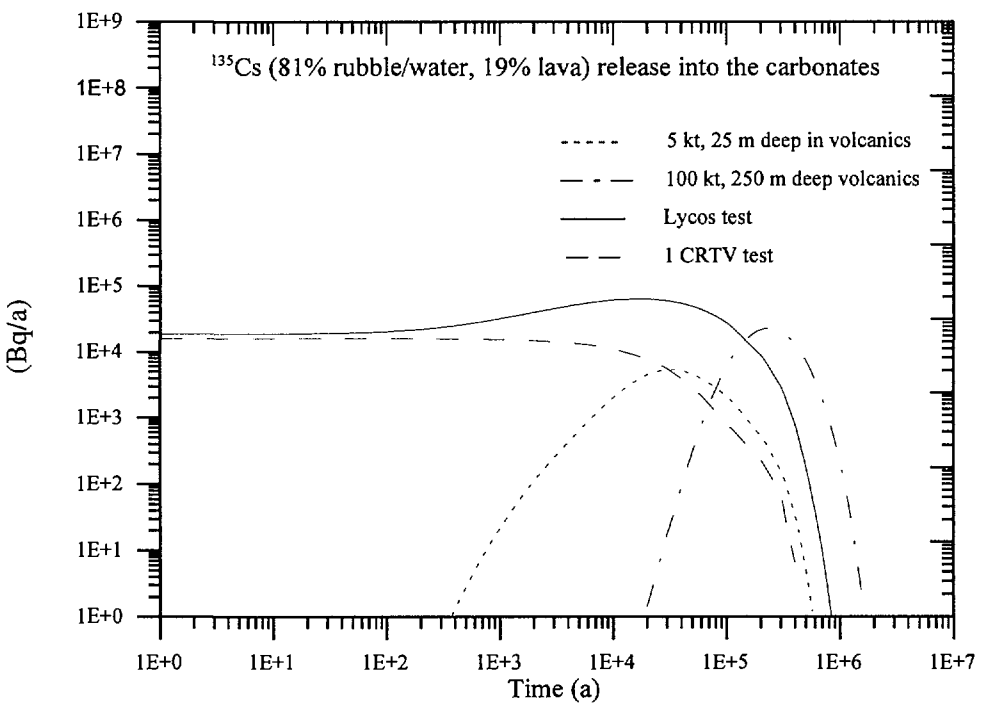

FIG. 85. *^{135}Cs release into the carbonates for different tests.*

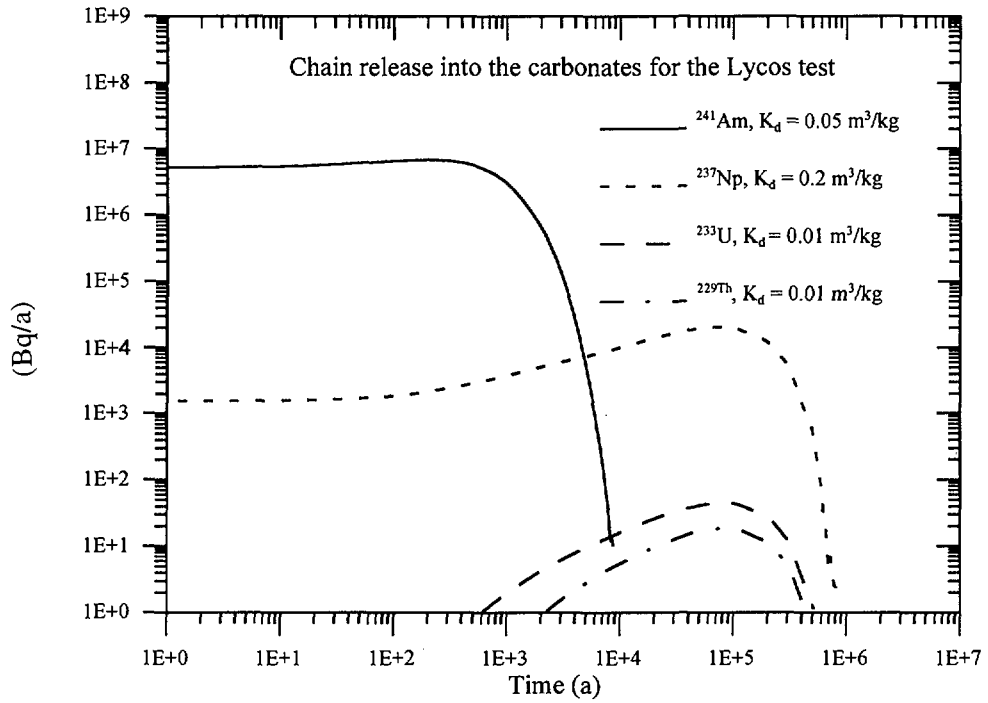

FIG. 86. Release of the ^{241}Am chain members into the carbonates forLycos test.

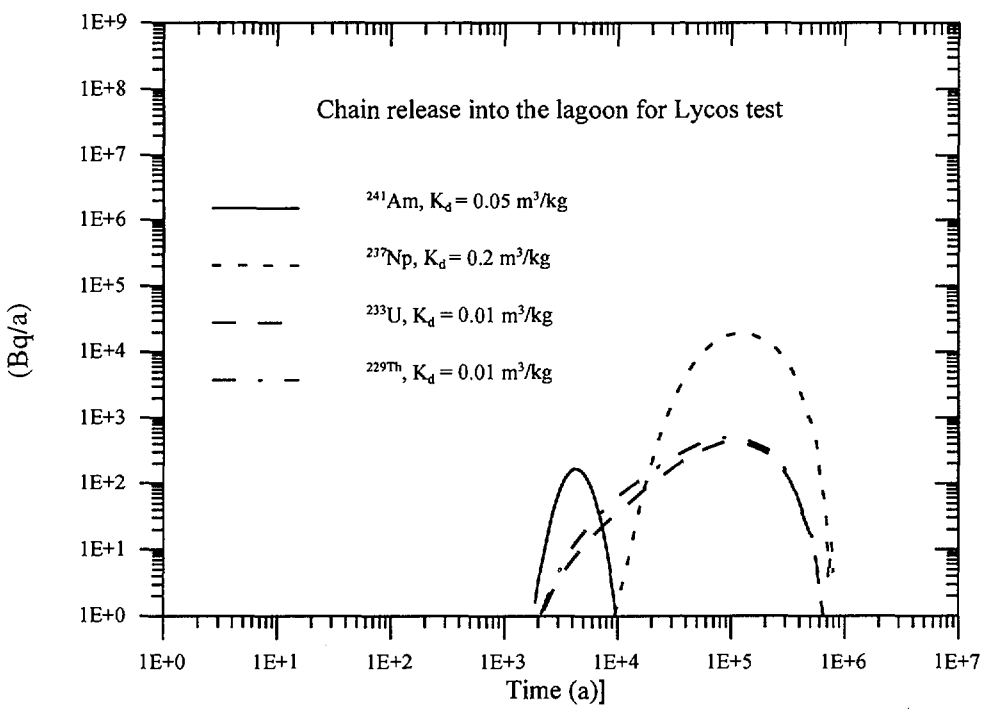

FIG. 87. Release of the ^{241}Am chain members into the lagoon for Lycos test.

interesting example. The strong effect of the decay of this radionuclide by about 4 orders of magnitude during its passage through the carbonate is clearly visible by comparison of Figs 83 and 84.

Amongst the sorbing radionuclides ^{59}Ni, ^{93}Zr, ^{107}Pd, ^{126}Sm, ^{135}Cs, ^{236}U, ^{237}Np and ^{242}Pu have long half-lives. The release rates of all these radionuclides to the lagoon are low and long lasting, as can be seen on the example presented in Fig. 85. The calculations have shown that these radionuclides are not of any radiological significance and, therefore, these results are presented merely for the sake of completeness.

This is also true for ^{237}Np as a chain member. The releases of the whole chain from ^{241}Am via ^{237}Np and ^{233}U to ^{229}Th have been calculated. The results in terms of releases into the carbonates and the lagoon are presented in Figs 86–87 for the Lycos test which has been shown to be the most relevant one from a radiological point of view. It can be seen that the highest releases from this test are in the order of 10^4 Bq/a for ^{237}Np after about 10^5 years.

5.3.5. Concluding remark

It is not possible to provide a quantitative estimate of the degree of conservatism contained in the results presented in this section. It has been mentioned earlier that very little site specific information is available and that parameter values have been assumed for the modelling in a simple approach with no consideration of temporal or spatial variability. Most importantly, the transport model has not been tested in the context of radionuclide migration in atolls. The model is, however, based on a large amount of work done in the context of civilian radioactive waste disposal.

The intention of the base case calculations was to calculate releases to the biosphere in a conservative way and overestimate the consequences by using conservative methods and parameter values, while avoiding the mistake of building conservatism upon conservatism such that the end result becomes totally unrealistic. In the given situation no effort was made to fit any parameters used in the model in order to improve the agreement between calculated and experimental data.

Recognising all of these limitations of the modelling calculations, we believe that the releases presented are reasonable but conservative estimates of the overall radionuclide releases from the geosphere of the atolls to the biosphere.

The modelling results of the radionuclide release through the geosphere were compared with the actually measured radionuclide inventories in underground waters (see Section 6). On this basis a refinement and adjustment of the modelling of radionuclide releases into the carbonates was made. Using estimates of the inventory of radionuclides in the carbonate and measurements of tritium release rates into the lagoon (obtained from the elevation in tritium concentration above the natural oceanic background, see Vol. 2 of this Technical Report) a simple, semi-empirical mixing model was developed to estimate maximum release rates to the lagoon and ocean (see Section 6.10).

6. UNDERGROUND WATER SAMPLING - MODEL VALIDATION AND REFINEMENT

Radionuclides deposited in the geological formation of the atolls of Mururoa and Fangataufa may be transported by water as a carrier through the geosphere to the biosphere. Such processes are often slow and take such long periods of time that estimates of releases from the underground rely on numerical models developed for such purpose. Because of the long time periods involved it is difficult to provide reasonable assurance that predicted releases represent the actual behaviour of radionuclides in a sufficiently precise manner.

The measurement of radionuclide concentrations in cavity-chimneys and monitoring wells at the Mururoa and Fangataufa Atolls provide very valuable information for the validation of these predictions. In addition, sampling of the monitoring wells provides an independent check of the concentrations of radionuclides reported by the CEA on both atolls. This verification step is important because many of the monitoring wells are located in the highly permeable karstic horizons.

A sampling campaign to collect water samples from monitoring and cavity-chimney wells on the atolls of Mururoa and Fangataufa was undertaken in late May and early June, 1997 by representatives of the International Atomic Energy Agency (IAEA) with the logistic support from the CEA and the French army. Two cavity-chimneys on the Mururoa atoll and nine monitoring wells in the carbonates on Mururoa and Fangataufa were selected for sampling by the IAEA. The sampling plan was developed by experts involved in the Study based on information provided by the CEA on the details of individual well constructions as well as previously measured radionuclide concentrations in these wells.

6.1. MONITORING WELL NETWORK

The CEA has monitored the concentration of radionuclides in waters beneath Mururoa and Fangataufa during nuclear testing on the atolls. Initially the wells consisted of open large diameter emplacement holes used for underground nuclear explosions. In 1986 testing moved from the rim to the lagoon and wells were subsequently sited in the lagoon. Samples were taken of pumped water during air-lift drilling. Emplacement holes were sampled before a nuclear test by use of sample bottles attached to a cable and hoist.

During the period from 1994 to 1996 a network of monitoring and cavity-chimney wells was installed on Mururoa and Fangataufa to support a long term monitoring programme on both atolls. This network of wells allows the distribution of radioactivity beneath the atolls to be determined spatially and concentration gradients mapped. Vertical wells were constructed in the northern rim of the Mururoa atoll as well as in previously investigated regions of the Mururoa and Fangataufa lagoon. Additionally, the vertical upper section of radiochemical post-shot holes were adapted for groundwater sampling after isolation from the cavity-chimney. Radionuclides targeted by the CEA for sampling and analyses included ^{3}H, ^{90}Sr, ^{137}Cs, and $^{239+240}Pu$.

Two types of monitoring wells have been constructed:

(i) wells ending in cavity-chimneys on Mururoa; and
(ii) monitoring wells constructed in the carbonate and volcanics within individual testing areas beneath the Mururoa and Fangataufa lagoons and beneath the Mururoa rim.

Wells ending in cavity-chimneys were directionally drilled into the side of a cavity-chimney. A sealed steel casing is installed over the full length of the drill hole to prevent contamination of the formation. A polyethylene tube with a 8 mm inner diameter is inserted into the cased borehole. At Céto an obstruction prevented the tube from being lowered beyond the entrance to the cavity-chimney.

The monitoring wells are constructed with an upper steel casing and a well head plug. They are otherwise open to the formation to total depth. These wells are equipped with a "polytube" which consists of a bundle of individual tubes each with a 4 mm inner diameter ending at different depths down the well. Up to four tubes end at each depth interval. In this way, waters from multiple intervals in the carbonate, the transition zone, and the basalt can be taken simultaneously to expedite sampling over the depth of the well. A plug separates the carbonate from the volcanic in the monitoring wells. Monitoring wells may also include re-entry holes, instrumentation holes and unused large diameter emplacement holes in addition to dedicated wells.

The characteristics of the selected monitoring wells are provided in Appendix V, Table V.1.

6.2. RADIONUCLIDE DISTRIBUTION IN THE CARBONATES

The underground water samples collected from the various wells on the two atolls provided a basis for the CEA to prepare maps for Mururoa and Fangataufa (Figs 88 and 89) which show the contours of the ^{3}H distribution in the carbonates and the ^{3}H, ^{90}Sr, and ^{137}Cs concentrations in the various monitoring wells.

Figure 88 shows zones on Mururoa where radioactivity is spread in the carbonates. The source of radioactivity are:

(i) nuclear tests in Areas 1, 2 and 3 carried out in the basalt, whose cavity-chimneys have reached the top of the volcanism;

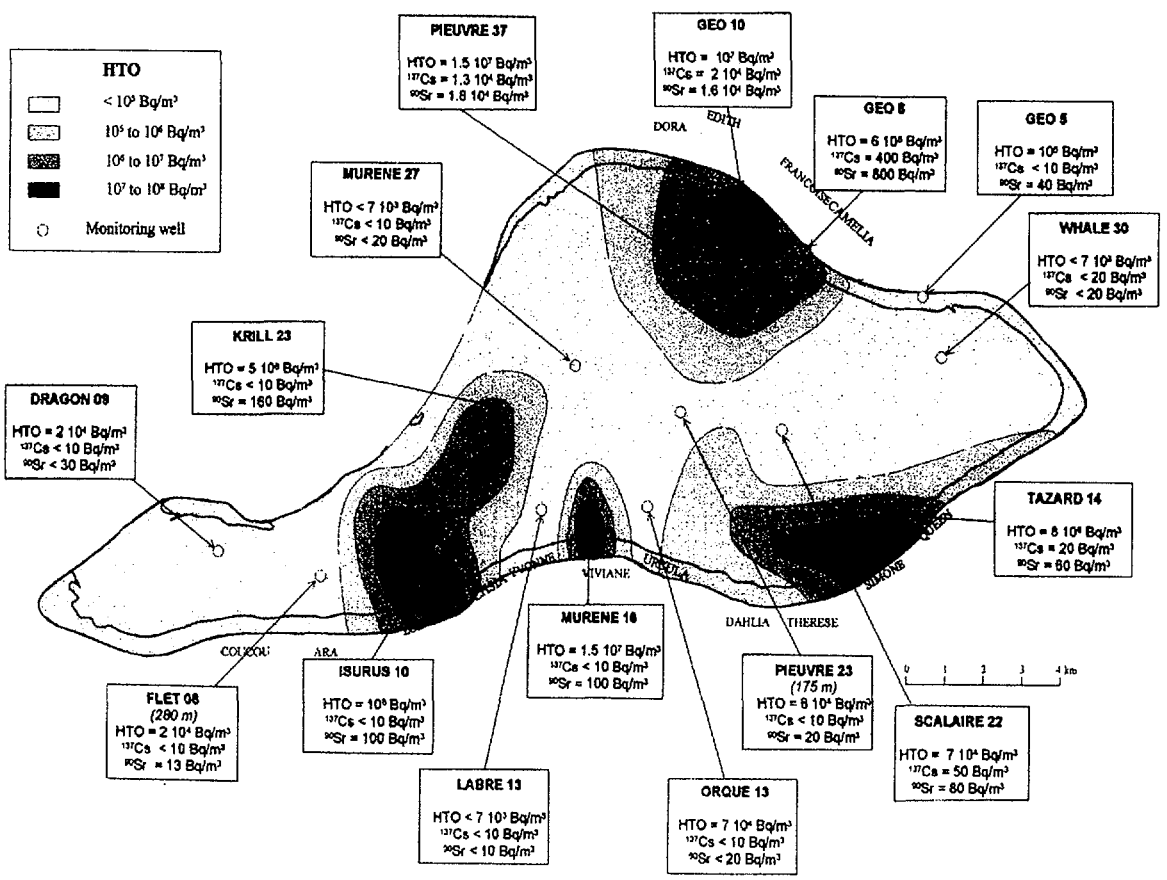

FIG. 88. Tritium contours and concentrations of radionuclides in monitoring wells at Mururoa. (From French Liaison Office Document No. 9.)

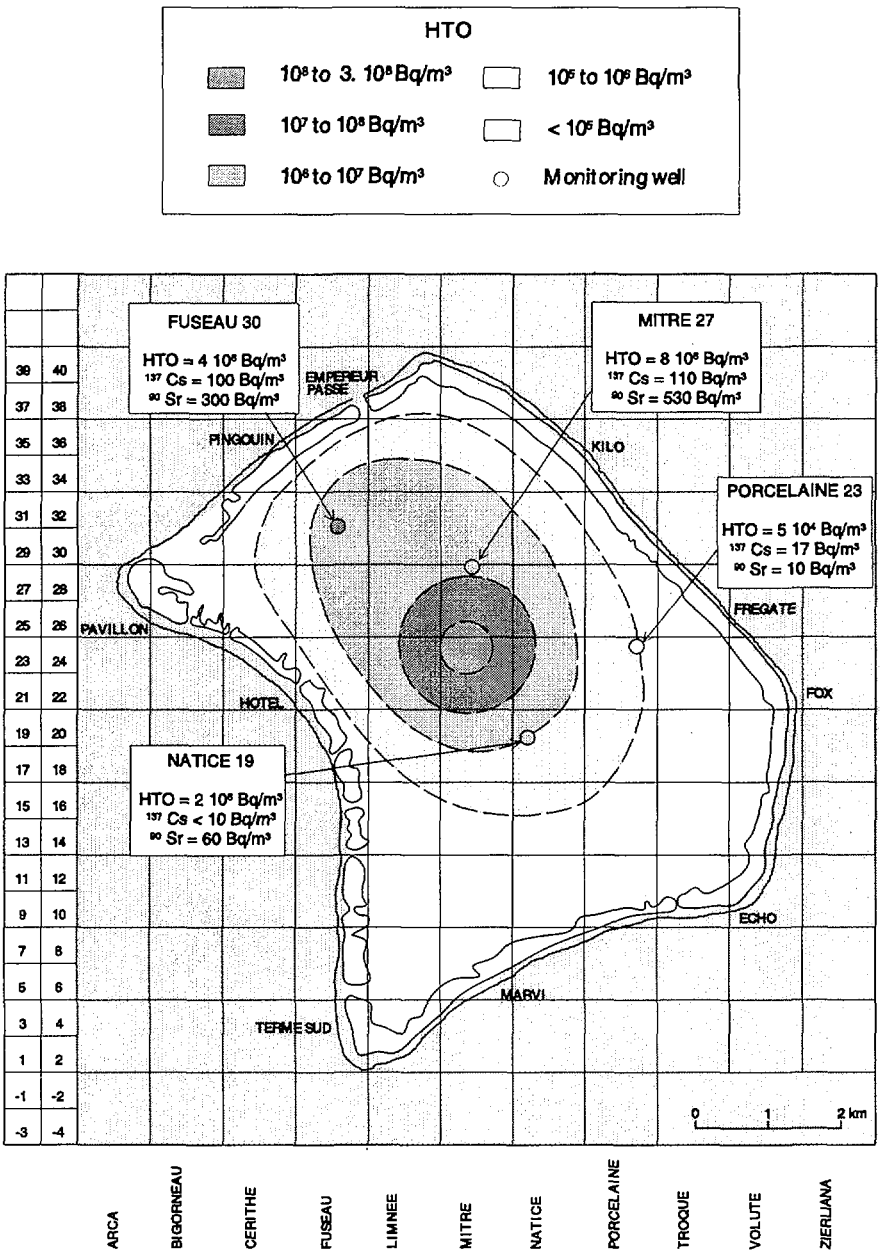

FIG. 89. Tritium contours and concentrations of radionuclides in monitoring wells at Fangataufa. (From French Liaison Office Document No. 9.)

(ii) large yield underground tests (Enée and Nestor under the coral rim in the Area 4 and Mégarée under the lagoon) whose volcanic cover did not sufficiently contain the radionuclides produced by these explosions; and

(iii) safety trials in the carbonate, where some of them went critical.

Figure 89 shows the radionuclide distribution beneath Fangataufa. The radionuclides in the carbonate originate from a single large test (Lycos) which is in hydrologic connection with the carbonate.

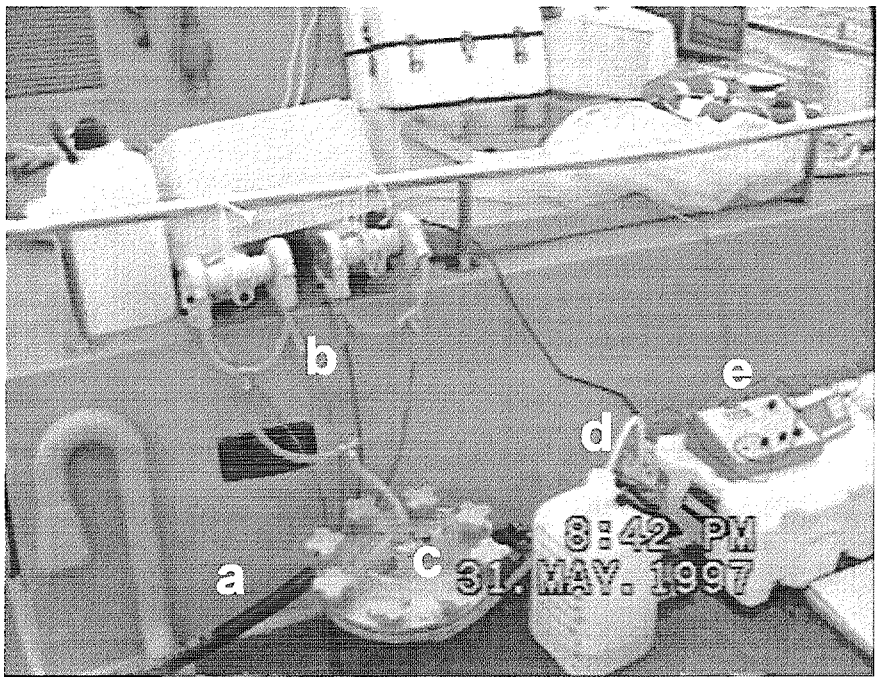

FIG. 90. Set-up of equipment for sampling of underground waters. a) polytube, b) peristaltic pumps, c) filter holder, d) Plexiglas cell for pH, temperature and Eh electrodes and e) electrode read outs.

FIG. 91. Pressurized gas cylinders used to verify sample collection depths.

6.3. UNDERGROUND WATER SAMPLING BY THE IAEA IN MAY AND JUNE, 1997

The IAEA organized and carried out, with technical and logistical support of the CEA and the French Army, a sampling campaign of underground waters on both atolls in May and June 1997. Access was offered to all the wells and the decision as to which wells to sample was made by the IAEA experts.

Two cavity-chimney wells associated with the Céto and Aristée tests on the Mururoa rim were sampled by the IAEA because they allow definition of the solution source term by direct measurement of radionuclide concentrations in solution (dissolved or as colloids). Monitoring wells were selected to intercept waters in the vicinity of the safety trials in the carbonate, nuclear tests with cavity-chimneys that ascended from the volcanics to the carbonate cover and nuclear tests with inadequate volcanic cover. One background location on the Mururoa rim was also selected outside the region affected by underground nuclear testing or the safety trials. Because the monitoring wells are open to the formation, the IAEA strategy for sampling targeted well horizons with the highest radionuclide concentration which in most cases was the deepest section of the carbonate which included the karst. Polytubes from this single interval were combined and continuously pumped.

Continuous pumping of the wells allowed the tubes to be sufficiently purged so that representative samples could be collected and changes in radionuclide and chemical concentrations could be monitored over the course of pumping. At the end of the sampling activity the sampling depth was verified by pressure testing with compressed air.

The IAEA selected radionuclides for analyses based on their production in a nuclear test, a minimum ten year half-life, relative mobility and toxicity. This list expands radionuclides monitored in the French programme and provides a comprehensive measure of the solution source term by including mobile, long lived and toxic species.

Furthermore, major cations and anions were analyzed and ^{3}H, pH, Eh, temperature and pumping rate were measured in the field. The sample collection depth was verified by a pressure test. As decided by the IAEA experts, waters were passed through a 450 nm filter so that the particulate fraction could be separated out. The residues on the filter were also analysed for their radionuclide and elemental composition.

The details of the sampling campaign, including the list of wells sampled, their characteristics and the sampling, sealing and shipping activities as well as the results of the analyses of samples are provided in Appendix V. The equipment used for sampling and pressure testing is shown in Figs 90 and 91.

6.4. FIELD DATA

Field measurements were carefully carried out and data thoroughly recorded and transferred into sample collection logs which are included in Appendix V.

Several field observations from the IAEA sampling expedition are notable.

First, during the sampling of some of the wells in the carbonate, Eh began to trend to higher values. The drift can be correlated to changes in tide. The increase in Eh is speculated to be the result of replacement of deeper waters at the sampling horizons with oxidized waters derived from shallower (near surface) levels after the passing of high tide. The tidal effect was particularly noticeable on the rim of the atolls. Such an effect was not observed during the sampling of the cavity-chimneys. In both cases (Aristée and Céto) Eh decreased with pumping time and stabilized at about $\pm$ 0 mV(SHE). Such Eh values were found to be considerably higher than the very low ones

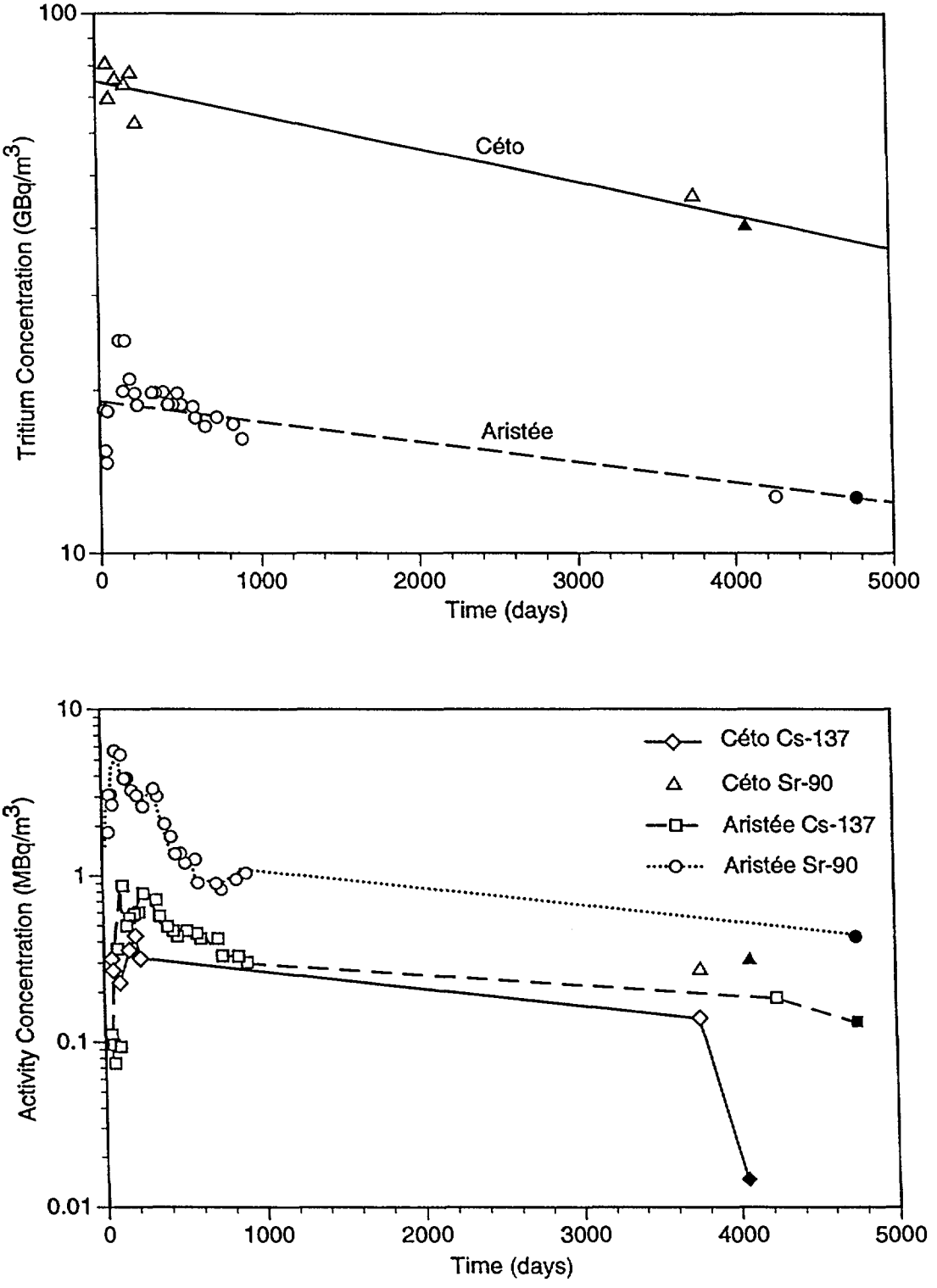

FIG. 92. Measured concentrations of radionuclides in Céto and Aristée cavity–chimneys corrected for decay back to time of test. French data (from French Liaison Office Document No. 8) are shown as open symbols and data from the Study as full symbols.

(~ - 600 mV) measured earlier by the CEA (French Liaison Office Document No. 8, 1996, p. 14). It is assumed to be likely that air entered the system, e.g. during sampling, and increased Eh since the earlier French measurements.

Second, the filter paper used in the in-line sampling system was variably charged with particulates. In some cases (Aristée, Céto, Fuseau 30, Géo 8, Géo 5) the paper had a distinctive reddish-brown colour from a heavy loading of ferric oxides and hydroxides; in other cases (Pieuvre 37, Tazard 14, Murène 16) the filter was loaded with smaller amount of retentates.

Third, tritium measurements made on pumped water samples taken after one, two and three "dead volumes" were produced from each well and also at the conclusion of each day's sampling. The concentrations remained approximately constant for all wells over the course of a day's pumping.

Finally, the field data suggest that the sampling tubes were sufficiently purged and the wells produced representative samples for the respective depth.

6.5. LABORATORY INVESTIGATIONS

Radiochemical and chemical analyses of the samples (waters and filter residues) collected during the IAEA sampling campaign from two cavity-chimneys and nine monitoring wells on the atolls of Mururoa and Fangataufa were performed by the IAEA Marine Environment Laboratory in Monaco and the Australian Nuclear Science and Technology Organization in Lucas Heights, near Sydney.

The analyses applied for the measurement of the relevant components of the waters and the solid materials include alpha and gamma counting, spectroscopy, accelerator mass spectrometry, chromatography, titration and requisite sample preparation. Detailed descriptions of the methods applied can be found in Appendix V, which also includes the results of the analyses (Tables V.4 to V.8).

6.6. RADIONUCLIDE ANALYSES

An essential component of the IAEA underground water sampling campaign is to provide an independent check of the concentrations of radionuclides reported by the CEA from monitoring wells and cavity-chimneys on Mururoa and Fangataufa. Furthermore, sampling allows the validation of model calculations by a comparison of measured and calculated data.

6.6.1. Cavity-chimney waters

The measurements carried out within the IAEA campaign (Appendix V, Table V.4) show that the water samples from the Céto and Aristée cavity-chimney wells have, as expected, the highest concentrations of radionuclides of any of the wells sampled on Mururoa and Fangataufa. This can be seen from the concentrations of ^{3}H, ^{90}Sr and ^{137}Cs as they developed in the cavity-chimney waters of Aristée and Céto since the time of the test explosion (Fig. 92).

Tritium dominates the radionuclide concentrations in the cavity-chimneys. ^{90}Sr, ^{137}Cs, ^{36}Cl, ^{129}I and ^{241}Am are also detected. $^{239+240}Pu$ was found to be below the detection limit of 0.008 mBq/L in Aristée and is very low in Céto (0.02 mBq/L). Very low concentrations of $^{239+240}Pu$ in the waters of the cavity-chimneys had been reported by the CEA. ^{241}Am was also detected but ^{237}Np was below detection limits. For ^{90}Sr and ^{137}Cs the IAEA measurements for Aristée were found to be by about a factor of 2 lower than the previously reported French data and are for Céto almost identical to the French data. Decay corrected ^{3}H concentrations are below concentrations previously measured by the CEA.

The IAEA measurements of radionuclide concentrations in the waters of the two cavity-chimneys (Aristée and Céto) confirm the data reported by the CEA or indicate that the French data are higher (Appendix V, Table V.9).

The measured radionuclide concentrations in the two cavity-chimneys can, in addition to the corroboration of the French data, be used as a calibration tool for the model calculations of radionuclide releases into the cavity-chimney waters.

Four parameters govern radionuclide concentrations in the waters of the cavity-chimneys:

(i) the yield of a test and design of the device;
(ii) the fractionation of the radionuclides between the lava and the rubble;
(iii) the release of radionuclides from the lava (leaching);
(iv) the sorption of radionuclides on the solid phase (rubble) expressed in K_d's; and
(v) the half-life of the respective radionuclides.

Sorption coefficients had been derived for this Study from existing investigations, chiefly from the former US basalt repository project and also the planned German Konrad repository (Section 4.2). The measured radionuclide concentrations in the waters of the cavity-chimneys can be used to calculate sorption coefficients in order to check the applicability of the K_d's derived from other repository projects to the given situation at the atolls. The method applied and the results achieved are provided in Appendix V, Section 6.4 and Table V.10.

In model calculations no sorption ($K_d = 0$) has been assumed for ^{3}H (as HTO), ^{129}I and ^{36}Cl. The sorption coefficients derived from the radionuclide concentrations show that there is a slight interaction between these radionuclides and the solid phase which is manifested in the small K_d's calculated for these elements.

The calculated K_d's confirm also the value applied for ^{90}Sr in the model calculations and suggest that the values for ^{137}Cs and, in particular for plutonium, are higher than the K_d's applied in model calculations.

In conclusion, the measurements of radionuclide concentrations in waters of the cavity-chimneys confirm that the sorption coefficients applied in model calculations will provide realistic or, for plutonium and ^{137}Cs, "conservative" results when applied to the atolls of Mururoa and Fangataufa.

The sorption coefficients(K_d's) are one of the four previously mentioned parameters governing radionuclide concentrations in waters of a cavity-chimney. The comparison between calculated and measured radionuclide concentrations in such waters allows an integral cross-check of all parameters governing the respective radionuclide releases. The comparision of the radionuclide concentrations measured in the waters of the Céto (4 kt) and the Aristée (6.8 kt) cavity-chimneys and the calculated values for a 5 kt test (12 years after the explosion) are compiled in Appendix V, Table V.11.

The calculated HTO concentrations reproduce the measured value of the Aristée water and slightly underestimates the respective Céto data. The measured ^{90}Sr, ^{137}Cs and ^{129}I concentrations are definitely lower than calculated. $^{239+240}Pu$ and ^{241}Am are by several orders of magnitude below the calculated values and the calculated ^{36}Cl concentration is between the two measured values.

The comparison of measured and calculated data demonstrates that releases of most of the radionuclides into the cavity-chimneys are overestimated in the calculations. In particular, the transuranic elements (plutonium and ^{241}Am) are drastically overestimated, whereas the ^{36}Cl and ^{3}H data are found to be roughly as calculated. These results demonstrate that the overall approach to the modelling of radionuclide releases into the cavity-chimney waters is applicable to the system although it is conservative for many radionuclides and very conservative for plutonium and ^{241}Am.

6.6.2. Waters from monitoring wells

The water samples from the monitoring wells contain, depending on their location, varying concentrations of radionuclides (Appendix V, Table V.4). The ^{3}H, ^{36}Cl and ^{129}I concentrations are lower by at least three or four orders of magnitude (up to about 10^{7} mBq/L) relative to the cavity-chimney wells (about 10^{10} mBq/L). The same is true for the ^{137}Cs and ^{90}Sr data, except the wells in and around Area 1 where the corresponding decrease in ^{90}Sr and ^{137}Cs between the cavity-chimney and monitoring wells is only one order of magnitude (cavity-chimney wells: 10^{5} mBq/L; monitoring wells: 10^{4} mBq/L) or less. As a matter of fact, plutonium isotopes, ^{241}Am and ^{237}Np are not detected in solution in any of the waters produced from the monitoring wells.

In general, good agreement is found between samples collected and analysed by the CEA and equivalent samples analyzed by the IAEA (Appendix V, Table V.9). Tritium shows nearly a one-to-one correspondence between the two sample groups, while for ^{137}Cs there is reasonable agreement with more inconsistency for three samples (Isurus 10, Mitre 27 and Tazard 14) with very low ^{137}Cs concentrations (less than 100 mBq/L). ^{90}Sr was not included in this suite of French measurements and, therefore, cannot be compared in the case of the May/June 1997 sampling campaign.

Table V.9 of Appendix V also includes data generated in the course of French sampling campaigns of 1996 and spring 1997. Although the data show some fluctuation, there is, in general, good agreement in the HTO, ^{137}Cs and ^{90}Sr concentrations throughout the three sampling campaigns. These "fluctuations" may be attributed to tidal influences or the sampling technique, because the IAEA pumped the wells whereas the French experts applied a vacuum chamber.

Thus, the IAEA sampling campaign confirms the French data. This applies to the sampling wells with higher radionuclide concentrations as well as to the "blank" Géo 5 well which is thought not to have been affected by underground tests.

It should be noted, however, that both the ^{137}Cs and ^{90}Sr concentration increased by a factor of 3 since the first measurement in Géo 8 (274 m, 276 m and 278 m) and Fuseau 30 (193 m), whereas Mitre 27 (239 m) showed a significant decrease for these two radionuclides. Furthermore, the data for Géo 10 seem to indicate increasing ^{90}Sr concentrations without showing an increase in ^{137}Cs. The few

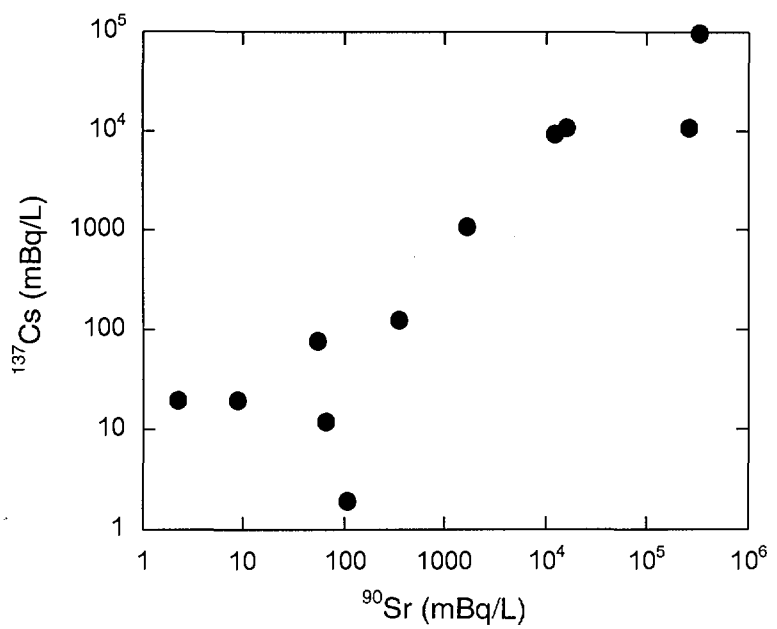

FIG. 93. Mururoa and Fangataufa cavity-chimney and monitoring well water analyses.

data and the variation in the data does not allow a firm conclusion in terms of signalling an increase (or decrease) in radionuclide concentrations in the carbonates. Such trends could be ascertained in a continuation of the monitoring activities in the carbonate which also would develop a better understanding of the behaviour of the radionuclides in the underground waters and the hydrological regime (including tidal effects) in the carbonates.

Furthermore, it seems that releases of ^{90}Sr and ^{137}Cs are geochemically controlled (e.g., ion exchange). This is demonstrated by a plot of ^{137}Cs over ^{90}Sr concentration (Fig. 93). At concentrations of about 100 mBq/L and higher there is a direct correlation between the two radionuclides suggesting that the releases are affected by similar processes.

It is evident that the highest ^{90}Sr and ^{137}Cs concentrations in the monitoring wells included in this sampling campaign are found in and around the Area 1. In Area 1 there is evidence for damage by the nuclear tests. Also, safety trials that went critical are in the carbonates of Area 1. These may be origins for the ^{90}Sr and ^{137}Cs found in the underground waters. Other wells with high ^{3}H concentrations, in particular Murène 16, Tazard 14 and Fuseau 30 have relatively low ^{137}Cs and ^{90}Sr concentrations, suggesting a more intact pathway through the geological strata with good sorbing properties.

The activation product ^{36}Cl and the fission product ^{129}I, both non-sorbing and highly soluble radionuclides, were found at rather low concentrations in the waters of the monitoring wells, except Géo 5 and Mitre 27 and Isurus 10 for ^{36}Cl. This is consistent with the fact that these wells also have the lowest ^{3}H concentrations, which is another non-sorbing radionuclide.

6.6.3. Analyses of the solid residues

In addition to the filtrate which passed through the 450 nm filter, the solid material found on the filter (Fig. 94) was analysed for its radionuclide content. These solids represent the material contained in about 50–100 L of water pumped through the filters in the course of the sampling activities.

The analyses of the solid material show that it is mostly an iron oxide/hydroxide and silikate based residue (Section 6.7). Such residues tend to scavenge or sorb all types of elements on their large and highly reactive surface and concentrate in particular highly sorbing elements.

It is therefore not surprising that plutonium and ^{241}Am but also ^{137}Cs are found in the residues of the cavity-chimney waters. Although the plutonium and ^{241}Am content associated to the pumped-up solid material is considerably higher than the plutonium and ^{241}Am dissolved in the water it does not necessarily mean that this material migrates through the geosphere towards the lagoon (or ocean). As the particle size of the solid is beyond the size of colloids it will sediment in stagnant waters whereas colloids ($\leq$450 nm) will be transported as dispersed particles with the liquid phase.

The results of the investigations show (Appendix V, Table V.5) that plutonium isotopes and ^{241}Am are found to be attached in measurable quantities to the solid residue of the two cavity-chimney waters and also the well waters taken at Fangataufa but not those taken at Mururoa. This difference between the Fangataufa and Mururoa wells cannot be explained by the relatively high total dry weight of solid material filtered from the Fangataufa waters, which are not high enough to explain this finding. Furthermore, the plutonium and ^{241}Am concentrations in the Fangataufa waters are below detection limits and therefore do not give reason to high concentrations on the solid material.

A speculative interpretation of this finding may be that plutonium and ^{241}Am containing material may have entered the monitoring well from the Fangataufa lagoon before the monitoring

radionuclide amounts on the solid phase are standardized to the volume of waters filtered. This shows that most of the plutonium is attached to the solid phase pumped up with the water. The ^{241}Am is almost evenly distributed between the solid and the liquid phase. Almost all of the ^{137}Cs is contained in the filtrate. The high plutonium and the low ^{137}Cs fraction on the solid material is in accordance with the chemical behaviour of the two elements.

Two aspects have to be taken into account when such comparisons are made.

First, the solid material may not be homogeniously dispersed in the water. Therefore, the averaged concentrations provided in Appendix V, Table V.6 may not reflect the real situation underground but they are very useful for the comparison.

Second, the question arises whether such solid material may cause an enhanced transport of rather immobile radionuclides, e.g. plutonium and ^{241}Am, through the geosphere and into the biosphere.

The rate of transport by water through geological formations depends on the particle size. Monomeric species can, of course, be transported by waters through geological formations. The interaction of such species with the geological formation retards the respective species in accordance with its sorption behaviour (K_d).

Macroscopic species, on the other hand, precipitate because the Brownian movement is not able to keep them dispersed in the aqueous phase. Such sedimentation occurs if species have sizes of $\geq$ 450 nm and if no other effects (e.g. tidal flow or heat convection) stir them up. The solid material collected on the 450 nm filter falls into the category of macroscopic species. It is considered to be a solid which will sediment and not migrate through the geosphere. Filtration of waters through a 450 nm filter is carried out in order to distinguish between dissolved or dispersed species and solid material. It has to be acknowledged that particles below 450 nm may be strained out once the filter loads up.

Colloidal species are in their sizes ($\leq$ 450 nm) between the monomeric and the macroscopic species. They are dispersed in aqueous phases, do not sediment and are able to migrate through the geosphere. Plutonium in near neutral natural waters, for example, is not stable in monomeric form. It polymerizes to form colloids (termed "real" colloids). Therefore, any measurement of plutonium sorption coefficients (K_d) in near neutral groundwaters only involves colloidal material. Elements such as plutonium may also be attached to other colloids (termed "pseudo" colloids), for example Fe oxides/hydroxides or organic molecules such as humic acids, which have sorption properties different from real colloids. In recent publications, there is much speculation about an accelerated radionuclide migration with colloids involved. Such considerations are stimulated by findings where radionuclides, including actinides, have migrated large distances in a relatively short period of time. One example is the migration of the association of actinides and relatively insoluble radionuclides downgradient of underground cavity-chimneys in fractured volcanic rocks at the Nevada Test Site (Kersting and Thompson, 1997). In this case, radionuclides have migrated in excess of 1000 m downgradient from a test over a thirty year interval.

In terms of Mururoa and Fangataufa, the measured radionuclide concentrations in the waters of the cavity-chimneys and the monitoring wells (Appendix V, Tables V.4, V.6 and V.11) as well as the K_d values calculated from these measurements (Appendix V, Table V.10) do not support the hypothesis of an accelerated plutonium or ^{241}Am transport by colloids. Nevertheless, a future monitoring programme may pay particular attention to dentifying such effects, should they occur in the future.

6.7. ELEMENTAL COMPOSITION

The chemical composition of the cavity-chimney and the monitoring well waters as well as the filtered solid material have been analyzed in addition to the radionuclide concentrations in such materials. Such analyses are important in terms of an interpretation of the radionuclide behaviour in the geosphere.

6.7.1. Cavity-chimney and monitoring well waters

The chemical composition of all the waters is related to the composition of sea waters. The waters of the monitoring wells in the carbonates have almost the same composition which is very similar to sea waters. The two cavity-chimneys waters (Céto and more specifically Aristée) have undergone alterations in their composition which are an indication of interactions between sea water and the volcanics as described in Guille et. al., 1996, pp. 142–145. Such alterations lead to an enrichment in Ca, Sr, Si, Al and Cl and to a depletion of Mg, K and sulphate. The composition of the waters did not reveal any anomalies which could enhance the transport of radionuclides through the geosphere. The waters, for example, do not show an elevated carbonate concentration that could decrease the K_d of plutonium through the formation of complexes. Although no special analyses were carried out for organic substances in the waters, the color of the waters did not indicate the presence of organics which could enhance the migration of plutonium, ^{241}Am etc. through the formation of complexes and colloids. The increased concentration of some elements (e.g., Na, Ca, Cl) and their influence on the K_d's of the respective radionuclides (e.g., Cs, Sr, I) had been taken into account when K_d's were derived for the model calculations.

6.7.2. Solid residues

The solid residue remaining on the 450 nm filter from the filtration of the waters was analyzed for 5 of the highly loaded filters in terms of overall mass and elemental composition (main cations only), in order to have an indication of the nature of such residues. Although the filter residue was clearly visible, the total amount is always below 1 g and in most cases below 0.1 g (Appendix V, Table V.5). It has been found that in all cases Fe and Si are the main constituents of the solid material. The Fe/Si ratio varies considerably in the various sampling locations. Al, Ca and Mg are also present in the residues whereas Mn concentrations are rather low. Fe (III) oxide/hydroxide is the predominant species which has a very low solubility limit whereas Fe (II) is reasonably soluble. The low Fe concentrations in the corresponding filtrates confirm this statement. This result indicates that Fe oxide/hydroxide cannot be present in the filtrate in colloidal form and act as a carrier for an enhanced transport of radionuclides through the geosphere.

It is well known in chemical engineering that Fe oxide/hydroxide precipitation scavenges other more soluble elements and purifies aqueous solutions. The resulting residue will be enriched with scavenged components whereas the aqueous phase will be depleted at the same time. The same effect occurs (or occurred) in the cavity-chimneys waters and the Fangataufa monitoring wells. The high radionuclide content attached to the solids filtered from these waters provides the evidence that the above mentioned scavenging of radionuclides by Fe oxides/hydroxides occurred. Formation of Fe oxide/hydroxide solids (>450 nm) will not enhance migration of radionuclides through the geosphere. In the case of the Fangataufa monitoring wells it seems to be unlikely that plutonium and ^{241}Am found on the solid material originate from the tests in the volcanics. The isotopic composition suggests that these elements may have been introduced into the respective wells from the lagoon before the wells were plugged.

6.8. FINDINGS FROM THE UNDERGROUND WATER SAMPLING

Results from underground water sampling on the atolls corroborate data provided by the CEA. In general, they validate the expected suite of radionuclides which comprise the solution source term

in the cavity-chimney or demonstrate that it was derived in a conservative way. The geochemical behaviour of these radionuclides follows predictions for the solution source term based on models of simplified radionuclide releases from the lava and rubble in the cavity-chimney of a nuclear test.

The apparent consistency of radionuclide concentrations measured in the monitoring wells by both, the CEA and the IAEA, suggests that representative concentrations are detected for most radionuclides. In this regard, the underground sampling programme achieved its primary purpose.

Additionally, the results from the monitoring wells indicate that in Area 1 ^{90}Sr and ^{137}Cs, additional to tritium, may be transported upwards from the cavity-chimneys in the volcanics and deposited in the carbonates. In eastern and northern testing areas on Mururoa, radionuclides have been introduced from those nuclear tests whose cavity-chimneys reach the top of the volcanism and are in hydrologic connection with the carbonate. In the southern and western testing areas radionuclides have been detected in the carbonate from tests with inadequate geologic cover. In Fangataufa, the majority of the radionuclides detected in the carbonate are from a single higher yield test in hydrologic connection with the volcanics.

Of particular concern are the plutonium safety trials in the carbonate formation. Each safety trial has a ~ 3.7 kg plutonium metal source term. Plutonium metal will oxidize and may form colloids that may be susceptible to transport through the geosphere. The low radionuclide concentrations in the waters of the monitoring wells do not indicate that such transport occurred.

The association of plutonium and ^{241}Am with Fe and Si rich, filterable solid material (>450 nm) was not investigated by the CEA. Such material would not be susceptible to migration from the cavity-chimneys through the volcanics because its particle size is beyond the size of colloids. The contamination of such solids with plutonium and ^{241}Am in the Fangataufa wells may be originated from the lagoon.

The results of the underground water sampling programme are important because they provide also a means to calibrate predictive models for radionuclide release from the geosphere. These models are complex and are based on a number of assumptions, including leaching of radionuclides from the lava, the solubility and sorption of radionuclides, the permeability and fracture geometry of the rock formations, and the Darcy velocity of the formation waters. In particular, the transition of the radionuclides in the lava and the rubble to the cavity-chimney waters defines which radionuclides are mobilized and determines resulting concentrations.

The measurement of radionuclide concentrations in the cavity-chimney waters provide evidence that the respective modelling approach is acceptable. It did not underestimate radionuclide concentrations. It overestimated the inventory of plutonium and ^{241}Am by orders of magnitude. A similar conclusion can be drawn from the derivation of sorption coefficients (K_d's) from the above mentioned measurements of radionuclide concentrations.

Measurements of radionuclide concentrations in the field, at varying distances from the working point of a nuclear explosion or a safety trial, provide a rigorous test of solubility and sorption limits selected to simulate radionuclide release and transport. Although field measurements provide a crucial validation step, one-time measurements are not diagnostic of the evolution of the hydrologic source term. Because of scientific interest, continued monitoring is preferred. Repetitive sampling provides a robust radiochemical baseline against which anomalies can be readily identified. This is particularly important for radionuclides with longer half-lives (i.e. plutonium) characterized by complex transport mechanisms.

TABLE XIII. FRENCH ESTIMATES (1996) OF INVENTORY OF RADIONUCLIDES IN CARBONATE ZONES (French Liaison Office Document No. 9, 1996)

	^{3}H (TBq)	^{137}Cs (GBq)	^{90}Sr (GBq)
Mururoa			
Northern Zone (Zone 1)	1100	1100	1600
SE Zone (Zone 2)	1300		30
South Zone (Zone 3)	170		2
SW Zone (Zone 4)	1500		150
Lagoon (Zone 5–7)	130		70
Total Mururoa	4200	1100	1850
Fangataufa	3000	80	250
Total (both atolls)	7200	1180	2100

6.9. RADIONUCLIDE INVENTORY IN CARBONATE

The good agreement between the French and IAEA results for underground water analyses is confirmation of the validity of the more extensive French underground sampling data. Using the concentration contours shown Figs 88 and 89, it is possible to roughly estimate the current inventory of ^{3}H, ^{137}Cs and ^{90}Sr in the carbonates. The French experts assume that the maximum measured concentrations in the karst waters extend over a water thickness of 10 m, equivalent to 50 m of dolomites with a porosity of 20% (French Liaison Office, Document No. 9, 1996). Table XIII gives the French estimates of the inventories of ^{3}H, ^{137}Cs and ^{90}Sr in the various carbonate zones, as depicted for Mururoa in Fig. 44 of the IAEA Main Report. These estimates strictly only apply to the lagoon-sides of the atolls since it is not possible to sample on the ocean-side. For the purpose of its own future analysis, the study team accepts these figures as reasonable estimates and probably accurate within a factor of 2–4.

The estimated combined release rate of tritium into the two lagoons is currently about 6–12 TBq/a (Vol. 5 of this Technical Report) or about 0.1–0.15% of the inventory given in Table XIII. It follows, therefore, that the releases into the lagoons have not significantly reduced the overall inventory of radionuclides in the carbonates.

6.10. REVIEW AND REFINEMENT OF GEOSPHERE TRANSPORT MODEL

6.10.1. Release into the carbonates

Figures 88 and 89 show that the tritium plume has dispersed to a far greater extent than predicted by pure advective transport. The tritium front has dispersed up to 4 km in 20 years (200 m/a), whereas the calculated pore velocities are of the order of 10 m/a. It is concluded, therefore, that dispersion (presumably through tide-induced flow in the karsts) dominates over advection. An important consequence of this conclusion is that radionuclides released from tests along the rim are as

likely to migrate towards the ocean as they are towards the lagoon. In further calculations, we shall assume that 50% of radionuclides released from tests along the rim are dispersed towards the ocean while the other 50% flows inwards and upwards to the lagoon. For tests under the lagoon, we assume 100% of the radionuclides migrate to the lagoon. This model, depicted in Fig. 95, is overly simplistic but it has the advantage that inventories in the lagoon-side and ocean-side zones determined in this manner, cannot be underestimated by more than a factor of two. Any other assumption could underestimate either the lagoon-side or ocean-side inventories by a greater factor.

Using the dual porosity transport model, estimates can be made of cumulative radionuclide inventories in the carbonates for comparison with the data shown in Table XIV. Estimates of cumulative releases of radionuclides into the carbonates at Mururoa and Fangataufa can be made by integration of the release rate curves (Figs 96 to 99). The model has also been used to predict the inventories in different zones of the carbonates as a function of time. From a comparison of predicted and measured inventories, a number of preliminary conclusions can be drawn on the appropriateness of the parameters used in the dual porosity model:

- A Darcy velocity of 20 m/a appears reasonable for the CRTV tests,

- For Category 2 ("leaky" tests), a Darcy velocity of 20 m/a is too high since the tritium inventories in the zones of the carbonate overlying Category 2 tests are significantly overestimated. This was not unexpectedly because the volcanic cover, although defective, should provide some resistance to flow. Closer agreement with measured values was obtained by using a Darcy velocity of 5 m/a for the three Category 2 tests at Mururoa and a Darcy velocity of 10 m/a for the Lycos test at Fangataufa. This is consistent with the French analyses which indicates that Lycos is the "leakiest" of the Category 2 tests (French Liaison Office Document No. 10, 1996)

- Table XIII shows that the northern zone at Mururoa is the source of almost all the ^{137}Cs and ^{90}Sr. Moreover, the $^{3}H/^{137}Cs$ and $^{3}H/^{90}Sr$ ratios in that zone are much lower than in other areas. This is strong evidence that the three Category 4 tests (safety trials that went critical), all of which were carried out in zone 1, are the dominant source of ^{137}Cs and ^{90}Sr since tritium is not a component of safety trials. The dual porosity model, with a Darcy velocity of 2 m/a and standard K_d values for basalt, underestimates the measured inventory of ^{137}Cs, and to a lesser

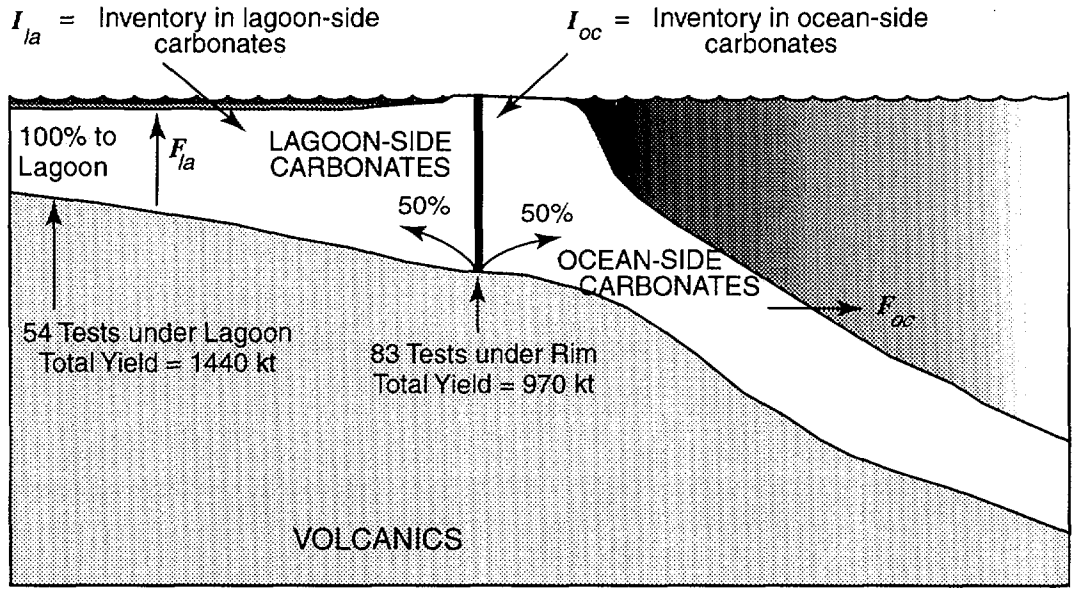

FIG. 95. Model for release of radionuclides into carbonates, lagoon and ocean.

TABLE XIV. PREDICTED INVENTORY (1996) OF RADIONUCLIDES IN LAGOON-SIDE CARBONATE ZONES USING MODIFIED PARAMETERS

	^{3}H (TBq)	^{137}Cs (GBq)	^{90}Sr (GBq)
Mururoa			
Northern Zone (Area 1)	2200	1160	4000
SE Zone (Area 2)	1400	240	2000
South Zone (Area 3)	360	60	500
SW Zone (Area 4)	1400	120	2900
Lagoon (Areas 5–7)	3100	90	2100
Total Mururoa	8460	1670	11500
Fangataufa	3000	140	4300
Total (both atolls)	11460	1810	15800

(Darcy velocity of 5 m/a for Category 2 tests on Mururoa and 10 m/a for the Lycos test on Fangataufa, K_d= 0 for ^{137}Cs and ^{90}Sr for Category 4 tests)

extent, ^{90}Sr from Category 4 tests. This is not unexpected because the basaltic sand used as packing around each test extends out to a diameter of about 1.6 m, whereas the diameter of the cavity in a Category 4 test is estimated to be about 14 m. In further calculations, it was decided to use a K_d of zero (no sorption) for ^{90}Sr and ^{137}Cs in these tests.

Using the dual porosity model and the modified parameters above, the inventory of ^{3}H, ^{90}Sr and ^{137}Cs can be calculated, as a function of time, for each zone on Mururoa (Figs 100–102). These predictions take account of decay of each radionuclide. Release into the lagoon is insignificant within this time-scale. The tritium curve (Fig. 100) shows two maxima, the first in 1982 from CRTV and "leaky" tests and the second in 2009 attributable to gradual release from the normal tests, mainly under the lagoon. Beyond that time, the inventory decreases steadily due to decay of tritium (half-life 12 years). The inventory of ^{90}Sr peaks at 14 TBq in 2014 (Fig. 101). The inventory of ^{137}Cs peaks at a much lower value (1.8 TBq in 2006) due to the high K_d for ^{137}Cs in the volcanics (Fig. 102). Most of the ^{137}Cs in the carbonates is attributable to the three safety trials that went critical. The predicted inventories in 1996 are shown in Table XIV.

A comparison of Tables XIII and XIV shows that the predicted inventories are all greater than the French estimates based on actual measurements, indicating that conservative parameters have been used in the dual porosity model. The predicted ^{90}Sr inventory is significantly higher than the measured value, suggesting that the chosen K_d value of 0.008 m^3/kg (8 L/kg) is too low. Moreover, the predicted tritium releases into the Mururoa lagoon (which are dominated by the Mégarée test and a large number of normal tests) appears to be too high, suggesting that the Darcy velocities chosen are probably too conservative.

It is possible to further adjust the model parameters in order to get closer agreement between measured and predicted inventories. The best agreement was obtained by assuming a K_d for ^{90}Sr of 0.07 m^3/kg for all tests (except for Category 4) and a Darcy velocity of 1 m/a and 0.1 m/a for the

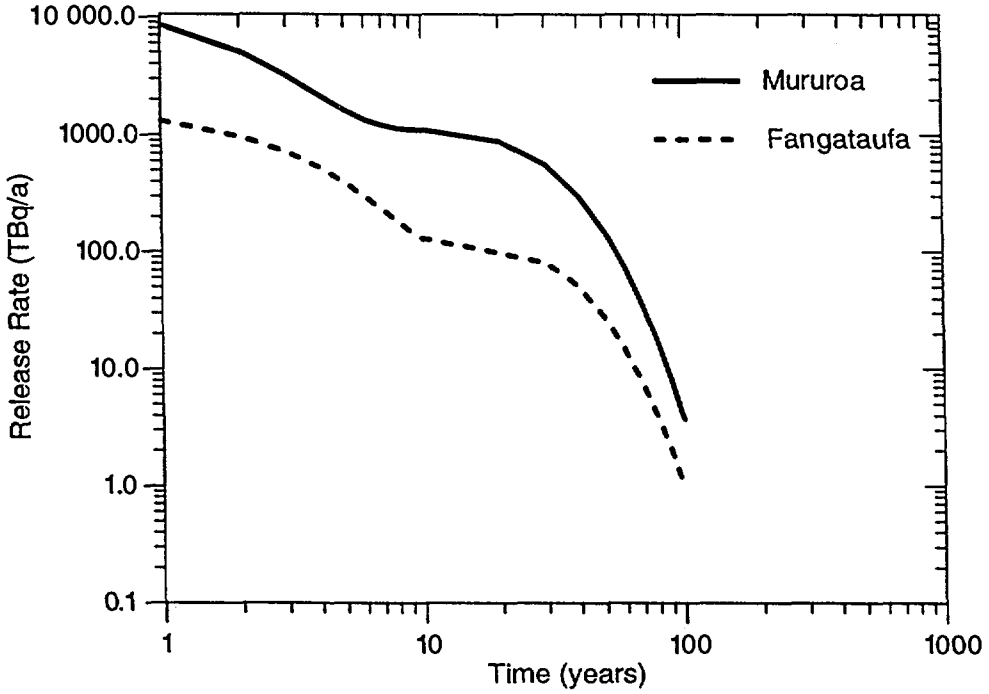

FIG. 96. Predicted rates of ^{3}H release into the carbonates at Mururoa and Fangataufa. Year 1 is 1979 for Mururoa and 1989 for Fangataufa.

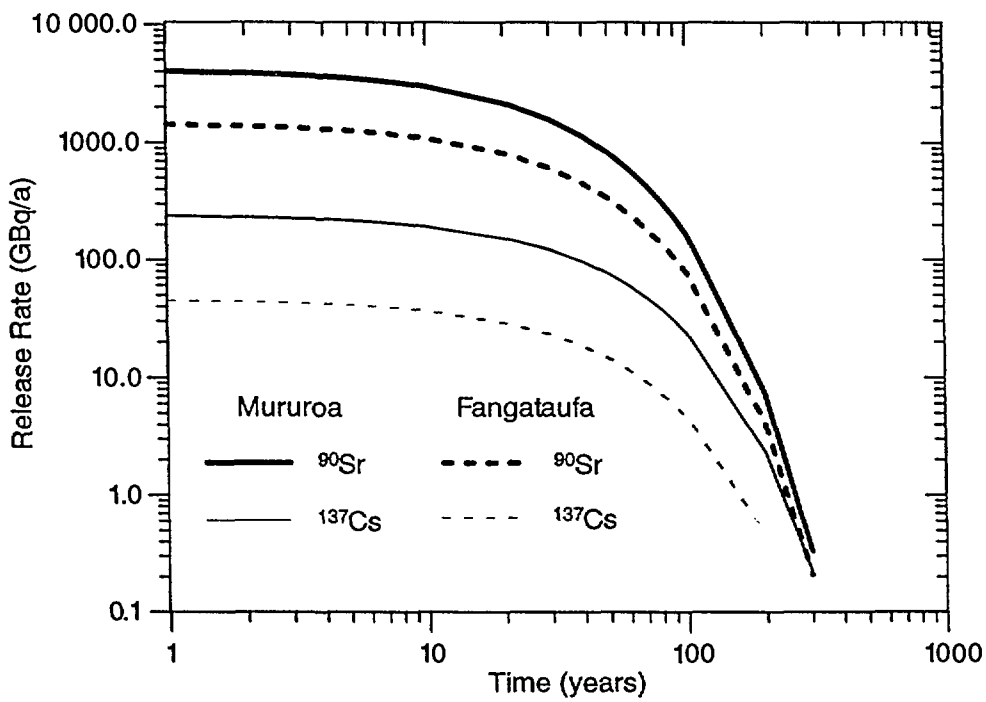

FIG. 97. Predicted rates of ^{90}Sr and ^{137}Cs release into the carbonates at Mururoa and Fangataufa. Year 1 is 1979 for Mururoa and 1989 for Fangataufa.

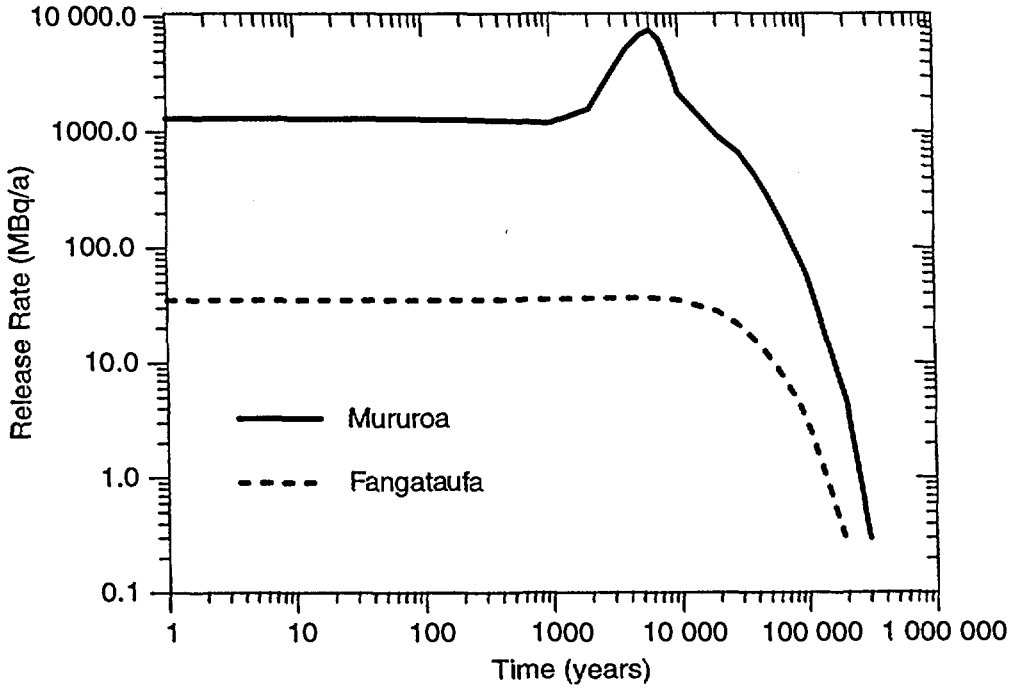

FIG. 98. Predicted rates of ^{239}Pu release into the carbonates at Mururoa and Fangataufa. Year 1 is 1979 for Mururoa and 1989 for Fangataufa.

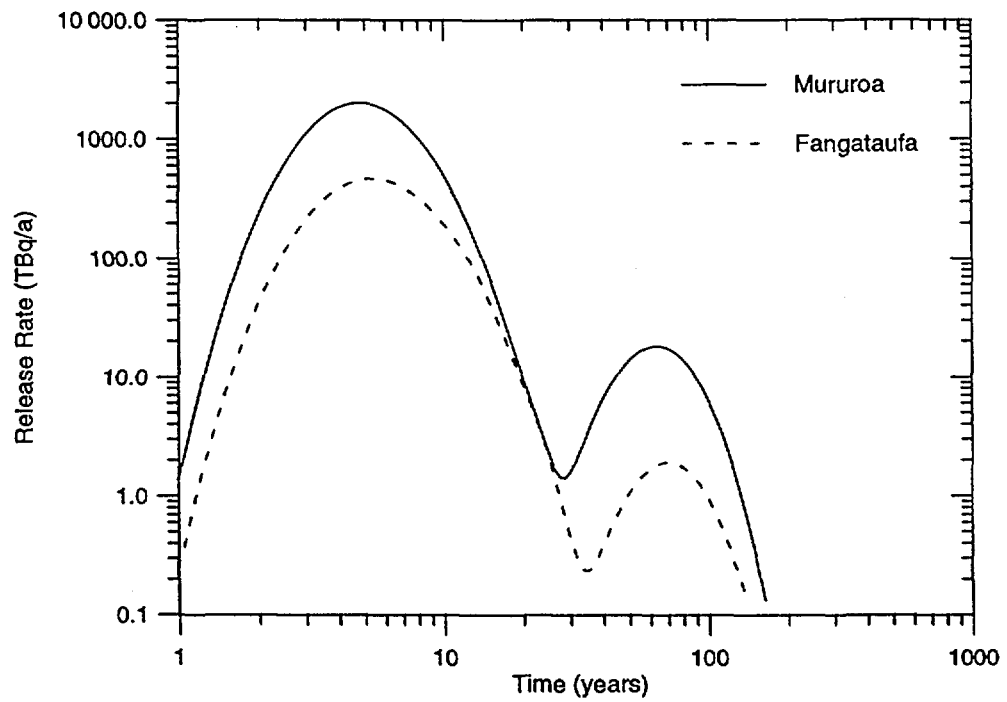

FIG. 99. Predicted rates of ^{3}H release into Mururoa and Fangataufa lagoons based on single porosity model in carbonate formations. Year 1 is 1979 for Mururoa and 1989 for Fangataufa.

TABLE XV. COMPARISON OF FRENCH ESTIMATES (1996) OF INVENTORY OF RADIONUCLIDES IN CARBONATE ZONES WITH PREDICTIONS FROM THIS STUDY FOR 1996 USING OPTMISED PARAMETERS

	^{3}H (TBq)		^{137}Cs (GBq)		^{90}Sr (GBq)	
	This Study	French	This Study	French	This Study	French
Mururoa						
Northern Zone (Area 1)	1500	1100	1160	1100	790	1600
SE Zone (Area 2)	920	1300	240		270	30
South Zone (Area 3)	260	170	60		60	2
SW Zone (Area 4)	1100	1500	120		350	150
Lagoon (Areas 5-7)	390	130	20		50	70
Total Mururoa	4170	4200	1600	1100	1520	1850
Fangataufa	2800	3000	140	80	500	250
Total (both atolls)	6970	7200	1740	1180	2020	2100

Mégarée and normal tests, respectively. The K_d of 0.07 m^3/kg is consistent with the value inferred from the concentration in the Céto cavity-chimney water (Appendix V, Table V.10). Figs 103 and 104 show the "optimised" inventory curves for ^{3}H and ^{90}Sr (the inventory for ^{137}Cs is virtually unchanged). The effect of the change in parameters is to reduce the predicted peak inventories and bring forward the year that they occur. Thus, the peak inventory for ^{3}H of 7000 TBq is predicted to have already occurred (in 1981). The peak inventory of ^{90}Sr (occurring in 2012) is reduced by a factor of about eight.

Table XV compares the French estimate of radionuclide inventories in 1996 with the predicted values for the lagoon-side carbonates using our model. The agreement is good and well within the range of probable uncertainties in French estimates based on actual measurements in the carbonates. Although the "optimised" values gave the best fit to the experimental data, this Study adopted the more conservative "modified" values (as per Figs 100 to 102) for the reference case.

6.10.2. Release into the lagoons and directly into the ocean

As noted earlier (see Section 3.3 and Appendices II and III), the mixing model is preferred over the single porosity model for modelling the release from the carbonates. If perfect mixing and no sorption is assumed within the karsts, the release rates to the lagoon (R_{lagoon}) or ocean (R_{ocean}) for each radionuclide can be described by the simple first-order equations:

$$R_{lagoon} = F_{lagoon} I_{lagoon}$$
$$R_{ocean} = F_{ocean} I_{ocean}$$

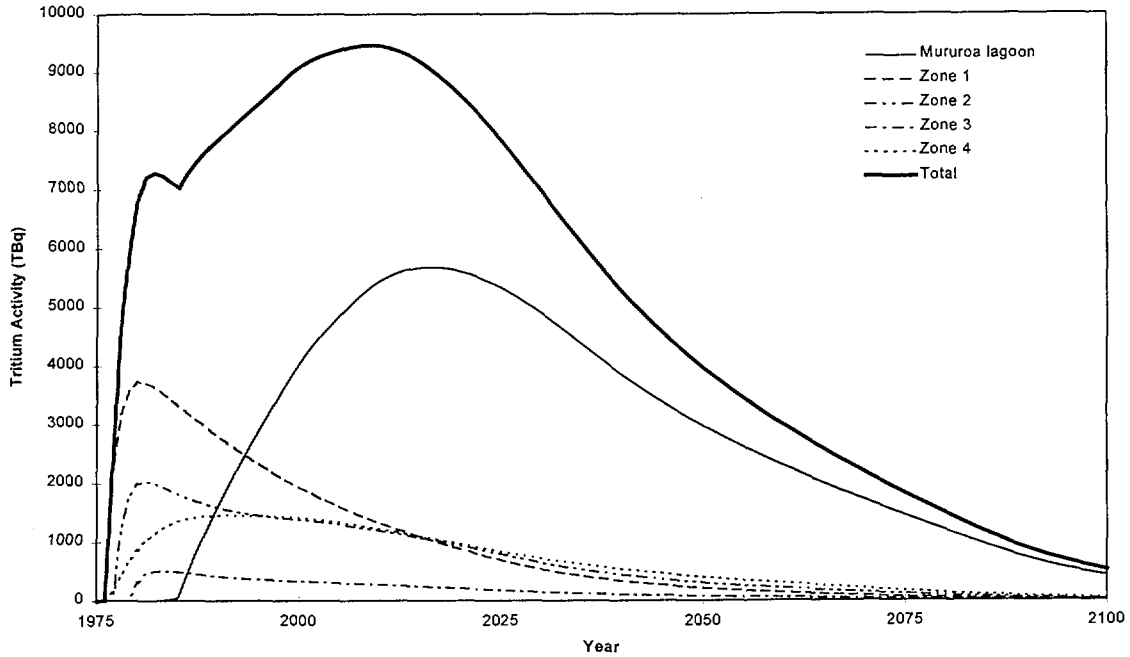

FIG. 100. Predicted ^{3}H inventory in different zones of Mururoa carbonates (based on "modified" parameters as per Table XIV).

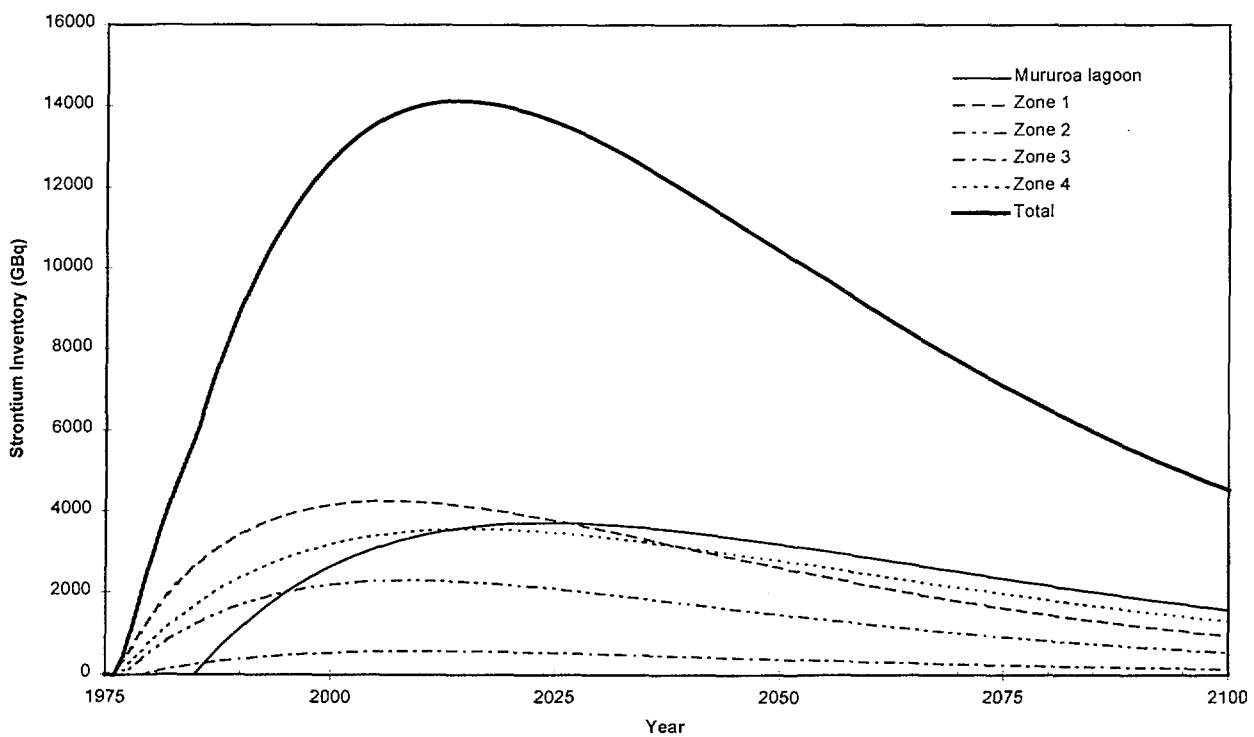

FIG. 101. Predicted ^{90}Sr inventory in different zones of Mururoa carbonates (based on "modified" parameters as per Table XIV).

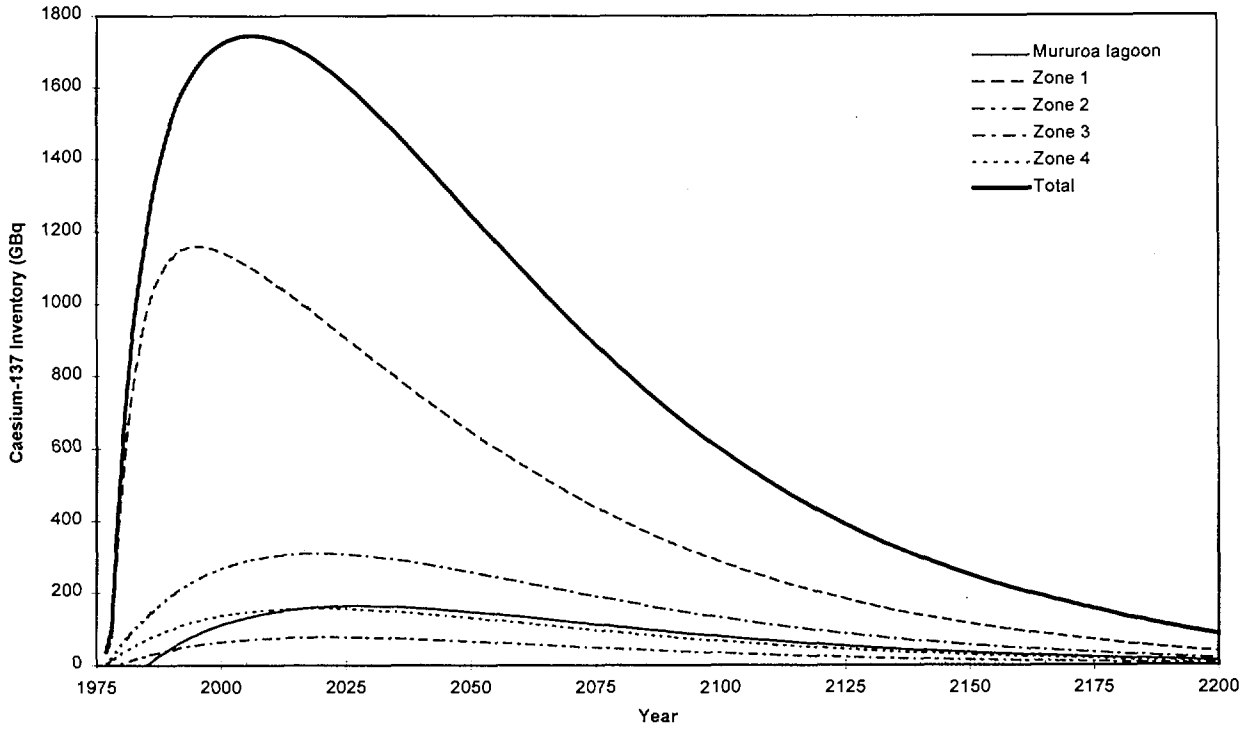

FIG. 102. Predicted ^{137}Cs inventory in different zones of Mururoa carbonates (based on "modified" parameters as per Table XIV).

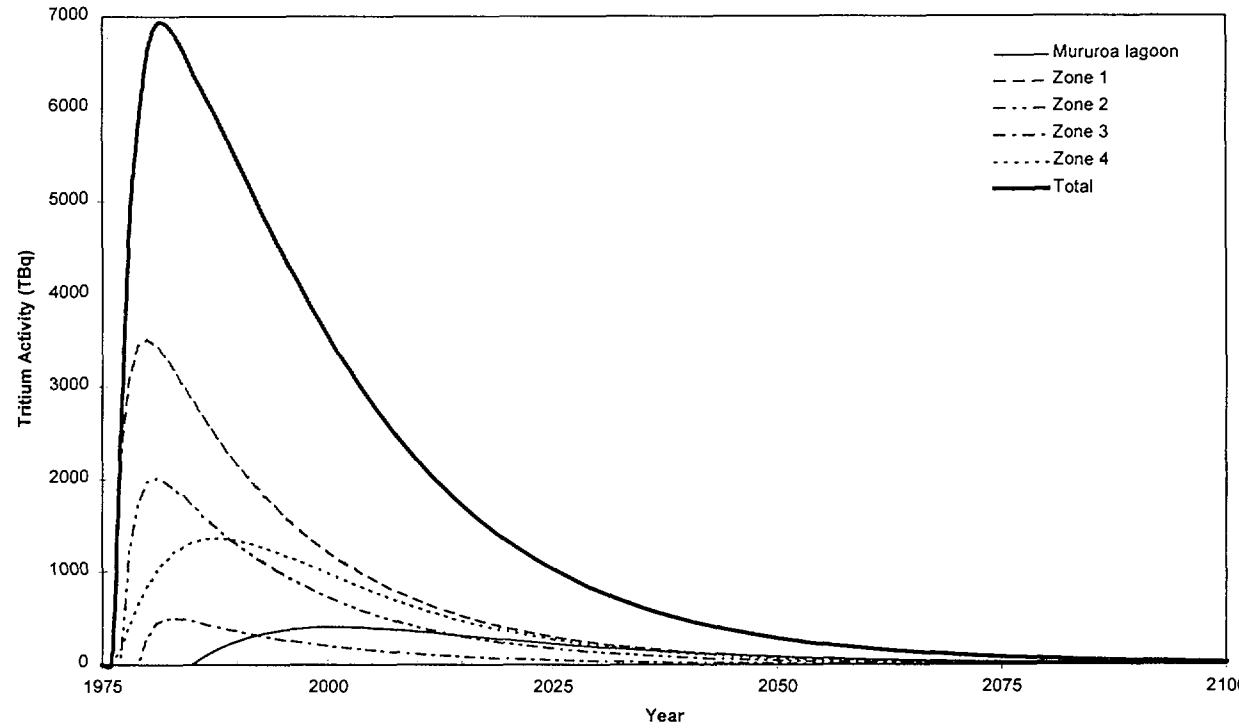

FIG. 103. Predicted ^{3}H inventory in different zones of Mururoa carbonates (based on "optimized" parameters as per Table XV).

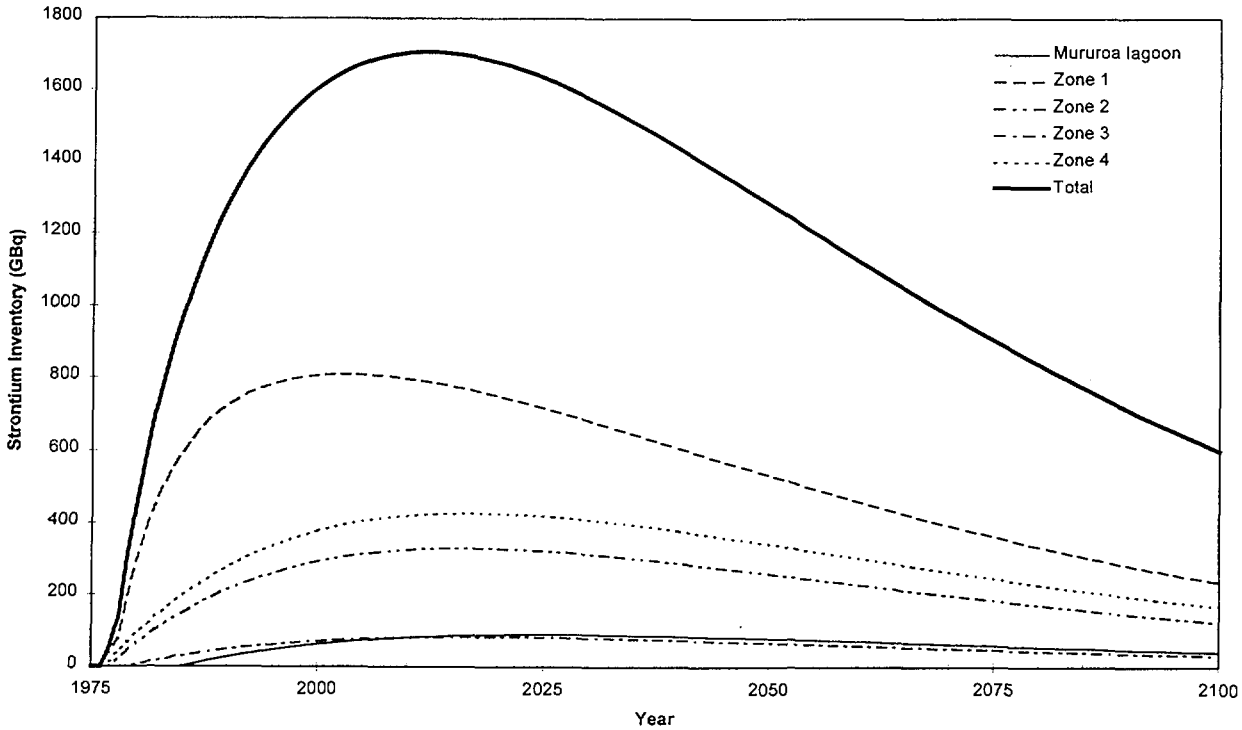

FIG. 104. Predicted ^{90}Sr inventory in different zones of Mururoa carbonates (based on "optimised" parameters as per Table XV).

where F_{lagoon} and F_{ocean} are the fractional releases from the lagoon-side and ocean-side carbonates per unit time, respectively, and I_{lagoon} and I_{ocean} are the corresponding inventories of each radionuclide. These equations can be applied to both Mururoa and Fangataufa atolls but direct release to the ocean at Fangataufa is assumed to be negligible.

Estimates of I_{lagoon} and I_{ocean} were computed using the dual porosity model with the following parameters (the "modified" case described in 6.10.1):

Darcy velocities:

Category 1 (normal) tests	1 m/a
Category 2 (leaky) tests	5 m/a, 10 m/a for Lycos
Category 3 (CRTV tests)	20 m/a
Category 4 and 5 (safety trials in carbonate)	2 m/a
Categories 6 and 7	1 m/a

K_d values in volcanics:

^{3}H	0
^{90}Sr	0.008 m^3/kg
^{137}Cs	0.3 kg m^3/kg
^{239}Pu	0.5 kg m^3/kg
^{90}Sr and ^{137}Cs (in carbonate)	0 for Category 4 tests only

The values of F_{lagoon} and F_{ocean} depend on the volumes and flow rates within the carbonates; F_{lagoon} is most accurately estimated from the inventory of tritium and the measured release rate to the lagoons as determined from the elevation in tritium concentration compared to the oceanic background. This effectively "anchors" the predicted release rates as at 1996 to the measured values in that year. It is, therefore, the most realistic estimate for tritium release to the lagoons but is more conservative for sorbing radionuclides (such as plutonium, ^{137}Cs and ^{90}Sr).

The best estimate of the current tritium release rate from the Mururoa lagoon based on the elevation in tritium concentrations above the oceanic background is 10 TBq/a (Vol. 5 of this Technical Report). Since the calculated inventory is 8460 TBq (Table XIV), 0.12% of the predicted tritium inventory in the lagoon-side carbonates was released to the Mururoa lagoon in 1996. Hence F_{lagoon} = 0.0012/a, which is reasonably consistent with estimates based on volumes and predicted flow rates (Section 6.5.2 of the IAEA Main Report).

F_{ocean} is more difficult to estimate because it is not possible to measure release rates directly to the ocean at a depth of about 300 m. However, F_{ocean} is almost certainly higher than F_{lagoon} because of the smaller volumes on the ocean-side and because tidal effects are likely to be stronger near the flanks. The lateral distance along the karsts to the ocean is not known precisely but is likely to be between 0.5 to 1 km. Having regard for the lateral spread of the front of the tritium plume inferred from concentration measurements under the lagoon, an average residence time on the ocean-side of about 20 years seems reasonable. This is equivalent to F_{ocean} = 0.05/a.

Estimates of release rates from the geosphere were determined for each radionuclide using a spreadsheet which computes the release rates into each zone of the carbonates based on the dual porosity model and then the cumulative inventory in each zone as a function of time (allowing for decay and release from the carbonates). L_{lagoon} and L_{ocean} can be varied as parameters but the chosen reference values were F_{lagoon} = 0.0012/a and F_{ocean} = 0.05/a.

Figures 105 to 108 show the predicted release rates to the Mururoa and Fangatuafa lagoons and directly to the ocean at Mururoa as a function of time for four radionuclides: ^{3}H, ^{90}Sr, ^{137}Cs and ^{239}Pu. For tritium (Fig. 105), the release rates to the Mururoa lagoon are predicted to be relatively constant between 1980 and 2025 with the peak value occurring in 2009. The peak tritium release rate into the Fangataufa lagoon is predicted to occur in 1999. The peak tritium release rate directly into the ocean of 320 TBq/a is predicted to have occurred in 1981.

The highest release rate of ^{90}Sr (300 GBq/a) directly into the ocean is predicted to have occurred in 1995 (Fig. 106). For the Mururoa and Fangataufa lagoons, the peak release rates of ^{90}Sr are much lower and are predicted to occur in 2015 and 2030, respectively. The curves for ^{137}Cs (Fig. 107) are similar in shape to those for ^{90}Sr but the absolute values are reduced by an order of magnitude because of the higher K_d for ^{137}Cs.

An important conclusion from this modelling is that future release rates of ^{3}H, ^{90}Sr and ^{137}Cs are unlikely to be significantly higher than the current release rates.

The release curves for ^{239}Pu (Fig. 108) are more complex and extend to much longer times because of its long half-life (24 000 years). The predicted release rates in the short term (to 100 years) are very low. In all cases, the peak release rates are predicted to occur from 5000 to 10 000 years in the future. The peak values of about 5 GBq/a are, however, less than the current release rates into the lagoons due to leaching of plutonium-bearing sediments.

A major uncertainty in estimating release rates directly to the ocean is the lack of quantitative information to support the chosen value of F_{ocean} = 0.05/a. Figs 109 to 112 show the effect of variation in this parameter (from 0.2 to 0.01/a) on the release to the ocean at depth. Although the value of F_{ocean} has a marked (almost linear) effect on the predicted pre-1996 release rates, it has a much smaller effect on release rates in the future. In particular increasing F_{ocean} to 0.2/a (corresponding to 20% release of the ocean-side inventory each year), increases future release rates by less than a factor of two.

Comparison of the release rates into the lagoons using the single porosity and mixing models shows that, as expected, the mixing model gives higher (i.e. more conservative) values for sorbing radionuclides (^{90}Sr, ^{137}Cs and ^{239}Pu).

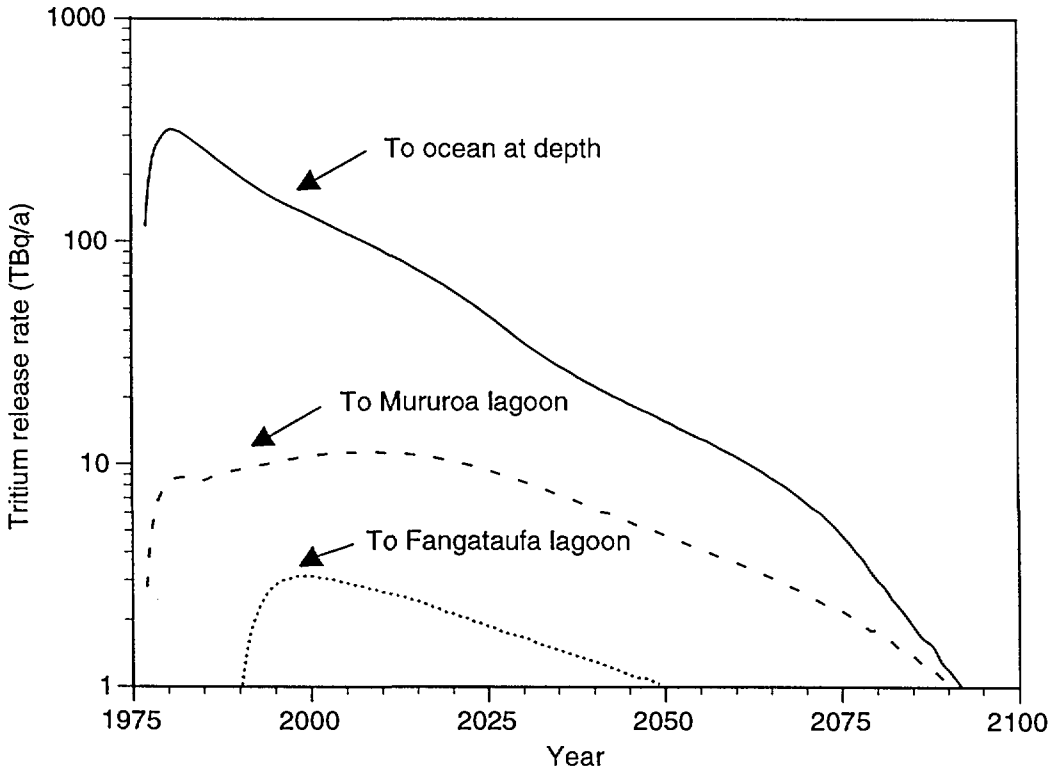

FIG. 105. Predicted ^{3}H releases into lagoons and directly into ocean.

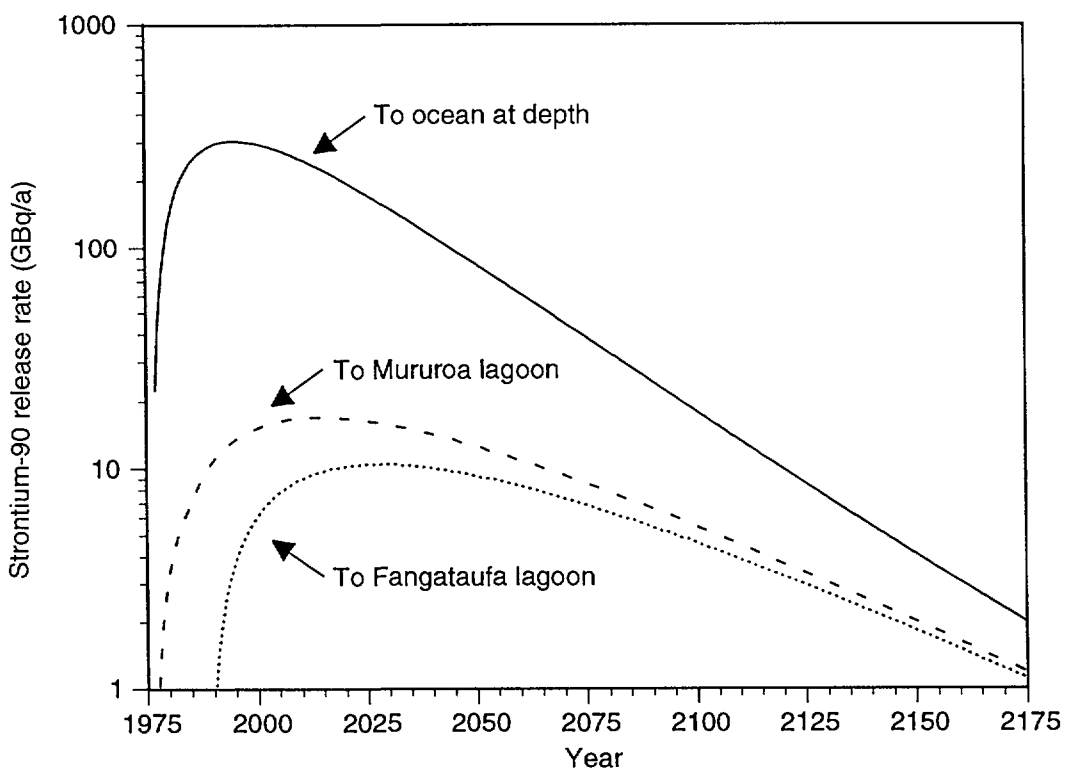

FIG. 106. Predicted ^{90}Sr releases into lagoons and directly into ocean.

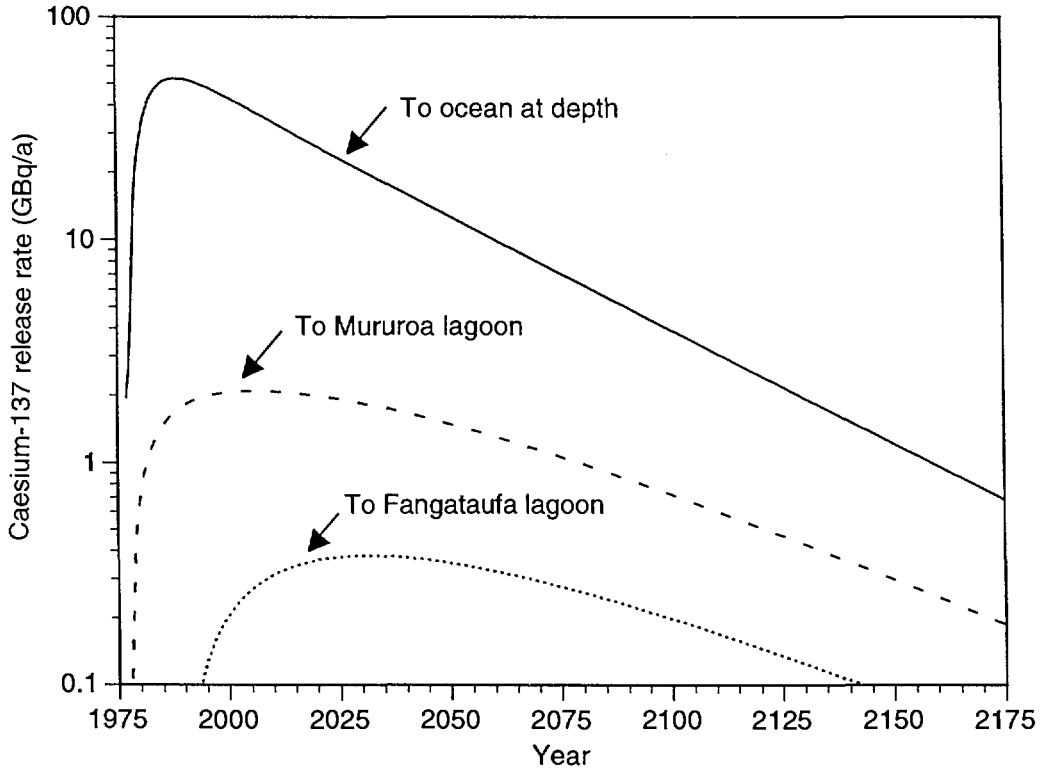

FIG. 107. Predicted ^{137}Cs releases into lagoons and directly into ocean.

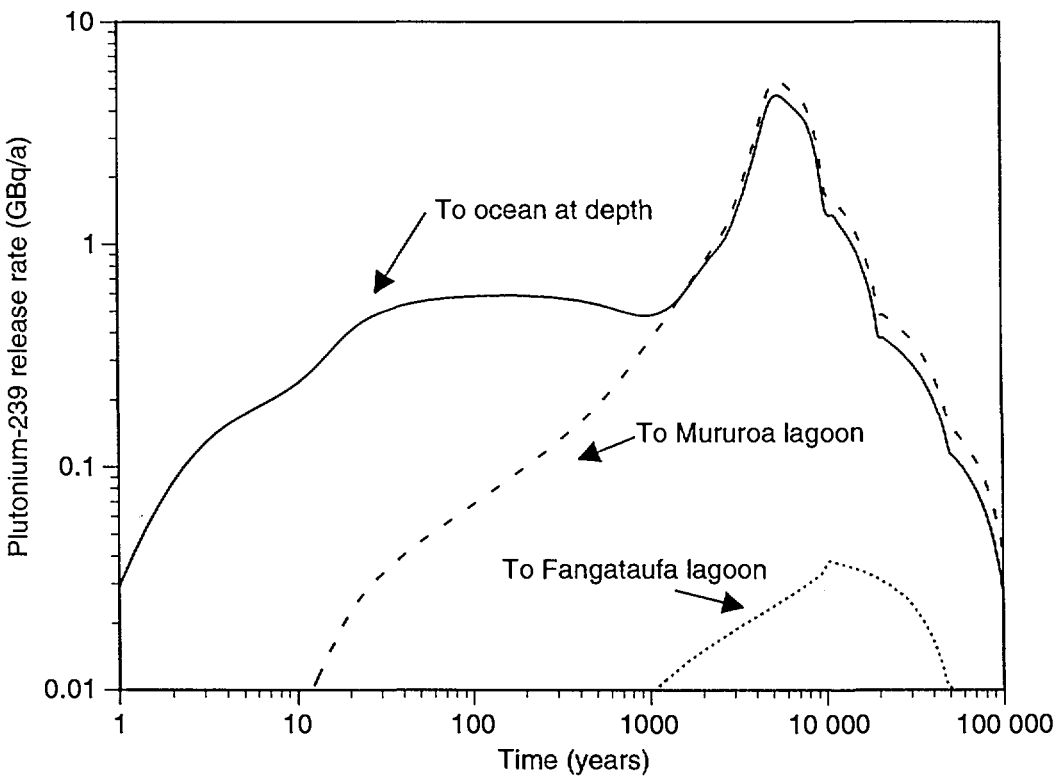

FIG. 108. Predicted ^{239}Pu releases into lagoons and directly into ocean.

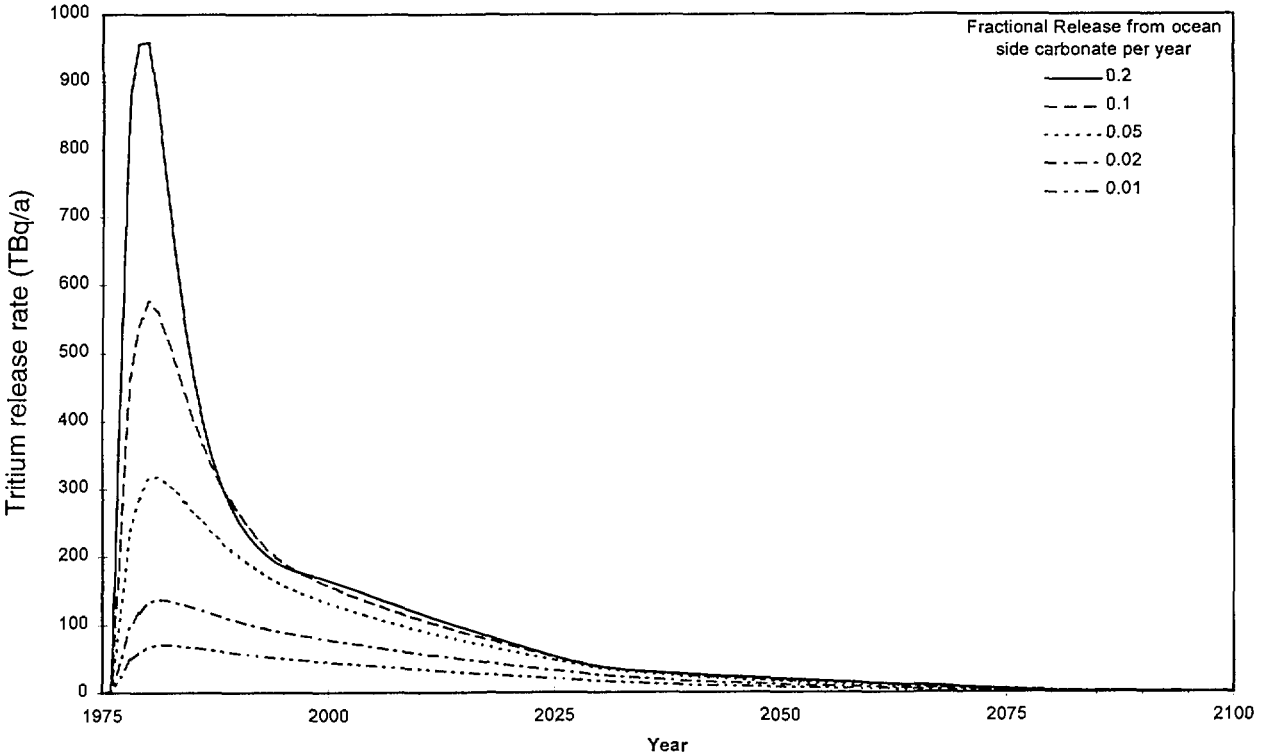

FIG. 109. Effect of fractional release rate from ocean-side carbonates on ^{3}H release directly to ocean.

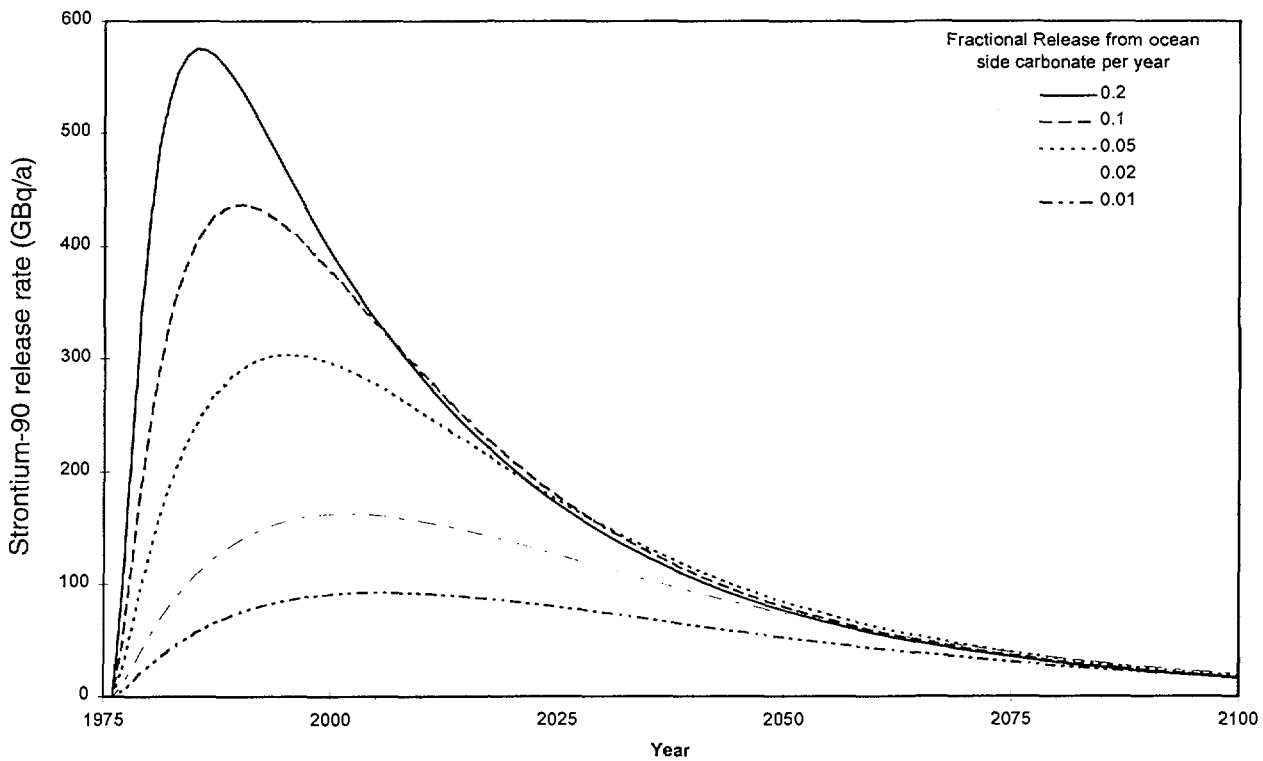

FIG. 110. Effect of fractional release rate from ocean-side carbonates on ^{90}Sr release directly to ocean.

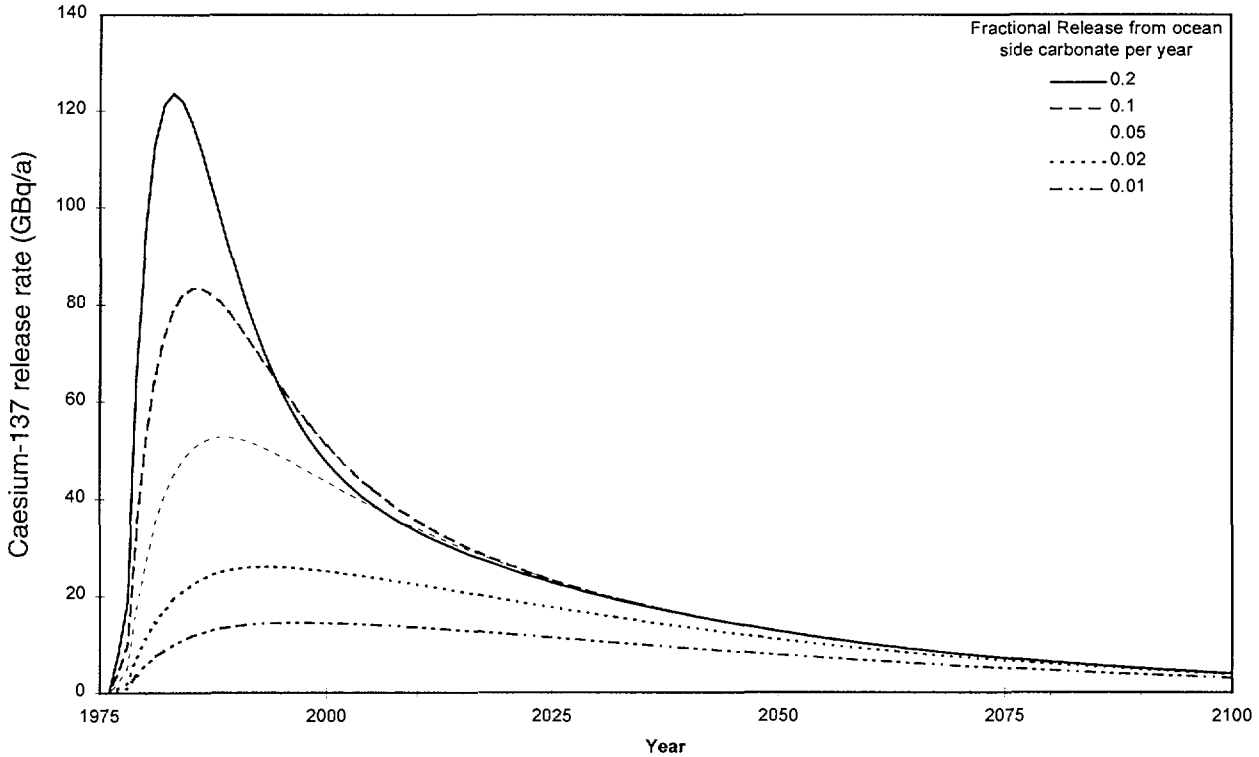

FIG. 111. Effect of fractional release rate from ocean-side carbonates on ^{137}Cs release directly to ocean.

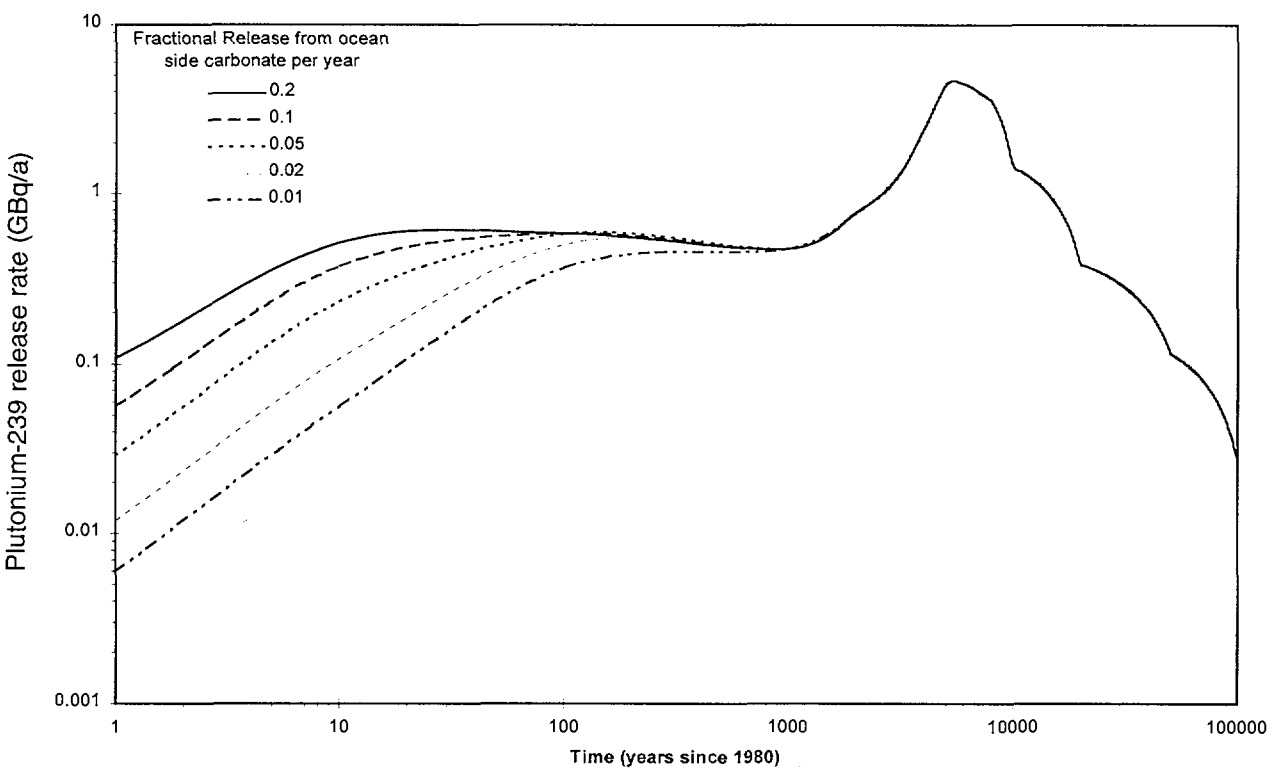

FIG. 112. Effect of fractional release rate from ocean-side carbonates on ^{239}Pu release directly to ocean

The release curves based on the mixing model with F_{lagoon} = 0.0012/a and F_{ocean} = 0.05/a (Figs 105 to 108) will be used as the source term for modelling of marine dispersion in the Vol. 5 of this Technical Report and the Main Report, Section 8.

6.11. COMPARISON WITH FRENCH MODELLING RESULTS

The geosphere transport modelling carried out by the French experts (French Liaison Office Document No. 10, 1996) differs from this Study in several respects. The French experts consider two cases, a "realistic" scenario where total confinement is assumed for all normal tests and a "pessimistic" scenario where a major anomaly is assumed for all tests. In this Study, transport through the volcanics is modelled more rigorously in that a dual porosity model is used and normal tests are integrated into the overall transport model. The major limitation in the dual porosity model is the need to assume a constant flow velocity but this has been overcome by choosing conservative values for the Darcy velocities.

The French "realistic" scenario is based on the estimated turnover rates for CRTV and leaky tests and safety trials with unclear yield that vary with time to simulate the effect of cooling within the cavity-chimneys. Values for K_d also vary depending on circumstances but typically range from 0.002–0.20 m^3/kg for ^{90}Sr, 0.05–0.4 m^3/kg for ^{137}Cs and 10 m^3/kg for ^{239}Pu. The K_d values for ^{90}Sr and ^{137}Cs are similar to those used in this Study but the French experts assume a much higher K_d for ^{239}Pu and also assume that plutonium and other actinides partition completely into the lava.

Table XVI compares the predicted peak inventories of ^{3}H, ^{90}Sr and ^{137}Cs using the two models. The year of the predicted peak is shown in brackets. In general, the agreement is fairly good although the peak releases are predicted to occur later in our Study because of the delayed release from normal tests which are not considered in the French "realistic" scenario.

TABLE XVI. COMPARISON OF ESTIMATES OF PEAK INVENTORIES (TBq) IN CARBONATES AND YEAR OF PEAK (in brackets)

	^{3}H TBq (year)	^{137}Cs TBq (year)	^{90}Sr TBq (year)
Mururoa			
This study*	14000 (1981)	2.6 (1995)	16 (2004)
French estimate	13000 (1978)	4.2 (1983)	17 (1983)
Fangataufa			
This study*	3200 (1999)	0.4 (2030)	10 (2029)
French estimate	2000 (1995)	0.05 (2000)	1.4 (2000)

* Lagoon-side plus ocean-side inventories.

French scientists have used a complex model to describe transport from the carbonates into either the lagoons or directly into the ocean (French Liaison Office Document No. 10, 1996). As indicated previously, the effect of tides is simulated by introducing the concept of an apparent diffusion coefficient. Flow and dispersion is assumed to occur predominantly within the karst system in the lower carbonates. In the upper carbonates, a very low effective porosity is used (0.1%) to simulate rapid transport along preferred pathways into the lagoon. The model requires estimates of many parameters: (a) apparent transverse and longitudinal diffusion coefficients, (b) thickness of the karst layer, (c) velocity in the karsts and (d) the effective porosity in the upper carbonates.

Appropriate parameters are estimated from data on the dispersion of tritium in the carbonates. No sorption is assumed in the carbonates for ^{90}Sr and ^{137}Cs (as in our mixing model).

Compared with our estimates, the French model predicts much smaller release rates of ^{3}H, ^{90}Sr and ^{137}Cs directly to the ocean. Because of the lack of pertinent data, it is not possible to determine which model is more realistic but the predictions of this Study are clearly more conservative. For release into the lagoons, the release rate versus time curves are fairly similar except that, in the French model, the maximum release rates have already occurred, whereas in our model they occur in the future due to delayed releases from normal tests. The French estimates of release rates into the lagoon tend to be higher than our estimates in the past and present but lower in the future. However, considering the differences in assumptions, the agreement can be considered reasonable.

The French experts consider three scenarios for long term modelling (beyond 100 years) where transport of plutonium is the dominant consideration. In both this Study and the French assessment, the four safety trials in the carbonate that did not go critical are considered to be the major potential contributor to releases because the plutonium is in a more available form. In the French analyses, the peak releases of plutonium generally occur from 100 to 10 000 years in the future (depending on the parameters used in the model) but are generally lower than those attributable to leaching of lagoon sediments. This Study has reached the same conclusion.

REFERENCES

AISSAOUI, D.M., BUIGUES, D., PURSER, B.H., "Model of Reef Diagenesis" (SCHROEDER, J.H., PURSER, B.H., Eds), Springer Verlag, Berlin (1986) 27–52.

ATKINSON, H.R., DAVIES, P.J., DAVY, D.R., HILL, L., McEWAN, A.C., Report of a New Zealand, Australian and Papua New Guinea Scientific Mission to Mururoa Atoll, Ministry of Foreign Affairs, Wellington, New Zealand (1984).

BARRILLOT, B., Les Essais Nucléaires Français 1960–1996, Centre de Documention et de Recherche sur la Paix et les Conflits (CDRPC), Lyon, France (1996).

BEAR, J., Dynamics of Fluids in Porous Media, American Elsevier, New York (1972).

BEJAN, A., Convection Heat Transfer, Second Edition, John Wiley & Sons, Inc., New York (1995).

BERG, I.Y., Radioactivity Trapped in Melt Produced by a Nuclear Explosion, Nuclear Technology 24 (1975) 85-100.

BERNER, U., Integrity of Concrete Plugs of Test Shafts, Rep. AN-44-96-11, Paul Scherrer Institut, Villigen, Switzerland (1996).

BOUCHEZ, J., LECOMTE, R., The Atolls of Mururoa and Fangataufa (French Polynesia), Vol. 2. Nuclear Testing: Mechanical, Lumino-thermal and Electromagnetic Effects, DIRCEN-CEA (1996).

BUIGUES, D., Mururoa and Fangataufa: Sea-Level Changes, Karstification and Atoll Morphology, Bull. Soc. Géol. France 169 (1996) 373–382.

BUIGUES, D., "Geology and Hydrology of Mururoa and Fangataufa, French Polynesia", Geology and Hydrology of Carbonate Islands (VACHER, H.L., QUINN, T.M., Eds.), Elsevier, Amsterdam (1997) 433–451.

CHOPPIN, G.R., KOBASHI, A., Marine Chem. 30 (1990) 241.

CHOPPIN, G.R., Redox Speciation of Plutonium in Natural Waters, J. Radioanalytical and Nuclear Chemistry 147 1 (1991) 109–116.

DELEERSNIJDER, E., TARTINVILLE, B., RANCHER, J., A simple model of the tracer flux from the Mururoa lagoon to the Pacific, Appl. Math. Lett. **10** (1997) 13–17.

DIERSCH, H.J., Interactive, Graphics-based Finite-element Simulation System FEFLOW for Modeling Groundwater Flow, Contaminant Mass and Heat Transport Processes, WASY Ltd., Berlin (1996).

FAIRHURST, C., BROWN, E.T., DETOURNAY, E., DE MARSILY, G., NIKOLAEVSKIY, V., PEARSON, J.R.A., TOWNLEY, L., (IGC), Stability and Hydrology Issues Related to Underground Nuclear Testing at French Polynesia, 2 Vols, Documentation Française, Paris (1998).

FETTER, C.W., Jr., Position of the Saline Interface Beneath Oceanic Islands, Water Resour. Res. 8 (1972) 1307–1314.

HADERMANN, J., HEER, W., The Grimsel (Switzerland) Migration Experiment: Integrating field Experiments, Laboratory Investigations and Modelling, Journal of Contaminant Hydrology 21 (1996) 87–100.

HADERMANN, J., PFINGSTEN, W., Source Term and Geosphere Transport Calculations for the Atolls of Mururoa and Fangataufa, Rep. TM-44-98-06, Paul Scherrer Institute (PSI), Villigen, Switzerland (1998); Internet: http://www1.psi.ch/~curti/Frameset home.html.

HAKANEN, M., HÖLTTÄ, P., Review of Sorption and Diffusion Parameters for TVO-92, Rep. YJT-92-14, Nuclear Waste Commission of Finnish Power Companies, Helsinki, Finland (1992).

HARRIES, J.R., Calf, G.E., Tritium Measurements in the Tasman Sea and the Southern Ocean. Aust. J. Mar. Freshwater Res. 31 (1980) 737-745.

HARTLEY, R.W., Release of Radionuclides to the Geosphere from a Repository for High-Level Waste, EIR-Bericht Nr. 554, Würenlingen, February 1985 and Nagra Technical Rep. 85-41, Baden, February 1985.

HASCHKE, J.M., "Hydrolysis of Plutonium", Transuranium Elements - A Half Century (MORSS, L.R., FUGER, J., Eds.), American Chemical Society, Washington, D.C., USA (1992) 416–425.

HASCHKE, J.M., Reactions of Plutonium and Uranium with Water: Kinetics and Potential Hazards, Rep. LA-13069-MS, Los Alamos National Laboratory, Los Alamos, New Mexico, USA (1995).

HENRY, H.R., Interfaces between Salt Water and Fresh Water in Coastal Aquifers. Water Supply Paper, US Geological Survey (1964).

HENRY, P., GUY, C., CATTIN, R., DUDOIGNON, P., SORNEIN, J.F., CARISTAN, Y., A Convective Model of Water Flow in Mururoa Basalts, Geochimica et Cosmochimica Acta, 60 12 (1996) 2087–2109.

HOCHSTEIN, M.P., O'SULLIVAN, M.J., Geothermal Systems Created by Underground Nuclear Testing, Proc. of the 7th New Zealand Geothermal Workshop, University of Auckland, New Zealand, 6-8 November, (1985) 149–154.

HOCHSTEIN, M.P., O'SULLIVAN, M.J., Geothermal Systems Created by Underground Nuclear Testing, Int. Scient. Symp. on a Nuclear Test Ban, Las Vegas, Nevada, USA, 15–16 January 1988.

ICHIKAWA, F., SATO, T., On the Particle Size Distribution of Hydrolyzed Plutonium(IV) Polymer, J. Radioanal. Nucl. Chem. 84 (1984) 269–275.

JAKOB, A., HADERMANN, J., RÖSEL, F., Radionuclide Chain Transport with Matrix Diffusion and Non-linear Sorption, Rep. 54, PSI, Villigen and Rep. NTB 90-13, Nagra, Baden (1989).

JAKOB, A., "Modelling Solute Transport using the Double Porous Medium Approach", Modelling in Aquatic Chemistry (GRENTHE, J., PINGDOMÈNEC, J., Eds.), OECD-Nuclear Energy Agency, Paris (1997) pp. 525–576.

JANKOVIC, I., High-Order Analytic Elements in Modeling Groundwater Flow, University of Minnesota, PhD Thesis (1997) p. 160.

KERSTING, A.B., The State of the Hydrologic Source Term, Rep. UCRL-ID-126557, Lawrence Livermore National Laboratory, Livermore, USA (1996).

KERSTING, A.B., THOMPSON, J.L., Near-field Migration of Radionuclides in the Subsurface at the Nevada Test Site: Evidence For Colloid Transport of Radionuclides Through Fractured Volcanic Rock, 214th American Chemical Society National Meeting, Division of Nuclear Chemistry and Technology, paper No. 076, September 7–11, Las Vegas, Nevada, USA (1997).

KESTER, D.R., DUEDALL, I.W., CONNORS, D.N., PYTKOWICZ, R.M., Preparation of Artificial Seawater, Limnol. Oceanogr. 12 (1967) 176.

KIM, J.I., Actinide Colloid Generation in Groundwater, Radiochimica Acta 52/53 (1991) 71–81.

LAI, M.G., GOYA, H.A., Radioactivity Release from Radionuclide Power Sources, III. Release from Plutonium Metal to Seawater, Rep. USNRDL-TR-1050, US Naval Radiological Defense Laboratory (1966).

MARSILY, G. de, Quantitative Hydrogeology, Groundwater Hydrology for Engineers, Academic Press, New York (1986) p. 440.

McCARTHY, J.F., ZACHARA, J.M., Subsurface Transport of Contaminants, Environ. Sci. Technol. 23 5 (1989) 496–502.

NAGRA, National Cooperative for the Disposal of Radioactive Waste, Kristallin-I, Conclusions from the regional investigation programmes for siting a HLW repository in the crystalline basement of Northern Switzerland, Technical Rep. 93-09E, Nagra, Wettingen, Switzerland (1994).

NIELD, D.A., BEJAN, A., Convection in Porous Media, Springer-Verlag, New York (1992) p. 408.

NITSCHE, H., MÜLLER, A., STANDIFER, E.M., DEINHAMMER, R.J., BECRAFT, K., PRUSSIN, T., GATTI, R.C., Dependence of Actinide Solubility and Speciation on Carbonate Concentration and Ionic Strength in Groundwater, Radiochimica Acta 58/59 (1992a) 27-32.

NITSCHE, H., ROBERTS, K., GATTI, R.C., PRUSSIN, T., BECRAFT, K., LEUNG, S., CARPENTER, S.A., NOVAK, C.F., Plutonium Solubility and Speciation Studies in a Simulant of Air Intake Shaft Water from the Culebra Dolomite at the Waste Isolation Pilot Plant, Rep. SAND 92-0659, Sandia National Laboratories, New Mexico, USA (1992b).

NITSCHE, H., The Importance of Transuranium Solids in Solubility Studies for Nuclear Waste Repositories, Mat. Res. Soc. Symp. Proc., Vol. 257 (1992c) 289–298.

NITSCHE, H., GATTI, R.C., STANDIFER, E.M., LEE, S.C., MÜLLER, A., PRUSSIN, T., DEINHAMMER, R.J., MAUER, H., BECRAFT, K., LEUNG, S., CARPENTER, S.A., Measured Solubilities and Speciations of Neptunium, Plutonium, and Americium in a Typical Groundwater (J-13) from the Yucca Mountain Region, Rep. LA-12562-MS., Los Alamos National Laboratory, New Mexico, USA (1993).

NITSCHE, H., ROBERTS, K., PRUSSIN, T., MÜLLER, A., BECRAFT, K., KEENEY, D., CARPENTER, S.A., GATTI, R.C., Measured Solubilities and Speciations from Oversaturation Experiments of Neptunium, Plutonium, and Americium in UE-25p #1 Well Water from the Yucca Mountain Region, Milestone Rep. 3329 - WBS1.2.3.4.1.3.1, Los Alamos National Laboratory, New Mexico, USA (1994a).

NITSCHE, H., ROBERTS, K., XI, R., PRUSSIN, T., BECRAFT, K., AL-MAHAMID, I., SILBER, H.B., CARPENTER, S.A., GATTI, R.C., NOVAK, C.F., Long-Term Plutonium Solubility and Speciation Studies in a Synthetic Brine, Radiochimica Acta 66/67, 3–8 (1994b).

OBERDORFER, J.A., HOGAN, P.J., BUDDEMEIER, R.W., Atoll Island Hydrogeology: Flow and Freshwater Occurrence in a Tidally Dominated System, Journal of Hydrology, 120 (1990) 327–340.

PENROSE, W.R., METTA, D.N., HYLKO, J. M., RINCKEL, L.A., The Reduction of Plutonium(V) by Aquatic Sediments, J. Environ. Radioactivity, **5** (1987) 169–184.

PERROCHET, P., TACHER, L., Mathematical Modelling of Hydrothermal Processes at Mururoa Atoll, Ecole Polytechnique Fédérale de Lausanne, Laboratoire de Géologie, Documentation Française (1998).

PETERSON, E., LIE, K., RIMER, N., NILSON, R., HIGGINS, G., "Thermodynamic Evolution of Nuclear Cavities", Containment of Underground Nuclear Explosions (Proc. Symp. Reno, 1991) Lawrence Livermore National Laboratory, Livermore, USA (1991) 257–274.

PROVOST, A.M., VOSS, C.I., NEUZIL, C.E., Glaciation and Regional Ground-water Flow in the Fennoscandian Shield, SKI Report 96:11, Swedish Nuclear Power Inspectorate (SKI), Stockholm, Sweden (1998).

PUIGDOMÈNECH, I., BRUNO, J., Plutonium Solubilities, SKB Technical Rep. 91-04, Swedish Nuclear Fuel and Waste Management Company (SKB), Stockholm, Sweden (1991).

RAEISI, E., MYLROIE, J.E., Hydrodynamic Behavior of Caves Formed in the Freshwater Lens of Carbonates Islands, Carbonates and Evaporites, 10 2 (1995) 207–214.

RAI, D., SERNE, R.J., Solution Species in Oxidizing Environments: I. Polymeric Pu(IV), Rep. PNL-SA-6994, Pacific Northwest Laboratory, Hanford, Washington, USA (1979) 1–9.

RAI, D., SWANSON, J.L., Properties of Plutonium(IV) Polymer of Environmental Importance, Nucl. Technol. 54 (1981) 107–112.

ROUGERIE, F., WAUTHY, B., The endo-upwelling concept: from geothermal convection to reef construction, Coral Reefs, **12** (1993) 19–30.

RUNDBERG, R.S., MITCHELL, A.J., TRIAY, I.R., TORSTENFELT, J.B., Size and Density of a Pu-242 Colloid, Mat. Res. Soc. Symp. Proc., Vol. 112 (1988) 243–248.

SAMADEN, G., DALLOT, P., ROCHE, R. Atoll d'Eniwetok. Système géothermique insulaire à l'état naturel. La Houille Blanche, **2** (1985) 143–151.

SERNE, R.J., RELEYA, J.F., The Status of Radionuclide Sorption-Desorption Studies Performed by the WRIT Program, Rep. PNL-SA-9787, Pacific Northwest Laboratory, Richland, WA, USA (1981).

SILVA, R.J., NITSCHE, H., Actinide Environmental Chemistry, Radiochimica Acta 70/71 (1995) 377–396.

SKI (Swedish Nuclear Power Inspectorate), Glaciation and Hydrology, Workshop on the impact of climate change and glaciations on rock stresses, groundwater flow and hydrochemistry - Past, present and future, SKI Rep. 97:13, Swedish Nuclear Power Inspectorate, Stockholm, Sweden (1997).

SMITH, D.K., A Review of Literature Pertaining to the Leaching and Sorption of Radionuclides Associated with Nuclear Expolosive Melt Glasses, Rep. UCRL-ID-113370, Lawrence Livermore National Laboratory, California, USA (1993).

SMITH, D.K., NAGLE, R.J., KENNEALLY, J.M., Transport of Gaseous Fission Products Adjacent to an Underground Nuclear Test Cavity, Radiochimica Acta 73 (1996) 177–183.

SWARTZ, J.H., Geothermal measurements on Eniwetok and Bikini Atolls, USGS Professional Paper 260-U (1958) 711–741.

TAZIEFF, H., Rapport d' Haroun Tazieff sur L'Ensemble de la Mission Scientifique en Polynésie Française (1982).

TOWNLEY, L.R., AQUIFEM-P: A Periodic Finite Element Aquifer Flow Model: User's Manual and Description, Version 1.0, CSIRO Division of Water Resources, Technical Memorandum 93/13 (1993) pp. 72, plus software.

TRIAY, I.R., HOBART, D.E., MITCHELL, A.J., NEWTON, T.W., OTT, M.A., PALMER, P.D., RUNDBERG, R.S., THOMPSON, J.L., Size Determination of Plutonium Colloids Using Autocorrelation Photon Spectroscopy, Radiochimica Acta 52/53 (1991) 127–131.

US CONGRESS – Office of Technology Assessment, The Environment of Underground Nuclear Explosions, Rep. OTA-ISC-414, US Government Printing Office, Washington DC, USA (1989) pp. 80.

VACHER, H.L., Dupuit-Ghyben-Herzberg analysis of strip-islands lenses, Geol. Soc. America Bull. 100 (1988) 508–591.

WILSON, C.V., BRUTON, C.J., Studies of Spent Fuel Dissolution Behavior Under Yucca Mountain Repository Conditions, Rep. PNL-SA-16832 (or UCRL-10023), Pacific Northwest Laboratory, Richland, Washington, USA (1989).

ZHAO, P., WRUCK, D.A., ROBERTS, K., PALMER, C.E.A., SILVA, R.J., Formation of Plutonium(IV) Colloids in Sodium Chloride Solutions of Low and High Ionic Strengths, Radiochimicha Acts, in press (1997).

APPENDICES I–VI

Appendix I

INFLUENCE ON GROUNDWATER FLOW OF HOLLOW SPHEROIDAL INHOMOGENEITIES IN A POROUS MEDIUM

It is instructive to examine the general influence of one or more heterogeneities in the rock structure on the permeability of the rock or rock mass. We will assume that the inhomogeneity can be represented as a spheroidal void, such as shown in Fig. I.1 below. The spheroid is an ellipsoid that is generated by revolving an ellipse around one of its axes. On the micro-scale, this void could, for example, represent pore spaces between grains in a porous medium or the solution cavities often found in carbonate rock. On the larger scale, the "void" could, for example, be a cavity-chimney of a nuclear explosion or a lava tube. The following results are based on studies by Jankovic 1997.

The inhomogeneities were represented in a potential flow simulation by spheroids of high permeability in a three-dimensional medium of average conductivity, i.e. of the order of 10^{-5} m/s. The computer code used for this purpose allows computation of heads only. Actual flow would occur along the local head gradient, i.e. perpendicular to the contours of constant heads.

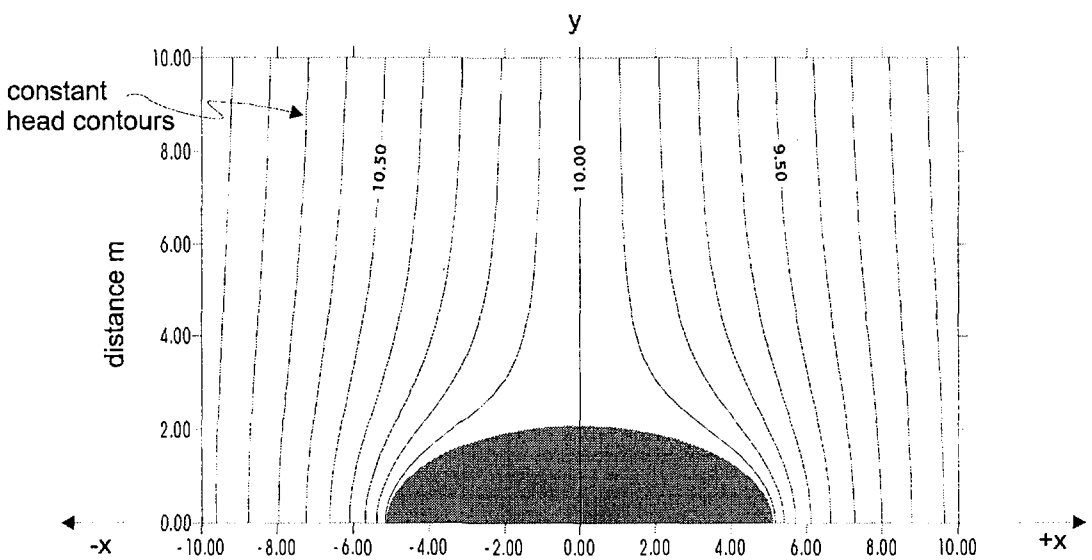

FIG. I.1. Head contours around a spheroidal cavity in a uniform flow field. Heads decrease from 11.00 m along the extreme left ordinate to 9.00 m along the extreme right hand ordinate.

Figure I.1 shows a typical result for flow around a highly conductive spheroidal cavity or void. The cross-section shown corresponds to the horizontal plane. The semi-major axis of the prolate spheroid is 5 m, the semi-minor axis is 2 m and it is centred on the xyz origin. A uniform flow is applied upstream (direction of -x) at a rate corresponding to a head drop of 10 cm per metre from left to right in the x direction, i.e. the direction of increasing x, along which the spheroid is aligned. The x-axis is also the axis of rotational symmetry for the spheroid.

In the absence of the cavity, a particle travelling in the water from left to right in the x direction, i.e. down the head gradient, would follow a path parallel to the x-axis, i.e. perpendicular to the local head contour. After the water-filled cavity, i.e. the "inhomogeneity", is introduced, the head

contours deviate around the cavity as shown in Fig. I.1. The same particle would now deviate towards the cavity, again in order to remain perpendicular to the local head contour. The quasi-hydrostatic pressure within the water-filled cavity tends to reduce the flow rate through it, but the very high conductivity allows the fluid to "rush" through the cavity from the higher head in the rock medium (on the left) to the lower head (on the right).

EQUIVALENT PERMEABILITY OF A POROUS MEDIUM CONTAINING AN INHOMOGENEITY

Using Jankovic's code (Jankovic 1997) the spheroidal inhomogeneity in Fig. I.1 can be surrounded by an imaginary stream "cell," using the method of images, discussed below. The cell is effectively a rectangular 'tube' of square cross-section placed symmetrically around the cavity, as shown in Fig. I.2. Flow along the cell is uniform from left (AA) to right (BB) as in Fig I.1.

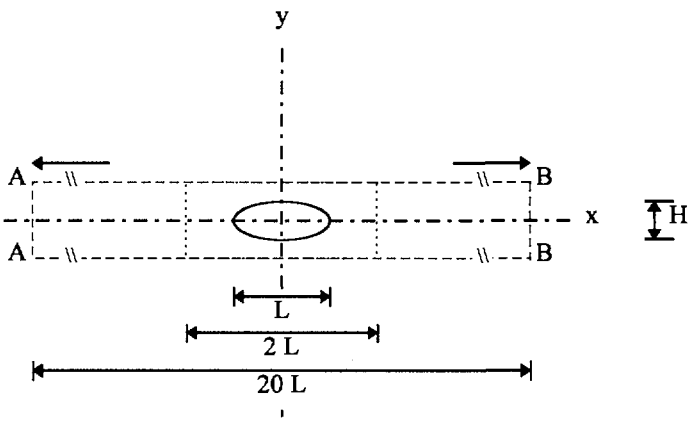

FIG. I.2. Rectangular stream cell, of variable length AB (2L-20L) with a square cross-section in yz plane (see Fig. I.6) and variable height BB, enclosing the spheroid of major axis L and minor axis H.

The pressure head acting on planes normal to the flow can be determined and, from this, a measure of the average head loss through the cell. Since the specific discharge (Darcy velocity) is given, this allows an "equivalent conductivity" k_e to be computed for the cell with the internal cavity. As the size of the cell around the single inhomogeneity is increased, the effect on the overall hydraulic conductivity (k) of the medium decreases progressively.

A series of computer runs were carried out for the spheroidal cavity of Fig. I.1, using cells of progressively increasing size to surround the spheroid. It was found that the equivalent conductivity (k_e) could be represented well by the expression

$$\frac{k}{k_e} = 1 - \frac{V_e}{V_t} \quad , \tag{1}$$

where

- k is the hydraulic conductivity of the medium,
- k_e is the equivalent conductivity of the cell (with cavity)
- V_e is the volume of the spheroid
- V_t is the volume of the cell.

As the volume of the cell (V_t), which could be considered as the space available between spheroidal inhomogeneities, becomes large compared to V_e, the effective conductivity k_e approaches the

conductivity of the medium (k) without inhomogeneities. The percentage error computed from the ratio

$$\frac{k_{e_{computed}} - k_{e_{Eq1}}}{k_{e_{Eq1}}} \tag{2}$$

for different sizes of cell, is shown in Fig. I.3. It can be seen that the error is less than 2% in all cases.

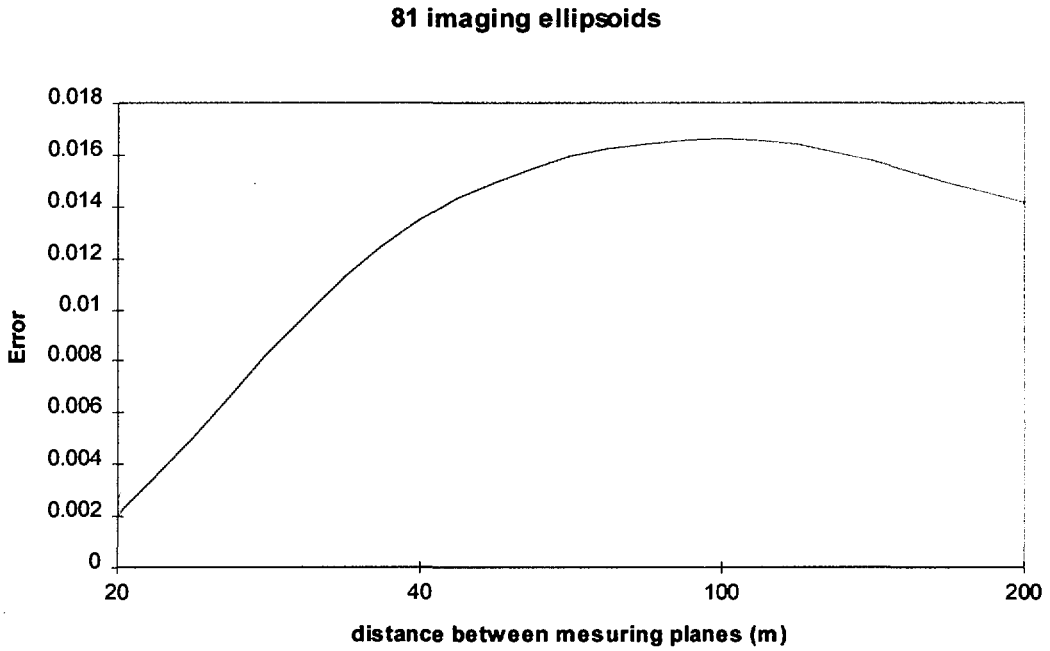

FIG. I.3. Error (as computed by Eq. 2) in the computed hydraulic conductivity (k) of a cell compared to the actual equivalent conductivity (k_e) for various sizes of the square-sided cell surrounding a single spheroidal cavity with a semi-major axis of 5 m and a semi-minor axis of 2 m (see Fig. I.1). The distance between the measuring planes AA and BB was varied between 2L = 20 m and 20L = 200 m (see Fig. I.2). Note: 81 imaging spheroids were used in the imaging procedure (see Fig. I.4).

Figure I.4 shows the arrangement of spheroids around the central spheroid.

A confirmation of this result is obtained by the three-diamensional finite element analysis of the "Influence of 137 Underground tests on long term hydrological regime" (see Section 3.2.6.3). Here, the following statement can be found:

> *With hydraulic conductivities of 10^{-4} m/s in all the damaged zones, for example, the total discharge into the lagoon is increased by less than 1%.*

Further details of the computational procedures used to arrive at this result are given in Jankovic (1997).

As mentioned in the discussion of Fig. I.1, the introduction of an inhomogeneity into the medium causes the potential flow field to deviate from the previously uniform pattern. In calculating the effect of the inhomogeneity on the resistance to flow in the medium we wish to ensure that this total flow through and past the inhomogeneity is "contained" within the imaginary boundaries the four sides of the rectangular cell shown in Fig. I.2. The flow enters the cell at one end (say AA) and leaves at the other (say BB). No fluid enters or leaves across the four sides. Thus, we must ensure that these sides are in fact no flow boundaries.

A technique frequently used to achieve this in an analysis is to introduce a second inhomogeneity which is identical to the first but displaced from it. This is a "mirror image" at the desired plane of symmetry as shown in Fig. I.4 (i).

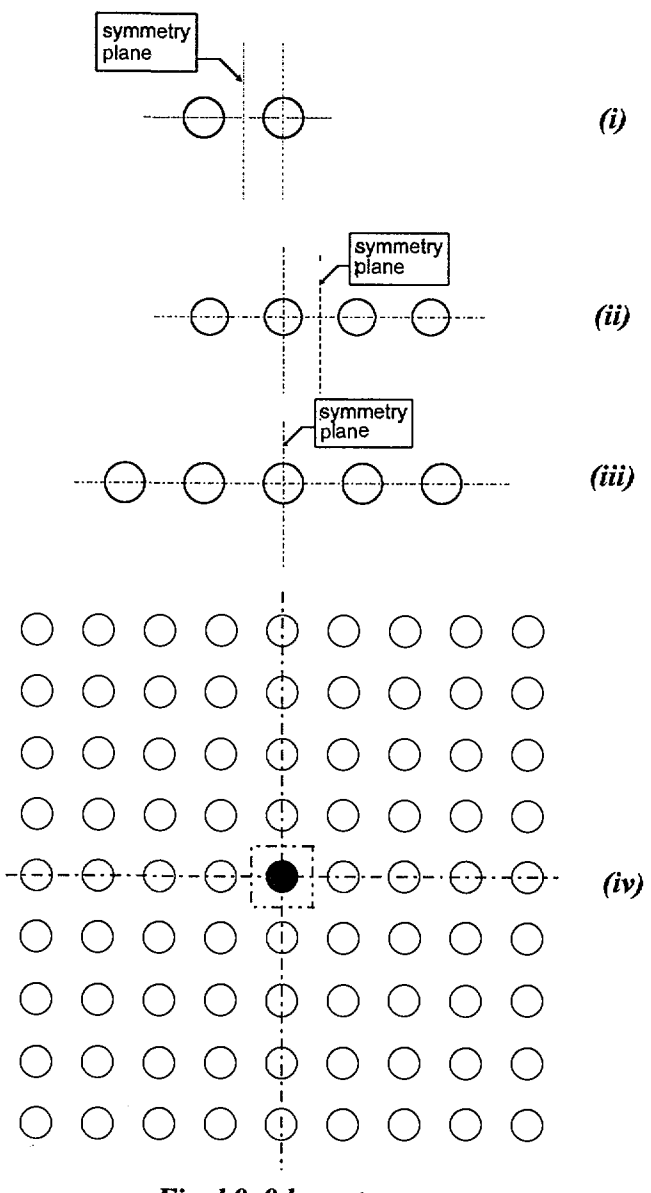

FIG. I.4. Successive steps of adding mirror image spheroidal inhomogeneities in order to establish rectangular no-flow boundaries for the stream cell shown in Fig. I.2.

Conditions of symmetry dictate that the plane mid-way between the two inhomogeneities will be a no-flow boundary, i.e. there will be no-flow normal to this plane.

Superposition of two inhomogeneities as shown in Fig. I.4 (ii) will similarly ensure that the plane mid-way between the four inhomogeneities will be a no-flow boundary. However, the process of going from I.4 (i) to I.4 (ii) destroys the symmetry along the plane in I.4 (i), since there are two inhomogeneities on the right of the original inhomogeneity and only one on the left. Addition of another inhomogeneity to the left as in I.4 (iii) would move the plane of symmetry to the axis of the original inhomogeneity, introducing a small degree of asymmetry to the flow along the planes of symmetry established in I.4 (i) and I.4 (ii), i.e. they are no longer strictly no-flow boundaries. This asymmetry along the previously symmetric boundaries can be reduced by introducing additional

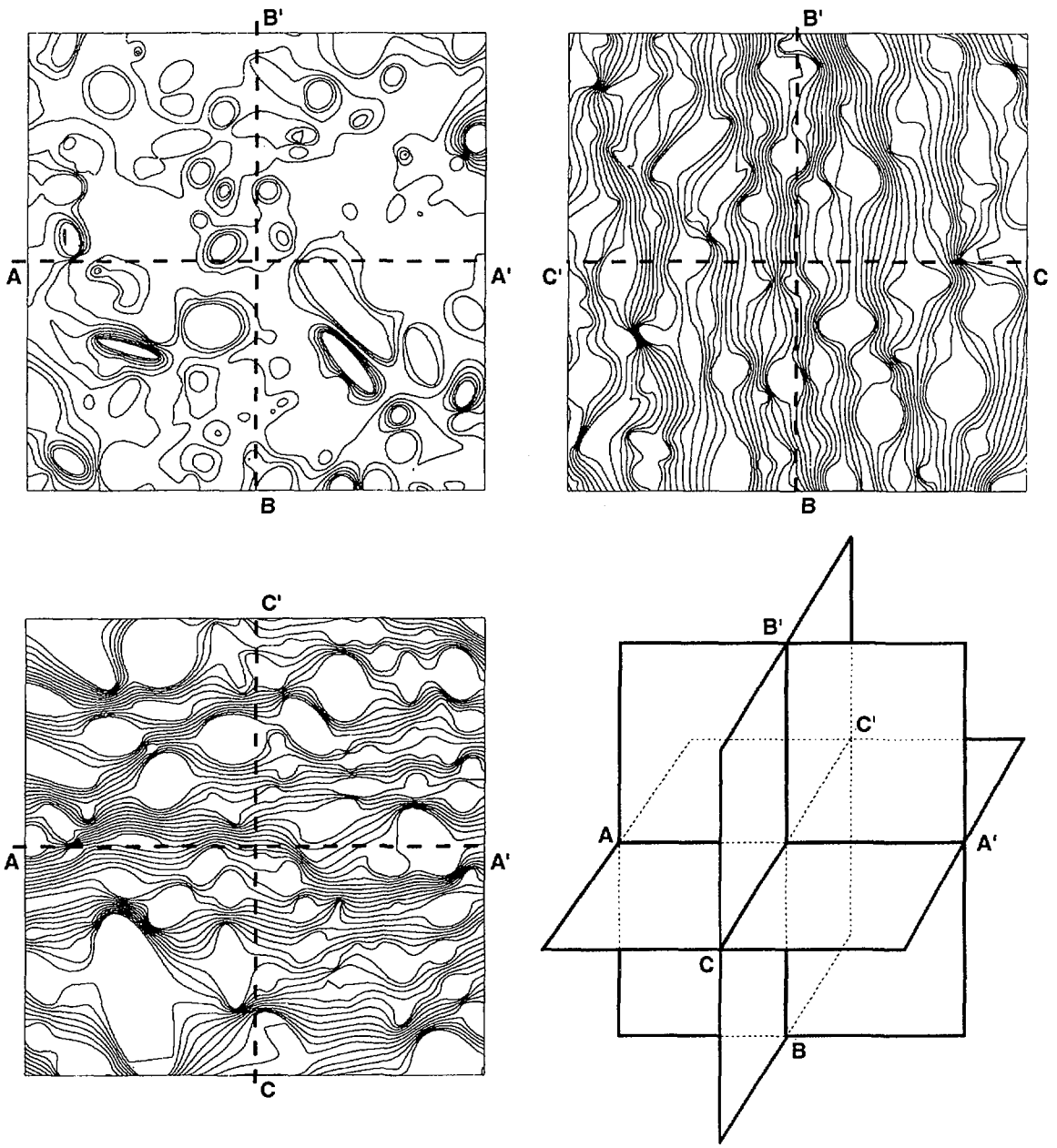

FIG. I.5. Intersections with constant head surfaces for 1000 spheroidal inhomogeneities in a uniform flow field. Inhomogeneities are, on average, 1000 times more permeable than the background. Flow is from C to C'.

inhomogeneities, along the same line as shown in Figs I.4 (i)–I.4 (iii). In this way the symmetry planes shown in Figs I.4 (i) and I.4 (ii) will tend to be restored as no-flow boundaries. Repeating the same process above and below the initial inhomogeneity, as shown in Fig. I.4 (iv), will similarly establish no-flow boundaries on the planes mid-way between the first layers of inhomogeneities above and below the initial inhomogeneity. The 9 × 9 array shown in Fig. I.4 (iv), established in this way, allows a very good approximation to the no-flow cell boundaries required for the stream cell shown in Fig. I.2. Variation of the centre to centre spacing between adjacent inhomogeneities will thus vary the size of the square cross-section of the cell. The distance upstream and downstream of the planar array of 81 inhomogeneities is varied from 2 L to 20 L as shown in Fig. I.2.

Figure I.5 shows three mutually orthogonal sections through a three-dimensional field of overall uniform flow containing 1000 spheroidal inhomogeneities. In this case, the inhomogeneities are, on average, 1000 times more permeable than the background.

The flow shown in Fig. I.6 is intended to represent groundwater flow around a series of cavity-chimneys from nuclear explosions aligned essentially perpendicular to the flow, which is directed from the slope of the atoll inward and upward to the lagoon. This arrangement of cavities is similar to the situation in rim test areas, especially on Mururoa. The axis AA' can be considered to be parallel to the rim shoreline, BB' is vertical. It is seen that the pattern of uniform flow is changed only in the immediate vicinity of the cavities, even for the two closest cavities. This indicates that there is very little hydrological interaction between cavity-chimneys, even when they are relatively close to each other.

In all cases (Figs I.1, I.5 and I.6) it can be seen that the distortion of the constant head contours, which would all be straight lines in the absence of the inhomogeneities, is significant only in the vicinity of the individual inhomogeneities.

LAVA TUBES

Lava tubes can be characterized as long, tunnel-like, voids sometimes formed in subaerial volcanics. They are formed *"as a result of the surface solidification of a lava flow during the last stages of its activity. A frozen crust forms over still mobile and actively flowing liquid rock as a result of surface cooling. A dwindling supply of lava may then cause the molten material to drain out from under the crust and leave long cylindrical tunnels"* (see **lava caves**, in Macropaedia, Vol. VI, p. 83, Encyc. Britt. (Chicago) 15th Ed. 1975).

Lava tubes may be up to several metres in diameter and can extend for kilometres in length. Impressive examples of lava tubes can be found on Hawaii and other recent volcanic islands. It has been suggested that lava tubes at depth in the volcanics could serve as fast conduits for flow of radionuclide contaminated groundwater from the vicinity of the explosion cavities towards the biosphere.

If lava tubes exist in Mururoa and Fangataufa, they will be located (as noted in the quotation above) in the subaerial volcanic series, which are found in the upper sections of the volcanics and hence above, or in the upper part of the cavity-chimneys. Since the radionuclide contaminated groundwater rises from the explosion sites towards the lagoon, lava tubes, which will be more or less horizontal, would appear to have the potential to serve as fast conduits for the contaminated groundwater.

It seems probable, however, that any such tubular voids would tend to become filled with sediments and also to collapse under the accumulated weight of overlying rock as the volcanic seamount subsides. CEA scientists indicate that no evidence of lava tubes has been found in any of the more than 300 drillholes associated with the underground tests on the atolls.

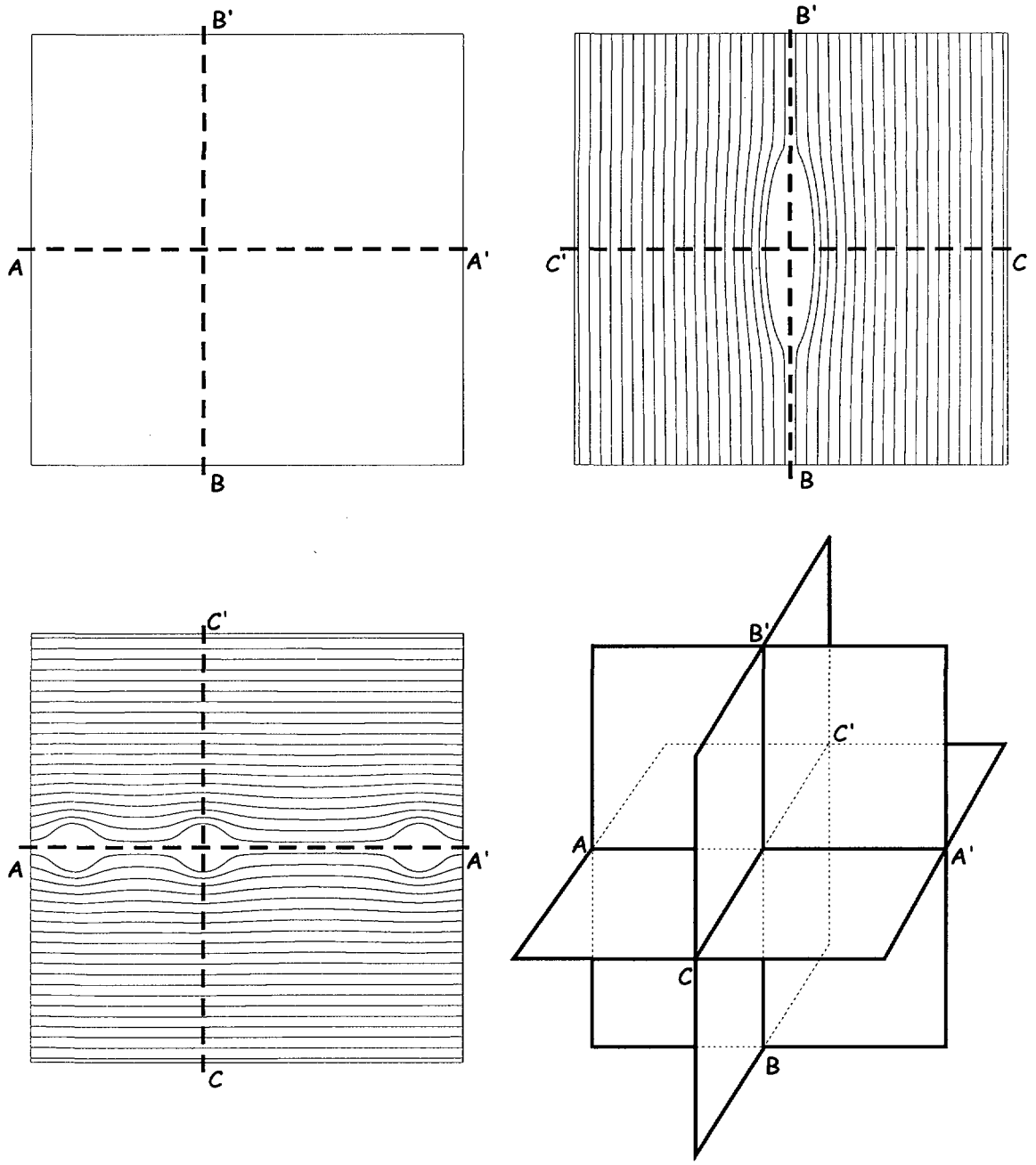

FIG. I.6. Effect of three spheroidal inhomogeneities on a previously uniform flow field. Flow is from C to C'.

If the lava tubes did not extend as an interconnected system across the full width of the atoll, their effect on the flow field would be restricted to the region of the lava tubes, i.e. forming one or more spheroidal inhomogenieties with an effect on the regional flow similar to that discussed earlier in this Appendix. Even the extension of one or more lava tubes as a continuous conduit across the atoll, which seems very improbable, would have a negligible influence compared to the extensive karst horizons in the overlying carbonates. The influence of the karsts is recognised and is considered in the analysis of radionuclide pathways to the biosphere. Thus, it can be assumed that any possible influence of lava tubes on the flow is effectively included in the effect of the karst horizons.

Appendix II

A MODEL OF TRITIUM RELEASE BASED ON MIXING IN THE CARBONATES

INTRODUCTION AND OBJECTIVE

In Section 3, we have described the major flow mechanism in the atolls, both in the volcanics and in the carbonates. We have also proposed a finite element model to predict (a) the flow under natural conditions, (b) the flow at a test site, (c) in the cavity-chimney, (d) in the volcanic cover (if it exists and is not damaged) and (e) in the carbonates. These calculations were made in steady state, i.e. neglecting any transient phenomena, in particular tidal effects.

In this section, we will make an attempt to further evaluate the flow and transport in the carbonates, taking into account in a simplified manner the effects of the tide. This will be done with a simple mixing model representing the carbonates. The major objective of this task is to try to support the assumptions and parameter values of the flow models in the volcanics, described in Section 3.2.7, by comparison with those HTO measurements that are available at the atoll scale, both in observation wells in the carbonates and in the lagoon waters. It was extremely important that these models were compared with actual radionuclide measurements to achieve some confidence in their predicted radionuclide releases to the environment.

FLUX OF HTO IN THE CARBONATES AND TO THE LAGOONS

Measurements of concentrations of HTO in the carbonates performed by both the IAEA and the CEA show very clearly that quite a large amount of HTO is present in the carbonates. We will establish our own estimate of this inventory, based on the measurements, but the order of magnitude is in the range of several 10^{15} Bq for each atoll. It is of interest to compare this figure with the current flux of HTO in the lagoons. This is easily done, as the average concentration of HTO in the lagoon water and their average daily flow in and out are known for 1996:

	Average HTO, 1996	Daily flow	Annual HTO flux in lagoons, 1996
Mururoa	1000 Bq/m^3	100×10^6 m^3/d	37×10^{12} Bq/a
Fangataufa	600 Bq/m^3	42×10^6 m^3/d	9×10^{12} Bq/a

In this table, we have used the daily flow in and out of the lagoons as estimated by the CEA. The IAEA produced also an estimate of these flows, partly based on a flow model developed for Mururoa by Deleersnijder et al. (1997). These estimates are lower than those of the CEA and may be valid for a situation after a storm. We therefore decided to keep the larger estimates given by the CEA, which are conservative as they maximise the release rate.

Even if we consider that the present flux has been maintained for 20 years, the cumulative amount of HTO having left the carbonates is of the order of 0.7×10^{15} Bq for Mururoa and 0.2×10^{15} Bq for Fangataufa, i.e. very small compared to the amount present in the carbonates and released by the volcanics. A large amount of HTO is thus stored in the carbonates and released very slowly to the lagoons.

The second observation is based on the maps of the HTO distribution in the carbonates (see Figs 88 and 89), particularly in Area 1 on Mururoa. The HTO seems to have "diffused" from the rim towards the interior of the lagoon over a distance of about 4 km during a period of 20 years. This is about 200 m/a, whereas the calculated horizontal pore velocities in the carbonates are of the order of less than 10 m/a. The most likely explanation for this spreading is lateral mixing due to the tidal effects, as discussed in Section 3.1.8. From this map, it is very difficult to determine whether some of

the HTO released to the carbonates has been transferred to the ocean or if most of it has spread towards the interior. From the steady state flow model the direction of the flow in the carbonates is towards the interior, thus supporting the assumption of no significant releases to the ocean. But the mixing due to tidal effects may have spread some of the HTO into the ocean as well. Based on a comparison of the amount of HTO released in Area 1 over the years and the amount still present in the carbonates, radioactive decay taken into account, the hypothesis of no release into the ocean is not incompatible with the measurements. In Area 4, however, the same analysis shows that some release to the ocean may have occurred, but this area is known to have been perturbed by mechanical instabilities, thus making it possible that communication in the carbonates between the rim and the ocean is easier. We do not imply that direct release to the ocean is impossible, in fact we believe that there is local evidence of it, but there is no hard information to estimate the flux of water to the ocean. We therefore take the conservative view that all transfer from the volcanics through the carbonates ends up in the lagoons.

The third observation is that the sampling of waters in the carbonates, as performed by both the CEA and the IAEA, seems to indicate a rather uniform concentration of HTO over several hundred metres vertically, at the various sampling points. Since these sampling points are within vertical boreholes, it is possible that the mixing that homogenized the HTO concentration vertically occurred only in the boreholes and not in the carbonates. However, we will say that it is compatible with the data that the HTO distribution is present not just in the karst layers, as assumed by the CEA, but over a significant thickness of the carbonates. Several different thicknesses will be considered. The potential cause for such an important vertical mixing has been described earlier: the tidal effect (see Sections 3.1.8). This assumption of large-scale mixing over a large thickness of the carbonates leads to an increase of the inventory of HTO in the carbonates compared to that given by the CEA. The CEA assumed that the measured HTO was only distributed over a 50 m dolomitic karst layer with a porosity of 20% at the bottom of the carbonates. The CEA assumption increases the rate of release of radionuclides from the volcanics and is obviously conservative.

A fourth consideration in support of the mixing model that will be presented below is based on the potential mechanisms of HTO transfer through the carbonates. We know from the hydrothermal modelling that the steady flow in the carbonates is at first horizontal and centripetal from the ocean towards the interior, and then vertically upwards. Vertical Darcy velocities in the carbonates are in the range of 0.5 to 2 m/a in the centre of the Mururoa Atoll as estimated by the IGC. Globally, in the 3-D modelling of Mururoa, the net flux of water to the lagoon has been estimated by the IGC to be 60 000 m^3/d, i.e. an average Darcy velocity over the 160 km^2 of the lagoon of 0.137 m/a. The porosity of the carbonates is in the order of 30%.

PISTON FLOW MODEL

If we assume vertical piston flow from the base of the carbonates to the lagoon over a thickness of 300 m the transfer time for HTO would be between 45 and 650 years. This is obviously incompatible with the data. HTO has been observed in the lagoons since 1987 and earlier data are not available. The piston flow model for transfer in the carbonates can thus be ruled out. A test of this model, with increased velocities and transfer times of 1 to 20 years, is nevertheless developed in Appendix III which shows that this model cannot account for the observed flux to the lagoon and the inventory.

ADVECTION - DISPERSION MODEL

Another model for transfer of HTO through the carbonates could be the advection - dispersion model in the vertical direction. This model accounts for the existence of preferential pathways in which the advective velocity could be much higher than the average. Using the same average advective velocity as in the piston flow model, a large dispersive term would make it possible to have

early breakthroughs, much before the advective front. In order to have breakthroughs in less than 10 years, it is necessary to use a very large longitudinal dispersivity in the advection - dispersion equation which would be in the order of 100 m or more. The dispersion coefficient is the product of the dispersivity and the average velocity. While such large dispersivities could be explained by the tidal effect, as suggested by the CEA and in Section 3.1.8, introducing them into the transport equation has the net effect that the early breakthroughs are followed by a rapid increase of the HTO flux to the lagoon, and thus of the concentration in the lagoon. This again contradicts the observations, as they indicate that the concentration in the lagoon seems to have been fairly constant over the last ten years, whereas the incoming flux of HTO from the nuclear test is increasing. A test of this model, exemplifying this behaviour, is developed in Appendix III. It shows the inability of this model to account for both the flux to the lagoon and the inventory.

Having ruled out both the piston flow and the advection - dispersion model, we suggest that a mixing model may be adequate to represent the transfer of HTO and other radionuclides through the carbonates. This model assumes that the horizontal areas where HTO has invaded the carbonates behave as well-mixed reservoirs, i.e. that the HTO spreads over a significant vertical thickness of the carbonates and is well-mixed with a homogeneous concentration over this thickness. Several thickness values will be considered. A small percentage of this water is transferred annually to the lagoons and accounts for the observed concentration in the lagoon water. This is plausible because of the mixing effect of the tides. It is not inconsistent with the few observations of a fairly homogeneous vertical, and locally horizontal distribution of HTO. It will be shown to be compatible with both the estimated releases of HTO from the volcanics and the flux of HTO to the lagoons. Because of the very large volume of water stored in the carbonates, the concentration in the carbonates builds up slowly, and the small average flux of HTO to the lagoon is approximately constant, thus providing an explanation for the absence of large variations of the concentration of HTO in the lagoons over the years. This model is in better agreement with the observations than the advective - dispersive model used by the CEA, which does not reproduce the almost constant level of HTO in the lagoons.

Is this mixing model for HTO transport in the carbonates in contradiction with the heat transfer model used by the IGC to account for the thermal profiles in the volcanics and carbonates? The answer is no. Indeed, the effect of mixing due e.g. to tidal fluctuations is much more significant for a tracer such as HTO than for heat, for which the temperature constantly equilibrates between water and solid. To confirm this, a thermal profile in the Mururoa atoll was calculated with the FEFLOW code with an artificial increase of the longitudinal thermal conductivity by taking a longitudinal thermal dispersivity of 10 000° m, equivalent to increasing the mixing. The results show very little difference in the thermal profile, confirming that intense mixing in the carbonates would not drastically change the thermal profile.

THE CARBONATES MIXING MODEL

We will now describe in detail the proposed mixing model of the carbonates. This model is made of three types of *reservoirs* in series.

a) The first reservoir is a cavity-chimney. It has been shown that within such a highly permeable cavity-chimney, a high velocity convective cell develops, causing an intense mixing within the cavity-chimney. The concentration of any radionuclide is assumed to be uniform within the cavity-chimney at all time. This well-mixed reservoir loses water through the top layer with a Darcy velocity v_D, either through the volcanic cover, if there is one (Category 1), or directly to the carbonates in the case of each of the four tests known to have leaking covers (Category 2) and for the CRTV tests (Category 3). The "categories" mentioned here are defined in Fig. 1 and Table 1 of this report. The flux of water coming out of the cavity-chimney is thus the product of this Darcy velocity and the horizontal area of the cavity-chimney, πR_c^2, where R_c is the radius of the cavity-chimney. By continuity, the cavity-chimney receives the same amount of water either from below or from the sides, which mixes rapidly. It is easy to establish that the

variation with time of the concentration in the cavity-chimney C(t), taking radioactive decay into account, is:

$$C(t) = C_0 Exp(-\Lambda t) \qquad (1)$$

with:

C_0 = Initial concentration in cavity $= A_0/(\pi R_c^2 H'_c \varepsilon)$

$$\Lambda = \lambda + \frac{v_D}{H'_c \varepsilon} \qquad (2)$$

where

Λ	decay constant (depletion of radionuclide) in a cavity
λ	decay constant of radionuclide (Ln2/T, T = half-life),
v_D	Darcy velocity above cavity-chimney,
H'_c	height of cavity-chimney, 5.66 × R_c, to take into account the volume of the lower hemisphere of the cavity,
ε	porosity in chimney, 30%,
A_0	initial HTO inventory of test, in Bq.

Note that if the radionuclide sorbs on the rubble in the cavity-chimney, then:

$$\Lambda = \lambda + \frac{v_D}{H'_c \varepsilon R} \qquad (3)$$

where

R is the retardation factor, see Section 5.

The flux of radionuclides leaving the cavity-chimney is thus $\pi R_c^2 v_D C(t)$, transferred to the carbonates. The time taken by this flux to reach the carbonate is a function of the thickness of the volcanic cover and of its porosity. For CRTV and Category 2 tests, with a damaged cover, this delay is zero. But for Category 1 tests we have seen that the most likely scenario, based on the interpretation of the filling rates of the cavity-chimneys, is that the volcanic cover has an increased permeability by a factor of ten compared to the undisturbed value. If this is the case, the fractures of the volcanic cover must have an effectively larger aperture than the undisturbed fractures. This is consistent with the mechanical interpretation of the consequences of a test. The transfer through the volcanic cover will take place through these fractures. A conservative estimate of the fracture porosity, also used in Section 5, is 1%, i.e. one fracture of 1 mm every 10 cm. With a Darcy velocity above a cavity-chimney estimated to be in the order of 1 m/a or more, at early times, and a thickness of cover on the order of some 100 metres, the delay between the flux leaving the cavity-chimney and reaching the carbonates is therefore in the order of one year. This delay will be ignored, even for the Category 1 tests. This is certainly conservative, but will be shown later to be consistent with the observations. This does not mean that the Category 1 tests release their content as quickly as the CRTV or Category 2 tests. The Darcy velocity above a CRTV or a Category 2 test is about 20 times larger than for a Category 1 test. This means that the thickness of the volcanic cover does not provide a delay for non-sorbing radionuclides, such as HTO, which leak into the carbonates at the rate of the flow crossing the cavity-chimney.

b) The second reservoir is the carbonate layer, which is assumed to extend over a selected horizontal area S and has a given thickness, which will be varied. A radionuclide flux enters

into this reservoir, which is assumed to be perfectly mixed by the tidal effects, from one of the cavity-chimneys, as determined in (a) above. A vertical radionuclide flux leaves this reservoir to the lagoon. Let v_D' be the vertical average natural Darcy velocity in the carbonates, directed upwards to the lagoon, which we have estimated with the 3-D model to be in the order of 0.137 m/a at Mururoa. Note that this Darcy velocity is much smaller than the one above a cavity-chimney because the heat in the cavity-chimney creates strong buoyancy forces. These forces are only local and the natural Darcy velocities at the large scale are essentially undisturbed by the tests. The flux entering the lagoon is thus $v_D'S$. Taking radioactive decay into account, the differential equation representing the evolution of the concentration $C'(t)$ in the carbonates as a function of time is:

$$\frac{dC'}{dt} = -\left(\lambda + \frac{v_D'S}{V}\right)C' + \frac{\pi R_c^2 v_D}{V}C(t) \qquad (4)$$

where

λ	decay constant of radionuclide (Ln2/T, T = half-life),
v_D'	the average Darcy velocity from the carbonates towards the lagoon,
S	is the horizontal area where mixing occurs in the carbonates,
V	is the volume of the carbonate reservoir,
V	L S ε', L thickness of reservoir, S area of the reservoir, ε' porosity of carbonates,
v_D	is the Darcy velocity above the cavity-chimney,
R_c	is the radius of the cavity-chimney,
$C(t)$	is the concentration of the radionuclide in the cavity-chimney, as given by (1).

The solution of this equation is:

$$C'(t) = \frac{\pi R_c^2 v_D C_0}{V(\Lambda - \Gamma)}\left[Exp(-\Gamma t) - Exp(-\Lambda t)\right] \qquad (5)$$

where

C_o	is the initial concentration in the cavity-chimney and
Γ	is the decay constant of the source term (carbonates), ($\Gamma = \lambda + v_D S/V = \lambda + v_D/L\varepsilon'$).

Note that the somewhat arbitrary selection of the area S over which the spreading of the radionuclides occurs is irrelevant as far as the flux to the lagoon is concerned. If this area is too large, the concentration in the carbonates will be smaller but the total flux to the lagoon will remain the same. As we will try to validate this model on both the observed concentrations in the carbonates and the flux in the lagoons this uncertainty in the area S is not important as far as the flux to the lagoon is concerned. It can be checked by comparing the calculated concentrations in the carbonates with the measured ones. This will lead to a credible estimate of the size of area S. Note also that the thickness L of the carbonates in which the mixing occurs is an adjustable parameter. The CEA assumed mixing over 50 m of dolomite with a porosity of 20% (French Liaison Office Document No. 9) to estimate the inventory of radionuclides in the carbonates. We will use 300 m, i.e. the full thickness of the carbonates, which is more conservative and also more consistent with the observed vertical distribution of radionuclides. Sensitivity tests with a smaller thickness will also be made. One could argue that the mixing occurs, for example, over 150 m instead of 300 m. In that case the net result would be a reduction of the inventory in the carbonates by a factor of two. That would lead to slightly

less constant concentrations in the lagoon which is contrary to the observations. We think the uncertainty in the concentration distribution in the carbonates is higher than a factor of two and will therefore keep the conservative 300 m thickness of the carbonate layer. However, the upper say 50 m of the carbonates may not participate in the mixing and may just be just short-circuited by a few fractures with low porosity (thus without delay). There is no data to further refine this model and we will therefore keep the simple and conservative approach described above. Note that a flux from the reservoir to the ocean could easily be added and would result in an increase of the constant Γ by the ratio of the additional flux leaving the reservoir to the reservoir volume.

However, the model needs to be further developed when several successive tests are considered, with fluxes arriving in the same carbonate reservoir but at different times and different rates. It can easily be shown that, in that case, the concentration C'(t) in the reservoir is given by:

$$C'(t) = A_0 Exp(-\Gamma t) + \sum_i A_i Exp[-\Lambda_i (t - t_i)]$$

with :

$$A_0 = \frac{C'(t_k) - \sum_{i=1}^{i=k} A_i Exp[-\Lambda_i (t_k - t_i)]}{Exp(-\Gamma t_k)} \qquad (6)$$

$$A_i = \frac{\pi (R^i_c)^2 v_D{}^i C^i_0}{V(\Gamma - \Lambda_i)}$$

where t_i is the time when a new test is carried out and all indices or superscripts i relate to the properties of the test i.

In the first expression, the summation over i is extended to all the tests prior to time t, and each time a new test is added, e.g. at time t_k, the constant A_0 is re-initialised using the above expression.

c) The third reservoir is the lagoon. It could be modelled as a well-mixed reservoir with a radionuclide flux entering from the carbonates as given by the second reservoir and a flux leaving the lagoon through the exchange with the ocean. Since the residence time in this third reservoir is in the order of tens of days and short compared to years for the other two, this third reservoir will not be modelled. We will compare only the flux leaving the carbonate reservoir towards the lagoon with the observed flux, as obtained by the product of the measured concentration in the lagoon and the annual flux of water transiting through the lagoon. As we have seen, this flux is relatively constant in time.

SELECTION OF PARAMETERS FOR THE TRANSPORT MODEL IN THE CARBONATES

The carbonate mixing model depends upon the following parameters, that need to be estimated:

C_0 is the initial concentration of HTO in each cavity-chimney. The yields of the tests and the initial inventory of HTO have all been estimated for classes of yields between 1 and 150 kt (see Vol. 3 of this Technical Report). The initial inventory of HTO was linearly interpolated between the different classes as given below:

Yield (kt)	0.45*	1	5	10	20	25	50	60	100	150
HTO inventory (TBq)	0	1 360	1 360	1 620	2 360	2 730	4 570	5 300	8 270	12 000

* Safety trials

The size of the cavity-chimney is given by assuming that $R_c = 12$ (yield)$^{1/3}$ and $H'_c = 5.66\ R_c$. The coefficient of 0.66 was added to the 5 R_c in order to take the volume of the half sphere of the initial spherical cavity into account. Inside the rubble-filled cavity-chimney, the porosity is 30%. Thus there is little uncertainty in C_0, except for the exact yield of each test where only the average yield is known. As we will compare average fluxes for a large number of tests, the uncertainty associated with the individual yields must average out.

The decay constant $\Lambda=\lambda+ v_D /(H_c\varepsilon)$ in the cavity-chimney is dependent only on the unknown Darcy velocity v_D, which applies to the fluid flow above the cavity-chimney. This Darcy velocity was estimated for several cases and was found to be almost independent of the yield of the test. The range of average Darcy velocities calculated for the first 10–50 years after a test, is as follows:

- Category 1 tests, with volcanic cover and permeability increase by a factor of ten: 0.1 to 1.3 m/a.
- Category 2 and 3 tests and CRTV tests or damaged cover: 20 to 40 m/a.

We decided to use as a base case the values 1 m/a for Category 1 tests and 20 m/a for Category 2 and 3 tests. These values are also used in the geosphere transport model presented in Section 5. The objective of the mixing model is in fact to check that these numbers are not unreasonable, on average. These Darcy velocities are therefore prescribed and not calibrated, but variations by a factor of two will be analysed. Note that for a given velocity, the larger the yield, the smaller is Λ, meaning that small cavities release their tritium faster than large cavities. Since the inventory and the total flux above a cavity do not scale with the yield, a zone with many small tests will release more tritium than one with a small number of large tests with the same total yield.

The decay constant $\Gamma=\lambda+ v_D' /L\varepsilon'$ in the carbonates depends on the average Darcy velocity v_D' in the carbonates at atoll scale, which have been estimated to be 0.137 m/a for Mururoa. We will use that number for both atolls and vary it by a factor of two for sensitivity analysis. As discussed earlier, we assume an average thickness L of the carbonates of 300 m and carry out a sensitivity study by varying it to 200 m, 100 m and 50 m. The porosity of the carbonates ε' is 30% without variation.

The last parameter is the horizontal area S over which the HTO spreads in the carbonates. This area will be estimated on the basis of the maps of HTO distribution developed from the sampling of monitoring wells (French Liaison Office Document No. 9 and Section 6, Figs 88 and 89). This is of course a parameter with a significant uncertainty because the number of sampling holes is small (16 on Mururoa and 4 on Fangataufa). The uncertainty may reach a factor of 2, but we have shown that this will only affect the calculated concentration in the carbonates and neither the flux to the lagoon nor the inventory. As this information is only available for 1996, we will estimate S for 1996, but it would not make any difference to use an area S that would grow with time, which is certainly the case, as the HTO spreads horizontally with time by tidal mixing. This parameter will also be varied by a factor of two.

In summary, the following set of uncertain parameters will be studied, for both atolls:

- Thickness of carbonates: 300 m, sensitivity 200 m, 100 m and 50 m;
- Vertical Darcy velocity at atoll scale: 0.137 m/a; sensitivity half or twice this value;
- Darcy velocity above cavity-chimney for Category 1 tests: 1 m/a; sensitivity half or twice this value.
- Darcy velocity above cavity-chimney for Category 2 and 3 tests: 20 m/a; sensitivity half or twice this value.

APPLICATION OF THE MIXING MODEL TO FANGATAUFA

On Fangataufa, the number of tests is small (10). All tests are Category 1 tests, exploded between 1975 and 1996, except Lycos, exploded on 27 November 1989, which is known to leak (Category 2 test). Estimates of the yield of each test is given in Vol. 3 of this Technical Report. The estimates shown below are consistent with the CEA totals.

Year	1975	1975	1988	1989	1989	1990	1990	1991	1995	1996
Name	Achille	Hector	Cycnos	Cysicos	Lycos	Cypselos	Hyrtacos	Periclymnos	Ploutos	Xouthos
Yield (kt)	20	20	103	74	87	100	118	106	97	46

Looking at the HTO distribution in 1996 (French Liaison Office Document No. 9 plus results of measurements made in the boreholes by IAEA in 1996–1997, Section 6, Fig. 89) we see that there is clearly one central leak of HTO under the lagoon, spreading towards the rim. This leak is most likely due to the Lycos test. The area S where the HTO is distributed extends according to this map over an area of 12 km^2 with an average concentration of 4×10^6 Bq/m^3. The flux to the lagoon is estimated to be 9×10^{12} Bq/a. The inventory in the carbonates is estimated to be 4.3×10^{15} Bq. This number is based on a 300 m thick layer of HTO containing carbonates with a porosity of 30% over an area of 12 km^2 with an estimated concentration of 4×10^6 Bq/m^3. This HTO inventory is a little bit larger than the CEA estimate of 3×10^{15} Bq (French Liaison Office Document No 9) which is loaded on 50 m of karst with a porosity of 20%.

It is assumed in the calculations that all tests were carried out on 1 January of the corresponding year and thus the concentrations were calculated accordingly. The concentration in the carbonates, the inventory in the carbonates and the flux into the lagoon have been calculated with the analytical Eq. (6) using a spreadsheet. The results are given in Fig. II.1, representing the HTO flux to the Fangataufa lagoon from the carbonates from 1975 to 2010. The curves of the HTO flux, the concentration and the total inventory in the carbonates have an identical shape since these are all proportional to the concentration. The conversion factors from flux to concentration and inventory are given on Fig. II.1. This Figure clearly shows that the 1989 Lycos test is indeed the major source of HTO in the carbonates and that the rapid increase in concentration occurred immediately after 1989.

Table II.1 compares the concentration, inventory and flux to the lagoon calculated with the results of the mixing model at Fangataufa for the base case and the sensitivity studies for the uncertain parameters. All numbers are calculated for the year 1996. After the base case, all the

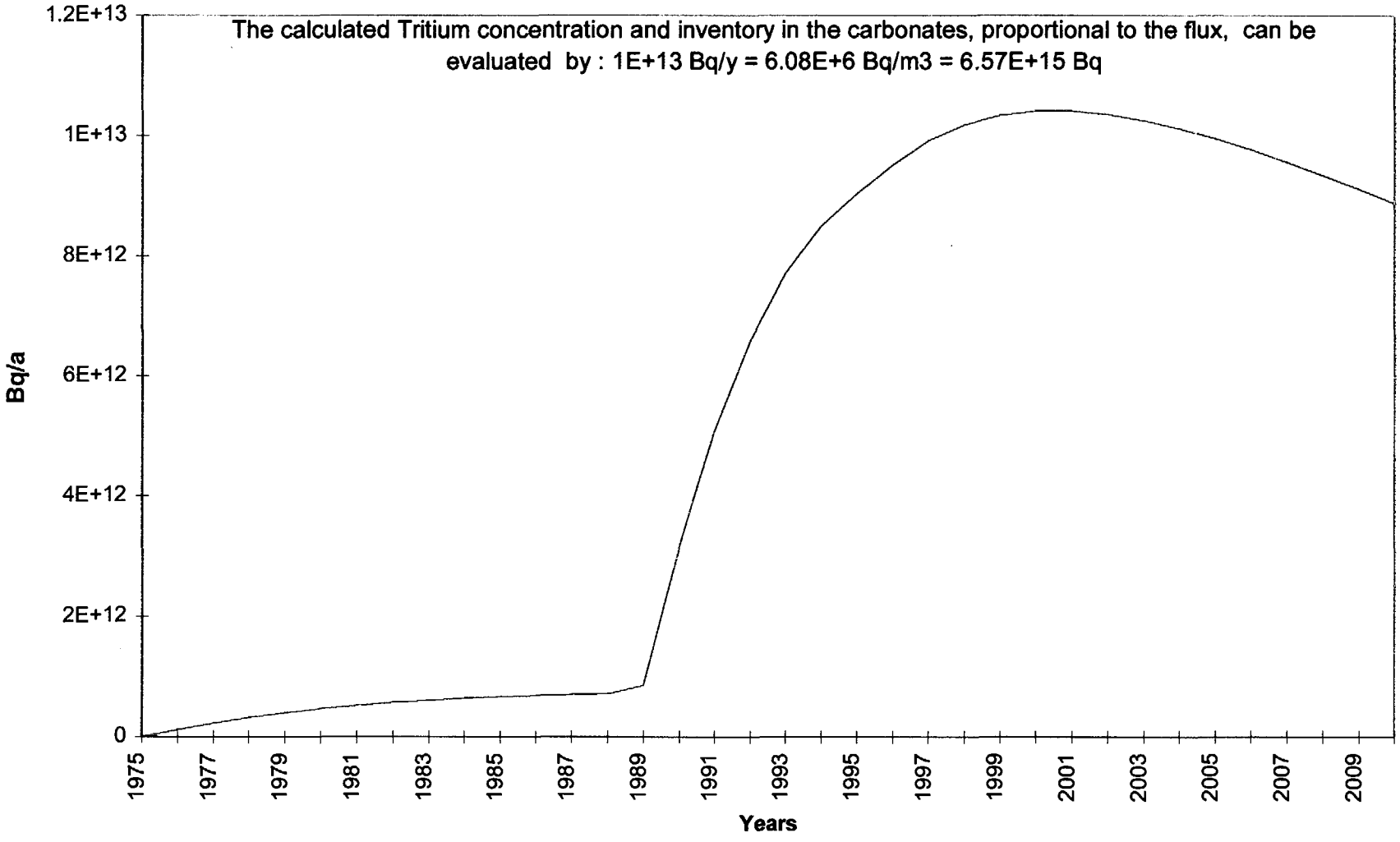

FIG. II.1. Tritium flux to the Fangataufa lagoon calculated with the mixing model, base case.

parameters are varied one by one by a factor of two, except the thickness of the carbonates, for which three values are tested, while all other parameters take their base case values.

TABLE II.1. MIXING MODEL HTO RESULTS FOR FANGATAUFA, FOR 1996, BASE CASE AND SENSITIVITY STUDY

Test case	Concentration in carbonates 10^6 Bq/m3	Flux to lagoon 10^{12} Bq/a	Inventory in carbonates 10^{15} Bq
Estimated values from observations	4	9	4.3 (3 in FLO* Doc. 9)
Base case, L = 300 m v_D' for Cat.1 = 1 m/a v_D' for Cat.2 = 20 m/a v_D' in carb. 0.137 m/a Area S 12 km^2	5.79	9.51	6.25
Reduced thickness, L = 200 m	8.65	14.2	6.23
Reduced thickness L = 100 m	17.1	28.2	6.16
Very low thickness L = 50 m	33.6	55.2	6.04
Reduced velocity v_D' = 0.5 m/a for Cat.1	4.71	7.75	5.09
Increased velocity v_D' = 2 m/a for Cat.1	7.75	12.7	8.37
Reduced velocity, v_D' = 10 m/a for Cat 2	4.66	7.66	5.03
Increased velocity v_D' = 40 m/a for Cat 2	6.54	10.8	7.06
Reduced velocity in carbonates v_D' = 0.5 × 0.137 m/a	5.81	4.77	6.27
Increased velocity in carbonates v_D' = 2 × 0.137 m/a	5.75	18.9	6.21
Reduced area S × 0.5	11.6	9.51	6.25
Increased area S × 2	2.89	9.51	6.25

* FLO: French Liaison Office

No attempt was made to calibrate the model. All base case parameters were selected a priori from earlier estimates. Nevertheless, the base case seems to be consistent with the observations.

The sensitivity study shows a large dependence on the thickness of the reservoir. A thickness of less than 300 m would require a significant decrease of all the fluxes from the volcanics for Category 1 and 2 tests. It appears therefore that the 300 m thickness leads to a conservative estimate of the fluxes passing from the volcanics to the carbonates. The sensitivity analysis of the velocities in the cavity-chimneys for Category 1 and 2 tests shows that these parameters are not very sensitive. However, the larger velocity values for both categories would give numbers that are too large for all three observations, while the smaller values would still be acceptable. The base case values for these cavity-chimney velocities therefore seem to be on the conservative side. The flux to the lagoon is very

sensitive to the average velocity in the carbonates, while the concentration and inventory are not, as expected. The base case average velocity in the carbonates is the only acceptable value. The area S of the HTO distribution in the carbonates is, as expected, totally insensitive to the flux to the lagoon and the inventory, while the concentration varies almost linearly with this parameter. The base case value seems to be the best choice and it is on the conservative side.

In summary, we believe that the carbonate mixing model with the selected Darcy velocities above the cavity-chimneys for the Category 1 and 2 tests is consistent with the data available at Fangataufa. It matches the measured flux of HTO to the lagoon and the measured HTO concentrations in the carbonates. There is no need to include into the model any leakage to the ocean. If such a leakage were added, e.g. of the same order of magnitude as the leakage to the lagoon, it would not significantly alter the results, as the total inventory transferred to the lagoon and thus to the ocean is negligible compared to the total inventory in the carbonates.

APPLICATION OF THE MIXING MODEL TO MURUROA

Looking at the HTO distribution in the carbonates in Mururoa, it is clear that a single application of the model to the whole atoll would be inefficient: several plumes of HTO can be seen, linked to the seven test zones, as defined in the French Liaison Office Documents. The same mixing model was thus applied successively to the seven areas, with the same parameters as for Fangataufa. For each zone, the area S and the average concentration of HTO were taken from the French Liaison Office Document No. 9 and the IAEA survey (Section 6, Fig. 88).

The average yield per zone, the number of tests and the years they were carried out (for periods of 5 years) are known from the French Liaison Office Documents for each Category (1, 2, and 3) of test. The tests were grouped for the calculations for the years 1978, 1984 and 1989 or placed at the exact years for the most recent ones. The yields of Category 2 tests were based on the data provided in Vol. 3 of this Technical Report.

TABLE II.2. PARAMETERS FOR THE CARBONATES MIXING MODEL FOR MURUROA

Area	1	2	3	4	5	6	7
Area S of HTO plume, km^2	10	8	2.5	4	4	4	4
Observed average HTO concentration, 10^7 Bq/m^3	1	1	1.5	1	≅0	1	1
Category 1 tests (Average Yield and number of tests)	2.4 kt 22 in 1978 5 in 1984 1 in 1990	5.5 kt 13 in 1978 14 in 1984	14.3 kt 3 in 1978 4 in 1984	35.2 kt 8 in 1978 12 in 1984	14.3 kt 7 in 1984 13 in 1989 1 in 1991	27.6 kt 7 in 1984 9 in 1989 2 in 1995	43 kt 5 in 1984 8 in 1989 1 in 1995
Category 2 tests			53 kt 1 in 1977 (Enée)	47 kt 1 in 1977 (Nestor)		54 kt 1 in 1985 (Mégarée)	
Category 3 (CRTV) tests	5 kt 7 in 1978	5 kt 4 in 1978	5 kt 1 in 1978				

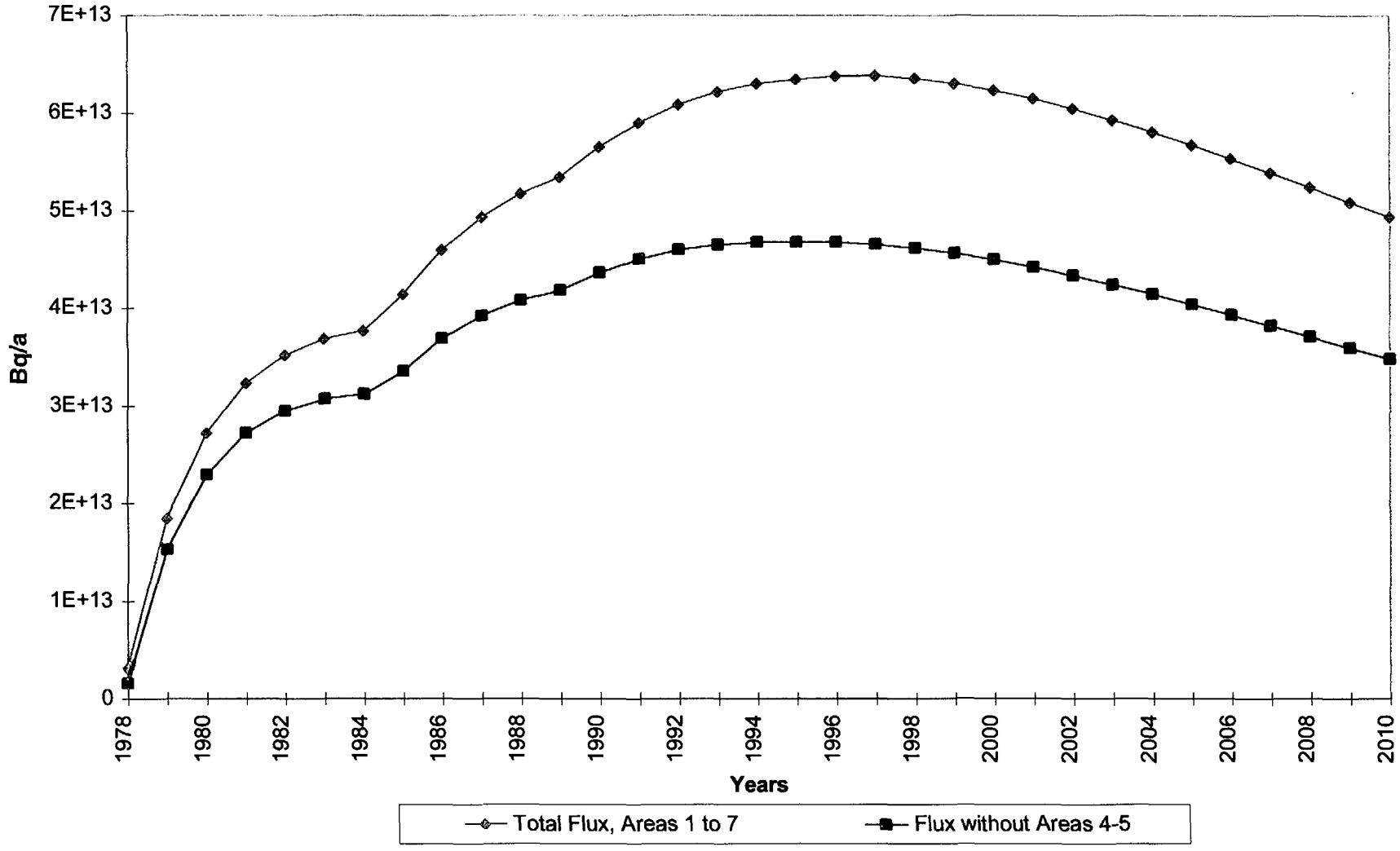

FIG. II.2. Tritium flux to the Mururoa lagoon calculated with the mixing model, base case.

Note that the "Enée" Category 2 test may not be in Area 3 but in Area 4. It is a Category C test (<150 kt) and there are no such tests in Area 3 according to the French Liaison Office Document No. 6. There is evidence of a significant leakage in the area of the Murène 16 observation hole, immediately to the north of Area 3, which is attributed to Enée. Alternatively, it could be a Category 2 test of Area 6.

Also note that in Area 5, the area S of the present distribution of HTO is apparently non-existent, unless some of the plumes attributed to Area 2 or 3 are due to some of the tests in Area 5. This is a difficulty in the present attempt of understanding the transfer in the carbonates, which will be discussed further. We used an area of 4 km^2 to define the reservoir.

From the observed HTO distribution summarised in Table II.2, one can calculate the total inventory in the carbonates at Mururoa. For consistency, we used a carbonates thickness of 300 m, over which the observed HTO concentration is assumed to be constant and a porosity of 30%. The inventory in the year 1996 is then 30×10^{15} Bq. This is larger than the French Liaison Office estimate (4.2×10^{15} Bq, see Document No. 9) because that is based on 50 m of carbonates. The HTO flux to the Mururoa lagoon is estimated to be 37×10^{12} Bq/a in 1996, using the observed concentration in the lagoon and the conservative French estimate of the daily flow.

TABLE II.3. MIXING MODEL HTO RESULTS FOR MURUROA, FOR 1996, BASE CASE AND SENSITIVITY STUDY

Test case	Conc. Area 1 10^7 Bq/m^3	Conc. Area 2 10^7 Bq/m^3	Conc. Area 3 10^7 Bq/m^3	Conc. Area 4 10^7 Bq/m^3	Conc. Area 5 10^7 Bq/m^3	Conc. Area 6 10^7 Bq/m^3	Conc. Area 7 10^7 Bq/m^3	Flux to Lagoon 1-7 10^{12}Bq/a	Invent. 1-7 10^{15} Bq	Flux to lagoon 1-3+6-7 10^{12}Bq/a	Invent. 1-3+6-7 10^{15} Bq
Estim. values	1	1	1.5	1	0	1	1	37	30	37	30 (4.2 in FLO* Doc.9)
Base case	1.1	1.0	1.6	2.0	1.1	1.7	1.0	63.8	41.9	46.9	30.8
L=200 m	1.7	1.5	2.4	3.0	1.6	2.6	1.5	95.1	41.7	69.8	30.6
L=100 m	3.2	2.9	4.6	5.9	3.2	5.1	3.0	186	40.8	137	29.9
L=50 m	6.1	5.6	8.7	11.4	6.2	10.0	5.9	358	39.2	262	28.7
v_D Cat. 2 10 m/a	1.1	1.0	1.5	2.0	1.1	1.6	1.0	62.8	41.2	45.9	30.2
v_D Cat. 2 40 m/a	1.1	1.0	1.6	2.0	1.1	1.8	1.0	64.0	42.1	47.1	30.9
v_D Cat. 1 0.5 m/a	0.8	0.7	1.3	1.3	0.6	1.2	0.5	42.4	27.8	32.4	21.3
v_D Cat. 1 2 m/a	1.5	1.5	2.1	3.3	2.0	2.7	1.9	98.4	64.6	69.4	45.6
$V_{carbo} \times 0.5$	1.1	1.0	1.6	2.0	1.1	1.7	1.0	32.1	42.2	23.6	31.0
$V_{carbo} \times 2$	1.1	1.0	1.6	2.0	1.1	1.7	1.0	126	41.4	92.4	30.4
S × 0.5	2.2	2.0	3.2	4.1	2.1	3.5	2.0	63.8	41.9	46.9	30.8
S × 2	5.6	5.1	7.9	10.1	5.4	8.7	5.1	63.8	41.9	46.9	30.8

* French Liaison Office.

RESULTS

Figure II.2 presents, for the base case, the evolution of the calculated HTO flux to the Mururoa lagoon with time, from 1978 to 2010. Table II.3 presents, for 1996, the calculated HTO concentration for each area, the total flux to the lagoon and the total inventory in the carbonates. The results obtained for the case that Areas 4 and 5 are excluded from the summation are provided for the flux of HTO to the lagoon (Table II.3 and Fig. II.2). The reasons for this exclusion will be explained below. The HTO inventory in the carbonates is also provided in Table II.2. The results of the base case calculations and the sensitivity studies are summarized in Table II.3. In the sensitivity studies, the major parameters were decreased or increased by a factor of two, except for the carbonate thickness, for which three values were considered. This is consistent with the approach taken in the application of the mixing model to Fangataufa.

DISCUSSION OF THE BASE CASE

In general, the calculated concentrations are in reasonable agreement with those observed, except for Areas 4 and 5.

For Area 4, the calculated concentration is larger than the estimate by a factor of two; this can be taken as a possible indication of the existence of a significant direct leakage from the carbonates to the ocean which may be likely in this area because the mechanical instability and the sliding that occurred may have facilitated communication between the carbonates and the ocean.

For Area 5, the calculated concentration is much higher than the concentrations measured in the two boreholes of that area (6 and 7 $\times$ 10^4 Bq/m^3). Note that this is one of the two areas (the others is Area 7) where no CRTV or Category 2 tests occurred. It could thus be concluded that the Darcy velocity of 1 m/a adopted for the Category 1 tests is too large. It is, however, consistent with the observations in Area 7, and in Area 1. Therefore we believe that either the sampling boreholes did not adequately represent the HTO concentration in Area 5 or the volcanic rock in this area is more resistant and provides a better confinement than in the other areas or that the tests may have been deeper. It can also be noted that the average yield of the Area 5 tests is only 14.3 kt and thus smaller than the test yields in Areas 6 and 7.

For Area 1, the calculated concentration is consistent with the observation. It is, however, interesting to realise that the present inventory of HTO in the carbonates cannot be attributed to the early CRTV tests only. Each CRTV test produced an estimated 1360 TBq of HTO. 18 years later, the HTO inventory of the 7 CRTV tests would be 3500 TBq, taking radioactive decay into account. For an area of 10 km^2 with a concentration of 10^7 Bq/m^3, a 300 m carbonate thickness and a porosity of 30%, the present inventory should be in the order of 9000 TBq. This is about three times higher than the HTO inventory of the CRTV tests after 18 years. It could be assumed that the area is only 3 km^2 or that the thickness of the carbonate mixing layer is only 100 m to explain the present HTO inventory. Although such interpretations cannot be totally ruled out, they are not really consistent with the observations. We think it is much more likely that the present HTO inventory is only in part due to the leakage of CRTV tests and that the results indicate the leakage of Category 1 tests. This interpretation would validate (or at least would not invalidate) the estimated Darcy velocity of 1 m/a in the undamaged volcanic cover. The Darcy velocity of 20 m/a for the CRTV tests cannot be validated in Area 1 at this late date because more than 90% of the HTO of each CRTV test would have leaked into the carbonates within 18 years if the Darcy velocity would only be 2.5 m/a. Note that there is no need to include any release of HTO to the ocean to match the observations, as indicated earlier for Fangataufa. If such a leakage would occur at the same order of magnitude as the leakage to the lagoon, it would not change the results significantly, as the fluxes are very small compared to the inventory.

For Area 6, the calculated concentration is slightly higher than the observations, indicating that the leakage may be over-estimated by the model.

In general, the base case value seems to be in reasonable agreement with the observations, particularly if the fluxes from Areas 4 and 5 are excluded from the summation. Even so, the calculated values are still conservative.

SENSITIVITY STUDY

The model is very sensitive to the carbonate thickness, and assuming a smaller thickness than 300 m would require an almost proportional reduction of the leakage from the volcanics. The sensitivity to the velocities above the cavity-chimneys is slight, but greater for the Category 1 tests, where the base case value seems the best choice. The Category 2 tests were too few (3) and old (1977 and 1988), and the Category 3 tests were too old (12 in 1978) and would not be a significant HTO source any more if compared to the possible releases from the very large number of Category 1 tests. This was not the case at Fangataufa where the Lycos test (Category 2) still had a significant effect on the HTO inventory. The sensitivity to the average Darcy velocity in the carbonates has a significant influence on the HTO flux to the lagoon. The sensitivity to the area S is also large. The base case values are the most likely ones and they are on the conservative side.

CONCLUSION

The approach used in this section to understand how radionuclides, released from the volcanics to the carbonates, eventually reach the environment is based on a simplified mixing model for the carbonates. It has been shown to be reasonably consistent with the observations without any calibration of parameters. All the parameters have been estimated independently or based on models developed earlier by the IGC.

The major difference with the model proposed by the CEA is that the carbonates act as a large reservoir for the radionuclides. We estimate that the total inventories in the carbonates are higher by a factor of 1.5 in Fangataufa and 5 in Mururoa than the ones given by the CEA, because we assumed that HTO was distributed at a constant concentration over the whole thickness of the carbonates (300 m). This is of course a very conservative assumption.

With this model and the associated assumptions, data available on the flux to the lagoon and the concentration in the carbonates have been used to evaluate the reasonableness of the rate of HTO release from the cavity-chimneys of Category 1, 2 and 3 tests. We conclude that the Darcy velocities of 1 m/a (for Category 1) and 20 m/a (for Category 2 and 3) can be used with some confidence to predict radionuclide releases from the volcanics to the environment. These Darcy velocities result in release rates from the volcanics that are higher than those assumed by the CEA. They also result in concentrations in the carbonates and inventories in the carbonates and fluxes to the lagoons higher than the observed ones. We believe that our estimates are reasonable and on the conservative side. Nevertheless, as a sensitivity study, even higher rates were used for radionuclide transport calculations presented in Section 5.

In this attempt of using measured radionuclide distributions in the carbonates and lagoons to validate assumptions and models, we have only used HTO data, although strontium, caesium and plutonium data are also available. This is because HTO is a perfect tracer of water which can be used to study and understand the hydrology of the atolls. The application of the mixing model to the above-mentioned radionuclides would have been complicated by the need to take retardation factors into account. The assumption of no delay for transfer from the top of the cavity-chimney to the carbonates, in case of the existence of a volcanic cover, would, for example, be no longer acceptable. However, radionuclide concentration data derived from model calculations (Section 5) have been

compared to in situ measurements. Retardation mechanisms and factors used in the geosphere transport model were validated (Section 6).

We have seen that direct release to the ocean cannot be ruled out with the present data. There is even evidence that it may occur in some areas, for example Area 4. Therefore, the calculations of the flux of radionuclides to the environment should be estimated by taking the release into the lagoon and into the ocean into account. The results of such investigations are presented in Section 6.10 for HTO, ^{90}Sr, ^{137}Cs and ^{239}Pu.

Appendix III

MODELS OF TRITIUM RELEASE BASED ON PISTON FLOW OR CONVECTION/ DISPERSION IN THE CARBONATES

In this Section, we develop two alternative models to the mixing model described in Appendix II, for the assessment of the tritium migration in the carbonates:

- a piston flow model; and
- a convection - dispersion model.

We show that neither of these models is able to correctly represent the observed fluxes and distribution of HTO at Mururoa and Fangataufa.

PISTON FLOW MODEL

The piston flow model is based on the assumption that the flux released to the carbonates, as given by the product of the concentration in the cavity-chimney (Eq. 1 in Appendix II) and the Darcy velocity in the cavity-chimney, is simply transferred to the lagoon with a time lag of 1, 2, 5, 10, 15 or 20 years. This is assumed to be the convective transfer time through the carbonates. Radioactive decay during this transfer is taken into account, but no mixing. The flux into the lagoon is then just the sum of all the releases from each group of tests, as described for the Mixing Model in Appendix II. The only parameter of this model is the transfer time, from 1 to 20 years, and of course the velocities in the cavity-chimney for Category 1 and Category 2 and 3 tests.

Four cases were run with the model, two for Mururoa, and two for Fangataufa. For each atoll, the base case calculation applies cavity-chimney velocities of 1 and 20 m/a, for Category 1 and Category 2 and 3 tests, respectively (Figs III.1 and III.3). The results for the base case show that the flux to the lagoon is about two orders of magnitude higher than the observed one.

The second case is run with velocities in the cavity-chimney that are reduced by a factor of 166, i.e. 0.006 and 0.12 m/a, for Category 1 and Category 2 and 3 tests, respectively. This is an approximate match to the observed flux to the lagoons (Figs III.2 and III.4). Even if the flux is of the correct order, the shape of the changes with time of this flux is neither consistent with the rather stable flux observed nor with the inventory in the carbonate which is about two orders of magnitude below the observations.

The piston flow model with its assumed rapid transit of the HTO flux from the volcanics to the lagoon is not consistent with the observations and therefore not a correct representation of reality.

CONVECTION - DISPERSION MODEL

The convection - dispersion model assumes convective plus dispersive transfer in the carbonates. For each group of tests, as used in the mixing model, the following analytical solution of the dispersion equation is used :

$$C(x,t) = \frac{C_0}{2}\,\mathrm{Exp}\left(\frac{v_C}{2D}\right)\mathrm{Exp}\,(-\Lambda t)\left\{\begin{array}{l}\mathrm{Exp}(-\beta x)\,\mathrm{Erfc}\left[\dfrac{x - t\sqrt{(v_D/\varepsilon)^2 + 4(\lambda-\Lambda)D/\varepsilon}}{2\sqrt{Dt/\varepsilon}}\right] \\ + \mathrm{Exp}(\beta x)\,\mathrm{Erfc}\left[\dfrac{x + t\sqrt{(v_D/\varepsilon)^2 + 4(\lambda-\Lambda)D/\varepsilon}}{2\sqrt{Dt/\varepsilon}}\right]\end{array}\right\}$$

Text cont. on p. 207.

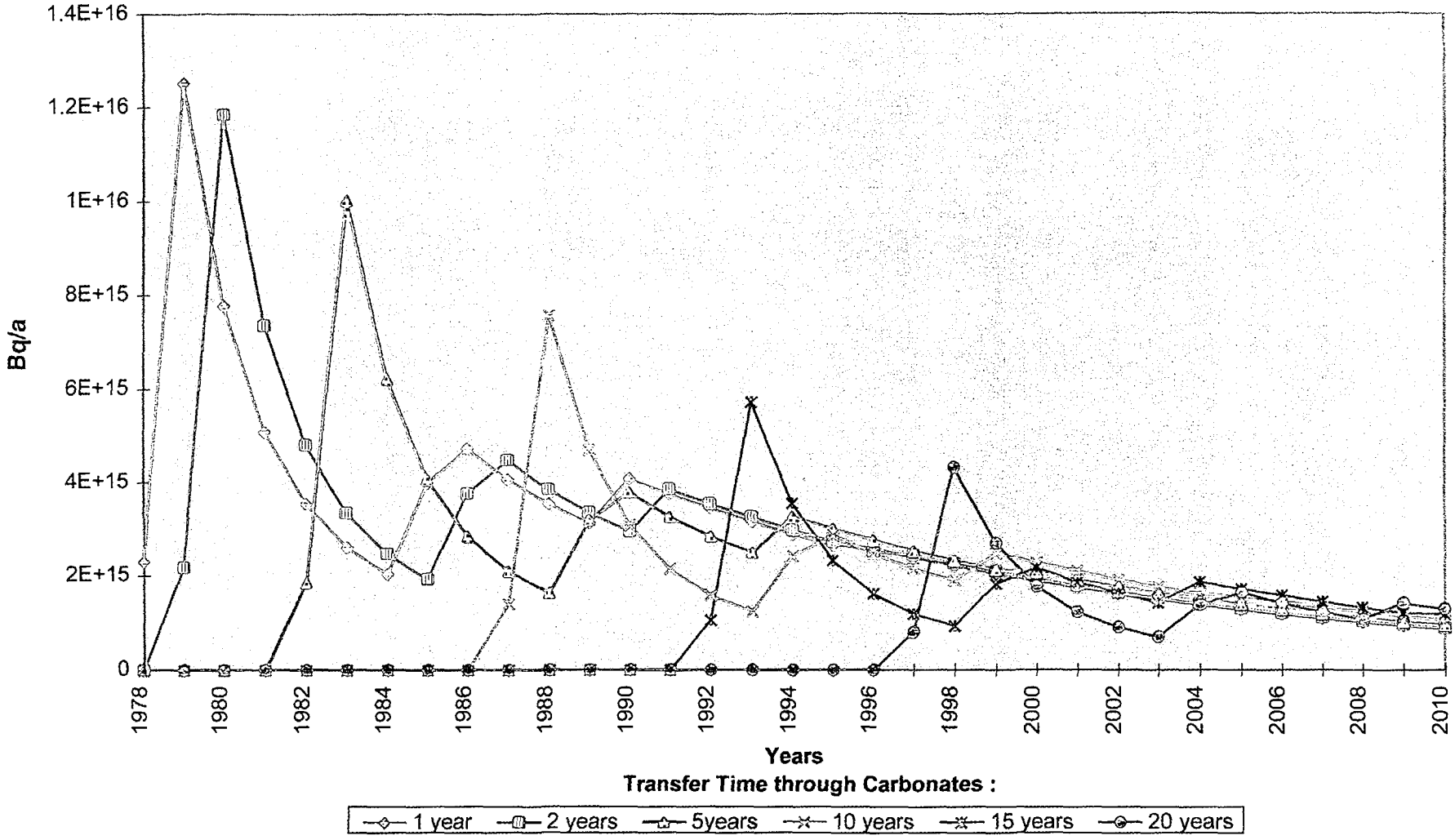

FIG. III.1. Tritium flux to the Mururoa lagoon calculated with the piston flow model, base case, Areas 1-7, Darcy velocities in the volcanics 1 and 20 m/a.

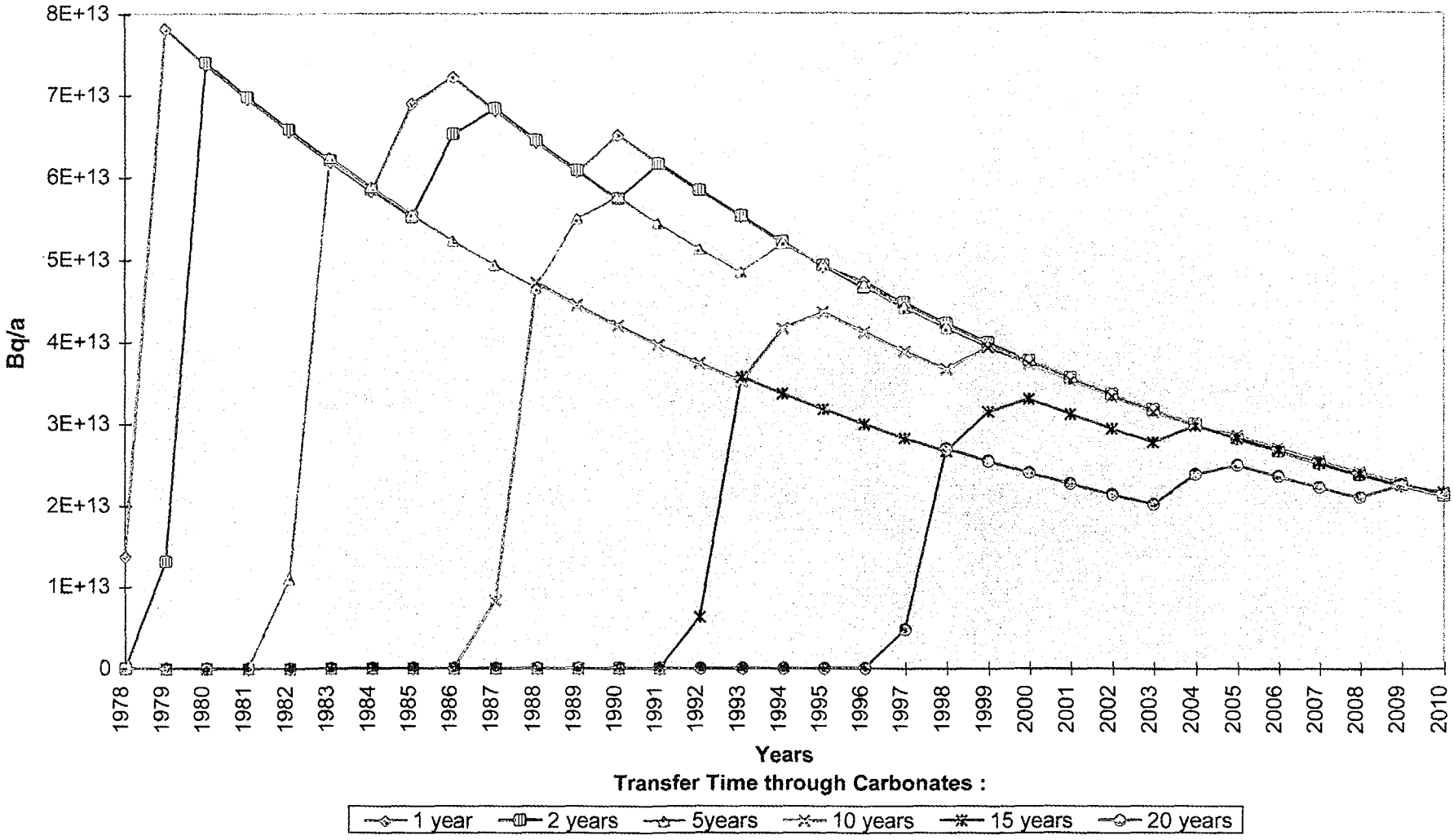

FIG. III.2. Tritium flux to the Mururoa lagoon calculated with the piston flow model, Areas 1–7, Darcy velocities in the volcanics 0.006 and 0.12 m/a.

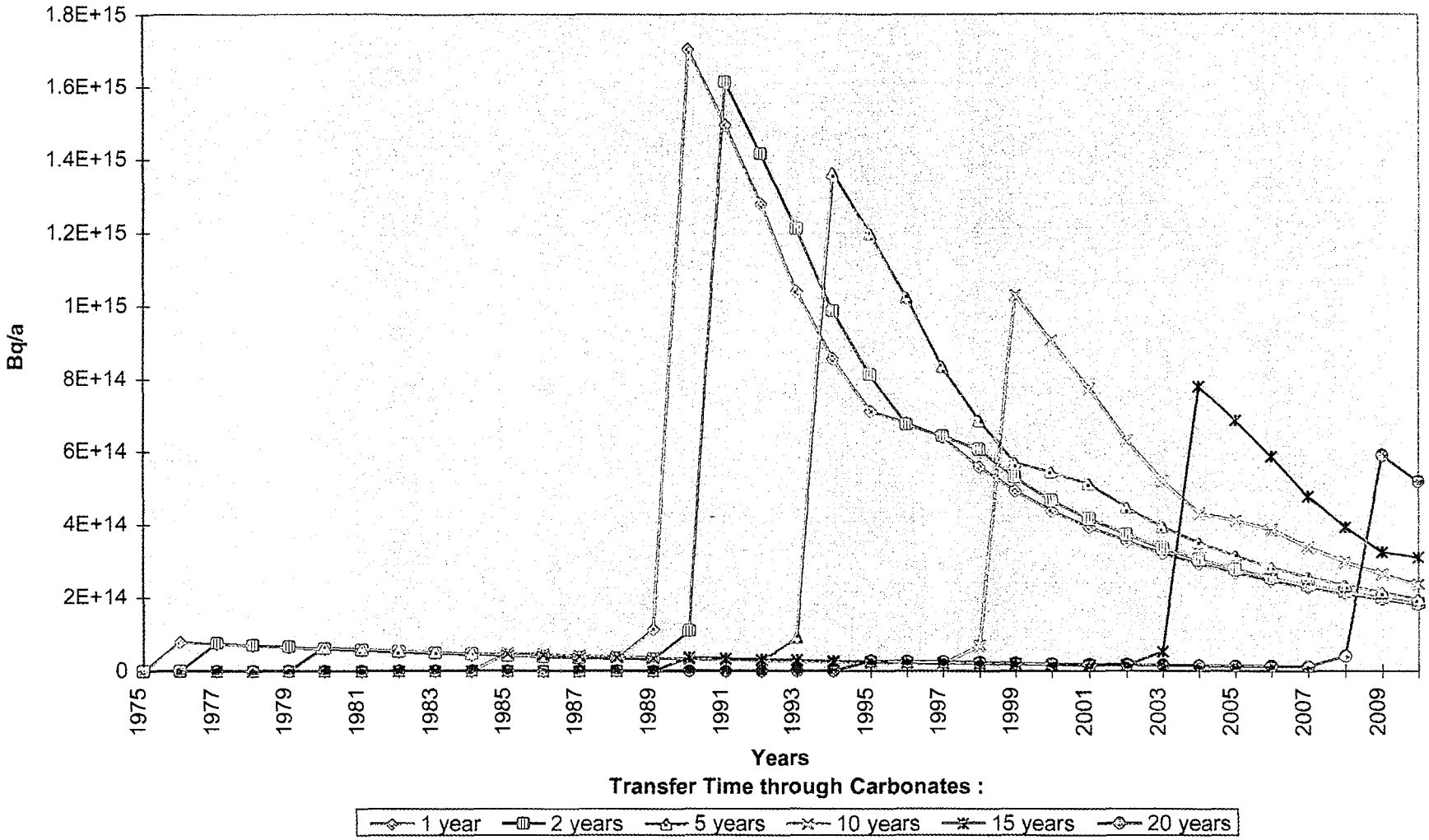

FIG. III.3. Tritium flux to the Fangataufa lagoon calculated with the piston flow model, base case, Darcy velocities in the volcanics 1 and 20 m/a.

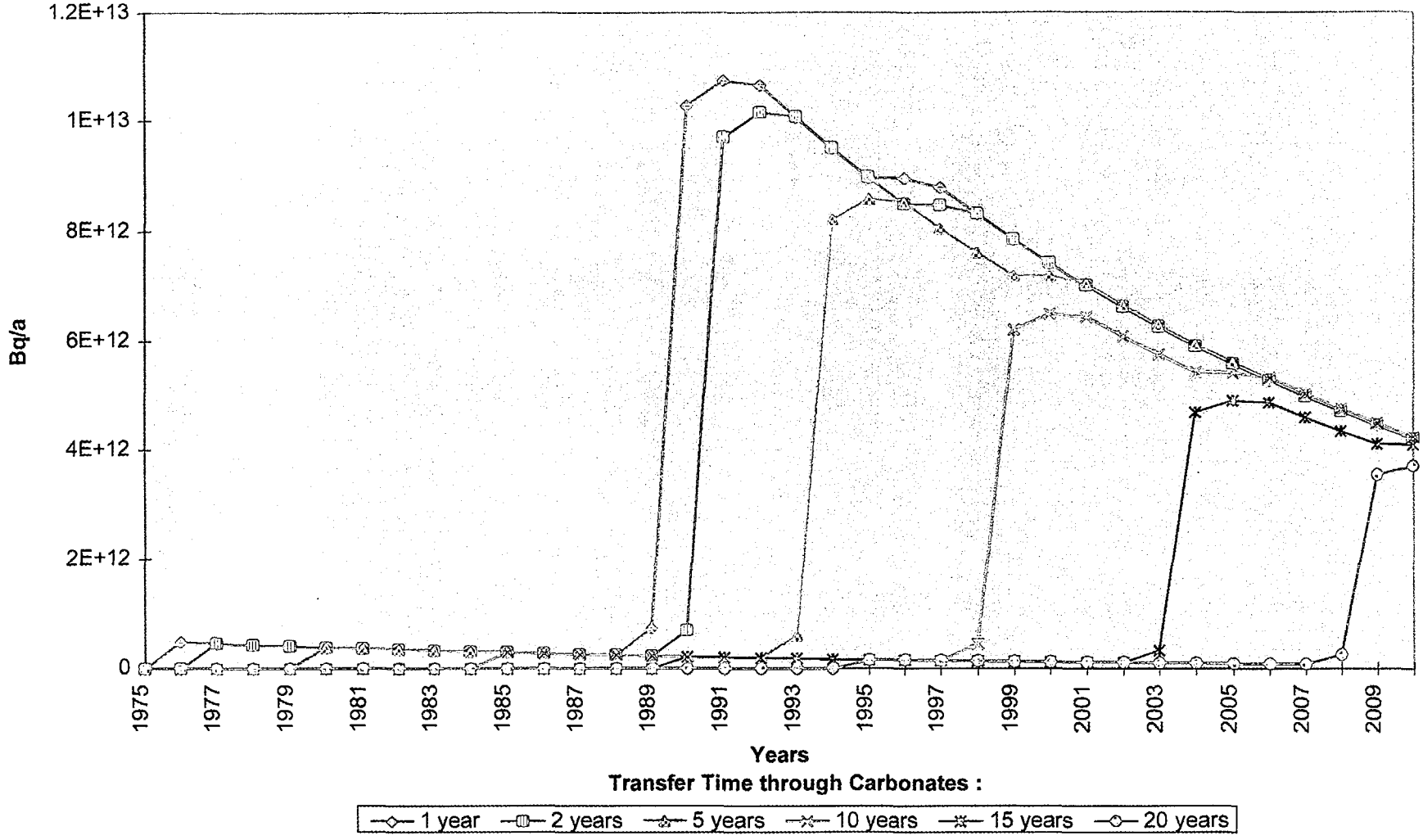

FIG. III.4. Tritium flux to the Fangataufa lagoon calculated with the piston flow model, Darcy velocities in the volcanics 0.006 and 0.12 m/a.

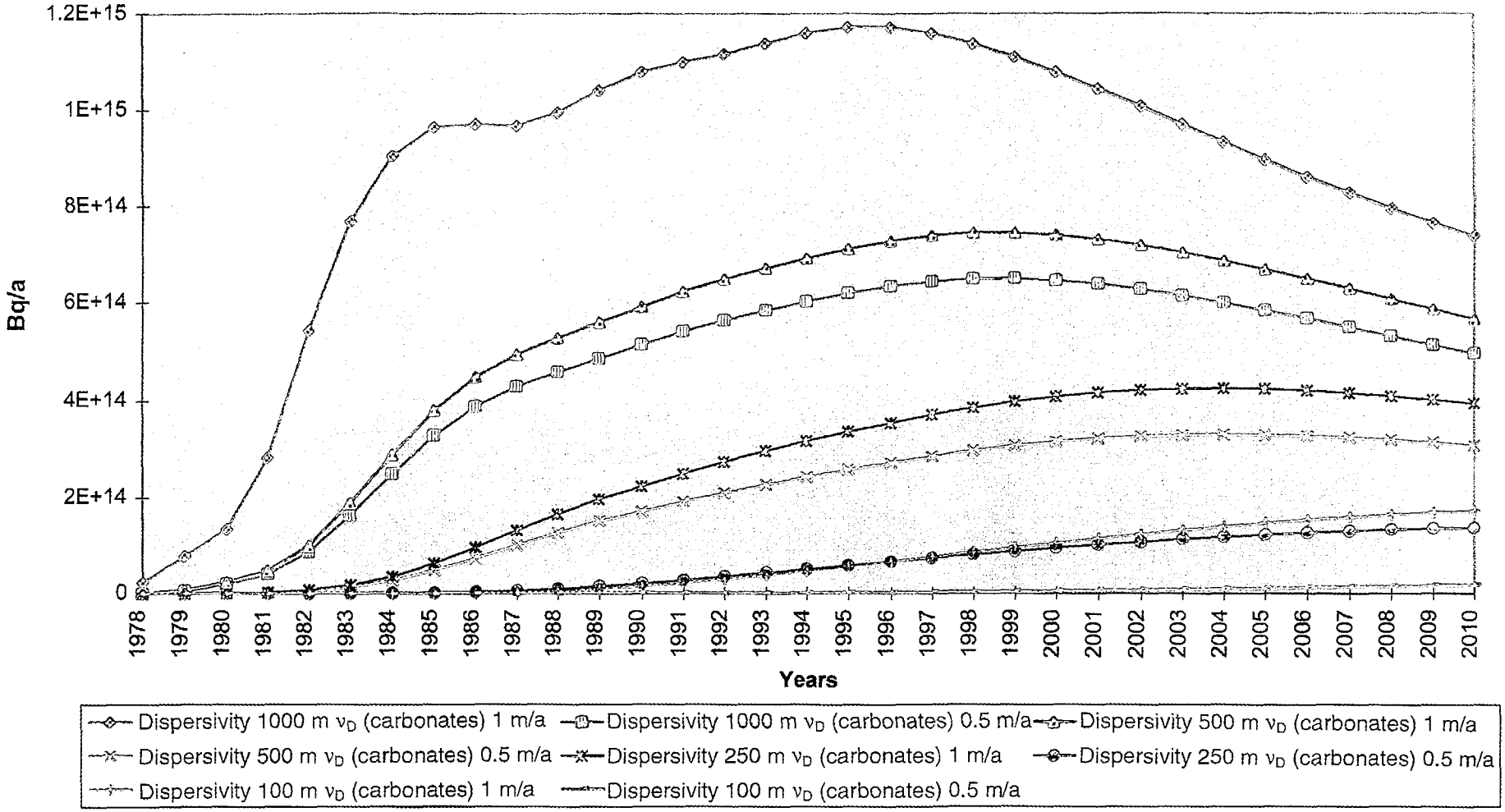

FIG. III.5. Tritium flux to the Mururoa lagoon calculated with the dispersion model; dispersivity and Darcy velocities in carbonates vary, velocities in the volcanics 1 and 20 m/a.

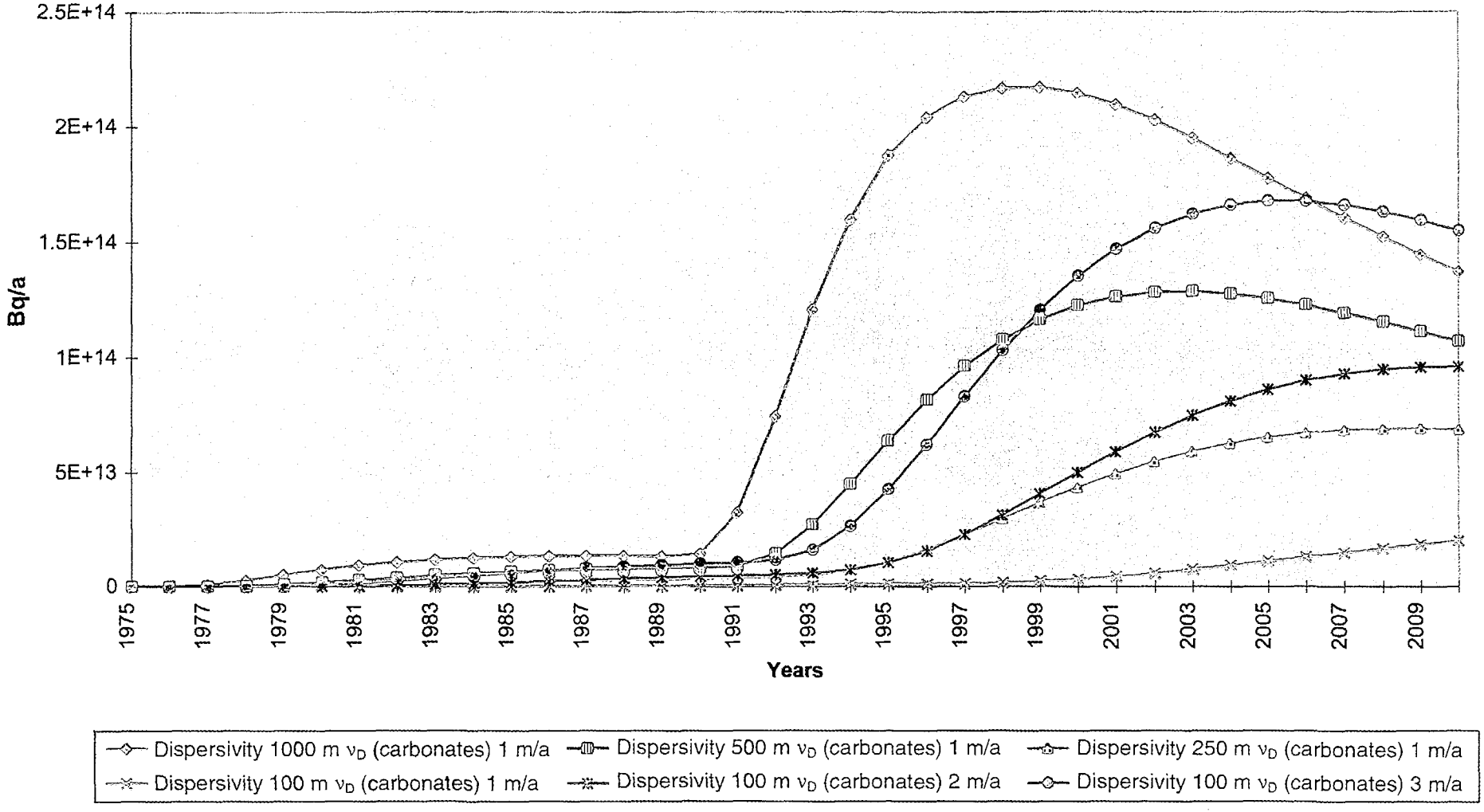

FIG. III.6. Tritium flux to the Fangataufa lagoon calculated with the dispersion model; dispersivities and Darcy velocities in carbonates vary, velocities in the volcanics 1 and 20 m/a.

where:

$$\beta = \sqrt{\left(\frac{v_D}{2D}\right)^2 + \frac{(\lambda - \Lambda)\varepsilon}{D}}$$

- λ is the decay constant of HTO,
- Λ is the decay constant of the source term (see Eq. 1 of Appendix II),
- D is the dispersion coefficient, product of the Darcy velocity v_D (m/s) and the dispersivity α (m),
- ε is the porosity,
- x is the distance, here the thickness of the carbonate layer,
- t is the time.

This equation is valid for an injection at decaying concentration $C_0Exp(-\Lambda t)$ at x=0. The flux coming from the volcanics is thus transformed into a flux reaching the lagoon. As for the piston flow model, all groups of tests are just summed up to calculate the total release to the lagoon. The parameters of the model are the Darcy velocity v_D and the dispersivity α, plus the Darcy velocities in the cavity-chimney of Category 1 and Category 2 and 3 tests.

The model was run for both atolls, with eight sets of parameters for Mururoa and six sets of parameters for Fangataufa. The Darcy velocity in the carbonates was varied between 0.5 m/a and 3 m/a, and the dispersivity between 100 m and 1000 m. The results show (Figs III.5 and III.6) an early release, as observed in the field, if dispersivities between 200 m and 1000 m are applied. In this case, however, the flux to the lagoon is too large. Furthermore, the calculations suggest that this flux is rapidly increasing which is contrary to the field observations. If the Darcy velocities in the cavity-chimneys are reduced to 0.002 m/a and 0.4 m/a (curves not shown), the calculated and the observed flux to the lagoon would match but the inventory in the carbonates would be by a factor of about 50 too low. Although the convection - dispersion model shows a much more smooth evolution of the flux to the lagoon with time, it is unable to match the field observations for both the inventory and flux to the lagoon.

CONCLUSION

The above two attempts to calibrate the classical piston flow and the convection - dispersion models against the observed HTO flux and distribution in the two atolls proved to be unsuccessful. This confirms that additional mixing is taking place in the carbonates which "spreads" the release of HTO in the carbonates. We believe that this mixing is due mainly to tidal fluctuations. The mixing model (Appendix II), which seems consistent with the field observations, is therefore a more approximate method of representing this mechanism.

Appendix IV

EXPERIMENTAL STUDIES OF PLUTONIUM SOLUBILITY IN VARIOUS WATERS

In the framework of several studies for the potential high level waste repository at Yucca Mountain, Nevada, and for the Waste Isolation Pilot Plant (WIPP) in Carlsbad, New Mexico, the solubility of plutonium was studied in laboratory experiments in different site-specific waters (Nitsche, et al., 1992a, 1992b, 1993, 1994a, and 1994b). The waters, their chemical composition and concentrations are listed in Table IV.1 together with the data for artificial sea water. Waters J-13 and UE-25p#1 come from two sources in the vicinity of Yucca Mountain, bracketing the range of expected waters at the repository horizon. Water from well J-13 is expected to be representative of the water composition of the unsaturated zone near the proposed emplacement area. Well UE-25p#1 taps the carbonate aquifer that underlies the emplacement horizon. The water from both wells is oxidising. Generally, radionuclide solubility studies under oxidising conditions lead to higher solubilities for a number of radionuclides than would occur under mildly or strongly reducing conditions. Waters AISinR and H-17 are simulant brines representing brines above or near the WIPP repository site, respectively.

TABLE IV.1. COMPOSITION OF WATERS FROM YUCCA MOUNTAIN, SIMULANT BRINES FROM THE WASTE ISOLATION PILOT PLANT (WIPP) AND ARTIFICIAL SEA WATER

	Concentration (m mol/L)				
	J-13[1,2]	UE-25p#1[1,3]	AISinR[4]	H-17[5]	Artificial Sea water[6]
Na^+	1.96	7.43	643.4	2397	479.3
K^+	0.14	0.34	8.2	30.7	10.1
Ca^{2+}	0.29	2.19	17.1	28.9	10.6
Mg^{2+}	0.07	1.31	21.5	74.1	54.5
SiO_2 (aq)	1.07	0.62	-	-	-
Carbonate (tot)	2.81	11.44	1.78	0.82	2.38
Cl^-	0.18	1.04	567.8	2482	558.7
SO_4^{2-}	0.19	1.34	79.6	75.0	28.9
F^-	0.11	0.18	-	-	0.05
pH	7.0	6.7	7.5	7.0	8.1
Eh (mV SHE)	700	360	-	-	-
Ionic Strength	- 3	- 20	- 862	- 3200	- 714

(1) Nitsche, et al., 1992a
(2) Nitsche, et al., 1993
(3) Nitsche, et al., 1994a
(4) Nitsche, et al., 1992b
(5) Nitsche, et al., 1994b
(6) Kester, et al., 1967

In the four different waters, plutonium solubility was studied from oversaturation by injecting excess soluble plutonium in a defined oxidation state into the water. Then the precipitation of the solubility-controlling solid and the attainment of steady-state solution conditions were followed over time. This has the advantage that the solubility controlling thermodynamic solid can form freely. No assumptions must be made about its nature as would be necessary when the solubility would be

TABLE IV.2. PU^{4+} SOLUBILITY CONCENTRATIONS IN WATERS FROM YUCCA MOUNTAIN AND SIMULANT BRINES FROM THE WASTE ISOLATION PILOT PLANT (WIPP)

pH	J-13	UE25-p#1	pH_{op}	AISinR	pH_{op}	H-17
	Concentration (mol/L)			Concentration (mol/L)		Concentration (mol/L)
7	$(2.3 \pm 1.4) \times 10^{-7}$	$(4.5 \pm 0.4) \times 10^{-7}$	7.5	$(2.5 \pm 1.3) \times 10^{-7}$	7.1	$(1.8 \pm 0.4) \times 10^{-7}$
8.5	$(2.9 \pm 0.8) \times 10^{-7}$	$(1.1 \pm 0.1) \times 10^{-6}$	-	-	-	-

from undersaturation where a predetermined solid is brought in contact with the water and the dissolution process is monitored over time.

All experiments were conducted under oxic conditions with a carbon dioxide pressure that was respective to the total dissolved carbonate concentration. The pH for the Yucca Mountain waters and the hydrogen ion concentration for the WIPP brines was controlled over the length of the experiment. Total concentrations of dissolved plutonium were monitored over time until steady-state conditions were established. Quantitative separation of the aqueous phase from any solids or suspended particles is necessary for an accurate assessment of dissolved concentration. For this process centrifugal filters with a calculated pore size of 4.1 nm were used. The filters were also tested for retention of dissolved plutonium due to sorption on the filter membrane. The aqueous plutonium oxidation state distribution was determined and the solid phase was characterised.

The steady-state solubilities listed in Table IV.2 were obtained by injecting Pu^{4+}-solution into the waters. The solids formed resembled amorphous green Pu(IV) polymer and did not show any crystallinity, except for the solid formed in AISinR brine. This solid showed some crystallinity in the X ray powder diffraction pattern which could not be assigned to any known plutonium solid. Pu(IV) polymer is known to absorb CO_2 which converts on the polymer surface to carbonate. From the chemical behaviour of the solids it was concluded that all the solids formed are mainly made from Pu(IV) polymer or amorphous $Pu(OH)_4$ containing also plutonium carbonate whose amount increases with increasing pH and carbonate content of the water. Plutonium carbonates have most likely a higher solubility than Pu(IV) polymer. This may explain the somewhat higher solubility in UE-25p#1 at pH 8.5 compared to J-13 groundwater. Due to the much higher concentration of CO_3^{2-} at that pH, a significantly larger formation of plutonium carbonate may take place. Furthermore, solubility experiments in AISinR and H-17 brine using Pu(IV) polymer solid from undersaturation also seem to prove this point. Here the dissolution reaction of Pu(IV) polymer (amorphous $Pu(OH)_4$) was monitored over time. The steady-state solution concentrations were $(8.2 \pm 1.6) \times 10^{-8}$ mol/L at an operational $pH_{op.}$= 7.5 and $(3.0 \pm 1.0) \times 10^{-8}$ mol/L at a $pH_{op.}$= 7.1 for AISinR and H-17 brine, respectively. The values are between one-half and one order of magnitude lower than those initially found in the Pu^{4+} experiment.

Appendix V

UNDERGROUND WATER SAMPLING IN MURUROA AND FANGATAUFA

V.1. INTRODUCTION

V.1.1. Background

Two test cavities at the Mururoa atoll and 20 monitoring wells in the carbonates or the top of the volcanics at Mururoa and Fangataufa are available for sampling of underground waters and subsequent analyses. Data on radionuclide concentrations in the cavities and the monitoring wells were available from the CEA. Access was offered to all the wells. The IAEA study team selected those wells to be sampled in the IAEA campaign.

V.1.2. Objectives

The sampling of underground waters has been initiated to gain information on the existing concentrations of radionuclides and other relevant constituents of waters potentially impacted by nuclear testing and to corroborate the French data. The results of the analyses of the waters provide input for and calibration of models of radionuclide transport and provide a basis for the calculation of future releases through the geosphere.

V.2. PLANNING FOR THE SAMPLING CAMPAIGN

Preparatory discussions on the execution of the sampling of underground waters were initiated in early 1997. The sampling was scheduled for 28 May–08 June 1997. The main elements of the sampling campaign were elaborated in a meeting in Vienna on 15 May 1997 in connection with the TG-A and TG-B meeting (participants: D. Levins, P. Povinec, D. Smith, J-F. Sornein, E. Warnecke). The most significant points of the May, 1997 planning session are summarized as follows:

(a) Analyses for the following radionuclides:

^{3}H, ^{14}C, ^{36}Cl, ^{90}Sr, ^{99}Tc, ^{129}I, ^{37}Cs, ^{237}Np, $^{239/240}Pu$-, ^{241}Am

(b) Sampling of cavity and monitoring wells:

- Cavities: Aristée and Céto on Mururoa.
- Monitoring wells: Géo 5, Géo 8, Géo 10, Isurus 10, Murène 16, Pieuvre 37, Tazard 14 on Mururoa and Fuseau 30, Mitre 27 on Fangataufa.

Samples are to be taken in the carbonates at the lowest depth (Mururoa) or in the upper karst (Fangataufa).

(c) Major cation and anion analyses

Na^{+}, K^{+}, Mg^{2+}, Ca^{2+}, Sr^{2+}, Si, $Fe^{2+/3+}$, Cl^{-}, SO_4^{2-}, CO_3^{2-}/HCO_3^{-},
total organic carbon and NO_3^{-} (in cavity waters only)

(d) Field measurements

pH, Eh, pumping rate, temperature, sampling depths, ^{3}H;

(e) Samples

10 L (acidified) for radionuclide analyses; 1 L (acidified) for elemental analyses; 1 L (non-acidified) for ^{129}I and ^{36}Cl analyses; 1 L (with $HgCl_2$) for ^{14}C analyses; 1 L for Pu analyses (from Aristée, Céto, Géo 10, Murène 16 and Pieuvre 37)

(f) Waters will be filtered through a 450 nm filter. Equipment will be provided by the CEA.

The actual sampling procedure deviated slightly from the plan. Last-minute sampling recommendations, some diverging, were received immediately before departure to Mururoa as well as during the sampling campaign. The timing of these directives precluded discussion prior to sampling and decisions on modifications had to be made in the field. The following changes were introduced:

(a) 20 L (acidified) for radionuclide analyses (from 29 May 1997 onward).

(b) 1 L (non-acidified) for elemental analyses as additional sample. This was increased to 10 L on 02 June 1997, except for Géo 8 (5 L).

V.3. THE FIELD PROGRAMME

V.3.1. Equipment

The sampling equipment comprised the sampling tubes(s) of a borehole, the peristaltic pump(s), a 450 nm filter, a ph/Eh/T measurement box and the sampling bottles. The following equipment was used:

(a) 2 Heydolph Rumo 100 peristaltic pumps with two "pump heads", each.

(b) Millipore filter box with 450 nm filters.

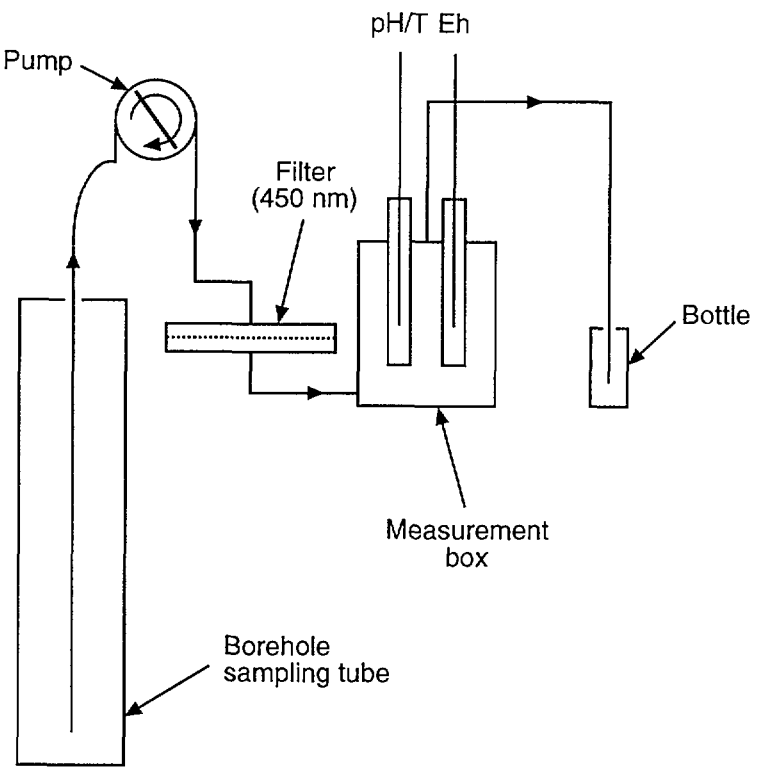

FIG. V.1. Equipment for sampling and filtration of underground waters.

(c) Schott pH electrode type N2042A and pH meter type Schott CG837 with temperature measurement.

(d) Schott pH buffer solutions for pH 7 or 6.87 and pH 4.

(e) Schott Eh electrode type Pt 61.

(f) Mettler - Toledo redox buffer solution with the following specification:

T (°C)	Ag/AgCl (mV)	SHE* (mV)
25	220	427
30	212	415

* SHE = *Standard hydrogen electrode*

(g) pH/Eh/temperature measurement box (Plexiglas).

(h) Polyethylene (PE) bottles of various sizes (100 ml, 1 L, 10 L and 20 L).

(i) Reagent grade HCl for preservative acid.

The equipment was configured in the following way for use in the sampling of waters (Fig. V.1):

(a) The peristaltic pumps were equipped with new pumping tubes for each sampling operation.

(b) The Millipore filter box was cleaned in the laboratory with water and a sponge, rinsed with distilled water and equipped with a new 450 nm filter prior to each day's sampling.

(c) The measurement box was washed in the laboratory with distilled water before each sampling operation.

(d) The pH and Eh electrodes were calibrated with the buffer solutions before and after sampling operations.

(e) The PE bottles were new as delivered from the factory. Each was rinsed twice with distilled water in the laboratory and taken to the sampling site with 50–100 ml of distilled water. This was discarded and the bottle rinsed with the sampling water before filling. The bottle for the ^{14}C analyses was rinsed with pentane instead of distilled water.

(f) The order in which samples were collected was invariant, except Aristée: radionuclides (acidified), elemental analyses (non-acidified), elemental analyses (acidified), ^{129}I and ^{36}Cl (non-acidified), ^{14}C ($HgCl_2$ preservative), Pu analyses (only for Aristée, Pieuvre 37, Céto, Géo 10), ^{3}H field measurement.

(g) Samples were collected with as little head-space as possible with allowance for volume changes during shipment.

(h) The filter box was opened at the end of the day and the still wet filter was sealed in a PE bottle prior to shipment. In all cases, except Aristée and Pieuvre 37, the filter was split between the IAEA and the French representative.

(i) Samples were sealed and stored in a secured, air conditioned room at the end of each day.

(j) ^{3}H samples were analysed from June 3 onward when the equipment became available to the IAEA.

V.3.2. Sampling sites

The sampling programme necessitated a variety of equipment and staff support. Inaccessible sampling sites on the Mururoa rim required helicopter service. Sampling sites in the lagoon needed a boat and divers to retrieve the sampling tubes which were anchored below the water surface. Sampling at Fangataufa (lagoon) required helicopter, boat and divers. This support, provided by the CEA and the French Army, has to be acknowledged with great appreciation.

The following sampling plan was elaborated in a meeting with the responsible persons in Mururoa on 27 May 1997:

Date	Location	Atolls	Specific needs
Wednesday, 28 May	Aristée	Mururoa	
Thursday, 29 May	Pieuvre 37	Mururoa	boat, divers
Friday, 30 May	Fuseau 30	Fangataufa	helicopter, boat, divers
Saturday, 31 May	Mitre 27	Fangataufa	helicopter, boat, divers
Sunday, 01 June	Céto	Mururoa	helicopter
Monday, 02 June	Géo 10	Mururoa	
Tuesday, 03 June	Géo 8	Mururoa	
Wednesday, 04 June	Isurus 10	Mururoa	boat, divers
Thursday, 05 June	Murène 16	Mururoa	boat, divers
Friday, 06 June	Tazard 14	Mururoa	boat, divers
Saturday, 07 June	Géo 5	Mururoa	
Sunday, 08 June	In reserve		

The sampling campaign was planned to start on 28 May at an accessible site on the Mururoa rim that would provide the opportunity to test the sampling procedure and equipment. Aristée was selected because the cavities were of highest priority for the study of the radiological situation at the atolls of Mururoa and Fangataufa.

On the second day (29 May 1997) it was intended to test the equipment at a location on the lagoon. Pieuvre 37 was selected because of its significance as a sampling point on the north rim.

On the next 2 days (30–31 May) boat, helicopter and divers were available to allow sampling of the two monitoring wells (Fuseau 30 and Mitre 27) at Fangataufa. Sampling at Fangataufa was prioritized because access depended on the weather conditions. Should weather conditions not allow sampling at these two dates, another 3 day slot would have been available for sampling at Fangataufa during the following week.

The other cavity, Céto, on Mururoa was selected as the next sampling point (01 June) because of its high priority. The necessary helicopter service was available on a Sunday.

The next two sampling points, Géo 10 and Géo 8, on Mururoa (02–03 June) were selected because of their high priority as sampling points on the north rim and their location on land. This would allow the best possible interaction between E. Warnecke who was going to leave Mururoa on 03 June (noon) and D. Smith who was scheduled to arrive at Mururoa on 02 June (noon) to take over responsibility for the sampling from E. Warnecke.

The next three samples (04–06 June) were then planned to be taken from monitoring wells on the Mururoa lagoon (Isurus 10, Murène 16, Tazard 14) followed by the sampling of Géo 5, on land (07 June).

TABLE V.1. CHARACTERISTICS OF THE SELECTED MONITORING WELLS

ARISTÉE

Type: Test cavity.
Drilling 8"1/2 vertical from the surface to 27 m, in 6"1/4 vertical from 27 m to 360 m, in turbo 6"1/4 (inclined) from 360 m to 675 m, inclined coring in HR diameter from 675 m to 720 m (ten meters below the bottom of the cavity).
Present configuration:
Casing 7" from the surface down to 26 m, cemented at the bottom.
Casing BW from the surface down to 713 m, slotted from the bottom up to 691 m, annular cemented in the volcanic covering.
The sampling point (at the end of the hose) is at 697 m (vertical depth) corresponding to 702 m (drilling length). It is located in the bottom part of the cavity, in the middle above the lava zone, 15 m below the working point of the test.

CÉTO

Type: Test cavity.
Drilling 8"1/2 vertical from the surface to 49 m, in 6"1/4 vertical from 49 m to 253 m, in turbo 6"1/4 (inclined) from 153 m to 545 m, inclined coring in HR diameter from 545 m to 585 m.
Present configuration:
casing 7" from the surface down to 575 m, slotted from the bottom up to 553 m, annular cemented in the volcanic covering.
The sampling point was initially in the bottom part of the cavity, in the middle above the lava zone, but it has progressively become more and more difficult to go down to this point with the sampling bottle.
It has been impossible to lower the sampling hose below 513 m. This point must correspond to a point where the casing is supposed to be collapsed and open in the chimney. This point is located at 507 m in vertical depth, in the middle of the chimney elevation, 10 m below the point where the trajectory enter in the chimney and 15 m from the vertical axis of the chimney.

PIEUVRE 37 (SHALLOW AND DEEP)

Type: Specific wells, one shallow (125 m) and one deep (315 m). Horizontal distance ~30 m
Lagoon depth: 47 m - Top of the volcanism: 305 m.
30" casing from the bottom of the lagoon to 80 m.
Well head obturator cemented in the 30" casing.
Open 27" hole from 80 m to 125 m or 315 m (bottom of the holes).
Shallow hole: One polytube is protected in a 5" tubing from the bottom of the lagoon to 111 m. This tubing is perforated from 91 m to 109 m. Sampling depths at 95 and 107 m (perforated tubing).
Deep hole: One polytube is protected in a 5" tubing from the bottom of the lagoon to 273 m. This tubing is perforated from 252 m to 272 m. Sampling depths at 260 m (perforated tubing), 285 and 300 m (open hole).

TABLE V.1. (cont.)

FUSEAU 30 (Fangataufa)

Type: Specific well.
Lagoon depth: 28 m - Top of the volcanism: 280 m.
30" casing from the bottom of the lagoon to 62 m.
Well head obturator cemented in the 30" casing.
Open 27" hole from 62 m to 281 m (bottom of the hole).
One polytube is protected in a 5" tubing from the bottom of the lagoon to 210 m. This tubing is perforated from 192 m to 210 m. Sampling depths at 193 (perforated tubing), 215, 255 and 268 m (open hole).

MITRE 27 (Fangataufa)

Type: re-entry hole of an experiment of the last campaign.
Lagoon depth: 42 m - Top of the volcanism: 267 m.
30" casing from the bottom of the lagoon down to 77 m.
Well head obturator cemented in the 30" casing.
Open 27" hole from 77 m to 260 m (bottom of the hole, after cementing of the lower part of the trajectory. Attempt to manage a chamber in the upper part of the volcanism failed).
One polytube is protected in a 3 1/2" tubing from the bottom of the lagoon to 237 m. This casing is perforated from 218 m to 237 m. Sampling depths at 232 (perforated tubing) and 239 m (open hole).

GÉO 10

Type: Instrumentation well (geophones).
12"1/4 hole cased in 9"5/8 from the surface down to 120 m.
8" 1/2 hole from 120 m down to 350 m, cased in 6"5/8 and cemented below 320 m.
Above the cemented zone, the 6"5/8 casing is perforated in the following zones: 140–149 m, 164–173 m, 228–237 m, 280–289 m, 307–316 m (carbonate zone).
A polytube is installed in the annular zone between the 6"5/8 casing and a 2"7/8 tubing. This tubing carries the instrumentation (geophones) cemented at ~ 340 m.
Sampling depth (polytube): 140, 167, 228, 282, 307 m.

GÉO 8

Type : Instrumentation well (geophones and tiltmeters).
12"1/4 hole cased in 9" 5/8 from the surface down to 83 m.
8" 1/2 hole from 83 m down to 463 m (bottom of the hole), cased in 7" and cemented below 310 m.
Above the cemented zone, the 7" casing is perforated in the following zones: 209–214 m, 273–278 m, 305–318 m (carbonate zone).
A polytube is installed in the annular zone between the 7" casing and a 2"7/8 tubing. This tubing carries the instrumentation (tiltmeters and geophones) cemented at the bottom of the hole.
Sampling depth (polytube): 211, 276, 307 m

TABLE V.1. (cont.)

ISURUS 10

Type: re-entry hole of an experiment of the last campaign.
Lagoon depth: 33 m - Top of the volcanism : 275 m.
Carbonate zone:
30" casing from the bottom of the lagoon down to 68 m.
Well head obturator cemented in the 30" casing.
Open hole (27") from 68 m to 277 m.
One polytube is protected in a 3 1/2" tubing from the bottom of the lagoon to 269 m. This casing is perforated from 259 m to 269 m. Sampling depths at 260, 265 (perforated tubing) and 275 m (open hole).
Volcanic zone:
Sampling chamber in a 12"1/4 open hole between 309 to 353 m (bottom of the hole, after cementing of the lower part of the trajectory). This chamber is isolated from the carbonate chamber by a cemented zone between 277 and 309 m.
One polytube is protected in a 3 1/2" tubing from the bottom of the lagoon to 312 m.
Sampling depths at 315, 330 and 345 m in the 12"1/4 open hole.

MURÈNE 16

Type: Large Diameter (60").
Lagoon depth: 43 m - Top of the transition zone: 254 m.
60" casing from the bottom of the lagoon down to 78 m.
Well head obturator cemented in the 60" casing.
Open hole without casing from 78 m to 296 m (bottom of the hole).
Polytube in the open hole. Sampling depths: 100, 185, 230, 285 m.

TAZARD 14

Type: specific well.
Lagoon depth: 42 m - Top of the volcanism: 299 m.
30" casing from the bottom of the lagoon to 72 m.
Well head obturator cemented in the 30" casing.
Open 27" hole from 72 m to 300 m (bottom of the hole).
One polytube is protected in a 5" (T2) tubing from the bottom of the lagoon to 210 m. This tubing is perforated from 192 m to 211 m. Sampling depths at 193 (perforated tubing), 245 and 290 m (open hole).

GÉO 5

Type: Instrumentation well (geophones).
12"1/4 hole cased in 9" 5/8 from the surface down to 80 m.
8" 1/2 hole from 80 m down to 301 m, cased in 7" and cemented below 267 m.
Above the cemented zone, the 7" casing is perforated in the following zones: 98–104 m, 148– 153 m, 183–188 m, 214–218 m, 227–232 m, 262—267 m (carbonate zone).
A polytube is installed in the annular zone between the 7" casing and a 2"7/8 tubing. This tubing carries the instrumentation (geophones)cemented at ~ 300 m.
Sampling depth (polytube): 102, 151, 187, 217, 230, 266 m.

All depths are related to the lagoon level (lowest tide).

The last day of the campaign (08 June) was kept in reserve to allow for changes in this plan if weather conditions should not allow sampling on one of these days. The actual sampling of underground waters was executed as planned.

V.4. UNDERGROUND WATER SAMPLING

V.4.1. Borehole description

The principle construction of the boreholes is described in the following paragraphs. A more detailed description of the wells is provided in Table V.1.

The two test cavities (Aristée and Céto) have a similar construction (Figs V.2 and V.3). Both cavities have been accessed from the side by a boring into the cavity. A PE tube with an inner diameter of 8 mm has been emplaced in the borehole. In the case of Aristée the tube is ending within the cavity 15 m below the firing point. The sampling point is located at 702 m (697 m vertical) depth. In the case of Céto the tube got stuck at the entrance of the borehole into the test cavity and could not be lowered further. The sampling point is located at 512 m (507 m vertical) depth.

The principle construction of the monitoring wells is given in Figs V.4 and V.5. Some of the wells have a sampling chamber in the volcanic rock (Fig. V.5) which is separated by a plug from the carbonates. Sampling of these deeper intervals was excluded from the IAEA sampling campaign which was designed only to take underground water samples from the karstic zone in the lowest accessible level in the carbonates or in the region of the upper karst in the case of the Fangataufa wells.

The monitoring wells are constructed with casing at the top only. For this reason waters from the various horizons can mix in the well bore. A rise and fall of the water levels in the wells with the tides has also been reported. The wells are equipped with a "polytube". This polytube consists of a bundle of individual tubes, each with an inner diameter of 4 mm. These 4 mm tubes end at different depths and allow the taking of water samples from different horizons. Up to four of these 4 mm tubes end at a certain depth and may be used in parallel for sampling in order to increase the volumetric flow of waters. The monitoring wells in the lagoon are plugged at the top against the introduction of surface waters. The polytube is anchored below the water surface (Fig. V.6) and has to be brought up to the boat by divers prior to sampling.

V.4.2. Sampling operations

The sampling tubes were connected to the elastic pumping tubes of the peristaltic pumps without fittings. Two pumps, each with two pump heads, were available and used as needed. Only one sampling tube was available in the case of the test cavities. Up to four sampling tubes were ending at any one specific depth in the monitoring wells. The maximum number of tubes was used for sampling in order to maximize the rate of the water flow.

After the pumping commenced one combined water volume in the tubes (termed "dead volume") was pumped off and discarded. Afterwards, the Millipore filter and the pH/Eh/temperature measurement box were connected to the pump. pH and Eh data were measured every fifteen or thirty minutes. Water samples for ^{3}H measurements were taken after one, two and three dead volumes were produced from the well and at the conclusion of each day's sampling. The water flow rate was recorded at the beginning and end of pumping. In the case that more than one tube was pumped both the individual and the combined flows were measured. The sampling of waters was started when pH/Eh values were proven to be constant. In practice sampling was started after the pumping of 3 dead volumes.

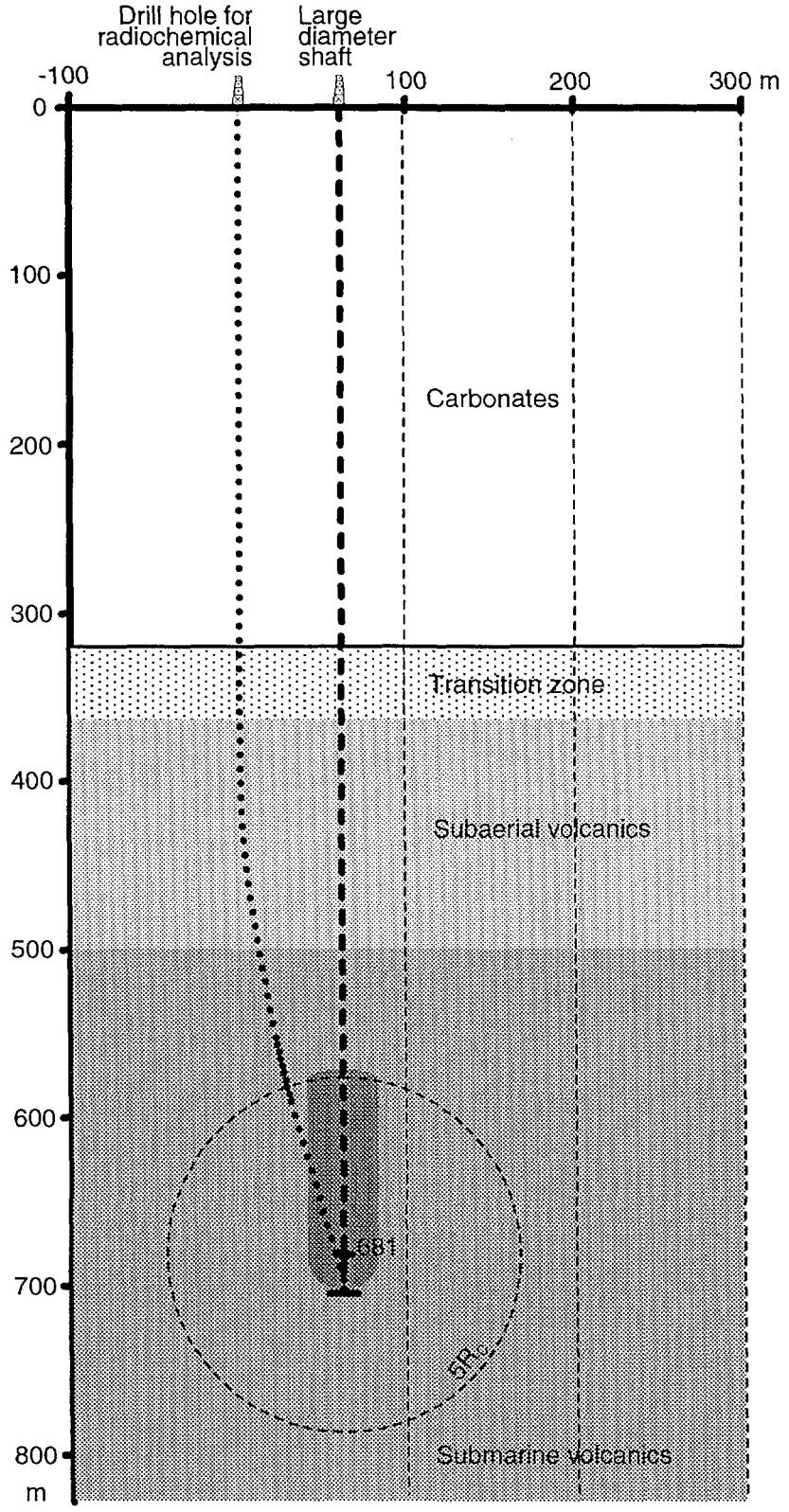

FIG. V.2. Aristée cavity-chimney and re-entry drillhole. Zero point depth: 681 m; sampling point at 702 m (697 m vertical depths); calculated cavity radius: 21 m; calculated chimney height: 110 m; yield: 6.8 kt. (From French Liaison Office Document No. 8, 1996.)

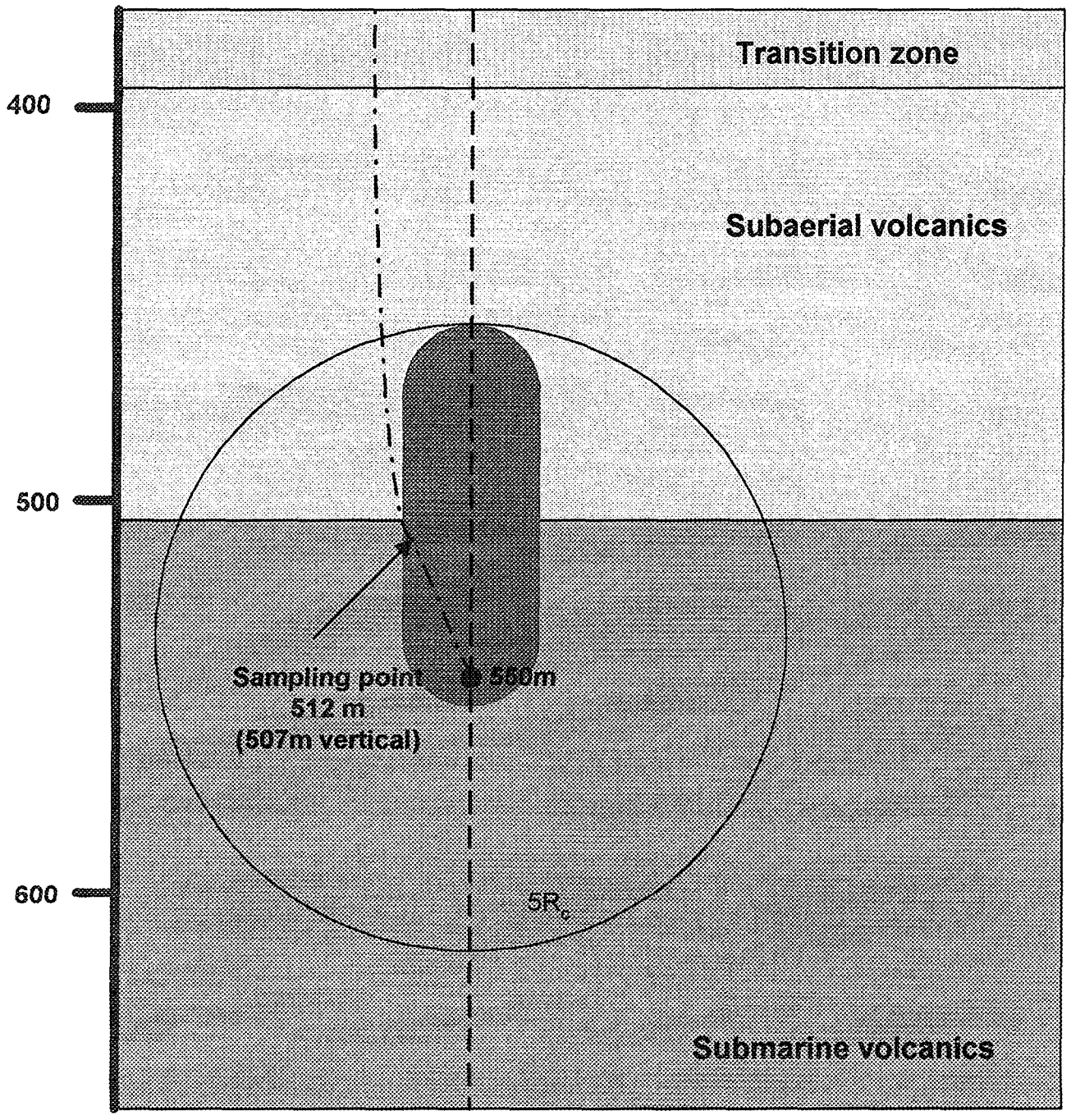

FIG. V.3. Céto cavity-chimney re-entry drillhole: sampling point at 512 m (507 m vertical).

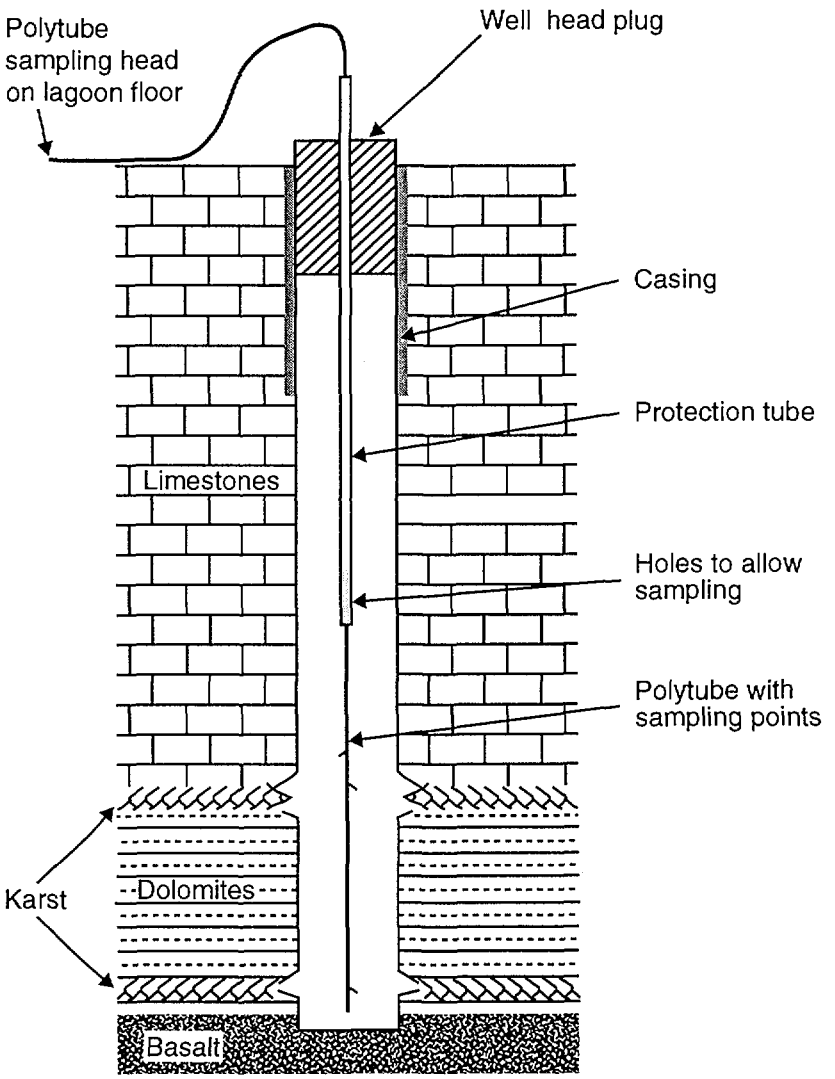

FIG. V.4. Typical long term monitoring well in carbonate formations. (From French Liaison Office.)

The water samples taken from the two cavities (Aristée and Céto) were checked during sampling for their surface dose rate with a portable dose meter. The surface dose rate was found to be about 2–3 times above the low natural background at the Mururoa atoll.

V.4.3. ^{3}H analyses

About 300 ml of underground water were distilled and the condensed vapour fraction was then sub-sampled (~ 10 ml) and mixed with 10 ml scintillation liquid (Pico Flour, Packard) for counting. Tritium free sea water was used for quenching and the counting time (100 minutes/sample) was determined according to CEA protocols.

V.4.4. Handling of samples

V.4.4.1. Sealing

At the end of each day the samples were sealed in order to prevent any compromise of sample integrity. The caps of the 10 L and 20 L containers were fixed to the body of the container using

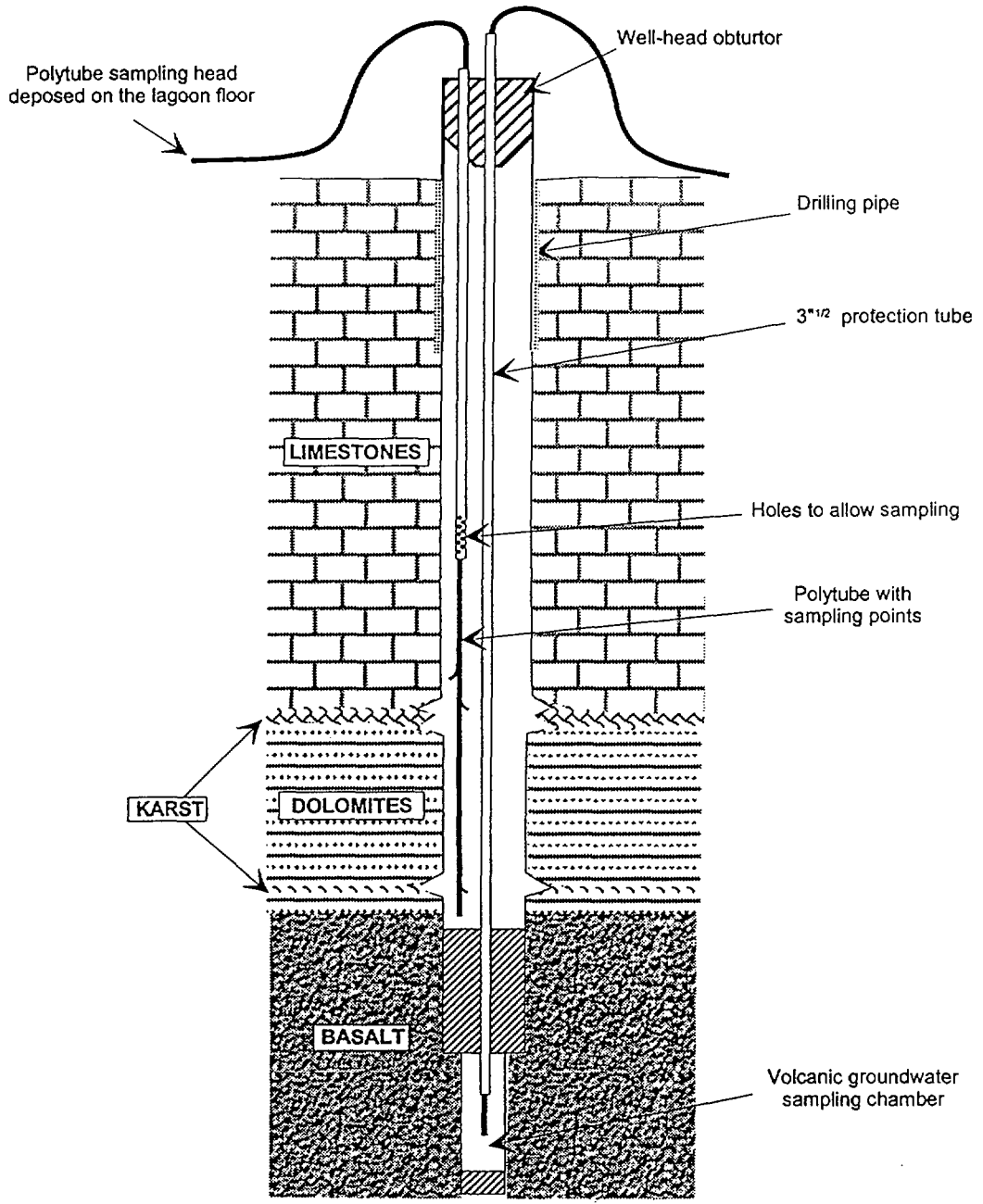

FIG. V.5. Typical long term monitoring well with a sampling chamber in the volcanics. (From French Liaison Office.)

standard sealing wire plus an IAEA seal. The 1 L bottles did not allow for this procedure and had to be sealed differently. As an interim measure the bottles were placed into a cardboard box which was bound over all sides with a seal wire and the ends were fused with an IAEA seal. For shipping each 1 L bottle was taped and then placed into a plastic bag. The open end of the plastic bag was sealed by heating. The same procedure was applied to the 450 nm filters which were collected in 100 ml bottles.

V.4.4.2. Storage and shipment

The sealed samples were stored in an air conditioned room in the dark. At the end of the sampling campaign all the sealed samples were placed into wooden boxes for shipping. Each box, after being nailed, was closed with two metal bands.

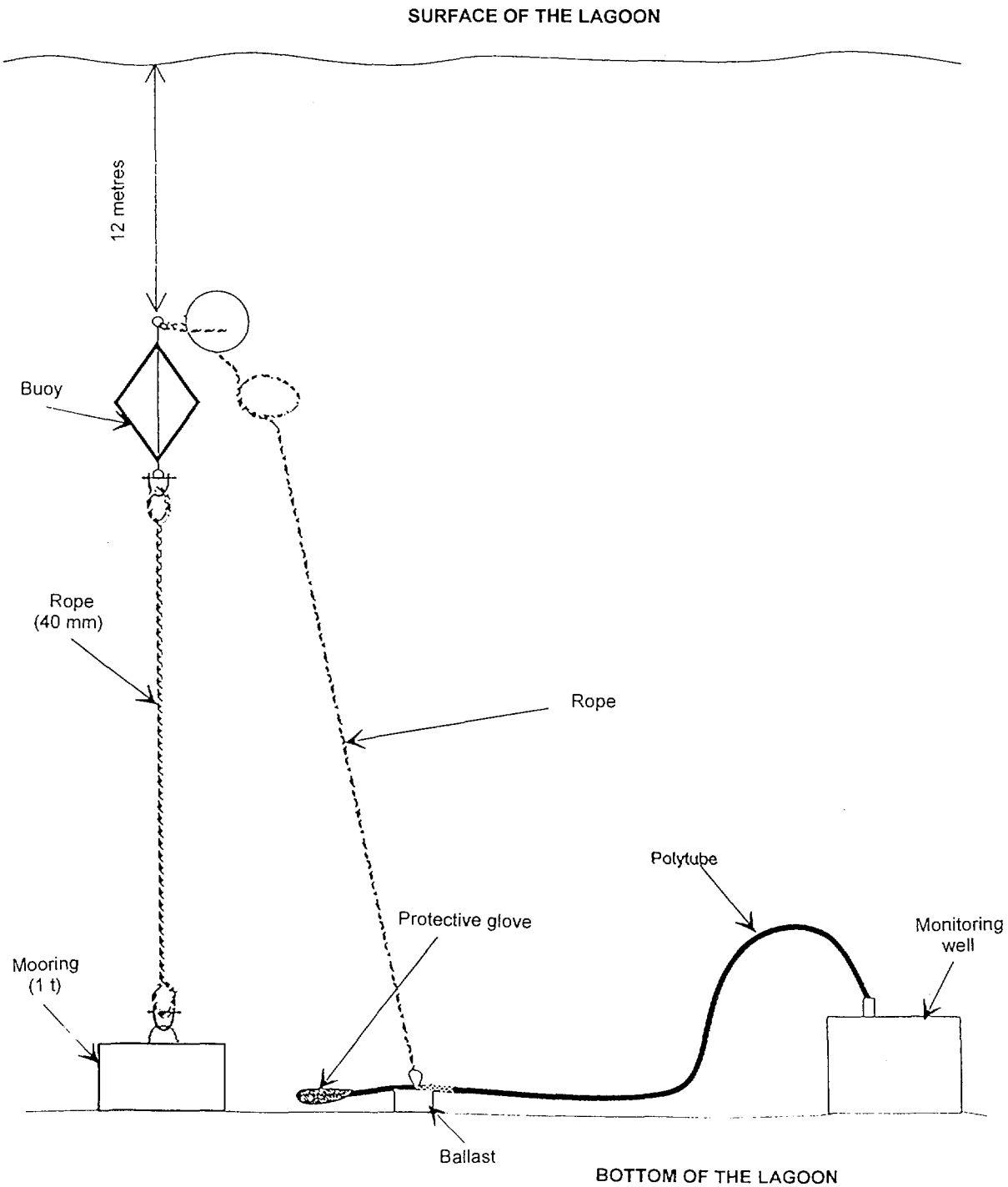

FIG. V.6. Schematic drawing of a sampling point in the lagoon. (From French Liaison Office.)

All the boxes were air transported from Mururoa to Paris. They were shipped on 9 June 1997 from Mururoa to Tahiti by airplane and on June 10 from Tahiti to Paris in the cargo compartment of a French military plane (COTAM). They were then sent from Paris to the IAEA-MEL, Monaco by surface transport. The 20 L sample and the filter remained in Monaco for radionuclide analyses and elemental analyses (filter). The samples taken for ^{129}I / ^{36}Cl analyses, ^{14}C analyses and elemental analyses (acidified and non-acidified) were stored at 4 degrees, kept in their plastic seals and shipped by airplane to the Australian Nuclear Science and Technology Organization (ANSTO), Lucas Heights, Australia. The four samples taken for Pu analyses were also kept at 4 degrees in their plastic seals and

shipped by airplane to the Lawrence Livermore National Laboratories, Livermore, USA. All samples were forwarded to the laboratories as taken and closed at the atolls without any further manipulation (e.g. opening of the bottles).

The sampling operations were carried out by E. Warnecke, IAEA (27 May–03 June 1997), D. Smith, Lawrence Livermore National Laboratory, USA (03–08 June 1997) and S. Mulsow, IAEA (27 May–08 June 1997).

V.5. SAMPLE COLLECTION LOGS

Sampling activities were recorded in sample collection logs which were completed for each well. Several specific items have bearing on the interpretation of the field data and are noted below.

(a) During the sampling of some of the waters from monitoring wells the Eh began to drift to higher values. The increase in Eh generally corresponds to changes in tide. The tide table is reproduced in Table V.2. Higher Eh is likely due to the replacement of deeper waters at the sampling horizons with oxidized waters derived from shallower (near-surface) levels during tidal intrusions. Changes in Eh have to be taken into account in the interpretation of the chemical analyses of the waters.

(b) The water temperature was measured in the measurement box. It reflects the ambient conditions (up to ~ 35°C) and not the water temperatures at sampling depth. The flow rate was not high enough to preserve down-hole temperatures.

(c) The knowledge of the pH and Eh values of the lagoon water may be important for the later review and interpretation of analytical results. Therefore, the pH and Eh data of the Mururoa lagoon water have been measured on 29 May, 5 June, and 6 June and the sea water on 7 June. The measured values are:

Date	pH	Eh(SHE)	Location
Thursday, 29 May	8.18	+368 mV	Pieuvre 37
Thursday, 05 June	8.17	+435 mV	Murène 16
Friday, 06 June	8.11	+449 mV	Tazard 14
Saturday, 07 June	8.81	+449 mV	Géo 5 (sea water)

The lagoon and sea water is more oxidizing and alkaline than the underground formation waters.

The records of the sampling operations for each well are provided in the attached sample collection logs. This provides the relevant information, in particular on the sampling location, the sample collection, the field parameters and comments on particular observations.

The development of pH, Eh and ^{3}H concentrations during sampling is provided in the attached log charts.

The Eh data are corrected in accordance with the calibration of the Eh electrode and are given against standard hydrogen electrode (SHE).

The tide table for the atolls is provided in Table V.2 for easy reference.

An overview of the characteristics of the cavities and monitoring wells sampled in 1997 is provided in Table V.3.

TABLE V.2. TIDE TABLE

Date	Low tide (hours)	Height (m)	High tide (hours)	Height (m)
27 May	00:32	0.45	06:59	0.9
	13:22	0.45	19:19	0.9
28 May	01:54	0.45	08:14	0.9
	14:29	0.45	20:37	0.9
29 May	03:10	0.45	09:20	0.95
	15:31	0.4	21:47	0.95
30 May	04:13	0.4	10:17	1
	16:27	0.35	22:47	1
31 May	05:07	0.4	11:07	1
	17:19	0.35	22:38	1.05
1 June	05:55	0.35	11:54	1
	18:08	0.3		
2 June	06:40	0.35	00:24	1.05
	18:55	0.3	12:40	1
3 June	07:24	0.35	01:07	1
	19:40	0.3	13:24	1
4 June	08:07	0.35	01:48	1.05
	20:23	0.35	14:08	1
5 June	08:50	0.4	02:29	1.05
	21:06	0.35	14:51	0.95
6 June	09:34	0.4	03:09	1
	21:47	0.4	15:35	0.95
7 June	10:19	0.45	03:50	0.95
	22:30	0.45	16:19	0.9

V.6. ANALYSES OF UNDERGROUND WATERS

All samples taken from the 11 sampling locations were analyzed as taken and closed at the atolls. The analytical investigations were carried out for the radionuclide content of the water samples and their chemical composition. The solid material on the 450 nm filters was characterized for chemical composition and radionuclide content. Two laboratories were involved in the analyses of the samples, i.e. the IAEA Marine Environment Laboratory (MEL) in Monaco and the Australian Nuclear Science and Technology Organization (ANSTO) in Lucas Heights, Australia. It happened that the equipment for the planned Pu analyses at the Lawrence Livermore National Laboratory was not available.

V.6.1. Radionuclide analyses

V.6.1.1. Methods

The radionuclide analyses, except ^{14}C, ^{36}Cl and ^{129}I, were carried out at the IAEA Marine Environment Laboratory (MEL), Monaco under P. Povinec. The respective analytical procedures are described in Vol. 1 of this Technical Report.

The analyses of ^{14}C, ^{36}Cl and ^{129}I were carried out by ANSTO, Lucas Heights, Australia. The ANSTO staff involved in the radionuclide analyses included M. Hotchkis, C. Tuniz and G. Jacobsen.

TABLE V.3. CHARACTERISTICS OF UNDERGROUND CAVITIES AND MONITORING WELLS SAMPLED IN 1997

Atoll	Well name	Site location	Facies	Drill's purpose	Casing	Tube type	Sampling depth (m)	Volume filtered (L)
Mururoa	Aristée	rim	basalt	experiment	*	single tube	702	100
	Céto	rim	basalt	experiment	*	single tube	513	92
	Géo 10	rim	carbonate	geophones	120 m	polytube	307/311	48
	Pieuvre 37	lagoon	transition	experiment	80 m	polytube	300	44
	Géo 8	rim	carbonate	geophones	83 m	polytube	274/276/278	54
	Tazard 14	lagoon	transition	experiment	72 m	polytube	245	68
	Murène 16	lagoon	transition	experiment	78 m	polytube	230	72
	Isurus 10	lagoon	carbonate	experiment	68 m	polytube	265	80
	Géo 5	rim	carbonate	geophones	80 m	polytube	215/230	50
Fangataufa	Fuseau 30	lagoon	transition	experiment	62 m	polytube	193	40
	Mitre 27	lagoon	transition	experiment	77 m	polytube	239	55

* The casing extends into the volcanic below the lava.

The ^{129}I and ^{36}Cl were measured by Accelerator Mass Spectrometry (AMS) at ANSTO. In AMS, the prepared sample is introduced into a negative ion source and the beams extracted are accelerated to MeV energies in a Tandem accelerator. Charge stripping in the terminal of a Tandem accelerator dissociates molecules which may otherwise interfere with mass spectrometry. This mechanism is coupled with medium resolving power devices before and after acceleration. The achievable sensitivity with AMS corresponds to about 10^6 atoms and is useful both to analyses at ultra-trace levels and to measurements of isotopic ratios.

For ^{129}I analyses by AMS, a known quantity of stable iodine carrier is added to the sample. The $^{129}I/^{127}I$ ratio is measured by AMS and the amount of ^{129}I in the original material can then be calculated. At ANSTO, iodide carrier was added to 0.5 L of sample water. The iodide was concentrated by anion exchange chromatography and eluted with sodium hypochlorite solution. The eluate was treated with concentrated HNO_3, hydroxylamine hydrochloride added and the iodine extracted into chloroform. Iodide was back extracted into a sodium metabisulphite solution. The chloroform extraction was repeated using sodium nitrite as the oxidant and back extracted as previously described. The iodide was then precipitated as AgI, washed and dried. AgI samples were mixed with equal quantities of Nb powder and loaded into sample holders for insertion into the AMS ion source. An accelerating voltage of 3.6 MV was used and iodine ions in the 5+ charge state were selected by a 90° analysing magnet. ^{129}I ions were further analysed using a 90° electrostatic analyser and counted in a Si surface barrier detector. The minimum detection limit was 50 nBq/L.

In the case of the underground waters the above-mentioned procedure was applied, except that samples were diluted by taking a small sub-sample and adjusting the quantity of iodide carrier, so as to ensure that the iodine isotopic ratio of the resulting material was within the range acceptable to the AMS instrument (ratio between 10^{-13} and 10^{-9}). Where necessary successive dilutions were performed.

The ^{36}Cl was measured by AMS at ANSTO. To maximise sensitivity, it is necessary to minimise the sulphur content of samples in order to reduce the counting rate from the stable isotope ^{36}S. Chloride was extracted by precipitation of AgCl from 2 mL of sea water. The AgCl was dissolved in ammonia solution and sulphates removed by precipitation as $BaSO_4$. After filtration the solution was neutralized and AgCl reprecipitated. This step was repeated to ensure that sulphur levels were reduced to a level acceptable for ^{36}Cl measurement.

AgCl samples were mixed with Ag powder and loaded into sample holders lined with AgBr. An accelerating voltage of 7.8 MV was used, with a carbon foil stripper in the terminal of the accelerator. Chlorine ions in the 7+ charge state were selected by a 90° analysing magnet. ^{36}Cl ions were further analysed using a Wien filter and detected in a gas-filled ionisation chamber which is capable of resolving ^{36}Cl from remaining ^{36}S ions. The minimum detection limit for measurements of seawater samples corresponds to 1 mBq/L, provided the processing has reduced the sulphur to an acceptable level.

In the case of the two test cavity samples, the samples were diluted by combining 40 mg of stable chlorine carrier with 2 µl of the water sample. This was necessary to ensure the chlorine isotopic ratio ($^{36}Cl/Cl$) of the resulting material was within the range acceptable to the AMS instrument (ratio between 10^{-14} and 10^{-11}). The other samples did not require dilution.

V.6.1.2. Results

The radionuclide concentrations measured in the underground water samples taken at the atolls are given in Table V.4 for the radionuclides specified in Section 2 of this Appendix, except ^{237}Np which was below detection limits in all samples and ^{99}Tc where data did not become available due to technical difficulties with the analyses.

TABLE V.4. RADIONUCLIDE CONCENTRATIONS (mBq/L) IN UNDERGROUND WATER SAMPLES

Atoll	Station	^{3}H	^{14}C	^{36}Cl	^{129}I	^{90}Sr	^{137}Cs	$^{239+240}Pu$	^{238}Pu	^{241}Am
Mururua	Aristée	$(6.1\pm 0.31) \times 10^{9}$	< 50	2.98×10^{3}	44.95	$(3.19 \pm 0.29) \times 10^{5}$	1.0×10^{5}	< 0.008	< 0.008	0.064 ± 0.016
	Céto	$(2.17 \pm 0.11) \times 10^{10}$	1280	3.1×10^{4}	16.87	$(2.54 \pm 0.15) \times 10^{5}$	$(1.12 \pm 0.8) \times 10^{4}$	0.02 ± 0.004	< 0.002	0.104 ± 0.014
	Géo 10	$(7.47 \pm 0.38) \times 10^{6}$	52	19	1.07×10^{-2}	$(1.6 \pm 0.1) \times 10^{4}$	1.1×10^{3}	< 0.03	< 0.02	< 0.003
	Pieuvre 37	$(8.45 \pm 0.42) \times 10^{6}$	< 32	1.7	1.17×10^{-2}	$(1.2 \pm 0.06) \times 10^{4}$	9.7×10^{3}	< 0.007	< 0.007	< 0.002
	Géo 8	$(1.4 \pm 0.07) \times 10^{6}$	< 32	5.4	4.31×10^{-3}	$(1.6 \pm 0.1) \times 10^{4}$	$(1.1 \pm 0.1) \times 10^{3}$	< 0.01	< 0.006	< 0.003
	Tazard 14	$(6.88 \pm 0.35) \times 10^{6}$	< 32	3	2.9×10^{-4}	53 ± 3.4	78.3 ± 7.0	< 0.005	< 0.006	< 0.005
	Murène 16	$(1.00 \pm 0.05) \times 10^{7}$	< 32	15	1.46×10^{-2}	103 ± 7	< 2	< 0.007	< 0.005	< 0.003
	Isurus 10	$(4.82 \pm 0.27) \times 10^{5}$	< 32	< 1	9.4×10^{-4}	64 ± 4.1	11.9 ± 0.2	< 0.004	< 0.007	< 0.005
	Géo 5	$(1.83 \pm 0.36) \times 10^{4}$	4.4	< 24.5	$< 5\times10^{-5}$	8.4 ± 1.3	20.3 ± 3.0	< 0.03	< 0.03	< 0.004
Fangataufa	Fuseau 30	$(3.44 \pm 0.18) \times 10^{6}$	< 32	3.1	1.02×10^{-2}	337 ± 21	127 ± 9	< 0.009	< 0.007	< 0.008
	Mitre 27	$(1.02 \pm 0.32) \times 10^{4}$	12	< 6	$< 5\times10^{-5}$	2.2 ± 1.2	19.7 ± 2.0	< 0.05	< 0.05	< 0.003

TABLE V.5. RADIONUCLIDE CONCENTRATIONS (mBq/g) IN PARTICULATES IN UNDERGROUND WATER SAMPLES

Atoll	Station	Total dw g*	$^{239+240}$Pu	^{238}Pu	^{241}Am	^{60}Co	^{125}Sb	^{137}Cs	^{155}Eu
Mururua	Aristée	0.084	235 ± 18	32 ± 3	44.4 ± 4.5	690 ± 80	7600 ± 200	4770 ± 90	1200 ± 400
	Céto	0.305	38.1 ± 3.2	3.9 ± 0.6	17.2 ± 1.7	160 ± 20	310 ± 50	4260 ± 80	<35
	Géo 10	0.086	< 0.2	< 0.2	< 0.7	<12	<35	<24	<45
	Pieuvre 37	0.023	< 3	< 3	< 4	<45	<90	<45	<90
	Géo 8	0.051	< 0.7	< 0.8	< 1	<20	<60	<20	<40
	Tazard 14	0.019	< 0.8	< 0.5	< 1	<100	<260	<100	<370
	Murène 16	0.042	< 1	< 0.7	< 0.8	<24	<70	<48	<100
	Isurus 10	0.043	<1	< 1	< 2	<46	<70	<23	<46
	Géo 5	0.128	< 0.4	< 0.2	< 0.6	<20	<40	<20	<40
Fangataufa	Fuseau 30	0.864	23.3 ± 2.0	8.9 ± 0.8	0.54 ± 0.11	<1	<3	<1	<2
	Mitre 27	0.198	24.3 ± 2.0	9.3 ± 0.8	1.15 ± 0.38	<20	<50	<20	<100

* Total dry weight of solid residue per filter in g.

TABLE V.6. RADIONUCLIDE CONCENTRATIONS STANDARDIZED TO VOLUME OF WATER FILTERED (mBq/L)

Atoll	Station	Volume filtered (L)	Filter size	$^{239+240}Pu$	^{238}Pu	$^{238}Pu/^{239+240}Pu$	^{241}Am	^{60}Co	^{125}Sb	^{137}Cs	^{155}Eu
Mururoa	Aristée	100	1	0.20 ± 0.01	0.027 ± 0.002	0.13 ± 0.01	0.037 ± 0.003	0.58 ± 0.06	6.38 ± 0.15	4.01 ± 0.07	1.01 ± 0.03
	Céto	92	0.5	0.25 ± 0.02	0.026 ± 0.003	0.10 ± 0.01	0.114 ± 0.012	1.06 ± 0.13	2.06 ± 0.34	28.24 ± 0.54	<0.2
	Géo 10	48	0.5	<0.0007	<0.0007		<0.002	<0.04	<0.1	<0.08	<0.1
	Pieuvre 37	44	1	<0.001	<0.001		<0.001	<0.02	<0.04	<0.02	<0.04
	Géo 8	54	0.5	<0.001	<0.001		<0.002	<0.03	<0.09	<0.03	<0.06
	Tazard 14	68	0.5	<0.0005	<0.0005		<0.001	<0.06	<0.1	<0.06	<0.2
	Murène 16	72	0.5	<0.001	<0.001		<0.001	<0.03	<0.09	<0.06	<0.1
	Isurus 10	80	0.5	<0.001	<0.001		<0.002	<0.05	<0.07	<0.02	<0.04
	Géo 5	50	0.5	<0.002	<0.001		<0.003	<0.1	<0.2	<0.1	<0.2
Fangataufa	Fuseau 30	40	0.5	1.01 ± 0.07	0.384 ± 0.023	0.38 ± 0.05	0.023 ± 0.003	<0.04	<0.12	<0.04	<0.08
	Mitre 27	55	0.5	0.17 ± 0.01	0.067 ± 0.005	0.39 ± 0.04	0.008 ± 0.001	<0.1	<0.2	<0.1	<0.5

The respective radionuclide concentrations in the solid material separated from the waters by a 450 nm filter are given in Table V.5. The data given in this table are corrected for the fact that in nine out of eleven cases the filter has been shared between the IAEA and the CEA so that only one half of the filter was available for the analyses of the solid residue.

From these data average concentrations of radionuclides per litre of filtered water have been derived (Table V.6). However, it should be taken into account that the solid residue is not homogeneously distributed in the waters. Most of the solid residue was pumped off with the initial waters but during the pumping operations the appearance of the waters changed in various cases from clear to reddish brown and back to clear again, possibly as a consequence of the tidal influence. This shows that the solid residue is not homogeneously distributed in the waters and the average concentrations given in Table V.6 do not reflect this fact.

V.6.2. Chemical analyses

V.6.2.1. Methods

The underground waters were analyzed for their chemical constituents at ANSTO. The ANSTO staff involved in the chemical analyses included N. Blagojevic.

The samples provided for chemical analyses were clear with the exception of the non-acidified Céto sample which contained substantial amount of brown sediment, which is an iron-based precipitate (Fe 53%, Si 9%, Ca 2.4%, Mg and Mn 0.1% each). All samples were subsampled and filtered through 450 nm membrane filters before analyses by either ICP/AES or Ion Chromatography.

The following methods were applied for analyses of the water samples:

(a) ICP/AES
Na, K, Mg, Ca, Sr, Si, Fe, Al (Perkin Elmer Optima 3000 DV, simultaneous ICP/AES)

(b) Ion Chromatography (Dionex)
Cl^-, SO_4^{2-}, NO_3^-

(c) Titration with HCl
Alkalinity (as CO_3^{2-})

The certified reference material (Seawater) CRM-SW Lot #690318 served as reference standard.

The filter residue of five sampling points (Aristée, Céto, Géo 5, Isurus 10 and Fuseau 30) has also been analyzed for the main elements by ICP/AES (see above).

V.6.2.2. Results

The results of the water analyses are given in Table V.7 in terms of concentrations of anions and cations in mg/L. It can be seen that all the waters from the carbonates are very similar to seawater composition. Relative to these samples, the two cavity samples (Céto and even more Aristée) are deficient in magnesium, potassium and sulphate and enriched in calcium, strontium, silicon, aluminium and chloride. These differences are an indication of alterations resulting from an interaction between the waters and the volcanics (Guille et. al., 1996, p.142–145).

The results of the analyses of the solid residues from five filters are provided in Table V.8. Only cations have been analyzed. The main components of these residues are Fe and Si which tend to form voluminous sludges with high scavenging capacities. Furthermore, there is a good representation of magnesium, calcium and aluminium in the solid residues.

Text cont. on p. 237.

TABLE V.7. CHEMICAL ANALYSES OF UNDERGROUND WATERS

		Concentration (mg/L)										
IAEA Code	Location	Ca	K	Mg	Na	Sr	SO_4^{2-}	Cl^-	Si	Al	Fe	Alk (as CO_3^{2-})
101401	Aristée	6220	70	32	6930	65	1150	22800	11.5	0.62	0.3	
101801	Céto	1930	168	710	11200	28	2660	22100	9.1	0.49	3.8	
101901	Géo 10	431	391	1230	11000	7.8	2730	20500	0.5	0.23	0.02	84
101501	Pieuvre 37	416	397	1310	10700	8	2250	20800	0.5	0.1	0.1	116
102001	Géo 8	426	392	1250	10700	7.5	2735	20600	0.1	0.17	<0.02	91
102301	Tazard 14	395	345	1200	10500	7.6	2690	18700	0.1	0.11	0.04	99
102201	Murène 16	402	366	1170	10100	7.7	2720	20100	<0.1	0.19	<0.02	96
102101	Isurus 10	407	371	1190	10300	7.7	2730	19300	0.3	0.14	0.02	90
102401	Géo 5	379	365	1170	10200	7.2	2630	19450	<0.1	0.13	<0.02	79
101601	Fuseau 30	389	377	1240	10200	7.3	2735	20000	<0.1	0.17	<0.02	101
101701	Mitre 27	393	396	1300	10500	7.2	2530	21300	<0.1	0.15	<0.02	93

TABLE V.8. ELEMENTAL ANALYSES OF THE SOLID RESIDUE FRACTION OF FIVE UNDERGROUND WATER SAMPLES

Stations	Fe(total) mg/g	Fe(exchangable) mg/g	Mg(total) mg/g	Mg(exchangable) mg/g	Mn(total) mg/g	Mn(exchangable) mg/g	Al mg/g	Ca mg/g	K mg/g	Si mg/g	Sr mg/g
Aristée	243.51	77.92	6.67	2.63	0.79	0.17	7.27	7.58	0.60	92.10	0.18
Céto	260.67	15.39	16.22	7.49	2.28	0.81	12.87	7.18	1.23	56.26	0.15
Isurus 10	370.61	36.73	3.42	1.15	0.17	0.04	4.72	1.08	0.55	42.69	0.09
Géo 5	410.85	29.16	4.51	0.99	0.77	0.05	2.46	0.38	nd	38.19	0.03
Fuseau 30	588.87	63.36	6.43	2.81	1.98	0.35	2.01	0.69	0.25	2.70	0.04

TABLE V.9. COMPARISON OF RADIONUCLIDE CONCENTRATIONS (mBq/L) IN UNDERGROUND WATERS

Mururoa

Aristée — 702 m (697 m vertical depth)

	French data* (see Doc. No. 8, Chapter II)	IAEA 28 May 1997
HTO	1.5×10^{10}	6.1×10^{9}
^{137}Cs	2×10^{5}	1.0×10^{5}
^{90}Sr	7×10^{5}	3.19×10^{5}

*Data reported 10 years after the test (with correction for decay); test date 12 June 1984.

Céto — 513 m (507 m vertical depth)

	French data* (see Doc. No. 8, Chapter II)	IAEA 1 June 1997
HTO	8×10^{10}	2.7×10^{10}
^{137}Cs	1×10^{5}	1.12×10^{4}
^{90}Sr	3×10^{5}	2.54×10^{5}

* Data reported 10 years after the test (with correction for decay); test date 6 May 1986.

Géo 10 — 307 m and 311 m

	French measurements			IAEA
	10 Oct. 1996	18 March 1997	2 June 1997	2 June 1997
HTO	1.2×10^{7}	4.2×10^{6}	7.6×10^{6}	7.47×10^{6}
^{137}Cs	1.56×10^{4}	2.8×10^{3}	9.1×10^{3}	1.1×10^{3}
^{90}Sr	690	5.3×10^{3}	N/A	1.6×10^{4}

Pieuvre 37 — 300 m

	French measurements			IAEA
	25 Nov. 1996	28 Feb. 1997	25 May 1997	29 May 1997
HTO	1.3×10^{7}	9.9×10^{6}	8.3×10^{6}	8.45×10^{6}
^{137}Cs	1.18×10^{4}	7.71×10^{3}	8.2×10^{3}	9.7×10^{3}
^{90}Sr	1.6×10^{4}	1.15×10^{4}	N/A	1.2×10^{4}

TABLE V.9. (cont.)

Géo 8 — 274 m, 276 m and 278 m

	French measurements			IAEA
	2 Oct. 1996	17 March 1997	3 June 1997	3 June 1997
HTO	7.3×10^5	5.6×10^5	1.4×10^6	1.4×10^6
^{137}Cs	378	324	790	1.1×10^3
^{90}Sr	N/A	668	N/A	1.6×10^4

Tazard 14 — 245 m

	French measurements			IAEA
	28 Nov. 1996	27 Feb. 1997	6 June 1997	6 June 1997
HTO	8.6×10^6	2.6×10^6	6.9×10^6	6.88×10^6
^{137}Cs	17.8	9	14.5	78.3
^{90}Sr	55.9	21.7	N/A	53

Murène 16 — 230 m

	French measurements			I A E A
	22 Nov. 1996	4 March 1997	5 June 1997	5 June 1997
HTO	1.1×10^7	1.1×10^7	1.0×10^7	1.0×10^7
^{137}Cs	< 4.5	< 3.4	< 2.5	< 2
^{90}Sr	99	95.7	N/A	103

Isurus 10 — 265 m

	French measurements			IAEA
	10 April 1996	13 March 1997	4 June 1997	4 June 1997
HTO	1.8×10^4	5.8×10^5	4.8×10^5	4.8×10^5
^{137}Cs	< 6.3	< 4.2	< 2.2	11.9
^{90}Sr	2.5	40.9	N/A	64

Géo 5 — 215 m and 230 m

	French measurements			IAEA
	30 Sept. 1996	17 March 1997	7 June 1997	7 June 1997
HTO	1.5×10^4	$8.8 / 7.3 \times 10^4$	1.7×10^4	1.83×10^4
^{137}Cs	8	5.5 / 6.2	15.5	20.3
^{90}Sr	11.4 / 12.8	10.8 / 34.1	N/A	8.4

TABLE V.9. (cont.)

Fangataufa

Fuseau 30 193 m

	French measurements			IAEA
	3 June 1996	7 March 1997	30 May 1997	30 May 1997
HTO	1.2×10^6	3.2×10^6	3.7×10^6	3.44×10^6
^{137}Cs	40.1	84.5	114	127
^{90}Sr	108	275	N/A	337

Mitre 27 239 m

	French measurements			IAEA
	17 Nov. 1995	8 March 1997	31 May 1997	31 May 1997
HTO	7.6×10^6	3.2×10^4	6.0×10^3	1.02×10^4
^{137}Cs	108	< 4.8	< 3.8	19.7
^{90}Sr	530	< 13.3	N/A	2.2

TABLE V.10. CALCULATED AND MEASURED RADIONUCLIDE CONCENTRATIONS IN CAVITY WATERS [mBq/L] (Céto, 4 kt; Aristée, 6.8 kt)

	Measured concentration		Calculated concentration* (5 kt test)
Radionuclide	Céto	Aristée	
HTO	2.17×10^{10}	6.1×10^9	5×10^9
^{90}Sr	2.54×10^5	3.19×10^5	2.5×10^6
^{137}Cs	1.12×10^4	1.0×10^5	1.9×10^5
^{129}I	17	45	1.1×10^2
$^{239+240}Pu$ tot	0.27	0.2	4.2×10^3
^{36}Cl	3.1×10^4	2.98×10^3	1.1×10^4
^{14}C	1.3×10^3	<50	3.0×10^6
^{241}Am tot	0.22	0.1	1.1×10^4

* 12 years after test.

TABLE V.11. SORPTION COEFFICIENTS (K_d) IN THE TEST CAVITIES DERIVED FROM UNDERGROUND WATER ANALYSES

	Céto	Aristée
Test date	06 May 1986	12 June 1984
Yield (kt)	4	6.8
R_{cavity}(m)	19.0	21.0
V_{cavity}(m)	28 731	38 792
$H_{chimney}$(m)	94	110
$V_{chimney}$(m^3)	120 972	171 795
V_{water}(m^3)	36 294	51 541
M_{rubble}(t)	211 714	300 658
Reference Date	06 June 1997	

		Inventory (Bq)		Inventory in rubble/ water (Bq)		Conc. no sorption (mBq/L)		Measured conc. (mBq/L)		Calculated Kd (L/kg)		This study Kd (L/kg)**
	F_{rubble}	Céto	Aristée	Céto	Aristée	Céto	Aristée	Céto	Aristée	Céto	Aristée	
HTO	1	3.00×10^{15}	1.50×10^{15}	1.61×10^{15}*	7.22×10^{14}*	4.44×10^{10}	1.40×10^{10}	2.17×10^{10}	6.10×10^{9}	0.18	0.22	0
^{90}Sr	0.60	8.00×10^{12}	3.00×10^{13}	3.68×10^{12}	1.32×10^{13}	1.01×10^{8}	2.56×10^{8}	2.54×10^{5}	3.19×10^{5}	68	137	≤100
^{137}Cs	0.75	2.00×10^{13}	4.50×10^{13}	1.16×10^{13}	2.50×10^{13}	3.20×10^{8}	4.85×10^{8}	1.12×10^{4}	1.00×10^{5}	4900	831	300
^{129}I	0.40	$8{,}57\times10^{6}$	1.93×10^{7}	3.43×10^{6}	7.71×10^{6}	95	150	17	45	0.79	0.40	0
$^{239+240}Pu$ (sol)	0.02	1.15×10^{13}	6.00×10^{12}	2.30×10^{11}	1.20×10^{11}	6.34×10^{6}	2.33×10^{6}	0.02	<0.008	5.43×10^{7}	$>4.99\times10^{7}$	500
$^{239+240}Pu$ (tot)	0.02	1.15×10^{13}	6.00×10^{12}	2.30×10^{11}	1.20×10^{11}	6.34×10^{6}	2.33×10^{6}	0.27	0.2	4.03×10^{6}	2.0×10^{6}	500
^{36}Cl	0.5	2.17×10^{9}	4.89×10^{9}	1.09×10^{9}	2.44×10^{9}	3.00×10^{4}	4.73×10^{4}	3.08×10^{4}	2.98×10^{3}	-0.44	2.55	0
^{14}C	1	1.14×10^{11}	2.57×10^{11}	1.14×10^{11}	2.57×10^{11}	3.14×10^{6}	4.99×10^{6}	1.3×10^{3}	<50	414	$>1.71\times10^{3}$	0
^{241}Am (tot)	0.02	4.14×10^{12}	2.16×10^{12}	8.13×10^{10}	4.23×10^{10}	2.24×10^{6}	8.21×10^{5}	0.22	0.1	1.74×10^{6}	1.41×10^{5}	50

* Corrected for decay.

** Note that the numerical value of K_d given in (m^3/kg) is lower by a factor of 1000.

V.6.3. Comparison of radionuclide concentrations in underground waters

Analytical data from French measurements and the IAEA investigations are provided in Table V.9 for ^{3}H (as HTO), ^{137}Cs and ^{90}Sr. These radionuclides were chosen for comparison of data as they are the main contributors to the total activity of the samples.

Monitoring of the Aristée and Céto cavities had already been carried out since after the tests had been conducted. Data on radionuclide concentrations in the cavities were provided in the French Liaison Office Document No. 8, Chapter II (Figs 4 and 5). The data reported for 10 years after the test (corrected for decay) and the respective results of the IAEA investigation of May/June 1997 are included in Table V.9.

Waters of the monitoring wells have been analysed since 1996. The French data for the locations sampled by the IAEA and the respective results can also be found in Table V.9.

It should be noted that the CEA representatives attending the IAEA sampling campaign took water samples of the sampling points selected by the IAEA. The IAEA sampling approach was to purge the respective tube and then sample a water representative for the respective sampling location. In this approach the first dead volume was always discarded. Then 2 more dead volumes were pumped off before the actual sampling began. The waters of these 2 dead volumes were collected by the CEA and analysed at Mururoa for HTO and ^{137}Cs. The CEA experts found that the HTO and ^{137}Cs results were in the expected order of magnitude and decided not to measure ^{90}Sr because the closure of their laboratory at Mururoa put time constraints on analytical investigations.

Furthermore, radionuclide concentrations measured in the test cavities (Aristée and Céto) were compared to the respective calculated inventories resulting from a 5 kt device 12 years after the test (Table V.10). The description of the calculations underlying this comparison is provided in Section 5 on Geosphere Transport.

V.6.4. Derivation of sorption coefficients (K_d) from the analyses of test cavity waters

The concentrations of radionuclides in waters taken from the cavity-chimneys provide the opportunity to derive sorption coefficient for the given systems and compare them to the sorption coefficients used in the modelling of radionuclide releases through the geosphere. The results of such a calculation are presented in Table V.10 together with the set of data necessary for such calculation.

Sorption coefficients are defined as the quotient of the concentration of a radionuclide in the solid phase over its concentration in the aqueous phase. It may be expressed in (L/kg) or (m^3/kg). In the latter case the numerical value is lower by a factor of 1000.

The relevant data for the derivation of sorption data are determined in the following way:

(a) The volume of water (V_{water}) and the mass of rubble (M_{rubble}) are calculated from the cavity data given in Table V.11.

(b) The total inventory in the rubble and water of a test cavity is calculated from the total inventory of the test minus the fraction of radionuclides contained in the lava. This is expressed in Table V.10 by the term "F_{rubble}". For example, F_{rubble} = 1 indicates that 100% of the radionuclide is in the rubble and water of the cavity-chimney and nothing is contained in the lava.

(c) If no sorption would occur the whole radionuclide inventory of the cavity-chimney would be in the water. The difference between the "no-sorption concentration" and the measured concentration of a radionuclide gives the amount of radionuclide attached to the solid phase (rubble). A division of this amount by the rock mass (M) results in the radionuclide concentration in the solid phase (rubble).

(d) Finally, the sorption coefficients are obtained by dividing the calculated concentration of a radionuclide in the rubble and the concentration in the water.

The calculated sorption coefficients and the sorption coefficients applied in the modelling of the radionuclide transport through the geosphere can be found at the right end of Table V.11. In most cases a remarkably good agreement is found between the calculted and applied sorption coefficients. The data used in model calculations are confirmed. In a few cases the sorption coefficients calculated from the actual measurement of radionuclides in the cavity-chimney waters are higher than the ones used in model calculations. This is particularly true for the sorption coefficients of plutonium and americium which are by 4–5 orders of magnitude higher than those applied in model calculations. Thus, the derivation of K_d values for these radionuclides (Section 4) was carried out in a very conservative way.

SAMPLE COLLECTION LOG 1

SAMPLE LOCATION							
Well	**ARISTEE**						
Depth	*702 m; 697 m (vertical depth)*						
Number of tubes	1						
Inner diameter	8 mm						
"dead volume"	35,3 L						
Pumping	start: 09:05 end: 16:22						
SAMPLE COLLECTION							
Date	**28-May-97**						
Time	15:40 - 16:16	15:18 - 15:22	15:23 - 15:26	15:27 - 15:30	15:32 - 15:35	15:36 - 15: 40	After 16:22
Sample number	10402	10401	10401	10401	10402	10402	Filter
Analyte	radionuclide analysis acidified	radionuclide analysis acidified	elemental analysis - non acidified	I-129; Cl-36	C-14	LLNL	radionuclide analysis
Preservatives	HCl	HCl	None	None	$HgCl_2$	None	None
Container	10 L PE flask	1 L PE flask	1 L PE Bottle	1 L PE Bottle	1 L PE Bottle	1 L PE Bottle	100 ml PE bottle
Amount collected	10 L	1 L	1 L	1 L	1 L	1 L	(See Comment 4)
Type of pump	Heydolph Rumo, 100 peristaltic pump						

CALIBRATION OF Eh ELECTRODE					
	Reading [mV]	Ag/AgCl [mV]	SHE* [mV]	T [°C]	Δ SHE* [mV]
Before sampling	176	212	415	30	239
After sampling	185	220	427	25	242

FIELD PARAMETERS				
Time	11:10	13:10	15:10	16:16
Pump rate [l / h]	20	18	18	18
^3H [Bq /m^3]	6.1 · 10 E 9	6.04 · 10 E 9	5.91 · 10 E 9	6.32 · 10 E 9
pH	7,01	7,81	7,91	7,92
Eh [mV (SHE*)]	+49	-7	-8	-6
Temperature [°C]	28	28	28	28

TIDE	high 08:14		low 14:29	
PRESSURE TEST (after sampling)	65,9 bar (compressed air)			
WEATHER (sun/rain/wind)	Partly sunny; partly cloudy; dry; no wind; 26-28°C			

COMMENTS

1) The first "dead volume" was discarded. It was dirty and full of precipitate.
2) The 450 nm filter and the Eh/pH/T measurement box were put into place at 11:20.
3) No degassing or precipitation was observed in the masurement box.
4) The filter contains the residue from about 100 L of sample water.

PREPARED BY

E. Warnecke
S. Mulsow

* SHE - Standard Hydrogen Electrode

SAMPLE COLLECTION LOG 2

SAMPLE LOCATION							
Well	**PIEUVRE 37**						
Depth	300 m						
Number of tubes	2 (black and red)						
Inner diameter	4 mm						
"dead volume"	3,8 L per tube; 7,6 L in total						
Pumping	start: 09:04	end: 15:30					
SAMPLE COLLECTION							
Date	**29-May-97**						
Time	12:10 - 14:40	14:44 - 14:51	14:51 - 15:00	15:00 - 15:08	15:09 - 15:17	15:18 - 15:27	After 15:30
Sample number	101502	101501	101501	101501	101502	101502	Filter
Analyte	radionuclide analysis-acidified	elemental analysis - acidified	elemental analysis - non acidified	I-129; Cl-36	C-14	LLNL	radionuclide analysis
Preservatives	HCl	HCl	None	None	$HgCl_2$	None	None
Container	20 L in card board box	1 L PE Bottle	1 L PE Bottle	1 L PE Bottle	1 L PE Bottle	1 L PE bottle	100 ml PE bottle (See comment 8)
Amount collected	20 L	1 L	1 L	1 L	1 L	1 L	
Type of pump	Heydolph Rumo, 100 peristaltic pump, 2 "pump heads"						

CALIBRATION OF Eh ELECTRODE					
	Reading [mV]	Ag/AgCl [mV]	SHE* [mV]	T [°C]	Δ SHE* [mV]
Before sampling	186	218	424	26	238
After sampling	176	209	410	32	234

FIELD PARAMETERS				
Time	10:10	11:00	12:00	15:30
Pump rate [l / h]	8,6	8,3	8,2	
^3H [Bq /m^3]	8.45 · 10 E + 6	8.17 E + 6	8.19 E + 6	8.39 E + 6
pH	7,45	7,48	7,52	7,18
Eh [mV (SHE*)]	+90	+57	+53	+73
Temperature [°C]	28	30	32	33

TIDE	high 15:31	low 09:20	
PRESSURE TEST (after sampling)	30,25 bar (compressed air)		
WEATHER (sun/rain/wind)	Sunny; no wind - about 28°C.		

COMMENTS

1) The first "dead volume" was discarded. The water was clear.
2) The 450 nm filter and the Eh/pH/T measurement box were installed at 10.04.
3) No degassing or precipitation was observed in the measurement box.
4) Eh readings: ± 3-7 mV.
5) Temperature of sample influenced by sunshine.
6) The pH and Eh were stable since 11:34 at about pH 7,50-7,52 and Eh +53 mV/+65 mV. It changed suddenly at 15:20; pH 7,18 and Eh +73 mV and increased in the last minutes of the sampling (see above: 15:30). Possibly a tidal influence
7) Measurement of the lagoon water: pH 8,18
   Eh + 368 mV (SHE)
   T 26°C
8) The filter contains the residue of about 44 L of sample water

PREPARED BY

E. Warnecke
S. Mulsow

* SHE - Standard Hydrogen Electrode

SAMPLE COLLECTION LOG 3

SAMPLE LOCATION						
Well	**FUSEAU 30 (Fangataufa)**					
Depth	193 m					
Number of tubes	3 (red, yellow and gray tube)					
Inner diameter	4 mm					
"dead volume"	2,43 L per tube; 7.3 L in total					
Pumping	start: 10:53	end: 14:32				
SAMPLE COLLECTION						
Date	**30-May-97**					
Time	12:45 - 14:08	14:08 - 14:12	14:13 - 14:17	14:18 - 14:22	14:23 - 14:27	After 14:32
Sample number	101602	101601	101601	101601	101602	Filter
Analyte	radionuclide analyses-acidified	elemental analyses - acidified	elemental analyses - non acidified	I-129; Cl-36	C-14	radionculide analysis
Preservatives	HCl	HCl	None	None	$HgCl_2$	None
Container	20 L in card board box	1 L PE Bottle	1 L PE Bottle	1 L PE Bottle	1 L PE Bottle	100 ml PE Bottle
Amount collected	20 L	1 L	1 L	1 L	1 L	(See comment 6)
Type of pump	Heydolph Rumo, 100 peristaltic pump; 2 pumps with 3 "pump heads".					

CALIBRATION OF Eh ELECTRODE					
	Reading [mV]	Ag/AgCl [mV]	SHE* [mV]	T [°C]	Δ SHE* [mV]
Before sampling	179	214	417	29	238
After sampling	180	216	421	27,5	241

FIELD PARAMETERS				
Time	11:30	12:05	12:35	14:32
Pump rate [l / h]	15,3	15,6	15,9	14,1
^3H [Bq / m^3]	3.44 · 10 E + 6	3.74 · 10 E + 6	3.75 · 10 E + 6	3.65 · 10 E + 6
pH	-	7,47	7,39	7,37
Eh [mV (SHE*)]	-	+186	+225	+246
Temperature [°C]	27	27	28	28

TIDE	high 10:17	low 16:27	
PRESSURE TEST (after sampling)	20,08 bar (compressed air)		
WEATHER (sun/rain/wind)	Rain (morning); sunny (afternoon); windy - 28°C		

COMMENTS

1) The first "dead volume" was discarded. Slight smell of H2S, light yellow color.
2) The 450 nm filter was installed at 11:35 but it was leaking. Reinstallation with new filter and installation of the measurement box behind the pump at 11:52.
3) No degassing or precipitation was observed in the measurement box. The color of the solution before the filter changed sometimes to yellow between 13:10 and 13:35.
4) The 3 "pump heads" produced slightly different amounts of water (5,25; 5,70 and 5,55 l/h; in total 16, 3 l/h whereas the combined flow was about 15, 3 l/h (at 11:30).
5) The pH was stable between 7,36 and 7, 40. The Eh increased from +186 mV (at 12:05) to +246 mV (at about 13:15) and was then stable around this value. This effect can be correlated to the tide.
6) Filter: orange colored precipitate (Fe III). The sludge results from a water volume of about 40 L.

PREPARED BY

E. Warnecke
S. Mulsow

* SHE - *Standard Hydrogen Electrode*

SAMPLE COLLECTION LOG 4

SAMPLE LOCATION						
Well	**MITRE 27 (Fangataufa)**					
Depth	239 m					
Number of tubes	4 (white, yellow, red and blue tube)					
Inner diameter	4 mm					
"dead volume"	3,00 L per tube; 12 L in total					
Pumping	start: 08:50 end: 12:10					
SAMPLE COLLECTION						
Date	**31-May-97**					
Time	10:50 - 11:50	11:51 - 11:54	11:55 - 11:58	11:58 - 12:01	12:02 - 12:05	After 12:10
Sample number	101702	101701	101701	101701	101702	Filter
Analyte	radionuclide analyses-acidified	elemental analyses - acidified	elemental analyses - non acidified	I-129; Cl-36	C-14	radionuclide analysis
Preservatives	HCl	HCl	None	None	$HgCl_2$	None
Container	20 L in card board box	1 L PE Bottle	1 L PE Bottle	1 L PE Bottle	1 L PE Bottle	100 ml PE bottle
Amount collected	20 L	1 L	1 L	1 L	1 L	(See comment 6)
Type of pump	Heydolph Rumo, 100 peristaltic pump					

CALIBRATION OF Eh ELECTRODE					
	Reading [mV]	Ag/AgCl [mV]	SHE* [mV]	T [°C]	Δ SHE* [mV]
Before sampling	182	215	420	28	238
After sampling	179	217	422	27	243

FIELD PARAMETERS				
Time	09:35	10:05	10:35	12:10
Pump rate [l / h]	20,3	20,4	20,4	20,4
^3H [Bq / m^3]	1.02 E + 4	4.20 E + 4	3.70 E + 3	≤ 5.6 E + 3
pH	8,15	8,18	8,2	8,19
Eh [mV (SHE*)]	+77	+67	+62	+105
Temperature [°C]	27	27	27	27

TIDE	high 11:07		low 17:19	
PRESSURE TEST (after sampling)	24,34 bar (compressed air)			
WEATHER (sun/rain/wind)	Cloudy; strong wind - boat could not return to Mururoa, T ~ 28°C			

COMMENTS

1) The first "dead volume" was discarded. Slight smell of H2S, black color; same gas bubbles.
2) The 450 nm filter and the Eh/pH measurement box were installed at 9:27.
3) No degassing or precipitation in the measurement box, clear solution after filter.
4) The Eh increased from about + 62 mV (SHE) to + 105 mV (SHE) after high tide. The Eh readings were very stable (± 1 mV).
5) The 4 "pump heads" produced 96; 96; 95 and 98 ml/min which is in total 366 ml/min. or 21;96 l/h. The combined flow was only 20.4 l/h.
6) Filter sludge results from a water volume of about 55 L.

PREPARED BY

E. Warnecke
S. Mulsow

* SHE - Standard Hydrogen Electrode

SAMPLE COLLECTION LOG 5

SAMPLE LOCATION							
Well	**CETO**						
Depth	513 m; 507 m (vertical)						
Number of tubes	1						
Inner diameter	8 mm						
"dead volume"	25,8 L						
Pumping	start: 09:02	end: 14:20					
SAMPLE COLLECTION							
Date	**01-Jun-97**						
Time	12:58 - 13:58	14:00 - 14:03	14:03 - 14:07	14:07 - 14:10	14:10 - 14:13	14:13 - 14:17	After 14:17
Sample number	101802	101801	101801	101801	101802	101802	Filter
Analyte	radionuclide analysis-acidified	elemental analyses - acidified	elemental analyses - non acidified	I-129; Cl-36	LLNL	C-14	radionuclide analysis
Preservatives	HCl	HCl	None	None	None	$HgCl_2$	None
Container	20 l in card board box	1 L PE Bottle	1 L PE Bottle	1 L PE Bottle	1 L PE Bottle	1 L PE Bottle	100 ml PE bottle
Amount collected	20 L	1 L	1 L	1 L	1 L	1 L	(See comment 5)
Type of pump	Heydolph Rumo, 100 peristaltic pump, 2 "pump heads"						

CALIBRATION OF Eh ELECTRODE	Reading [mV]	Ag/AgCl [mV]	SHE* [mV]	T [°C]	Δ SHE* [mV]
Before sampling	181	217	422	27	241
After sampling	180	217	422	27	242

FIELD PARAMETERS				
Time	10:26	11:40	12:55	14:17
Pump rate [l / h]	22,2	22,2	22,5	20,6
^3H [Bq / m^3]	2.17 · 10 E + 10	2.02 · 10 E + 10	2.1 · 10 E + 10	2.13 · 10 E + 10
pH	7,28	7,31	7,33	7,35
Eh [mV (SHE*)]	+48	+22	+15	+9
Temperature [°C]	28	27	27	27

TIDE	high 18:08	low 11:54		
PRESSURE TEST (after sampling)	49,8 bar (compressed air)			
WEATHER (sun/rain/wind)				

COMMENTS

1) The water was slightly yellow (Fe III).
2) The 450 nm filter and the Eh/pH/T measurement box were installed at 10:10.
3) Pressure verification of sampling depth 49,8 bar in a second attempt because the first failed.
   Probelms to find clear evidence of sampling depth.
4) Some degassing was observed .
5) The precipitate on the filter results from a volume of 92 L of water.

PREPARED BY

S. Mulsow

* SHE - Standard Hydrogen Electrode

SAMPLE COLLECTION LOG 6

SAMPLE LOCATION							
Well	**GEO 10**						
Depth	307 m and 311 m						
Number of tubes	2						
Inner diameter	4 mm						
"dead volume"	3,9 L per tube; 7,8 L in total						
Pumping	start: 08:54 end: 16:30						
SAMPLE COLLECTION							
Date	**02-Jun-97**						
Time	12:02 - 14:24	14:28 - 15:50	15:50 - 15:58	15:58 - 16:08	16:08 - 16:15	16:15 - 16:23	After 16:30
Sample number	101902	101902	101901	101901	101902	101902	Filter
Analyte	radionuclide analyses acidified	elemental analyses - non-acidified	elemental analyses acidified	I-129; Cl-36	C-14	LLNL	radionuclide analyses
Preservatives	HCl	None	None	None	$HgCl_2$	None	None
Container	20 L in card board box	10 L PE Bottle	1 L PE Bottle	1 l PE Bottle	1 l PE Bottle	1 l PE Bottle	100 ml PE Bottle
Amount collected	20 L	10 L	1 L	1 L	1 L	1 L	(See comment 7)
Type of pump	Heydolph Rumo, 100 peristaltic pump, 2 "pump heads"						

CALIBRATION OF Eh ELECTRODE					
	Reading [mV]	Ag/AgCl [mV]	SHE* [mV]	T [°C]	Δ SHE* [mV]
Before sampling	182	214	417	29	235
After sampling	186	217	422	27	236

FIELD PARAMETERS				
Time	10:55	11:25	11:55	16:30
Pump rate [l / h]	8,1	8,2	8,1	7,65
^3H [Bq / m^3]	7.47 · 10 E 6	7.58 · 10 E 6	7.54 · 10 E 6	7.88 · 10 E 6
pH	7,66	7,65	7,66	7,65
Eh [mV (SHE*)]	+50	+52	+52	+169
Temperature [°C]	28	29	29	28

TIDE	high	12:40	low	18:55
PRESSURE TEST (after sampling)	31,15 bar (compressed air)			
WEATHER (sun/rain/wind)	Sunny			

COMMENTS

1) The first "dead volume" was discarded. Gas bubbles were found in the solution before the pump. The solution was at the beginning almost clear and became yellow at 10:55. It was clear after the filter.
2) The 450 nm filter and measurement box were installed at 10:14. The filter leaked and was reinstalled at 10:36
3) No degassing or precipitation in the pH/Eh measurement box.
4) The Eh increased from about + 52 mV (SHE) to + 169 mV (SHE) after the high tide.
5) The 2 "pump heads" produced 138 ml/min and 142 ml/min. The combined flow was 280 ml/h which is 8,4 l/h. The flow decreased to 8,1 l/h after filtering. It decreased at 16:25 to 7,65 l/h.
6) The Eh readings were ± 4 to ± 7 mV.
7) The filter contains the residue from about 48 L of sample water.

PREPARED BY

E. Warnecke
S. Mulsow

* SHE - Standard Hydrogen Electrode

SAMPLE COLLECTION LOG 7

SAMPLE LOCATION						
Well	**GEO 8**					
Depth	*274 m, 276 m and 278 m*					
Number of tubes	3					
Inner diameter	4 mm					
"dead volume"	3,5 L per tube; 10,5 L in totall					
Pumping	start: 09:22	end: 14:37				
SAMPLE COLLECTION						
Date	**03-Jun-97**					
Time	11:40 - 13:40	13:40 - 14:02	14:03 - 14:07	14:07 - 14:12	14:12 - 14:17	After 14:37
Sample number	102001	102001	102001	102001	102002	Filter ?
Analyte	radionuclide analayses acidified	elemental analyses - non-acidified	elemental analyses acidified	I-129; Cl-36	C-14	radionuclide analyses
Preservatives	HCl	None	HCl	None	$HgCl_2$	None
Container	20 L in card board box	10 L PE Bottle	1 L PE Bottle	1 L PE Bottle	1 L PE Bottle	100 ml PE bottle
Amount collected	20 L	5 L	1 L	1 L	1 L	(See comment 5)
Type of pump	Heydolph Rumo 100, peristaltic pump; 3 "pump heads".					

CALIBRATION OF Eh ELECTRODE					
	Reading [mV]	Ag/AgCl [mV]	SHE* [mV]	T [°C]	Δ SHE* [mV]
Before sampling	189	218	425	26	236
After sampling	190	218	425	26	235

FIELD PARAMETERS				
Time	10:25	11:10	11:35	14:17
Pump rate [l / h]	13,5	?	?	13,5
^3H [Bq / m^3]	1.4 · 10 E 6	1.43 · 10 E 6	1.42 · 10 E 6	1.35 · 10 E 6
pH	7,91	7,94	7,95	7,92
Eh [mV (SHE*)]	319	202	200	207
Temperature [°C]	26	28	28	29

TIDE	high	13:24	low	19:40
PRESSURE TEST (after sampling)	28.13 bar	(compressed air)		
WEATHER (sun/rain/wind)	Sunny, warm, no clouds			

COMMENTS

1) First dead volume discarded.
2) Gas bubbles noted in poly tubes before reaching pump.
3) Solution clear - no reddish color.
4) 10:33 connect 450 nm filter; 14:26 disconnect filter.
5) Total of 54 liters of fluid passed through the 450 nm filter.

PREPARED BY

D. Smith
E. Warnecke
S. Mulsow

* SHE - Standard Hydrogen Electrode

SAMPLE COLLECTION LOG 8

SAMPLE LOCATION						
Well	**ISURUS 10**					
Depth	265 m					
Number of tubes	4					
Inner diameter	4 mm					
"dead volume"	3,5 L per tube; 14 L in total					
Pumping	start: 08:57	end: 14:35				
SAMPLE COLLECTION						
Date	**04-Jun-97**					
Time	12:22 - 13:40	13:40 - 14:17	14:17 - 14:20	14:20 - 14:25	14:25 - 14:29	After 14:29
Sample number	101202	101201	101201	101201	101202	Filter
Analyte	radionuclide analayses acidified	elemental analyses - non-acidified	elemental analyses acidified	I-129; Cl-36	C-14	radionuclide analyses
Preservatives	HCl	None	HCl	None	$HgCl_2$	None
Container	20 L in card board box	10 L PE Bottle	1 L PE Bottle	1 L PE Bottle	1 L PE Bottle	100 ml PE Bottle
Amount collected	20 L	10 L	1 L	1 L	1 L	(See comment 5)
Type of pump	Heydolph Rumo 100, peristaltic pump; 4 "pump heads"					

CALIBRATION OF Eh ELECTRODE					
	Reading [mV]	Ag/AgCl [mV]	SHE* [mV]	T [°C]	Δ SHE* [mV]
Before sampling	192	218	425	26	233
After sampling	185	215	420	28	235

FIELD PARAMETERS				
Time	10:10	11:10	12:17	14:30
Pump rate [l / h]	16.6			15.8
^3H [Bq /m^3]	4.82 · 10 E 5	4.89 · 10 E 5	4.81 · 10 E 5	4.82 · 10 E 5
pH	7,92	7,92	7,92	7,93
Eh [mV (SHE*)]	66	126	158	188
Temperature [°C]	30	30	31	29

TIDE	high 14:08	low 20:23	
PRESSURE TEST (after sampling)	26.27 bar (compressed air)		
WEATHER (sun/rain/wind)	Sunny, high clouds, showers (afternoon)		

COMMENTS

1) First dead volume discarded.
2) No gas bubbles noted in poly tubes before reaching pump.
3) Solution initially had a reddish color, but cleared after first dead volume.
4) 09.35 connect 450 nm filter, 14:35 disconnect filter.
5) Total of 80 liters passed through the 450 nm filter.

PREPARED BY

D. Smith
S. Mulsow

* SHE - Standard Hydrogen Electrode

SAMPLE COLLECTION LOG 9

SAMPLE LOCATION						
Well	**MURENE 16**					
Depth	230 m					
Number of tubes	3					
Inner diameter	4 mm					
"dead volume"	2,9 L per tube; 8,7 L in total					
Pumping	start: 08:49 end: 14:06					
SAMPLE COLLECTION						
Date	**05-Jun-97**					
Time	11:27 - 12:49	12:51 - 13:40	13:40 - 13:44	13:44 - 13:48	13:48 - 13:52	After 13:50
Sample number	102202	102201	102201	102201	102202	Filter
Analyte	radionuclide analayses acidified	elemental analyses - non-acidified	elemental analyses acidified	I-129; Cl-36	C-14	radionuclide analyses
Preservatives	HCl	None	None	None	$HgCl_2$	None
Container	20 L in card board box	10 L PE Bottle	1 L PE Bottle	1 L PE Bottle	1 L PE Bottle	100 ml PE Bottle
Amount collected	20 L	10 L	1 L	1 L	1 L	(See comment 6)
Type of pump	Heydolph Rumo 100, peristaltic pump; 3 "pump heads"					

CALIBRATION OF Eh ELECTRODE	Reading [mV]	Ag/AgCl [mV]	SHE* [mV]	T [°C]	Δ SHE* [mV]
Before sampling	184	217	422	27	238
After sampling	178	212	415	30	237

FIELD PARAMETERS				
Time	09:35	10:35	11:22	14:00
Pump rate [l / h]	13.6			13,5
^3H [Bq /m^3]	1.0 · 10 E + 7	1.01 · 10 E + 7	9.89 · 10 E + 6	1.0 · 10 E 7
pH	7,26	7,18	7,19	7,19
Eh [mV (SHE*)]	227	202	200	215
Temperature [°C]	27	29	30	30

TIDE	high 14:51	low 21:06		
PRESSURE TEST (after sampling)	23.71 bar (compressed air)			
WEATHER (sun/rain/wind)	Sunny, warm, occasional high clouds			

COMMENTS

1) First dead volume discarded.
2) No gas bubbles noted in poly tubes before reaching pump.
3) Solution clear, even in first dead volume.
4) 450 nm filter was clear at the end of the day.
5) 09:38 connect 450 nm filter; 13:56 disconnect filter.
6) Total of 72 liters passed through the 450 nm filter.
7) Measurement of lagoon water: pH 8,17
   Eh +435 mV (SHE)
   T 26°C

PREPARED BY

D. Smith
S. Mulsow

* SHE - Standard Hydrogen Electrode

SAMPLE COLLECTION LOG 10

SAMPLE LOCATION						
Well	**TAZARD 14**					
Depth	245 m					
Number of tubes	4					
Inner diameter	4 mm					
"dead volume"	3,1 L per tube; 12.4 L in total					
Pumping	start: 08:17 end: 13:18					
SAMPLE COLLECTION						
Date	**06-Jun-97**					
Time	11:08 - 12:22	12:22 - 13:00	13:00 - 13:04	13:04 - 13:08	13:08 - 13:11	After 13:11
Sample number	102302	102301	102301	102301	102302	Filter
Analyte	radionuclide analayses acidified	elemental analyses - non-acidified	elemental analyses acidified	I-129; Cl-36	C-14	radionuclide analyses
Preservatives	HCl	None	HCl	None	$HgCl_2$	None
Container	20 L in card board box	10 L PE Bottle	1 L PE Bottle	1 L PE Bottle	1 L PE Bottle	100 ml PE Bottle
Amount collected	20 L	10 L	1 L	1 L	1 L	(See comment 7)
Type of pump	Heydolph Rumo 100, peristaltic pump; 4 "pump heads"					

CALIBRATION OF Eh ELECTRODE	Reading [mV]	Ag/AgCl [mV]	SHE* [mV]	T [°C]	Δ SHE* [mV]
Before sampling	189	218	425	26	236
After sampling	178	210	413	31	235

FIELD PARAMETERS				
Time	09:15	10:12	11:05	13:11
Pump rate [l / h]	15,8			17,0
^3H [Bq /m^3]	6.88 · 10 E + 6	6.84 · 10 E + 6	6.89 · 10 E + 6	6.93 · 10 E + 6
pH	6,82	7,28	7,31	7,32
Eh [mV (SHE*)]	172	138	141	130
Temperature [°C]	27	27	28	30

TIDE	high	15:38	low	21:47
PRESSURE TEST (after sampling)	24.95 bar (compressed air)			
WEATHER (sun/rain/wind)	Rain (morning); the rest a bit sunny and little wind.			

COMMENTS

1) First dead volume discarded.
2) No gas bubbles noted in poly tubes before reaching pump.
3) Solution clear - no reddish color.
4) 450 nm filter slightly reddish at end of the day.
5) Eh/pH cell had slight leak in morning; repaired.
6) 09:18 connect 450 nm filter; 13:17 disconnect filter.
7) Total of 68 liters passed through the 450 nm filter.
8) Measurement of lagoon water: pH 8,11
   Eh +449 mV (SHE)
   T 26°C

PREPARED BY

D. Smith
S. Mulsow

* SHE - Standard Hydrogen Electrode

SAMPLE COLLECTION LOG 11

SAMPLE LOCATION						
Well	**GEO 5**					
Depth	215 m and 230 m					
Number of tubes	2					
Inner diameter	4 mm					
"dead volume"	2,7 L and 2,9 L, total 5,6					
Pumping	start: 09:30 end: 17:58					
SAMPLE COLLECTION						
Date	**07-Jun-97**					
Time	13:29 - 16:02	16:02 - 17:20	17:20 - 17:28	17:28 - 17:36	17:36 - 17:45	After 14:45
Sample number	102402	102401	102401	102401	102402	Filter
Analyte	radionuclide analayses acidified	elemental analyses - non-acidified	elemental analyses acidified	I-129; Cl-36	C-14	radionuclide analyses
Preservatives	HCl	None	HCl	None	$HgCl_2$	None
Container	20 L PE Bottle	10 L PE Bottle	1 L PE Bottle	1 L PE Bottle	1 L PE Bottle	100 ml PE Bottle
Amount collected	20 L	10 L	1 L	1 L	1 L	(See comment 6)
Type of pump	Heydolph Rumo 100, peristaltic pump; 2 "pump heads"					

CALIBRATION OF Eh ELECTRODE					
	Reading [mV]	Ag/AgCl [mV]	SHE* [mV]	T [°C]	Δ SHE* [mV]
Before sampling	188	214	417	29	229
After sampling	190	220	427	25	237

FIELD PARAMETERS				
Time	10:35	12:30	13:17	17:45
Pump rate [l / h]	6,0			6.9
^3H [Bq /m^3]	1.83 · 10 E + 4	1.64 · 10 E + 4	1.52 · 10 E + 4	1.89 · 10 E + 4
pH	7.69	7,71	7,7	7,76
Eh [mV (SHE*)]	245	240	250	279
Temperature [°C]	X33	36	35	26

TIDE	high 16:19		low 22:30	
PRESSURE TEST (after sampling)	22.07 bar (compressed air)			
WEATHER (sun/rain/wind)	Sunny all day and very hot up to 36°C; afternoon a bit windy and some showers (few minutes) after 4 p.m.			

COMMENTS

1) Had diffculty producing initially from this well; only 2 of 3 poly tubes were employed. Moved sampling station over sea-wall to lower head difference and facilitate pumping.
2) First dead volume discarded.
3) Solution was very reddish-brown throughout the day.
4) 10:45 connect 450 nm filter; 17:58 disconnect filter.
5) Due to low pump rate (6.0 to 7.0 L/hour), pumped into darkness when sampling was completed.
6) Total of 50 liters passed through the 450 nm filter.
7) Measurement of sea water: pH 8,81
   Eh +449 mV (SHE)
   T 26°C

PREPARED BY

D. Smith
S. Mulsow

* SHE - Standard Hydrogen Electrode

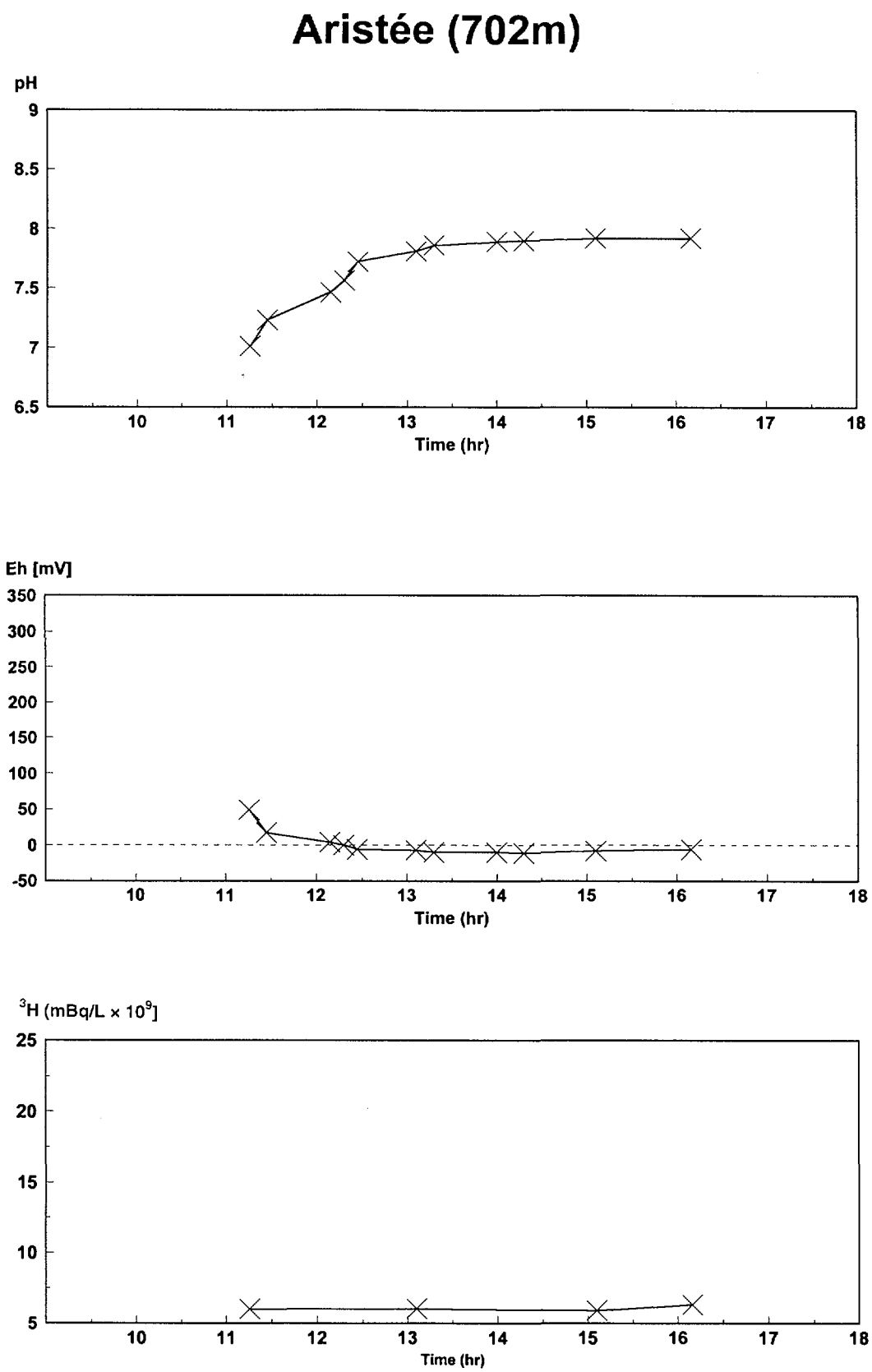

Log Chart 1: Development of pH, Eh and ^{3}H concentration during sampling (28 May 1997)

Pieuvre 37

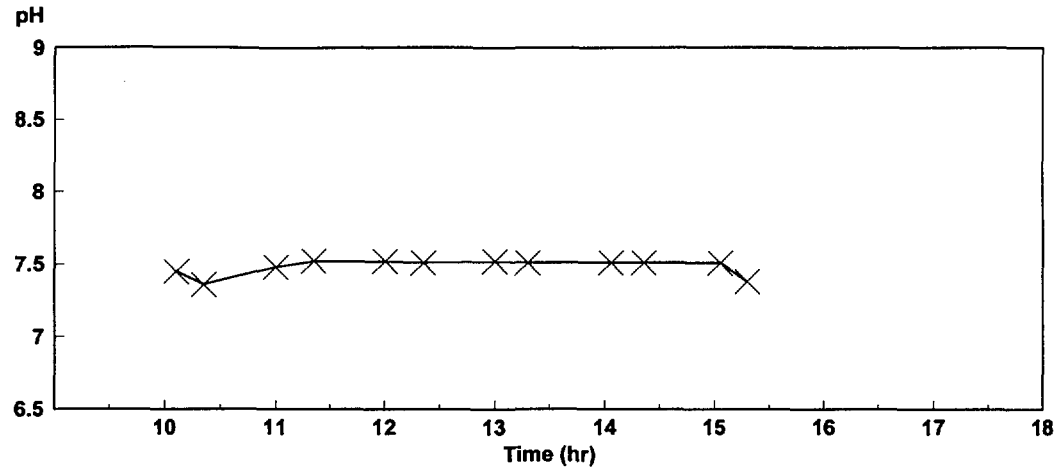

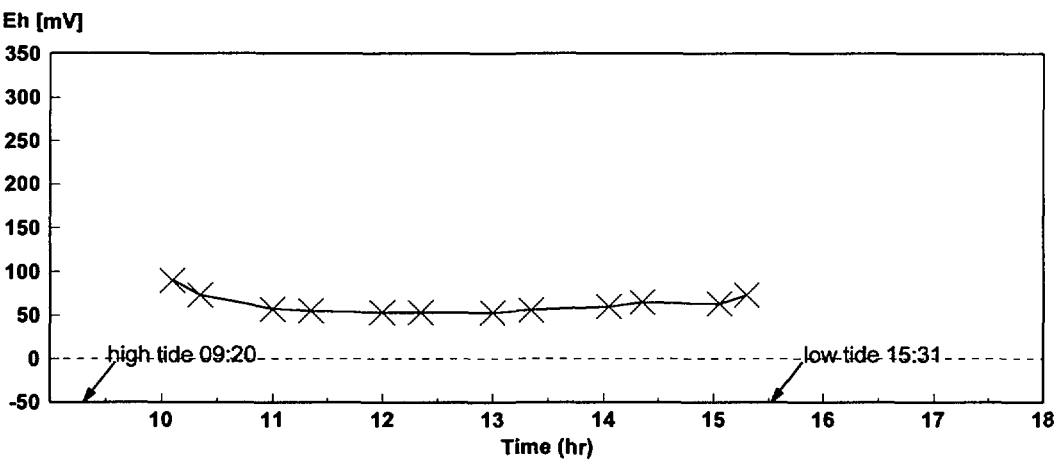

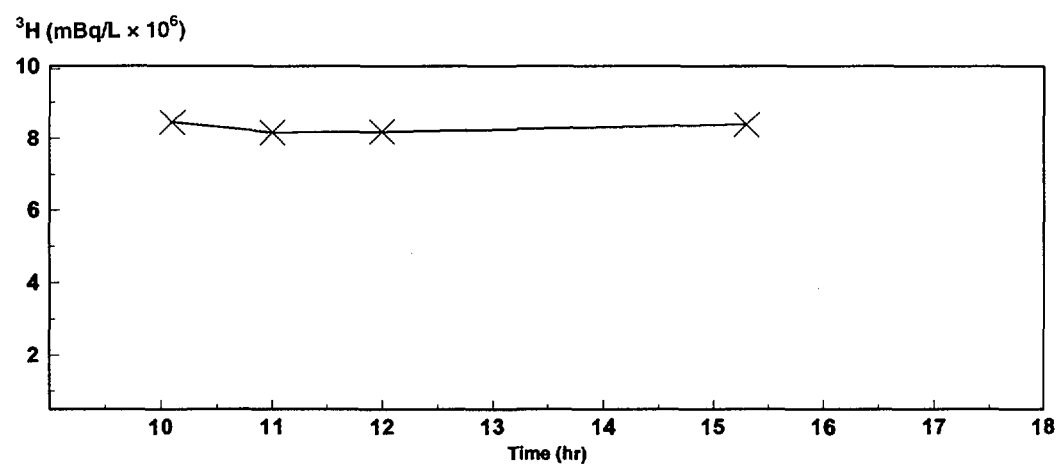

Log Chart 2: Development of pH, Eh and ^{3}H concentration during sampling (29 May 1997)

Fuseau 30 (Fangataufa)

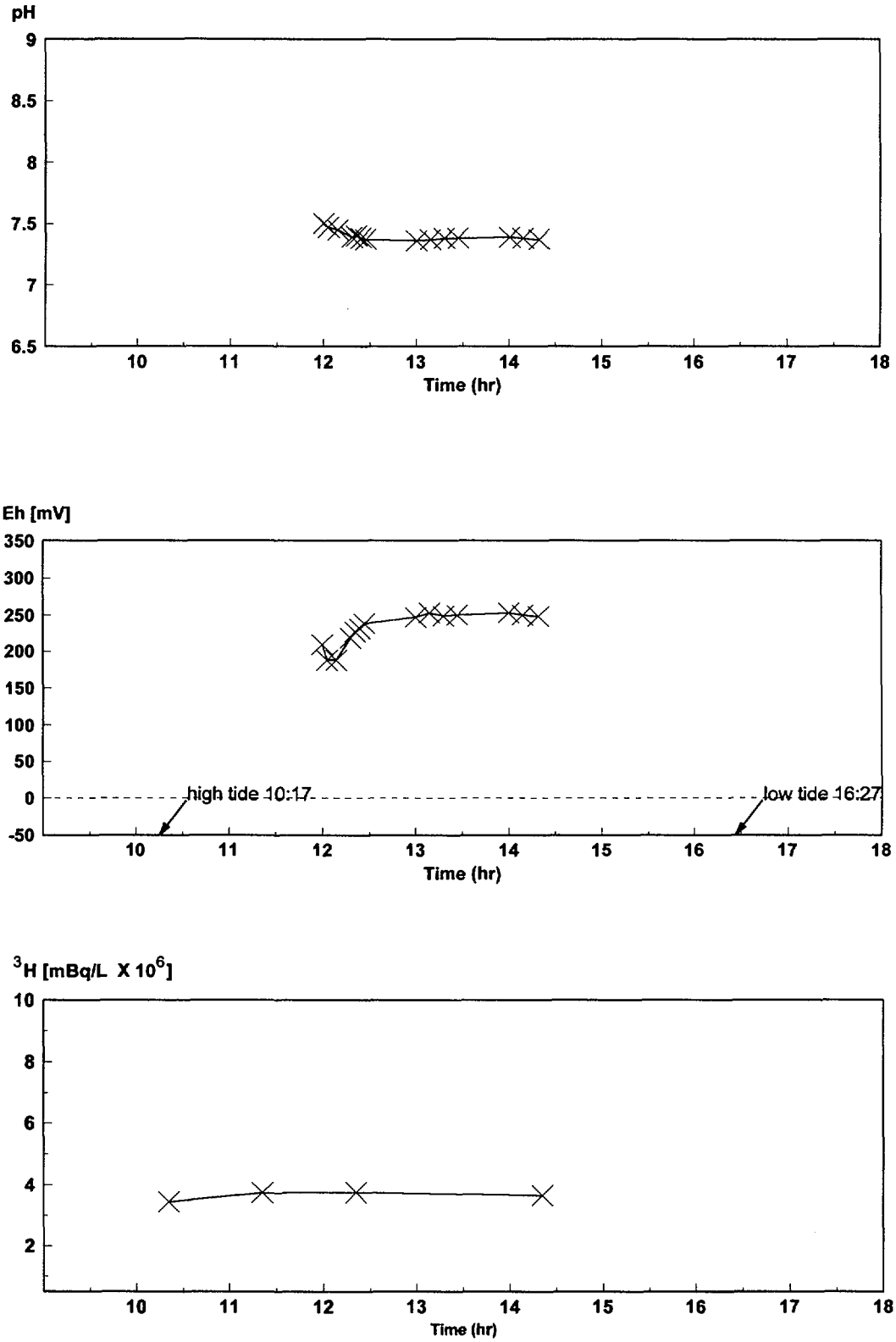

Log Chart 3: Development of pH, Eh and ^{3}H concentration during sampling (30 May 1997)

Mitre 27 (Fangataufa)

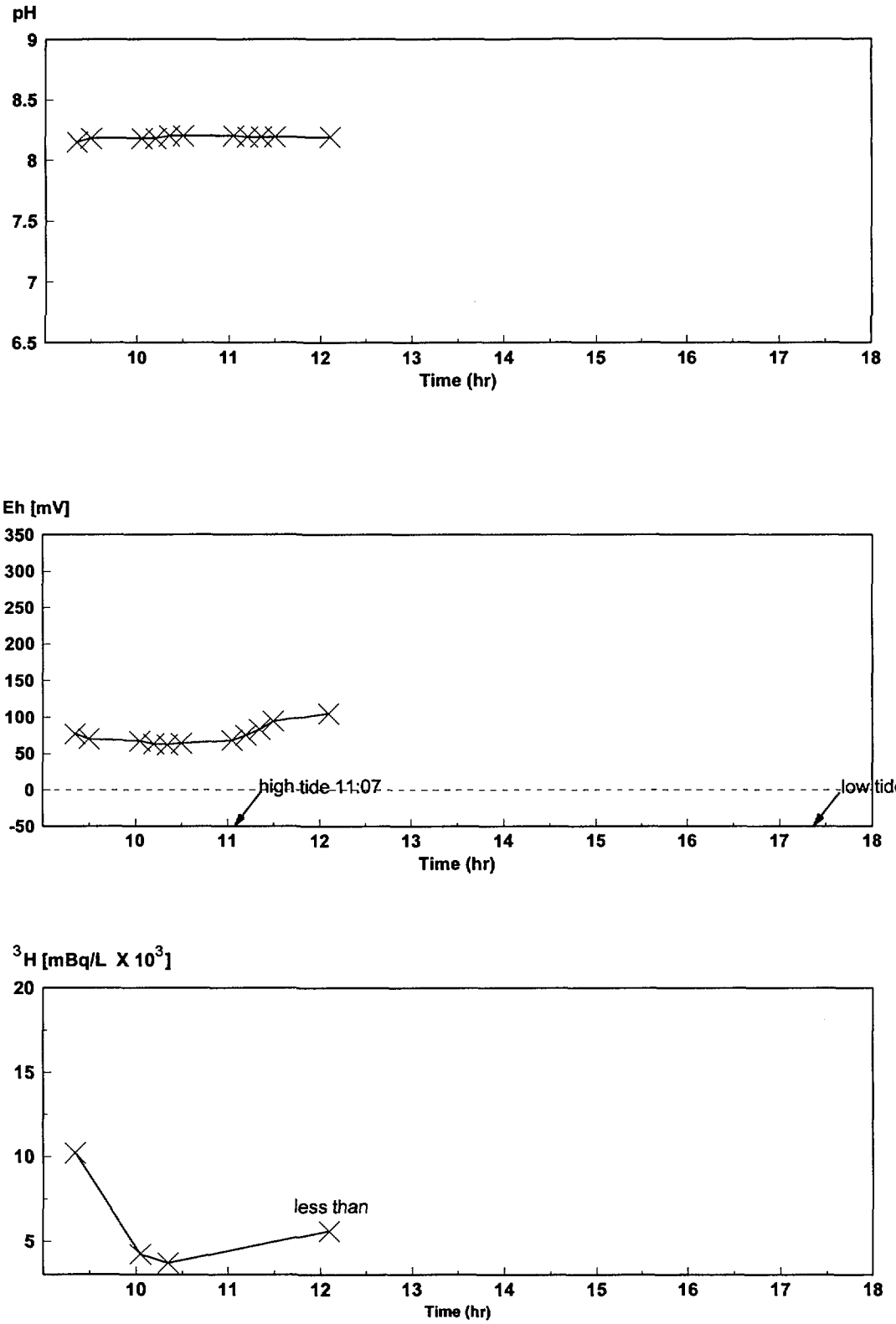

Log Chart 4: Development of pH, Eh and ^{3}H concentration during sampling (31 May 1997)

Céto (513m)

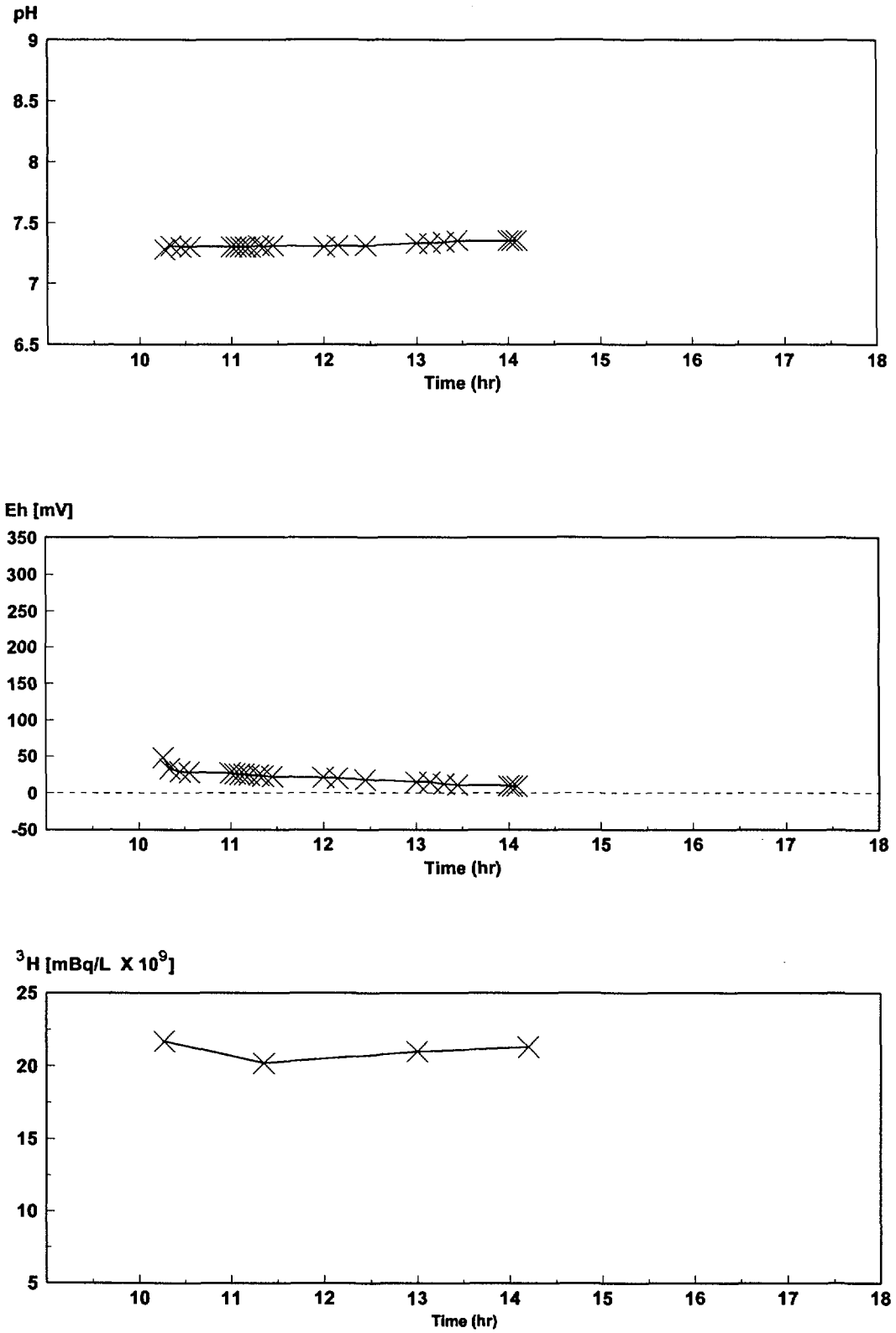

Log Chart 5: Development of pH, Eh and ^{3}H concentration during sampling (01 June 1997)

Géo 10

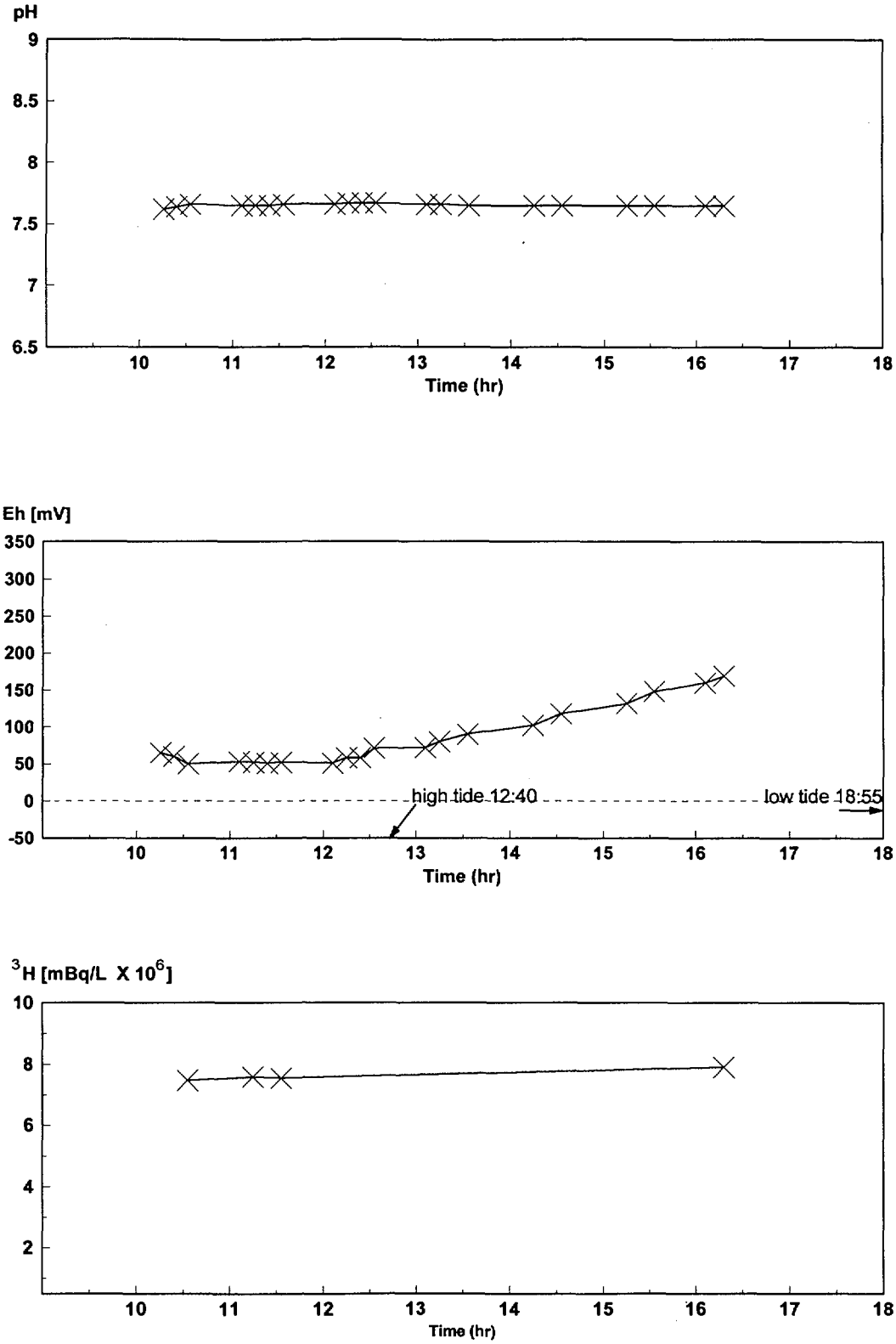

Log Chart 6: Development of pH, Eh and ^{3}H concentration during sampling (02 June 1997)

Géo 8

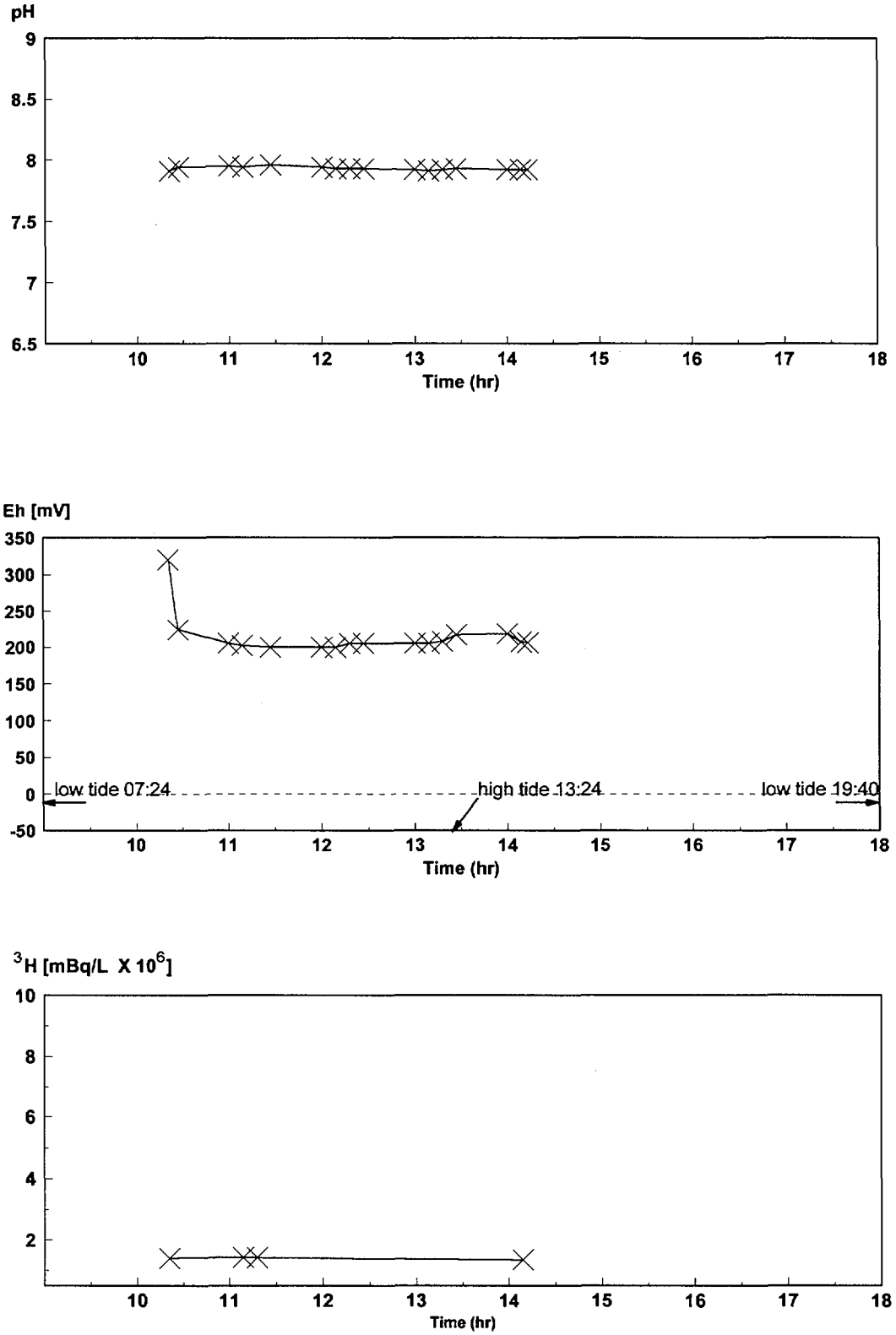

Log Chart 7: Development of pH, Eh and ^{3}H concentration during sampling (03 June 1997)

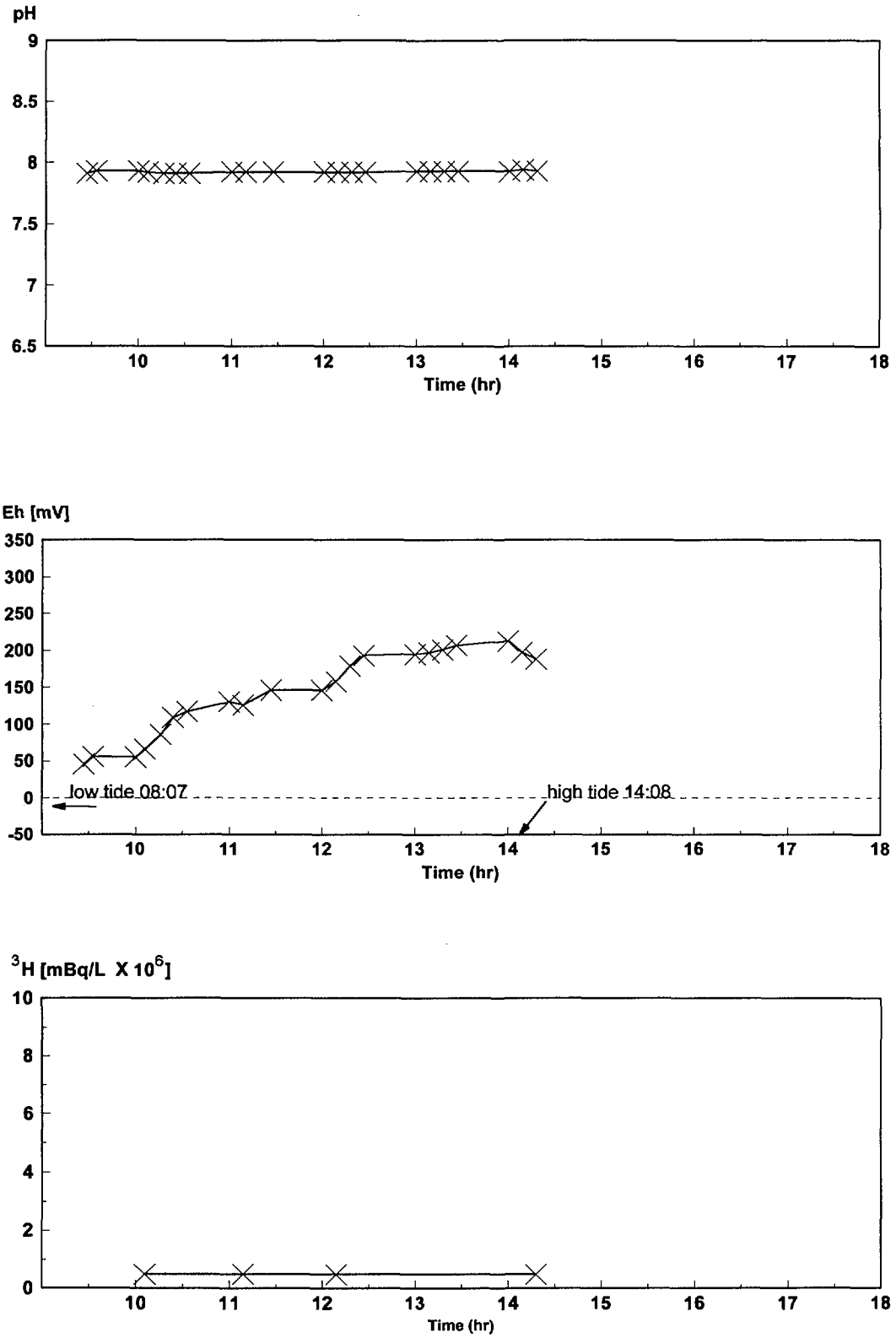

Log Chart 8: Development of pH, Eh and ^{3}H concentration during sampling (04 June 1997)

Murène 16

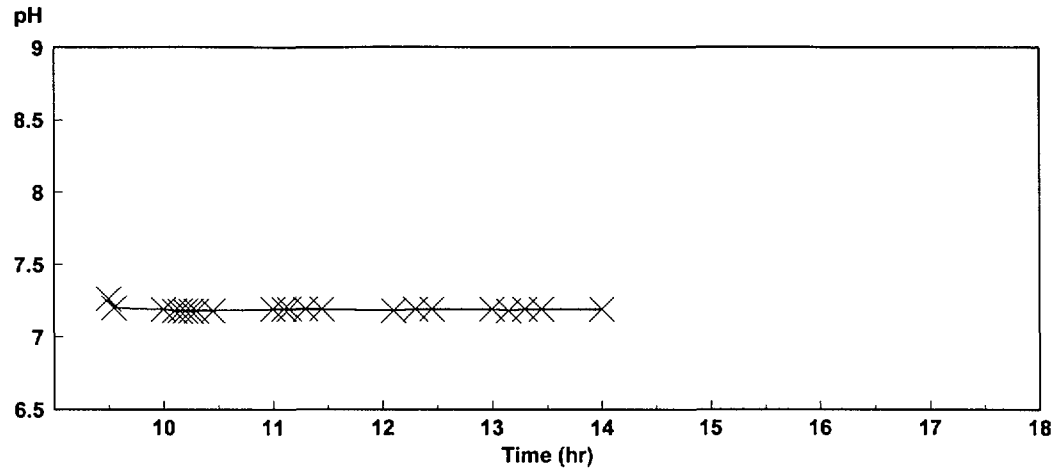

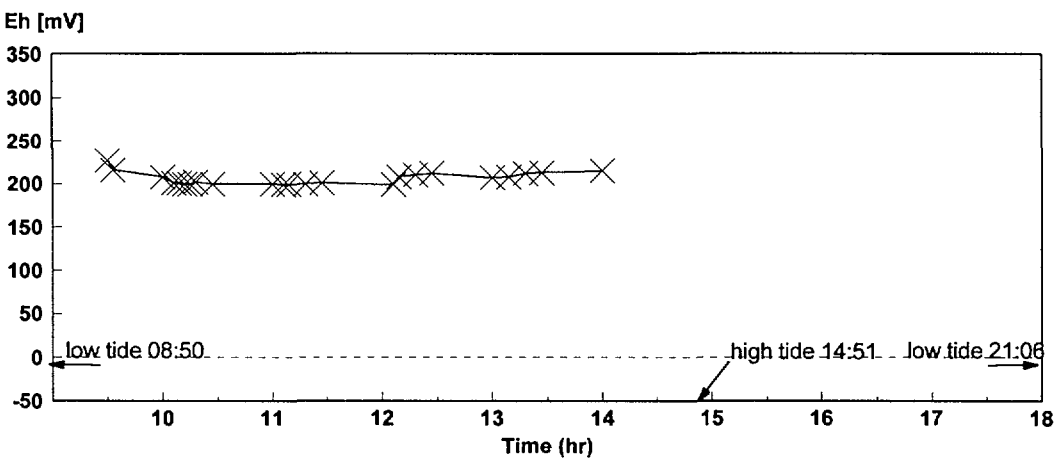

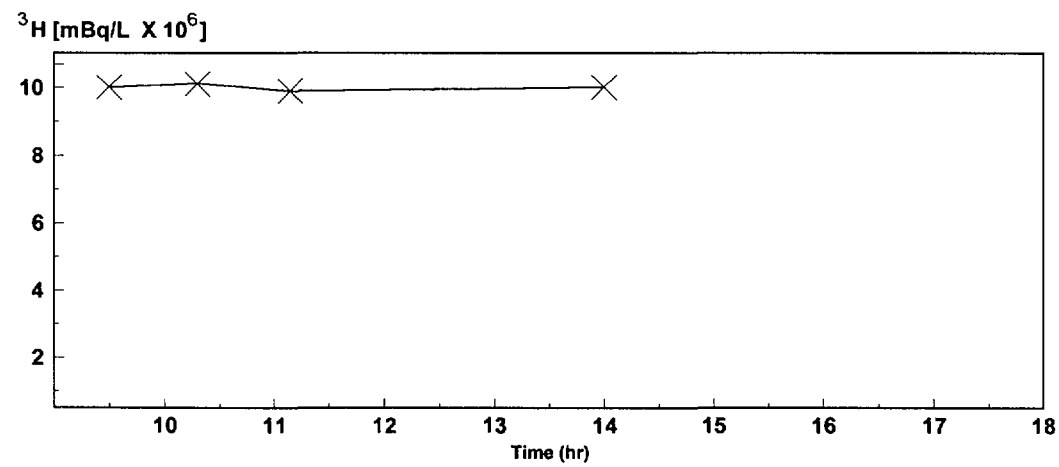

Log Chart 9: Development of pH, Eh and ^{3}H concentration during sampling (05 June 1997)

Tazard 14

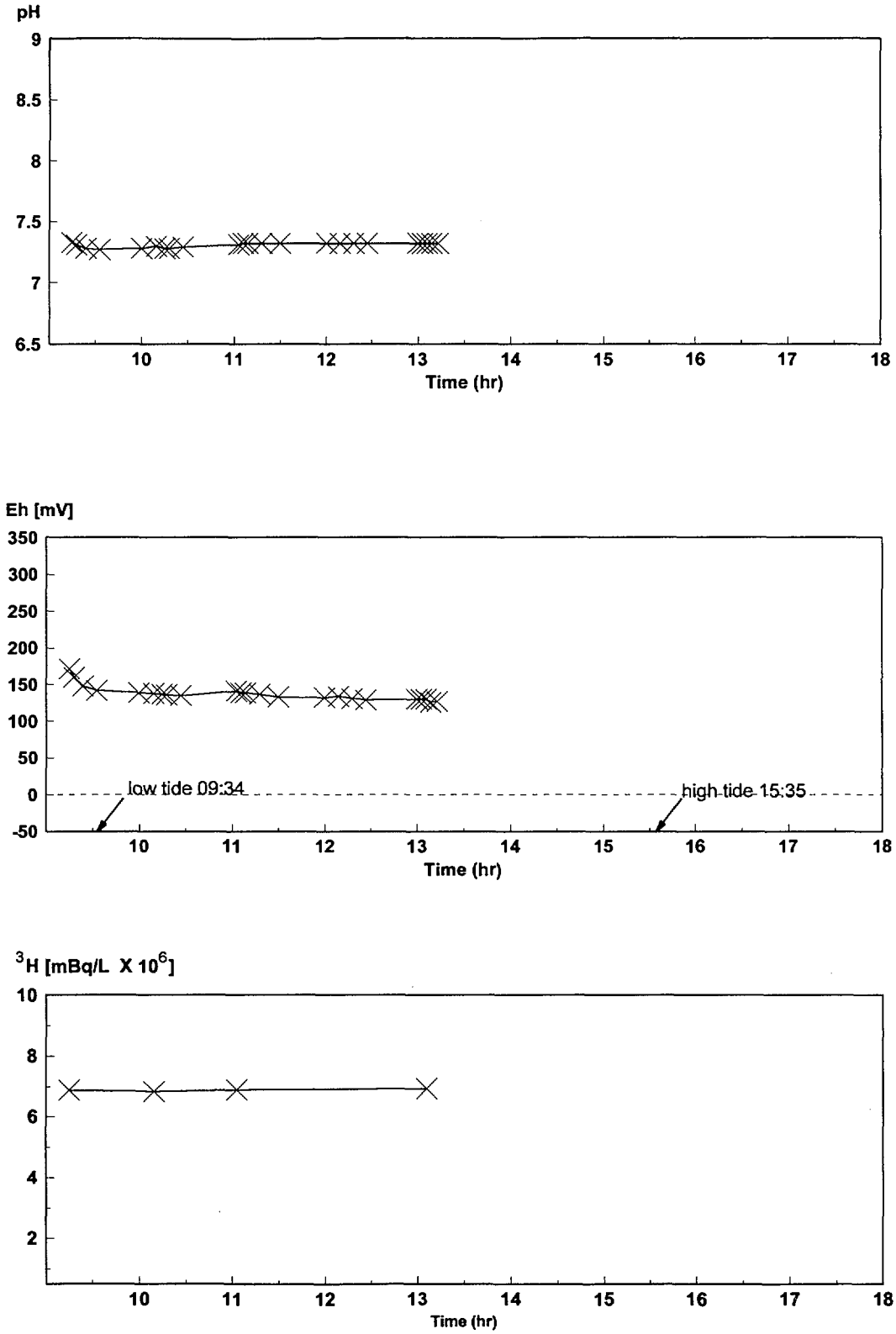

Log Chart 10: Development of pH, Eh and ^{3}H concentration during sampling (06 June 1997)

Gèo 5

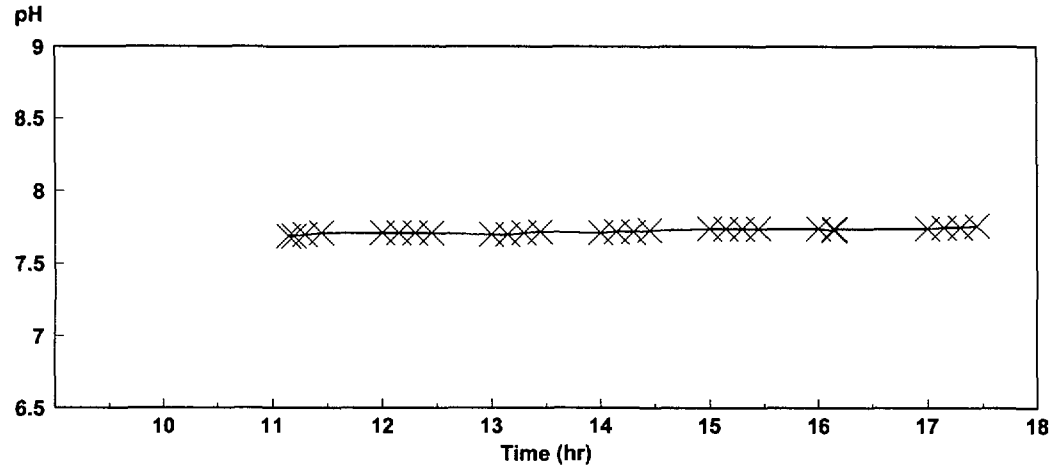

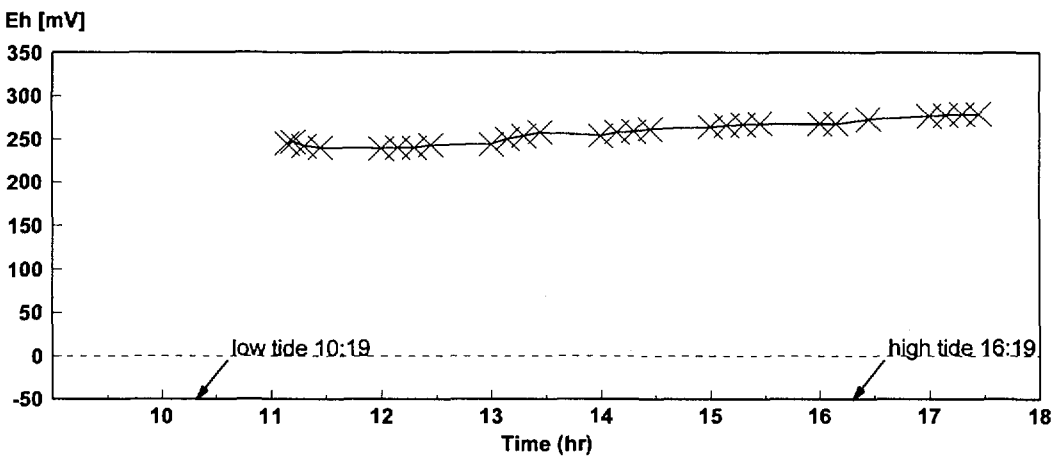

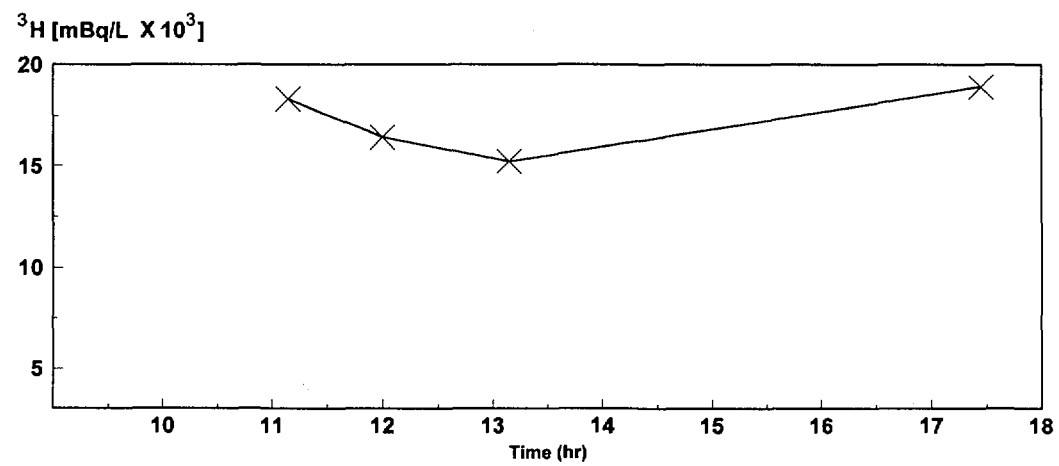

Log Chart 11: Development of pH, Eh and H concentration during sampling (07 June 1997)

Appendix VI

EXCERPT FROM CHAPTER 3 OF THE ATKINSON REPORT (1984)

Venting and Long-Term Leakage from the Underground Test Sites

3.1. INTRODUCTION

In this report venting refers to the loss of radioactivity from the intended geological confinement at the time of detonation, while leakage is restricted to the transport of radioactivity by water over any period of time after the vitrified material has cooled. As a consequence, venting is concerned with the inventory of fission and activation products arising from the detonation (or daughter products formed within a very short period) whereas leakage is also concerned with radionuclides that may take a considerable time (e.g. 1000 years) to grow in from the decay chain that was originated by a product of the detonation.

This chapter is divided into four parts:

- *Venting*
- *Long-term leakage*
- *Comparison with high-level radioactive waste repositories*
- *Conclusions*

3.2. VENTING

Radionuclides which, if detected at the surface, demonstrate that venting has occurred fall into three categories:

- *those that are short lived and are concentrated in marine organisms (e.g., ^{131}I in algae)*
- *those with moderate half-lives but which are not concentrated by marine organisms (e.g., ^{85}Kr, ^{3}H)*
- *those of long half-lives which may or may not be concentrated by marine organisms but which are present as well in global fallout (e.g., ^{90}Sr, ^{137}Cs)*

Because of the time that had elapsed between the then most recent French underground tests and the visit by the Mission, detection of the first class of radionuclides was not possible. For detection of the third class of radionuclides as evidence of venting, a prerequisite is a data base covering pre- and post-detonation sampling periods. This too was not an option on the minimal nature of the venting that occurs at Mururoa concentrated on ^{3}H and ^{85}Kr.

For radionuclides to be liberated during venting, they must be either volatile or have volatile precursors. Samples collected by the Mission were also analysed for other radionuclides that are produced with a high yield and have moderately long half-lives and large accumulation factors in marine organisms (e.g., ^{106}Ru). None of these radionuclides was found and, under the circumstances, none was expected.

3.2.1 Evidence of Venting

Within the sampling regime permitted, only one simple experiment could be construed as attempted verification of the claim [presumably by CEA scientists] *that no significant venting occurs at the time of nuclear detonation in their series of underground tests.*

In this experiment, which was sited ~1 km west of the industrial area and between the lagoon and the road to Viviane, an auger hole was drilled into the coral to a depth of ~1 m. Vinyl tubing was inserted to a depth of 62 cm, the borehole then filled with rice grains to about 10 cm from the top. A coral dust-water slurry was used to complete the filling of the borehole and mounded at ground surface.

The experiment was done on an incoming tide. The arrangement was intended to minimise the amount of atmospheric air passing vertically down the borehole and to maximise the amount of coral interstitial air driven by the incoming tide to the sampling tube. If venting from underground tests led to an increase in the amount of gaseous and volatile fission products then the concentration of these contaminants would be higher in the interstitial air than in atmospheric air.

Air was drawn from the sampling tube at 20 l min^{-1} for 170 minutes. It passed first through chemical absorbers to remove water and carbon dioxide and then through a bed of activated charcoal, to absorb noble gases, for example naturally occurring radon and, if present, the fission product ^{85}Kr.

In the event, ^{85}Kr could not be detected above the level of radon originating from the naturally occurring radium in the activated charcoal.

Water vapour absorbed on the desiccant was driven off by heat and condensed, 32.5 g was recovered. For the sampled air volume of 3400 l, this corresponds to a relative humidity of ~56% at 20°C. Clearly the desire to sample only interstitial air was only partially met.

The tritium (^{3}H) concentration in the absorbed water vapour was 0.5 Bq ml^{-1} which corresponds to 4.8 Bq m^{-3} in the sampled air. An acceptable derived air concentration (DAC) for members of the general public exposed continuously to tritiated water vapour is 2.7 kBq m^{-3} (1/100 of the occupational DAC), a factor of 560 times higher than that measured.

Levels of ^{3}H in southern hemisphere oceanic waters are largely due to atmospheric weapon testing in the northern hemisphere. They peaked in 1965 and have been decreasing since 1974 with a halving time of about five years.

Tritium levels for surface waters from the Tasman Sea, sampled in 1979, were reported to be in the range of 1.5-1.8 tritium units (Harries and Calf, 1980). (1 TU = 0.12 Bq l^{-1}.) Were it not for weapon testing by France, the tritum level in surface waters near Mururoa would be about 1.0 Bq l^{-1} - a factor of 5000 times lower than that measured in the absorbed water vapour.

Two explanations for the elevated tritium levels are offered:

(a) Venting of volatile and gaseous fission products through or past the back-filled drill hole used for placing the weapons for the underground test series - which the French admit does occur to a limited degree.

(b) A groundwater transport time from the basalt to the lagoon that is much shorter than deduced from the claimed flowrate in basalt (~1 m y^{-1}) and the assumed distance (<500 m) between the top of the chimney and the limestone subsequent to an underground test.

A systematic lagoon sampling programme immediately after an underground test series would be needed in order to choose between these alternative explanations.

3.3. *LONG-TERM LEAKAGE*

Migration of radionuclides from the underground test sites is dependent on the availability of the radioactivity to leaching processes and on the availability and movement of water which has access to the radionuclides.

The estimated percentage of radioactivity contained, over the short term, in the vitrified material covers a wide range, from Tazieff's reported but unconfirmed 99.9% of fission products to 75% one minute after detonation (Berg, 1975). Most published reports merely state that 'most' of the radioactivity is trapped. Radioactivity condensed on the chimney rubble and walls is more readily leachable than that present within the vitrified material.

3.5. *CONCLUSIONS*

Venting of gaseous and volatile fission products from the underground test sites does occur at the time of detonation. The radionuclides vented include ones other than the noble gases (which are admitted by the French) and there is evidence that their magnitude is greater than would be expected simply through the back-packing of the placement bore being "less than perfect."

PARTICIPANTS IN THE STUDY

INTERNATIONAL ADVISORY COMMITTEE

Chairman

de Planque, E.G.
(former Commissioner of the United States Nuclear Regulatory Commission)
Independent consultant,
Potomac, Maryland,
United States of America

Members from IAEA Member States

Beninson, D.J.
(former Chairman of the International Commission on Radiological Protection)
Autoridad Regulatoria Nuclear,
Buenos Aires, Argentina

Clarke, R.
(Chairman of the International Commission on Radiological Protection)
National Radiological Protection Board,
Chilton, Oxfordshire,
United Kingdom

Garnett, H.
Australian Nuclear Science and Technology Organisation,
Lucas Heights, New South Wales,
Australia

Holm, G.E.G.
Radiation Physics Department,
Lund University Hospital,
Lund, Sweden

Karyono, H.S.
Nuclear Minerals Development Centre,
National Atomic Energy Agency,
Jakarta, Indonesia

Kaul, A.
Bundesamt für Strahlenschutz,
Salzgitter, Germany

Matushchenko, A.
Commission for Radiation Protection,
Moscow, Russian Federation

Numakunai, T.
Institute of Radiation Measurements,
Tokai, Japan

Poletti, A.
Department of Physics,
University of Auckland,
Auckland, New Zealand

Ex officio members from intergovernmental organizations

Bennett, B.
United Nations Scientific Committee on the Effects of Atomic Radiation,
Vienna

Fraser, G.
Directorate General XI/C/1,
European Commission,
Luxembourg

Fuavao, V.A.
(South Pacific Forum)
South Pacific Regional Environment Programme,
Apia, Western Samoa
(at present with the Office of the FAO Sub-Regional Representative for the Pacific, Apia)

Kreisel, W.
Health and Environment,
World Health Organization,
Geneva

TASK GROUP A
(Evaluation of the current radiological situation)

Chairman

McEwan, A.
National Radiation Laboratory,
Christchurch, New Zealand

Members

Aarkrog, A.
Risø National Laboratory,
Roskilde, Denmark

Fujimoto, K.
National Institute of Radiological Sciences,
Chiba, Japan

Gangaiya, P.
University of the South Pacific,
Suva, Fiji

Lokan, K.
Australian Radiation Laboratory,
Melbourne, Victoria,
Australia

Robison, W.L.
Lawrence Livermore National Laboratory,
Livermore, California,
United States of America

Schönhofer, F.
(Austria)
Chairman, Terrestrial Working Group

Woodhead, D.
(United Kingdom)
Chairman, Aquatic Working Group

Observer

Janssens, A.
Directorate General XI/C/1,
European Commission,
Luxembourg

Simon, S.
(former consultant to the Government of the Republic of the Marshall Islands)
Private consultant,
Reno, Nevada,
United States of America

Participating IAEA staff

Danesi, P.R.
Maillard, D.
Makarewicz, M.
Ouvrard, R.
Valkovic, V.
Zeiller, E.

TERRESTRIAL WORKING GROUP
(Radioactive material in the terrestrial environment)

Chairman

Schönhofer, F.
Federal Institute for Food Control and Research,
Vienna, Austria

Sampling and Surveillance Campaign in the Terrestrial Environment

Participating experts

Colgan, T.
Instituto del Medio Ambiente,
Centro de Investigaciones Energéticas, Medioambientales y Tecnológicas (CIEMAT),
Madrid, Spain
(at present with the Radiological Protection Institute of Ireland, Dublin, Ireland)

Cooper, M.
Australian Radiation Laboratory,
Melbourne, Victoria,
Australia

Green, N.
National Radiological Protection Board,
Chilton, Oxfordshire,
United Kingdom

Romero, M.L.
Instituto del Medio Ambiente,
Centro de Investigaciones Energéticas, Medioambientales y Tecnológicas (CIEMAT),
Madrid, Spain

Schönhofer, F.
Federal Institute for Food Control and Research,
Vienna, Austria

Participating laboratories

Agency's Laboratories,
International Atomic Energy Agency,
Seibersdorf

Centro de Isótopos,
Havana, Cuba

Environmental Measurements Laboratory,
United States Department of Energy,
New York, N.Y.,
United States of America

Federal Institute for Food Control and Research,
Vienna, Austria

Institute for Inorganic Chemistry,
University of Vienna,
Vienna, Austria

Institute of Radiobiology,
Minsk, Belarus

Instituto del Medio Ambiente,
Centro de Investigaciones Energéticas, Medioambientales y Tecnológicas (CIEMAT),
Madrid, Spain

Jožef Stefan Institute,
Ljubljana, Slovenia

National Radiological Protection Board,
Chilton, Oxfordshire,
United Kingdom

Norwegian Radiation Protection Authority,
Østerås, Norway

Physikalisch-Technische Bundesanstalt,
Braunschweig, Germany

Radiochemistry Group,
Central Veterinary Laboratory,
Addlestone, Surrey,
United Kingdom

AQUATIC WORKING GROUP
(Radioactive material in the aquatic environment)

Chairman

Woodhead, D.
Centre for Environment, Fisheries and Aquaculture Science,
Lowestoft, Suffolk,
United Kingdom

Sampling and Surveillance Campaign in the Aquatic Environment

Participating experts

Blowers, P.
Centre for Environment, Fisheries and Aquaculture Science,
Lowestoft, Suffolk,
United Kingdom

Dahlgaard, H.
Risø National Laboratory,
Roskilde, Denmark

Hamilton, T.
Lawrence Livermore National Laboratory,
Livermore, California,
United States of America

Szymczak, R.
Radiochemical Oceanography Group,
Australian Nuclear Science and Technology Organisation,
Lucas Heights, New South Wales,
Australia

Woodhead, D.
Centre for Environment, Fisheries and Aquaculture Science,
Lowestoft, Suffolk,
United Kingdom

Participating IAEA staff

Ballestra, S.
Huynh-Ngoc, L.
Osvath, I.
Povinec, P.

Participating laboratories

Australian Nuclear Science and Technology Organisation,
Lucas Heights, New South Wales,
Australia

Australian Radiation Laboratory,
Melbourne, Victoria,
Australia

Centre for Environment, Fisheries and Aquaculture Science,
Lowestoft, Suffolk,
United Kingdom

Federal Fisheries Research Centre,
Hamburg, Germany

IAEA Marine Environment Laboratory,
International Atomic Energy Agency,
Monaco

Institute of Geological and Nuclear Sciences,
Lower Hutt, New Zealand

Isotope Hydrology Laboratory,
International Atomic Energy Agency,
Vienna

Lawrence Livermore National Laboratory,
Livermore, California,
United States of America

National Radiation Laboratory,
Christchurch, New Zealand

Risø National Laboratory,
Roskilde, Denmark

TASK GROUP B
(Evaluation of the potential long term radiological situation)

Chairman

Levins, D.M.
Australian Nuclear Science and Technology Organisation,
Lucas Heights, New South Wales,
Australia

Members

Aoki, K.
Kamaishi Site Office,
Radioactive Waste Management Project,
Power Reactor and Nuclear Fuel Development Corporation,
Iwate, Japan

Beninson, D.J.
(replacing E. D'Amato)
Autoridad Regulatoria Nuclear,
Buenos Aires, Argentina

Cooper, J.
National Radiological Protection Board,
Chilton, Oxfordshire,
United Kingdom

De Geer, L.-E.
(Sweden)
Chairman, Working Group 3

Fairhurst, C.
(United States of America)
Chairman, Working Group 4

Jones, R.
United States Department of Energy,
Germantown, Maryland,
United States of America

Kürsten, M.
(retired from) Bundesanstalt für Geowissenschaften
und Rohstoffe,
Hanover, Germany

Mittelstaedt, E.
(Germany)
Chairman, Working Group 5

Smith, D.
Lawrence Livermore National Laboratory,
Livermore, California,
United States of America

Observer

Girardi, F.
Joint Research Centre,
European Commission,
Ispra, Italy

WORKING GROUP 3
(Source term)

Chairman

De Geer, L.-E.
National Defence Research Establishment,
Stockholm, Sweden
(at present with the Preparatory Commission for the
Comprehensive Nuclear-Test-Ban Treaty Organization,
Vienna)

Members

Beck, H.
Environmental Measurements Laboratory,
United States Department of Energy,
New York, N.Y.,
United States of America

Comley, C.
AWE Blacknest,
Brimpton, Berkshire,
United Kingdom

Dubasov, Y.V.
V.G. Khlopin Radium Institute,
St. Petersburg, Russian Federation

WORKING GROUP 4
(Geosphere radionuclide transport)

Chairman

Fairhurst, C.
University of Minnesota,
Minneapolis, Minnesota,
United States of America

Members

de Marsily, G.
Université de Paris,
Paris, France

Hadermann, J.
Paul Scherrer Institute,
Villigen, Switzerland

Nitsche, H.
Forschungszentrum Rossendorf eV,
Dresden, Germany

Sastratenaya, A.S.
National Atomic Energy Agency,
Jakarta, Indonesia

Townley, L.
Commonwealth Scientific and
Industrial Research Organisation,
Perth, Western Australia,
Australia

Underground Water Sampling Campaign

Participating expert

Smith, D.
Lawrence Livermore National Laboratory,
Livermore, California,
United States of America

Participating IAEA staff

Mulsow, S.
Warnecke, E.

Participating laboratories

Australian Nuclear Science and Technology Organisation,
Lucas Heights, New South Wales,
Australia

IAEA Marine Environment Laboratory,
International Atomic Energy Agency,
Monaco

WORKING GROUP 5
(Marine modelling)

Chairman

Mittelstaedt, E.
Federal Maritime and Hydrographic Agency,
Hamburg, Germany

Members

Deleersnijder, E.
Catholic University of Louvain,
Louvain, Belgium

Scott, M.
University of Glasgow,
Glasgow, United Kingdom

Tomczak, M.
Flinders Institute for Atmospheric and Marine Sciences,
Flinders University,
Adelaide, South Australia,
Australia

Yoon, J.-H.
(Republic of Korea)
Research Institute for Applied Mechanics,
Kyushu University,
Fukuoka, Japan

Co-opted members

Osvath, I.
IAEA Marine Environment Laboratory,
International Atomic Energy Agency,
Monaco

Povinec, P.
IAEA Marine Environment Laboratory,
International Atomic Energy Agency,
Monaco

Rajar, R.
University of Ljubljana,
Ljubljana, Slovenia

Togawa, O.
IAEA Marine Environment Laboratory,
International Atomic Energy Agency,
Monaco

FRENCH LIAISON OFFICE

Corion, G. (August 1996 onwards)
Direction des Centres d'expérimentations nucléaires,
Armées, France

Delcourt, P. (until August 1996)
Direction des Centres d'expérimentations nucléaires,
Armées, France

Goutière, G. (until September 1996)
Commissariat à l'énergie atomique,
Arpajon, France

Sornein, J.-F. (September 1996 onwards)
Commissariat à l'énergie atomique,
Bruyères-le-Châtel, France

TECHNICAL ILLUSTRATOR

Wildner, B. (Australian Nuclear Science and Technology Organisation)

IAEA SECRETARIAT

Project Management

Project Manager
González, A.J.

Technical Project Manager
Fry, R.M.

Analytical Project Managers
Baxter, M. (until November 1997)
Danesi, P.R.
Povinec, P. (November 1997 onwards)

Scientific Secretaries

Task Group A
Linsley, G.

Terrestrial Working Group
Danesi, P.R.

Aquatic Working Group
Povinec, P. (October 1996 onwards)
Valković, V. (until October 1996)

Task Group B
Webb, G.

Working Group 3
McKenna, T.

Working Group 4
Warnecke, E.

Working Group 5
Baxter, M. (until November 1997)
Povinec, P. (November 1997 onwards)

Administrative Assistant
Boldizsar, R.

Computer Assistant
Hinterleitner, G.

Technical Writers and Editors

Barraclough, I.
Davies, M.
Delves, D.
Flitton, S.P.
Robinson, C.

MEETINGS

29–31 January 1996
Informal technical consultation meeting, Vienna

28–29 March 1996
Initial meeting of Task and
Working Group Chairmen of International Advisory Committee (IAC) and
French Liaison Office, Montlhéry, France

11–12 April 1996
Meeting of Chairmen of Task and Working Groups, Vienna

13–14 April 1996
First formal meeting of IAC, Vienna

13–15 May 1996
First meeting of Task Group A (TG-A), Monaco

19–21 June 1996
First meeting of Working Group 5 (WG-5), Monaco

22, 24 June 1996
First meeting of Working Group 4 (WG-4), Paris

1–2 July 1996
First meeting of Working Group 3 (WG-3), Paris

2–3 July 1996
First meeting of Task Group B (TG-B), Paris

10–13 September 1996
First review and co-ordination meeting of IAC Chairman with TG Chairmen and WG-5 Chairman, Vienna

29 September–2 October 1996
Second meeting of WG-3, Stockholm

2–4 December 1996 (Suva, Fiji) and
4–6 December 1996 (Papeete, Tahiti)
Second formal meeting of IAC

24–27 February 1997
Second meeting of WG-4, Paris

18–21 April 1997
Second meeting of WG-5, Monaco

12–14 May 1997
Second meeting of TG-B, Vienna

14–16 May 1997
Second meeting of TG-A, Vienna

15–16 August 1997
Third meeting of WG-4, Vienna

20–22 August 1997
Third meeting of TG-B, Vienna

25–27 August 1997
Third meeting of WG-5, Monaco

17–19 September 1997
Second review and co-ordination meeting of IAC Chairman with TG and WG Chairmen, Vienna

24–28 November 1997
Meeting of TG Chairmen, Vienna

3–5 February 1998
Third formal meeting of IAC, Vienna

98-01634